PHOTOGRAPH THIS SHEET

AD-E 800 764

AD A 953074

LEVEL

INVENTORY

Bomb Penetration Project

DOCUMENT IDENTIFICATION

Contract DA29-005 eng-280

15 Jun. 51

DISTRIBUTION STATEMENT A

Approved for public release;
Distribution Unlimited

DISTRIBUTION STATEMENT

ACCESSION FOR		
NTIS	GRA&I	☒
DTIC	TAB	☐
UNANNOUNCED		☐
JUSTIFICATION		
(15 June 1951)		
BY		
DISTRIBUTION /		
AVAILABILITY CODES		
DIST	AVAIL AND/OR SPECIAL	
A/1		

DISTRIBUTION STAMP

Released

COPY INSPECTED 2

UNANNOUNCED

DTIC
ELECTE
FEB 28 1984
S D
D

DATE ACCESSIONED

84 02 27 132

DATE RECEIVED IN DTIC

PHOTOGRAPH THIS SHEET AND RETURN TO DTIC-DDA-2

DTIC FORM OCT 79 70A

DOCUMENT PROCESSING SHEET

AD E800 764

ADA953074

Bomb Penetration Project

Colorado School of Mines
Research Foundation, Inc.

C. W. Livingston and F. L. Smith

Golden, Colorado, 15 June 1951

APPROVED FOR PUBLIC RELEASE: NO LIMITATION
ON DISTRIBUTION

CONFIDENTIAL
UNCLASSIFIED

C

Regraded UNCLASSIFIED

by authority of DoD Dir. 5200.10 Date 22 Sept 63
(Document authorizing the change)

UNCLASSIFIED
CONFIDENTIAL

E

COLORADO SCHOOL OF MINES RESEARCH FOUNDATION, INC.
GOLDEN, COLORADO

20 April, 1951

Charles H. McNutt, Colonel, Corps of Engineers
District Engineer
Albuquerque District, Corps of Engineers
P.O. Box 1538
Albuquerque, New Mexico

Dear Sir:

In compliance with contract No. DA-29-005 eng-280 entered into between the Colorado School of Mines Research Foundation and the Albuquerque District, Corps of Engineers, on 15 June, 1950, we submit herewith our report, together with the specified number of copies of the appendix to the report.

Contract No. DA-29-005 eng-280 provided for the field work, laboratory work, analysis and compilation of data in connection with the "Bomb Penetration Project" as outlined on 15 February, 1950 by the Protective Construction Branch, Engineering Division (Military Construction), Office, Chief of Engineers, Department of the Army.

Fundamentals of penetration obtained during the course of the field and laboratory work are presented herein and should prove helpful in designing fortifications to resist penetration and in designing and selecting bombs for attack.

Respectfully submitted,

V. L. Mattson

V. L. Mattson, Director
Colorado School of Mines
Research Foundation, Inc.

CONFIDENTIAL UNCLASSIFIED

RESTRICTED

Reclassified To
By Author [illegible] neers
[illegible] MAY 12 1954
Date

BOMB PENETRATION PROJECT

Colorado School of Mines Research Foundation, Inc.

C. W. Livingston and F. L. Smith

"This document contains information affecting the national defense of the United States within the meaning of the Espionage Act, 50 U.S.C., 31 and 32, as amended. Its transmission or the revelation of its contents in any manner to an unauthorized person is prohibited by law."

Golden, Colorado, 15 June 1951

UNCLASSIFIED

CONFIDENTIAL

CONTENTS

	Page
Abstract	i
Summary	iii
Part A—Introduction	1
Section I—The Problem	1
1. Nature of the Problem	1
2. Objectives of the Bomb Penetration Project	1
3. Personnel and Acknowledgements	3
Section II—Field Procedure	5
1. Site Selection	5
2. Field Procedure	9
a) Target Preparation, Access Roads	9
b) Diamond Drilling, Specimen Preparation, and Core Logging	9
c) Auger Drilling	15
d) Surveying and Topographic Mapping	15
e) Target Layout and Target Marking	16
f) Bombing and Communications	19
g) Crater Mapping and Crater Photographs	25
h) Excavation	25
i) Damage Surveys and Field Analysis	33
j) Bomb Recovery and Disposal	33
Section III—Geologic Report	37
1. Regional Geology	37
a) Introduction	37
b) Stratigraphy	37
b-1) Pre-Cambrian Rocks	37
b-2) Pennsylvanian Rocks	38
b-3) Permian Rocks	38
b-4) Triassic Rocks	38
b-5) Jurassic Rocks	38
b-6) Cretaceous Rocks	39
b-7) Tertiary Rocks	39
b-8) Quaternary Rocks	39
c) Structure	39
c-1) Folds	40
c-2) Faults	40
d) Geologic History	40

CONTENTS—(Continued)

	Page
2. Geology of the Granite Site Target Area	43
3. Geology of the Sandstone Site Target Area	45
4. Petrographic Report	47
a) The Zuni Granite	47
a-1) General Description	47
a-2) Mineralogy	47
a-3) Alteration	48
b) Lamprophyre (Vogesite) Dikes in Zuni Granite	49
b-1) General Description	49
b-2) Mineralogy	49
c) The Dakota Sandstone	51
c-1) General Description and Mineralogy	51
Section IV—Physical Rock Tests	53
1. Test Procedure	53
2. Porosity—Total and Apparent	53
3. Apparent Specific Gravity	54
4. Tensile Strength	56
5. Modulus of Rupture	58
6. Compressive Strength	60
7. Impact Toughness	61
8. Scleroscope Hardness	63
9. Elastic Constants—Dynamic Method	67
10. Velocity of Sound and Seismic Velocity	69
11. Elastic Constants, Static Method	69
12. Triaxial Compression Tests	71
13. Summary of Results	74
Part B—Ballistic Data	77
Section I—Bomb Characteristics and Nominal Dimensions	77
1. Introduction	77
2. Description of Bombs Used in the Tests	77
Section II—Bomb Ballistics	81
1. Striking Velocity	81
2. Angle of Fall	81
Part C—Penetration Tests in Zuni Granite	83
Section I Test Procedure	83
1. Detail Layout of the Granite Site	83

CONTENTS—(Continued)

	Page
2. Description of the Tests in Granite	83
3. Vertical Penetration of 1600 AP, 2000 SAP, and 25,000 SAP Bombs in Granite	85
4. Crater Shape as Related to Impact Energy	87
5. Path Shape as Related to Impact Energy	91
6. Damage to 1600 AP, 2000 SAP, and 25,000 SAP Bombs	92
Part D—Penetration Tests in Dakota Sandstone	99
Section I—Test Procedure	99
1. Detail Layout of the Sandstone Site	99
2. Description of the Tests in Sandstone	99
3. Vertical Penetration of 1600 AP, 2000 SAP, and 2000 GP Bombs in Dakota Sandstone	100
4. Crater Shape as Related to Impact Energy	100
5. Path Shape as Related to Impact Energy	104
6. Damage to 1600 AP, 2000 SAP, and 2000 GP Bombs	105
Part E—Laboratory Experiments and Stress Analysis	113
Section I—Model Bombing Experiments	113
1. Introduction	113
2. Comparison of Penetration of Various Bombs	114
3. Effect of Sectional Density and of Sectional Pressure Upon Penetration at Constant Kinetic Energy	117
4. Effect of Compressive Strength Upon Penetration	118
5. Variation of Penetration with Kinetic Energy	119
6. Variation of Penetration with Angle of Impact	123
Section II—Stress-Coat Experiments	125
1. Introduction	125
2. Summary of Experimental Results—Aluminum Alloy Models	126
2a) Areas of Equal Strain	126
2b) Stress Trajectories	129
3. Summary of Experimental Results—Allite Models	131
3a) Area of Compression Spalling—90-Degree Angle of Impact	131
3b) Area of Compression Spalling at Various Angles of Impact	133
Section III—Stresses and Displacements Produced in a Semi-Infinite Solid by a Concentrated Force at the Surface	137
1. Introduction	137

CONTENTS—(Continued)

	Page
2. Notation	137
3. Stress and Coordinate Conventions	138
4. The Problem	138
5. Stress-Strain Relations	138
6. Displacements and Stresses	139
7. Principal Stresses and Directions	142
8. Horizontal and Vertical Component Stress for $y = 0$	143
9. Explanation of Tables and Computations	144
10. Maximum Shear Contours	145
11. Stress Trajectories	146
12. Principal Stress Contours	146
13. Illustrative Applications of the Diagrams	146
Section IV—Metallurgical Studies	151
1. Introduction	151
2. Flow Lines and Strain Lines	152
3. Flow-Metal Droplets	152
4. Microstructure	152
5. Hardness Changes	153
Section V—Photoelastic Studies of Stress Distribution in the Medium	155
1. Introduction	155
2. Comparison of Mathematical and Photoelastic Results	156
3. The Use of Gelatin as a Photoelastic Material	159
4. Comparison of the Stress Distribution in the Medium at the Noses of 2000 SAP and 25,000 SAP Bombs	160
5. Stress Distribution in the Medium at Various Stages of Penetration of a 1600 AP Bomb	164
Section VI—Photoelastic Studies of the Stress Distribution in the Bomb	169
1. Introduction	169
2. Maximum Shear Stress Distribution in the Nose of a 1600 AP Bomb	169
3. Maximum Shear Stress Distribution in the Nose of a 25,000 SAP Bomb	172
4. Maximum Shear Stress Distribution in the Nose of a 2000 SAP Bomb	172
5. Maximum Shear Stress Distribution in the Nose of a 2000 GP Bomb	174
6. Summary	175

CONTENTS—(Continued)

	Page
Part F—Analysis and Conclusions	177
Section I—A Theory of Penetration of Projectiles in Rock	177
1. Introduction	177
2. Rock Failure at Impact	177
2a) Effect of Kinetic Energy	177
2b) Displacement of the Overburden	179
2c) Effect of Nose Shape	179
2d) Effect of Bomb Diameter	179
2e) Effect of Physical and Elastic Properties of the Rock	182
3. Crushing Failure as Related to Depth	183
4. Failure in Combined Shear and Tension	188
4a) Characteristics of the Zone of Shearing	188
4b) Characteristics of the Zone of Tension Slabbing	191
5. A Theory of Rock Failure	193
Section II—The Influence of Geology and Topography Upon Penetration	195
1. The Influence of Soil Cover	195
2. The Influence of Joints, Faults, and Bedding Planes	195
3. Comparison of the Elastic Properties of Dakota Sandstone and Zuni Granite as Related to Penetration and Path Shape	198
4. The Influence of Topography and Striking Angle Upon Penetration and Path Shape	205
Section III—Review and Analysis of Penetration Formulas and Derivation of the Livingston Penetration Formula	207
1. Review and Analysis of Penetration Formulas	207
2. Zuni Granite and Dakota Sandstone Prototype Composite Curves	209
3. Dakota Sandstone Prototype Rock and Prototype Bomb Curves	210
3a) Correction for the Bomb Diameter	210
3b) Nose Correction Factors	211
4. Relation of Sectional Pressure and Sectional Density to Penetration in Rock	212
5. Increased Resistance to Penetration as a Function of Depth, Striking Velocity, and Kinetic Energy	212
6. The Livingston Penetration Formula	213
7. Extrapolation of the Data	216
8. Use of the Formula	216

CONTENTS—(Concluded)

	Page
Section IV—The Effect of Bombing on Underground Installations	223
1. Accuracy of Bombing	223
2. Preliminary Discussion	223
3. Comparison of Various Bombs for Damage to Underground Openings	226
4. Attack or Defense of Any Underground Opening	227
Section V—Conclusions	231
1. The Livingston Penetration Formula	231
2. Effect of the Bomb Upon the Rock	235
3. Effectiveness of an Underground Installation	239
4. Effect of the Rock Upon the Bomb	239
5. Selection of Bombs for Attack	242
6. Recommendations	243
Table of Errata	Back of Book

ILLUSTRATIONS

Figure		Page
1	Index Map	Following 4
2	Photograph, The Paxton Springs Granite Site	6
3	Photograph, The 600-Foot-Diameter Clearing at the Putney Mesa Sandstone Site	7
4	Diamond-Drill Hole Pattern and Hole Numbers	Following 8
5	Photograph, Underground Diamond Drill Adapted for Surface Drilling	8
6	Photograph, Diamond Drill Rig in Operation	10
7	Photograph, Logging Diamond Drill Cores	11
8	Diamond Drill Core Log	Following 12
9	Diamond Drill Core Log	Following 12
10	Photograph, Cutting Specimens from the Drill Cores to Length for Physical Rock Tests	12
11	Photograph, Original Target Layout of Granite Site	13
12	Photograph, Bull's-eye Target Pattern at the Granite Site	14
13	Photograph, The Target Layout and Grid Road Pattern at the Putney Mesa Sandstone Site	14
14	Photograph, Weapons Carrier Converted to Spray Truck for Target Marking	17
15	Photograph, Loading Black Volcanic Cinders into Weapons Carrier	17

ILLUSTRATIONS—(Continued)

Figure		Page
16	Photograph, Spreading Cinders Along Boundaries of 150-foot Market Square	18
17	Photograph, Bull's-eye Target Outlined with Volcanic Cinders	18
18	Spotting Map, Granite Site Following	20
19	Spotting Map, Sandstone Site Following	20
20	Photograph, Layout of the Ground Control Station, "Brass Nob," Granite Site	21
21	Photograph, The Plotting Table and Spotting Map	21
22	Photograph, The Granite Target as Viewed from Observation Station "Fred's Pipe"	22
23	Photograph, Close-up of the VHF Radio Equipment	23
24	Photograph, The Sandstone Site Viewed from Observation Station "Easy" at the Conclusion of the Tests	24
25	Photograph, Portable Headframe for Crater Excavation	26
26	Photograph, Crater Headframe Detail and Accessories	26
27	Photograph, Above-Ground Muck Pile, Apparent Crater 19	27
28	Photograph, Portable Headframe in Place for Sinking Crater 19	27
29	Photograph, Shaft Timbering and Spiling, Bomb 19	28
30	Photograph, Condition of Rock Near Collar Set, 25,000 SAP Bomb 20	30
31	Photograph, Shaft Timber Details, Bomb 20	30
32	Crater No. 17 Following	30
33	Photograph, Measuring Compaction of Inert Filler in a 2000 SAP Bomb	31
34	Photograph, Damage to Casing of a 2000 GP Bomb Released from 16,000 Feet Above the Sandstone Target	31
35	Photograph, Collecting Specimens of Flowed Metal From the Nose of a Bomb	32
36	Photograph, Cutting Specimens for Metallurgical Studies	32
37	Photograph, Dragging Bombs to Disposal Area	34
38a	Photograph, Hoisting a 25,000-Pound Bomb From its Crater	35
38b	Photograph, Lowering Bomb to Ground in a 90-Degree Position	35
38c	Photograph, Lifting the 25,000-Pound Bomb in a Horizontal Position	36
38d	Photograph, Securing Bomb on a Lowboy	36
39	Geologic Map—South of Grants, Valencia County, New Mexico Following	38
40	General Stratigraphic Table of Area Near Grants, New Mexico Following	38
41	Geologic Map of Granite Site Target Area Following	42

p

ILLUSTRATIONS—(Continued)

Figure		Page
42	Photograph, Panoramic View Showing Granite Core of Zuni Uplift	42
43	Geologic Column of Section a-a' East of Granite Site Following	42
44	Photograph, The Granite Surface at the Paxton Springs Bombing Site	44
45	Geologic Map of Sandstone Site Target Area Following	44
46	Cross-Section of Sandstone Target Looking North, Section b-b' Following	44
47	Geologic Section c-c' Looking East, Sandstone Target Site Following	44
48	Photograph, View Looking North Toward Sandstone Target	46
49	Geologic Column of Section d-d'—South of Sandstone Target Following	46
50	Photograph, Bent and Fractured Grains of Plagioclase	50
51	Photograph, Elongated, Pod-Shaped Cluster of Quartz Grains	50
52	Photograph, Coarse Laths of Sericite Formed from Hydrothermal Alteration	51
53	Table, Specific Gravity and Porosity of Specimens of Dakota Sandstone and Zuni Granite	55
54	Photograph, Tension Specimen and Grip Assembly	56
55	Table, Tensile Strength of Specimens of Dakota Sandstone and Zuni Granite	57
56	Photograph, Modulus of Rupture Test	58
57	Table, Modulus of Rupture of Specimens of Dakota Sandstone and Zuni Granite	59
58	Table, Compressive Strength of Specimens of Dakota Sandstone and Zuni Granite	61
59	Photograph, C.S.M. Impact Apparatus	63
60	Table, C.S.M. Impact Test, Impact Toughnett of Specimens of Dakota Sandstone and Zuni Granite	64
61	Table, U. S. Bureau of Mines (Page) Impact Test, Impact Toughness of Specimens of Dakota Sandstone and Zuni Granite	64
62	Photograph, Recording-Type Shore Sclerescope, Model C	65
63	Table, Sclerescope Hardness and Coefficient of Restitution for Specimens of Dakota Sandstone and Zuni Granite—Diamond-Pointed Hammer	66
64	Table, Elastic Constants for Dakota Sandstone and Zuni Granite—Dynamic Method	68
65	Table, Young's Modulus and Poisson's Ratio First Loading Cycle Following	70
66	Graph, Simple Compression Tests—Granite Following	70

ILLUSTRATIONS—(Continued)

Figure		Page
67	Graph, Simple Compression Tests — Dakota Sandstone Following	70
68	Graph, Young's Modulus and Poisson's Ratio—Dakota Sandstone and Zuni Granite Following	70
69	Table, Triaxial Compressive Strength—Dakota Sandstone, Weathered Zuni Granite, and Unweathered Zuni Granite	72
70	Photograph, Test Specimens of Dakota Sandstone Showing Manner of Failure	73
71	Mohr Diagrams—Dakota Sandstone and Zuni Granite Following	74
72	Table, Summary of Physical and Elastic Properties of Dakota Sandstone and Zuni Granite Following	74
73	Photograph, 1600-Poung Armor-Piercing AN-MK-1 Bomb	77
74	Bomb, 1600 lb AP, AN-MK-1—Characteristics and Nominal Dimensions Following	78
75	Photograph, 2000 SAP, AN-M 103 Bomb	79
76	Bomb, 2000 lb SAP, AN-M 103—Characteristics and Nominal Dimensions Following	80
77	Photograph, 2000 GP, AN-M66A2 Bomb	79
78	Bomb, 2000 lb GP, AN-M66A2—Characteristics and Nominal Dimensions Following	80
79	Bomb, 25,000 SAP, T28E4—Characteristics and Nominal Dimensions Following	80
80	Graph, Altitude Above Target vs Striking Velocity—1600 AP Bomb Following	82
81	Graph, Altitude Above Target vs Striking Velocity—2000 SAP Bomb Following	82
82	Graph, Altitude Above Target vs Striking Velocity—25,000 SAP Bomb Following	82
83	Graph, Altitude Above Target vs Striking Velocity—2000 GP Bomb Following	82
84	Graph, Striking Velocity vs Height of Target Following	82
85	Graph, Altitude Above Target vs Angle of Fall—1600 AP Bomb and 25,000 SAP Bomb Following	82
86	Graph, Altitude Above Target vs Angle of Fall—2000 GP Bomb and 2000 SAP Bomb Following	82
87	Topographic Map—Granite Site Following	84
88	Diagram of Crater Measurements Following	84
89	Ballistic and Crater Data—Zuni Granite Following	84
90	Graph, Vertical Penetration vs Impact Energy—Zuni Granite Following	84
91	Photograph, Control of Rebound by Joint Planes	86
92	Photograph, Path of Bomb 13 Leaving Crater	87

R

ILLUSTRATIONS—(Continued)

Figure		Page
93	Photograph, Apparent Crater 1600 AP Bomb 1—Altitude Above Target 9200 Ft	88
94	Photograph, Effect of Impact Energy Upon Crater Shape—Scale Models of Craters 3, 5, and 9—1600 AP Bombs	89
95	Photograph, Effect of Impact Energy Upon Crater Shape—Scale Models of Craters 11, 18, and 16—2000 SAP Bombs	90
96	Effect of Energy on Path Shape—Granite Following	90
97	Crater No. 19 Following	90
98	Crater No. 20 Following	90
99	Photograph, Fins and Rear of Bomb Body—25,000 SAP—Altitude of Release 18,000 Ft	92
100	Photograph, Typical Condition of Cap and Base Plate of 2000 SAP and 1600 AP Bombs After Impact	93
101	Photograph, 1600 AP Bomb Released from 18,000 Ft Above Granite Site	93
102	Photograph, Nose of 1600 AP Bomb Released from 18,000 Ft Above Granite Target	94
103	Photograph, 2000 SAP Bomb 16 Showing Slight Gouging of Nose—Altitude of Release 30,000 Ft	95
104	Photograph, Crack in Body of 25,000 SAP Bomb 20—Altitude of Release 26,000 Ft	96
105	Photograph, Putney Mesa Sandstone Bombing Site	98
106	Topographic Map—Sandstone Site Following	100
107	Ballistic and Crater Data—Dakota Sandstone Following	100
108	Ballistic and Crater Data—Dakota Sandstone Following	100
109	Graph, Vertical Penetration vs Impact Energy—Dakota Sandstone Following	100
110	Photograph, Plaster Models of Craters 24, 22, and 28. Produced by 1600 AP Bombs in Dakota Sandstone	101
111	Photograph, Plaster Models of Craters 33, 38, and 32. Produced by 2000 SAP Bombs in Dakota Sandstone	102
112	Photograph, Plaster Models of Craters 48, 39, and 46. Produced by 2000 GP Bombs in Dakota Sandstone	103
113	Table, Ratio of Crater Radius R to Crater Depth D for 1600 AP, 2000 SAP, and 2000 GP Bombs in Dakota Sandstone	104
114	Effect of Energy on Path Shape—Sandstone Following	104
114a	Table, Angle "V" as a Function of Impact Energy for Various Bombs	105
115	Photograph, 1600 AP Bomb 28 Released from 30,000 Ft Above the Sandstone Target	106
116	Photograph, 2000 SAP Bomb 30 Released from 30,000 Ft Above the Sandstone Target	106
117	Photograph, Sequence of Damage of 2000 GP Bombs Released from 7000, 8700, 18,000, and 30,000 Ft Above the Sandstone Target	107

S

ILLUSTRATIONS—(Continued)

Figure		Page
118	Photograph, Longitudinal Rupture Associated with Bulge of Bomb Nose	108
119	Photograph, Rupture and Loss of Filling—2000 GP Bomb 39—Altitude of Release 18,000 Ft	109
120	Photograph, 2000 G PBomb Released from 30,000 Ft Above the Sandstone Target	109
121	Photograph, C.S.M. Model Bombing Apparatus	112
122	Graph, Effects of Bomb Properties on Penetration	Following 116
123	Graph, Penetration in Zonolite Mixtures of Various Strengths	Following 118
124	Graph, Cement-Zonolite Mixes—Penetration vs Tensile Strength	Following 118
125	Graph, Cement-Zonolite Mixes—Penetration vs Compressive Strength of Mix	Following 118
126	Graph, Penetration vs Compressive Strength	Following 120
127	Graph, Penetration vs Kinetic Energy—Calseal Mixture	Following 120
128	Photograph, Plaster Model After Impact—SAP Model Bomb	121
129	Photograph, Plaster Model After Impact—AP Model Bomb	122
130	Graph, Penetration vs Kinetic Energy—Molding Plaster	Following 122
131	Graph, Poisson's Ratio and Young's Modulus—Molding Plaster	Following 122
132	Graph, Variations of Penetration with Angle of Impact	Following 122
133	Photograph, Hesselbacher Apparatus for Determining Dynamic Strain Patterns in Stress-Coat	126
134	Photograph, Dynamic Strain Pattern in a Stress-coat Model by Impact of 25,000 SAP Model Bomb	127
135	Photograph, Dynamic Strain Pattern—Impact of 1600 AP Model Bomb	128
136	Table, Depth and Areas of Equal Minimum Tensile Strain	129
137	Graph, Area and Depth of Tension Zone vs Kinetic Energy—Stress-Coated Models	Following 128
138	Stress Trajectories—Stress-Coat Model	Following 130
139	Photograph, Area of Flaking Below Model GP Bomb	130
140	Graph, Area and Depth of Compressive Zone vs Kinetic Energy—2000 GP Bomb	Following 130
141	Photograph, Compression Spalling and Tension Cracks—Impact Model of a 2000 SAP Bomb	132
142	Graph, Area of Flaking—2000 SAP Bomb—Surface Impact	Following 132
143	Photograph, Dynamic Strain Pattern at 65-Degree Angle of Impact	134

T

ILLUSTRATIONS—(Continued)

Figure		Page
144	Photograph, Dynamic Strain Pattern at 90-Degree Angle of Impact	135
145	Stress Conventions	Following 138
146	Principal Stress Conventions	Following 142
147	Table, Stresses in Dimensionless Form	Following 144
148	Maximum Shear Contours—Case I	Following 144
149	Maximum Shear Contours—Case II	Following 144
150	Maximum Shear Contours—Case III	Following 144
151	Maximum Shear Contours—Case IV	Following 144
152	Stress Trajectories—Case I	Following 146
153	Stress Trajectories—Case III	Following 146
154	Principal Stress Contours—Case I	Following 146
155	Principal Stress Contours—Case III	Following 146
156	Figure to Accompany Example I, Part 13	Following 148
157	Photograph, Distribution of Metal Droplets—Nose of AP Bomb	151
158	Metallurgical Studies—1600 AP Bomb—Metal Droplets	Following 152
159	Metallurgical Studies—2000 GP Bomb	Following 152
160	Hardness of GP Bombs After Impact (Shore Scleroscope)	Following 152
161	Photograph, Photoelastic Apparatus and Loading Frame	156
162	Two-Dimensional Stresses for 60° Loading	Following 156
163	Photograph, Shear Contours as Determined Photoelastically in the Medium Below a Model 25,000 SAP Bomb	158
164	Shear Contours in 2- and 3-Dimensional Bodies	Following 158
165	Photograph, Gelatin Model Loading Frame	161
166	Photograph, Stress Distribution in the Medium at the Nose of a 2000 SAP Bomb	162
167	Photograph, Stress Distribution in the Medium at the Nose of a 25,000 SAP Bomb	163
168a	Photograph, Shear Stress Distribution at Nose of 25,000-pound Model Bomb	165
168b	Photograph, Shear Stress Distribution at Nose of 2000-pound SAP Model Bomb	166
169	Shear Contours and Stress Trajectories in the Medium—1600 AP Bomb	Following 166
170	Stress Trajectories at Nose—2000 SAP Bomb	Following 166
171	Photograph, Maximum Shear Stress Distribution in the Nose of a 1600 AP Bomb	170
172	Photograph, Maximum Shear Stress Distribution in the Nose of a 25,000 SAP Bomb	171

ILLUSTRATIONS—(Continued)

Figure		Page
173	Photograph, Maximum Shear Stress Distribution in the Nose of a 2000 SAP Bomb	173
174	Photograph, Maximum Shear Stress Distribution in the Nose of a 2000 GP Bomb	174
175 a & b	Photograph, Fragmentation in Granite as Related to Impact Energy	178
176 a & b	Photograph, A Comparison of Fragmentation of Dakota Sandstone Relative to the Bomb Diameter	180
177 a & b	Photograph, The Influence of Rock Type Upon Fragmentation—2000 SAP Bombs; Release Altitude 30,000 Feet	181
178 a & b	Photographs, Crushing Failure as Related to Depth	184
178 (c)	Photograph, Crushing Failure as Related to Depth	185
179	Photograph, Crushed Zone in Footwall of 2000 SAP Bomb 11—Altitude of Release, 9200 Feet—Target, Zuni Granite	186
180	Photograph, Crushed Zone at Nose of 25,000 SAP Bomb 19—Altitude of Release, 18,000 Feet—Target, Zuni Granite	187
181	Photograph, Rock Failure Within the "Zone of Shearing"; Stage 1—Path Cracks	189
182	Photograph, Rock Failure Within the "Zone of Shearing"; Stage 2—Rock Burst and Release of Strain Energy	190
183a	Photograph, Characteristics of the "Zone of Crushing"	192
183b	Photograph, Characteristic of the "Zone of Tension Slabbing"	192
184	Sketches to Illustrate a Theory of Rock Failure	Following 192
185	Sketches Showing the Effect of Jointing Upon Crater Shape and Bomb Path	Following 196
186	Photograph, The Influence of Faulting Upon the Path of a Bomb	196
187	Photograph, Effect of Bedding in Sandstone Upon Penetration	199
188	Photograph, Effect of Bedding Upon Vertical Penetration	199
189a	Photograph, Rebound of 1600 AP Bomb in Zuni Granite	201
189b	Photograph, Rebound of 1600 AP Bomb in Dakota Sandstone	201
190	Graph, Path Length vs Kinetic Energy—1600 AP and 2000 SAP Bombs—Sandstone and Granite	Following 202
191	Graph, Vertical Penetration vs Kinetic Energy—1600 AP and 2000 SAP Bombs—Sandstone and Granite	Following 202
192	Table, Ratios of Penetration in Zuni Granite and Dakota Sandstone—1600 AP and 2000 SAP Bombs	204
193	Path of 1600 AP Bombs Referred to a 65° Line of Action	Following 204
194	Vertical Deviation, I_N, for Up-dip, Level, and Down-dip Bombing	206

ILLUSTRATIONS—(Concluded)

Figure		Page
195	Graph, Normal Penetration vs. Kinetic Energy—1600 AP and 2000 SAP Bombs—Sandstone and Granite	Following
196	Composite Path Length, Prototype Granite and Sandstone Curves, 1600 AP and 2000 SAP Bombs	Following 210
197	Composite Normal Penetration Prototype Granite and Sandstone Curves, 1600 AP and 2000 SAP Bombs	Following 210
198	Composite Vertical Penetration Prototype Granite and Sandstone Curves, 1600 AP and 2000 SAP Bombs	Following 210
199	Graph, Nose Correction Factor versus Caliber Radius of Head	Following 210
200	Penetration versus Kinetic Energy Prototype Bombs—Prototype Rock	Following 210
201	Values of Q_{NR} in the Livingston Penetration Formula	Following 214
202	Values of Q_P in the Livingston Penetration Formula	Following 214
203	Extrapolation of Penetration Data	Following 216
204	Horizontal Displacement as Influenced by the Inclination of the Target Surface	Following 220
205	Table, Quantities Used in Predicting Damage to an Underground Opening	Following 224
206	Damage to an Underground Opening by Various Bombs	Following 224
207	Table, Figure of Merit for Various Bombs to Give Destruction in Sandstone	Following 226
208	Table, Figure of Merit for Various Bombs to Give Tension in Sandstone	Following 226
209	Figure of Merit for Various Bombs to Give Destruction in Granite	Following 226
210	Figure of Merit for Various Bombs to Give Tension in Granite	Following 226

CONTENTS OF APPENDIX

PART A—DIAMOND DRILL LOGS

Logs of the following diamond drill holes:

GRANITE	SANDSTONE
G—0—0	S—0—0a
G—0—1	S—0—0b
G—0—2	S—0—1
G—0—3	S—0—2
G—I—13a	S—0—3
G—I—13b	S—0—4
G—I—13c	S—III—0
G—I—14	S—III—5
G—III—0	S—III—6
G—III—5	S—VI—0
G—III—6	S—VI—7
G—VI—0a	S—VI—8
G—VI—0b	S—IX—0
G—VI—0c	S—IX—9
G—VI—8	S—IX—10
G—VI—8a	S—XII—0
G—IX—0	S—XII—11
G—IX—9a	
G—IX—9b	
G—XII—0	
G—XII—11	
G—XII—12	
G—1000	

PART B—TRIANGULATION SYSTEM AND TOPOGRAPHIC MAPS

1—Triangulation Map—Paxton Springs Granite Site
Triangulation Map—Putney Mesa Sandstone Site

2—Topography—Granite Site; 1-Foot Contour Interval
Topography—Sandstone Site; 1-Foot Contour Interval

3—Topography—Granite Site; 5-Foot Contour Interval
Topography—Sandstone Site; 5-Foot Contour Interval

PART C—CRATER MAPS

Granite Craters 1 through 20
Sandstone Craters 21 through 50

PART D—STRESS ANALYSIS COMPUTATION TABLES

ABSTRACT

✦ ✦ ✦

The Colorado School of Mines Research Foundation undertook a Bomb Penetration Project, a project designed and sponsored by the Protective Construction Branch, Office, Chief of Engineers, U. S. Army, as a coordinated undertaking by the U. S. Airforce and the Army Corps of Engineers to determine the penetration of inert bombs into representative types of rocks. In the field, bombs of various types were dropped on "hard" Paxton Springs granite and on "soft" Putney Mesa sandstone. Data were taken to provide evidence for a study of the effect of the bomb on the medium and of the effect of the medium on the bomb. The field data were supplemented by laboratory tests of the physical and elastic properties of the rocks, by model bomb experiments, by photoelastic model tests, by mathematical analysis of stress distributions, by metallurgical studies of the bomb metal, and by the development of a theory of rock failure and a theory of penetration. As a result of the analysis of the data and of the development of the theory, a penetration formula was evolved. This formula, the Livingston Penetration Formula, is thought to be valuable in the design and selection of bombs to reduce enemy fortifications and in the design of fortifications to resist enemy bombs.

SUMMARY

The object of the Bomb Penetration Project was to study the penetration of inert bombs into representative "hard" and "soft" rocks in an effort to gain knowledge, both from field and from laboratory investigations, which would contribute to an understanding of rock failure and would prove useful in designing fortifications to resist attack and in designing and selecting bombs for attacking underground installations.

The field investigations comprised two parts:

(1) An analysis of the effect of the bomb on the rock.

A thorough study was made of the cracks in the rock, the manner of rock failure, and the influence of physical and geologic properties of rocks upon crater shape and bomb path. During the field work a theory of bomb penetration was developed, and evidence was accumulated in support of this theory.

(2) An analysis of the effects of the rock upon the bomb .

The various critical dimensions of the bomb were compared before and after the drop, the compaction of the inert material in the bomb was measured, photographs and measurements were taken to record distortion or damage to the casing, specimens of flowed metal were collected, and specimens were cut from the bombs for metallurgical study.

Target sites for the tests were ultimately selected for the "hard" rock tests in the Paxton Springs granite and for the "soft" rock tests in the Putney Mesa sandstone, both in the vicinity of Grants, New Mexico. The target areas were cleared and smoothed, access roads were completed, auger drillings were made, and marker areas and bull's-eye targets were laid out. Diamond drill hole positions were patterned over the target areas, and NX and EX cores were drilled to obtain specimens for physical rock tests. Cores were logged and specimens prepared for laboratory study. To determine absolute target elevation, height of drop, angle of fall, and angle of impact for each bomb drop, survey controls were established using U.S.G.S. and U.S.C.G.S. bench marks, and topographic maps were then plotted. During scheduled periods of bombing, radio control was maintained between a ground control station and the plane over the target. The point of impact of each bomb dropped during the tests was reported to a central plotting station from observation points and thus located on a block-grid system established both on a map and on the ground.

Each bomb crater was photographed to record the distribution and size of rock fragments relative to the line of flight, and then mapped in plan and cross-section. The bombs were recovered from the craters by use of various equipment and procedures. As excavation proceeded, a series of cross-section drawings and of photographs were made. After a bomb had been completely exposed, a damage survey was conducted to obtain information useful in analyzing the results of the tests. Bombs were then pulled from the craters and, if necessary, excavation was continued until the crater had been cleared to solid rock at the bottom. Bombs were then dragged to a bomb disposal site or sent to the ballistic research laboratory. Crater maps prepared for all bombs dropped during the

program recorded information obtained from topographic mapping, auger drilling, and diamond drilling before the bomb was dropped; from the apparent crater immediately after the bomb was dropped; from the true crater as excavation proceeded; from the damage surveys and field analyses after excavation was complete; and from ballistic data obtained from research after the completion of the field work.

Because the geologic processes that act upon rock masses affect the penetration in the medium, detailed analyses were made of (1) the stratigraphy, structure, and geologic history of the region; (2) the geology of the granite site target area; and (3) the geology of the sandstone site target area. Petrographic studies of the mineralogy and alteration of the Zuni granite, the lamprophyre dikes in the Zuni granite, and the Dakota sandstone were made to assist in the interpretation of tests of the physical properties of the rocks.

Because weathering and alteration influence the physical properties of granite, the granite cores were divided into two groups, weathered granite and unweathered granite. Tests were then made in various laboratories to determine the following physical and elastic properties of the sandstone, weathered granite, and unweathered granite cores: total and apparent porosity, apparent specific gravity, tensile strength, modulus of rupture, compressive strength, impact toughness, sclerescope hardness, Young's modulus, modulus of rigidity, Poisson's ratio, velocity of sound and seismic velocity, and triaxial compressive strength. (The physical and elastic properties of the specimens are tabulated in Fig. 72.)

Ballistic data were gathered for each of the 50 bombs dropped during the test project. Certain critical dimensions were recorded, curves were drawn in which striking velocity was plotted against altitude above target, and graphs were prepared to show the relationships among plane speed, release altitude above the target, and angle of fall.

At the Paxton Springs granite site, essentially three 1600 AP and three 2000 SAP bombs were released at each of three different altitudes, and two 25,000 SAP bombs were released at 18,000 and 26,000 feet respectively. At the Putney Mesa sandstone site, essentially three 1600 AP bombs, three 2000 SAP bombs, and three 2000 GP bombs were released at each of three different altitudes. For each bomb dropped, data were taken to provide evidence for study of (1) vertical penetration, without attempting to correct for soil thickness, topography, obliquity, or geological properties of the rock; (2) crater shape as related to impact energy; (3) path shape and length as related to impact energy; and (4) damage to nose, body, cap and base plate, and fins of each bomb. Crater maps and diagrams of bomb paths were constructed for both the granite and sandstone tests, and ballistic and crater data were tabulated.

The results of field work showed that penetration of a given type of bomb dropped from a given altitude upon a rock target varied greatly, depending upon the physical and geologic properties of the rock at the point of impact and upon the striking angle as influenced by topography. It was also evident that compressive strength alone could not be used as a basis for predicting penetration. Therefore, model bombing experiments were conducted in the Barodynamics Laboratory of the Colorado School of Mines to investigate various properties of bombs and various properties

of the medium upon penetration. The primary purpose of the model bombing experiments was to obtain evidence pointing towards the specific fundamental property of any material that can be used as a penetration index. Model bombs, model materials, and testing apparatus were selected to provide variations in striking velocity, kinetic energy, sectional density or sectional pressure of various bombs, angle of obliquity at which the bomb struck, tensile and compressive strength, and elastic properties of the medium. Laboratory tests were made to study depth of penetration of various bombs in a weak model material of constant strength, the effects of sectional density and of sectional pressure upon penetration at constant kinetic energy, the effect of compressive strength upon penetration, the variation of penetration with kinetic energy, and the variation of penetration with angle of impact.

Another type of model experiment was utilized in "Stress-coat" testing of models. Columbia resin CR-39 and aluminum alloy models were coated with Stress-coat and tested to determine (1) the direction of principal stress in the medium caused by impact of a model bomb at various angles of obliquity, (2) the effect of various depths of penetration and of various types of bombs upon the stress distribution, and (3) experimental data useful in analyzing field results.

A mathematical analysis of the stresses and displacements produced in a semi-infinite solid by a concentrated force at the surface was prepared. From this mathematical analysis, curves were drawn for various cases of angle of fall and Poisson's ratio, from which maximum shear, stress trajectory, and principal stress can be read for each of the cases.

Both macroscopic and microscopic metallurgical tests were made to investigate the effects of bomb impact and penetration upon the metal of which the bombs were constructed. Specimens were tested to determine flow lines, stress lines, structure of flowed-metal droplets, and changes in composition or hardness.

Photoelastic studies were made to supplement the mathematical analysis of the stress distribution in the interior of a semi-infinite solid due to a concentrated force at the surface and to investigate the more complex phenomenon of stress distribution in such a solid due to a force applied at various points and in various directions below the surface. Both Columbia resin CR-39 models and gelatin models were used. Data were gathered for two-dimensional stresses at various angles of loading, for shear contours in two- and three-dimensional bodies, for shear contours and stress trajectories in the medium, and for stress trajectories in the medium at the nose of the bomb.

Preliminary photoelastic studies were made of the stress distribution at the nose and near the juncture of the nose and the cylindrical portion of the bomb body. These two-dimensional photoelastic studies of the maximum shear stress distribution in the nose of a 1000 AP bomb, a 25,000 SAP bomb, a 2000 SAP, and a 2000 GP bomb indicated how each of the four types of bombs dropped in the Bomb Penetration Project could be improved and what their relative strengths are.

As a result of the combined analyses of the field results ,the laboratory results, the mathematical and photoelastic results, and the physical and elastic properties of the rock, a theory of penetration was evolved. The theory of penetration proposes that penetration of projectiles in rocks occurs as a result of rock failure. Penetration begins when rock failure begins and ceases when rock failure ceases. Therefore a study was made of rock failure.

Rock failure, it is proposed, takes several forms, depending upon a number of factors. At impact, failure is either by plastic flow or by crushing and fragmentation. The limits of the zone of failure depend upon the kinetic energy of the bomb, the shape of the nose, the diameter of the bomb, and the physical and elastic properties of the rock.

Rock failure is thought to occur in a sequence of three stages and to involve three zones of failure—a "zone of crushing," a "zone of shearing," and a "zone of tension slabbing." In general the zone of crushing lies nearest the bomb, the zone of shearing begins at the zone of crushing and extends outwardly to the zone of tension slabbing, and the zone of tension slabbing extends to the surface . For a given type of bomb dropped on a given type of rock, the amount of fine material is a measure of the proportion of rock that has failed by crushing. The amount of fine material increases with the impact energy of the bomb; decreases as the sharpness of the nose increases, but increases as the cross-sectional area of the bomb increases; and (when the bomb is dropped from a given altitude with a given kinetic energy) depends upon the elastic properties of the rock and upon the stress range rather than upon simple compressive strength.

The zone of shearing is characterized by two stages of failure: one stage in which the rock fails because of the energy transmitted from the bomb to the medium; the other stage in which the energy imparted to the medium causes the rock to burst into the cavity behind the bomb as in a "rock burst" in a deep mine.

The energy with which the cavity fails causes rock to be carried upward and forces rock from the zone of crushing and from the first stage of shearing failure into "O" (onion), "R" (radial), and "I" (inward) cracks typical of the zone of tension slabbing. The attitudes of these three types of fractures coincide with the three directions of maximum principal stress. Since the principal stress directions change as the bomb penetrates the medium, the attitude of the fractures depends upon the stress distribution at the instant at which the factures formed.

The sequence of failure involves three stages. Stage 1 is characterized by crushing failure. In stage 2 the zone of shearing and the zone of tension slabbing predominate. That ratio of the crater radius to the crater depth (r/d ratio) reaches a maximum. O cracks form within the zone of shearing but progress beyond into the zone of tension slabbing. I cracks form normal to the O cracks, and R cracks radiating about the axis of the bomb form perpendicular to the other two systems of fracture. In Stage 3 a decrease in the r/d ratio is due both to increased resistance to rock failure with increased depth and to a reduction in the extension beyond the zone of shearing of the fractures that characterize tension slabbing. The rockburst zone is confined principally to the footwall of the bomb path and to the region considerably below the ground surface. The downward ad-

vance of the rock-burst zone follows the release of compressive stresses in the medium at the tail of the bomb equal in magnitude to the compressive stresses in the medium at the nose of the bomb.

The sequence of rock failure and the zones involved are illustrated diagrammatically in Fig. 184.

From consideration of the phenomena of rock failure and of the influence of geology and topography upon penetration, the Livingston Penetration Formula is proposed as a means by which the depth of penetration of various types and sizes of bombs into rock masses can be predicted:

$$P = \frac{1 - m_x}{2.484\, m_x} \cdot \frac{N}{d} \cdot Q$$

If it is desired to compute the path length in rock to the point of normal penetration, the formula takes the form

$$P_{RM} = \frac{1 - m_x}{2.484\, m_x} \cdot \frac{N}{d} \cdot Q_P$$

If it is desired to compute the normal penetration in rock, the formula takes the form

$$N_R = \frac{1 - m_x}{2.484\, m_x} \cdot \frac{N}{d} \cdot Q_{NR}$$

where

P_{RM} is path length of any given bomb in rock X, measured to the point of maximum normal penetration, feet

Q_P is path length of a 1.0-foot-diameter prototype bomb in a prototype rock, feet

N_R is the maximum depth of penetration measured normal to the rock surface of any given bomb in rock X, feet

Q_{NR} is the normal penetration of a 1.0-foot-diameter prototype bomb in a prototype rock, feet

m_x is Poisson's ratio of rock X at 5000 pounds per square inch, the stress range at which failure occurs in simple compression for Dakota sandstone, the prototype rock.

N is the nose factor

d is the diameter of the bomb, feet.

The first term of the Livingston Penetration Formula

$$\frac{1 - m_x}{2.484\, m_x}$$

is referred to as the "rock factor." It is a measure of the lateral stress in the medium, and the lateral stress in the medium is a function of Poisson's ratio and of the axially applied force. Neither the axial force nor Poisson's ratio is a constant. Moreover, Poisson's ratio is dependent upon the stress range; therefore, it is necessary to establish a prototype stress range and a prototype rock. By means of the rock factor term it is possible to predict penetration in any type of rock from any part of the world.

The second term of the Livingston Penetration Formula

$$\frac{N}{d}$$

involves the nose factor and the bomb diameter. It was shown that the form of the stress contours and the degree of fragmentation depended upon the sharpness of the nose of the bomb. The second term states that penetration varies inversely as the diameter of the bomb. This relation was determined from photoelastic studies and is at variance with the sectional pressure formulas in which penetration is said to vary inversely as the square of the diameter of the bomb. Model experiments in which sectional pressure and sectional density were the only variables showed that penetration is independent both of sectional pressure and of sectional density at a given impact energy.

The third term of the formula, the "Q" term, expresses the path length, or the normal penetration of a prototype bomb in a prototype rock. The term expresses empirically the effect of two factors: the decrease in kinetic energy of the bomb between impact and maximum penetration, and the increased resistance to penetration with depth.

The theory of penetration, as presented, should aid in the design and selection of bombs to reduce enemy fortifications and in the design of fortifications to resist enemy bombs. The specific conclusions and recommendations reached as a result of the investigations that constitute this project are presented in detail in the last parts of this report.

PART A—INTRODUCTION

SECTION I—THE PROBLEM

1—Nature of the Problem

The Bomb Penetration Project was designed and sponsored by the Protective Construction Branch, Office, Chief of Engineers, U. S. Army, as a co-ordinated undertaking by the U. S. Airforce and the Army Corps of Engineers to determine the penetration of inert bombs into representative types of rocks. The purpose of the project was to supplement available information on effects of underground explosions and to determine the relative effectiveness of specific bombs for attacking enemy installations. A total of 50 inert bombs was dropped during the tests by flying missions originating at Edwards Airforce Base, Muroc, California. Four types of bombs—1600 AP, 2000 SAP, 2000 GP, and 25,000 SAP—and two types of rocks were tested.

One type of rock was selected from the group of "hard" rocks—granite, basalt, or hard limestone—and the other type of rock was selected from the group of "soft" rocks—shale or soft sandstone. Because of previous experience, which had shown that general-purpose bombs deformed or ruptured when dropped from high altitudes, the 2000 GP bombs were tested at the "soft" rock site only. Two SAP 25,000-pound T28E4 bombs were available for the tests, and these were to be dropped in the "hard" rock group.

Inasmuch as granite had been selected from the "hard" rock group and sandstone from "soft" rock group for the Underground Explosion Test Program, the same two rock types were favored for the Bomb Penetration Test Project. However, basalt, limestone, and shale sites were considered during the site investigation, which embraced the entire western part of the United States. Suitable sites were eventually located near Grants, New Mexico, in Zuni granite and in Dakota sandstone.

Previously, experiments had been conducted to determine the penetration of projectiles into concrete slabs, soils, and armor. As a result of experiments in this country and in England, several empirical formulas were available for the bomb penetration tests in rock. Because of the lack of homogeneity in rock masses, which is a result of the geologic processes that have acted upon them, it must be recognized that the number of variables affecting penetration is greater than for any of the materials previously tested.

2—Objectives of the Bomb Penetration Project

The Bomb Penetration Project resolves itself into two parts: 1) a study of the effect of the bomb on the rock and 2) a study of the effect of the rock upon the bomb. The field work was supplemented by laboratory work in which 1) the rock and the stress distribution in the rock and 2) the bomb and the stress distribution in the nose portion of the bomb were studied.

The objectives of our study of the rock and the effect of the bomb upon the rock are to determine answers to the questions:

1) How does a rock fail as a result of bomb impact?

2) Is the method of failure the same in granite as in sandstone?

3) How are the physical and elastic properties of rocks related to their ability to resist penetration?

4) What determines the shape of the path of a bomb in rock?

5) Is penetration a function of the sectional pressure or of the sectional density of a bomb?

6) Does the resistance to penetration increase with depth?

7) What factors determine the size and shape of a bomb crater in rock?

8) How do geologic planes of weakness influence the crater shape and the depth of bomb penetration?

9) How and why does "tunneling" of a bomb in rock occur?

10) What geologic and topographic conditions minimize the penetration of a bomb into rock and provide the maximum protection against attack?

11) What types of damage to underground installations in sandstone and granite are possible using the types of bombs dropped in the test program?

12) What is the relative effectiveness of various types of bombs in damaging underground installations?

13) Do all sandstones or granites behave alike? How can the results of the Bomb Penetration Project be applied to similar rocks?

14) Can the theory of penetration of bombs be used to improve the design of fortifications?

15) How can the vulnerable portal area of an underground installation best be protected against bombing?

Our objectives in the study of the bomb and of the effect of the rock upon the bomb are to determine:

1) Which of the various types of bombs tested is most effective for penetrating rock?

2) Can the design of bombs be improved to increase their penetration into rocks?

3) At what altitude can low-order detonation be expected when bombing with general-purpose bombs?

4) Can the design of general-purpose bombs be improved to minimize low-order detonation?

5) What structural changes and hardness changes take place in the metal of the bomb upon impact?

6) What is the stress distribution in the nose and in the forward part of the cylindrical portion of each of the types of bombs tested?

7) Can the shape of the nose and the distribution of metal be improved to increase the strength of the various bombs tested without increasing the weight of the bombs?

8) What future types of bomb will be most effective against underground installations?

3—Personnel and Acknowledgements

The assistance and co-operation of the following persons engaged in the field and laboratory work as staff of the Colorado School of Mines Research Foundation, Inc., in conducting the Bomb Penetration Test Project is gratefully acknowledged:

Director, C.S.M. Research Foundation, Inc.	V. L. Mattson
Project Manager, Bomb Penetration Project	C. W. Livingston
Assistant Project Manager	F. L. Smith
Field Engineer	R. L. Wood
Site Engineer	P. O. Yingst
" "	G. T. Bator
Engineer and Senior Draftsman	L. Borasio
Consulting Geologist	Dr. V. L. Kelley
Field Geologist	F. T. Quiett
" "	F. D. MacKenzie
Junior Geologist	R. E. Becker
Consulting Metallurgist	S. L. Smith
Petrographer	Dr. W. H. Wagner
"	Dr. T. H. Kuhn
Mathematician	W. H. Jurney
Photoelastician	Dr. C. N. Zangar
" "	Dr. M. J. Pandya
Editor	E. G. Fisher
Bookkeeper	H. Kelsey
Junior Engineer	H. L. Shivley
" "	W. F. Schwenn
" "	B. B. Chomiak
" "	R. L. Carmichael
" "	W. McGregor, Jr.
" "	H. K. Van Poolen
" "	R. Soares
" "	R. C. Johnson
" "	J. C. Tiffany
" "	J. H. Bright
Physical Rock Tests	J. H. Wyatt
" " "	A. W. Buell
" " "	W. A. Colburn
Laboratory Technician	S. Diker
" "	A. D. Gray
Photographer	W. Winters
"	J. Shoaf
Draftsman	L. S. Conder
Stenographers	Mrs. R. C. Johnson
"	Mrs. B. J. Clausen

The assistance of Mr. R. J. Lyman, Chief, and of Ben Camp, Planning Division, Albuquerque District, Corps of Engineers, in making available facilities of the Corps of Engineers at Albuquerque is deeply appreciated.

The rock data obtained by Val Jones, J. W. Demmitt, and J. H. Hanson of the structural laboratory of the United States Bureau of Reclamation, Denver, Colorado, from simple compression—strain tests and from triaxial tests of specimens of Zuni granite and Dakota sandstone were very useful in the analysis of results. The use of the facilities and personnel of the structural laboratory of the United States Bureau of Reclamation is greatly appreciated.

The services of Dr. Leonard Obert, Mr. Maurice Shelton, Mr. Louis L. Dashiell, and Mr. Hugh B. Sheppard and the use of facilities of the Applied Physics Branch of the United States Bureau of Mines at College Park, Maryland, are greatly appreciated. The Bureau of Mines data include impact toughness, Young's modulus, modulus of rigidity, specific damping capacity, apparent Poisson's ratio, and velocity of sound.

Ballistics data essential to the analysis of results were obtained through the office of Alden P. Tabor, Director, Ballistics Research Laboratories, Aberdeen Proving Ground, Maryland.

Major Donald G. Bussey, Chief of Armament Branch, Edwards Airforce Base, Muroc, California, was in charge of field operations of the Bomb Penetration Project for the United States Airforce. The excellent assistance and co-operation of Major Bussey and the following airforce personnel are greatly appreciated:

Pilot	Col. F. J. Ascani
"	Maj. D. G. Bussey
"	Maj. F. K. Everest, Jr.
"	Maj. G. Askounis
"	Capt. W. W. Sellers
"	Lt. W. R. Coleman
Observers	1st Lt. E. P. Brown
"	S/Sgt. W. R. Hardin
Bombardier	Capt. R. L. Filson

Captain R. W. Harris of Kirtland Field, Albuquerque, New Mexico, assembled the VHF air-to-ground radio equipment and was most helpful in arranging for equipment used for air-to-ground communications.

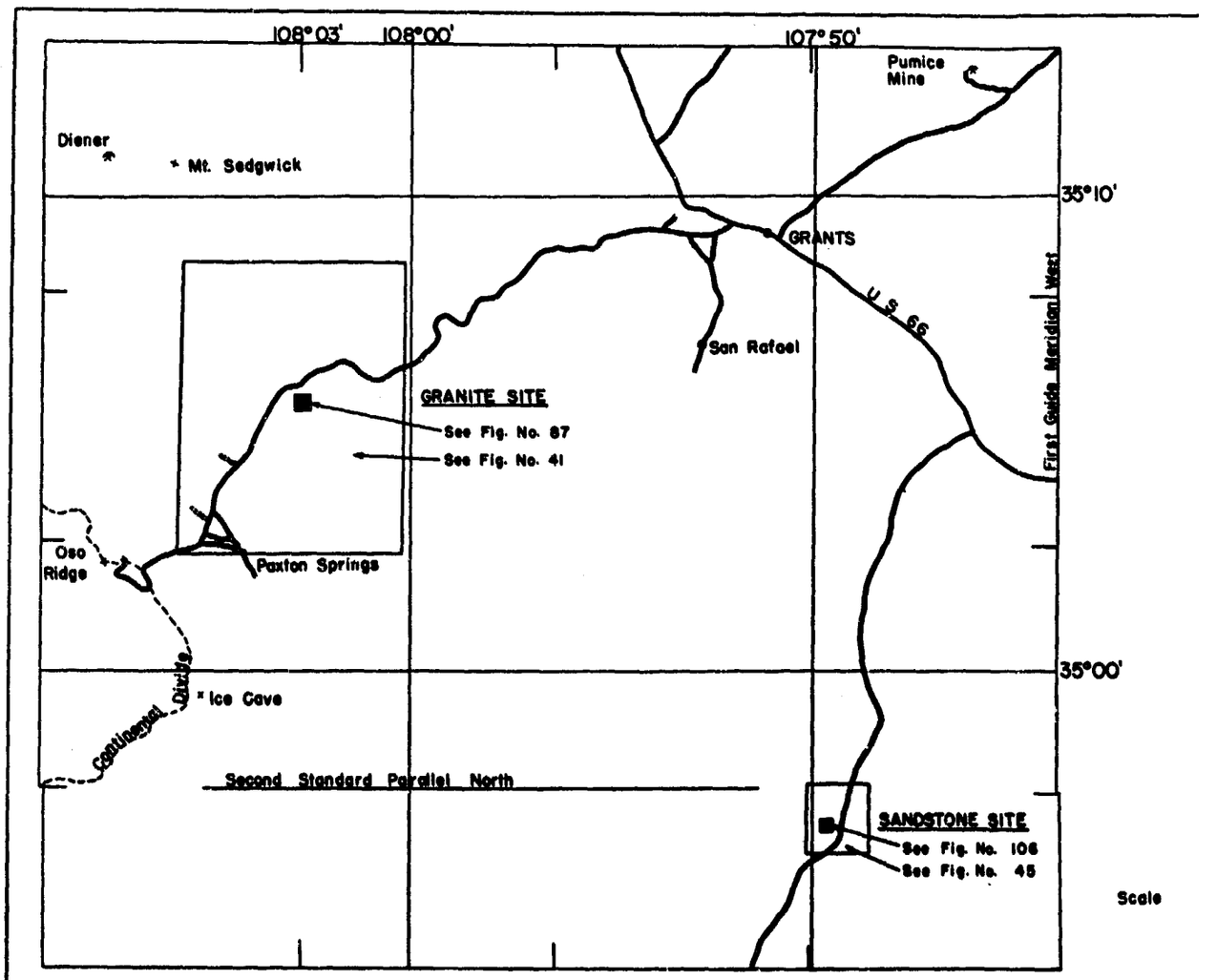

-BOMB PENETRATION PROJECT-
COLORADO SCHOOL OF MINES
RESEARCH FOUNDATION, INC.

INDEX MAP

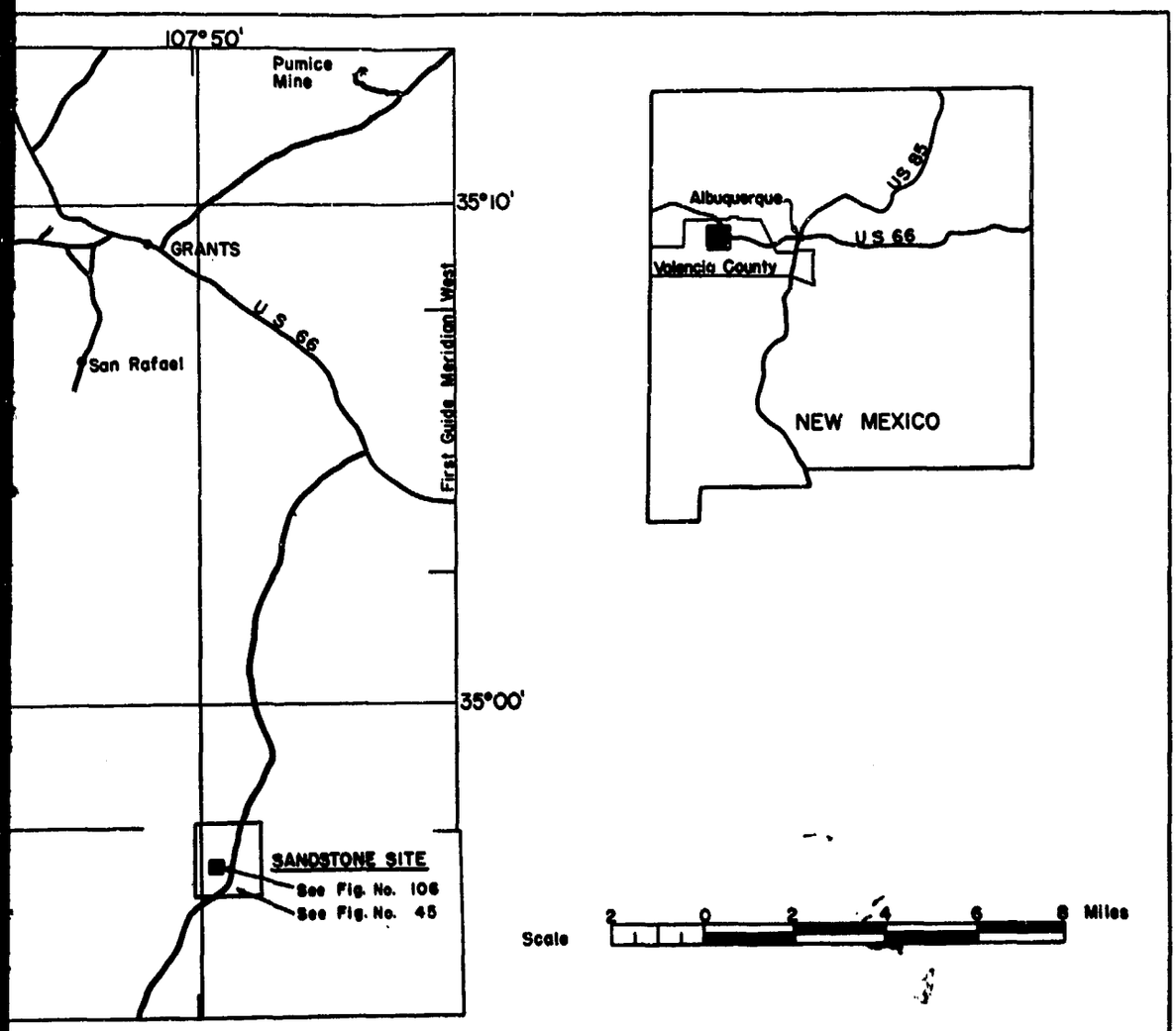

INDEX MAP

Scale Shown Date 10-11-50
Fig. No. 1 By RLW

Fig. 1

2

SECTION II—FIELD PROCEDURE

1—Site Selection

Preliminary site selection surveys were conducted by the North Pacific, South Pacific, and Southwestern Division offices to determine the availability of suitable sites for tests in accordance with the following site requirements:

1) One hard-rock site from the group comprising granite, basalt, or hard limestone and one soft-rock site from the group comprising shale or soft sandstone to be located within fairly close geographic proximity of each other.

2) The sites to be 4000 feet in diameter, as flat as possible, free of large stones and boulders, with a minimum of overburden. The rock to be as homogeneous as possible to a depth of approximately 40 feet, and within the target area to be free from large cracks and faults.

3) The minimum distance from any habitation to be 2 miles. The minimum distance from a town or city to be 5 miles. The airline distance from Edwards Airforce Base, Muroc, California, to be not more than 1200 miles.

4) The cites preferably to be within 25 miles from a town and preferably to have good roads for access by truck.

Suitable sites were located by the Seattle District, south of The Dalles, Oregon, and west of Twin Falls, Idaho; by the Los Angeles District west of Gila Bend, Arizona, and north of Tuba City, Arizona; by the Sacramento District, east of Castledale, Utah, and south of Delta, Utah; and by the Albuquerque District, near Vaughn and near Grants, New Mexico.

The Utah and New Mexico sites were visited by I. O. Thorley, Chief of the Protective Construction Branch, O.C.E., and C. W. Livingston, consultant. As a result of their examination, sites were tentatively selected near Mt. Sedgwick, southwest of Grants, New Mexico. These selections were contingent upon the results of an exploratory diamond drilling program and upon additional geologic work. The results of the diamond drilling at the soft rock site proved to be unsatisfactory. Accordingly, the Mr. Sedgwick area was abandoned temporarily, and a search for a suitable soft rock site was resumed in the vicinity of Vaughn, New Mexico, where a suitable hard rock site had been located. Again it proved impossible to meet the program requirements for a soft rock site, and the Vaughn area was abandoned.

A possible sandstone site was located in the Glorieta sandstone member of the San Andreas formation in the Bluewater-Toltec region, west of Grants, New Mexico. At the beginning of field work by Colorado School of Mines Research Foundation, Inc. it was intended to use the Bluewater-Toltec sandstone site and the Mt. Sedgwick granite site. Because of the abundance of timber to be removed from the Mt. Sedgwick granite site and the lack of suitable observation points, Research Foundation personnel continued the site search in the Grants area and located the Paxton Springs granite site, the site which was used for bomb drops in granite.

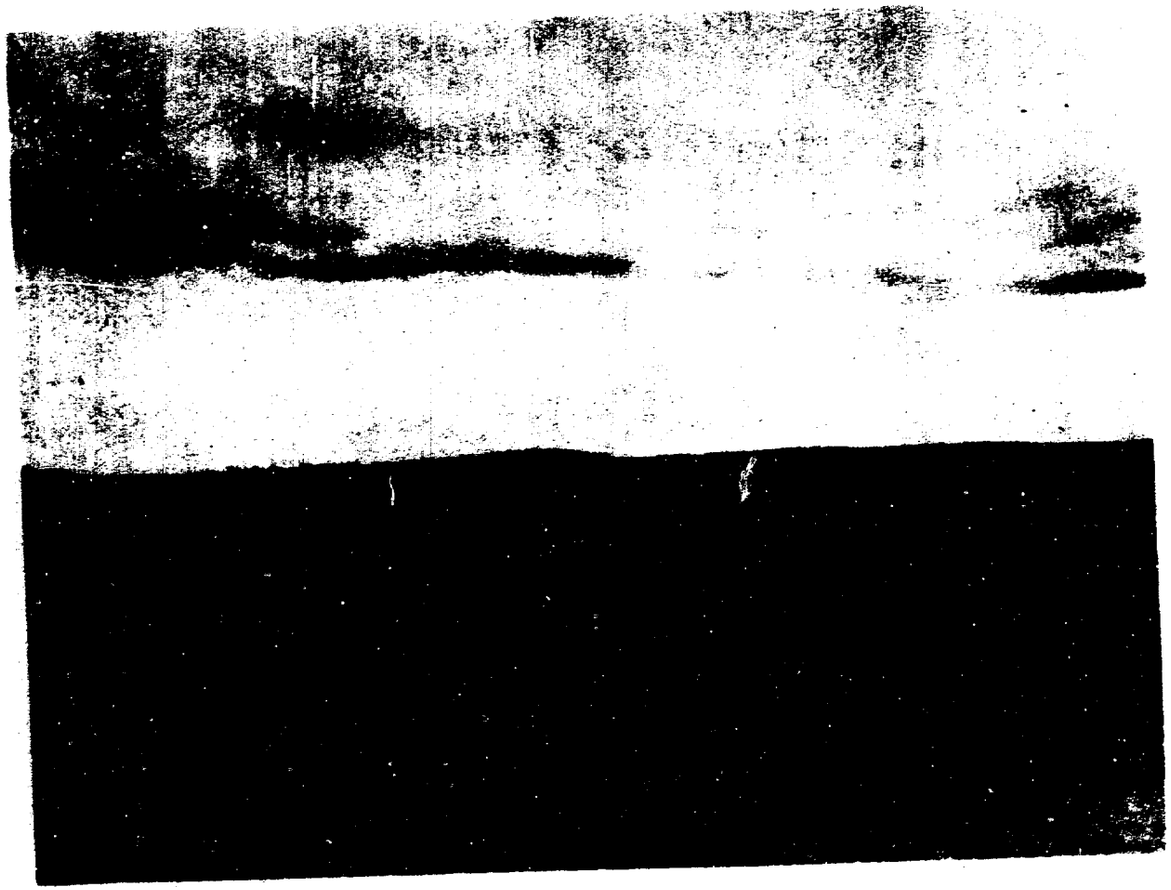

Fig. 2

The Paxton Springs Granite Site

Fig. 3

The 600-Foot-Diameter Clearing at the Putney Mesa Sandstone Site

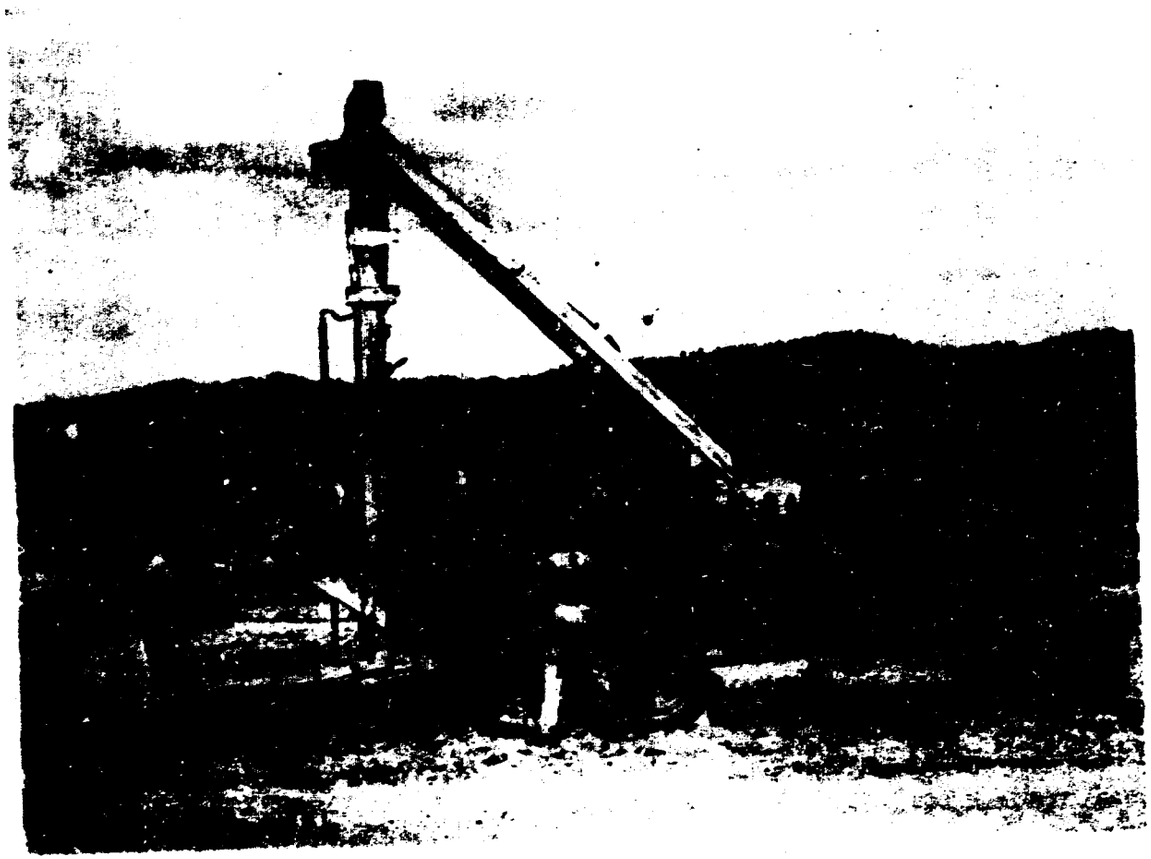

Fig. 5
Underground Diamond Drill Adapted for Surface Drilling

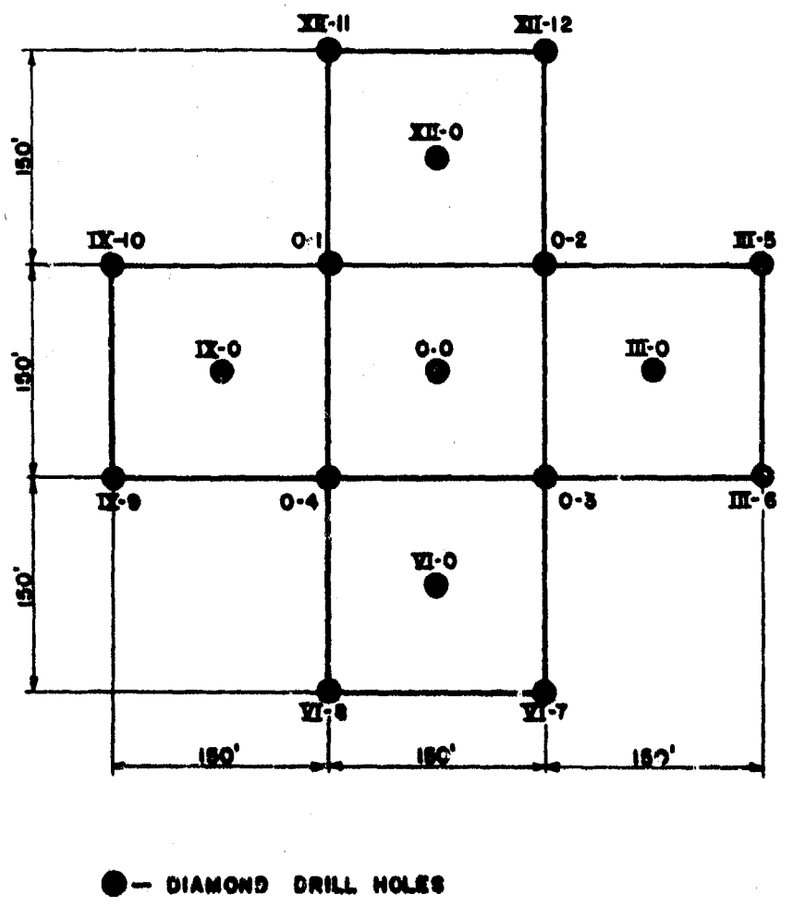

● — DIAMOND DRILL HOLES

-BOMB PENETRATION PROJECT- CSM RESEARCH FOUNDATION, INC.

Scale 1" = 100' Date 2-22-51

Fig. No. 4 By LB

DIAMOND-DRILL HOLE PATTERN AND HOLE NUMBERS

Fig. 4

As the detailed geological work proceeded at the Bluewater-Toltec sandstone site, it became evident that the proposed target surface had been beveled by erosion and that limestone lenses were present in the Glorieta sandstone. Accordingly, the search for a more suitable sandstone site in the Grants area continued. As a result of this search the Putney Mesa sandstone site in the Dakota sandstone formation was located.

Fig. 1, an Index Map, shows the location of the Paxton Springs granite site and the Putney Mesa sandstone site in relation to Grants and Albuquerque.

2—Field Procedure

a) Target Preparation, Access Roads

At the Paxton Springs granite site merchantable timber, consisting of sound trees 12 inches in diameter or over, was removed from a 300-foot-diameter target circle and from the four 150-foot marker circles by the U. S. Forest Service. Trees from 4 inches to 12 inches in diameter were removed by A. E. Blevins, a lumberman from Grants, New Mexico, under authority of a purchase order from the Albuquerque District, Corps of Engineers. Brush and trees smaller than 4 inches in diameter were removed from the target and marker areas by the Colorado School of Mines Research Foundation, Inc. The target area was broadened to a 400-foot-diameter circle and the area was smoothed with a bulldozer blade. A grid pattern of roads was built through the granite site, and access roads were built to connect the target and marker areas, the observation points, and the State road between Grants and Paxton Springs. The photograph, Fig. 2, taken from Brass Nob observation point shows the granite site target area after the timber had been cleared and the roads completed.

The Putney Mesa sandstone site was thickly covered with pinon and scrub cedar. As a result of experience with bombing at the granite site, it was decided to increase the size of the central cleared area to 600 feet in diameter, but to keep the four marker areas the same size and the same distance apart. As at the granite site, a grid system of roads was bulldozed through the target area, and the area was divided into lines and rows of 150-foot square blocks. The block boundaries were marked on the ground by means of sign posts placed along each side of the grid roads and at the block corners within the 600-foot-diameter target circle.

The photograph, Fig. 3, shows the 600-foot-diameter central cleared area at the Putney Mesa sandstone site. The contrasting background of green trees and buff sandstone simplified the problem of target marking. After the trees had been cleared from the center target area, the wind-blown sand on top of the Dakota sandstone was smoothed off to a uniform thickness with the bulldozer blade.

b) Diamond Drilling, Specimen Preparation, and Core Logging

Because of the variability in physical and elastic properties of rock specimens from the same drill holes or from adjacent drill holes and because of the difficulty of moving diamond drill equipment in and out of the target area during bombing, it was decided to drill the target area on a regular co-ordinate pattern before any bombs were dropped, rather than to drill alongside each of the bomb craters afterwards. The

hole spacing and the distribution between EX and NX holes were computed from the core requirements adjusted to the footage of recoverable and usable core. The hole depths were based upon the expected depths of bomb penetration using a Modified Petrie Formula and values of K equals 2 for sandstone and K equals 1 for granite. The pattern of drilling was adapted to the original idea of using 150-foot square targets. Figure 4 shows the drill pattern and drill hole numbers used at the granite and the sandstone sites.

Diamond drill hole positions were staked out on the ground with transit and steel tape. At the granite site, holes were bored through the overburden with an auger at the staked position and cased with 4-inch or 6-inch casing. Because of the shallowness and unconsolidated nature of the overburden (a wind-blown sand) at the Putney Mesa sandstone site, it was unnecessary to use the same procedure. Instead, the sand was shoveled aside and the drill holes were collared on bare sandstone.

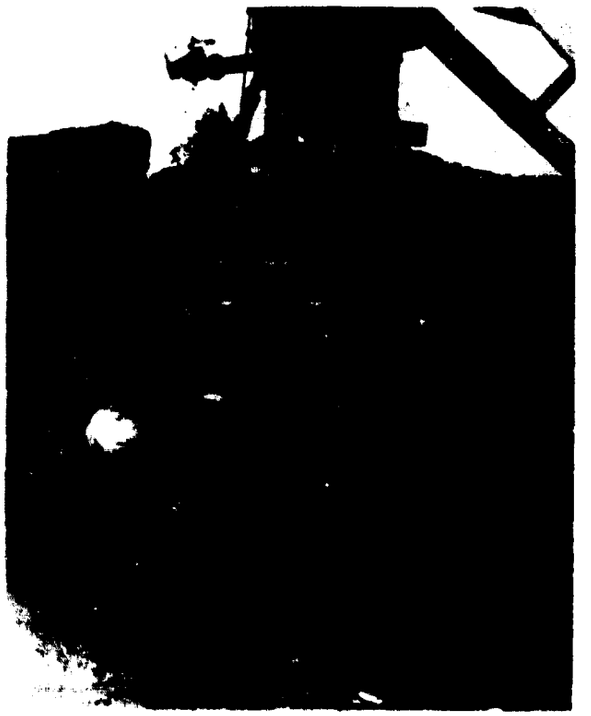

Fig. 6
Diamond Drill Rig in Operation

Two underground-type diamond drills designed for column mounting, one a Joy-Sullivan HS-15 and the other an Ingersoll-Rand Explorer type drill, were used for drilling the target site to obtain cores for physical rock testing. Drills of the air-operated, screw-feed type were adapted for surface drilling by being mounted on a framework bolted to the rear bumper of a 6x6 truck-mounted compressor unit as shown in the photograph, Fig. 5. The truck was backed up over the cased drill hole and jacked-up off its springs, and the rear axles were blocked.

Holes of both NX and EX size were drilled to obtain specimens of the desired size for physical rock testing. The photograph, Fig. 6, shows one of the rigs in operation with EX rod, E to N adapter, and NX double-tube core barrel. A "Truco" beveled, round-nose coring bit followed by a reaming shell was used for drilling both sandstone and granite. The drilling rate was 3 feet per hour of actual drilling time in granite and 5 feet per hour in sandstone. The compressed-air supply of the truck-

Fig. 7
Logging Dia nd Drill Cores

mounted, 105-cfm compressor unit of each drill rig was supplemented by operating a 215-cfm trailer-mounted compressor with two discharge lines from the receiver, one feeding into the receiver of each of the 105-cfm compressors.

A drill crew consisted of a runner and a helper. Drilling was done on two shifts at each site. Laying pipe, erecting light lines, and other preparatory work were done on the day shift whenever possible.

Diamond drill cores were logged in the field office at Grants, New Mexico, (see photograph, Fig. 7). A typical diamond drill core log for a drill hole in granite is presented as Fig. 8, and a typical log of a sandstone drill hole is presented as Fig. 9. During the process of logging, the core recovery of each drill run was computed and recorded in column 1 of the drill log. Column 2 shows the number and the position in the hole of samples taken for physical rock tests. The columns to the right of the description show the distribution of the specimens for testing.

Fig. 10

Cutting Specimens from the Drill Cores to Length for the Physical Rock Tests

Core Recovery	Sample Number	Graphic Scale	Graphic Log	Description	USBM	USBR
		2		Cement plug		
				2.4'		
27.2%		4		7 small pieces of broken, weathered, granite gneiss		
				4.6'		
57.1%	1, 2, 11, 3, 4	6, 8		Core all from weathered zone. Feldspars altered to clay. 45° joint between samples 1 and 2. Vertical joint above sample 3. Numerous breaks caused by drilling.		4
				9.5'		
95%	5, 6, 7	10, 12, 14		This core is still in the weathered zone. Below sample 6 there is a horizontal joint followed by a vertical joint. Recovery between samples 6 and 7 limited to small broken pieces.		
				14.5'		
90%	8, 9, 10, 11, 12, 21	16, 18, 20		Between 8 and 9 alteration of micas to chlorite, alteration of feldspars stops and chloritization begins. Rock becomes more dense. 60° joint between sections 10 and 11.		
				19.5' Bottom hole.		

Elevation of Collar 7793.3'
Core Size NX
Total Recovery 77.2%

-BOMB PENETRATION PROJ
Scale 1" = 3ft. Date
Dwg. No. 8 By
L

Graphic Log	Description	USBM	USBR	CSM Mining	CSM Physics	CSM PE	CSM Geology
	Cement plug						
2.4'							
	7 small pieces of broken, weathered, granite gneiss						
4.6'							
	Core all from weathered zone. Feldspars altered to clay. 45° joint between samples 1 and 2. Vertical joint above sample 3. Numerous breaks caused by drilling.			1 2 3			1†
			4				
9.5'							
	This core is still in the weathered zone. Below sample 6 there is a horizontal joint followed by a vertical joint. Recovery between samples 6 and 7 limited to small broken pieces.			5			
14.5'				7			
	Between 8 and 9 alteration of micas to chlorite, alteration of feldspars stops and chloritization begins. Rock becomes more dense. 60° joint between sections 10 and 11.			8 9 10 11 12			
19.5'	Bottom hole.						2†

-BOMB PENETRATION PROJECT- C S M RESEARCH FOUNDATION, INC.

Scale 1" = 3ft. Date

Dwg. No. 8 By

DIAMOND DRILL CORE LOG

Location NE corn. Area VI Hole No. 0-0-3

FIG. 8

1

2

Core Recovery	Sample Number	Graphic Scale	Graphic Log	Description	USBM
				Overburden	
				1.4'	
83%	9, 10	2, 4		At the surface and down 0.5 feet there are 60° joints. Good core, constant composition to 5.0 feet.	
				5.0'	
895%	11, 12, 13	6, 8		Sandstone becomes calcareous from approximately 6.0 feet to 6.9 feet. Small veinlets of calcite in this layer. Irregular joint pattern just above calcareous layer.	
		10		10.0'	
75%	14, 15, 16	12		Good core of constant composition.	
		14		14.0'	
80%	17, 18, 19, 20	16, 18		Good core of constant composition with a few small open joints at irregular intervals.	
				19.1' Bottom.	
		20			

Fig. No. 9

Elevation of Collar 6954.3
Core Size NX
Total Recovery 79.0%

BOMB PENETRATION
Scale 1" = 3ft. Date 2-1
Fig. No. 9 By FDI

USBM	escription	USBM	USBR	CSM Mining	CSM Physics	CSM PE	CSM Geology
	ace and down 0.5 feet there are Good core, constant composition		9				
				10			
	comes calcareous from approximately 6.9 feet. Small veinlets of calcite er. Irregular joint pattern just reous layer.			11			
			12				
				13			
	f constant composition.			14			
			15				
			16				
	f constant composition with a few joints at irregular intervals.		17				
			18				
			19				
			20				

Fig. No. 9

TION
te 2-19-
by FDM

-BOMB PENETRATION PROJECT- C S M RESEARCH FOUNDATION, INC.

Scale 1" = 3ft. Date 2-19-51

Fig. No. 9 By FDM

DIAMOND DRILL CORE LOG

Location SW corn. Area 0 Hole No. S-0-4

Fig. 9

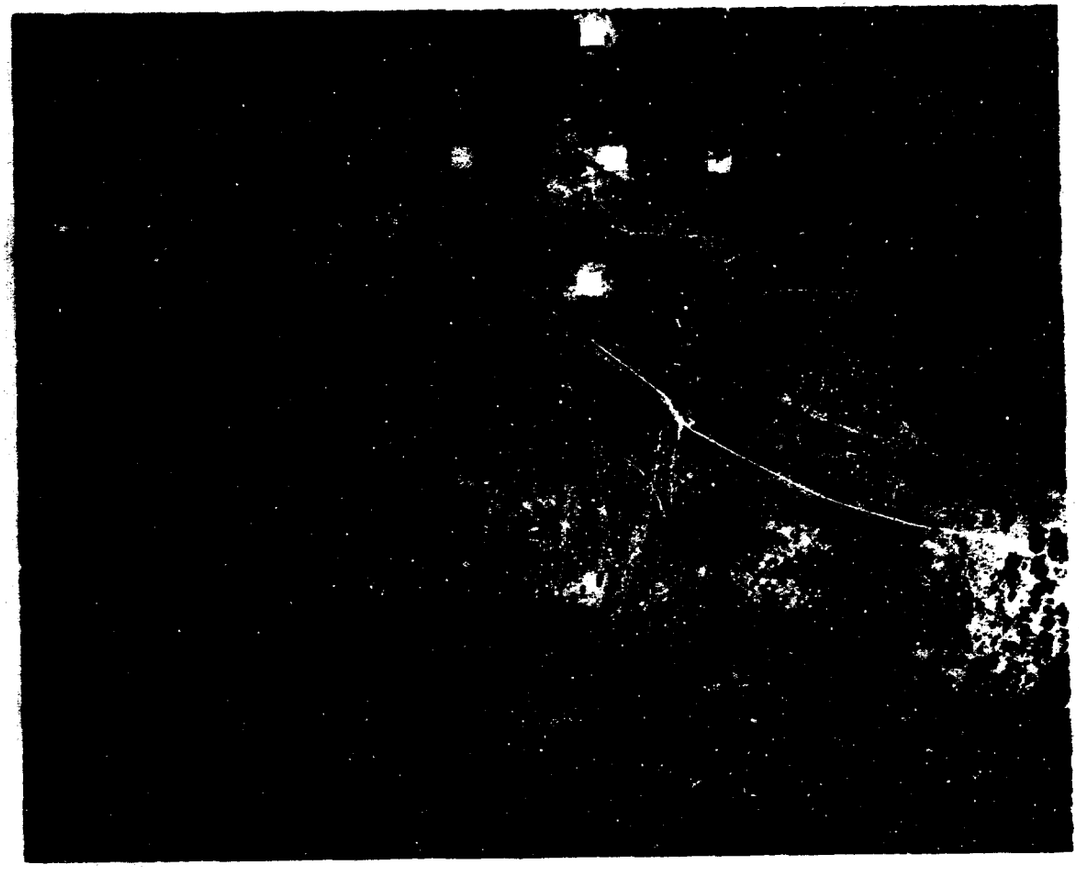

Fig. 11

Original Target Layout of Granite Site

Fig. 12
Bull's-eye Target Pattern at the Granite Site

Fig. 13
The Target Layout and Grid Road Pattern at the Putney Mesa Sandstone Site

Tests were made at the United States Bureau of Mines Laboratory in College Park, Maryland, at the structural laboratory of the United States Bureau of Reclamation in Denver, Colorado, and in the Mining Department, Physics Department, Petroleum Engineering Department, and the Geology Department of the Colorado School of Mines in Golden, Colorado. A complete set of drill logs is contained in the appendix to this report. (See Appendix, Part A.)

Specimens were cut from the drill cores at the positions marked on the core and on the core log. The photograph, Fig. 10, shows the process of cutting the specimens to proper length using a water-cooled diamond blade on an electrically driven "Skilsaw." Using the device shown in the photograph, it was possible to cut off the specimen with the ends square and ready to use in the testing machine. A carborundum blade was used in place of a diamond blade when cutting speciments of sandstone.

c) Auger Drilling

The depth of overburden at various places throughout the target area first was determined by auger drilling during site selection to make certain that the thickness of overburden was not so great that the site would be unsuited to the Bomb Penetration tests. Again, after the targets were laid out in their final position on the ground, lines of auger holes were drilled on a 75-foot coordinate pattern covering the central cleared area. In places where the overburden proved to be thickest, the bulldozer scraped off the high spots. At the sandstone site, the thickness of the wind-blown sand could be estimated approximately without auger drilling. The center target area was smoothed with the bulldozer blade first; then a pipe probe, rather than an auger, was used to determine the thickness of the overburden. The position of the auger holes and of the probe holes is recorded on the topographic maps.

d) Surveying and Topographic Mapping

In order to determine the absolute target elevation, the height of drop, the angle of fall, and the angle of impact for each bomb drop, it was necessary to establish both horizontal and vertical survey control at each target site. Coast and Geodetic Survey triangulation stations were the starting bases for horizontal control.

Triangulation surveys were chosen as the fastest, easiest, and most accurate method of providing horizontal control because of the distances involved and the type of terrain and vegetation present. Primary and secondary base lines were established at convenient points, and the triangulation net was broadened to include the target area and the observation areas. (See Appendix, part B, for maps of the triangulation system.) Three observation points were selected so as to provide complete visibility of the bombing target at each site and spaced in such a manner as to assure a high degree of spotting accuracy. The observation points were made a part of the triangulation network. At the granite site, the triangulation system began at the primary base line and ended at the secondary base line. Stations on the U. S. Geological Survey triangulation system were tied into the Research Foundation system at convenient points. At the sandstone site a secondary base line was unnecessary because "Rock" and "Ledge," two U.S.G.S. stations whose coordinates

and elevations were known, were sufficiently close to the target area to be usable in checking the closure of the sandstone site triangulation system.

Vertical control at the granite site was established by running a series of closed, precise-level loops from U.S.C.G.S. bench mark P47-1934, which was located 2 miles south of the target area. Two concrete bench marks were established in the target area, and the elevations of other triangulation, traverse, and topographic control points were recorded as a part of the final loop of the precise level system.

At the sandstone site the distance to the nearest accessible U.S.C.G.S. bench mark was 14 miles. The elevations of the U.S.G.S. triangulation stations "Rock" and "Ledge," both close to the target area, were known. Because of the distances involved, and considering the accuracy with which the altitude of the airplane on the bomb run could be determined, it was decided to establish vertical control from U.S.G.S. "Rock" by triangulation. As a rough check on the triangulation levelling, barometric levels were carried from the Santa Fe depot at Grants to the site several times during the period of field work.

Topographic maps of the central cleared area of the granite site (see Appendix, Part B) and of the sandstone site (see Appendix, Part B) were constructed to a scale of 1 inch equals 30 feet using a 1-foot contour interval. Topographic maps of the entire target and marker area of the granite site (see Appendix, Part B) and of the sandstone site (see Appendix, Part B) were constructed to a scale of 1 inch equals 50 feet, using a 5-foot contour interval.

e) Target Layout and Target Marking

Various target layout patterns were considered by representatives of the Protective Construction Branch, Office, Chief of Engineers, and of the Colorado School of Mines Research Foundation, Inc. before the beginning of field work. It was finally decided to provide several 150-foot square bombing targets and four 150-foot square markers spaced so as to positively identify the target. The pattern originally used at the granite site consisted of five 150-foot squares arranged in the form of a cross within the central cleared area and one 150-foot square marker in the center of each of four 300-foot-diameter cleared marker areas 500 feet out from the center of the center target. The 150-foot square targets within the central cleared area were referred to as the 12 o'clock, 3 o'clock, 6 o'clock, 9 o'clock, and zero targets. The 12 o'clock target was the north arm of the cross, and the zero target was the center of the cross. The targets were staked out and diamond drill holes placed in the center and at the four corners of each 150-foot square.

In the aerial photograph, Fig. 11, the 6 o'clock target and the four markers are in white. The 12 o'clock, 3 o'clock, and zero targets have been outlined with black cinders. An additional target at the 1 o'clock position was outlined in anticipation of possible future needs. The grid road pattern driven through the target area for access functions much in the same manner as the four markers to identify the target from the air. After the first few bombing missions were completed, Lt. Filson, the bombardier, suggested that the target shape be changed to a circle in order to eliminate the possibility of aiming at a marker square rather

Fig. 14
Weapons Carrier Converted to Spray Truck for Target Marking

Fig. 15
Loading Black Volcanic Cinders into Weapons Carrier

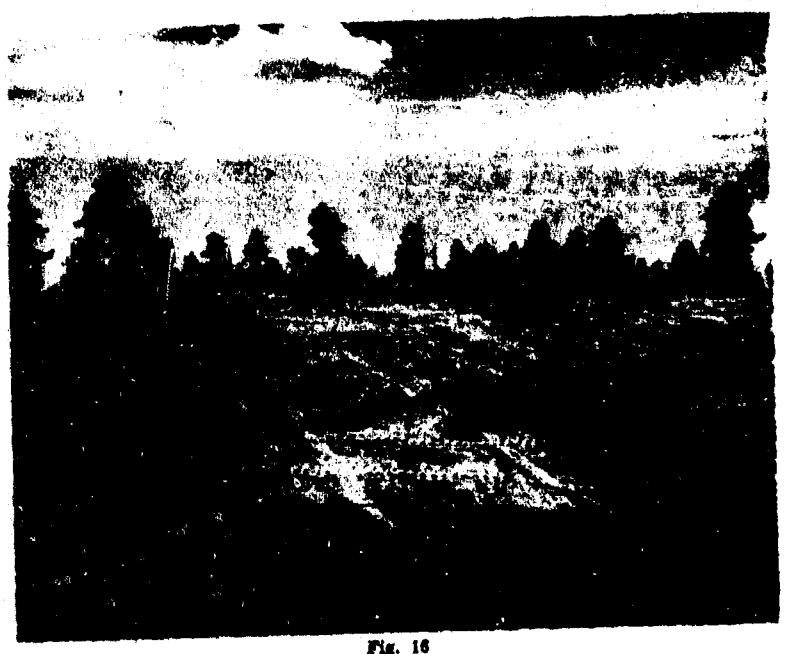

Fig. 16
Spreading Cinders Along Boundaries of 150-foot Marker Square

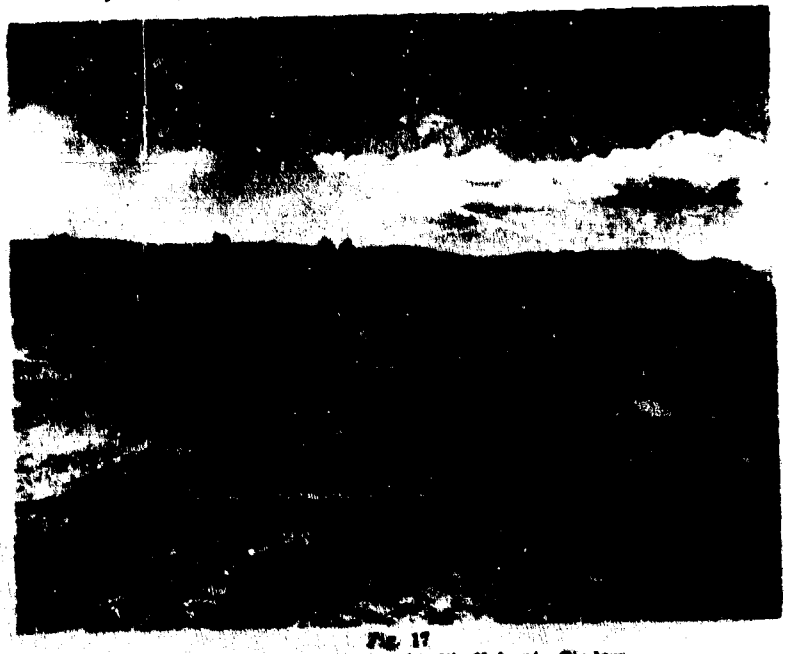

Fig. 17
Bull's-eye Target Outlined with Volcanic Cinders
The pumice bags have been distributed preliminary to spreading all the pumice by hand.

than a target square. Acting upon this suggestion, a 150-foot-diameter bull's-eye was placed in the 2 o'clock position as shown in the aerial photograph, Fig. 12. The black center of the bull's-eye is 40 feet in diameter.

As a result of bombing experience at the granite site, the target layout at the sandstone site was further modified as shown in the aerial photograph, Fig. 13. The four marker areas are slightly in excess of 300 feet in diameter, and because of the contrasting background of the buff sandstone and the green trees, the 150-foot white squares were eliminated. Because of the thick growth of cedar and pinon, the number of grid roads through the target area and the size of the center target clearing were increased. The bull's-eye was the same size as that used at the granite site. It was placed slightly off-center in the 600-foot-diameter central cleared area. The off-center placement of the target was based upon the observation that most of the bombs at the granite site over-shot rather than undershot the target. However, at the sandstone site it would have been just as well to center the bull's-eye in the clearing, for as many bombs fell short as fell long.

Various materials for marking the targets were tried. It was determined from these experiments that white was visible from the greatest distance and that a white target was sharpest when outlined with black. Flour, pumice, and mixtures of flour and pumice were tried. A pumice deposit was being mined near Grants, New Mexico, and a substantial supply of 325-mesh pumice was available. Since commercial demand for this grade of pumice is not great, the price is much lower than that of other grades. The price was much less than that of any other suitable material.

By experiment it was determined that pumice turned a buff color when wet, but that it would stick to the ground better if put on wet rather than dry. The addition of flour to the wet pumice reduced the tendency of the mixture to blow away. Placed on wet, a mixture would dry in a few hours, and as it dried the buff color would change to white. The first method used for marking the granite site targets was to pump a water suspension of pumice through spray nozzles as shown in the photograph, Fig. 14. This method proved to be slow and produced an erratic covering. The afternoon New Mexico cloudbursts were capable of destroying such a target marking in a few minutes.

The method of target marking that was finally used was to distribute bags of pumice over the target, then break the bags and spread the pumice dry on the dew-covered ground an hour before the bomber was due to arrive at the target.

A deposit of volcanic cinders was conveniently located at the edge of the granite site target. The black cinders were used to outline the white targets on the ground. Three stages of marking a target are shown in Figs. 15, 16, and 17. Figure 15 shows the cinders from the volcanic cinder deposit being hand-shoveled into the back of a weapons carrier. Figure 16 shows the cinders being spread along the boundaries of a previously staked 150-foot marker square. Figure 17 shows a bull's-eye target with bags of pumice distributed preparatory to spreading the pumice by hand.

f) Bombing and Communications

The target areas at both the granite and the sandstone site were

just inside the boundaries of the Civil Aeronautic Administration "Green-4 airlane" and also within the 150-mile-radius Los Alamos defense zone. To complicate the situation further, the state road to the granite site was a main access road used by the Forest Service for fire fighting. The scheduled period of bombing coincided with the maximum fire hazard period. As it happened, several forest fires broke out in the surrounding area during the season, and the Forest Service requested the Colorado School of Mines Research Foundation to make available a bulldozer and fire-fighting equipment if a situation developed that they could not handle.

The problem of air clearance was solved by meetings of representatives of the Air Force, the Civil Aeronautics Administration, the Albuquerque District Corps of Engineers, and the Research Foundation. The procedure worked out in these meetings was as follows: A bombing schedule was agreed upon, and all bombing during any scheduled day was to be accomplished before noon. The bomber plane was to report its estimated arrival time over the target to Acomita radio. All commercial and military aircraft were to be routed to the south of the granite target and to the north of the sandstone target. Before each bomb release, the pilot of the bombing plane would be required to obtain a clearance from Acomita radio and a clearance from the ground crews. Only one bomb was to be dropped on each bomb run.

It was essential to the success of the Bomb Penetration Project that each bomb crater be marked on the ground immediately after impact, and that any unusual condition be immediately reported to the central control station so that the height of release could be modified if the situation warranted doing so.

Spotting maps were constructed in advance of the tests, and the spotting accuracy was checked by using dynamite charges to simulate the effect of a bomb burst. Figure 18 is a spotting map of the granite site, and Fig. 19 is a spotting map of the sandstone site. The position of points of impact of all of the bombs dropped during the test is represented by the black dots numbered according to the C.S.M. bomb number. Angles left or right from a flag at the center of the central cleared area to the point of impact were simultaneously measured by means of transits set up at three observation-triangulation stations. Results were reported by SCR-4 "Horsie-talkie" radio to a central plotting station located at the main ground control station. The intersection on the spotting maps of the three lines from the observation stations located the point of impact. The result was radioed to "Rover," a weapons-carrier team of two men, whose duty it was to enter the bombing area, mark the crater, inspect general-purpose bombs for casing failure, and retire from the area before the next bomb run began. As may be observed by inspection of the spotting maps, the point of impact is defined by a block-grid system established both on the map and on the ground. The point of impact of Bomb 5, for example, would be described as within the southwest corner of block G8. (See Fig. 18.)

At each observation station one man in addition to the transit operator was assigned to watch for low-flying aircraft. Road blocks were established to regulate traffic into and out of the area on bombing days. Each road block was equipped with a SCR-4 "Horsie-talkie" radio so

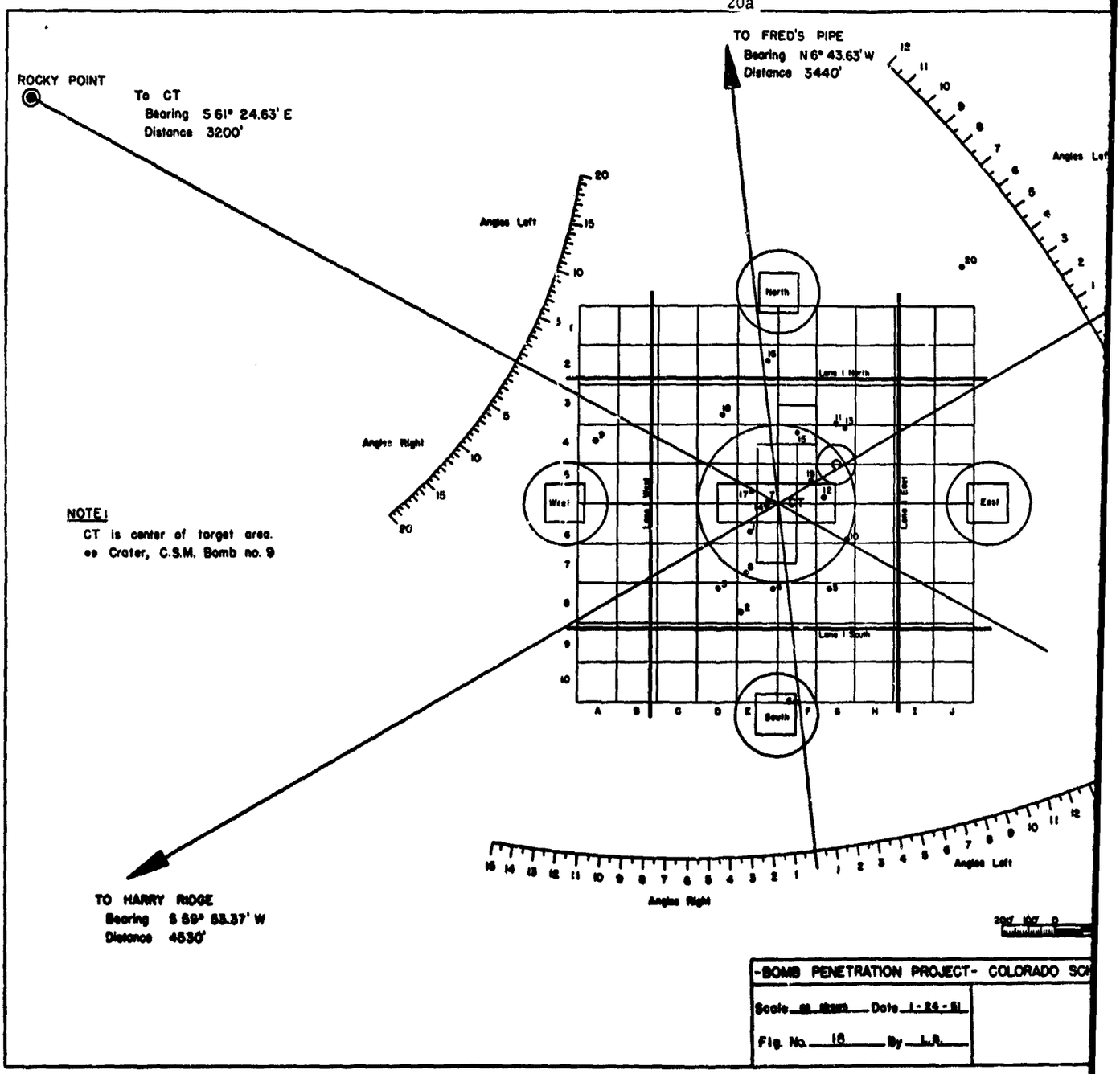
ROCKY POINT
To CT
Bearing S 61° 24.63' E
Distance 3200'
TO FRED'S PIPE
Bearing N 6° 43.63' W
Distance 3440'
Angles Left
Angles Right
North
South
West
East
Lane I North
Lane I South
Lane I West
Lane I East
CT
A B C D E F G H I J
NOTE:
CT is center of target area.
•• Crater, C.S.M. Bomb no. 9
TO HARRY RIDGE
Bearing S 59° 53.37' W
Distance 4630'
-BOMB PENETRATION PROJECT- COLORADO SC
Scale as shown Date 1-24-51
Fig. No. 18 By L.R.

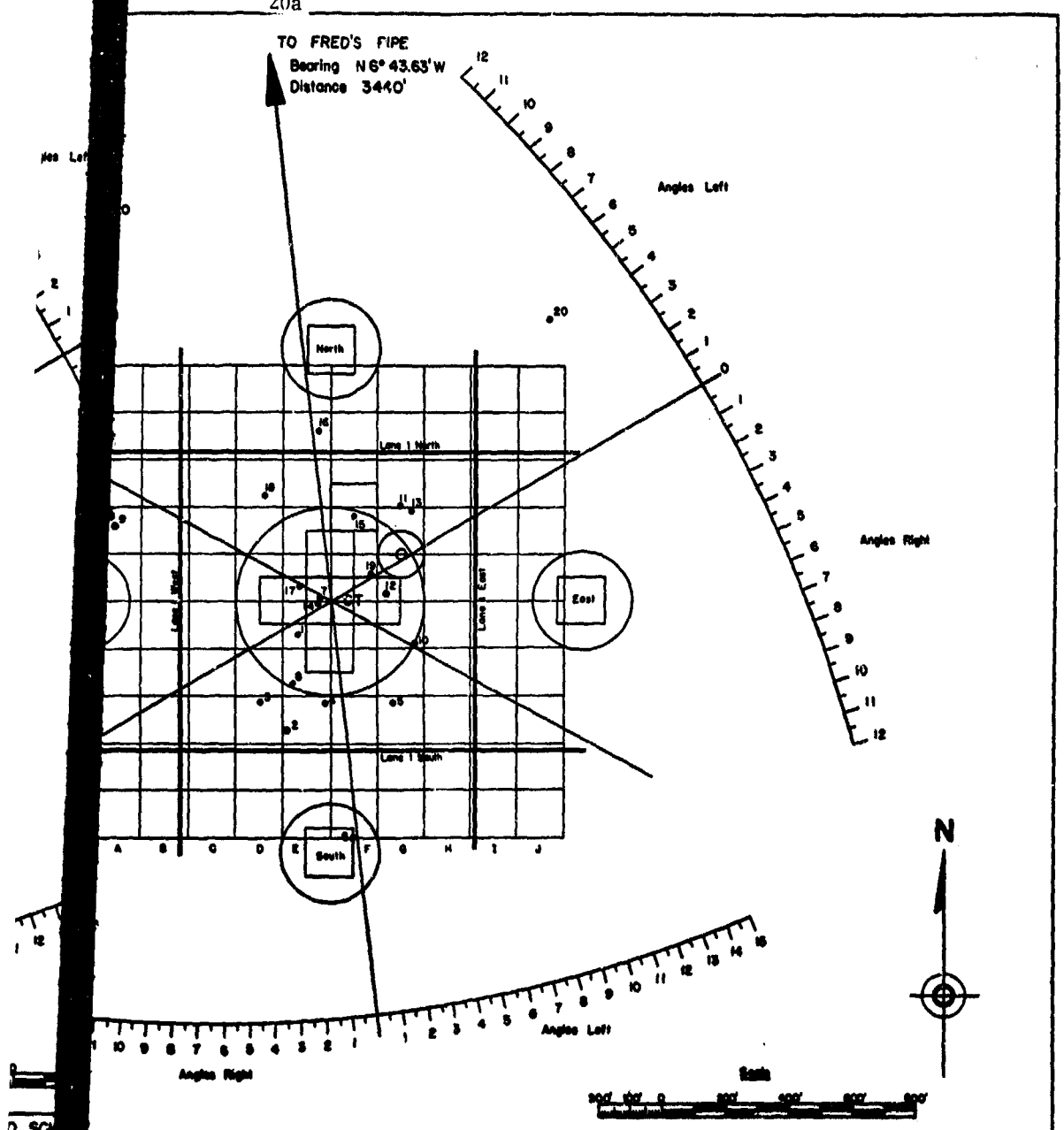

-BOMB PENETRATION PROJECT- COLORADO SCHOOL OF MINES RESEARCH FOUNDATION, INC.

Scale as shown Date 1-26-61	SPOTTING MAP
Fig. No. 18 By L.B.	GRANITE SITE

Fig. 18

2

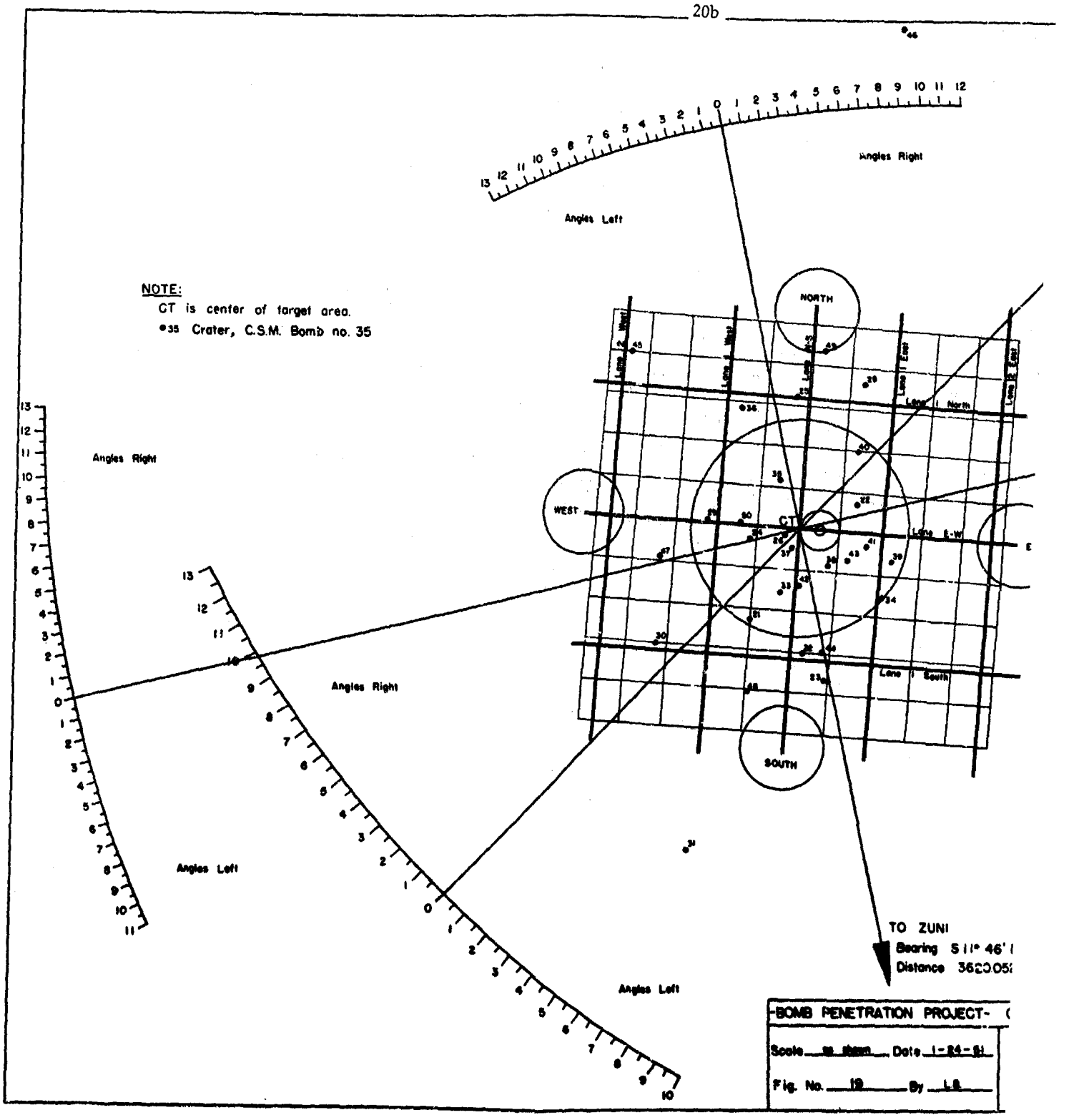
NOTE:
CT is center of target area.
•35 Crater, C.S.M. Bomb no. 35
Angles Right
Angles Left
NORTH
WEST
SOUTH
CT
Lane 1 North
Lane E-W
Lane 1 South
TO ZUNI
Bearing S 11° 46'
Distance 3620.05
-BOMB PENETRATION PROJECT-
Scale as shown Date 1-24-51
Fig. No. 19 By LB

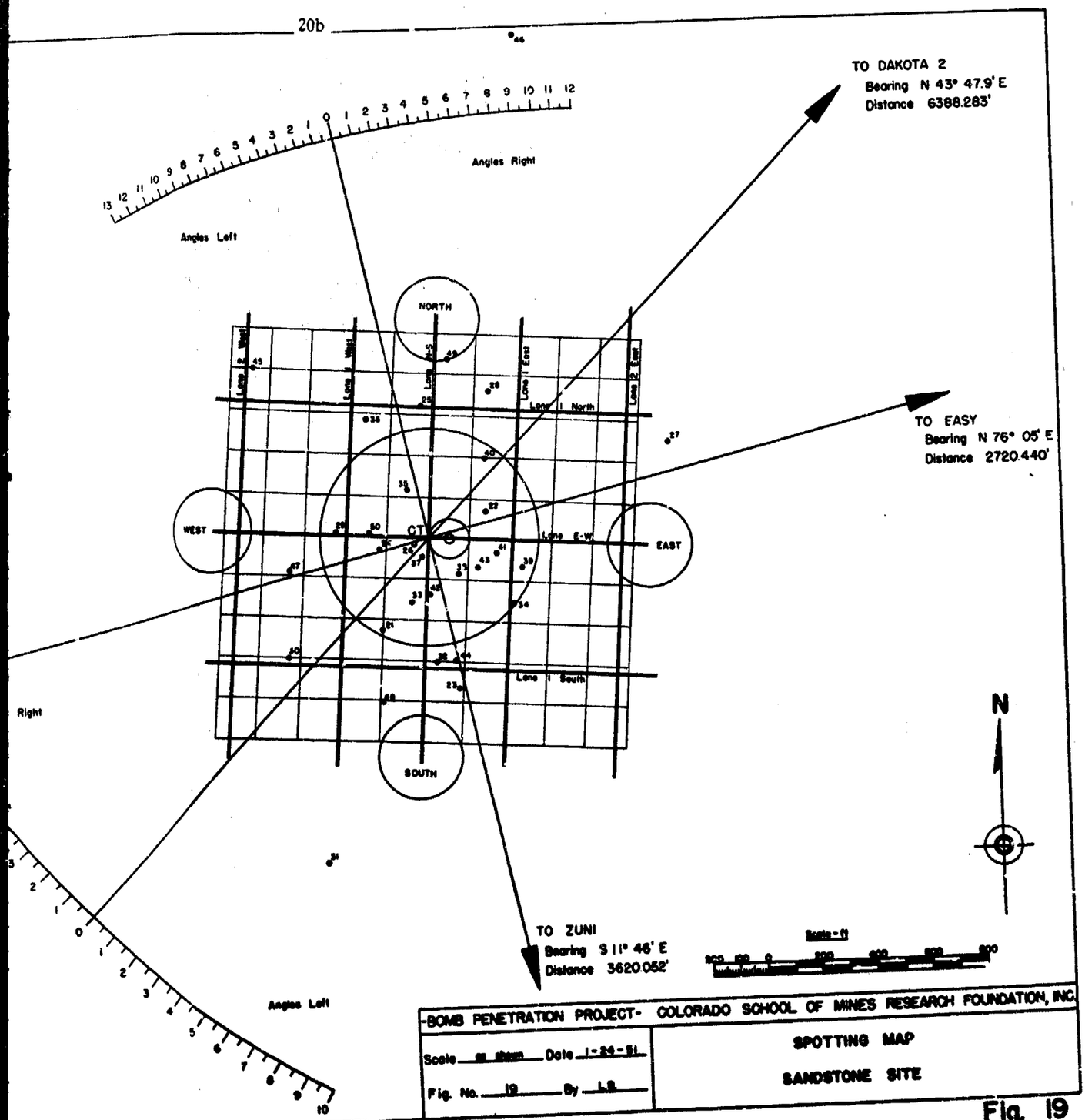

BOMB PENETRATION PROJECT- COLORADO SCHOOL OF MINES RESEARCH FOUNDATION, INC.

Scale as shown Date 1-24-51	SPOTTING MAP
Fig. No. 19 By LB	SANDSTONE SITE

Fig. 19

2

Fig. 20
Layout of the Ground Control Station, "Brass Nob," Granite Site

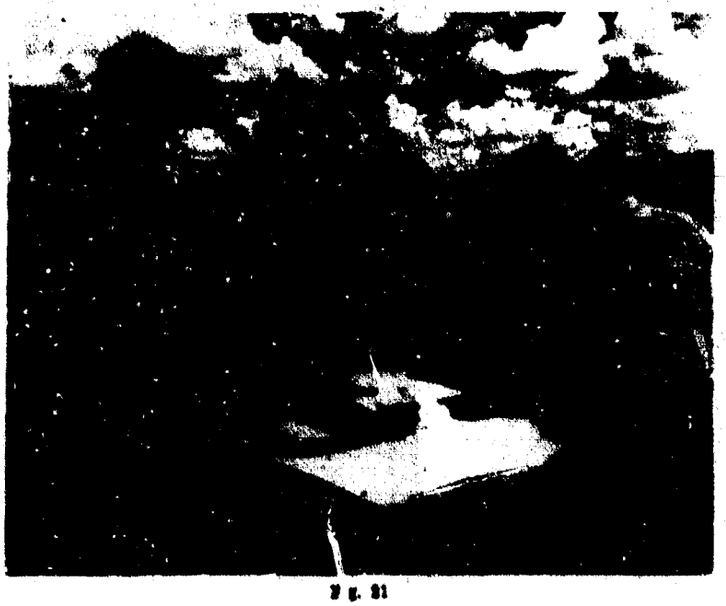

Fig. 21
The Plotting Table and Spotting Map

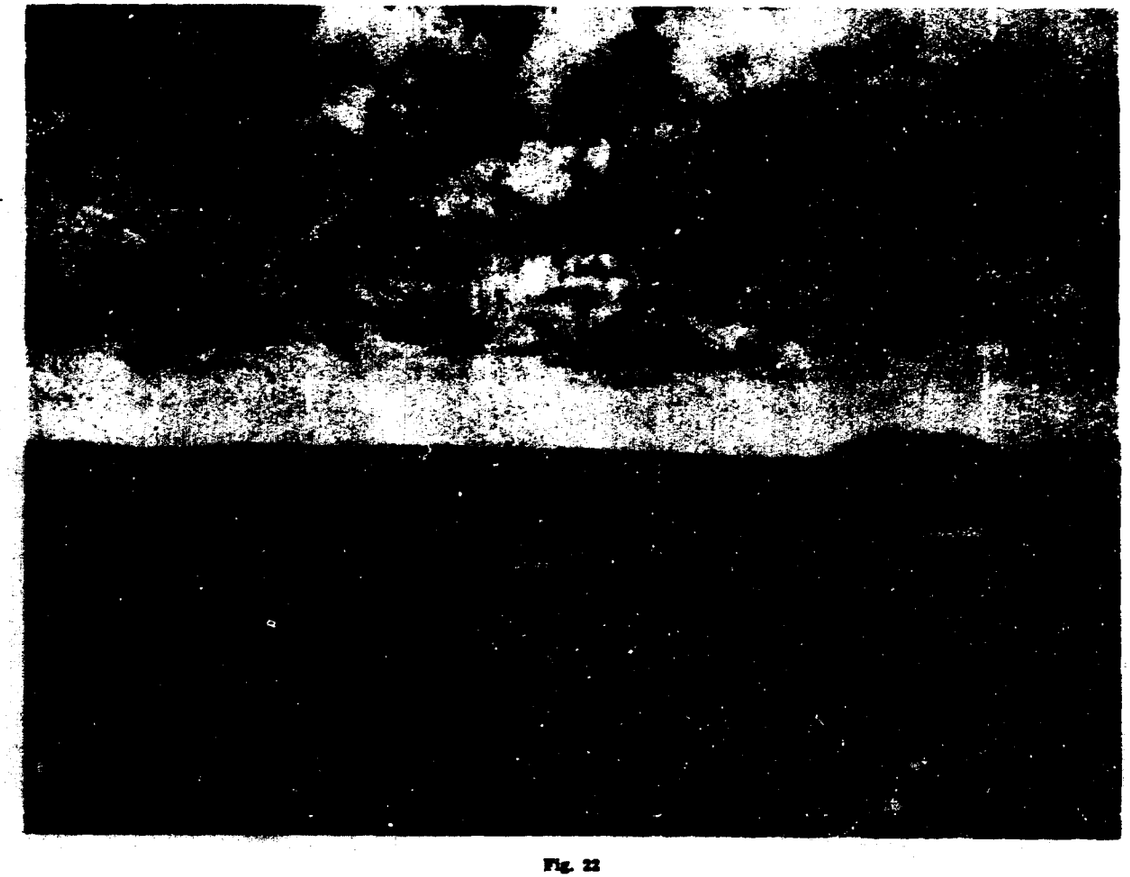

Fig. 22
The Granite Target as Viewed from Observation Station "Fred's Pipe"

that it was possible to communicate with the main control station or with any one of the ground crews in the bombing area.

Figure 20 is a view of the layout of the main control station at the granite site. The plotting table is in the center. The VHF air-to-ground radio truck is to the left of the plotting table. The weapons carrier to the right is equipped with "Horsie-talkie" radio and is used by the "Rover" team. The weapons carrier to the left is an emergency standby. The photograph, Fig. 21, a close-up of the spotting table, shows the manner in which the coordinates of the point of impact were determined after receiving the angles left or right from each of the observation stations. Each thumbtack on the board is an observation station, and each string represents the line of sight from the observation station to the point of impact. Readings were repeated if an excessively large triangle of error resulted.

The photograph, Fig. 22, is a close-up of the radio equipment used for air-to-ground communication after the tests had progressed somewhat. This setup is superior to the pickup truck mounting shown in Fig. 20. The entire setup was covered with a tent when not in use. The batteries were charged while in use, and also after each period of bombing, by means of the C-10 APU gasoline-engine-driven generator set, which is located to the right in the photograph. A low-frequency radio receiver

Fig. 23
Close-up of the VHF Radio Equipment

Fig. 24

The Sandstone Site Viewed from Observation Station "Easy" at the Conclusion of theTests. "Rover" is alongside the target. The bombing plane is overhead.

was used for a standby in case of VHF radio failure. A "Horsie-talkie" set was conveniently placed so that messages received on "Dog" or "Able" channels of the VHF radio could be relayed to the ground communications system. Arrangements were made with the pilot so that communications from the plane to the main control center using the 5500 frequency of the "Horsie-talkie" ground communications system was possible at all times while the plane was over the target.

At the beginning of each day of bombing, the program for the day was reviewed by the pilot and the project manager as the plane approached the experimental area. The plane speed, the plane heading, the altitude of release, the bomb type, the bomb weight, and the critical dimensions of the bomb were radioed to the ground control station immediately following each release. Plans for the following day or for the uncompleted portion of the tests were discussed while the plane was still within radio range after the day's mission had been completed.

The photograph, Fig. 23, is a view of the granite site target from observation station "Fred's Pipe." The target, three of the markers, and most of the access and grid roads were visible from this station. Similar views of the bombing area from other angles were obtained by observers at other stations designated on the spotting maps. The photograph, Fig. 24, is a view of the standstone site from observation station "Easy." This view was taken after the tests were completed. "Rover" is alongside the target, and the bombing plane is overhead.

g) Crater Mapping and Crater Photographs

Each apparent bomb crater was photographed to record the distribution and size of rock fragments relative to the line of flight, and then mapped in plan and cross section using a transit for elevations and cross sections and a plane table for plan mapping. The center of each apparent crater was selected, and two cross-section lines at right angles to each other were passed through this point. One line, designated the A-B line, was set parallel with the line of flight; the other, designated the C-D line, was set at right angles to it. A series of stakes at 25-foot or 50-foot intervals was set on each line to serve as reference points for horizontal and vertical control.

As excavation proceeded, a series of crater cross sections was taken along the AB and CD lines. Photographs of the crater were taken at intervals as the bomb was exposed. (See subsection i, Damage Surveys.)

h) Excavation

The amount of drilling and blasting necessary to recover the bombs from the craters was much less than anticipated. Generally the rock was so heavily shattered that the bombs could be recovered from all but the deepest craters without the use of explosives. The shallow craters were sufficiently broad that the bombs could be recovered without timbering. Craters of intermediate depth required timber support but did not require drilling and blasting. Deep craters required both blasting and timber support. The excavation and removal of the two 25,000-pound SAP bombs was a major undertaking which required the use of standard shaft-sinking methods in heavy ground.

59289

Fig. 25
Portable Headframe for Crater Excavation

Fig. 26
Crater Headframe Detail and Accessories

Fig. 27
Above-Ground Muck Pile, Apparent Crater 19

Fig. 28
Portable Headframe in Place for Sinking Crater 19

The heavily shattered rock from shallow craters was hand-shoveled onto the bank at the edge of the crater. Periodically the muck pile was shoved out of the way with a bulldozer. Deeper craters which could not be cleaned by hand shoveling direct to the surface were mucked out using a small sinking bucket and the portable headframe shown in the photograph, Fig. 25. The headframe was so designed and constructed that it could be skidded into position adjacent to the crater, then pulled across the top of the open crater without toppling into it. Each headframe was provided with a 1-ton chain hoist, a ½-ton sinking bucket, a sheave block, an air tugger hoist, and a complete drilling outfit including a pressure water tank. When the accessory equipment was placed in position on the bulkhead platform (shown in the photograph, Fig. 26), the center of gravity of the headframe was low and to the rear, and all necessary excavation equipment was readily available on a single unit. The 6 x 6 compressor truck used to move the headframe contained air-hose reels and was used to supply compressed air during both the drilling and the mucking cycles.

Fig. 29
Shaft Timbering and Spiling, Bomb 19

Excavation procedure at the two 25,000-pound SAP craters was adapted to the equipment used to excavate the 48 other craters and based somewhat upon the depth of penetration in granite using the modified Petrie formula and a value of K equals 2. The actual penetration was much greater than expected, and if this had been known at the time, different equipment would have been provided.

The first step in the excavation of the two 25,000-pound SAP bombs was to remove the above-ground-level muck from the apparent crater with a D-8 bulldozer. The photograph, Fig. 27, is a view of the above-ground muck pile at the granite site resulting from the release of a 25,000-pound SAP bomb at 18,000 feet above the target. The photograph was taken at right angles to the line of flight and from the 3 o'clock position. The pile is roughly 40 feet long and 4½ feet high at the apex.

Next, the heavily shattered rock to a depth of 6 feet within the apparent crater was dozed away. When the dozer reached a depth too great to dig further, it leveled an area 16 feet square. A crib of logs was built on this area, and the headframe was skidded onto the crib. (See Fig. 28.) A collar set was placed about 2 feet inside of the crib. The wall plates of this set—that is, the long timbers placed parallel to the line of flight—were made long enough to give a good bearing into the sides of the crater. Muck was taken out from within the collar set until the sides started to cave. Spiling was then set and driven, and was worked down as excavation proceeded. The heavily shattered ground required timber sets to be placed at close intervals. The photograph, Fig. 29, shows the method of timbering and spiling.

As excavation proceeded, the shaft was converted from a vertical shaft to an incline shaft, because of the path of the bomb. The hanging-wall of the inclined shaft was badly broken and difficult to support. At the change in direction, the hanging-wall timbers were placed skin-to-skin. Below the center of gravity of the bomb, the shaft set was converted from a 4-piece to a 3-piece set and the excavation was made entirely above the footwall of the bomb. The legs of the 3-piece sets were blocked to the sides of the bomb, and the portion of the bomb below the center of gravity rested directly on the rock. The lateral blocks were knocked out in a retreating fashion, beginning at the lowest block, just before the bomb was hoisted out of the shaft.

The excavation of Bomb 20, a 25,000-pound SAP bomb released from 26,000 feet above the target was conducted much in the manner described in preceding paragraphs. Because of the greater path length, the steeper angle of fall, and the slight deviation (or yaw) measured in a vertical plane, the percentage of the total length of the shaft in ground extremely difficult to support was much less than for Bomb 18. A shaft much larger in cross section was sunk, and heavy drilling and blasting were required beginning at the collar set.

The photograph, Fig. 30, shows the condition of the rock immediately below the collar set. The long axis of the shaft is parallel to the line of flight, which is indicated by the horizontal level rod. The broken rock in the skaking bucket and to the left was produced by blasting the corner of the shaft to square it up. The jagged horizontal fracture on the far side of the shaft is one of a series of open horizontal fractures along the path of the bomb. The fine muck between the 2- and 4-foot

Fig. 30
Condition of Rock Near Collar Set, 3½,000 SAP Bomb 20

Fig. 31
Shaft Timber Details, Bomb 20

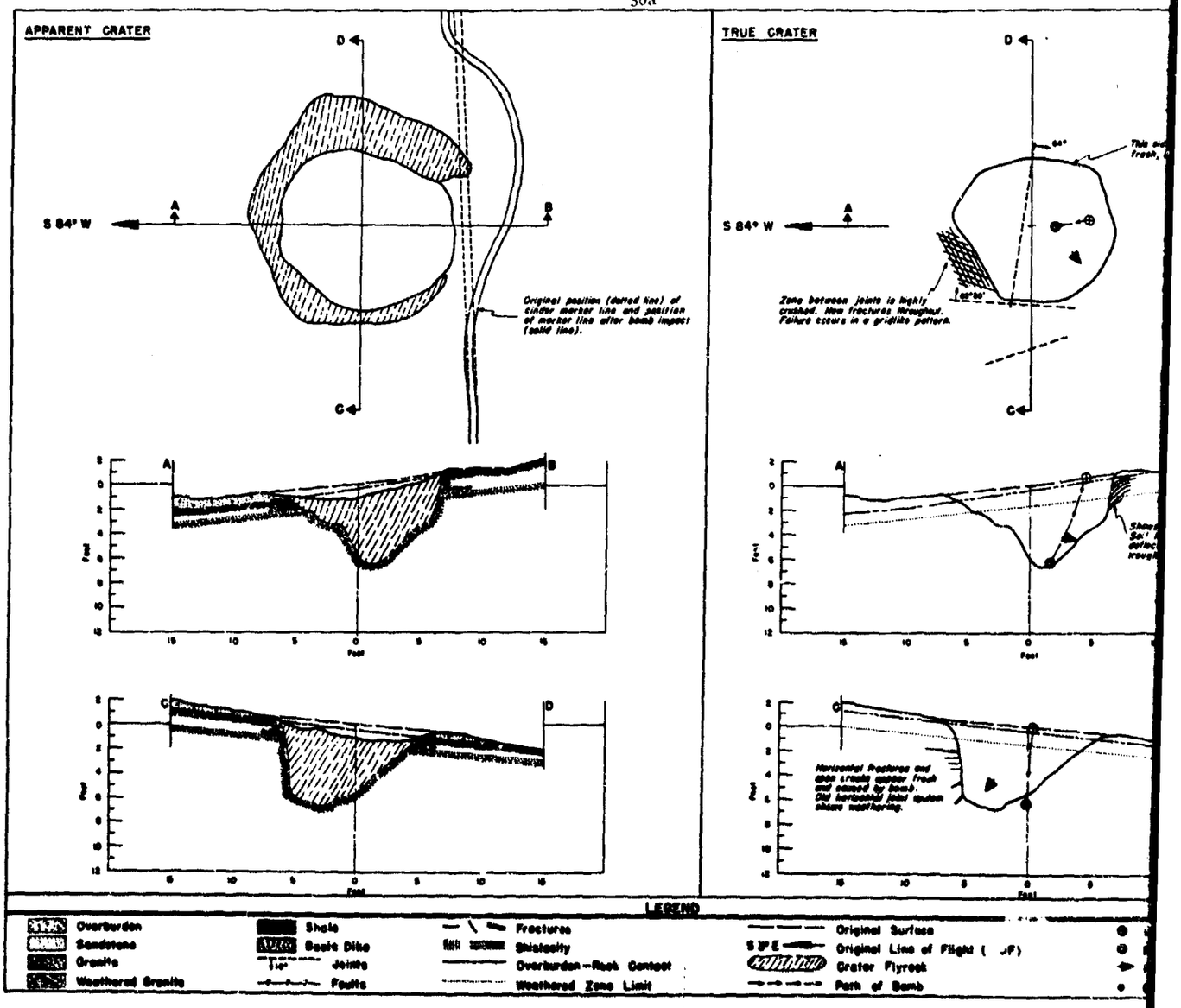
APPARENT CRATER
TRUE CRATER
S 84° W
Original position (dotted line) of cinder marker line and position of marker line after bomb impact (solid line).
Zone between joints is highly crushed. New fractures throughout. Failure occurs in a gridlike pattern.
Horizontal fractures and open cracks appear fresh and caused by bomb. Old horizontal joint system shows weathering.
Feet
LEGEND
Overburden
Sandstone
Granite
Weathered Granite
Shale
Basic Dike
Joints
Faults
Fractures
Shistosity
Overburden—Rock Contact
Weathered Zone Limit
Original Surface
Original Line of Flight
Crater Flyrock
Path of Bomb

TRUE CRATER

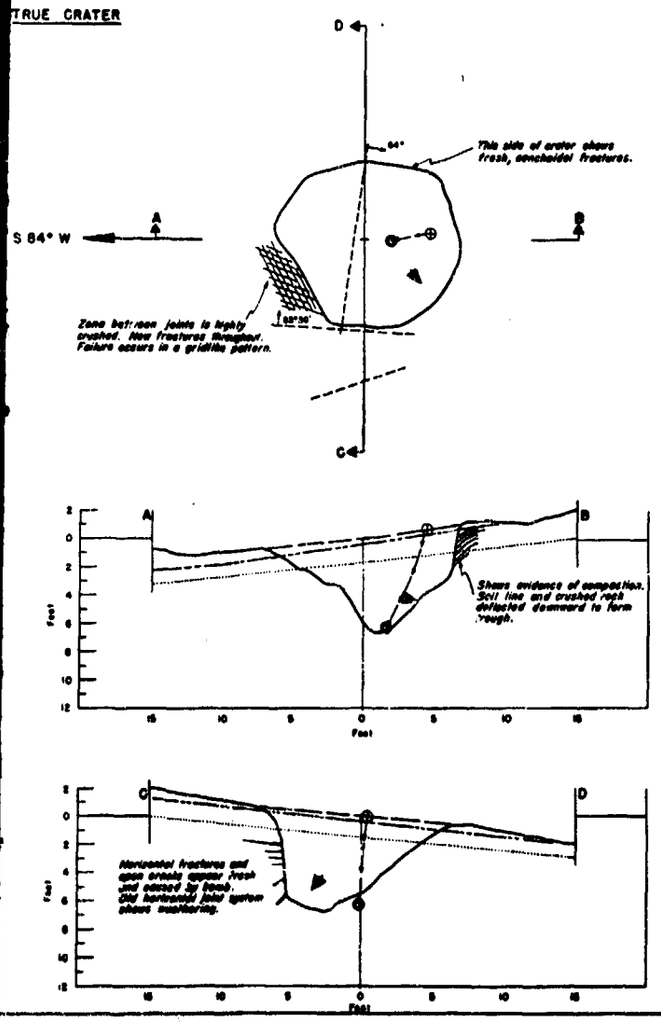

SECTION ON PATH OF BOMB

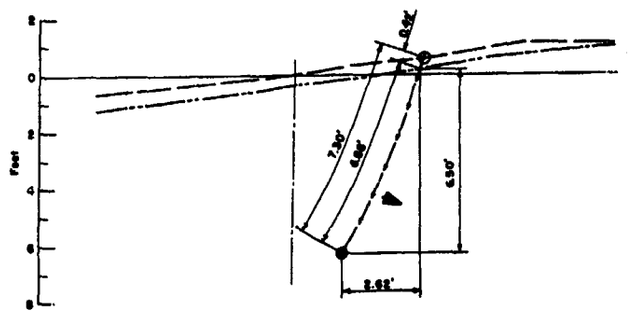

-BOMB PENETRATION PROJECT- OSM RESEARCH FOUNDATION, INC.

Original Surface
S 3°E Original Line of Flight (LOF)
Crater Flyrock
Path of Bomb
Point of Impact
Point of Maximum Penetration
Final Nose Position
Center of Gravity of Bomb

CRATER NO. 17

Fig. No. 32

2

Fig. 33
Measuring Compaction of Inert Filler in a 2,000 SAP Bomb

Fig. 34
Damage to Casing of a 2000-Pound General-Purpose Bomb
Released from 16,000 Feet above the Sandstone Target

Fig. 35
Collecting Specimens of Flowed Metal from the Nose of a Bomb

Fig. 36
Cutting Specimens for Metallurgical Studies

marks on the horizontal level rod marks the path of the bomb through the rock. After the fine material was mucked out, an opening was formed below the general level of the shaft bottom, and this opening served in place of the cut holes in a standard shaft round.

The photograph, Fig. 31, shows details of timbering near the face in the inclined portion of the shaft below the heavily shattered surface crater-zone. As may be observed, spiling was unnecessary, the hanging-wall was tightly lagged, the shaft timbers were closely spaced, and a horizontal, 4-piece timber-set was used. The timbers were cut from trees removed from the bombing area during target clearing. The base plate of the bomb is visible in the photograph, and the deviation of the bomb in a horizontal direction at a right angle to the line of flight may be inferred from the position of the bomb relative to the direction of the timbers.

i) Damage Surveys and Field Analysis

After a bomb had been completely exposed as a result of the excavation procedure described and before the bomb had been disturbed from the position at which it came to rest, a damage survey was conducted to obtain specific information useful in analyzing the results of the tests. Figure 32 is a typical crater map which records the details of the apparent crater, the true crater, and the true path of the bomb. The crater map, as presented, records information obtained from topographic mapping, auger drilling, and diamond drilling before the bomb was dropped; from the apparent crater immediately after the bomb was dropped; from the true crater as excavation proceeded; from the damage surveys and field analysis after excavation was complete; and from the damage surveys and field analysis after excavation was complete; and from ballistic data obtained from the Ballistic Research Laboratories, Aberdeen Proving Ground, after the completion of field work. A complete set of crater maps for all bombs dropped during the test program is a part of the appendix. (See Appendix, Part C.)

The field analysis consisted of two parts: part a) an analysis of the effects of the bomb on the rock and part b) an analysis of the effects of the rock upon the bomb. The analysis, part a), consisted of an intense study of the cracks in the rock, the manner of rock failure, and the influence of physical and geologic properties of rocks upon crater shape and bomb path. During the field analysis a theory of bomb penetration was developed and evidence was accumulated in support of the theory. The analysis, part b, consisted of comparing various critical dimensions of the bomb before and after dropping, measuring the compaction of the inert material in the bomb (see Fig. 33), taking photographs and measurement of the bombs to record distortion or damage to the bomb casing (see Fig. 34), collecting specimens of flowed metal (see Fig. 35), and cutting specimens from the bombs for metallurgical studies (see Fig. 36).

j) Bomb Recovery and Disposal

The bombs were pulled from the craters and additional excavation was done where required. The surveys were continued until the crater was completely cleaned to solid rock in the bottom. The 1600 AP and

2000 SAP bombs were skidded from their respective craters using the winch of a weapons carrier or truck or using a chain hooked to a D-8 bulldozer. The bulldozer was used to drag all except the 25,000-pound bombs to a disposal area at each site, (see Fig. 37) where they were photographed in two positions at right angles to each other, before being shoved into a wide trench and covered with 6 to 10 feet of earth.

The two 25,000-pound, T28E4, SAP bombs were hoisted from their craters with a crane, lowered to the ground after a 90-degree swing, picked up again in a horizontal position, and lowered into place and secured on a lowboy. (See Fig. 38a, b, c, d.) The transfer from the lowboy to a Santa Fe Railroad flat car was done with the same equipment and crew. The two 25,000-pound bombs were shipped by rail from Grants, New Mexico, to Watertown Arsenal, New York, for further study by the Department of Ordnance.

Fig. 37

Dragging Bombs to Disposal Area

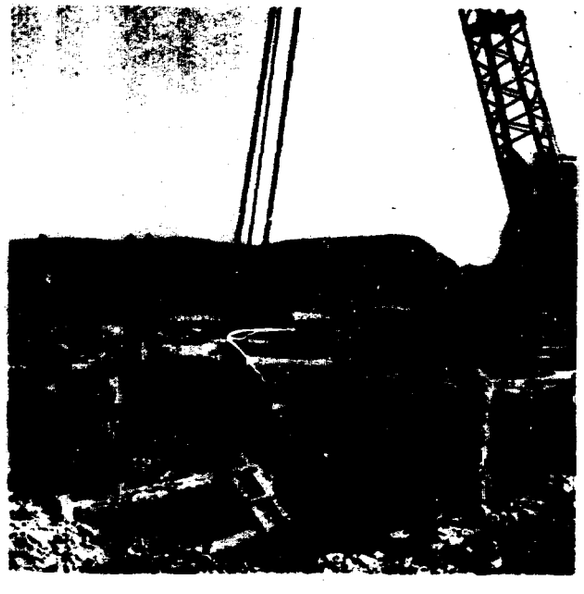

Fig. 38a
Hoisting a 25,000-Pound Bomb from Its Crater

Fig. 38b
Lowering Bomb to the Ground in a 90-Degree Position

Fig. 38c
Lifting the 25,000-Pound Bomb in a Horizontal Position

Fig. 38d
Securing Bomb in Place on a Lowboy

SECTION III—GEOLOGIC REPORT

1—Regional Geology—By V. C. Kelley

a) Introduction

The area with which this report is generally concerned covers about 384 square miles and lies in northwestern New Mexico and in the north central part of Valencia County. As may be observed from the regional geologic map, Fig. 39, the Zuni Mountains constitute most of the area, but parts of the north end of the Valencia volcanic field and Putney Mesa are also included. U. S. Highway 66 and the Santa Fe Railroad cross the northeastern edge of the area, and the region is generally accessible by dirt or gravel side roads, the principal one of which is New Mexico Highway 53.

The area lies in the Datil physiographic section of the Colorado Plateau Province. The altitudes range from 6,400 feet in the San Jose Valley near Grants to about 9,300 feet at Mount Sedgwick, the highest peak in the Zuni Mountains. The altitude of the lava-capped mesas along the eastern edge of the area ranges from 7,000 to 7,500 feet.

The rocks of the region range in age from pre-Cambrian to Recent. Pre-Cambrian granite, gneiss, and schist form the core of the Zuni Mountains. Permian strata are the principal rocks overlying the pre-Cambrian core, and they form the flanks and slopes of the Zuni Uplift. Weak Triassic strata form the principal bedrock of the valleys, and Jurassic and Cretaceous rocks make up the slopes of the mesas in the eastern part of the area. Basalt flows of early Quaternary (?) age cap the eastern mesas, and similar flows of late Quaternary age cover the valley bottoms surrounding the highlands.

The principal structural elements of the region are the Zuni Uplift and the Mount Taylor syncline. The eastern end of the Zuni Mountains is a part of the northwestward-trending Zuni Uplift, which is about 80 miles long and 35 miles wide. Along the eastern edge of the area Jurassic and Cretaceous strata in the slopes of the mesas are a part of the western limb of the Mount Taylor syncline.

b) Stratigraphy

The general stratigraphy of the region is outlined in the accompanying table (Fig. 40). The sedimentary section from the pre-Cambrian to and including the Upper Cretaceous totals about 6000 feet in thickness. It consists mostly of marine and continental clastic sediments which were formed either marginal to highlands or on marine shelves. Much greater thicknesses of almost all the formations are to be found to the north and east of the Zuni region.

b-1) Pre-Cambrian Rocks

The pre-Cambrian rocks form the core of the Zuni Mountains, and their outcrops generally mark the axis of the range. The dominant rock is granitoid and consists of tourmaline granite, granite gneiss, mica schist,

and metarhyolite porphyry. Smaller patches of amphibolite, diorite, gabbro, and quartzite are scattered through the granitoid rocks.

The principal foliation of the metamorphic terranes is west-northwest. Locally, however, considerable variation from this trend is to be noted, and at the Paxton Springs granite site a foliation trend of about N. 43 E. is pronounced.

b-2) Pennsylvanian Rocks

Locally a thin interval of Pennsylvanian rocks that are probably the equivalent of the Madera limestone lies nonconformably upon the deeply eroded pre-Cambrian rocks. The Madera in the Zuni Mountains consists of reddish conglomerate, sandstone, siltstone, and light-gray, marine limestone. It is the product of a short, late transgression of the Pennsylvanian seas which were widespread and of longer duration in nearby areas.

b-3) Permian Rocks

The Permian rocks consist of units that are Wolfcamp and Leonard in age. The lowermost unit is the Abo formation (Wolfcamp) which is a floodplain deposit that spread over the area following the regression of the Pennsylvanian Madera sea. The Yeso formation (Leonard) overlies the Abo formation. The Yeso formation was probably laid down under marine conditions. Thin marine limestone and gypsum beds are intercalated with the abundant sandstone and siltstone. The more massive lower one-third of the formation is mapped in many places in New Mexico as the Meseta Blanca member, whereas the upper part has been designated as the San Ysidro member.

The Glorieta sandstone and the San Andres limestone intertongue, and together they are often mapped simply as the San Andres formation. In the eastern end of the Zuni Mountains, the San Andres limestone member makes up about three-fourths of the formation, whereas in the western part of the mountains the Glorieta sandstone member is dominant. The limestone beds commonly contain marine fossils.

b-4) Triassic Rocks

The Triassic rocks of the eastern end of the Zuni Mountains are all of late Triassic age and are probably best designated as the Chinle formation. The formation is a floodplain deposit and its bedding is irregular and channeled. It is a soft formation, and outcrops are meager; it underlies the broad valleys surrounding the mountains and mesas.

b-5) Jurassic Rocks

The Jurassic rocks are most prominently represented by units of the San Rafael group, although a thin interval of Glen Canyon rocks represented by the Wingate and Kayenta may be present. The Glen Canyon rocks, if present within the map area (Fig. 30), do not crop out because they are covered by Quaternary basalt and alluvium.

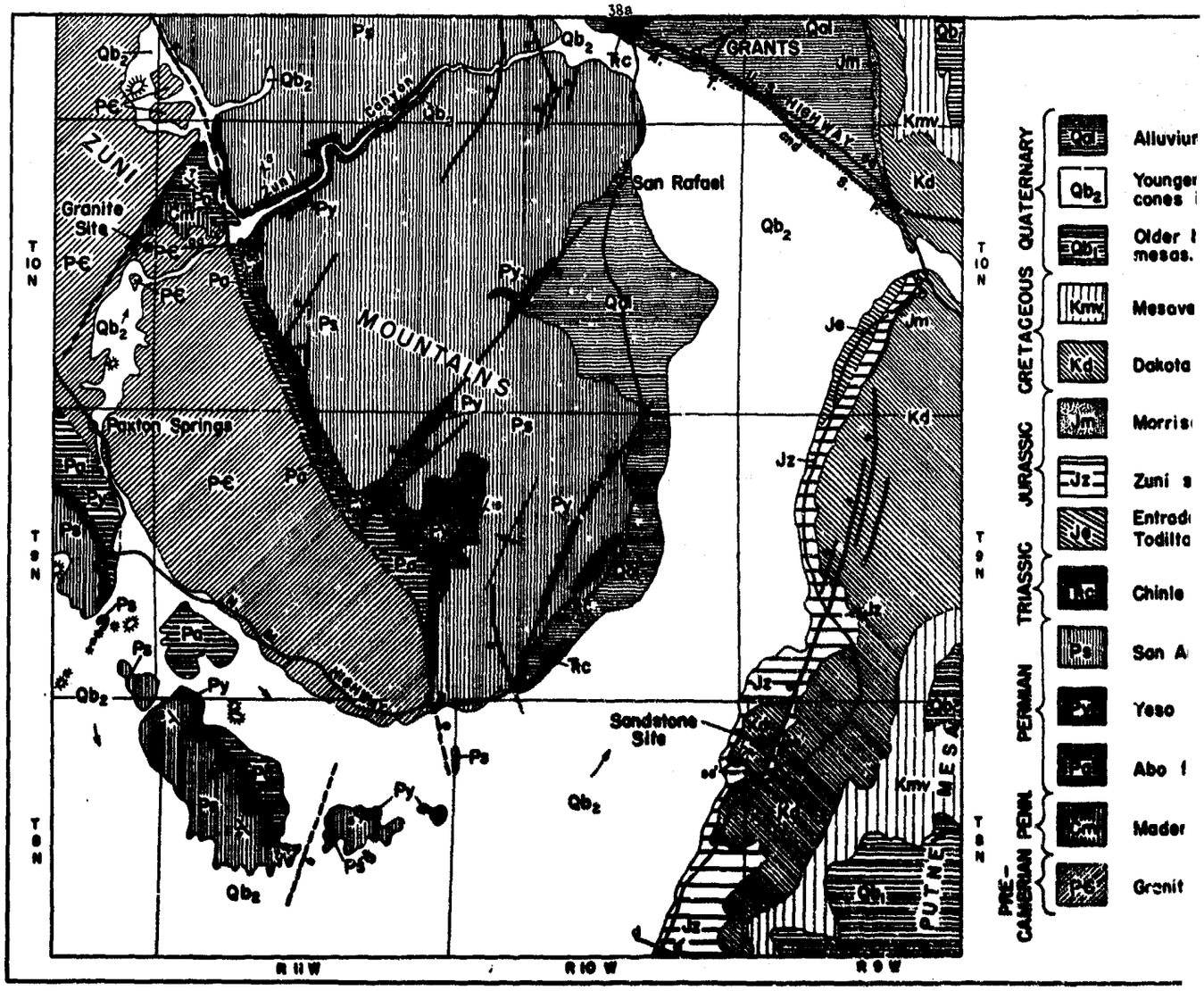
GRANTS
HIGHWAY
ZUNI
MOUNTAINS
San Rafael
Granite Site
Paxton Springs
Sandstone Site
PUTNEY MESA
T 10 N
T 9 N
T 8 N
R 11 W
R 10 W
R 9 W
QUATERNARY
CRETACEOUS
JURASSIC
TRIASSIC
PERMIAN
PENN.
PRE-CAMBRIAN
Alluviu
Younger cones
Older mesas.
Mesave
Dakota
Morris
Zuni s
Entrad Todilto
Chinle
San A
Yeso
Abo
Mader
Granit

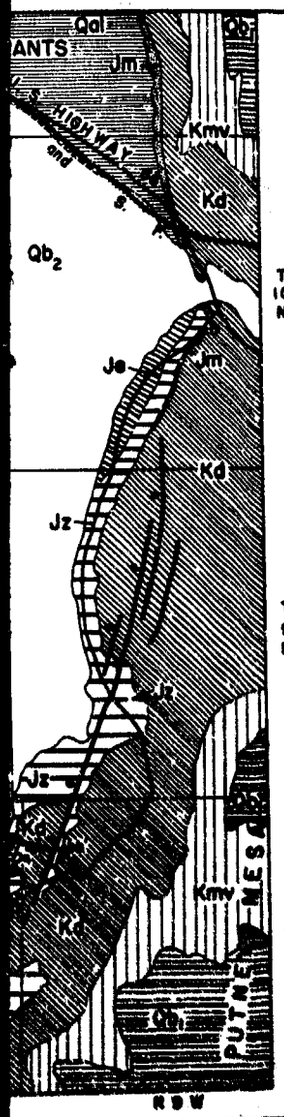

EXPLANATION

ROCKS

Age	Symbol	Description
QUATERNARY	Qal	Alluvium, valley fill.
	Qb_2	Younger basalt flows and cones in valleys.
	Qb_1	Older basalt flows on mesas.
CRETACEOUS	Kmv	Mesaverde formation.
	Kd	Dakota sandstone.
JURASSIC	Jm	Morrison formation.
	Jz	Zuni sandstone.
	Je	Entrada sandstone including Todilto limestone at top.
TRIASSIC	Mc	Chinle formation.
PERMIAN	Ps	San Andres formation.
	Pw	Yeso formation.
	Pa	Abo formation.
PENN.	Cm	Madera limestone.
PRE-CAMBRIAN	Pc	Granite, gneiss, and schist.

SYMBOLS

- Fault, with downthrown side; dashed where uncertain.
- Strike and dip of beds.
- Axis of syncline.
- Location of geologic columns. Not to scale. See Figs. 43, 45, 46, and 48.

SCALE

0 1 2 3 4 5 6 7 Miles

-BOMB PENETRATION PROJECT- CSM RESEARCH FOUNDATION, INC.

Scale: Shown Date: 2-12-81

Figure 39 By VOK-LB

GEOLOGIC MAP - SOUTH OF GRANTS, VALENCIA COUNTY, NEW MEXICO

Fig. 39

2

System and Series	Formation		Thickness (feet)	Description
Quaternary	Basalt		0-100	Basalt of valleys and mesas; plugs, cones, and flows.
Tertiary	Rhyolite and andesite		900	Andesite and rhyolite tuff; breccia, flows, and plugs.
Upper Cretaceous	Mesaverde formation	Upper Gibson coal mem.	46	Shale, siltstone, sandstone, and coal.
		Hosta sandstone member.	300	Massive sandstone.
		Lower Gibson coal mem.	350	Gray shale, carbonaceous shale, coal, and sandstone.
		Dalton sandstone mem.	100	Massive, blocky, cross-bedded sandstone.
		Dilco coal member.	150	Sandy shale, thin limestone, and coal.
		Gallup sandstone mem.	65	Massive, clean, white sandstone.
	Mancos shale	Satan tongue	0-300	Sandy shale
		Mulatto tongue	0-250	Sandy shale and sandstone.
		Lower Mancos shale mem.	800	Dark-gray to black marine shale.
	Dakota sandstone		50-150	Coarse sandstone and conglomerate with shale interbeds.
Jurassic	Morrison formation		0-50	Varicolored shale and light-buff sandstone.
	Zuni sandstone		370	Massive, cross-bedded, white to light-buff sandstone.
	Todilto limestone		5-10	Thin-bedded, dark-gray limestone.
	Entrada sandstone		150	Massive white and tan-brown sandstone.
	Carmel formation		20	Red and tan-brown friable sandstone and siltstone.
	Wingate sandstone		50	Red and tan-brown sandstone.
Triassic	Chinle formation		1500	Red, brown, gray shale, siltstone and sandstone.
Permian	San Andres formation		270	Gray to dark-gray massive limestone; yellowish-brown ss.
	Yeso formation		500-600	Tan-brown, fine-grained ss. little limestone and gypsum.
	Abo formation		400-550	Red-brown siltstone and sandstone, irregular bedding.
Pennsylvanian	Madera limestone		35	Gray limestone, reddish shale, and basal conglomerate.
Pre-Cambrian	Pre-Cambrian.			Granite, gneiss, and schist.

Fig. 40

General Stratigraphic Table of Area Near Grants, New Mexico

The San Rafael group crops out prominently and includes in ascending order the Carmel formation (?), Entrada sandstone, Todilto limestone, and Zuni sandstone. If the Carmel is present, it is covered. The Entrada sandstone (Wingate of older reports) crops out in a narrow band at the base of the north end of Putney Mesa. By some geologists it is thought to be a transgressive sandstone which was deposited by a minor advance of the late Jurassic sea that widely deposited the thin Todilto limestone. Some of the overlying Zuni sandstone has been mapped in adjoining areas to the east as a part of the Morrison formation. The massive cliff formed by the Zuni sandstone along the east side of the area may contain representatives of the Morrison as well as units mapped as the Bluff and Junction Creek sandstones in southwestern Colorado and Utah. A thin wedge of typically varicolored Morrison shale overlies the Zuni sandstone locally in the area.

b-6) Cretaceous Rocks

Owing to the reconnaissance nature of the field work, the Cretaceous rocks of this area are mapped into two units, the Dakota sandstone and the Mesaverde formation. The entire sequence belongs to the Upper Cretaceous and consists of intertonguing marine and swamp-formed continental units. The lowermost unit of the Upper Cretaceous is the Dakota sandstone. It consists in this area of several coarse-grained thick sandstone beds intercalated with thin black shale units. A relatively thick black shale slope-forming unit above the Dakota ledges could with more detailed mapping be delineated as the Mancos shale. However, on the accompanying map it is included with the Dakota. The Mesaverde coal-bearing formation that is mapped above the Dakota also contains tongues of the marine Mancos shale.

b-7) Tertiary Rocks

In the southwestern part of Mount Taylor, rhyolite, andesite, and basalt intrusives and extrusives occur and are probably of middle or late Tertiary age (Hunt, 1938). These are not included on the accompanying map. The older, mesa-capping basalt flows designated as Qb_1 on the map may be of late Tertiary age. No Tertiary sedimentary rocks are preserved in the area.

b-8) Quaternary Rocks

The Quaternary rocks consist of two kinds, Pleistocene or Recent basalt flows and Recent valley alluvium. A rather remarkable flooding of the valley bottoms around the highlands has resulted from eruptions of low-viscosity lavas from cones in the Zuni Mountains and to the northwest of Grants.

c) Structure

The structure of the Zuni Mountain region consists principally of folds and faults. Folds dominate over faults, and whereas the fold axes are generally tens of miles in length, the faults are rarely more than a few miles in length.

c-1) Folds

The principal fold is the northwesterly elongated Zuni Domal uplift which tends northwesterly. The structural relief of this feature is about 5500 feet. The Zuni Uplift is generally asymmetrical, with the steep limb on the southwest side. Along the southeastern end of the Zuni dome the east limb descends into the Mount Taylor or McCarty's syncline, the axis of which trends north and lies a few miles east of the eastern edge of the accompanying map. Lesser folds that are superimposed upon the larger regional features are uncommon and obscure. One such fold, a north-northeasterly trending syncline, is shown on the accompanying map. Lesser folds that are superimposed upon the larger regional features are uncommon and obscure. One such fold, a north-northeasterly trending syncline, is shown on the accompanying map near the southeast end of the Zuni Mountains. The regional dips on the flanks of the major folds are rarely more than 10 to 20 degrees.

c-2) Faults

Two sets of faults occur in the region south of Grants—those whose strikes are north-northwest and those whose strikes vary from north-northeast to northeast. All are high-angle faults and are probably normal faults.

The principal fault of the area strikes generally north-northwest along the northeast flank of the Zuni dome. It is downthrown on the northeast side as much as several hundred feet. The Abo and Yeso formations are dropped against the pre-Cambrian rocks. Other lesser faults roughly parallel this major fault along the Zuni Uplift.

Most of the other faults of the area strike northeasterly. These occur both in the Zuni Mountains and in Putney Mesa. Some of these faults are downthrown on the west side and others are downthrown on the east side, but neither type is the throw more than a few tens of feet, or exceptionally, one or two hundred feet. The most abundant and prominent joint set in the sedimentary rocks of this region is parallel to the north-northeasterly faults. The joints and faults of this trend are undoubtedly related, and the faults may be considered as members of the joint set along which displacement is relatively large.

d) Geologic History

The long pre-Cambrian history of the Zuni Mountains is rather imperfectly known and is much obscured because of covering of the pre-Cambrian rocks by younger rocks. It appears, however, that clastic sediments and volcanic products accumulated in the region in pre-Cambrian time. Probably in late pre-Cambrian time the region was subjected to compressive forces which impressed within the depths of the crust a west-northwesterly foliation upon these rocks. Closely following and perhaps nearly accompanying this deformation, masses of granite were intruded into the older terrain, and the older foliation trends were locally diverted or new trends were formed. The entire region, in common with much of the southwestern part of the United States, was eventually eroded to a low base in late pre-Cambrian time.

During most of Paleozoic time the Zuni Mountain region appears

to have been a rather stable highland area which, although perhaps contributing some sediment to seas to the north and south, never was uplifted greatly.

In late Pennsylvanian times, shallow seas transgressed the Zuni area for a short time, only to be pushed back by the seaward growth of floodplain deposits in early Permian time. During the remainder of Permian time the region appears to have remained close to the transitional environment between sea and land. With the advent of Triassic time the region appears to have been at first a stable upland and then in late Triassic time the site of great floodplain accumulations that probably were derived mostly from the south. During Jurassic time erosion followed by continental and near-shore aeolian deposition and finally floodplain and lacustrine accumulation took place. The Jurassic deposits were derived largely from a slowly rising arch to the south of the Zuni area.

Widespread erosion affected the area during early Cretaceous time as the southerly highland continued its gradual rise. During late Cretaceous time the seas again transgressed the area from the south, east, and north, and as the area gradually sank concurrently with the gradually rising source area to the southwest and west, marine and nonmarine sediments accumulated to a thickness of several thousand feet to form the Dakota, Mancos, and Mesaverde formations.

Throughout the long interval between pre-Cambrian and Tertiary time the Zuni area was affected only by broad epeirogenic warping. Sediments which accumulated upon this gently undulating surface were essentially parallel or only locally sub-parallel in their arrangement. In early Tertiary time the region began to be deformed in more accentuated or accelerated manner. It appears from geologic evidence in adjoining areas that the Zuni Uplift may have been largely formed by the end of Eocene time. The trend of the Zuni Uplift appears to have been influenced or determined in part by the direction of the late Paleozoic highland trends, and both may have inherited structural trends from the pre-Cambrian structure.

During middle Tertiary time the entire area was rather deeply eroded, and wide pediment surfaces were formed. The Mount Taylor volcanic pile was built upon this surface in late Tertiary time. Broad regional uplift, accompanied and followed by erosion which etched most of the present valleys and landscape features, occurred in late Tertiary and early Quaternary time. In late Pleistocene or early Recent times numerous central vents erupted great floods of basalt which flowed down the modern valleys.

Tectonic activity in the Zuni area has been long and varied. The pre-Cambrian rocks in the core of the Zuni Uplift have been affected by many deforming stresses that were both tangential and radial with reference to the earth's crust. It may be said, however, that the dominating directions of tangential forces have been northerly and southerly. The deformation is the result of two principal periods of activity, one in late pre-Cambrian time and the other in early Tertiary time. The region appears to have been little affected by the late Tertiary tectonics which so profoundly affected the central New Mexico area along the Rio Grande Valley. There is no geologic evidence to suggest that the Zuni Mountain area is under stress at the present time.

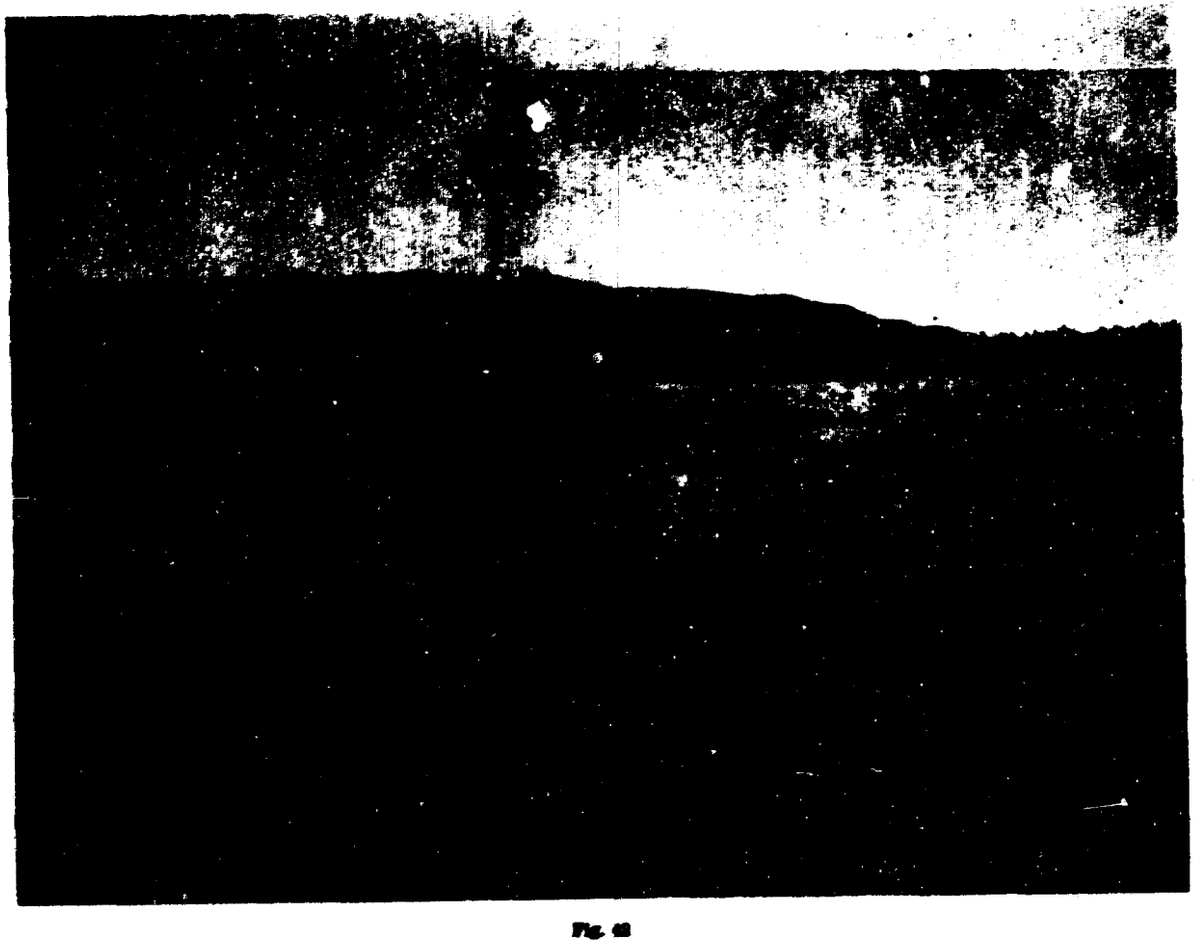

Fig. 42
Panoramic View Showing Granite Core of Zuni Uplift

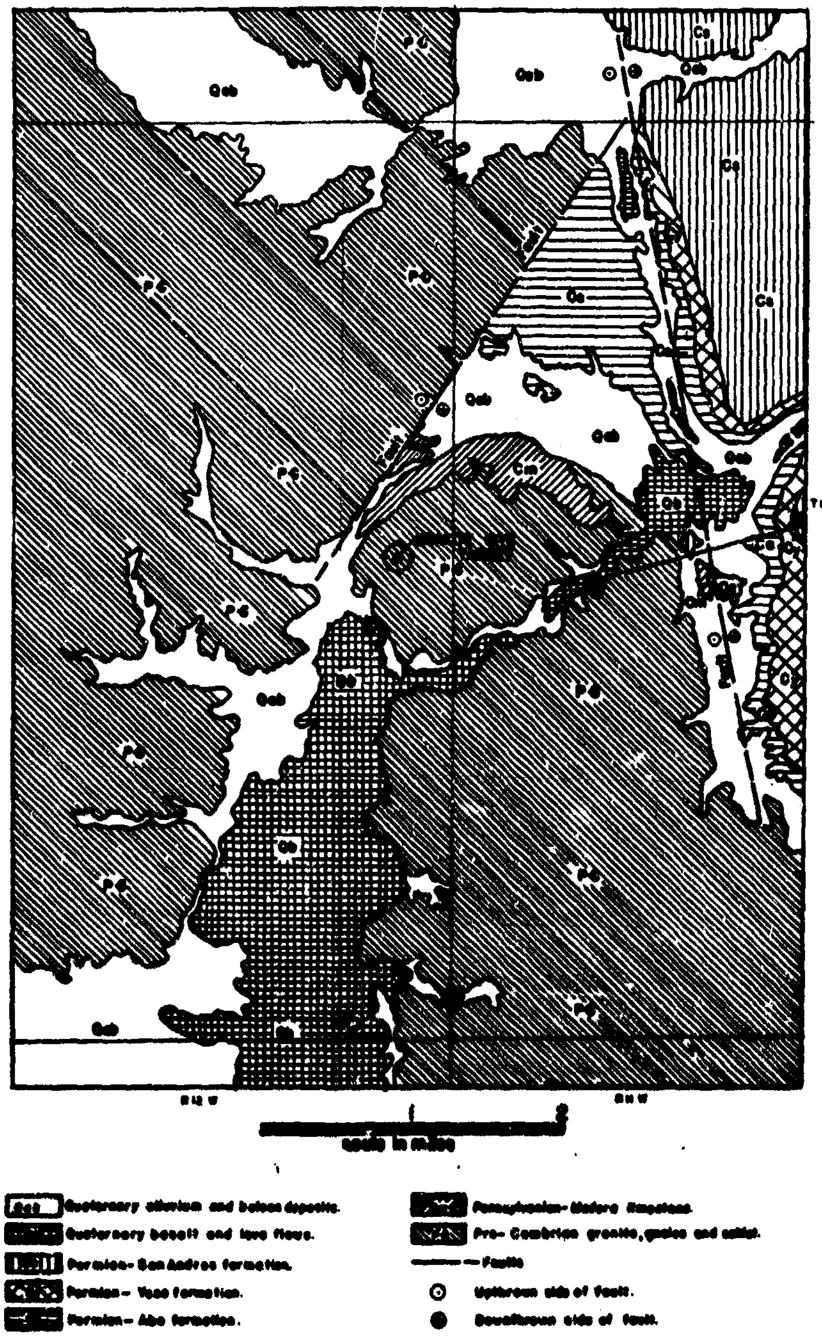

-BOMB PENETRATION PROJECT- C S M RESEARCH FOUNDATION, INC.

Scale 1in=1/2mi Date 1-9-50

Fig. No. 41 By FDM

- GEOLOGIC MAP OF GRANITE SITE
TARGET AREA-

Fig. 41

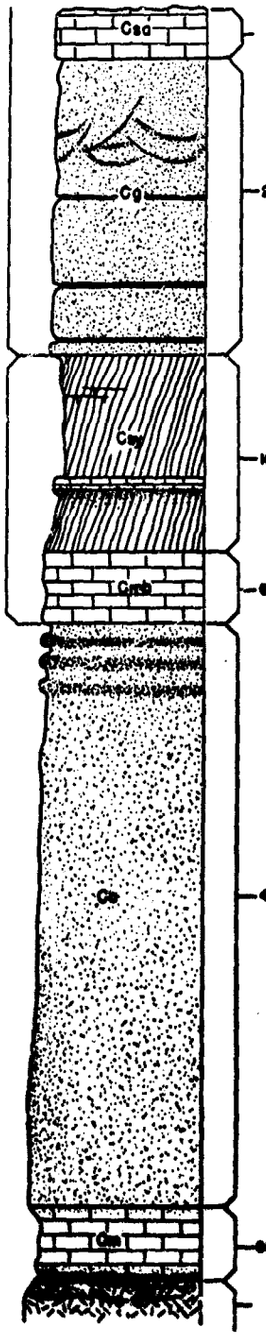

SAN ANDRES (Permian)

YESO (Permian)

SAN ANDRES Limestone: A massive, fine grained, equigranular limestone, gray to buff color, sharp irregular surfaces indicating chemical weathering. Fossils fairly abur

245' GLORIETA Sandstone: A light buff-white, medium-grained, equigranular sandstone. Cross-beddi portion of formation. A series of thinly laminated lenses of shale are

164' SAN YSIDRO Formation: A series of strata consisting of easily eroded, grayish-white gypsum and dark gray limestone. A very soft, fine grained, yellow sandstone is located

60' MESETA BLANCA Limestone: A dense, equigranular limestone. gray colored and in part red.

405' ABO Sandstone: (Permian) An irregular bedded, brownish-red, ferruginous sandstone. Top section is banded r layer being the more resistant forms shelves or benchs.

60' MADERA Limestone: (Pennsylvanian) A dark brick-red, fine-grained, equigranular limestone.

PRE-CAMBRIAN Granite, gneiss, schist.

-BOMB PENETRATION F	
Scale 1in=60ft.	Date 9-14-60
Fig No. 43	By FDM

sharp

y abund stone: A massive, fine grained, equigranular limestone, gray to buff color, sharp irregular surfaces indicating chemical weathering. Fossils fairly abundant.

-bedding

le are tone: A light buff-white, medium-grained, equigranular sandstone. Cross-bedding in top portion of formation. A series of thinly laminated lenses of shale are present.

n and

cated a ation: A series of strata consisting of easily eroded, grayish-white gypsum and thin-bedded dark gray limestone. A very soft, fine grained, yellow sandstone is located at base of limestone.

l.

CA Limestone: A dense, equigranular limestone. gray colored and in part red.

nded re

An irregular bedded, brownish-red, ferruginous sandstone. Top section is banded red and white, the white band or layer being the more resistant forms shelves or benchs.

ION PR

-60

one: A dark brick-red, fine-grained, equigranular limestone.

Granite, gneiss, schist.

-BOMB PENETRATION PROJECT- C S M RESEARCH FOUNDATION, INC.	
Scale 1in=80ft. Date 9-14-60 Fig. No. 43 By FDM	- GEOLOGIC COLUMN OF SECTION e-e' EAST OF GRANITE SITE-

Fig. 43

2

2.—Geology of the Granite Site Target Area

Figure 41 is a geologic map of the locality adjacent to the granite site target. The Index Map, Fig. 1, and the map showing the regional geology, Fig. 39, may be referred to for the location of the granite site target relative to Grants, New Mexico, and relative to the broader geologic features discussed in preceding paragraphs.

The pre-Cambrian basement rocks of the target area have been exposed by erosion of the uplifted Zuni Mountain region. Figure 42 is a panoramic view of the north edge of the target area showing the granite core of the Zuni Uplift (to the right in the photograph), Permian strata in the background, Quaternary basalt flows in the middle distance, and Quaternary alluvium in the foreground. The steep slopes are on the geologic map of the granite site target area (Fig. 41). The uppermost sedimentary beds in the photograph are the lower members of the San Andres limestone (see table, Fig. 40).

The stratigraphic sequence and the measured thickness of sedimentary rocks lying between the granite and the San Andres formation are presented in the geologic column, Fig. 43. The formation thicknesses were measured on the steep slope to the left center in the panoramic view.

Immediately above the granite surface lies a thin layer of sandstone conglomerate which represents the base of the Pennsylvanian Madera limestone. Remnants of the sandstone conglomerate are present at the edges of the granite target; and the distribution of the remaining part of the Madera, the Abo, the Meseta Blanca, the San Ysidro, the Glorieta sandstone, and the San Andres limestone are shown on the geologic map.

The presence of remnants of sandstone conglomerate close to the bombing targets implies that erosion has not deeply dissected the pre-Cambrian granite. A thin cover of alluvium, to a maximum thickness of 3 feet, overlies the granite surface; where the alluvium is thickest, the degree of weathering of the granite has been greatest. The granite surface below the alluvium is relatively smooth. The photograph, Fig. 44, shows the nature of the rock surface where it is free from overburden and likewise relatively free from weathering.

Thin pegmatite dikes oriented similarly to the joints in the granite or parallel to the flow lines in the granite are present to a minor extent. In some places the flow lines in the granite are so well developed that the granite might be more properly classified as a gneissic granite. A 10-foot-wide lamprophyre dike (vogesite) passes through the target area beneath alluvium. It was discovered beneath the alluvium after one bomb struck squarely in it and another penetrated into it from the adjacent granite. The dip of the dike is nearly vertical and the strike is such that the like did not intersect any of the diamond drill holes. The lamprophyre dike is possibly one of many feeder channels through which the Quaternary lava poured upward to flood valleys in Recent geologic time.

The detail geology and fracture pattern of the granite within the target area have been mapped on the topographic map which is intro-

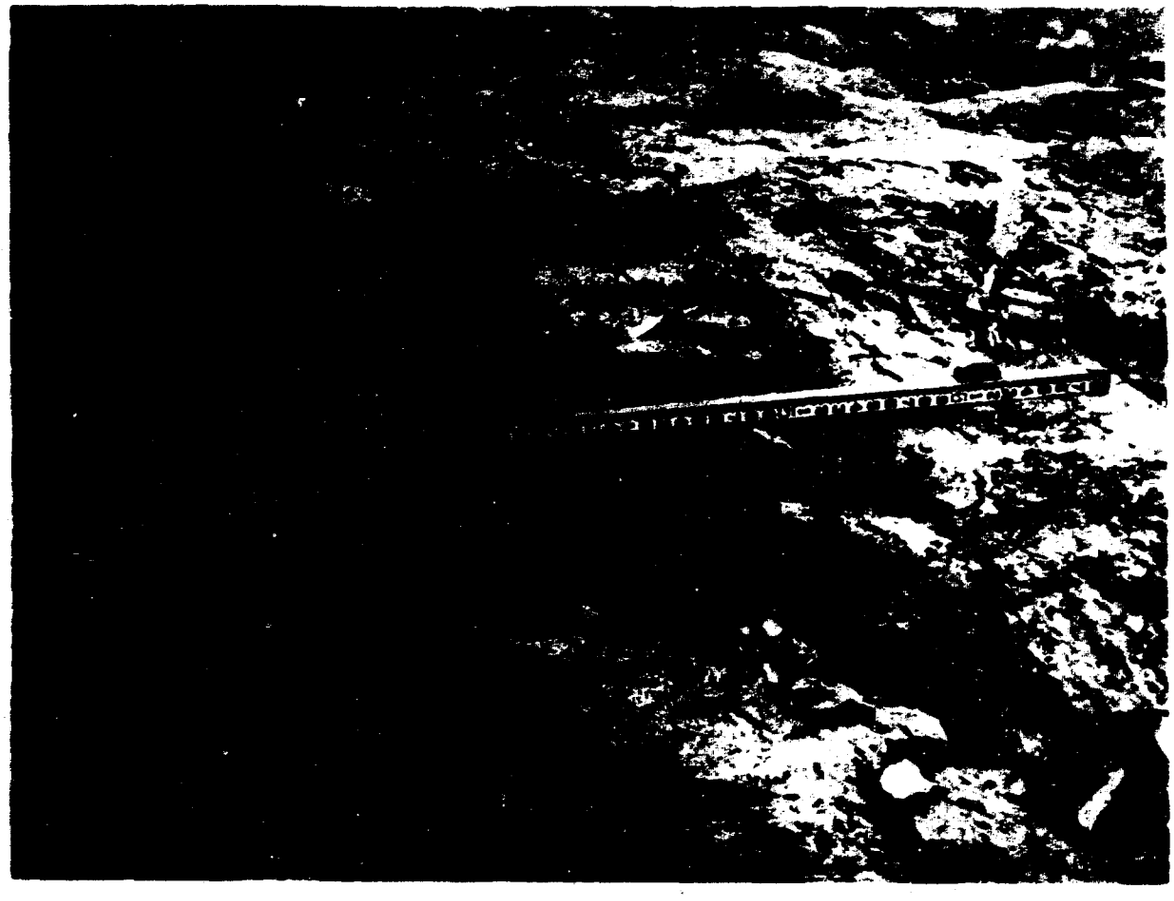

Fig. 44

The Granite Surface at the Paxton Springs Bombing Site

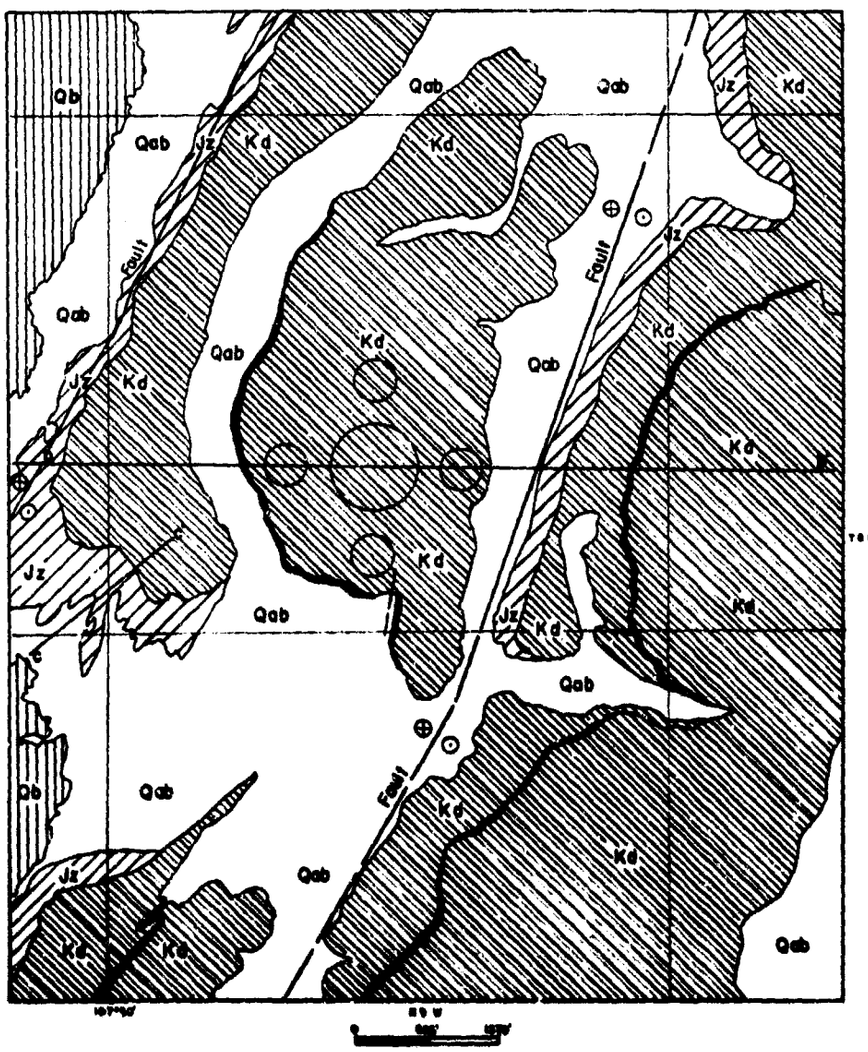

Qab Quaternary alluvium deposits.

Qb Quaternary basalt and lava flows.

Jz Jurassic- Zuni sandstone.

Kd Cretaceous- Dakota sandstone.

Cretaceous- Dakota shale.

Faults.

Upthrown side of fault.

Downthrown side of fault.

BOMB PENETRATION PROJECT – CSM RESEARCH FOUNDATION, INC.

Scale 1in= 5.25 ft. Date 11-7-50

Fig.No. 45 By FDM

–GEOLOGIC MAP OF SANDSTONE SITE TARGET AREA–

Fig. 45

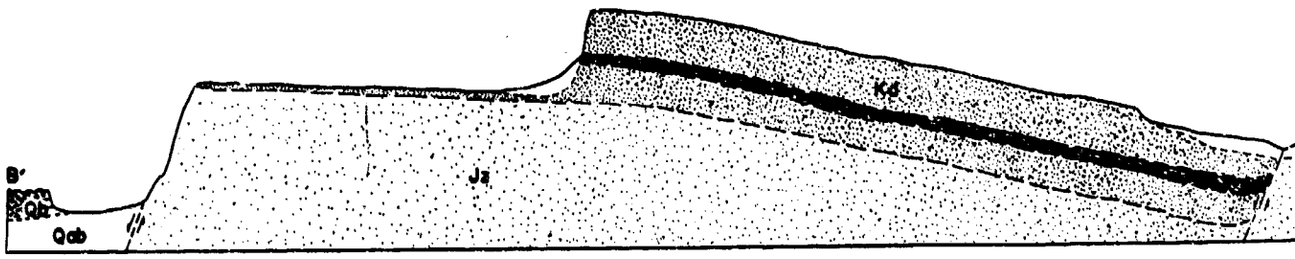

Kd—DAKOTA Sandstone (Cretaceous)

Jz—ZUNI Sandstone (Jurassic)

Qab-ALLUVIUM (Quaternary)

Qb—BASALT (Quaternary)

Horizontal Scale —

Vertical Scale —

-BOMB PENETRATION PRO	
Scale 1" = 200' Date 8-12-50	CR
Fig. No. 46 By FDM	

Kd—DAKOTA Sandstone (Cretaceous)

Jz—ZUNI Sandstone (Jurassic)

Qab-ALLUVIUM (Quaternary)

Qb—BASALT (Quaternary)

Scale — ft

Horizontal Scale — 100 0 200 400 600 800 1000

Vertical Scale — 50 100 200 300 400

100 0

-BOMB PENETRATION PROJECT- C S M RESEARCH FOUNDATION, INC.

Scale 1" = 300' Date 8-18-50

Fig. No. 46 By FDM

CROSS-SECTION OF SANDSTONE TARGET LOOKING NORTH SECTION b-b'

Fig. 46

2

DAKOTA Formation: (Upper Cretaceous)

Yellow-buff, massive, equigranular sandstone. Sand grains are subangular to round, approximately one-sixty fourth inch in diameter. Fucoid markings are present along the bedding planes located near the contact zone of the shale and upper member of sandstone. A one foot lenticular layer of calcareous sandstone is located about three feet from surface of the target area. A few fossils (pelecypods) are present. The sandstone is fairly resistant to erosion.-

Shale members are gray-black, soft and very friable, thinly laminated, easily decomposed. Formation is 132 feet in thickness.

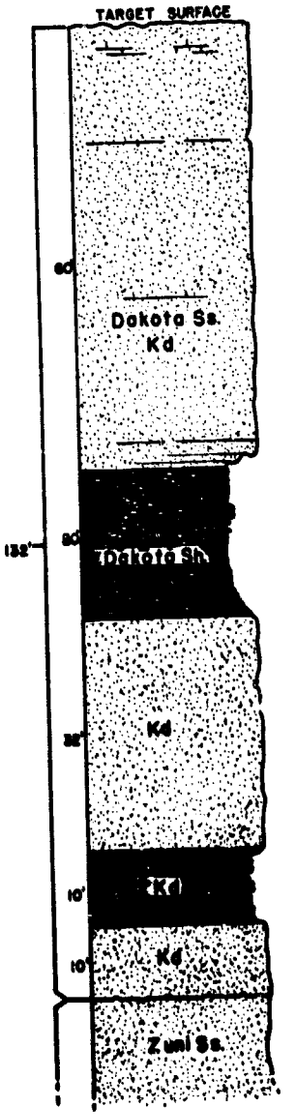

BOMB PENETRATION PROJEC	
Scale 1in.=10ft. Date 9-29-50	
Fig.No. 47 By FDM	

ation: Yellow-buff, massive, equigranular sandstone.
ous) Sand grains are subangular to round, approximately one-sixty fourth inch in diameter.
Fucoid markings are present along the bedding planes located near the contact zone of the shale and upper member of sandstone. A one foot lenticular layer of calcareous sandstone is located about three feet from surface of the target area. A few fossils (pelecypods) are present. The sandstone is fairly resistant to erosion.-
Shale members are gray-black, soft and very friable, thinly laminated, easily decomposed.
Formation is 132 feet in thickness.

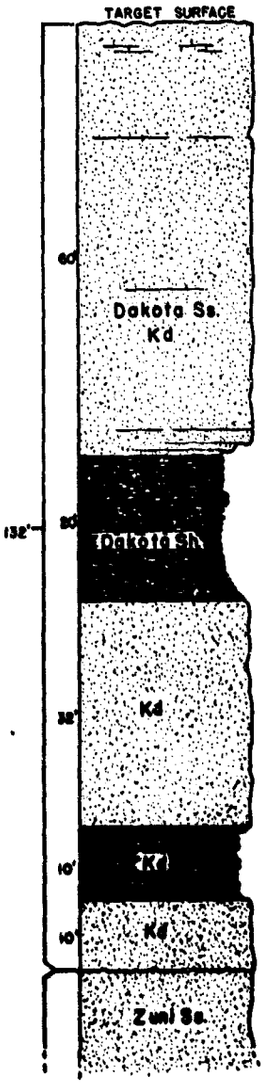

-BOMB PENETRATION PROJECT- C S M RESEARCH FOUNDATION INC.	
Scale 1in.=10ft. Date 9-29-50 Fig.No. 47 By FDM	-GEOLOGIC SECTION c-c' LOOKING EAST SANDSTONE TARGET SITE-

Fig. 47

2

duced in Part C. The influence of geologic features upon the path and penetration of bombs into granite is described in Part F, Section II.

3—Geology of the Sandstone Site Target Area

The location of the Putney Mesa Sandstone Bombing Site is shown on the Index Map, Fig. 1, and on the regional geology map, Fig. 39. The site is in section 6, R. 9 W., T. 8 N. of Valencia County, and is accessible by New Mexico State Highway 117.

Figure 45 is a geologic map of the locality in the immediate vicinity of the sandstone target, and Fig. 46 is a geologic cross section through the target area. From the plan and cross section and other geologic evidence to be cited it may be observed that the target surface can be placed stratigraphically in the lower part of the Cretaceous Dakota sandstone. The sand member upon which the target surface rests is 60 feet thick. The stratigraphy of the beds immediately below the target surface is shown in detail in geologic column CC', (Fig. 47), which was measured at the edge of the target area along the cliff face at the position marked in the photograph, Fig. 48. As shown in the geologic column, the thick sand member rests upon a shale bed 20 feet thick. The slope at the base of the vertical cliff in the photograph marks the position of the shale. The base of the Dakota sandstone formation and the contact between the Dakota and the Zuni sandstone are shown in the photograph.

Referring to the general stratigraphic table (Fig. 40) of the area near Grants, New Mexico, it can be seen that the Dakota sandstone is far above the sedimentary rock at the granite site, stratigraphically. As much as 3600 feet of sedimentary rock may lie below the target surface between the base of the Dakota formation and the pre-Cambrian basement rocks. The thickness of the sedimentary rocks lying stratigraphically below the Dakota sandstone and above the Permian formations was measured south of the sandstone target at the position of geologic column DD', shown on the regional geology map (Fig. 39). The results are recorded in the geologic column DD', Fig. 49.

The target surface of the sandstone bombing site is a gentle-dip slope formed between two normal faults. The faulting is related to the uplift of the Zuni Mountains, and 2 miles north of the target a basalt dike cuts through the Dakota sandstone and marks a channel through which lava escaped to flood the valley. As a result of the tectonic forces the Dakota sandstone has developed a system of steeply dipping joints which influence the results of the bombing experiments.

Within the thick sandstone member below the target surface minor bedding planes are spaced at irregular intervals. The bedding planes are marked by clay-shale partings which are seldom more than 1 or 2 inches thick. In places, the sandstone between the shale partings is cross-bedded, but the cross-bedding is not a conspicuous feature. The clay cementing material of the sandstone became the principal component of the rock at intervals as the sandstone was deposited. The bands in which clay predominates are now designated as shale partings. In places throughout the sandstone, the clay is present as small pellets or galls; at other places the clay appears as ribbons which have been distorted by differential compaction. Near the target surface, roots have

Fig. 48

View Looking North Toward Sandstone Target; Small Fault Indicated by Arrow on the Right

DAKOTA Sandstone: A massive yellow-buff colored sandstone, equigranular and compact, very resistant to erosion. Surface weathers brown on exposure. Lower portion has two thinly laminated layers of shale. Bottom of formation is conglomeritic. Formation is 64 feet in this locale but thicker elsewhere. It is of the Upper Cretaceous in age.

ZUNI Sandstone: Top 67 feet is composed of a medium grained, equigranular, white calcareous sandstone. grains are loosely cemented. Surface weathers round. — Middle member is a massive, equigranular, buff colored sandstone. Sand grains are well cemented. Joints are vertical and form high, smooth-faced cliffs. Some cross-bedding present.
Bottom member is a massive, cross-bedded, buff sandstone, with shale lenses located at bottom. Formation is formed of continental clastics of Jurassic age.

TODILTO Limestone: This formation is represented locally as a white, calcareous conglomerate. Pebbles are loosely cemented and cross-bedded. Not very resistant to erosion. Jurassic in age.

CHINLE Formation: A dense, maroon, thin bedded, arenaceous and calcareous siltstone easily eroded. Probably of Triassic age.

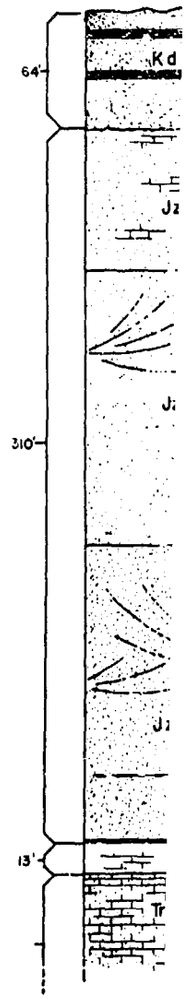

-BOMB PENETRA

Scale 1in=30ft. Date 9-

Fig. No. 49 By FD

llow-buff colored sandstone, equigranular and compact, very
rosion. Surface weathers brown on exposure. Lower portion has
minated layers of shale. Bottom of formation is conglomer-
on is 64 feet in this locale but thicker elsewhere. It is of
Cretaceous in age.

is composed of a medium grained, equigranular, white
sandstone. grains are loosely cemented. Surface weathers
dle member is a massive, equigranular, buff colored sand-
grains are well cemented. Joints are vertical and form high,
d cliffs. Some cross-bedding present.
mber is a massive, cross-bedded, buff sandstone, with
located at bottom. Formation is formed of continental
Jurassic age.

tion is represented locally as a white, calcareous congl-
Pebbles are loosely cemented and cross-bedded. Not very
to erosion. Jurassic in age.
maroon, thin bedded, arenaceous and calcareous siltstone
roded. Probably of Triassic age.

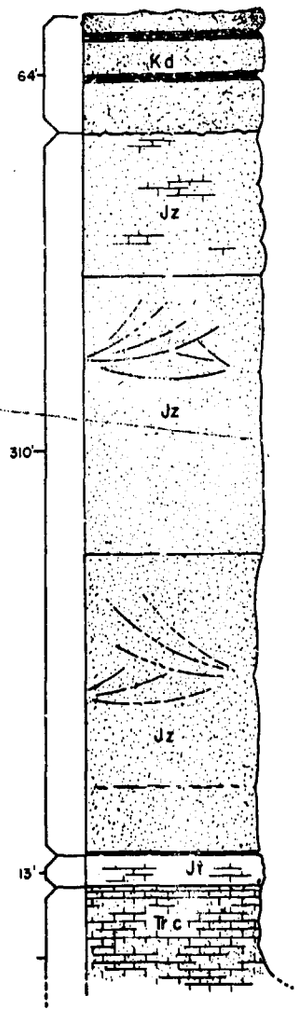

-BOMB PENETRATION PROJECT- CSM RESEARCH FOUNDATION, INC.	
Scale 1in=30ft. Date 9-14-50 Fig. No. 49 By FDM	- GEOLOGIC COLUMN OF SECTION d-d' SOUTH OF SANDSTONE TARGET-

Fig. 49

2

penetrated through the vertical joints and spread out horizontally in the partings.

4—Petrographic Report—By T. H. Kuhn and W. R. Wagner

a—The Zuni Granite

a-1) General Description

The Zuni granite at the Paxton Springs Site is a medium-to-coarse-grained, pink to pinkish- and greenish-gray rock, varying in mineral composition from granite to quartz monzonite. Most specimens have the mineral constituents of a granite. The pink color of the granite is due to the abundance of pink orthoclase feldspar, whereas the greenish-gray rocks owe their color to a predominance of such secondary minerals as chlorite and epidote. The texture in hand specimen is typically granitic or granular. Slight but readily visible lineation is produced by the alignment of slightly elongated quartz aggregates and by the alignment of the dark minerals, such as biotite mica and hornblende.

a-2) Mineralogy

The Zuni granite is approximately 25 per cent quartz, 45 per cent orthoclase, 10 per cent oligoclase, 10 per cent biotite, 5 per cent hornblende, and 3 per cent augite and muscovite. The remaining 2 per cent of the rock consists of the secondary minerals chlorite, epidote, sericite, kaolin, magnetite, and hematite, and the accessory minerals garnet, zircon, allanite, and apatite. The rock is extensively altered, and several types of alteration are present; namely chloritization, epidotization, sericitization, kaolinization, and silicification. In thin section, the granite most commonly has an irregular, cataclastic texture with most mineral grains bent, fractured, or stretched (Fig. 50). This deformation is also indicated by the quartz, which has undulatory extinction. Individual mineral grains vary in average size from 0.5 millimeter to over 2.0 millimeters. However, some of the feldspar grains have a length of approximately 1 centimeter. Quartz universally occurs as clusters of randomly oriented smaller grains (0.5 millimeter in diameter) with all clusters elongated into pod-shaped masses about 1 centimeter long (Fig. 51).

Quartz. The quartz is colorless to white. Normally it occurs as small grains clustered into elongate pod-like forms; however, in all specimens there is a late-stage quartz in the form of replacement blebs or as miscroscopic veinlets cutting all other minerals. Most quartz grains show undulatory extinction.

Orthoclase. Orthoclase is the most abundant mineral. A few grains show Carlsbad twinning, but normally the grains are not twinned. The mineral is so thoroughly altered to sericite and kaolin by hydrothermal or late-stage solutions that it is difficult in some sections to determine the original grain boundaries, (Fig. 52).

Oligoclase. Oligoclase is much less abundant than orthoclase in seven of the eight sections studied, but like orthoclase, it is severely altered. The oligoclase alteration products are epidote, sericite, and kaolin. In most cases the mineral is twinned after the Albite Law, but in some sec-

tions a combination of Albite and Carlsbad twinning was noted. In many grains the alteration is so complete that twinning shows only as indistinct shadows.

Biotite. Biotite varies in amount throughout the sections but is present to some extent in all. It is greenish-brown in color and occurs as small lath-shaped flakes or as stretched and bent clusters. In three specimens, the biotite forms reaction rims around cores of hornblende. In one section the augite core is rimmed with hornblende and the hornblende in turn is bordered by biotite. Much of the biotite is altered to chlorite and magnetite.

Muscovite. In most sections, primary muscovite occurs either as single, colorless, lath-like flakes or as clusters. In one section it is equal in amount to biotite, but generally it is only a minor constituent of the rock. The late-stage muscovite closely resembles sericite, although it is much larger in grain size than the sericite formed from the alteration of feldspar.

Hornblende. Hornblende is the common green pleochroic variety. In three of the specimens it occurs single, as small, single, irregular grains; in aggregates of small grains; or as cores in biotite clusters. Much of the hornblende is altered to chlorite, epidote, and magnetite.

Augite. Augite is rare; where found, it shows as minute cores in hornblende aggregates.

Secondary Minerals. Chlorite, magnetite, epidote, sericite, kaolin (clay minerals), and hematite are abundant secondary minerals in all sections. Chlorite and magnetite result from the breakdown of biotite. Epidote forms as an alteration product of hornblende and plagioclase, and the sericite and kaolin alter from the feldspars. Hematite forms from magnetite.

Accessory Minerals. Zircon, apatite, garnet, magnetite, and allanite are minor, (totaling 2 per cent or less) but ever-present minerals in the rock. They occur as minute, euhedral crystals along the borders or enclosed in other minerals.

a-3) Alteration

Sericitization and Kaolinization. Since the easily replaced feldspars make up nearly 50 per cent of the rock, their alteration products are most abundant. From the amount and thoroughness of the kaolinization and sericitization, it is evident that these products are the result of extensive hydrothermal action. To the unaided eye, the only noticeable result of the hydrothermal action is a bleaching effect, but under the microscope the feldspars show as a mass of fine sericite flakes in a matrix of brownish-gray kaolin.

Chloritization. Upon the addition of water, biotite mica alters to chlorite, and magnetite also is commonly formed by the same process. Where considerable biotite is present, the change to chlorite tends to give the rock a greenish cast.

Epidotization. Epidote, an alteration product of hornblende, augite, or calcic plagioclase, is a prominent secondary mineral of the rock. In abundance, it is next to sericite and kaolin. In the Zuni granite, there seems to be more epidote present than could form from the primary basic minerals present. It is possible that the altering solutions added some epidote by replacement.

Silicification. Silicification is evident as a minor alteration process in all sections, and is chiefly indicated by quartz filling microscopic fractures, though feldspar and other minerals are replaced to a minor extent by quartz.

b—Lamprohyre (Vogesite) Dikes in Zuni Granite

b-1) General Description

Although dikes are not abundant in the Zuni granite at the target site, one lamprophyre dike cuts the target and was penetrated by two bombs. Near the surface where weathering agents are abundant in the soil cover, the lamprophyre is heavily altered and essentially has the physical characteristics of the overburden. Downwardly, as the degree of weathering progressively decreases, the lamprophyre grades into a dense rock that is exceedingly tough. The rock breaks into plates or sheets parallel to the faintly visible schistosity.

In hand specimens the lamprohyre dike rock is extremely fine-grained, and almost aphanitic. It is dark green to gray-green when freshly broken, but weathers to a rusty brown color.

b-2) Mineralogy

The mineral content of the lamprophyre is as follows:

Primary Minerals		Secondary Minerals	Accessory Minerals	
Hornblende	— 50%	Chlorite	Magnetite	— 5%
Biotite	— 20%	Hematite	Quartz)	
Augite	— 20%		Orthoclase)	5%
Total	90%		Total	10%

From the mineral content the dike rock is a member of the lamprophyre group and is most correctly termed a vogesite.

The texture in the section is fine-grained porphyritic. The phenocrysts range in size from 0.3 millimeter to 1.0 millimeter with the average about 0.5 millimeter. They occur in a definite sub-parallel orientation in the fine-grained (0.10 millimeter average) matrix. Post-crystallization deformation is indicated by the attitude of the planes of schistosity, by bent and fractured biotite cleavages, and by an interpenetrating system of microfractures. Some of the fractures are filled with quartz; others contain hematite, apparently weathered from magnetite.

Chlorite and hematite are formed during the alteration process. The

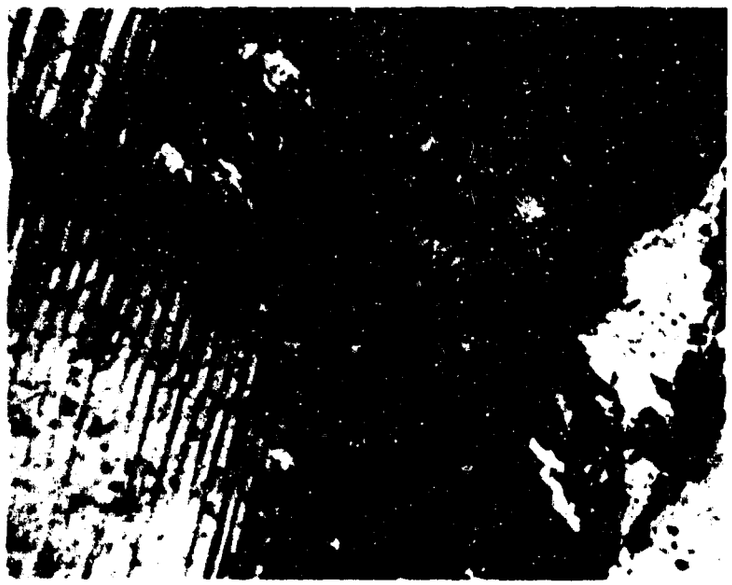

Fig. 50
Bent and Fractured Grains of Plagioclase (P), with Some of the Fractures Filled with Muscovite (M) and Epidote (E). X 120, enlarged 2½ diameters.

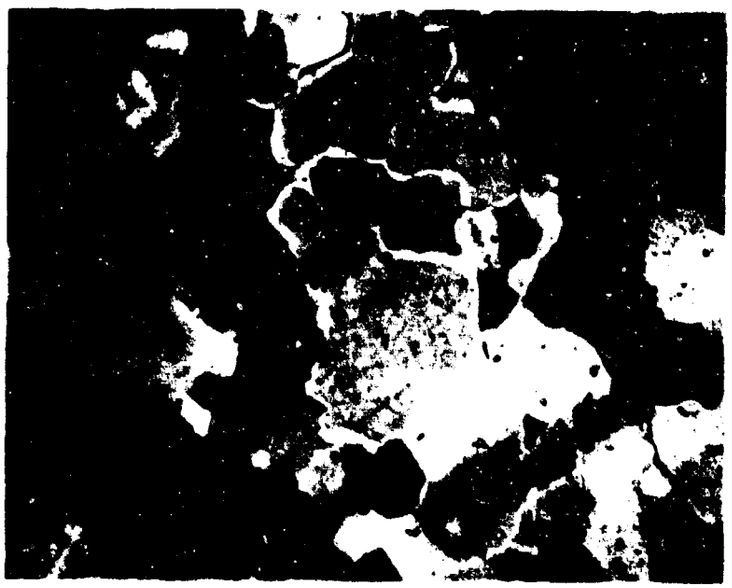

Fig. 51
Elongated, Pod-shaped Cluster of Quartz Grains. X 120, enlarged 2½ diameters.

chlorite forms rims on, and irregular areas within hornblende and biotite; the hematite comes from the breakdown of magnetite, which is present in abundance.

c—The Dakota Sandstone

c-1) General Description and Mineralogy

The Dakota sandstone is a fine-grained cream to light buff sandstone. The sand grains are angular and are of nearly equal dimensions in three directions. For the most part, the rock is friable, although some specimens are better consolidated. The cementing material is finely divided clay minerals, in part slightly stained by hematite. The sand grains compose roughly 90 percent of the sandstone and the clay cement the remaining 10 percent. The distribution of the clay cement throughout the sandstone is irregular.

The mineral grains of the sandstone are quartz, feldspar, magnetite, biotite, and muscovite. A few scattered grains of zircon and tourmaline were observed in thin section. Quartz predominates and constitutes 90 percent of the mineral grains. Plagioclase feldspar constitutes 5 per cent, muscovite 3 percent, and magnetite the remaining 2 percent of the mineral grains.

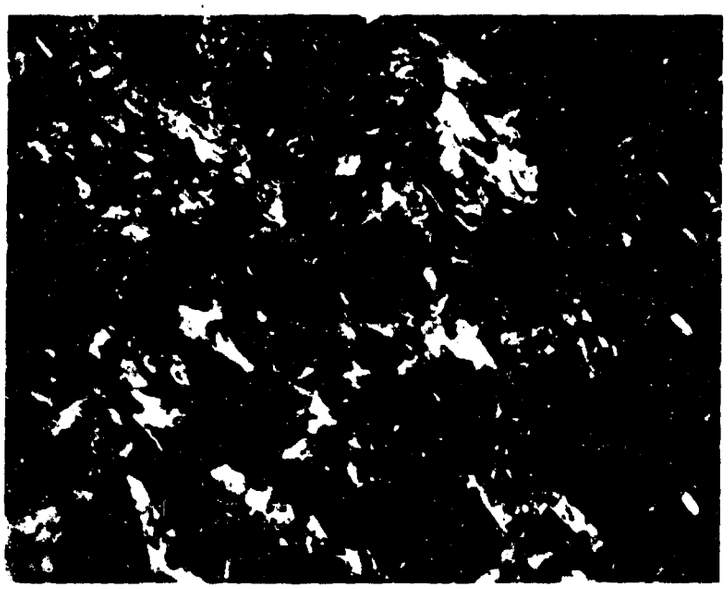

Fig. 52

Coarse Laths of Sericite Formed from the Hydrothermal Alteration of Orthoclase Feldspar. The whole grain of feldspar is altered. X 120, enlarged 2½ diameters.

SECTION IV—PHYSICAL ROCK TESTS

1—Test Procedure

Diamond drilling was directed toward obtaining representative specimens of the rocks below the target surfaces which were of suitable lengths for various physical rock tests and which were free from joints or other natural surfaces of weaknesses. As may be observed from the drill logs (see Appendix, Part A), the Dakota sandstone bed below the surface of the sandstone target is remarkably uniform in composition. However, the physical properties of the granite cores from the Paxton Springs granite site vary greatly as a result of the nature and extent of weathering and alteration. The degree of weathering bears a direct relation to the thickness of the overburden, and is greatest where the overburden is thickest. Bare, exposed rock surfaces within the target have been least affected. As may be expected, the degree of alteration varies considerably from hole to hole and also from the collar of any given hole downward.

The effect of weathering and of all the types of alteration described in the petrographic report, except silicification, is to weaken the tensile and compressive strength of the rock and to modify its elastic properties. It is necessary, therefore, to appraise the individual results obtained from each of the various physical rock tests of the granite specimen relative to the degree of alteration. Accordingly, the granite specimens have been divided into two groups—weathered granite and unweathered granite. The division was made by visual comparison. It is now evident from the results of the physical rock tests that each group might have been further subdivided, but the practical value of further subdivision is doubtful.

The specimen numbers in the following tables which summarize the results of the several tests may be used in combination with the diamond drill logs in the appendix to show the elevation below the collar of the drill hole from which the specimen was cut, and the geologic description of the specimen.

2—Porosity—Total and Apparent

Porosity is the interstitial void space in the rock, expressed as a percentage of the external volume of the rock specimen. Two types of porosity are recognized: closed-pore porosity and open, or communicating-pore, porosity. Open, or communicating, porosity is known as "effective" porosity by petroleum engineers. The sum of the open- and closed-pore porosities is known as the total porosity.

In this study the total porosity was considered to be of primary importance. However, porosity was determined by two different methods in the laboratories of the Colorado School of Mines. In the Petroleum Engineering laboratories the total porosity was determined using a Russel Porosimeter and employing the technique described in detail in Series I and Series II Experiments.[1] In the Physics laboratory, the "Apparent" porosity was determined. The procedure for determining apparent porosity established by the A.S.T.M. uses the following formula:

[1]Report of the Colorado School of Mines, Series I and Series II Experiments, Underground Explosion Test Program, pp. 19-20, Jan. 1949. (Restricted).

$$P = \frac{M_w - M_o}{d_w V} \times 100$$

where,

P = apparent porsity, percent

M_w = weight of water-saturated specimen

M_o = weight of oven-dried specimen

V = external volume

d_w = density of water

The results of the porosity determination have been combined with the results of the specific gravity determination and are presented together in Fig. 53.

3—Apparent Specific Gravity

Apparent specific gravity was determined in the Petroleum Engineering laboratory and the Physics laboratory of the Colorado School of Mines and in the laboratories of the Applied Physics Branch of the U. S. Bureau of Mines using the procedure establishing by the A.S.T.M. for natural building stone. Apparent specific gravity is calculated using the formula:

$$\text{Apparent specific gravity} = \frac{M_o}{M_w - M_s}$$

where,

M_o = weight of oven-dried specimen

M_w = weight of wet specimen after water immersion

M_s = weight of specimen suspended in water

As may be observed from the tabular data, Fig. 53, the numerical average apparent specific gravity of the Dakota sandstone member immediately below the target surface of the Putney Mesa sandstone site is 2.13. The average apparent porosity of the sandstone is 16.4 percent and the average total porosity is 16.5 percent. The apparent specific gravity of the Dakota sandstone and the total porosity of the Dakota sandstone are essentially the same as for the Navajo sandstone at the Buckhorn Wash Underground Explosion Test site. The porosity and apparent specific gravity are essentially the same as for sandstone from other parts of the United States tested by the U. S. Bureau of Mines. The very slight difference between the apparent porosity and the total porosity of the sandstone indicates—as the petrographic study also indicates—that the pores are open and communicating.

The average apparent specific gravity of the Zuni granite below the target surface of the Paxton Springs granite site is 2.77. This value is somewhat higher than that of most granites. This fact is substantiated by the petrographic study, and may possibly be explained by the recrystallization and reorientation of the mineral grains as a result of metamorphic processes. An almost complete lack of pore space between the mineral

Dakota Sandstone				Weathered Zuni Granite				Zuni Granite			
Specimen	Apparent Specific Gravity	Apparent Porosity	Total Porosity	Specimen	Apparent Specific Gravity	Apparent Porosity	Total Porosity	Specimen	Apparent Specific Gravity	Apparent Porosity	Total Porosity
C	2.12	-	20.0	200	2.74	-	0.00	142	2.75	-	0.00
D	2.13	-	16.5	145	2.75	-	0.00	48a	2.76	-	0.40
29	2.12	-	13.0	144	2.71	0.00	-	A	2.75	-	0.00
54	2.13	-	15.9					B	2.73	-	0.00
78	2.14	-	17.4					-	2.81	0.00	-
209	2.17	-	16.3					-	2.73	0.00	-
-	2.13	15.7	-					-	2.68	0.00	-
213	2.13	16.9	-					30	2.75	0.00	-
44	2.14	15.9	-					60	2.77	0.00	-
31	2.12	17.1	-					143			
-	2.13	16.9	-					167			
119	2.14	15.7	-					195	2.80		
28								199			
49								201			
53	2.12							202			
59											
163											
186											
Avg.	2.13	16.4	16.5		2.73	0.00	0.00		2.77	0.00	0.10

Fig. 53

Specific Gravity and Porosity of Specimens of Dakota Sandstone and Zuni Granite

grains exists in both the weathered and the unweathered specimens. It would appear from the available data that a slight volume increase takes place during the weathering process.

4—Tensile Strength

Tensile strength tests were conducted using NX diamond drill cores cut to a length of 8 inches and air-dried at room temperature for two weeks. Core diameters were measured to the nearest 0.01 inch. Each specimen was clamped into grips of the type designed by the Bureau of Reclamation. These grips consist essentially of a split steel tube lined with a section of rubber belting, which is clamped to the specimen by a wide 3-piece steel bolted clamp. (See Fig. 54.) The grips are screwed into spherically seated blocks on the testing machine so that the load is applied axially. The rate of loading was maintained at 100 pounds per square inch per minute.

It may be observed from the tabular data, Fig. 55, that the average tensile strength of Dakota sandstone is 63 pounds per square inch, the average strength of the weathered granite is 1003 pounds per square inch, and the average strength of unweathered granite is 1905 pounds per square inch. The weathering process results in a substantial decrease in the tensile strength of the granite specimens. However, the tensile

Fig. 54

Tension Specimen and Grip Assembly

Dakota Sandstone		Weathered Zuni Granite		Zuni Granite	
Specimen Number	Tensile Strength, psi	Specimen Number	Tensile Strength, psi	Specimen Number	Tensile Strength, psi
10	39	28	1501	15	2231
48	63	87	826	80	1804
90	66	88	682	81	2190
122	63			82	2033
124	31			83	1269
161	41				
166	42				
55	107				
65	66				
77	31				
106	90				
175	56				
194	35				
202	158				
83	50				
197	76				
208	61				
Avg.	63		1003		1905

Fig. 55

Tensile Strength of Specimens of Dakota Sandstone and Zuni Granite

strength of the weathered Zuni granite is more than twice as great as that of the unaltered Unaweep granite of the Underground Explosion Test site. The tensile strength of the unweathered Zuni granite is more than five times as great as that of the Unaweep granite.

5—Modulus of Rupture

Both NX and EX diamond drill cores were used for modulus of rupture tests. The NX cores were cut to a length of 6 inches and supported on knife edges 5 inches apart, and the EX cores were cut to a length of 4 inches and supported on knife edges 3 inches apart. The load was applied midway between supports. The granite specimens were placed upon the supports in such a manner that the load was applied normal to the flow lines or normal to the trend of the mineral grains. The photograph, Fig. 56, shows the setup for determining the modulus of rupture of an NX granite drill core.

The specimens were air-dried at room temperature for two weeks before testing. The ends of the specimens were cut off with either a diamond or carborundum blade, but not polished. The diameters of the specimens were measured to the nearest 0.01 inch.

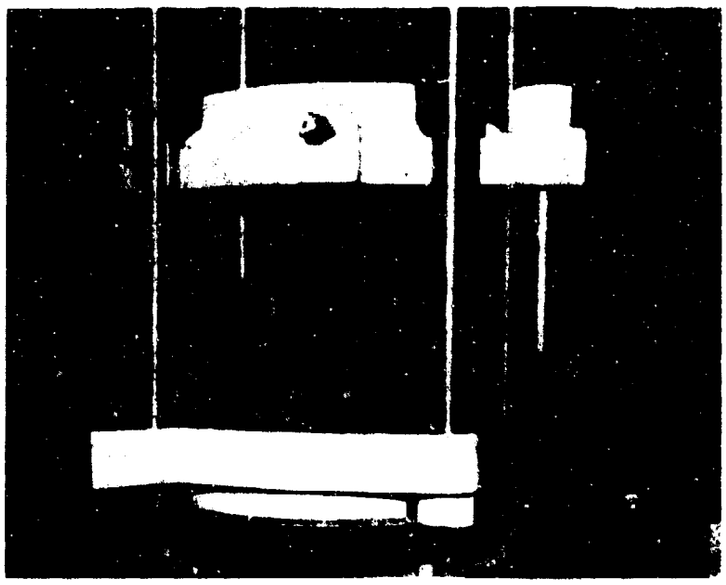

Fig. 56
Modulus of Rupture Test

Modulus of Rupture was calculated from the formula:

$$R = \frac{8WL}{\pi D^3}$$

where,

R = modulus of rupture

W = applied load, pounds

L = span between centers of knife edges, inches

D = diameter of specimen, inches

It may be observed from the tabulated results in Fig. 57 that the average modulus of rupture of the Dakota sandstone is 355 pounds per square inch, that of weathered granite is 2261 pounds per square inch, and that of the unweathered Zuni granite is 5434 pounds per square inch. The ratio between the moduli of rupture of unweathered and weathered granite is roughly the same as the ratio of the tensile strengths of the two rock types. When the results are compared with results for similar rocks in other localities, the Dakota sandstone appears to be a normal sandstone, but the Zuni granite is stronger and tougher than the normal.

Dakota Sandstone		Weathered Zuni Granite		Zuni Granite	
Specimen	Modulus of Rupture	Specimen	Modulus of Rupture	Specimen	Modulus of Rupture
14	515	-	773	-	-
58	299	151	1418	148	5285
74	286	165	1418	163	4769
152	269	27	3546	10	5466
179	377	86	3427	12	5274
182	481	89	1764	18	5965
198	260	139	3480	21	6349
				91	4527
Avg.	355		2261		5434

Fig. 57
Modulus of Rupture of Specimens of Dakota Sandstone and Zuni Granite

6—Compressive Strength

Sandstone diamond drill cores of NX size and granite diamond drill cores of both NX and EX sizes were used for simple compression tests. The ends of the test specimens were cut normal to the axis of the core so that the length-to-diameter ratio was 1 to 1. The ends of the granite cores were lapped perpendicular to the axis of the core and tested for smoothness until a water film on the lapped surface showed full contact with a smooth glass plate. The procedure was modified for the sandstone specimens because it was impossible to polish the loosely cemented sand grains and because the silicon carbide used for polishing was permanently imbedded in the clay matrix. The ends of the sandstone specimens were smoothed against the flat surface of a fine carborundum grinding wheel and checked in the same manner as the granite cores for uniform contact over the bearing surfaces.

Both granite and sandstone cores were air-dried at room temperature for two weeks after the end surfaces had been prepared, then tested in simple compression in a Tinius-Olsen testing machine. The specimen was centered between a 6-inch spherically mounted block in the fixed head of the testing machine and a fixed block in the movable head. The rate of loading was maintained at 100 pounds per square inch per second.

From the test results tabulated in Fig. 58 it may be observed that the average strength of the Dakota sandstone in simple compression is 5015 pounds per square inch, that of the weathered Zuni granite is 9142 pounds per square inch, and that of the unweathered Zuni granite is 24,565 pounds per square inch.

If the Dakota sandstone of the Putney Mesa bombing site is compared with the Navajo sandstone of the Underground Explosion Test site on a basis of tensile and compressive strengths alone, it may be concluded that the Dakota sandstone is relatively weak and friable, because the compressive strength of the Navajo sandstone (9938 pounds per square inch) is roughly twice that of the Dakota sandstone and the tensile strength is 4.6 times as great.

If the strength of the Zuni granite of the Paxton Springs bombing site is compared with that of the Unaweep granite of the Underground Explosion Test site, it is apparent that the compressive strength of the weathered Zuni granite below the target surface is only 10 percent less than that of the Unaweep granite, and the compressive strength of the unweathered Zuni granite is 2.3 times as great as that of the Unaweep granite. When the average tensile strengths of the rocks from the two sites are compared, it is apparent that the tensile strength of the weathered Zuni granite is 2.4 times as great as that of the Unaweep granite, and the tensile strength of the unweathered Zuni granite is 4.6 times as great as that of the Unaweep granite.

When the compressive strength of the Zuni granite is compared with the compressive strength of other granites in the United States, it is apparent that the Zuni granite falls within the normal range. Many granites are stronger in compression, and many are weaker. It appears that silicification increases the compressive strength of the Zuni granite, and that sericitization, kaolinization, chloritization, and epidotization decrease it.

Dakota Sandstone		Weathered Zuni Granite		Unweathered Zuni Granite	
Specimen	Compressive Strength, psi	Specimen	Compressive Strength, psi	Specimen	Compressive Strength, psi
36	6169	1	9730	11	20,573
42	4261	2	8118	13	21,184
92	2989	3	7241	27	15,235
98	3628	5	8243	27-A	26,411
100	5067	7	14345	61	30,331
102	5444	35	7534	89	25,579
108	3098	36	7006	90	21,963
112	5783	37	9953	91	17,681
117	3074	38	10398	91-A	31,506
126	3989	39	8855	92	31,948
22	5080			24	37,866
43	2288			44	21,627
46	4434			54	26,525
63	5205			56	17,006
76	4420			62	30,314
84	5254			63	19,409
95	2645			65	22,458
136	7312				
141	2568				
184	6255				
33	4749				
59	8675				
60	6227				
66	7617				
67	6756				
68	4420				
71	5922				
82	7089				
Avg.	5015		9142		24,565
Standard Deviation	1626		2019		6,032

Fig. 58

Compressive Strength of Specimens of Dakota Sandstone and Zuni Granite

7—Impact Toughness

Impact toughness was determined in the laboratories of the United States Bureau of Mines by a method known as the Page Impact Test

and by a method developed in the laboratories of the Mining Department of the Colorado School of Mines using a cantilever-type impact-loading device. The Page Impact Test involves dropping a weight from successively higher heights upon a rounded plunger of 1-centimeter radius of curvature until such a height is reached that the specimen is fractured or broken. The toughness is expressed by the height (per unit area) at which failure occurs. The C.S.M. Impact Test involves releasing one end of a pivoted steel beam which falls in an arc and strikes the specimen. The steel beam is fitted with a tup which strikes a flat steel disc resting on top of the specimen. The angle through which the beam rotates is successively increased until failure results. The number of drops on a given specimen is held at a minimum by means of preliminary experiments to determine the range of failure. Impact toughness is expressed by the kinetic energy (per unit area) at which failure occurs.

The specimens for the Page Impact Test and the C.S.M. Impact Test were similarly prepared. Specimens were cut to a length-diameter ratio of 1 to 1 and prepared as described previously for the compression tests. The granite and sandstone cores used in the C.S.M. tests were air-dried for 11½ weeks at room temperature.

Figure 59 is a photograph of the C.S.M. impact apparatus. The axis about which the beam rotates is equipped with a transit vertical circle and vernier so that the angle of fall can be determined to the nearest minute. The height of the platform which supports the specimen is adjustable in increments of 1 inch by selecting the proper steel plate to bring the beam in nearly a horizontal position at the instant of contact. A zero reading is taken on the vernier with the tup in contact with each specimen, and a reading is taken again with the beam raised and about to be released. The beam is so designed that additional weights can be added directly over the impact tup if necessary. The kinetic energy of each drop is computed using the weights and moments of the component parts and the sine of the angle of fall. Impact toughness is computed from the formula:

$$\text{Impact Toughness} = \frac{\text{Kinetic Energy (ft-lb.)}}{\text{Cross Section Area of Specimen (in}^2\text{)}}$$

It may be observed from the results tabulated in Fig. 60 that the average impact toughness of the Dakota sandstone is 24.95 foot-pounds per square inch, of the weathered Zuni granite is 54.01 foot-pounds per square inch, and of the unweathered Zuni granite is 54.28 foot-pounds per square inch. The ratios between the strength of unweathered Zuni granite and Dakota sandstone is 30.2 to 1 in tension, 4.9 to 1 in compression, and 2.17 to 1 in impact toughness. Considering the results of the impact tests, it appears that the Dakota sandstone is tougher relative to Zuni granite than the ratios between the tensile and compressive strengths would indicate.

Specimens for impact toughness tests and specimens for compressive strength tests were prepared in the same manner, and in many instances the manner of failure was identical. Presumably, then, we may assume that the average compressive strength of the unweathered Zuni granite of 24,565 pounds per square inch for static loading is equivalent to 54.28 foot-pounds per square inch in dynamic loading; also that the average compressive strength of the Dakota sandstone of 5015 pounds per square inch is equivalent to 24.95 foot-pounds per square inch in dynamic loading.

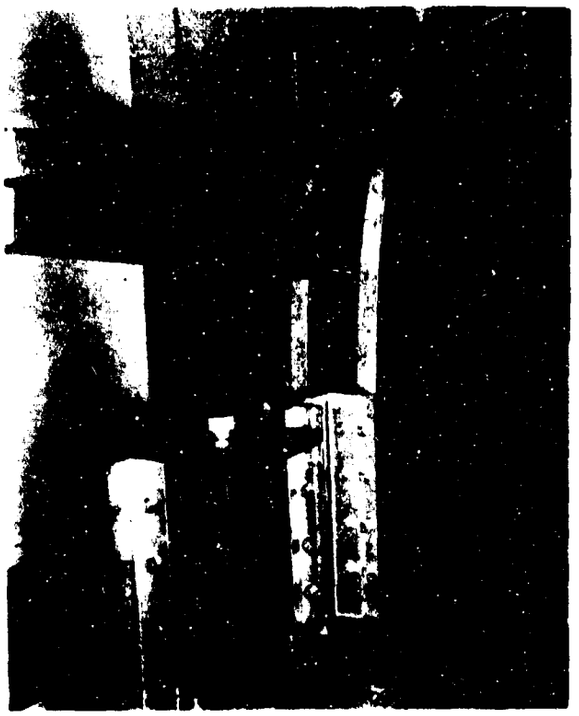

Fig. 59
C.S.M. Impact Apparatus

Although the number of weathered Zuni granite specimens available for impact toughness testing is smaller than desired, it is of interest to note that the toughness of the weathered and of the unweathered granite is practically the same.

The results of the Page Impact Test are tabulated in Fig. 61. The difference in results between the Page Tests by the U. S. Bureau of Mines and the C.S.M. Impact Tests is, perhaps, due to the shape of the striker.

8—Sclerescope Hardness

The Shore Sclerescope measures the hardness of a rock specimen by the height of rebound of a diamond-pointed hammer dropped vertically on the polished rock surface. Two types of Shore Sclerescopes are available, and both types were used in this work. In one type the hammer

Dakota Sandstone		Weathered Zuni Granite		Zuni Granite	
Specimen Number	Impact Toughness (ft-lb/in.^{2})	Specimen Number	Impact Toughness (ft-lb/in.^{2})	Specimen Number	Impact Toughness (ft-lb/in.^{2})
123	14.57	8	54.80	57	51.59
126-A	18.95	301	50.74	66	59.32
135	22.75	302	54.98	68	56.75
144	23.94	303	55.52	75	27.87
151	28.89			76	58.02
153	28.09			132	58.02
162	28.01			133	59.06
163	26.72			133-A	58.02
170	28.32			146	58.50
174	29.28			199	55.61
Avg.	24.95 ft-lb/in.^{2}		54.01 ft-lb/in.^{2}		54.28 ft-lb/in.^{2}

Fig. 60

C.S.M. Impact Test
Impact Toughness of Specimens of Dakota Sandstone and Zuni Sandstone

Dakota Sandstone		Weathered Zuni Granite		Zuni Granite	
Specimen Number	Impact Toughness (in./sq in.)	Specimen Number	Impact Toughness (in./sq in.)	Specimen Number	Impact Toughness (in./sq in.)
70				19	
79	num.			22	num.
173	avg.			23	avg.
106				26	
133	1.0			29	15.0
142				64	
143	Standard			115	Standard
148	Deviation			131	Deviation
155	43%			151	29%
165				136	

Fig. 61

U. S. Bureau of Mines (Page) Impact Test
Impact Toughness of Specimens of Dakota Sandstone and Zuni Granite

is dropped from a height of ¾ inch above the rock surface, and the height of rebound is recorded on a dial-type gauge. In the other type, a very light hammer is dropped from a much greater height, and the rebound of the hammer is observed through a graduated glass tube. The non-recording type is shown in the photograph, Fig. 62.

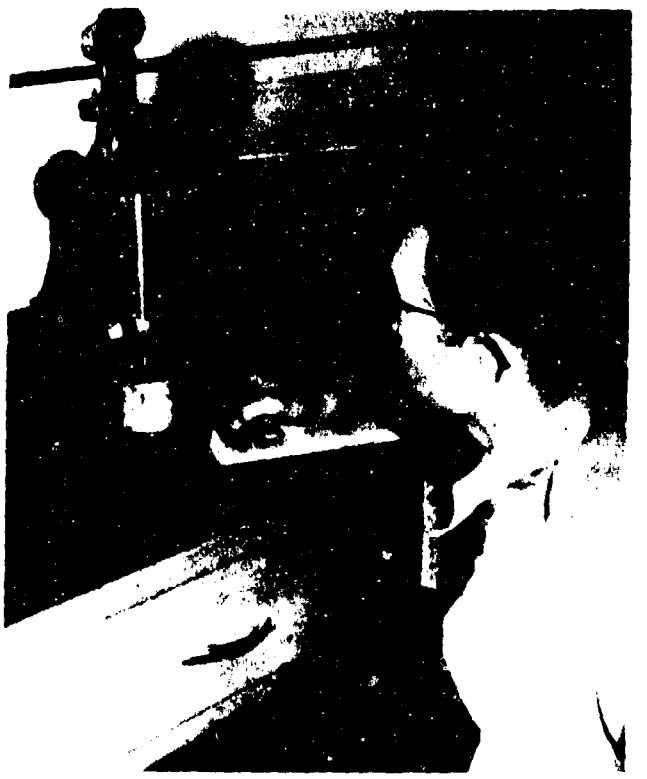

Fig. 62
Non-Recording-Type Shore Sclerescope, Model C

Specimens were prepared from NX diamond drill cores and the ends were polished and tested as described for compression specimens; in fact, the compression tests were run using the same specimens previously used for sclerescope hardness. The sclerescope hardness of each specimen of Dakota sandstone and Zuni granite is the average of 20 readings on each specimen. The readings were taken with the points of impact spaced uniformly and arranged in two mutually perpendicular rows of ten each.

The sclerescope hardness scale bears a direct relation to the Brinell

hardness scale for metals. The scale reading may be converted to inches by dividing by a constant.

In Fig. 63 are tabulated both the average height of rebound in sclerescope hardness units and the average coefficient of restitution for each specimen. The coefficient of restitution is determined from the formula

$$e=\left(\frac{h_2}{h_1}\right)^{1/2}$$

where

e = coefficient of restitution

h_2 = height of rebound

h_1 = height of drop.

Dakota Sandstone			Weathered Zuni Granite			Unweathered Zuni Granite		
Specimen	Coef. of Restitution	Hardness	Specimen	Coef. of Restitution	Hardness	Specimen	Coef. of Restitution	Hardness
33	0.398	19.03	1	0.637	48.65	11	0.888	94.65
59	0.446	23.85	2	0.636	48.55	13	0.897	96.60
60	0.406	19.83	3	0.706	59.85	27	0.835	83.80
66	0.414	20.55	5	0.689	57.00	27-A	0.869	90.55
67	0.404	19.58	7	0.815	79.65	61	0.924	102.40
68	0.433	22.50	35	0.767	70.65	89	0.872	91.35
71	0.429	22.05	36	0.667	53.40	90	0.890	95.10
82	0.393	18.55	37	0.723	62.75	91	0.901	97.35
			38	0.675	54.70	91-A	0.886	94.15
			39	0.660	52.30	92	0.890	95.15
			8	—	76.05			
			301	—	52.90			
			302	—	55.00			
			303	—	47.30			
Avg.	0.415	20.74		0.698	58.48		0.885	94.11

Fig. 63

Sclerescope Hardness and Coefficient of Restitution for Specimens of Dakota Sandstone and Zuni Granite—Diamond-Pointed Hammer

From the tabular data it may be observed that the average sclerescope hardness of the Dakota sandstone is 20.74, of the weathered Zuni granite is 58.48, and of the unweathered Zuni granite is 94.11. The coefficients of restitution in the same order are 0.415, 0.698, and 0.885. The sclerescope hardness and the compressive strength of rocks appear to be closely related, but the relation does not appear to be a straight-line function.

9—Elastic Constants—Dynamic Method

Elastic constants of Dakota sandstone and of Zuni granite were determined in the laboratories of the United States Bureau of Mines at College Park, Maryland, in accordance with procedure described in U.S.B.M. Report of Investigation 3891.

a) Young's Modulus

In the dynamic method, Young's modulus is computed from the formula

$$E = V_l^2 d$$

where

E = Young's modulus

V_l = longitudinal velocity of sound

d = density of the rock.

The longitudinal velocity of sound is computed from the formula

$$V_l = 2f_1 L$$

where

f_1 = fundamental longitudinal frequency

L = length of the specimen

b) Modulus of Rigidity

The modulus of rigidity, or the ratio of the shearing stress to shearing strain, is computed from the formula

$$G = V_t^2 d$$

where

G = modulus of rigidity

V_t = torsional velocity of sound

d = density of rock.

The torsional velocity of sound is computed from the formula

$$v_t = 2f_t L$$

where

f_t = fundamental torsional frequency

L = length of specimen.

c) Apparent Poisson's Ratio

Apparent Poisson's ratio is computed from the formula

$$m = \frac{E}{2G} - 1$$

where

m — apparent Poisson's ratio

E = Young's modulus

G — modulus of rigidity.

d) Tabulation of Elastic Constants—Dynamic Method

The elastic constants as determined by the United States Bureau of Mines using the dynamic method are as follows:

Dakota Sandstone				Unweathered Zuni Granite			
Specimen No.	Young's Modulus, E	Modulus of Rigidity, G	Apparent Poisson's Ratio, m	Specimen No.	Young's Modulus, E	Modulus of Rigidity, G	Apparent Poisson's Ratio, m
28 49 53 59 163 186	0.780×10^6	0.400×10^6	-0.024	143 167 195 199 201	11.9×10^6	4.7×10^6	0.27
Standard Deviation	13.0	13.0	—		4.9	2.5	19.0

Fig 64

Elastic Constants for Dakota Sandstone and Zuni Granite—Dynamic Method

10—Velocity of Sound and Seismic Velocity

The longitudinal bar velocity of sound is determined by measuring the fundamental resonance frequency of a cylindrical bar. The frequency multiplied by twice the length of the bar equals the longitudinal bar velocity. The longitudinal velocity in an unlimited solid medium is related to the longitudinal bar velocity by Poisson's ratio as follows:

$$\frac{V_u}{V} = \left(\frac{1 - m}{1 - m - 2m^2}\right)^{1/2}$$

where

V_u = velocity of sound in unlimited medium

V = longitudinal bar velocity, and

m = Poisson's ratio.

Values of the longitudinal bar velocity, V, as determined by the U. S. Bureau of Mines for Dakota sandstone and Zuni granite are as follows:

	Bar Velocity	
	Longitudinal, fps	Torsional, fps
Dakota sandstone	5,210	3,730
Zuni granite	17,800	11,100

When m = 0.20, the ration V_u to U is 1.1, and the longitudinal velocity of sound in an unlimited granite medium is

$$1.1 \times 17{,}800 = 19{,}580 \text{ feet per second.}$$

When m = -0.024, the ratio V_u to V is 1.0 and the longitudinal velocity of sound in an unlimited Dakota sandstone medium is 5,210 feet per second.

11—Elastic Constants, Static Method

Specimens of Dakota sandstone, weathered Zuni granite, and unweathered Zuni granite were tested in the Structural Laboratory of the Bureau of Reclamation in simple compression to obtain Young's modulus and Poisson's ratio, and in the triaxial testing machine to determine the triaxial compressive strength and the equation of Mohr's envelope. Using values of Young's modulus and Poisson's ratio determined from strain measurements in the simple compression tests, the bulk modulus, the shear modulus, and the relative volume change $\Delta V/V_o$ were computed from the Bureau of Reclamation data.

Specimens of weathered granite, unweathered granite, and Dakota sandstone were first subjected to an initial loading cycle in which longitudinal and lateral strain measurements were taken. Later the loads were carried to failure. In most cases the first cycle strains nearly coincide with the second cycle. SR-4 strain gauges in pairs were placed longitudinally and horizontally on opposite sides of the specimen.

Using the strain measurements from the initial loading cycle, Young's modulus and Poisson's ratio were computed for three granite and three sandstone specimens. Results are tabulated in Fig. 65. The stress-strain curve shows increased linearity with decrease in weathering and alteration. Since the strain measurements of the sandstone and weathered granite specimens show definite curvature, the modulus was computed from the average slope of the stress-strain curve between the limits of the accompanying stress range. In other words, the reported value is a tangent modulus that adheres very closely to the measured strain curve within the indicated stress limits. Likewise, Poisson's ratio is the ratio of the slopes of the measured curves within the indicated stress range.

Figures 66 and 67 show extended longitudinal and lateral stress-strain curves observed from the final loading cycle of the elasticity specimens. Some irregularities occur at high load in the case of unweathered granite specimens 14 and 84T, which may be due to local failure near the strain gauges and should not be considered representative of the material.

The extremely large lateral strains near the failure point of the sandstone and weathered granite may be due to a change from decreasing to increasing volume in preparation for failure. At this point the lateral strains are increasing at a rate several times greater than the longitudinal.

Using the stress-strain curves, Figs. 66 and 67, values of Young's modulus were calculated for stress intervals of 1000 pounds per square inch using the formula:

$$E = \frac{S}{e_l}$$

where

E = Young's modulus

S = applied stress

e_l = longitudinal strain

Similarly, using the stress-strain curves, Poisson's ratio was calculated for the same stress intervals from the formula:

$$m = \frac{e_t}{e_l}$$

where,

m = Poisson's ratio

e_t = lateral strain

e_l = longitudinal strain.

The computed values for sandstone, weathered granite, and unweathered granite are presented graphically in Fig. 68. The diagrams

Dakota Sandstone				Weathered Zuni Granite				Unweathered Zuni Granite			
Specimen No.	Stress Range, psi	Young's Modulus 10^6 psi	Poisson's Ratio	Specimen No.	Stress Range, psi	Young's Modulus, 10^6 psi	Poisson's Ratio	Specimen No.	Stress Range, psi	Young's Modulus, 10^6 psi	Poisson's Ratio
15	0- 200	0.49	0.00	33	0- 400	0.94	-0.03	84T	0- 400	10.30	0.15
	200- 400	0.47	0.01		400- 800	0.98	-0.01		400- 800	10.69	0.16
	400- 600	0.60	0.02		800-1200	1.13	0.01		800-1200	11.12	0.17
					1200-1600	1.33	0.05		1200-1600	11.58	0.17
16	0- 200	0.51	0.05		1600-2000	1.36	0.13		1600-2800	12.08	0.18
	200- 400	0.54	0.05		2000-2800	1.47	0.26				
	400- 600	0.48	0.06					14	0-2800	11.12	0.18
21	0- 200	0.34	0.06								
	200- 400	0.31	0.10								
	400- 600	0.[illegible]	0.16								
	600- 800	0.51	0.20								
	800-1000	0.62	0.23								
	1000-1200	0.77	0.26								

Fig. 65

Young's Modulus and Poisson's Ratio First Loading Cycle

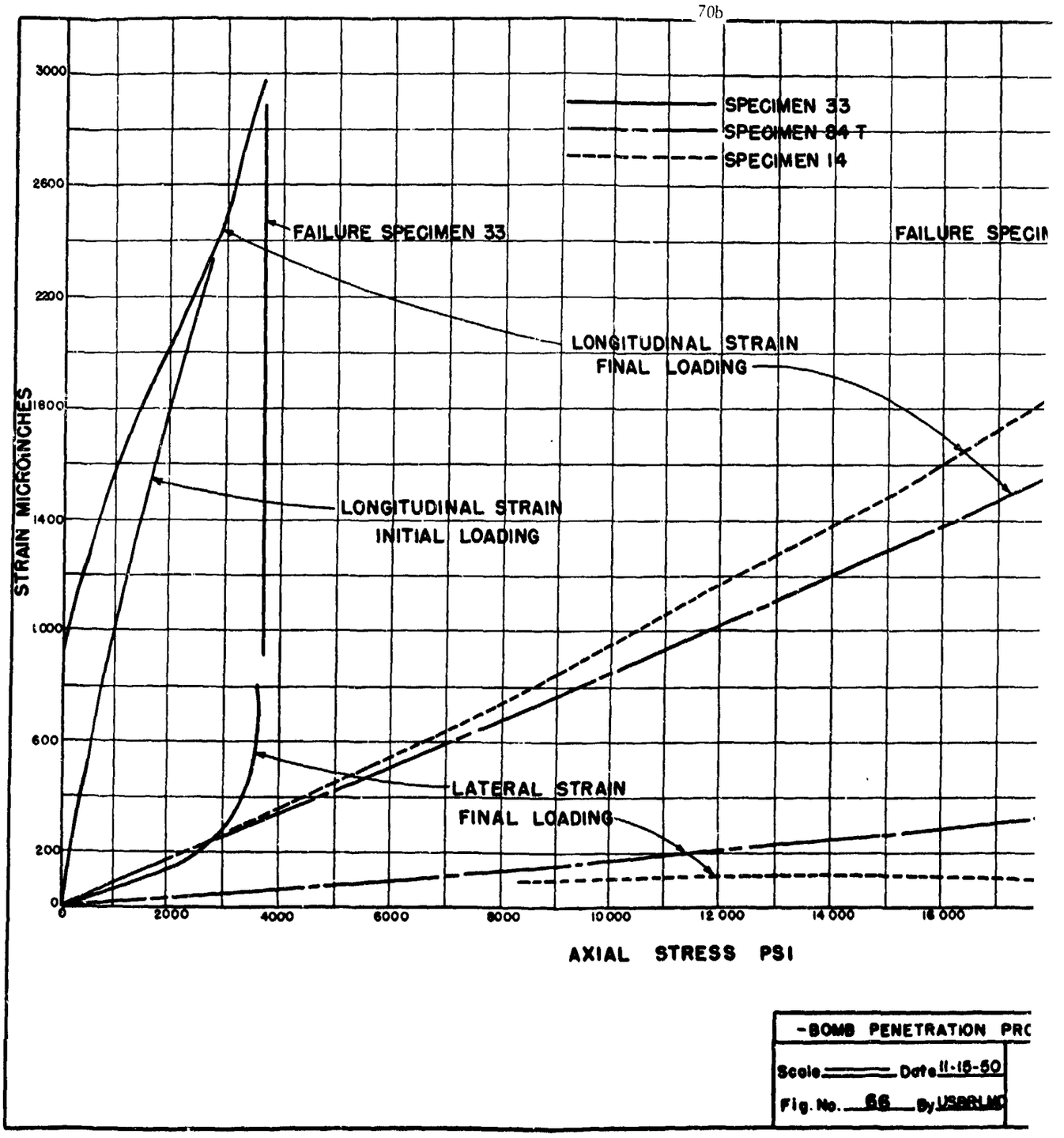
SPECIMEN 33
SPECIMEN 84 T
SPECIMEN 14
FAILURE SPECIMEN 33
FAILURE SPECIM
LONGITUDINAL STRAIN
FINAL LOADING
LONGITUDINAL STRAIN
INITIAL LOADING
LATERAL STRAIN
FINAL LOADING
STRAIN MICROINCHES
3000
2600
2200
1800
1400
1000
600
200
0
0
2000
4000
6000
8000
10 000
12 000
14 000
16 000
AXIAL STRESS PSI
-BOMB PENETRATION PRO
Scale
Date 11-15-50
Fig. No. 66
By USBRLMD

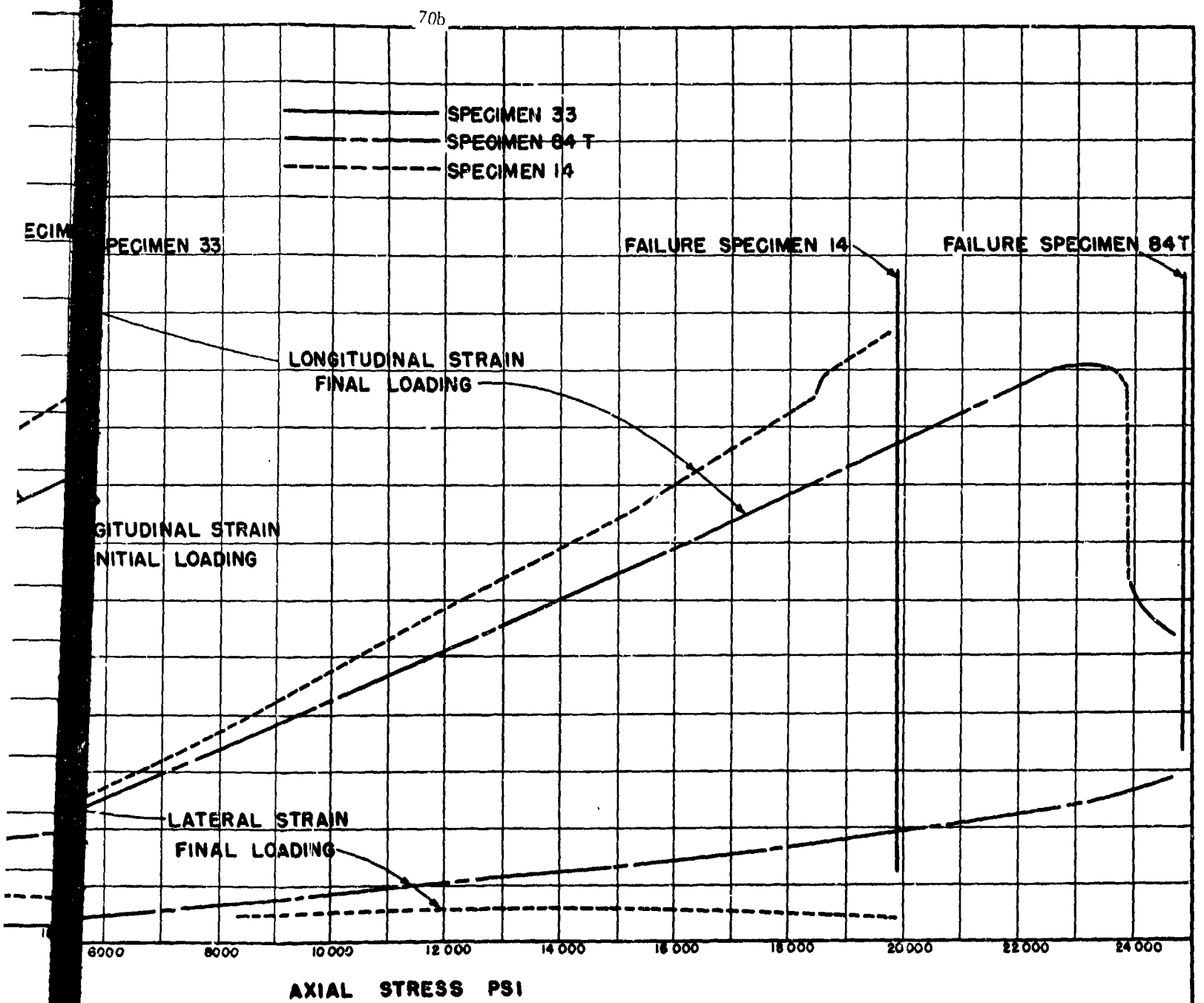

-BOMB PENETRATION PROJECT- CSM RESEARCH FOUNDATION, INC.

Scale ——— Date 11-16-50
Fig. No. 66 By USDRLMC

SIMPLE COMPRESSION TESTS
GRANITE

Fig. 66

2

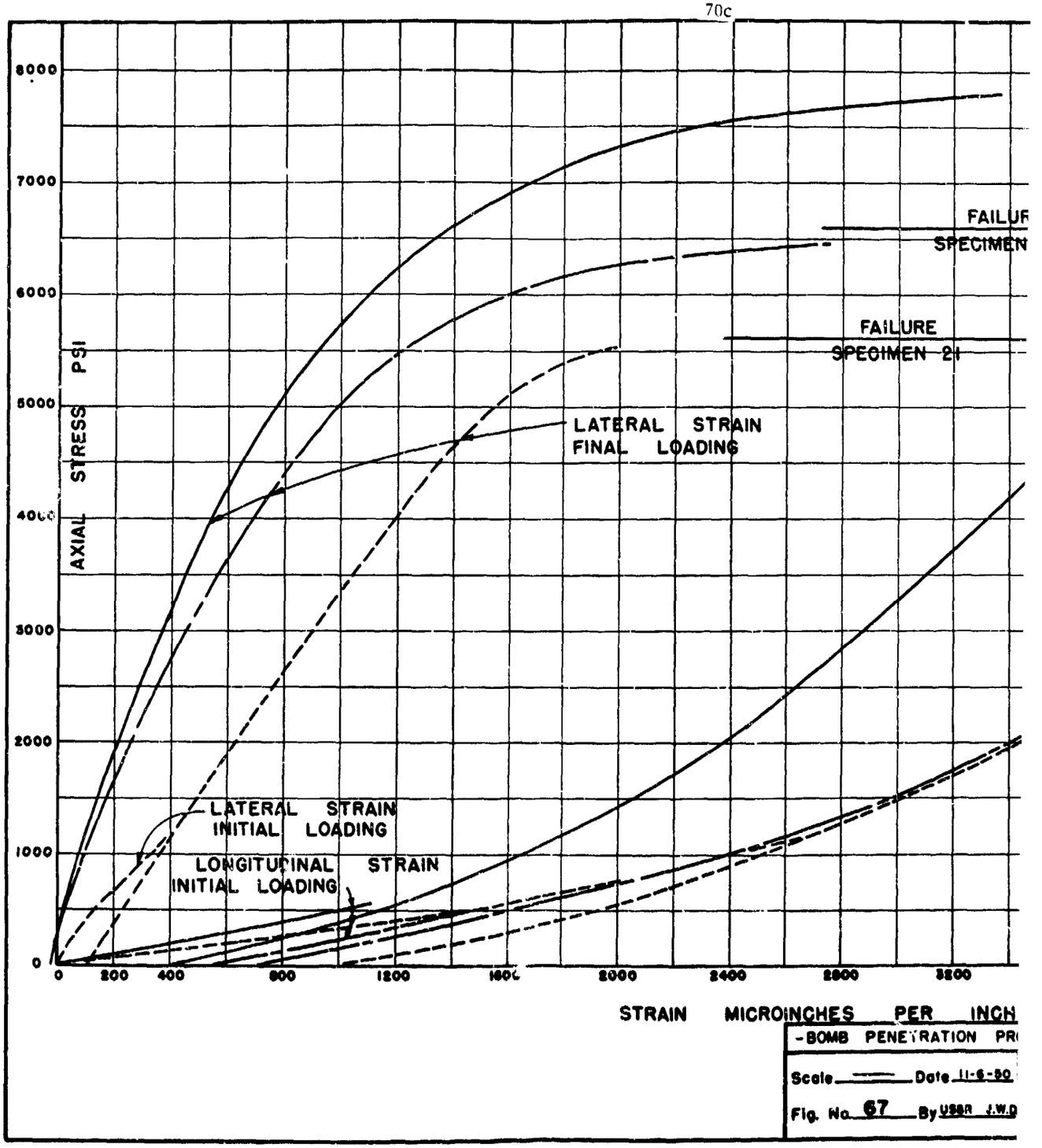
8000
7000
6000
5000
4000
3000
2000
1000
0
AXIAL STRESS PSI
0
200
400
600
1200
1600
2000
2400
2800
3200
STRAIN MICROINCHES PER INCH
FAILUR
SPECIMEN
FAILURE
SPECIMEN 21
LATERAL STRAIN
FINAL LOADING
LATERAL STRAIN
INITIAL LOADING
LONGITUDINAL STRAIN
INITIAL LOADING
-BOMB PENETRATION PR
Scale
Date 11-6-50
Fig. No. 67
By USSR J.W.D

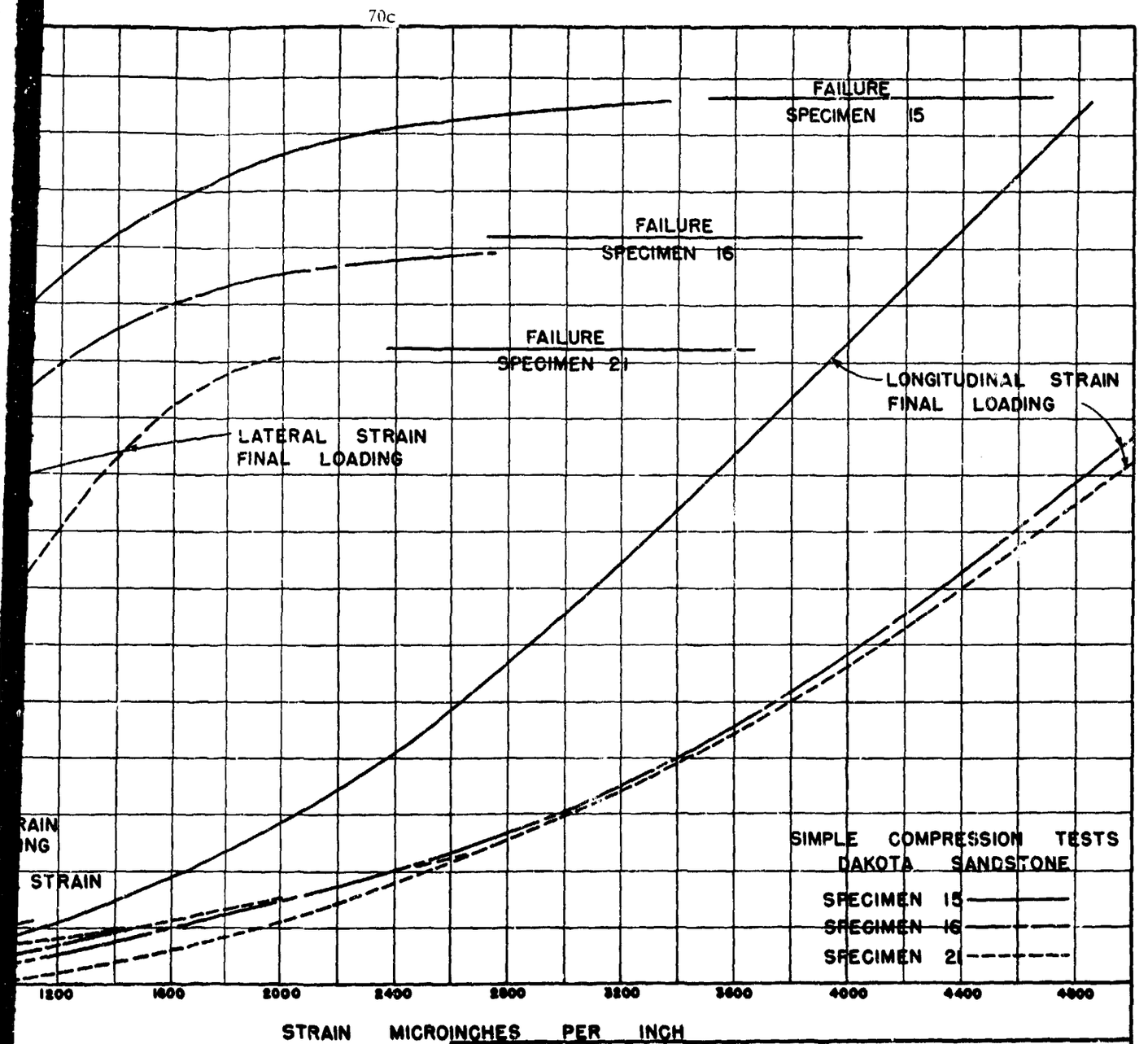

-BOMB PENETRATION PROJECT- C S M RESEARCH FOUNDATION, INC.

Scale ——— Date 11-6-50

Fig. No. 67 By USBR J.W.D

SIMPLE COMPRESSION TESTS
DAKOTA SANDSTONE

Fig. 67

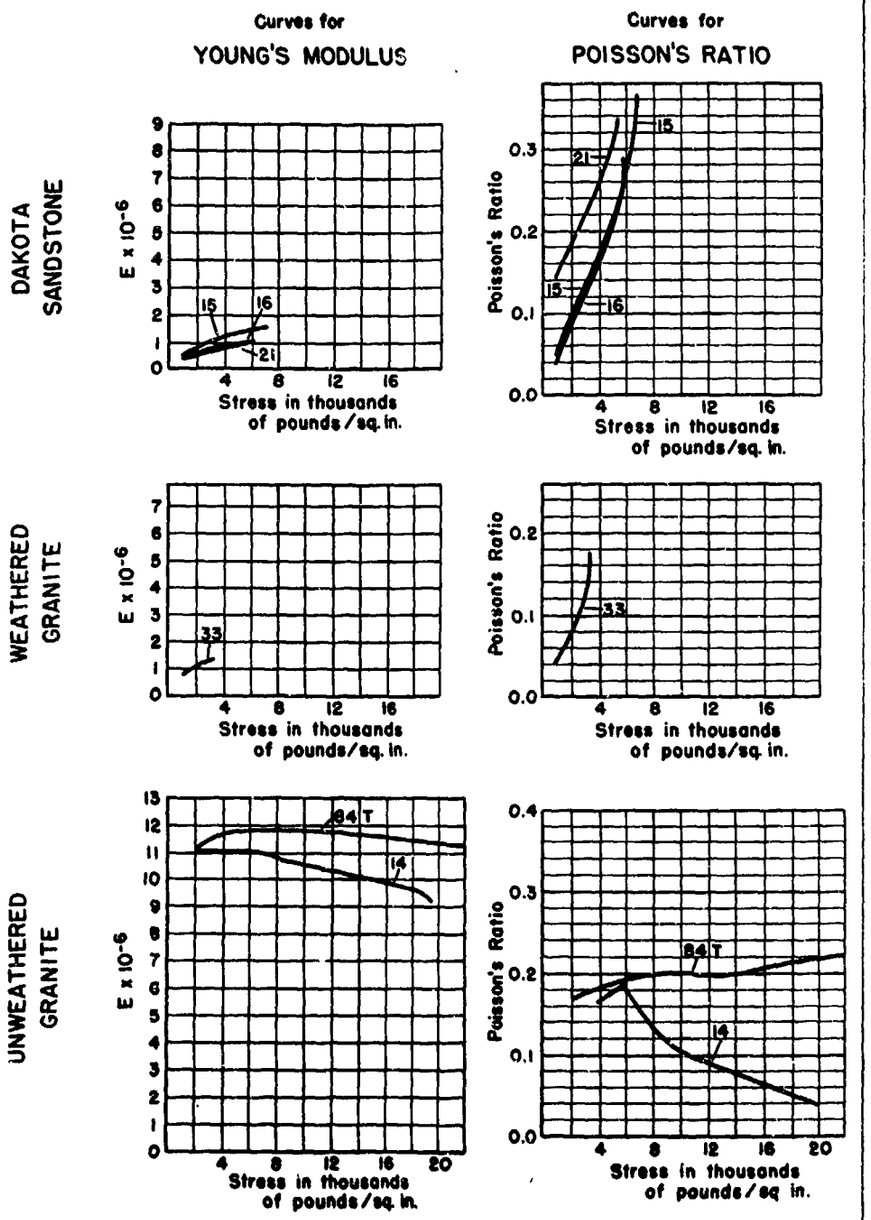

-BOMB PENETRATION PROJECT- C S M RESEARCH FOUNDATION, INC.

Scale ——— Date 3-9-61 Fig. No. 68 By ADG.	YOUNG'S MODULUS AND POISSON'S RATIO- DAKOTA SANDSTONE AND ZUNI GRANITE

Fig. 68

are arranged so that Young's modulus and Poisson's ratio of the three rock types can be compared readily. It may be observed that the so-called elastic constants are not constants but are variables which depend upon the stress range. Values of Young's modulus for unweathered granite decrease in the higher stress range, whereas values of Young's modulus for weathered Zuni granite and Dakota sandstone increase. Unweathered granite specimen 84T shows the least variation. Values of Poisson's ratio for unweathered granite either decrease (specimen 14) or increase at a moderate rate in the higher stress range, whereas values of Poisson's ratio for weathered granite and Dakota sandstone increase much more rapidly. At the point of failure in simple compression the value of Poisson's ratio for Dakota sandstone is 1.63 times that of unweathered granite.

At 24,600 pounds per square inch, the average compressive strength of the unweathered Zuni granite, (see Fig. 58) the maximum value of Poisson's ratio that might be inferred from presently available data is 0.232. In the same stress range it is evident from inspection of Fig. 68 that the Dakota sandstone would behave plastically. Thus, Poisson's ratio for the sandstone would approach 0.50 and the ratio of Poisson's ratios for the two rocks would approach a maximum of 2.2.

12—Triaxial Compression Tests

Triaxial compression tests of specimens of Dakota sandstone, weathered Zuni granite, and unweathered Zuni granite were conducted by the United States Bureau of Reclamation in the structural laboratory at Denver. Specimens of each rock type were tested in groups of three subjected to the same lateral load. The zero lateral load member of each triaxial group provided stress-strain data used in calculating Young's modulus and Poisson's ratio. The lateral load was introduced by means of a hydraulic pump to NX diamond drill core specimens fitted with a rubber jacket inside the triaxial testing cylinder.

The confining lateral load on the outside of the jacketed specimens was added in increments of 250 pounds per square inch to specimens of Dakota sandstone and in increments of 1000 pounds per square inch to specimens of weathered and unweathered Zuni granite. As the confining lateral load increased, the longitudinal stress at the failure point likewise increased. The lateral stress is referred to as S_3 and the longitudinal stress at failure is referred to as S_1. Values of S_3 and corresponding values of S_1 for each of the three types of rocks are tabulated in Fig. 69.

The relations of the principal stresses at failure and the shear equations for a segment of Mohr's envelope as determined by the Coulomb formula[1] were computed by the method of least squares, and the results for each of the three rock types are tabulated in Fig. 69. Other test data have shown that Mohr's envelope is curved in the general case and prudence should be exercised in extrapolating values far beyond the test ranges. Fig. 70 is a photograph of a group of test specimens of Dakota sandstone which shows the manner of failure.

[1]Basic Structural Research Laboratory Report No. SP-9. A Revised Method of Interpretation of Triaxial Compression Tests for the Determination of Shearing Strength. U. S. Bureau of Reclamation.

Dakota Sandstone			Weathered Zuni Granite			Unweathered Zuni Granite		
No.	S_1 psi	S_3 psi	No.	S_1 psi	S_3 psi	No.	S_1 psi	S_3 psi
21	5610	0	33	3700	0	84T	24880	0
16	6595	0						
15	7830	0						
9	8090	250	4	12560	1000	2	32470	1000
47	9290	250						
35	9760	250						
20	12290	500	34	14450	2000	1	34030	2000
50	13250	500						
25	13570	500						
34	12450	750				84B	37420	3000
39	13760	750						
40	14030	750						
12	15300	1000				85	49180	4000
17	16650	1000						
18	16900	1000						
99	16120	1250						
23	16210	1250						
30	17570	1250						
Relation of S_1 and S_3 $S_1 = 7110 + 8.6S_3$			Relation of S_1 and S_3 $S_1 = 4510 + 5.8S_3$			Relation of S_1 and S_3 $S_1 = 24360 + 5.6S_3$		
Mohr's Envelope $Y = 1210 + 1.3X$			Mohr's Envelope $Y = 940 + 1.0X$			Mohr's Envelope $Y = 5140 + 1.0X$		

Fig. 69

Triaxial Compressive Strength
Dakota Sandstone, Weathered Zuni Granite, and Unweathered Zuni Granite

The equation giving the relation of the principal stresses at failure is of the form:

$$S_1 = C + AS_3$$

where

S_1 = longitudinal principal stress at failure, pounds per square inch

C = simple compressive strength, pounds per square inch

A = a constant

S_3 = lateral principal stress at failure, pounds per square inch.

Fig. 70
Test Specimens of Dakota Sandstone Showing Manner of Failure

Referring to the equations tabulated in Fig. 69 and to Fig. 58 for average compressive strengths, the results compare as follows:

	C, psi	Average Compressive Strength, psi
Dakota Sandstone	7,110	5,015
Weathered Zuni Granite	4,510	9,142
Unweathered Zuni Granite	24,360	34,565

It is apparent from this comparison that the results of the triaxial tests on the unweathered Zuni granite substantiate the results of the compression tests and that the assumption of a straight line $S_1=24,360 + 5.6S_3$ is reasonably accurate. It is apparent that the number of specimens of weathered granite in the triaxial tests is insufficient to draw any definite conclusions. It is also apparent that the slope of Mohr's envelope for Dakota sandstone is a curve rather than a straight line. Values of S_1 computed using the equation for Dakota sandstone, $S_1=7110 + 8.6S_3$ are perhaps too high in the range 0 pounds per square inch to 500 pounds per square inch lateral load, and in the range beyond 1250 pounds per square inch lateral load. Perhaps this relation is due to the plastic nature of the Dakota sandstone in the high stress range.

The equation of Mohr's envelope is of the form:

$$Y = c + X \tan \phi$$

where

Y = shear stress at failure, pounds per square inch

c = unit cohesive strength, pounds per square inch

X = accompanying normal stress, pounds per square inch

ϕ = angle of interval friction

$\tan \phi$ = slope of line representing Mohr's equation

Inspection of the equation of Mohr's envelope shows that c, the unit cohesive strength, equals the strength of the rock in pure shear when X equals zero. Therefore from the equation of Mohr's envelope the pure shear strengths of the three types of rocks are as follows:

	Pure Shear Strength, psi
Dakota Sandstone	1210
Weathered Zuni Granite	940
Unweathered Zuni Granite	5140

The data of Fig. 69 for Dakota sandstone and for unweathered Zuni granite have been used to construct the Mohr diagrams of Fig. 71. The diagrams have been plotted to the same scale, so that the envelope of rupture for the two rock types may be compared visually. It may be observed that the slope of Mohr's envelope is much steeper for sandstone than for unweathered Zuni granite, and it may be inferred that the strength of the sandstone becomes greater than that of the granite as the lateral load increases.

13—Summary of Results

The arithmetic mean of each of the physical rock tests, the standard deviation, and the coefficient of variation have been determined statistically and are presented in summary form in Fig. 72.

A dispersion of test data about the arithmetic mean is to be expected, and the "standard deviation" is one means of expressing this dispersion. The standard deviation is expressed by the formula

$$\sigma = \sqrt{\frac{\text{Sum}\,(x^2)}{N}}$$

where,

σ = the standard deviation

x = the deviation from the arithmetic mean

N = the number of test specimens.

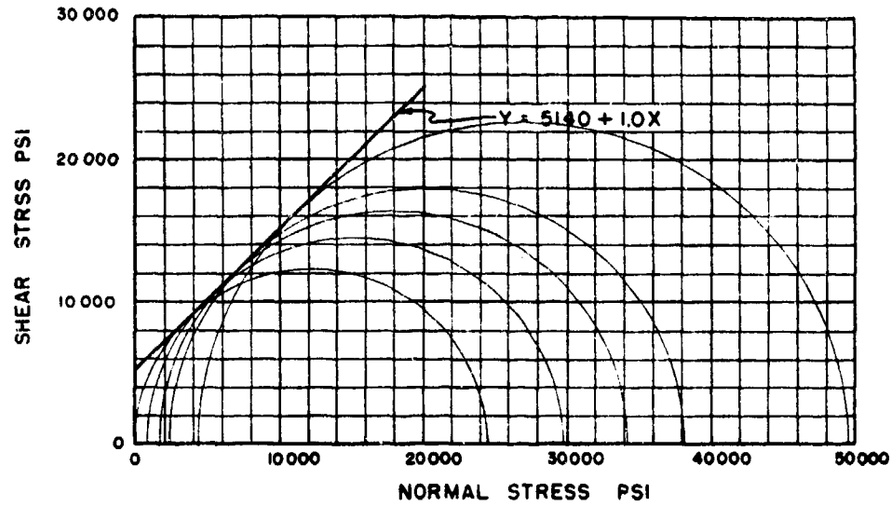

UNWEATHERED GRANITE SPECIMENS; 84T, 2, 1, 84B, & 85

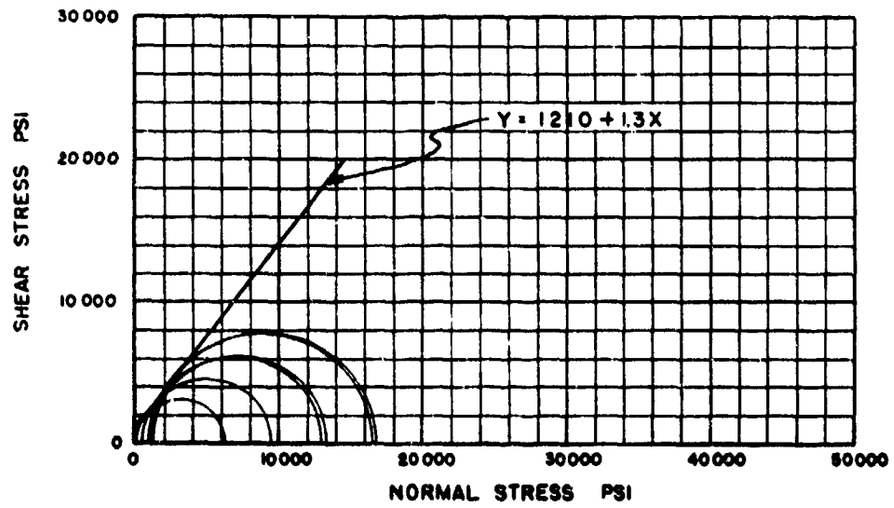

DAKOTA SANDSTONE SPECIMENS

-BOMB PENETRATION PROJECT- C S M RESEARCH FOUNDATION, INC.

Scale ——— Date 11-17-60	MOHR DIAGRAMS
Figure 71 By [redacted]	DAKOTA SANDSTONE & ZUNI GRANITE

Fig. 71

Physical Property	Dakota Sandstone			Weathered Zuni Granite			Zuni Granite		
	Mean Value	Standard Deviation σ	Coef. of Variation %	Mean Value	Standard Deviation σ	Coef. of Variation %	Mean Value	Standard Deviation σ	Coef. of Variation %
Specific Gravity	2.13	0.01	0.5	2.73	0.02	0.6	2.77	0.04	1.3
Apparent Porosity (percent)	16.4	0.62	3.8	0.00	-	-	0.00	-	-
Total Porosity (percent)	16.5	2.07	12.6	0.00	-	-	0.10	0.17	173.0
Tensile Strength (psi)	63	31	49.2	1003	357	35.6	1905	352	18.5
Modulus of Rupture (psi)	355	97	27.3	2261	1094	48.4	5434	516	9.5
Compressive Strength (psi)	5015	1626	32.4	9142	2019	22.1	24,565	6032	24.6
Impact Toughness (ft-lb/in^2)	24.95	4.65	18.7	54.01	1.91	3.5	54.28	9.45	17.4
Impact Toughness (in./in.^{2})	1.0	-	43.0	-	-	-	15.0	-	29.0
Coef. of Restitution	0.415	0.018	4.2	0.698	0.054	7.7	0.885	0.022	2.5
Sclerescope Hardness	20.74	1.67	8.1	58.48	9.90	16.9	94.11	4.63	4.9
Young's Modulus (psi) Poisson's Ratio	See Figs. 64, 65, 68			See Figs. 64, 65, 68			See Figs. 64, 65, 68		
Velocity of Sound (fps)	Long.= 5210, Tors.= 3730			-	-	-	Long.= 17,800, Tors.= 11,100		
Seismic Velocity (fps)	Longitudinal = 5120			-	-	-	Longitudinal = 19,580		
Equation of Mohr's Envelope	Y = 1210 + 1.3X			Y = 940 + 1.0X			Y = 5140 + 1.0X		
Relation of Prin. Stresses	S_1 = 7110 + 8.6S			S_1 = 4510 + 5.8S_3			S_1 = 24,360 + 5.6S_3		

Fig. 72

Summary of Physical and Elastic Properties of Dakota Sandstone and Zuni Granite

Thus, the standard deviation is the quadratic mean of the deviations from the arithmetic mean and is the root-mean-square of the deviations. The standard deviation is affected by the value of every test, and is an absolute measure.

The "coefficient of variation" is a measure of dispersion that is useful where the units and the sizes of the averages differ. It may be expressed in the form of an equation:

$$V = \frac{\sigma}{x} 100$$

where,

V coefficient of variation

σ the standard deviation

x the arithmetic mean.

Thus, the coefficient of variation is a means of expressing the standard deviation as a percentage of the arithmetic mean.

Values of the elastic constants have not been included in the table, because the so-called "elastic constants" are not constants but are variables depending upon the stress range. The reader is referred to Figs. 64, 65, and 68 wherein Young's modulus and Poisson's ratio as determined by the sonic method are recorded, and variations of Young's modulus and Poisson's ratio in the stress range to failure are presented graphically.

PART B—BALLISTIC DATA

SECTION I—BOMB CHARACTERISTICS AND NOMINAL DIMENSIONS

1—Introduction

A total of 50 inert bombs was dropped in the Bomb Penetration Test Project; 20 were dropped at the Paxton Springs granite site, and 30 were dropped at the Putney Mesa sandstone site. Of the 20 bombs dropped on the granite target, 9 were 1600-pound armor-piercing AN-MK-1 bombs, 9 were 2000-pound semi-armor-piercing M 103 bombs, and 2 were 25,000-pound semi-armor-piercing bombs. Of the 30 bombs dropped on the sandstone target, 9 were 1600-pound armor-piercing AN-MK-1 bombs, 9 were 2000-pound semi-armor-piercing M 103 bombs, and 12 were 2000-pound general-purpose AN-M66 A2 bombs.

2—Description of Bombs Used in the Tests

Photographs of the bombs used in the tests were furnished by Edwards Airforce Base, Muroc, California. Detail drawings of the several types of bombs were furnished by the Department of Ordnance through the

Fig. 73
1600-Pound Armor-Piercing AN-MK-1 Bomb

Protective Construction Branch, Office, Chief of Engineers. Each of the bombs was weighed and assigned an airforce number. Certain critical dimensions were measured at Edwards Airforce Base before the bombs were loaded into the bomb racks of the bombing plane. Each bomb was assigned a C.S.M. number at the instant of release. The C.S.M. number is the number referred to repeatedly in this report.

2a—The 1600 AP, AN-MK-1 Bomb

Figure 73 is a photograph of the 1600 AP, AN-MK-1 bomb with its attached fin.

Figure 74 shows certain critical dimensions which were taken from Department of Ordnance drawings numbers 328867 and 328870. The maximum variations between the actual weight and the nominal weight was 54 pounds—the actual weight being greater than the nominal. The actual weight of each bomb is recorded on a summary data sheet of the bombs dropped at each test site. The differences between the actual and nominal dimensions were negligible. The sectional pressure is found by the formula

$$S=\frac{4W}{\pi d^2}$$

where,

S = sectional pressure

W = weight, pounds

d = diameter, inches

The sectional pressure of 10.40 as recorded on the outline drawing is computed using the nominal weight and the nominal dimensions, whereas actual dimensions and actual weights have been used in the analysis and in the field data summary sheets.

Similarly, the sectional density of 0.583 as recorded on the outline drawings refers to nominal dimensions and nominal weights, whereas the actual dimensions and actual weights have been used in the analysis and in the field data summary sheets. The sectional density of a bomb is given by the formula

$$D=\frac{W}{d^2}$$

where

D = sectional density

W = weight, pounds

d = diameter, inches

The caliber radius head has been computed from the nominal dimensions and equals the radius of the ogive, R, divided by the diameter of the bomb, d. The caliber radius head of the 1600 AP bomb is 2.

The slenderness ratio equals the length in calibers, or equals the

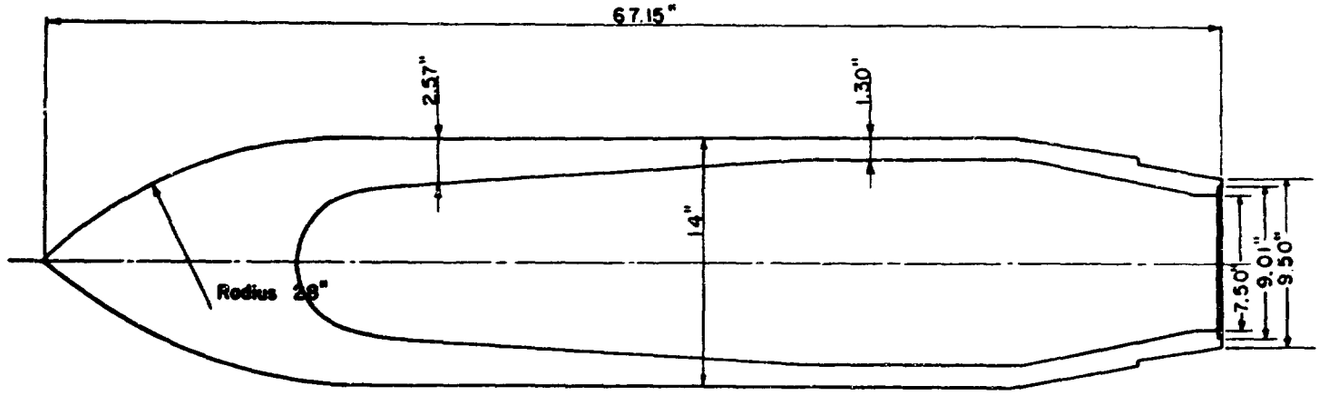

Weight (W)	=	1600 lb	Sectional Pressure (S)	=	10.40
Diameter (d)	=	14"	Caliber radius head $\left(\frac{R}{d}\right)$	=	2
Length (L)	=	67.15"	Sectional Density (D)	=	0.583
Radius ogive (R)	=	28"	Slenderness Ratio $\left(\frac{L}{d}\right)$	=	4.80
Weight, Cost TNT	=	215 lb	Charge / Weight Ratio (%)	=	13.4

-BOMB PENETRATION PROJECT-
COLORADO SCHOOL OF MINES
RESEARCH FOUNDATION INC.

BOMB, 1600LB AP, AN-MK-I
CHARACTERISTICS & NOMINAL DIMENSIONS

Scale 1" = 8" Date 2-22-51
Fig. No. 74 By LB

Fig. 74

Fig. 75
2000 SAP, AN-M 103 Bomb

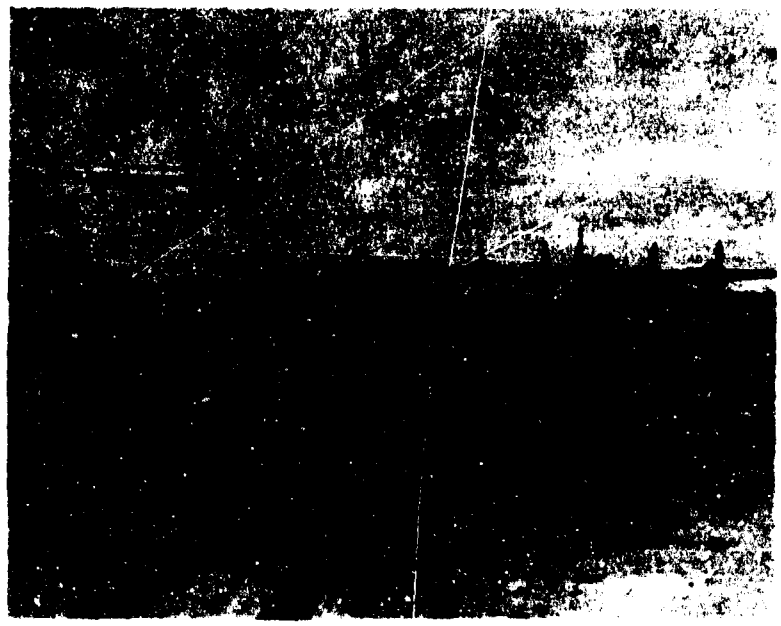

Fig. 77
2000 GP, AN-M66A2 Bomb

length divided by the diameter of the bomb. The slenderness ratio of the 1600 AP bomb is 4.80.

2b—The 2000 SAP, AN-M 103

Figure 75 is a photograph of a 2000 SAP, AN-M 103 bomb used in the Bomb Penetration Tests with a M117A1 fin assembly. Figure 76 shows certain critical dimensions which were taken from Ordnance drawings numbers 82-0-133 and 82-3-582. The greatest variation in weight was 79 pounds heavier than the nominal weight. The maximum difference between the actual and nominal length was 0.44 inch, and the largest difference in diameter was 0.35 inch. The nominal sectional pressure of the 2000 SAP bomb is 7.24 and the sectional density 0.302.

2c—The 2000 GP, AN-M66A2 Bomb

Figure 77 is a photograph of a 2000 GP, AN-M66A2 bomb used in the Bomb Penetration Tests with a T143 fin assembly. Figure 78 shows certain critical dimensions which were taken from Ordnance drawings numbers 82-0-76 and 82-3-366. The deviation of the actual weights and dimensions from the nominal was greater than for other types of bombs used in the tests. The maximum increase in length was 0.6 inch and the maximum increase in diameter was 0.18 inch.

The nominal sectional pressure of the 2000 GP bomb is 4.77, and the nominal sectional density is 0.162.

2d—The 25,000 SAP, T28E4 Bomb

Figure 79 shows the characteristics and nominal dimensions of the 25,000 SAP, T28E4 bomb used in the Bomb Penetration Tests with a T115E1 fin assembly. The dimensions were taken from Ordnance drawings numbers TAM2749, TAM2751, TAM2152, TAM2753, and TAM2754. The largest deviation from the nominal weight was 265 pounds.

The nominal sectional pressure is 31.08 and the nominal sectional density is 0.763.

A photograph of the bomb and fin assembly before dropping is not available. However, Figs. 38b, 38a, and 33d show Bomb 19 (C.S.M. number) as it was being removed from the crater.

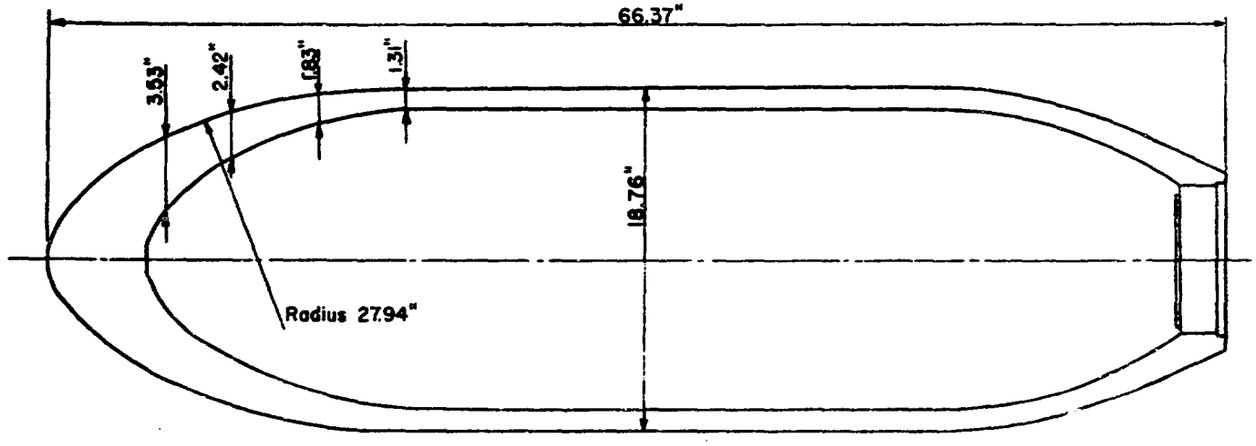

Weight (W)	=	2000 lb	Sectional Pressure (S)	=	7.24
Diameter (d)	=	18.76"	Caliber radius head $\left(\frac{R}{d}\right)$	=	1.49
Length (L)	=	66.37"	Sectional Density (D)	=	0.302
Radius ogive (R)	=	27.94"	Slenderness Ratio $\left(\frac{L}{d}\right)$	=	3.54
Weight, Cast TNT	=	556.48 lb	Charge/Weight Ratio (%)	=	27.8

NOTE: Used with M117A1 Fin Assembly.

-BOMB PENETRATION PROJECT- COLORADO SCHOOL OF MINES RESEARCH FOUNDATION INC.	BOMB, 2000LB SAP, AN-M103 CHARACTERISTICS & NOMINAL DIMENSIONS	Scale 1" = 5" Date 2-22-51 Fig. No. 76 By LB

Fig. 76

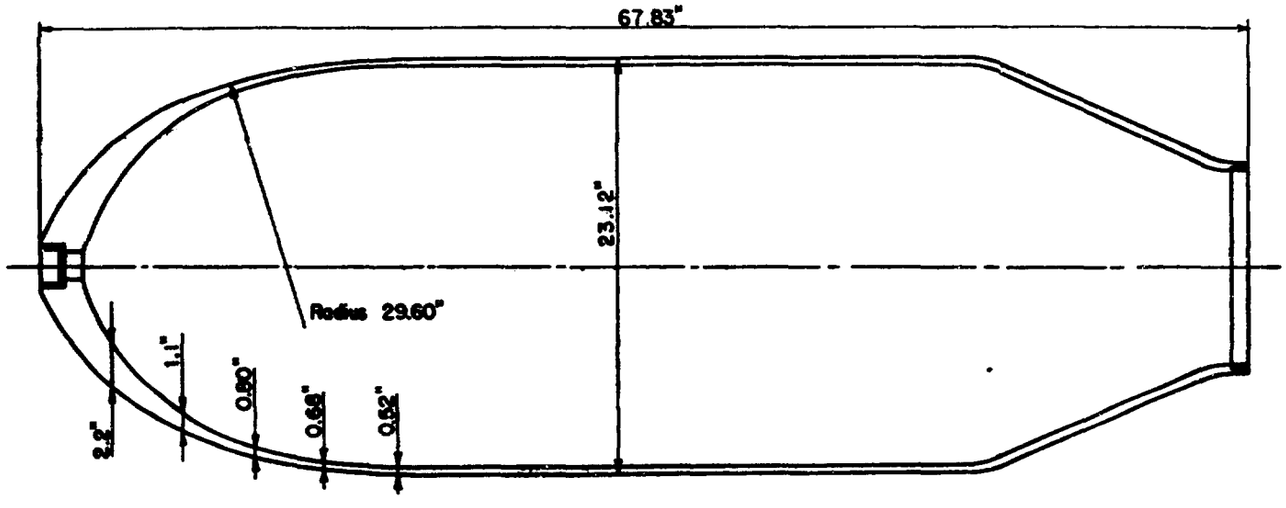

Weight (W)	=	2000 lb	Sectional Pressure (S)	=	4.77
Diameter (d)	=	23.12"	Caliber radius head $\left(\frac{R}{d}\right)$	=	1.28
Length (L)	=	67.83"	Sectional Density (D)	=	0.162
Radius ogive (R)	=	29.60"	Slenderness Ratio $\left(\frac{L}{d}\right)$	=	2.93
Weight, Cast TNT	=	1045.6 lb	Charge/Weight Ratio (%)	=	52.3

NOTE: Used with T143 Fin Assembly.

-BOMB PENETRATION PROJECT- COLORADO SCHOOL OF MINES RESEARCH FOUNDATION INC.	BOMB, 2000LB GP, AN-M66A2 CHARACTERISTICS & NOMINAL DIMENSIONS	Scale 1" = 6" Date 2-22-51 Fig No. 78 By LB

Fig. 78

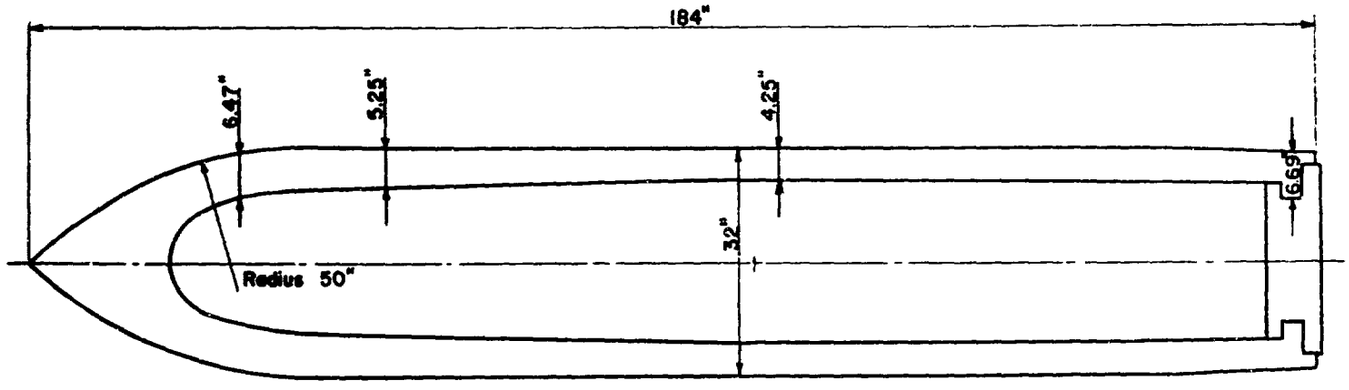

Weight (W)	=	25,000 lb	Sectional Pressure (S)	=	31.08
Diameter (d)	=	32"	Caliber radius head $\left(\frac{R}{d}\right)$	=	1.56
Length (L)	=	184"	Sectional Density (D)	=	0.763
Radius ogive (R)	=	50"	Slenderness Ratio $\left(\frac{L}{d}\right)$	=	5.75
Weight, Cast TNT	=	3860 lb	Charge/Weight Ratio (%)	=	15.44

NOTE: Used with T115E1 Fin Assembly.

-BOMB PENETRATION PROJECT- COLORADO SCHOOL OF MINES RESEARCH FOUNDATION INC.	BOMB, 25,000LB SAP, T 28 E 4 CHARACTERISTICS & NOMINAL DIMENSIONS	Scale 1" = 20" Date 2-22-51 Fig No 79 By LB

Fig. 79

SECTION II—BOMB BALLISTICS

1—Striking Velocity

The elevation of the Paxton Springs granite site target is 7800 feet, and the elevation of the Putney Mesa sandstone site target is 6950 feet. Using tabular data for level bombing with 1600 AP, 2000 SAP, and 25,000 SAP, bombs furnished on December 18, 1950, by the Ballistics Research Laboratories, Aberdeen Proving Ground, Maryland, and based upon a target elevation of 6950 feet above sea level, curves were drawn by the C.S.M. Research Foundation in which striking velocity was plotted against altitude above target.

Figures 80, 81, and 82 show the relation between striking velocity in feet per second and altitude above target in feet for 1600 AP, 2000 SAP, and 25,000 SAP bombs respectively, and for true air speeds of 250, 300, and 350 miles per hour. The 25,000 SAP bombs were dropped at the granite site only. Therefore, the striking velocity shown in Fig. 82 must be corrected for the 7800-foot target elevation. However, the Ballistics Research Laboratories state that "a height of target of 7800 feet would increase the striking velocity by less than 5 feet per second and would decrease the striking angle by less than 1 degree."

Figure 83 shows the relation between striking velocity in feet per second and altitude above target in feet for 2000 GP, AN-M66A2 bombs with T143 fins based upon a target elevation of 7800 feet. The general-purpose bombs were dropped on the sandstone site only (target elevation 6950) and the striking velocities obtained from the graph must be corrected to the 6950-foot target elevation. "A height of target of 6950 feet would decrease the striking velocity by less than 5 feet per second and would increase the striking angle by less than 1 degree."

An examination of the curves for striking velocity as a function of height of drop shows that the striking velocity increases with the height of drop and also increases with the air speed of the plane at the instant of release. An increase in the air speed causes relatively less increase at a high altitude than such an increase of speed causes at a lower altitude. The curves also show that the terminal velocity, or velocity the bomb attains at a time when the air resistance is equal to the force of gravity and no further increase in velocity takes place, has not been reached for any of these bombs.

Figure 84 has been reproduced from graphs furnished by the Ballistics Research Laboratory to show the effect of target elevation upon the striking velocity of 1600 AP, 2000 SAP, 25,000 SAP, and 2000 GP bombs.

2—Angle of Fall

Figure 85 is a graph showing the relation between plane speed, release altitude above the target, and angle of fall for level bombing with 1600 AP and 25,000 SAP bombs. The curves for the 2000 GP bomb are based upon a target elevation of 7800 feet, whereas the curves for the 2000 SAP bomb are based upon a target elevation of 6950 feet. Data for Figs. 85 and 86 were obtained from the Ballistics Research Laboratory.

Curves exhibiting the angle of fall at various air speeds and heights of release show that the angle of fall increases with an increase in height of drop and decreases with an increase of the air speed. If the bomb were to strike at its terminal velocity, and if that terminal velocity consisted only of a vertical velocity component, the angle of fall at impact would be 90 degrees. The angle of fall at any particular instant is that angle whose tangent is the ratio of the vertical to the horizontal components of the velocity.

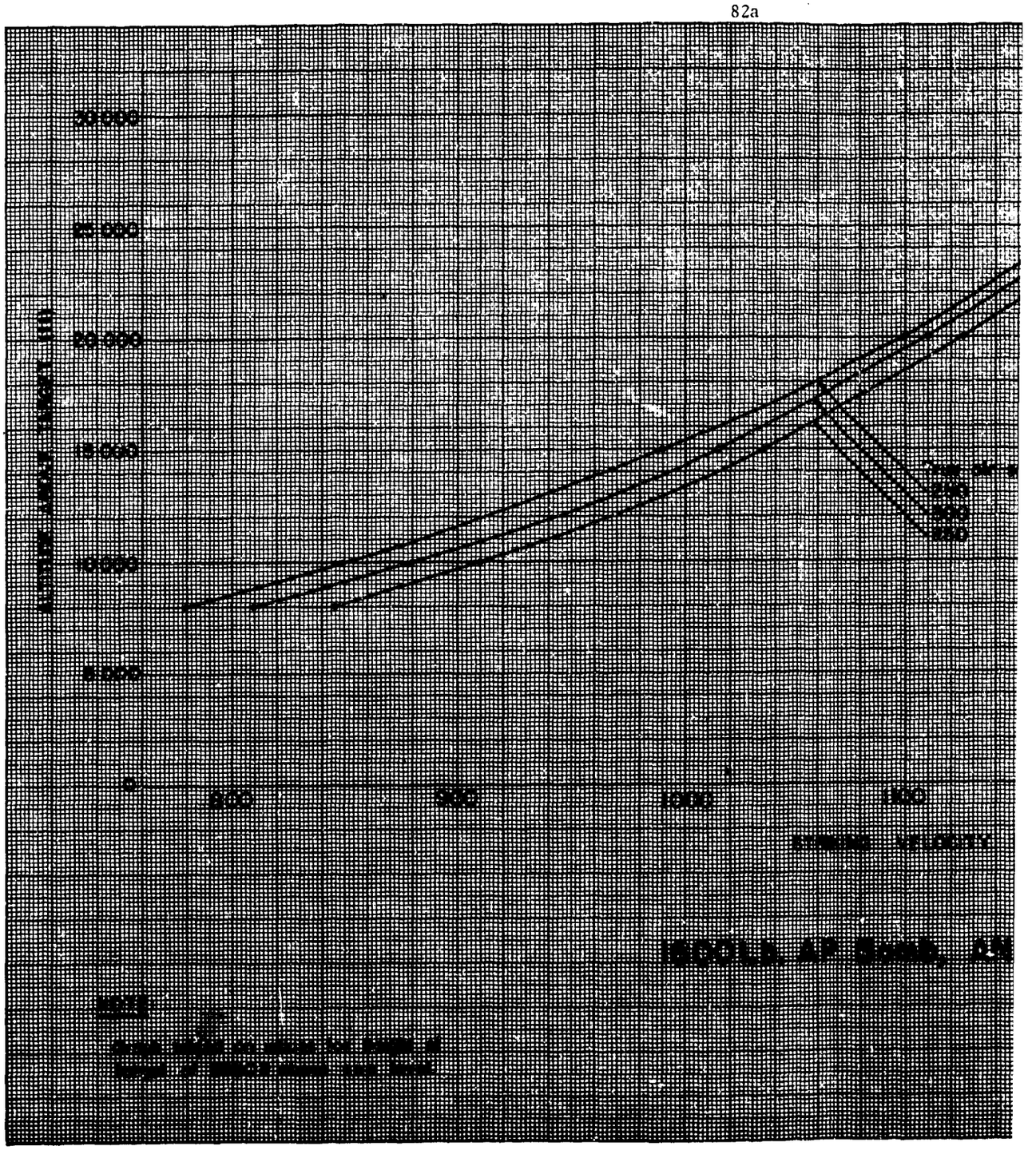
30 000
25 000
20 000
15 000
10 000
5 000
0
500
1000
1500
STRING VELOCITY

82a

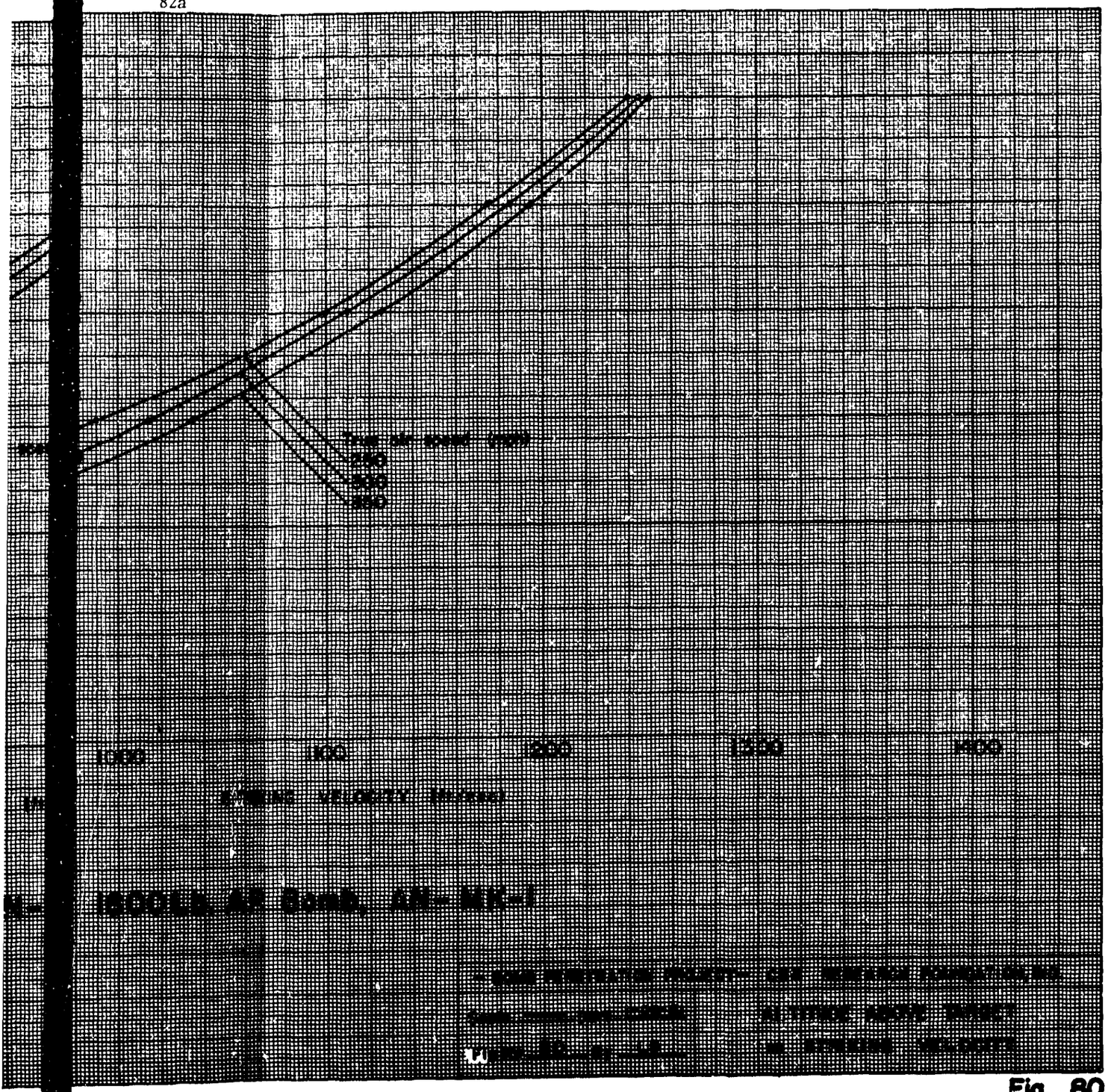

Fig. 80

2

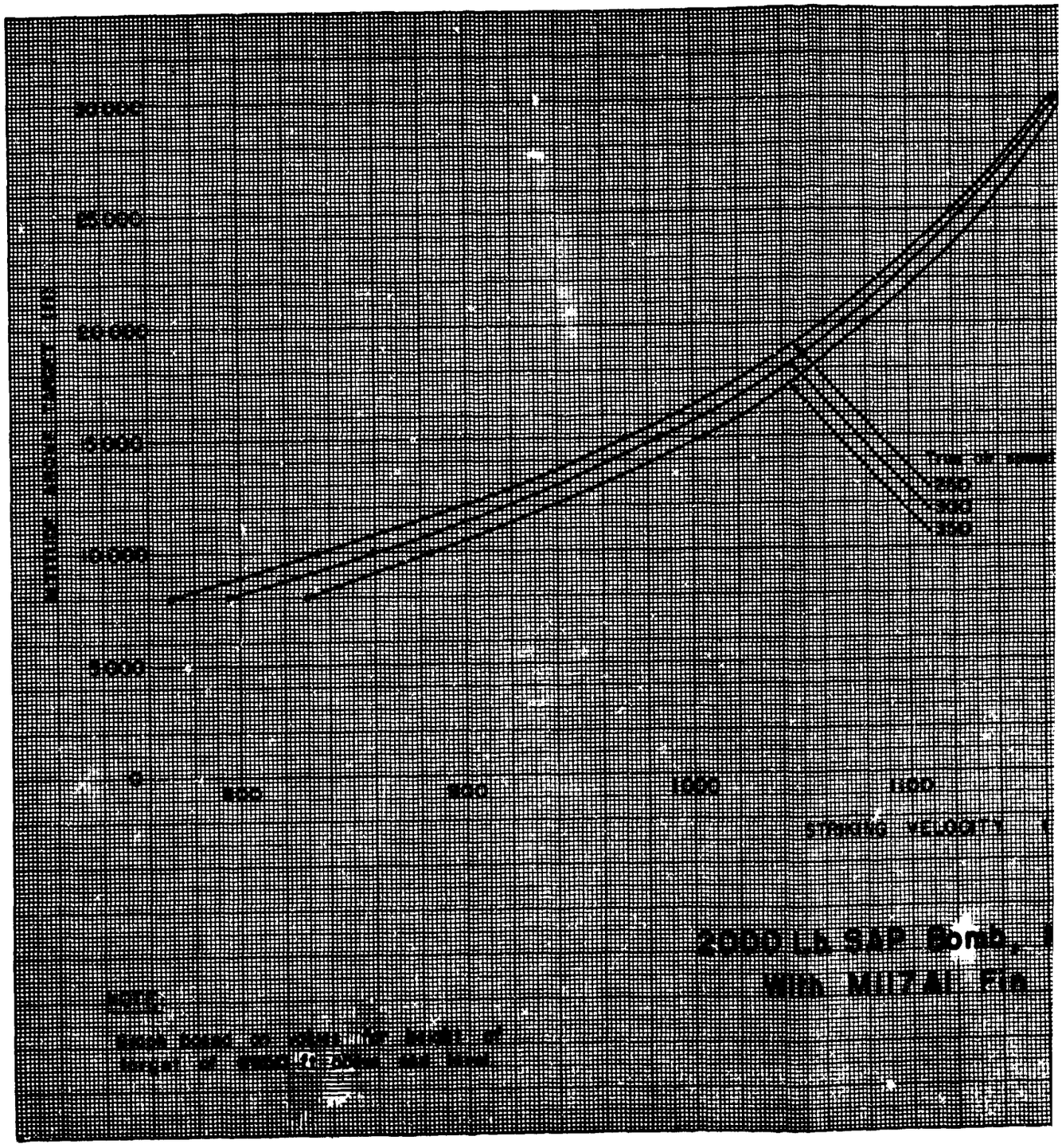

2000 Lb SAP Bomb,
With M117A1 Fin

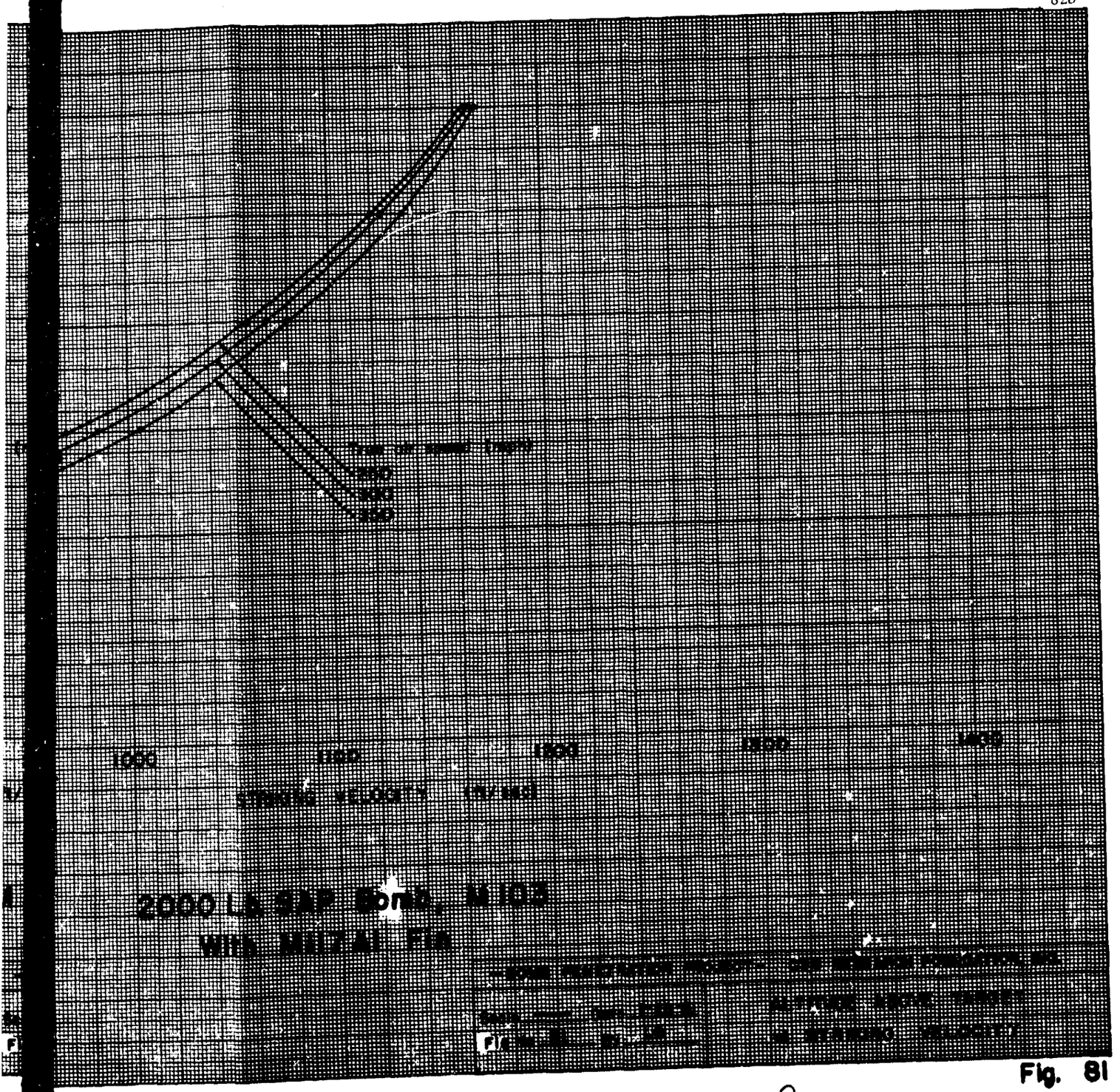
1000
1100
1200
1300
1400
STRIKING VELOCITY
2000 Lb. SAP Bomb, M103
With M117A1 Fin

Fig. 81

2

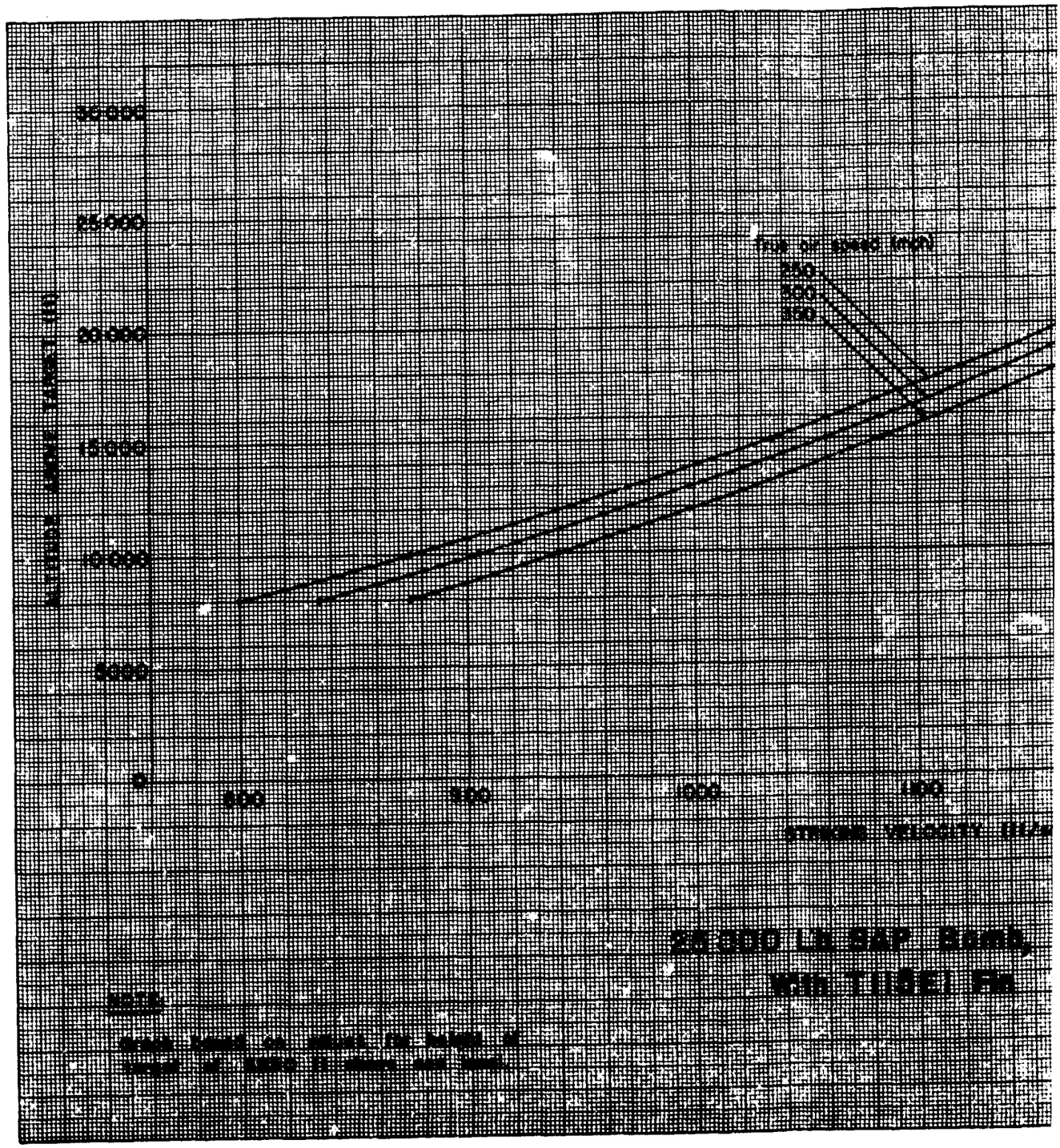

30,000
25,000
20,000
15,000
10,000
5000
0
500
1000
1100
True air speed (mph)
250
300
350
25,000 Lb SAP Bomb,
With T110E1 Fin
NOTE:

82c

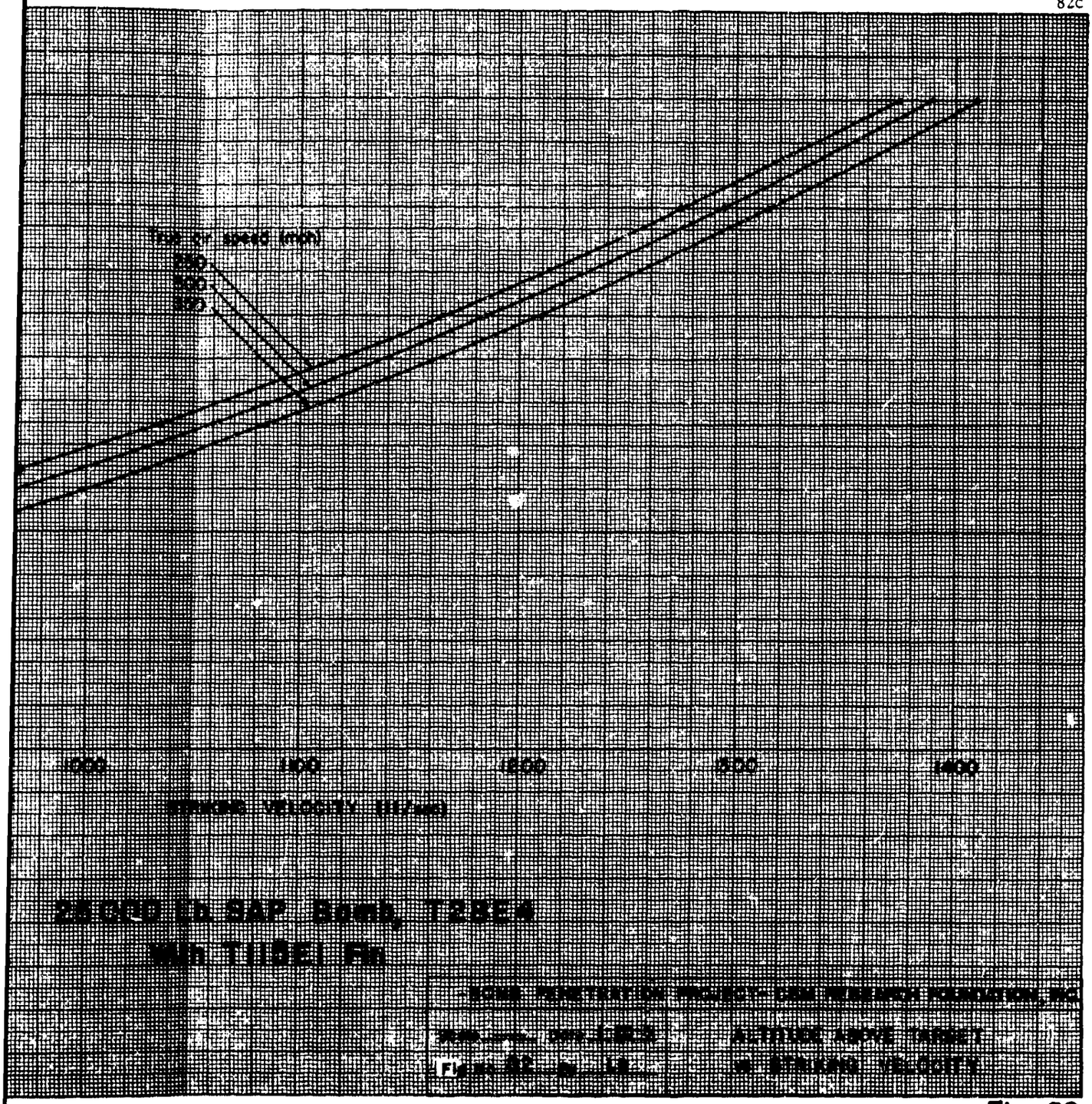

True air speed (mph)
250
500
750
1000
1100
1200
1300
1400
STRIKING VELOCITY (ft/sec)
25000 Lb. SAP Bomb, T28E4
With T115E1 Fin
BOMB PENETRATION PROJECT - CBM RESEARCH FOUNDATION, INC.
ALTITUDE ABOVE TARGET
vs. STRIKING VELOCITY

Fig. 82

2

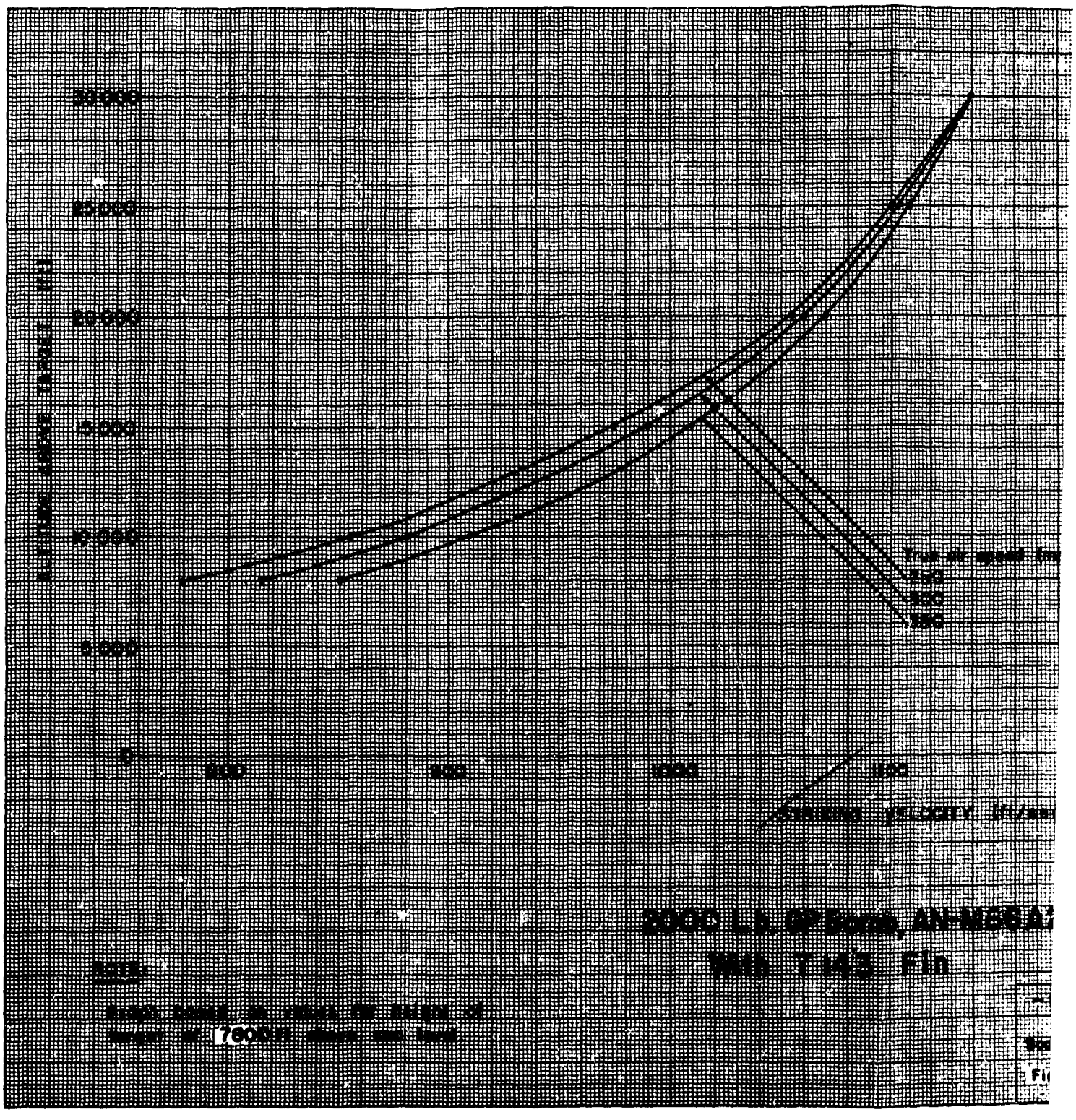
30,000
25,000
20,000
15,000
10,000
5,000
0
900
1000
1100
True air speed
STRIKING VELOCITY
2000 Lb. GP Bomb, AN-M66A2
With T143 Fin
NOTE:

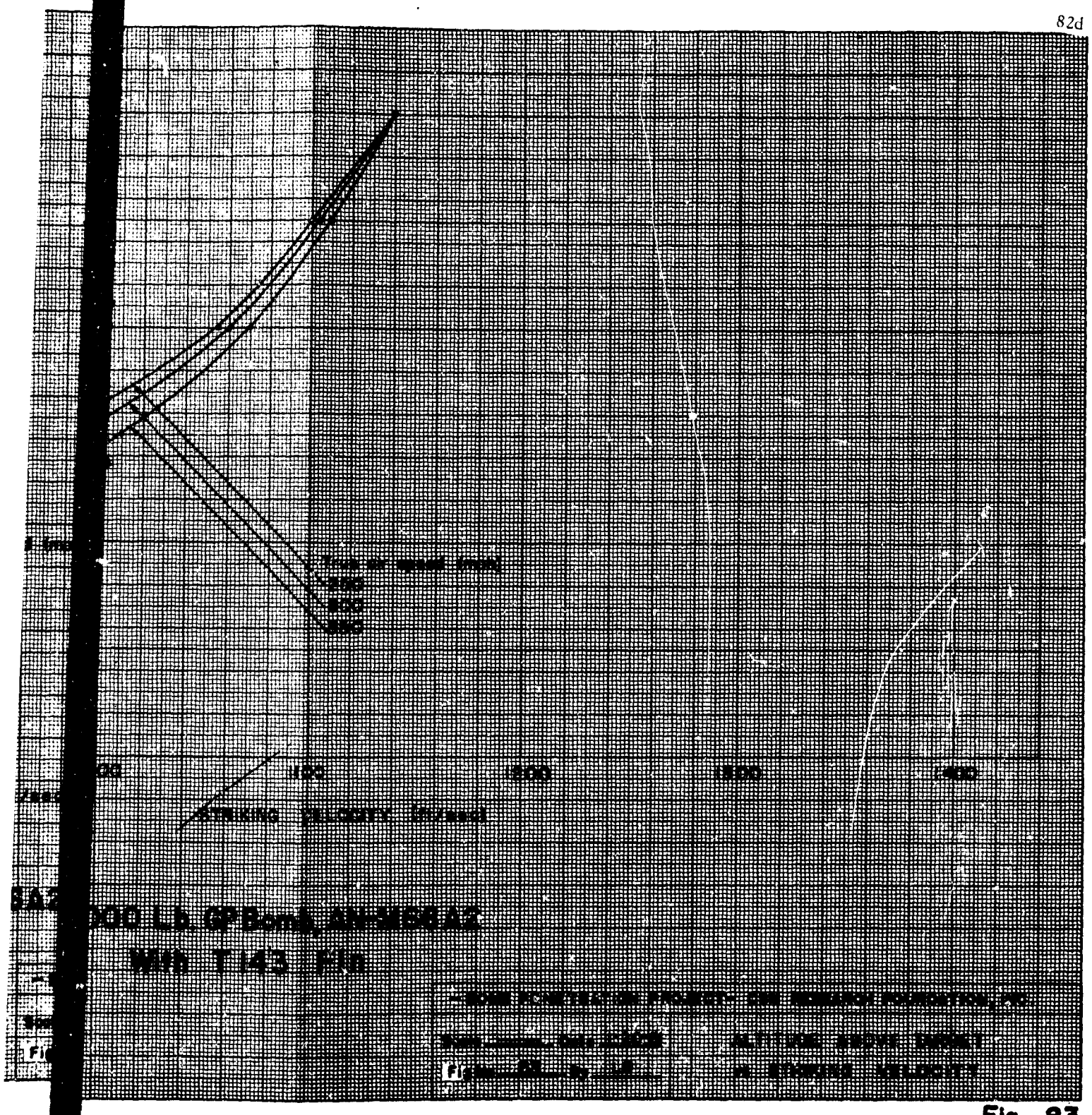
True air speed (mph)
200
300
350
1100
1200
1300
1400
STRIKING VELOCITY (ft/sec)
000 Lb. GP Bomb, AN-M66A2
With T143 Fin
ALTITUDE ABOVE TARGET
vs STRIKING VELOCITY

Fig. 83

2

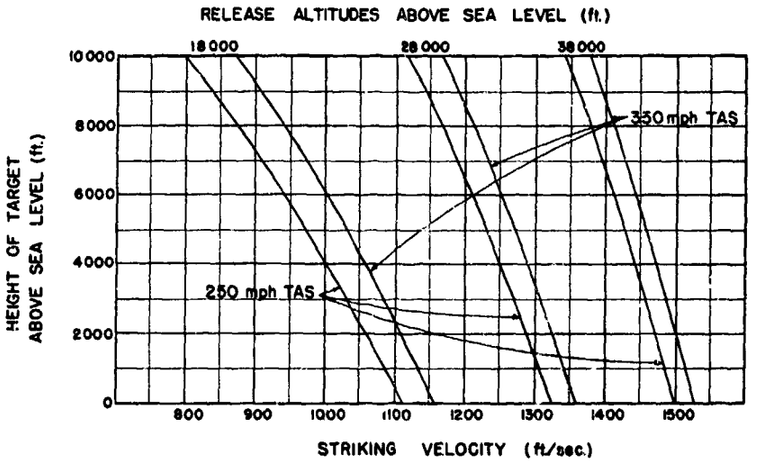

BOMB, SAP, 25000 Lb., T28E4
W/FIN ASSEMBLY, T115E1

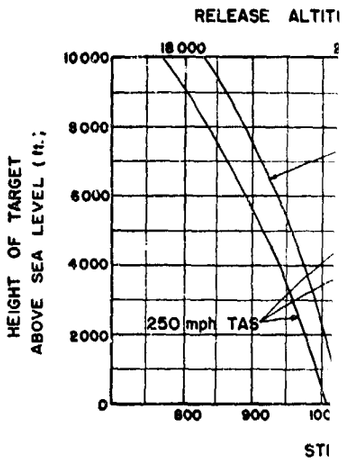

BOMB, SAP,
W/FIN ASSE

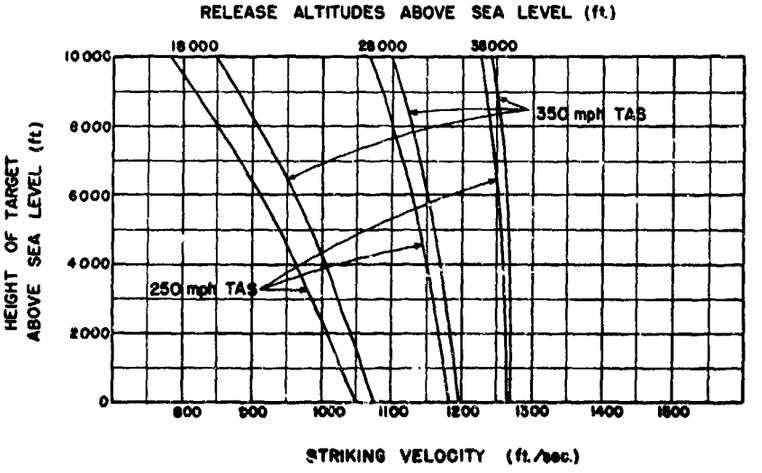

BOMB, AP, 1600 Lb., AN-Mk I

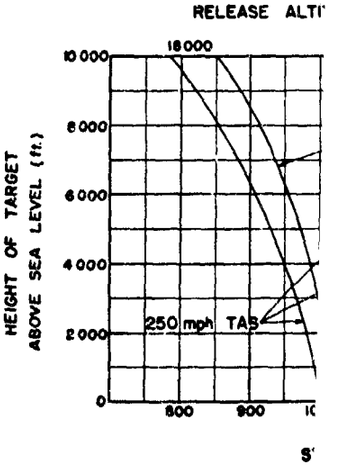

BOMB, GP,
W/FIN ASS

-BOMB PENETRATION PROJ	
Scale ———	Date 2-20-51
Fig. No. 84	By LB

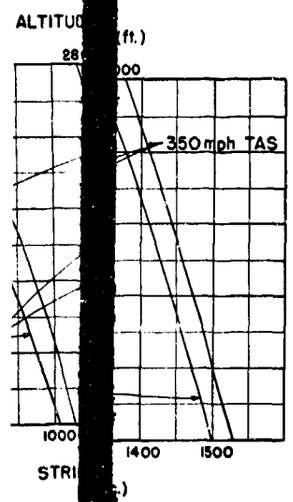

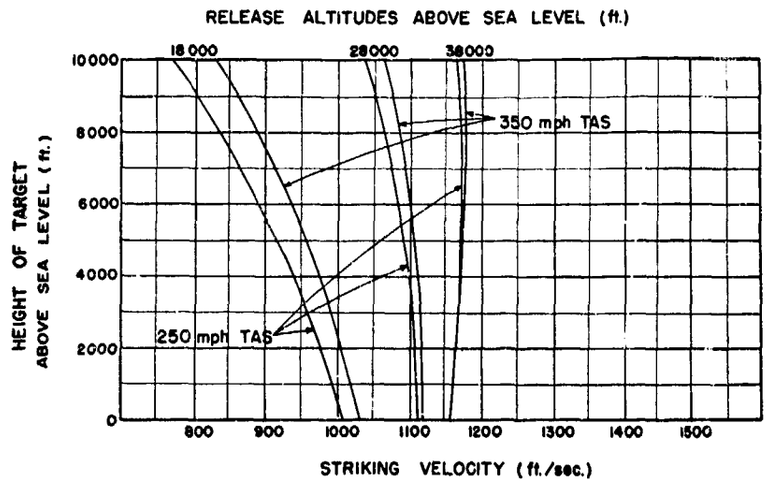

BOMB, SAP, 2000 Lb., M 103
W/FIN ASSEMBLY, M117A1

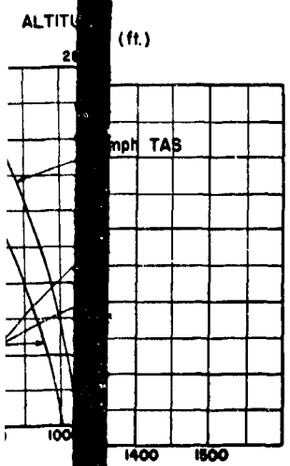

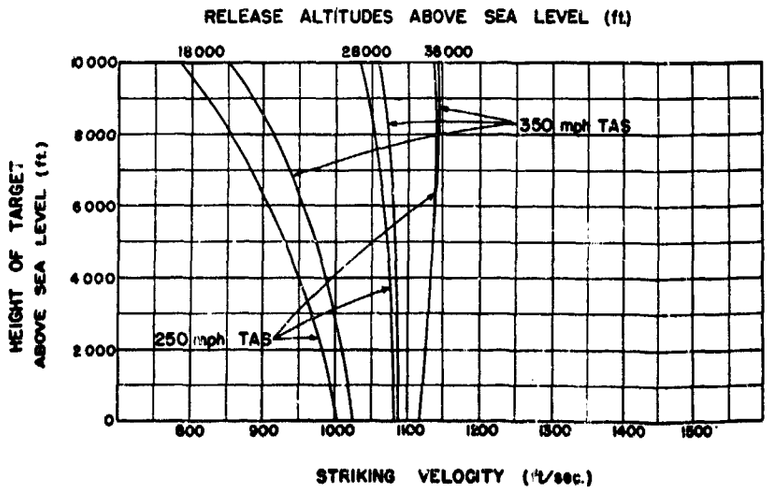

BOMB, GP, 2000 Lb., AN-M66A2
W/FIN ASSEMBLY, T143

-BOMB PENETRATION PROJECT- C S M RESEARCH FOUNDATION, INC.	
Scale ——— Date 2-20-51 Fig. No. 84 By LB	STRIKING VELOCITY vs HEIGHT OF TARGET

Fig. 84

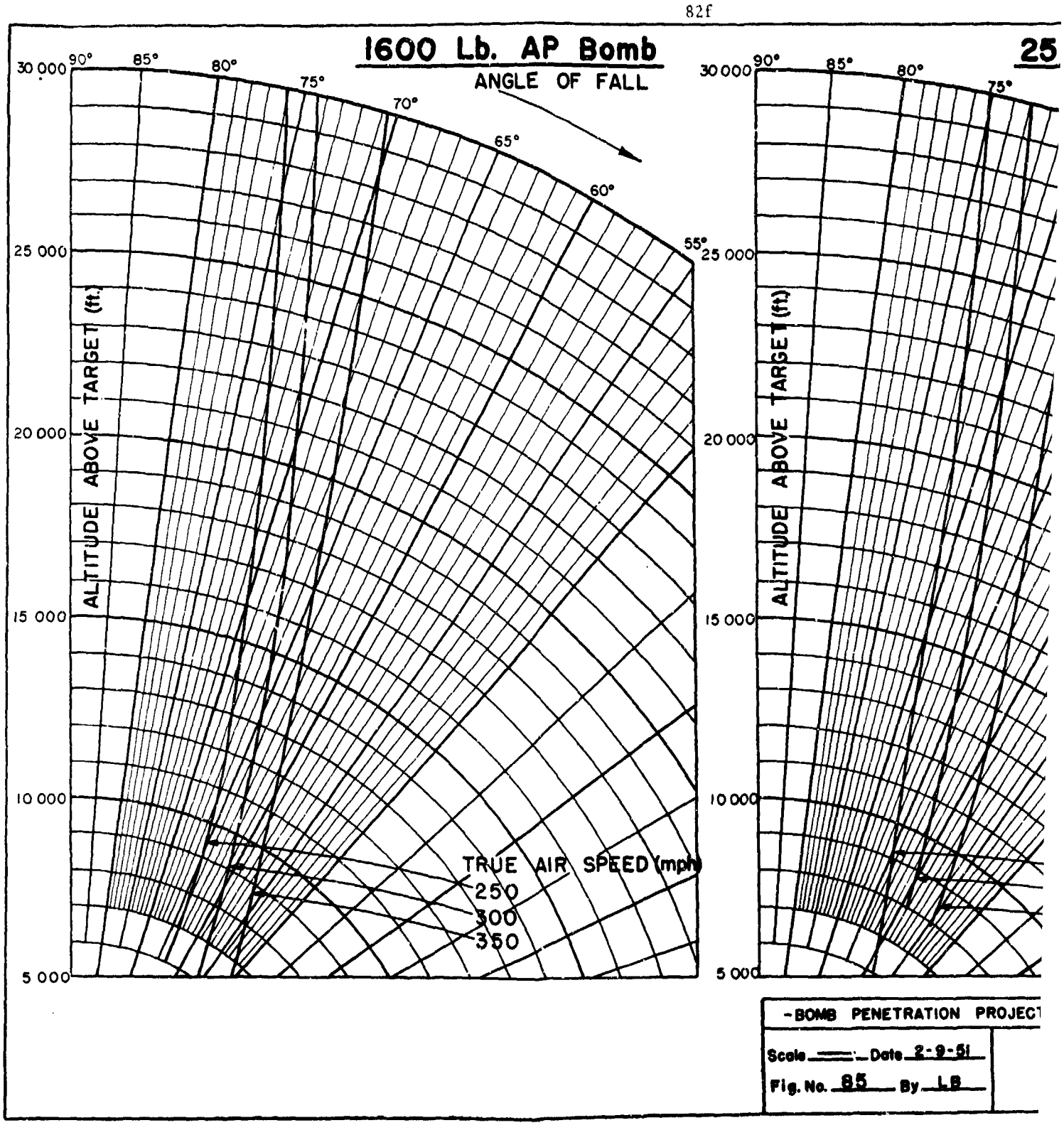
1600 Lb. AP Bomb
ANGLE OF FALL
90°
85°
80°
75°
70°
65°
60°
55°
30 000
25 000
20 000
15 000
10 000
5 000
ALTITUDE ABOVE TARGET (ft.)
TRUE AIR SPEED (mph)
250
300
350
25
-BOMB PENETRATION PROJECT
Scale
Date 2-9-51
Fig. No. 85
By LB

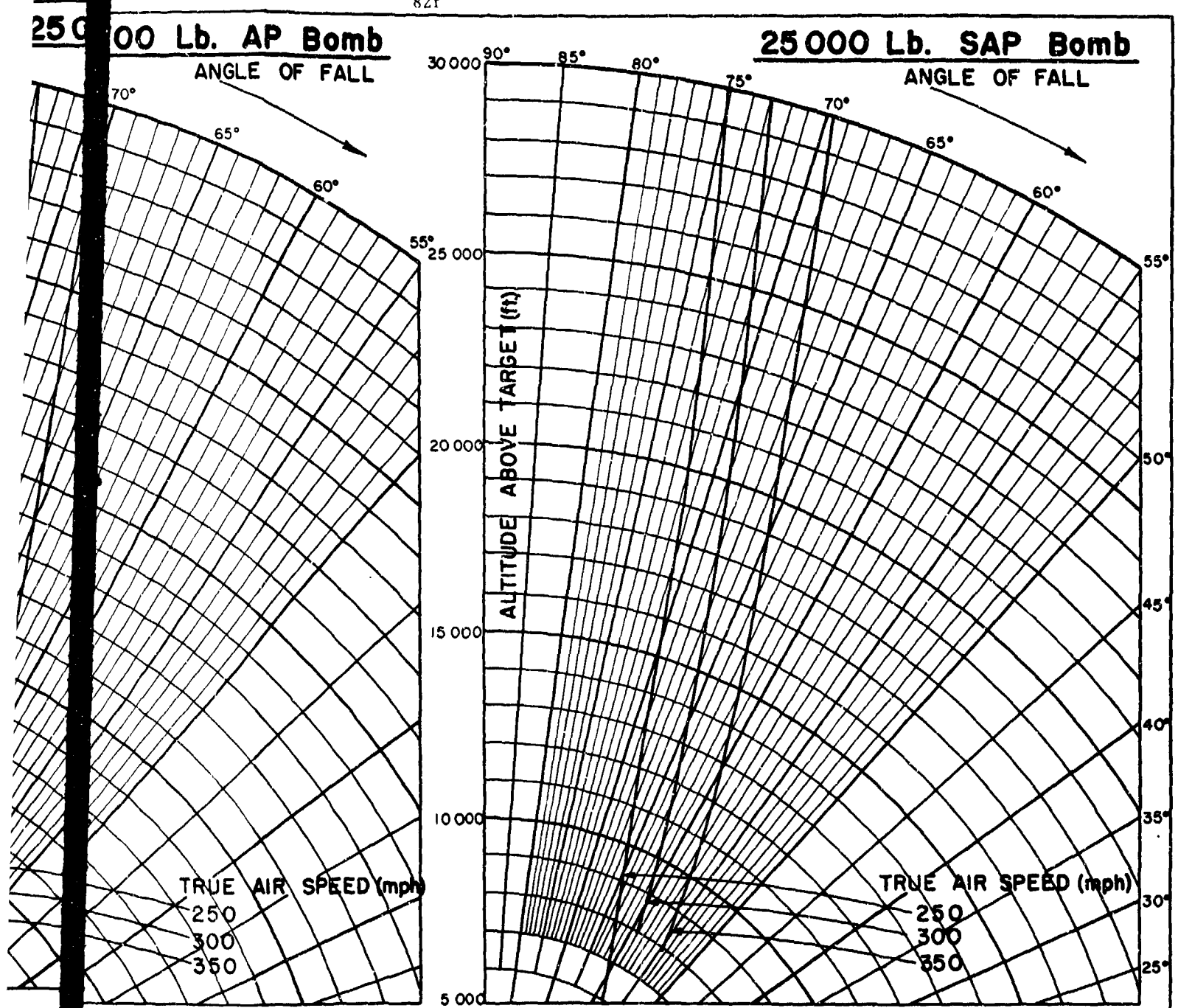

-BOMB PENETRATION PROJECT- CSM RESEARCH FOUNDATION, INC.

Scale ——— Date 2-9-51

Fig. No. 85 By LB

ALTITUDE ABOVE TARGET vs ANGLE OF FALL

Fig. 85

2

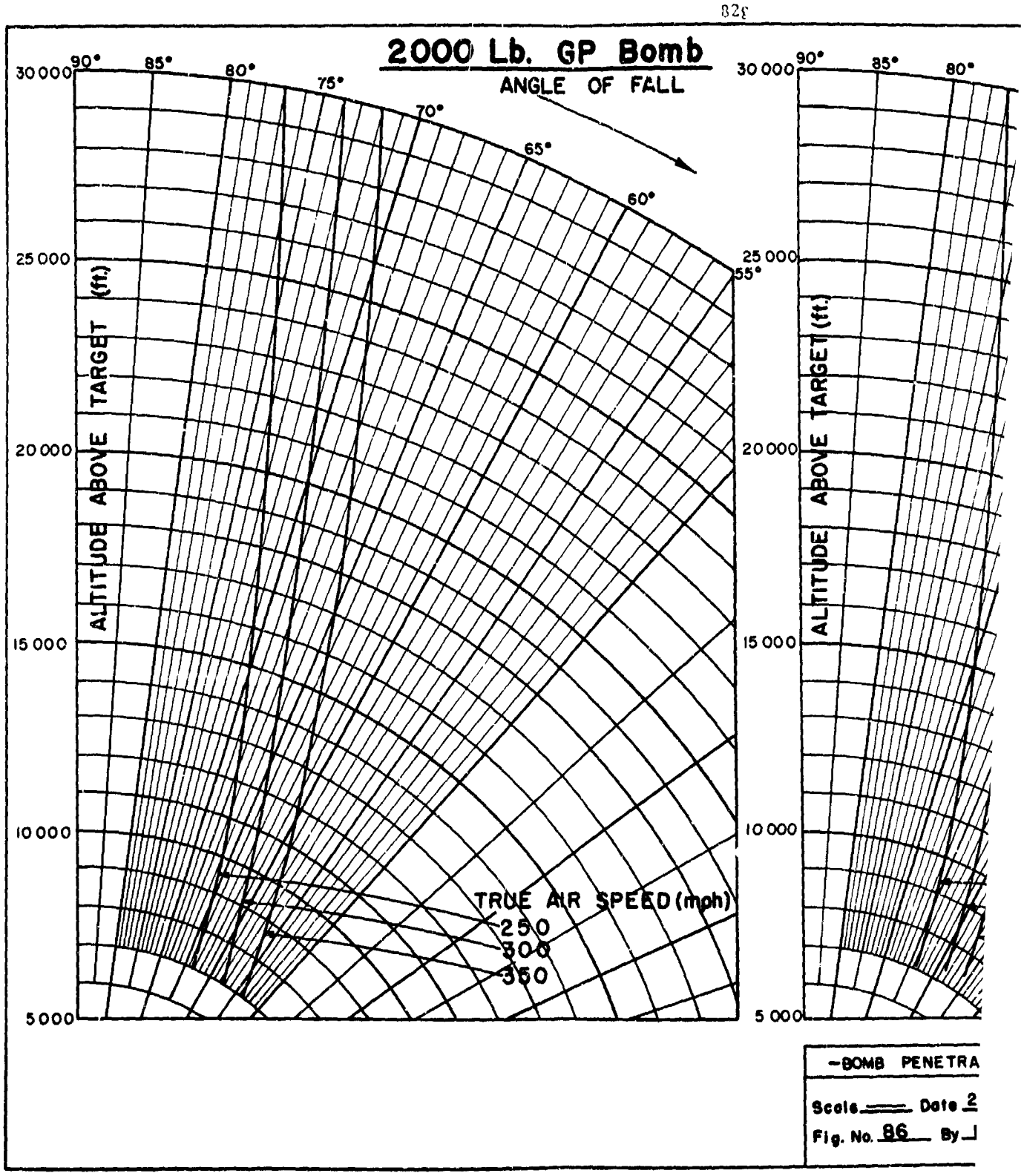
2000 Lb. GP Bomb
ANGLE OF FALL
90°
85°
80°
75°
70°
65°
60°
55°
30 000
25 000
20 000
15 000
10 000
5000
ALTITUDE ABOVE TARGET (ft.)
TRUE AIR SPEED (mph)
250
300
350
-BOMB PENETRA
Scale
Date 2
Fig. No. 86
By

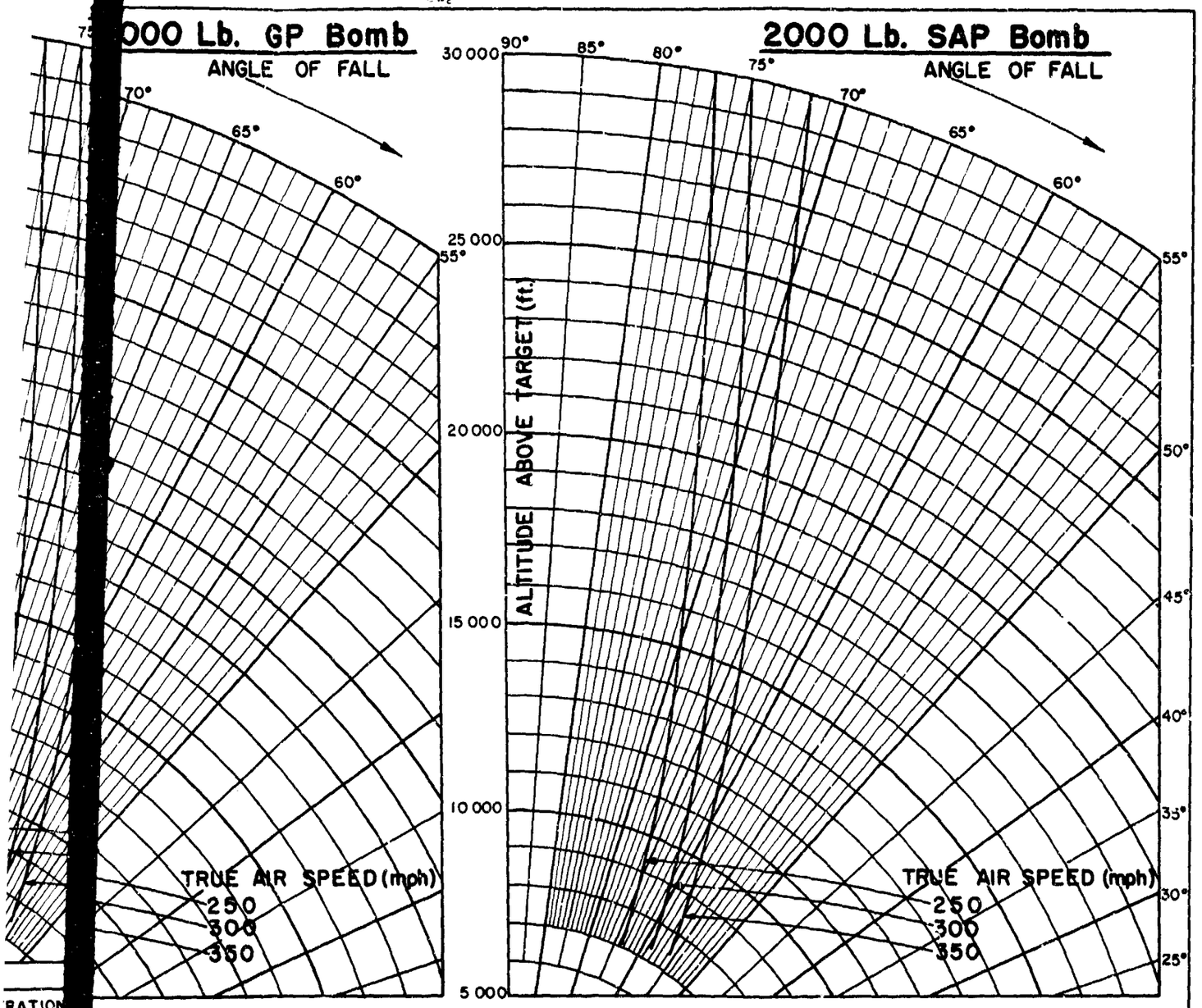

—BOMB PENETRATION PROJECT— C S M RESEARCH FOUNDATION, INC.	
Scale ——— Date 2-9-51 Fig. No. 86 By LB	ALTITUDE ABOVE TARGET vs ANGLE OF FALL

Fig. 86

2

PART C—PENETRATION TESTS IN ZUNI GRANITE

SECTION I—TEST PROCEDURE

1—Detail Layout of the Granite Site

Figure 87 is a topographic map of the Paxton Springs granite site reduced in scale from the map presented in the appendix. (See Appendix, part B.) The reader is referred also to Figs. 11 and 12, aerial photographs of the granite site target area. The topographic map shows the target and marker layout, the access and grid roads through the target, and the location and elevation of each point of bomb impact. The contour interval is 5 feet. The centers of the several bomb craters are the intersections of the crater cross-section lines AB and CD, and the bomb crater is marked with the C.S.M. bomb number. The direction of the line of flight is always along the AB section line from B to A. The bearing and the direction of the line of flight are shown adjacent to the number designating the crater number or the bomb number. Detail maps of each crater are presented in the appendix and may be oriented to the topographic map if desired by use of the AB and CD axes. The topography of the central part of the target area was mapped in greater detail than that of the area in Fig. 87, and is available in the appendix at a 1-foot contour interval.

The topographic map was used as a base map for detailed geologic mapping of the Zuni granite. Because of the large scale reduction, the detail geology is not shown in Fig. 87, but the joint orientation is shown by a clock diagram and a strain ellipse adjacent to each of the granite outcrops. The theoretical attitude of longitudinal joints parallel to the major axis of the ellipse, cross joints parallel to the minor axis of the ellipse, and diagonal joints at 45 degrees to the minor axis are indicated within the ellipse. By comparing the theoretical attitude with the attitude of the lines in the clock diagram, it is possible to identify the joints within the outcrop area and to observe the relative abundance of any joint set and the dispersion of orientation. The long axis of the ellipse is thought to coincide with the direction of maximum strain during emplacement of the granite and during mountain building.

2—Description of the Tests in Granite

Nine 1600 AP bombs, nine 2000 SAP bombs, and two 25,000 SAP bombs were dropped at the granite site. One of the 25,000 SAP bombs was released at 18,000 feet above the target; the other, because of engine trouble which prevented attaining a higher altitude, was released at 26,000 feet above the target. The 1600 AP and the 2000 SAP bombs were released from 9200 feet, 18,000 feet, and 30,000 feet above the target. Because of clouds forming over the target it was necessary to drop one of the 2000 SAP bombs at 14,000 feet rather than at 30,000 feet, the intended height of release. Essentially, three 1600 AP and three 2000 SAP bombs were released at each of three different altitudes.

Figure 88 is a diagram illustrating such terms as "ground ring," "up-surge area," "6 o'clock position," and "hanging-wall" and "footwall," show-

ing the various measurements that were made to record the path of the bomb and the depth of penetration of the bomb. The procedure followed in mapping craters and making damage surveys in the field has been described in Part A, Section II.

Evidence used in determining the point of impact as recorded in the field has been supplemented by use of ballistic data not available at the time of field mapping. In some craters, a trough-shaped path with a diameter corresponding to the bomb diameter, or a remnant of such a trough, was present. In these craters it was a relatively simple task to locate the impact point and map the crater with confidence. In other craters, the rock was crushed so badly that the only evidence of the path of the bomb was the relative amount of crushing and fragmentation at various points. In most craters the point of maximum bomb penetration was determined by the nose of the bomb being in place, or by a mold of the bomb nose in the rock.

The field evidence was reviewed in the drafting laboratory. Scale models were constructed of each bomb and the path was tested using the known line of flight and the known angle of fall at impact. Two assumptions were made in drawing the path. First, it was assumed that no deviation from the line of impact (see sketch) took place in soil less than 2 feet thick. Second, it was assumed that one-fourth of the curvature occurred in the first half of the distance between the point of impact and the point of maximum vertical penetration and three-fourths occurred in the remaining half of the distance.

The crater map for Bomb 17, Fig. 32, is typical of evidence recorded on the crater maps of each bomb dropped at the granite site. Similar maps for each of the craters are part of the appendix to this report. (See Appendix, part C.)

The measurements shown diagrammatically in Fig. 88 together with the essential ballistic data for each of the bombs dropped at the granite site are tabulated on the data sheet, Fig. 89. The data sheet is divided into flight and ballistic data on the left and crater measurements on the right. The bombs are referred to in this report by the C.S.M. bomb number. Bombs of the same type and dropped from the same altitude are arranged in the data sheet by groups, and each group is assigned a group number. Most of the items of the data sheet are self-explanatory, but the following explanation may clarify certain points; the points discussed are arranged in the order of the column headings.

The actual weight of the bomb includes the weight of the fin and the fuses. Weighing was done at Edwards Airforce Base. The striking velocity and the angle of fall were taken from the ballistics data presented in Part B, Section II.

The time of fall given in the column is a rough approximation only; it was measured with a stop watch as an aid in taking pictures on the ground. The energy of the bomb is the kinetic energy of the bomb plus the

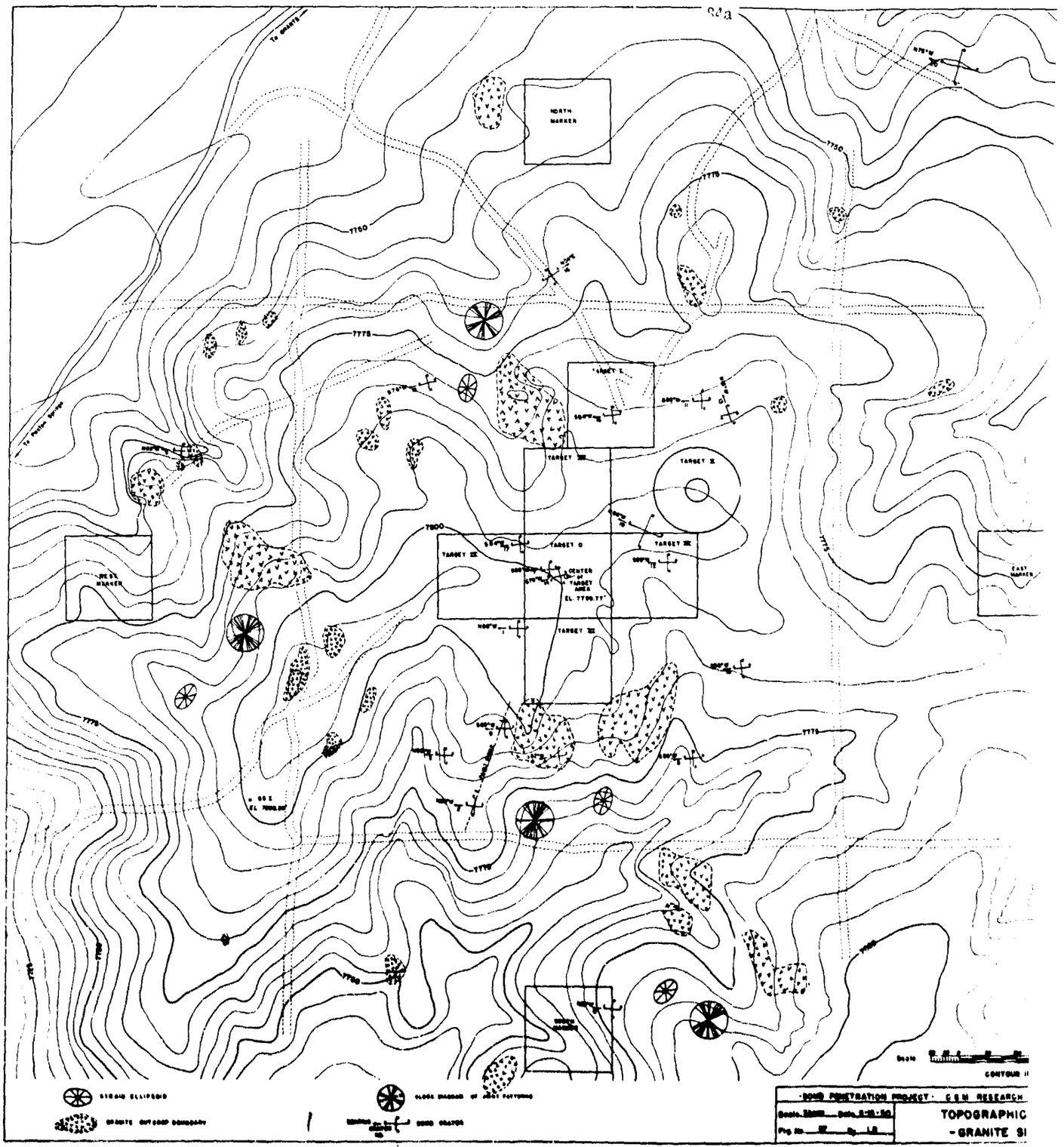

NORTH MARKER
TARGET I
TARGET II
TARGET III
TARGET IV
TARGET V
TARGET VI
TARGET VII
TARGET VIII
CENTER OF TARGET AREA
EL. 7799.77'
WEST MARKER
EAST MARKER
7750
7775
7800
To Grants
To Paxton Springs
STRAIN ELLIPSOID
GRANITE OUTCROP BOUNDARY
CLOCK DIAGRAM OF JOINT PATTERNS
DOME CRATER
DOME PENETRATION PROJECT - C S M RESEARCH
TOPOGRAPHIC
- GRANITE SI

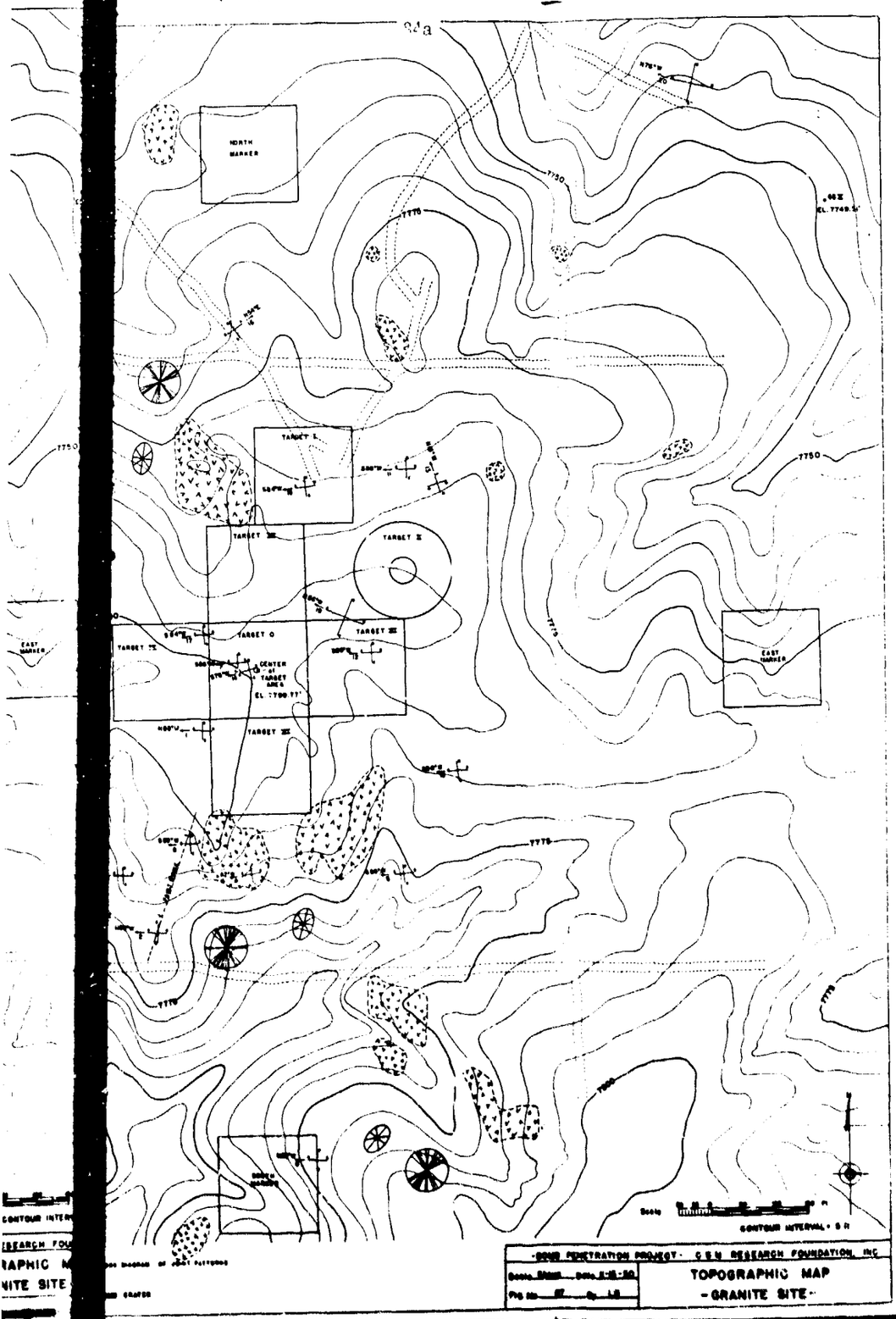

NORTH MARKER
TARGET I
TARGET II
TARGET III
TARGET O
CENTER of TARGET AREA
EL. 7700.77'
EAST MARKER
7750
7775
7770
Scale
CONTOUR INTERVAL = 5 ft
-DOME PENETRATION PROJECT- C S M RESEARCH FOUNDATION, INC
TOPOGRAPHIC MAP
-GRANITE SITE-

2

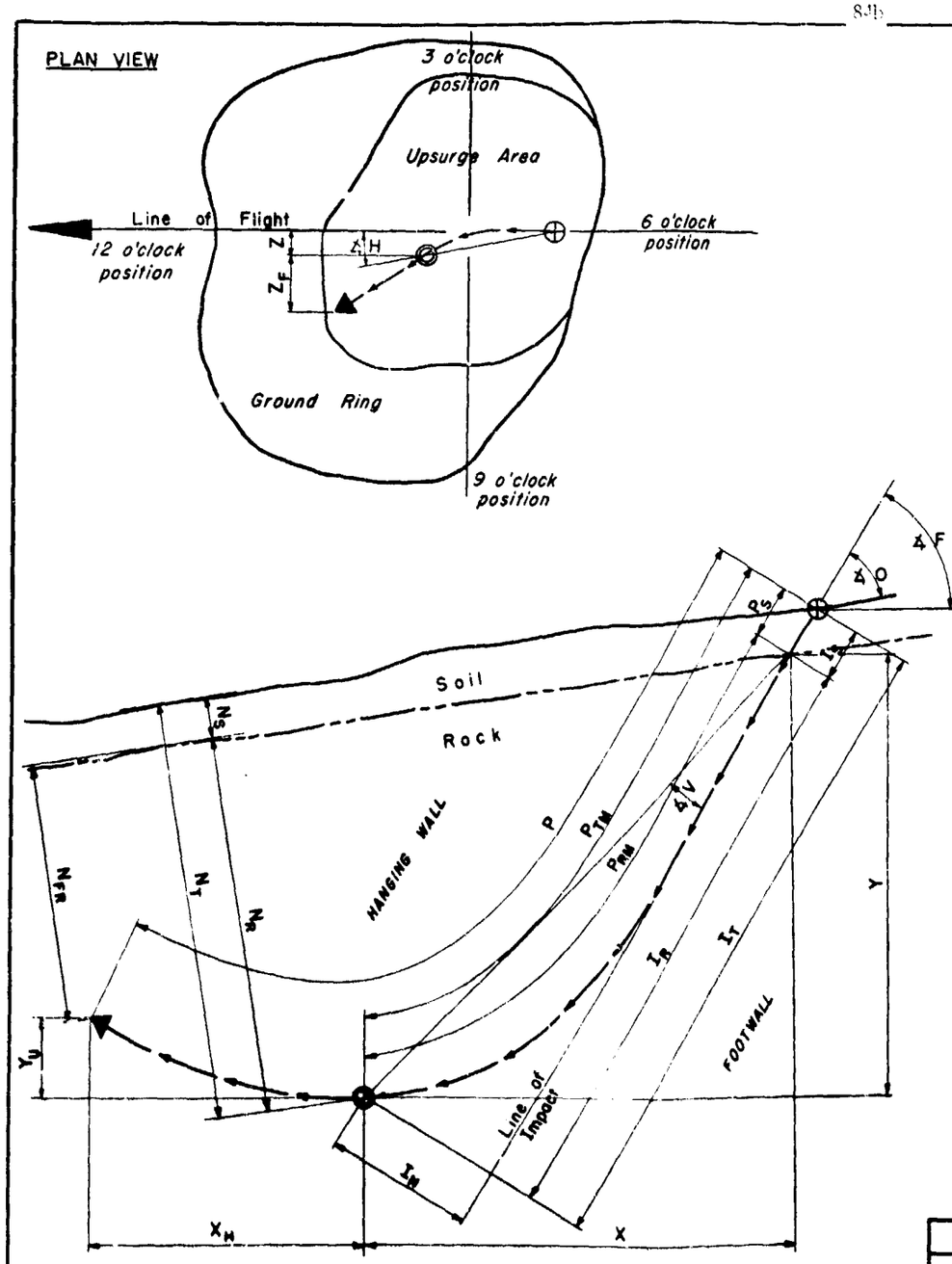

SECTION ON PATH OF BOMB

LEGEND

- X - Horizontal displac
- X_H - Horizontal displac final position
- Y - Vertical displac
- Y_U - Vertical displac final position
- Z - Horizontal devia penetration
- Z_F - Horizontal devia
- N_{FR} - Penetration norm
- P_S - Path length in
- P_{RM} - Path length in
- P_{TM} - Path length, s penetration
- P - Total path len
- N_S - Normal thickne
- N_R - Normal thickne
- N_T - Normal thicknes
- I_S - Inclined distanc line of impact
- I_R - Inclined distanc line of impact
- I_T - Inclined distanc along line of
- I_N - Perpendicular d at maximum p
- ∡F - Angle of fall
- ∡O - Angle of impac
- ∡H - Angle of horiz
- ∡V - Vertical deviat impact
- ⊕ - Point of impa
- ◎ - Point of maxir
- ← - Final nose po
- ←← - Path of bomb

NOTE: - All measuremer

-BOMB PENETRATION PR
Scale NONE Date 1-3-51
Fig. No. 88 By LB

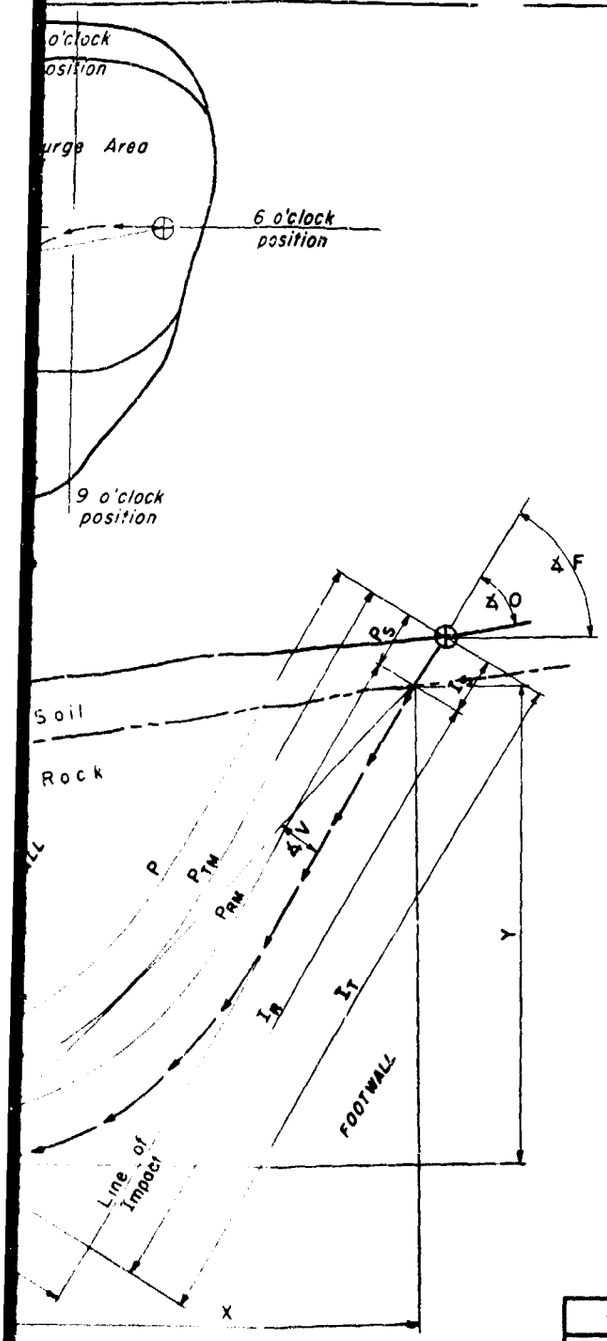

ON PATH OF BOMB

LEGEND

- X - Horizontal displacement of nose at maximum penetration, (rock)
- X_H - Horizontal displacement of nose, maximum penetration to final position
- Y - Vertical displacement of nose at maximum penetration, (rock)
- Y_U - Vertical displacement of nose, maximum penetration to final position
- Z - Horizontal deviation from line of flight to maximum penetration
- Z_F - Horizontal deviation, maximum penetration to final position
- N_{FR} - Penetration normal to rock surface at final position
- P_S - Path length in soil along arc
- P_{RM} - Path length in rock along arc at maximum penetration
- P_{TM} - Path length, soil and rock, along arc at maximum penetration
- P - Total path length along arc
- N_S - Normal thickness of soil at maximum penetration
- N_R - Normal thickness of rock at maximum penetration
- N_T - Normal thickness, soil and rock, at maximum penetration
- I_S - Inclined distance, at maximum penetration, in soil, along line of impact
- I_R - Inclined distance, at maximum penetration, in rock, along line of impact
- I_T - Inclined distance, at maximum penetration, soil and rock, along line of impact
- I_N - Perpendicular distance from line of impact to bomb nose at maximum penetration
- $\measuredangle F$ - Angle of fall
- $\measuredangle O$ - Angle of impact
- $\measuredangle H$ - Angle of horizontal deviation from line of flight
- $\measuredangle V$ - Vertical deviation at maximum penetration from line of impact
- ⊕ - Point of impact
- ◎ - Point of maximum penetration
- ← - Final nose position
- ←← - Path of bomb nose

NOTE: - All measurements to nose of bomb

-BOMB PENETRATION PROJECT- C S M RESEARCH FOUNDATION, INC.	
Scale NONE Date 1-3-51 Fig. No 88 By LB	DIAGRAM OF CRATER MEASUREMENTS

2 Fig. 88

BALLISTIC DATA															CRATER MEASUR															
GROUP NUMBER	C.S.M. BOMB NO.	DATE OF DROP (MAR.)	MISSION NUMBER	AIR FORCE BOMB NUMBER	TYPE OF BOMB	ACTUAL WEIGHT OF BOMB (lb)	PLANE'S AIR SPEED (mph)	ALTITUDE ABOVE TARGET (ft)	STRIKING VELOCITY (fps)	ANGLE OF FALL (°)	TIME OF FALL (sec)	PLANE'S BEARING	ENERGY OF IMPACT ($ft\cdot lb \times 10^6$)	IMPACT POINT	IMPACT ELEVATION (ft)	ANGLE OF IMPACT (°)	X	X_H	Y	Y_U	Z	Z_F	N_{FR}	P_S	P_{RM}	P_{TM}	P	N
I	1	9	2	3	AP	1652	274	9200	845	63	23	N58W	18.35	M6	7802	66	5.20	0	5.90	0	0	0	6.05	1.65	7.72	9.37	9.37	1
	2	9	2	9	AP	1652	272	9200	843	63	23	S84W	18.26	E8	7783	77 1/4	5.90	0	9.07	0	0.20	0	9.10	1.40	10.85	12.25	12.25	1
	3	9	2	2	AP	1642	274	9200	845	63	—	N58W	18.24	D	7786	56	4.00	0	7.33	0	0.70	0	6.22	0.20	8.11	8.31	8.31	0
II	4	9	2	7	AP	1638	305	18000	1077	68	32	S82W	29.55	E7	7784	78	3.78	0	3.95	0	0.70	0	4.15	1.25	5.25	6.50	6.50	1
	5	9	2	1	AP	1648	304	18000	1077	68	31	S86W	29.73	G8	7772	60	6.20	0	9.22	0	1.25	0	7.35	1.28	11.40	12.68	12.68	2
	6	9	2	8	AP	1640	307	18000	1079	68	29	N86W	29.70	—	7777	71	4.62	-1.95	4.85	3.00	1.[illegible]	0.15	1.95	0	6.70	6.70	10.20	0
III	7	7	1	4	AP	1642	332	30000	1250	72	42	S88W	39.91	O	7796	74 3/4	3.70	0	14.14	0	1.45	0	14.50	1.58	14.70	16.28	16.28	1
	8	7	1	5	AP	1646	350	30000	1252	70 1/2	42	S89W	40.14	E7	7793	68 1/2	8.90	0	9.88	0	1.80	0	9.80	0.75	13.52	14.27	14.27	0
	9	7	1	6	AP	1646	354	30000	1253	70 1/2	41	N85W	40.21	A4	7748	55 1/2	3.68	0	8.80	0	0.20	0	7.82	1.40	9.50	10.90	10.90	1
IV	10	11	3	11	SAP	2058	271	9200	824	62 1/2	22	S86W	21.73	H7	7786	64 1/4	6.50	0	7.22	0	0.22	0	7.28	0.65	9.72	10.37	10.37	0
	11	11	3	12	SAP	2056	279	9200	827	62	22	S88W	21.87	O3	7786	68 1/2	3.42	0	3.75	0	0.90	0	3.85	2.10	5.15	7.25	7.25	1
	12	11	3	13	SAP	2053	300	9200	836	60 1/2	22	S89W	22.32	III	7793	58	4.23	4.28	4.15	0.95	1.70	1.35	2.90	0.95	5.90	6.85	11.20	0
~~IV~~	14	14	4	16	SAP	2060	280	14000	957	66 1/2	27	S76W	29.35	M6	7800	68	4.90	0	5.15	0	2.60	0	5.77	1.40	7.22	8.62	8.62	
V	13	11	3	10	SAP	2056	311	18000	1044	68	31	N16W	34.86	O4	7787	66 1/2	3.25	—	4.00	—	—	—	3.85	2.58	5.15	7.73	7.73	
	15	14	4	18	SAP	2075	303	18000	1040	68 1/2	30	S84W	34.91	F4	7786	70 1/2	6.68	0	7.42	0	4.10	0	7.25	2.10	10.02	12.12	12.12	
	18	14	4	15	SAP	2079	302	18000	1040	68 1/2	32	S76W	34.98	D3	7783	76	3.38	3.40	5.40	5.15	0.40	3.15	0.75	0.55	6.40	6.95	13.20	
VI	16	14	4	17	SAP	2047	340	30000	1172	71 1/2	43	N54W	43.74	E2	7771	71 1/2	2.65	0	3.30	0	0	0	3.35	1.32	4.25	5.57	5.57	
	17	14	4	14	SAP	2079	340	30000	1172	71 1/2	42	S84W	44.42	E5	7796	63 1/2	2.62	-2.00	6.50	1.75	0.50	3.00	4.60	0.42	6.88	7.30	10.00	
VII	19	18	5	19	SAP	25265	310	18000	1144	67	31	N66W	514.40	F5	7796	67	14.90	0	22.30	0	1.00	0	22.20	0.90	26.80	27.70	27.70	
	20	20	6	20	SAP	25215	311	26000	1320	70 1/2	—	N76W	683.50	—	7742	70 1/2	15.10	0	38.00	0	6.00	0	37.60	1.10	40.70	42.00	42.00	

NOTES

(1) Bombs 2 and 8 hit in a lamprophyre dike.

(2) Abnormally thick weathered zone.

(3) Hit side of an outcrop and bounced back.

(4) Highly sheared zone.

(5) Highly schistose area.

(6) Bomb flew out of crater with high remaining energy. Final resting place 1620' N 11 E from impact point.

(7) Abnormal weather

(8) The total volume

ASURE CRATER MEASUREMENTS

P	Ns		X_H	Y	Y_U	Z	Z_F	N_{FR}	P_S	P_{RM}	P_{TM}	P	N_S	N_R	N_T	I_S	I_R	I_T	I_N	ΔH	ΔV	CRATER VOLUME IN ROCK (cu ft)	CRATER VOLUME IN SOIL (cu ft)	CRATER VOLUME TOTAL (cu ft)	CRATER RADIUS "R" (ft)	CRATER DEPTH "D" (ft)	R/D RATIO	NOTES	C.S.M. BOMB NO.
9.37	1.6	0	0	5.90	0	0	0	6.05	1.65	7.72	9.37	9.37	1.62	6.05	7.67	1.65	7.60	9.25	1.85	0	13 3/4	204	121	325	4.89	7.40	0.661		1
2.25	1.2	0	0	9.07	0	0.20	0	9.10	1.40	10.85	12.25	12.25	1.20	9.10	10.30	1.40	10.70	12.13	1.23	1 1/2L	6 1/2	166	117	283	4.49	10.50	0.428	(1)	2
8.31	0.4	0	0	7.33	0	0.70	0	6.22	0.20	8.11	8.31	8.31	0.42	6.22	6.64	0.20	8.09	8.29	0.35	10 L	2 1/2	135	33	168	4.30	6.60	0.652		3
6.50	1.1	8	0	3.95	0	0.70	0	4.15	1.25	5.25	6.50	6.50	1.15	4.15	5.30	1.25	4.52	5.77	2.28	10 1/2R	26 3/4	147	96	243	4.84	5.20	0.931	(2)	4
2.68	2.2	0	0	9.22	0	1.25	0	7.35	1.28	11.40	12.68	12.68	2.25	7.35	9.60	1.28	11.00	12.28	2.20	11 1/2L	11 1/4	235	62	297	4.99	11.40	0.438		5
0.20	0	2	-1.95	4.85	3.00	1.05	0.15	1.95	0	6.70	6.70	10.20	0	4.92	4.92	0	6.13	6.13	2.66	13 L	23 1/2	202	0	202	5.22	4.00	1.305	(3)	6
6.28	1.4	0	0	14.14	0	1.45	0	14.50	1.58	14.70	16.28	16.28	1.40	14.4	15.8	1.58	14.65	16.23	-0.30	23 1/2R	-3	116	94	210	3.68	16.00	0.230	(4)	7
4.27	0.5	0	0	9.88	0	1.80	0	9.80	0.75	13.52	14.27	14.27	0.50	9.80	10.30	0.75	12.25	13.00	5.05	11 3/4L	22 1/2	327	79	406	3.59	8.50	0.422	(1)	8
0.90	1.1	8	0	8.80	0	0.20	0	7.82	1.40	9.50	10.90	10.90	1.18	7.82	9.00	1.40	9.53	10.93	0.55	3 R	3 1/4	235	85	320	4.62	9.50	0.486		9
0.37	0.	0	0	7.22	0	0.22	0	7.28	0.65	9.72	10.37	10.37	0.65	7.28	7.93	0.65	9.40	10.05	2.48	2 L	14 3/4	286	57	343	5.27	8.00	0.659	(5)	10
7.25	1.	2	0	3.75	0	0.90	0	3.85	2.10	5.15	7.25	7.25	1.87	3.85	5.72	2.10	3.85	5.95	1.50	15 1/4R	21 1/4	103	142	245	4.82	5.90	0.817		11
11.20	0.	3	4.28	4.15	0.95	1.70	1.35	2.90	0.95	5.90	6.85	11.20	0.70	4.15	4.85	0.95	5.80	6.75	1.70	23 3/4L	16 1/4	289	78	367	5.92	5.30	1.116		12
8.62	1.	0	0	5.15	0	2.60	0	5.27	1.40	7.22	8.62	8.62	1.87	5.27	7.14	1.40	6.70	8.10	2.32	32 L	19	375	254	629	6.30	7.40	0.851		14
7.73	2.	5	—	4.00	—	—	—	3.85	2.58	5.15	7.73	7.73	2.35	3.85	6.20	2.58	4.85	7.43	1.60	0	18 1/4	186	401	587	7.86	6.10	1.288	(6)	13
12.12	2.	8	0	7.42	0	4.10	0	7.25	2.10	10.02	12.12	12.12	2.30	7.25	9.55	2.10	9.30	11.40	3.68	37 3/4L	21 1/2	146	176	322	5.08	10.00	0.508	(7)	15
13.20	1.	8	3.40	5.40	5.15	0.40	3.15	0.75	0.55	6.40	6.95	13.20	1.60	4.72	6.32	0.55	6.25	6.80	1.25	6 3/4R	11 1/4	247	30	277	5.92	6.20	0.955		18
5.57	1.	5	0	3.30	0	0	0	3.35	1.32	4.25	5.57	5.57	1.18	3.35	4.53	1.32	4.00	5.32	1.48	0	20 1/4	112	154	266	6.00	4.60	1.304		16
10.00	3.	2	-2.00	6.50	1.75	0.50	3.00	4.60	0.42	6.88	7.30	10.00	0.35	6.15	6.50	0.42	6.95	7.37	0.55	11 L	4 1/2	369	30	399	6.00	7.10	0.845		17
27.70	0.	0	0	22.30	0	1.00	0	22.20	0.90	26.80	27.70	27.70	0.80	22.20	23.00	0.90	26.30	27.20	4.95	3 3/4L	10 3/4	-	-	-	-	-	-	OK (8)	19
42.00	1.	0	0	38.00	0	6.00	0	37.60	1.10	40.90	42.00	42.00	1.05	37.60	38.60	1.10	40.90	42.00	0	23 1/2R	0	-	-	-	-	-	-	OK (8)	20

weatheri

l volume

high remaining energy. Final resting place
nt.

(7) Abnormal weathering and some structural control.

(8) The total volume of rock broken was not excavated.

BOMB PENETRATION PROJECT- CSM RESEARCH FOUNDATION, INC.

Scale — Date 2-18-51
Fig. No. 89 By LB

BALLISTIC & CRATER DATA
ZUNI GRANITE

2

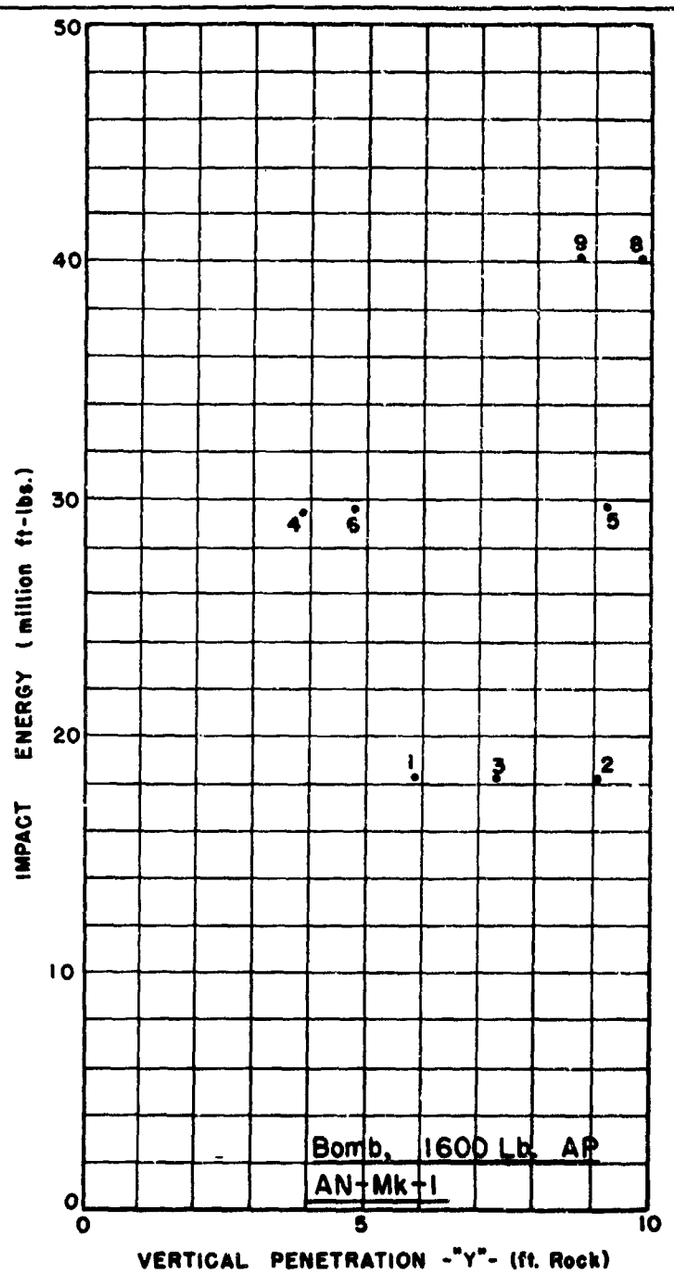
IMPACT ENERGY (million ft-lbs.)
VERTICAL PENETRATION -"Y"- (ft. Rock)
Bomb, 1600 Lb. AP
AN-Mk-1

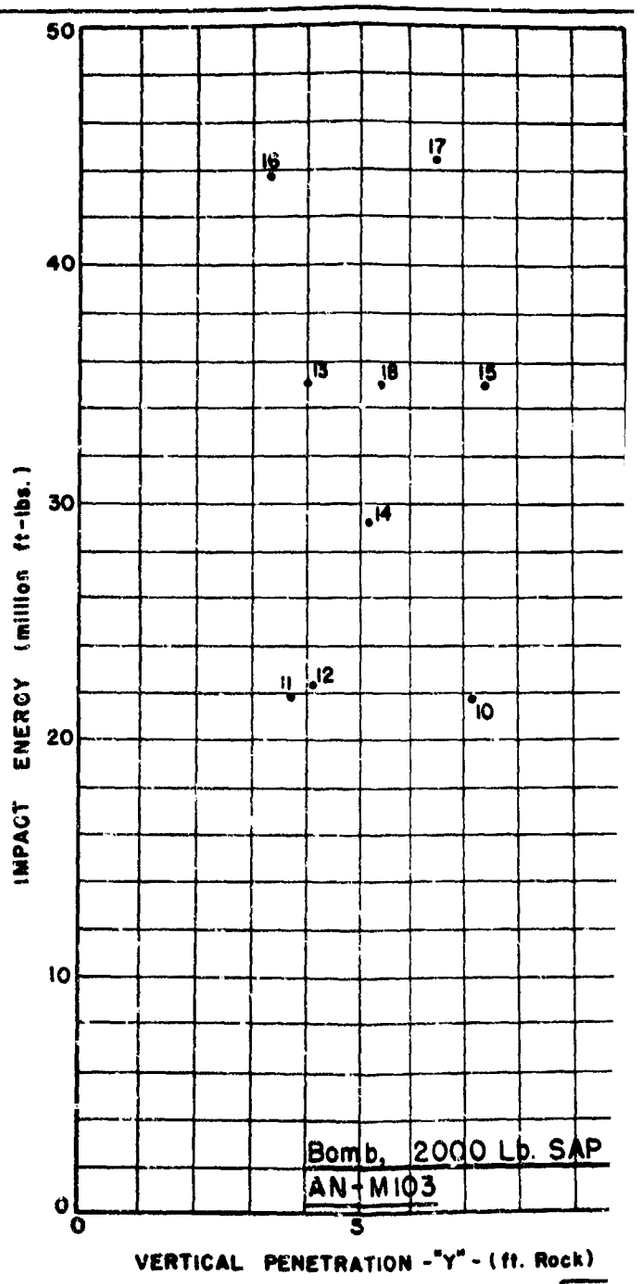
IMPACT ENERGY (million ft-lbs.)
VERTICAL PENETRATION -"Y"- (ft. Rock)
Bomb, 2000 Lb. SAP
AN-M103

-BO
Sca
Fig.

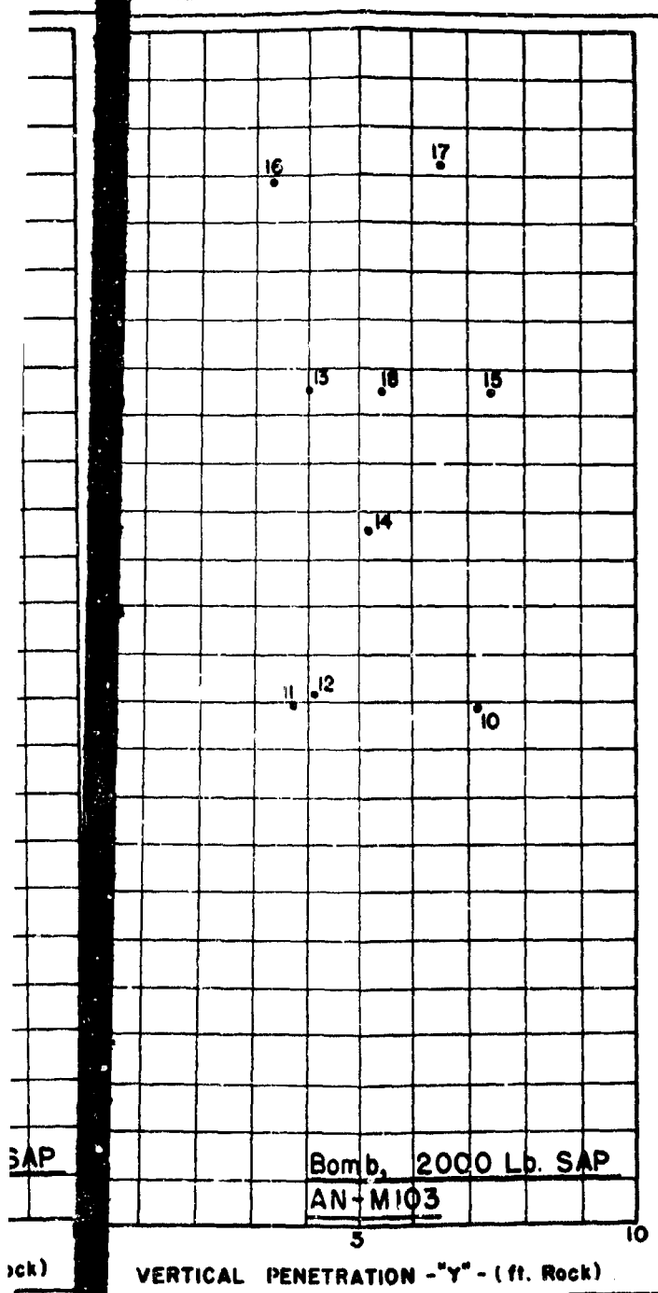

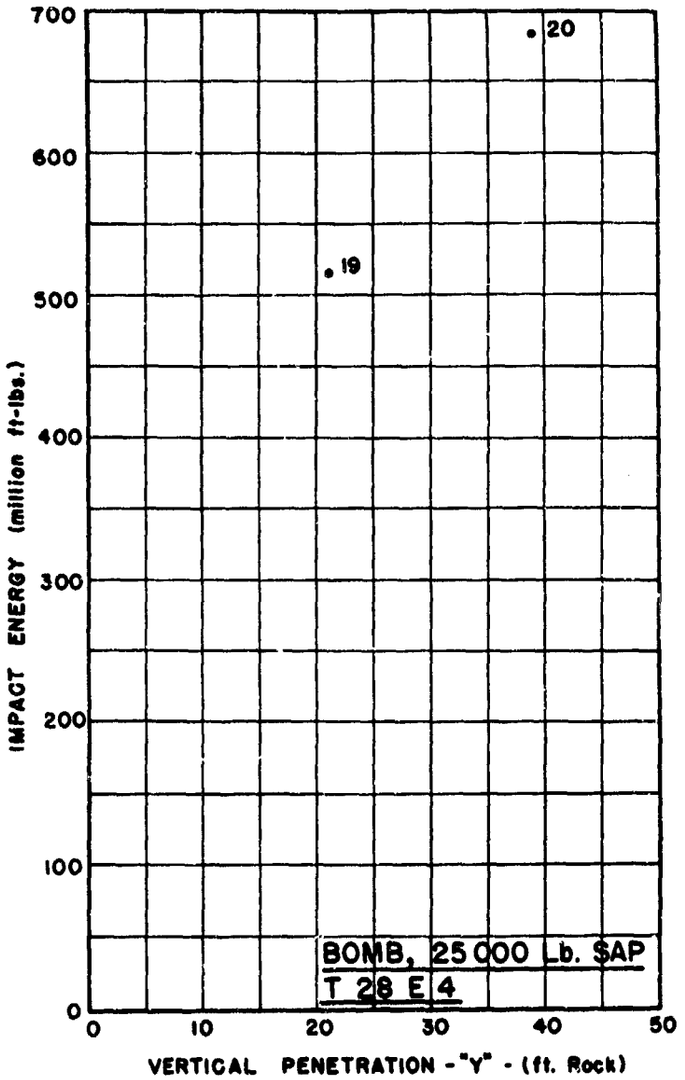

-BOMB PENETRATION PROJECT- GSM RESEARCH FOUNDATION, INC.

Scale ——— Date 3-7-51

Fig. No. 90 By LB

VERTICAL PENETRATION vs IMPACT ENERGY
—ZUNI GRANITE—

Fig. 90

2

fin at impact. In some instances the fins were knocked off at impact. The energy at impact equals

$$KE=\frac{w}{2g}V^2$$

where

w = weight of bomb, fuse, and fins, pounds

V = impact velocity, feet per second

g = 32.14 feet per second per second at latitude 35 degrees N.

In the table, impact energy is given in millions of foot-pounds, and in the preliminary analysis no correction was made for possible loss of the fins, because dispersion was so great that a correction at this stage would be of little value.

The impact point column refers to the coordinate system on the spotting map. (See Fig. 18.) The angle of impact differs from the angle of fall and includes a topography correction. (See Fig. 88.)

The columns X through ΔV are defined and illustrated in the diagram of crater measurements (Fig. 88). Crater volumes in rock, in soil, and in rock and soil were determined from plaster models constructed to scale from the plan and cross section. The volumes were computed using the weight and density of galena required to fill the specified portion of the cavity in the model.

The crater radius, R, is the radius of a circle whose area equals the area of the plan view of the crater. Crater areas were measured with a planimeter. The crater depth, D, is the distance to the deepest point in the crater measured normal to the ground surface. The quantity R/D is the ratio of the radius, as defined, to the depth, as defined.

3—Vertical Penetration of 1600 AP, 2000 SAP, and 25,000 SAP Bombs in Granite

The dispersion of data for test drops in granite is greater than for the test drops in sandstone. A high dispersion should not be interpreted as indicating that certain data should be eliminated; rather it should be recognized that the dispersion is caused by variations in the geologic properties of the rock and that in a normal granite a wide variation in geologic properties is truly representative of the rock type. It is difficult to determine the cause for the difference in penetration between bombs of the same type released from the same altitude at the same plane speed and striking the same type of rock, but the explanation must be related to the physical and the elastic properties of the rock.

Of the several measurements summarized on the data sheet it seems preferable at this phase to compare vertical penetration at various values of kinetic energy rather than to make any of several other possible comparisons. In Fig. 90 the vertical penetration of 1600 AP, 2000 SAP, and 25,000 SAP bombs in granite has been plotted against impact energy. The vertical penetration equals the Y distance in Fig. 89. No attempt has been

made to correct for soil thickness, topography, obliquity, or geologic properties of the rock. Geologic features had a pronounced effect upon 1600 AP Bombs 2, 4, 6, 7, and 8. Semi-armor-piercing bombs show a tendency to rebound from the crater. Bomb 13 bounced and came to rest 1620 feet from the point of impact. Bomb 16 bounced and came to rest 20 feet from the crater.

Bouncing occurs after penetration; it is not a simple matter of rebound at impact. The rebound for Bomb 16 might be described as resulting from the rebound of the "wedge" of rock containing the bomb. The "wedge" was formed by intersecting and inward-dipping joint planes. The photograph, Fig. 91, shows the joint system in the Zuni granite that controlled the rebound of Bomb 16 and the manner in which the wedge of rock was removed, leaving the crater nearly clean. The rebound of Bomb 13 was influenced by jointing, but the effect of the joints was to displace the nose of the bomb horizontally and thus rapidly increase the vertical deviation of the bomb from the line of flight. The photograph, Fig. 92, shows the path of Bomb 13 leaving the crater.

Penetration is less where rebounding occurs than where it does not occur. Moreover, the decrease in vertical penetration due to rebounding is not constant, but varies with the energy remaining in the bomb as it emerges from the crater. It may be noted by referring to Fig. 90 that the

Fig. 91
Control of Rebound by Joint Planes

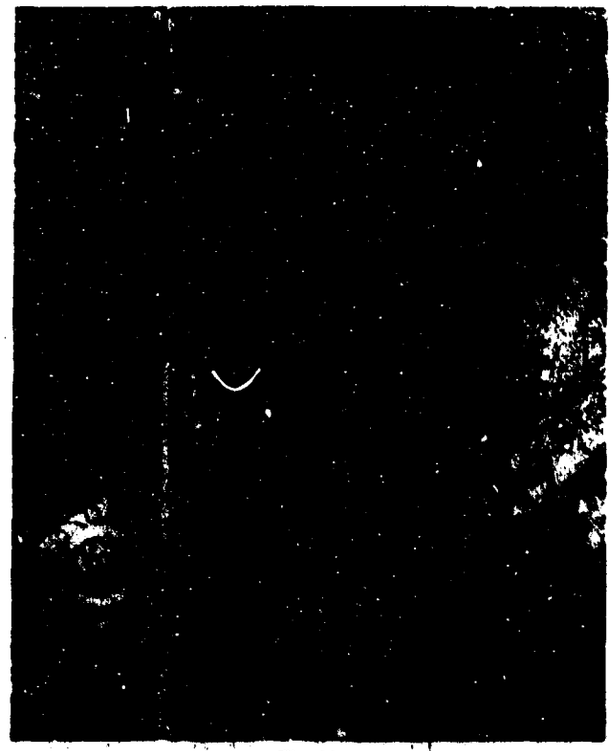

Fig. 92
Path of Bomb 13 Leaving Crater

penetration of SAP Bombs 13 and 16 is less than that of other SAP bombs released from the same altitude.

The penetration data for the two 25,000-pound semi-armor-piercing bombs dropped at the granite site are compiled in Fig. 89, Group VII. Maps of the resulting craters are included in the appendix of this report and in Figs. 97 and 98. Because of the expense involved, only two 25,000 SAP bombs were dropped. Vertical penetration of Bomb 19, released from 18,000 feet above the target, and Bomb 20, released from 26,000 feet above the target, is plotted against impact energy, in Fig. 90. The fins of both bombs remained attached to the full depth of penetration.

4—Crater Shape as Related to Impact Energy

Figure 93 is a photograph of the apparent crater of Bomb 1, a 1600-pound armor-piercing bomb released 9200 feet above the target. The

view is taken from the 6 o'clock position looking in the direction of the line of flight. The level rod on the ground is parallel to the line of flight. The near end of the level rod is slightly to the right of the point of impact. The depressed area to the left of the level rod is the "upsurge area," and the rest of the flyrock is part of the "ground ring." The broken material within the ground ring consists predominantly of chunks of overburden and pieces of near-surface rock. The broken material within the upsurge area is much finer than that in the ground ring and consists predominantly of rock that has risen along the path of the bomb. The ground ring is elongated at right angles to the line of flight; the amount of flyrock to the rear of the point of impact is negligible.

The crater maps in the appendix show the apparent and the true craters for each bomb dropped during the tests. The distribution of flyrock is shown by the shape of the ground ring on each crater map and is influenced by the topography and by the geologic features within the crater area.

The photographs, Figs. 94 and 95, show how the crater shape changes with an increase in energy. There seems to be a tendency for the R/D ratio to increase with increasing energy until a certain critical energy is reached; the R/D ratio then begins to decrease. Figure 94 is arranged so that a comparison of the crater shapes produced by 1600-pound AP

Fig 93
Apparent Crater 1600 AP Bomb 1
Altitude Above Target 2300 Ft.

Fig. 94

Effect of Impact Energy Upon Crater Shape
Scale Models of Craters 3, 5, and 9
1600 AP Bombs

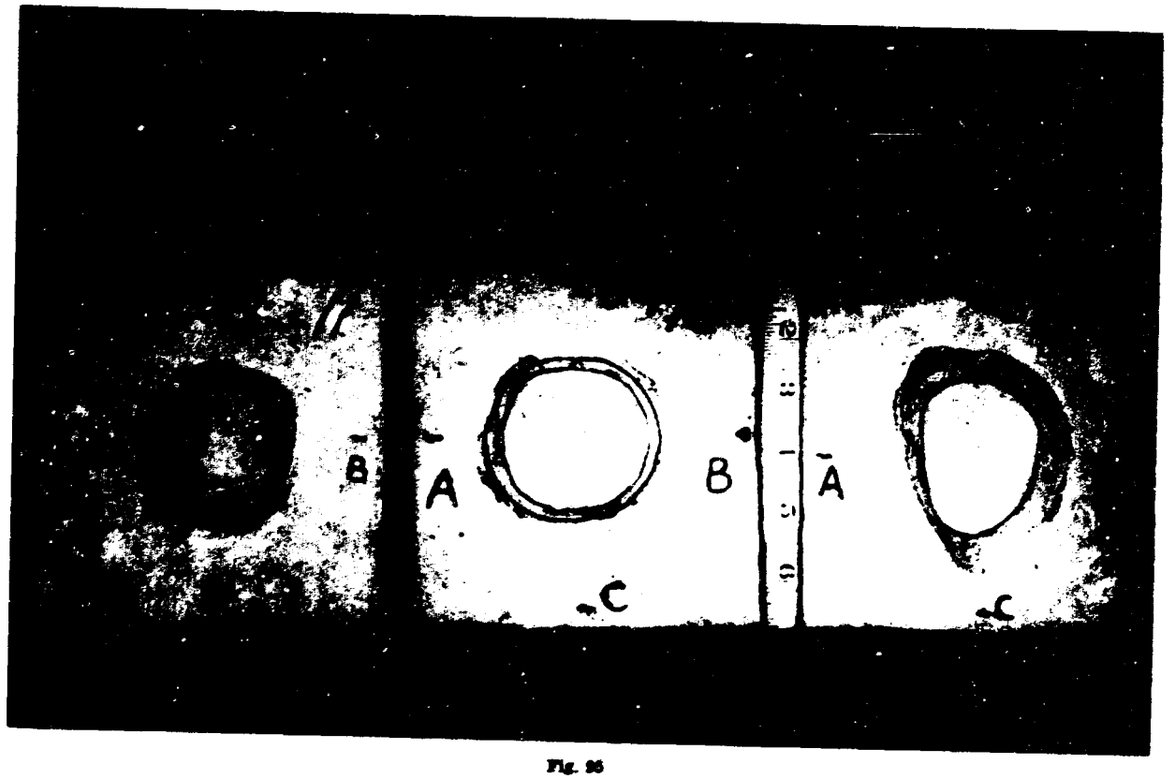

Fig. 26

Effect of Impact Energy Upon Crater Shape
Scale Models of Craters 11, 18, and 16
2000 SAP Bombs

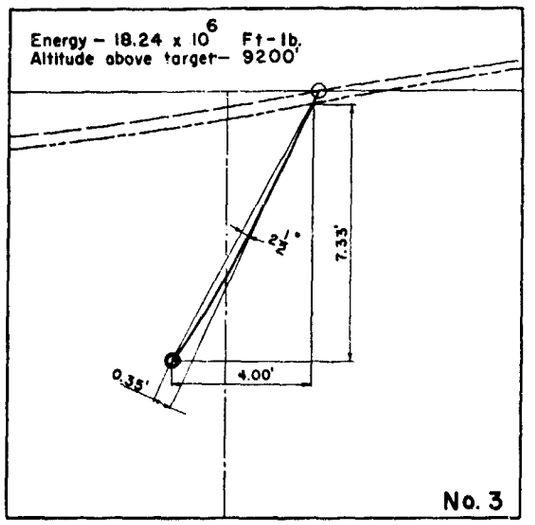

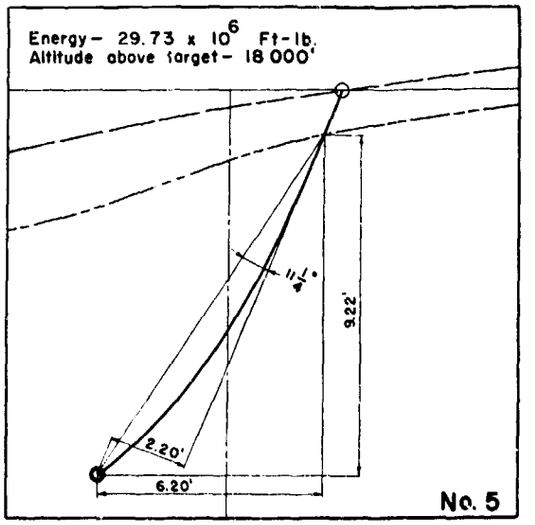

1600 LB. AP BOMB, AN-MK-1

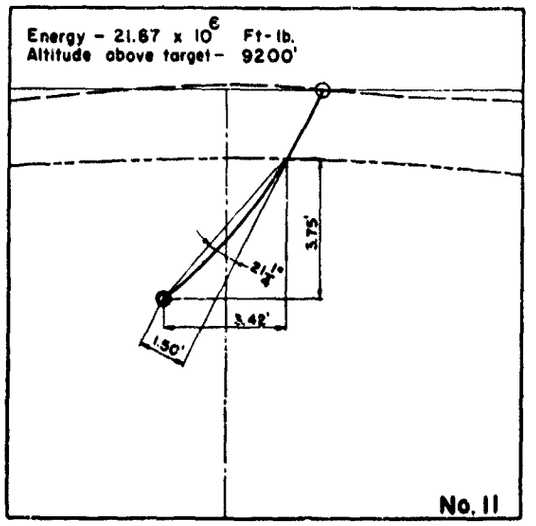

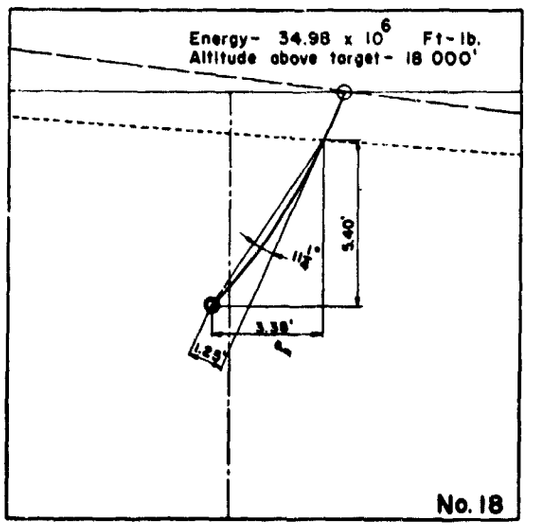

2000 LB. SAP BOMB, AN-M 10

-BOMB PENETRATION

Scale Shown Date 2-22-5

Fig. No. 96 By LB

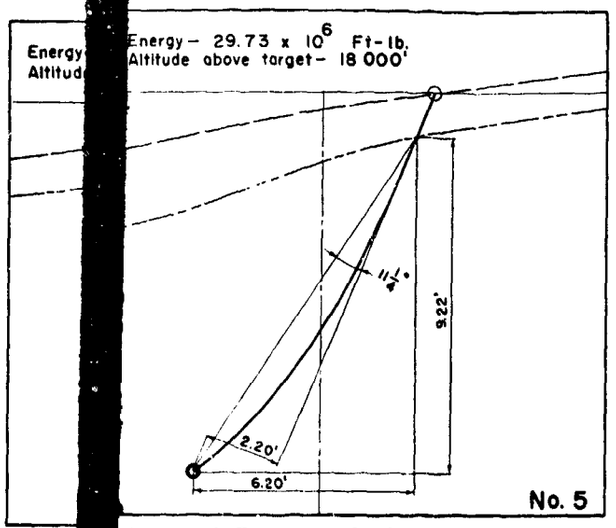

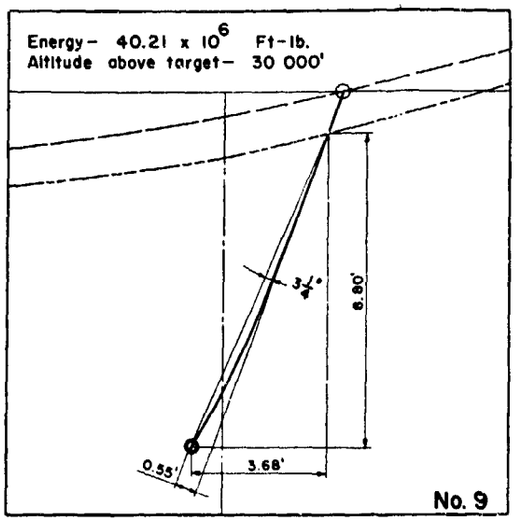

LB. AP BOMB, AN-MK-1

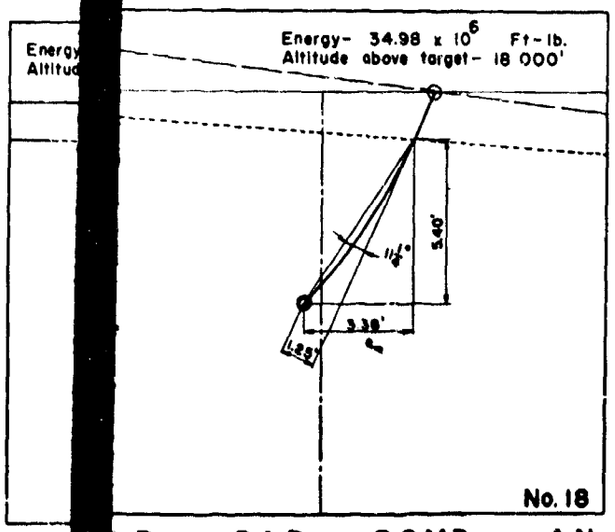

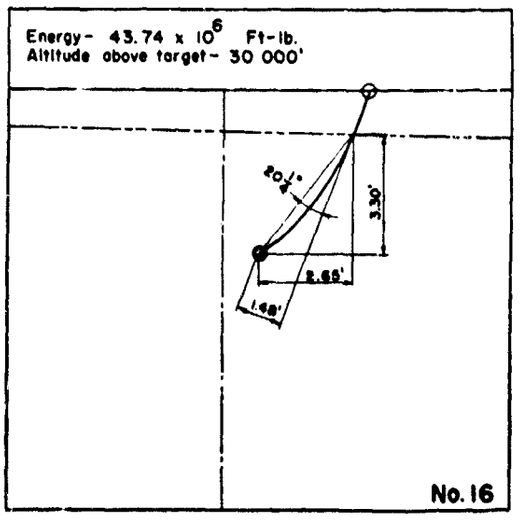

LB. SAP BOMB, AN-M103

-BOMB PENETRATION PROJECT- CSM RESEARCH FOUNDATION, INC.	
Scale Shown Date 2-22-51 Fig. No. 96 By LB	EFFECT OF ENERGY ON PATH SHAPE -GRANITE-

Fig. 96

2

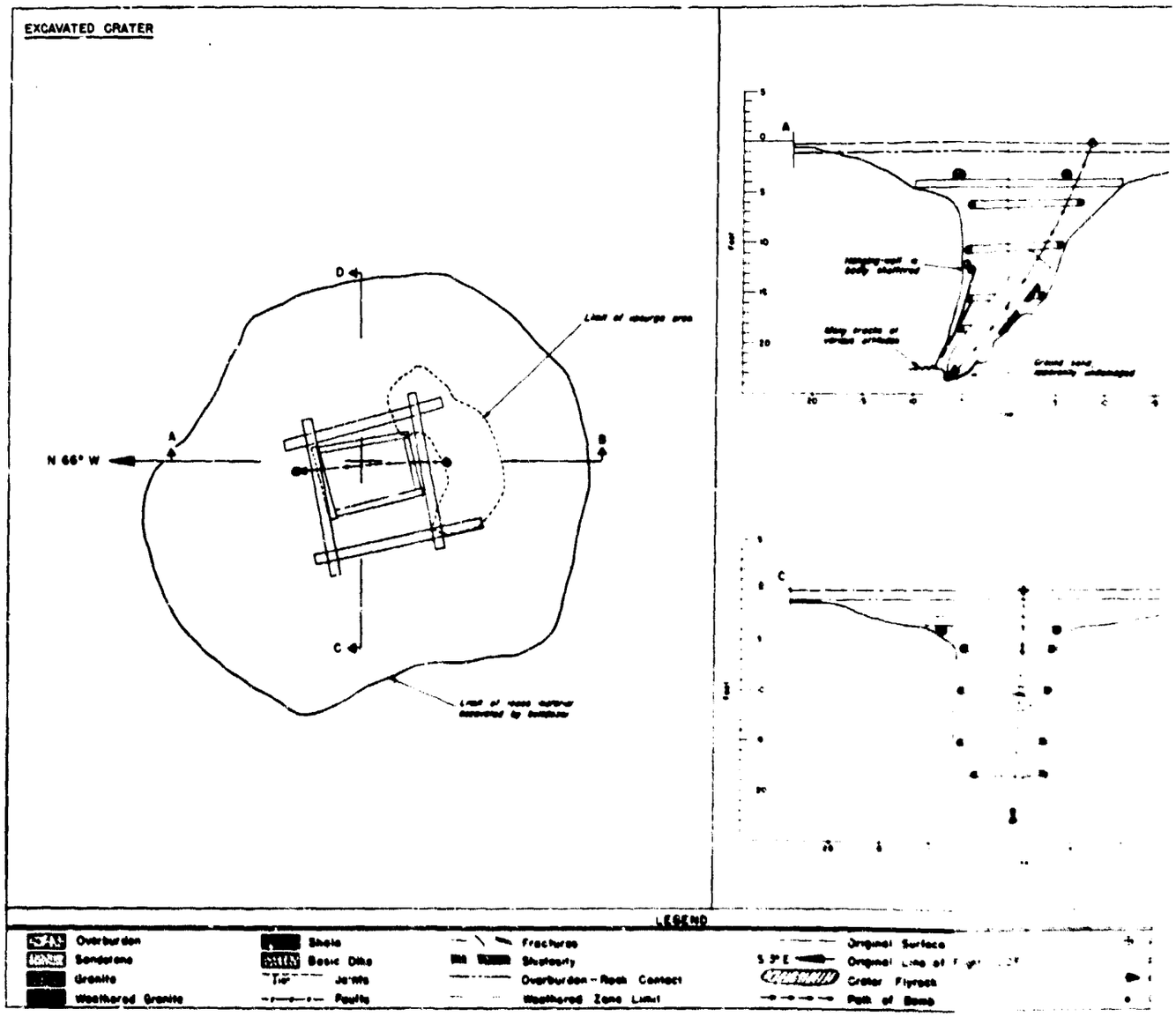
EXCAVATED CRATER
N 66° W
A
B
C
D
LEGEND
Overburden
Sandstone
Granite
Weathered Granite
Shale
Basic Dike
Joints
Faults
Fractures
Shistosity
Overburden - Rock Contact
Weathered Zone Limit
Original Surface
Crater Flyrock
Path of Bomb

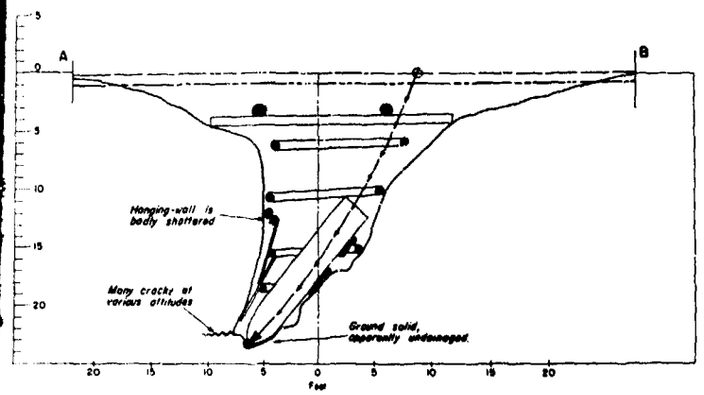

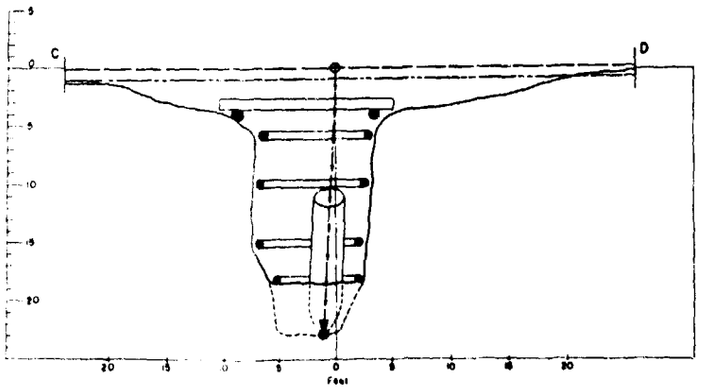

SECTION ON PATH OF BOMB

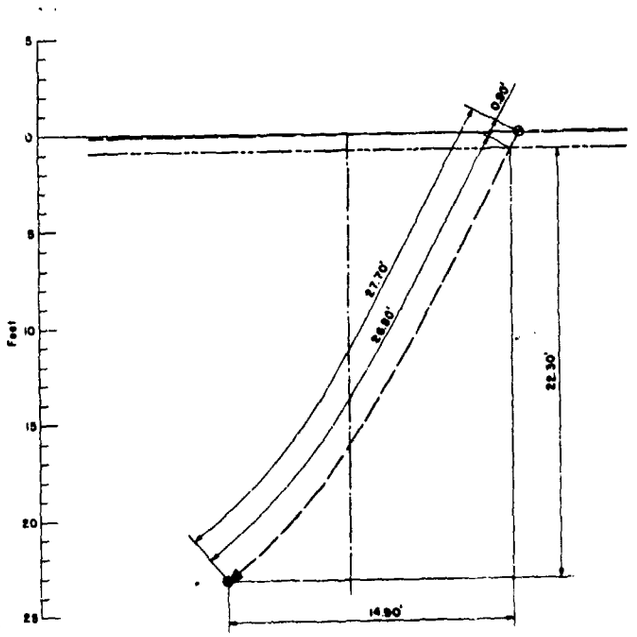

- BOMB PENETRATION PROJECT - C S M RESEARCH FOUNDATION, INC

Original Surface
S 5° E Original Line of Flight (LOF)
Crater Flyrock
Path of Bomb
Point of Impact
Point of Maximum Penetration
Final Nose Position
Center of Gravity of Bomb

CRATER NO. 19

Fig. No. 97

2

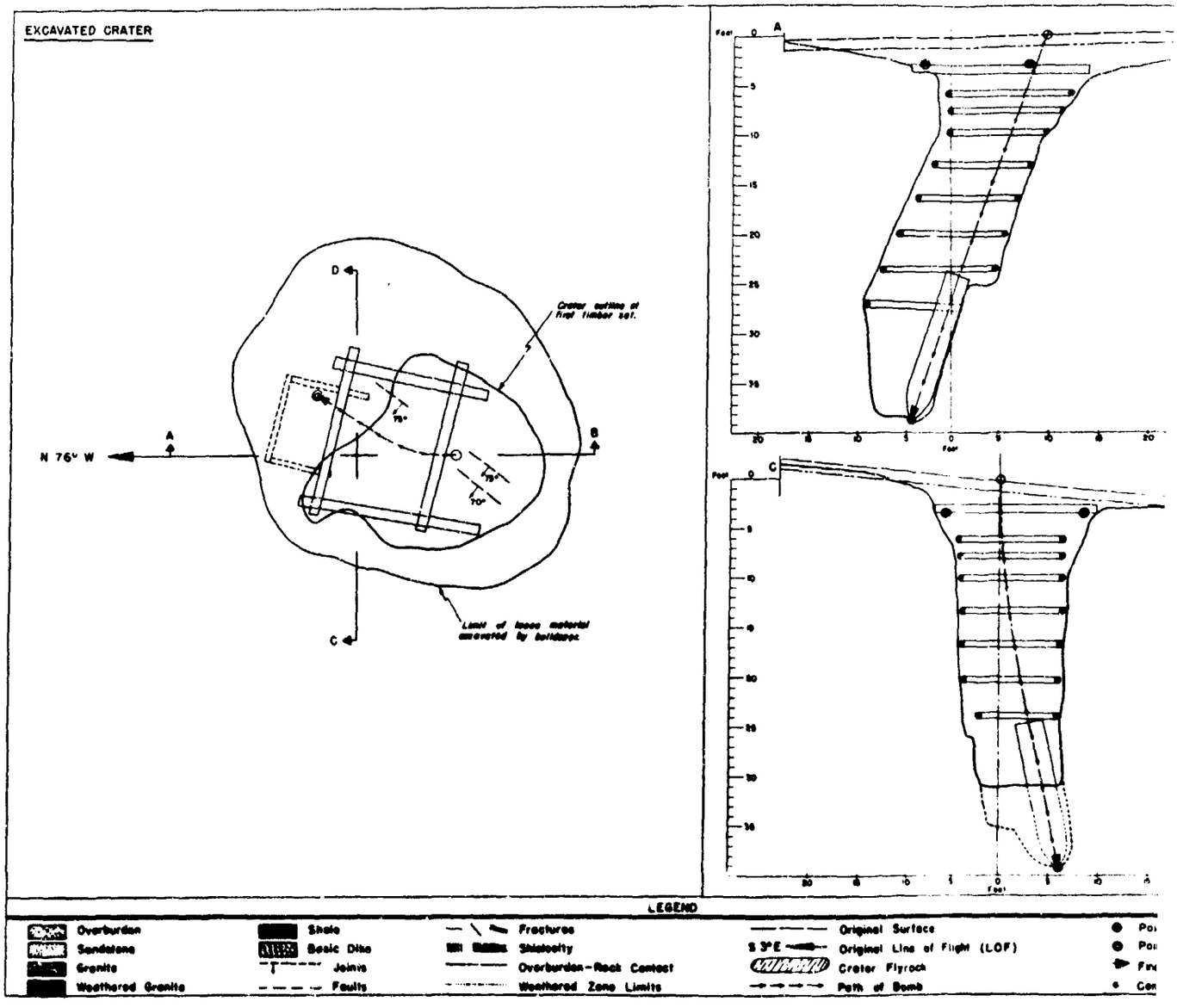
EXCAVATED CRATER
D
A
B
C
N 76° W
Crater outline at first timber set.
Limit of loose material excavated by bulldozer.
A
C
Feet
LEGEND
Overburden
Sandstone
Granite
Weathered Granite
Shale
Basic Dike
Joints
Faults
Fractures
Shatterbelt
Overburden-Rock Contact
Weathered Zone Limits
Original Surface
S 3°E Original Line of Flight (LOF)
Crater Flyrock
Path of Bomb

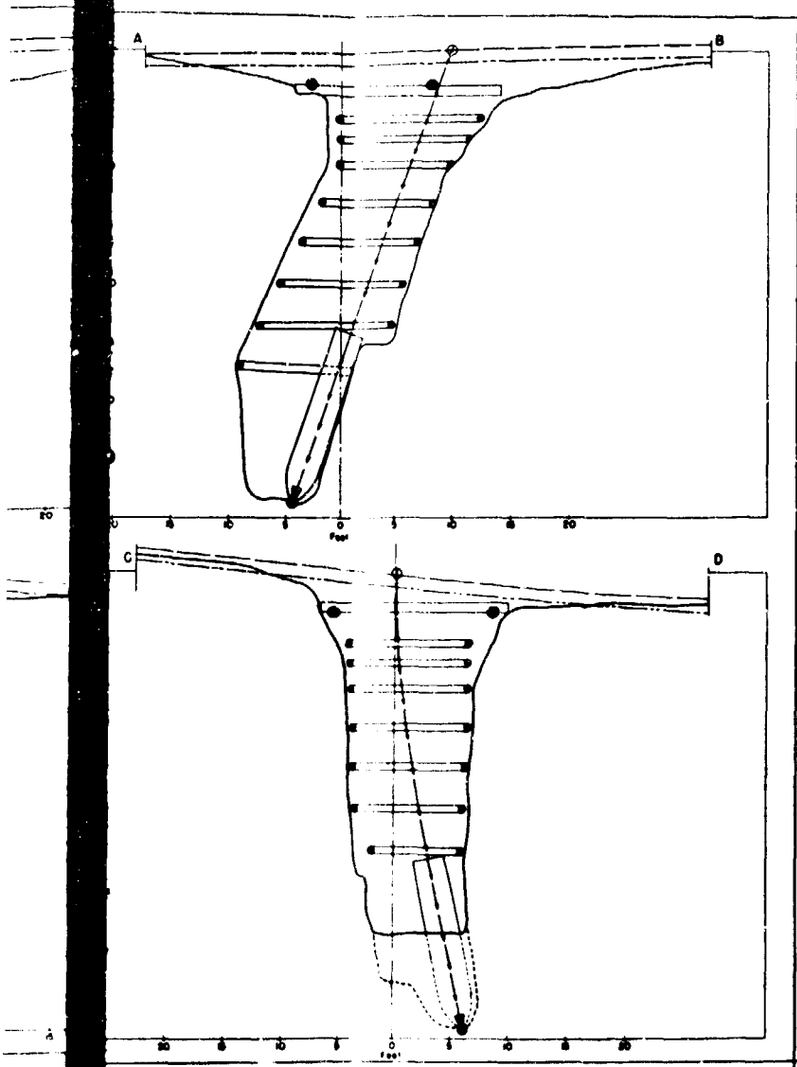

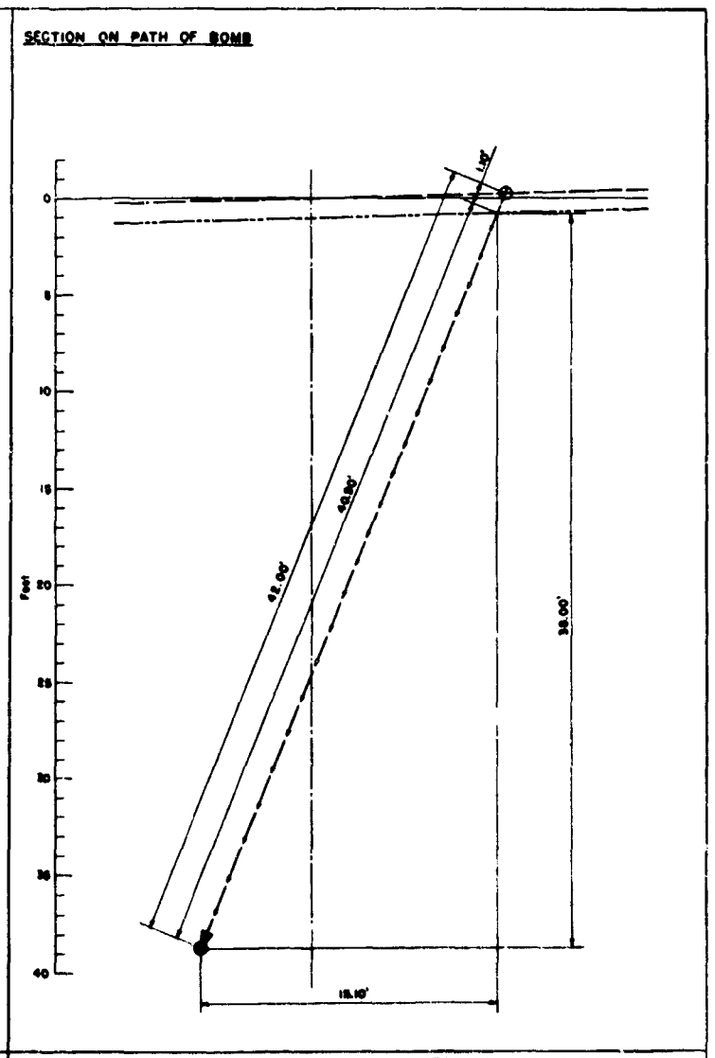

Original Surface
3°E Original Line of Flight (LOF)
Crater Flyrock
Path of Bomb
Point of Impact
Point of Maximum Penetration
Final Nose Position
Center of Gravity of Bomb

-BOMB PENETRATION PROJECT- C S M RESEARCH FOUNDATION, INC

CRATER NO. 20

Fig. No. 98

2

bombs dropped from altitudes of 9200, 18,000, and 30,000 feet may be obtained visually. Figure 95 is similarly arranged for 2000-pound SAP bombs, with the height of drop increasing to the right. The line of flight is the AB line on the models, and the numbers on each block are the C.S.M. bomb numbers. Cross sections along the AB lines are oriented in their proper position and rest on top of the model block. The soil-rock contact is shown by a heavy line in the model. In the model of Crater 18 two lines are shown: one represents the soil-weathered rock contact; the other represents the weathered-rock—unweathered-rock contact.

The additional cost necessary to determine the crater shape of the two 25,000-pound SAP bombs prevented the accumulation of similar data for the 25,000-pound SAP bombs, but it is unlikely that any additional fundamentals would have been learned.

5—Path Shape as Related to Impact Energy

A very noticeable change in the path of a bomb crater occurs with an increase in impact energy. There is a decided tendency for the path length to behave in the same manner as the crater shape; i.e., the length of the path increases up to a certain critical point; then a further immediate increase in impact energy results in a reduced rate of penetration, and perhaps in a reduced depth of penetration. The relations are the subject of a series of investigations that are discussed in the Analysis.

The paths of 1600 AP Bombs 3, 5, and 9 are shown in the top half of Figure 96, and the paths of 2000 SAP Bombs 11, 18, and 16 are shown in the bottom half. Angle V, a measure of the curvature of the path, is summarized for the two types of bombs at energies corresponding to release altitudes of 9200, 18,000, and 30,000 feet as follows:

Bomb Type	Bomb No.	Impact Energy, million ft-lb	V, degrees
1600 AP	3	18.24	2¼
1600 AP	5	29.73	11¼ max.
1600 AP	9	40.21	3¼
2000 SAP	11	21.87	21¼
2000 SAP	18	34.98	11¼ min.
2000 SAP	16	43.74	20¼

Curvature in the path can only be caused by the forces that resist the bomb as it passes downward into the medium. Because the momentum of the bomb decreases with depth, a change in the curvature denotes a change in the deviation and in the magnitude of the resisting forces. It will be noted from Fig. 96 and from the foregoing table that the behavior of the armor-piercing and the semi-armor-piercing bombs differs. The curvature of the path of the armor-piercing bomb first increases, then decreases with higher energies; whereas the curvature of the path of the semi-armor-piercing bomb first decreases, then increases. We conclude, therefore, that the resisting forces are functions not only of the rock properties and of the depth of action, but also of the bomb shape.

Figures 97 and 98 show the paths of the two 25,000 SAP bombs in

granite. It will be noted that the curvature of Bomb 20, which was released from the higher altitude, is less than that of Bomb 19. The path of the 25,000 SAP bombs is much more like that of the 1600 AP bomb than the 2000 SAP. The slenderness ratios and the nose curvature of the three types of bombs dropped at the granite site are:

Bomb	Slenderness Ratio L/D	Caliber Radius Head
25,000 SAP	5.75	1.56
1,600 AP	4.80	2.00
2,000 SAP	3.54	1.49

We conclude that the slenderness ratio is the bomb characteristic that governs the curvature of the bomb path.

6—Damage to the 1600 AP, 2000 SAP, and 25,000 SAP Bombs

Damage to the 1600 AP, 2000 SAP, and 25,000 SAP bombs striking

Fig. 90
Fins and Rear of Bomb Body
25,000 SAP Bomb—Altitude of Release 18,000 Ft

Fig. 100
Typical Condition of Cap and Base Plate of 2000 SAP and 1600 AP Bombs After Impact

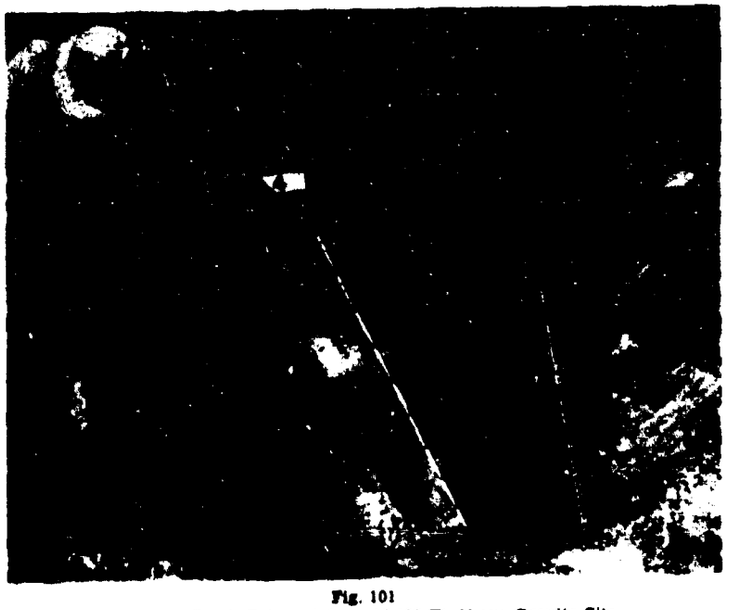

Fig. 101
1600 AP Bomb Released from 18,000 Ft Above Granite Site

Fig. 102
Nose of 1600 AP Bomb Released from 18,000 Ft Above Granite Target

in granite was slight. The fins of the 1600 AP and 2000 SAP bombs were knocked off and badly crumpled at the impact, but the fins of each of the 25,000 SAP bombs remained attached to the bomb body for the full depth of penetration. The condition of the fins of 25,000 SAP Bomb 19, which was released at 18,000 feet over the target, is shown in the photograph, Figure 99. Only random fragments of the fins of the 1600 AP and 2000 SAP bombs were found. Figure 100 shows the condition of the rear of Bomb 16, a 2000 SAP bomb, after impact. The cap and base plate of all 2000 SAP and all 1600 AP bombs were found to be in a condition similar to that of Bomb 16 regardless of the altitude of release and regardless of whether the impact occurred in granite or in sandstone.

The photograph, Fig. 101, shows the condition of the rear portion of the body of Bomb 4, a 1600 AP bomb, released from 18,000 feet above the target. The photograph was taken from the 6 o'clock position, and the level rod is parallel to the line of flight. The scratches and the fused scale on the bomb body are on the footwall side of the bomb. The bomb has

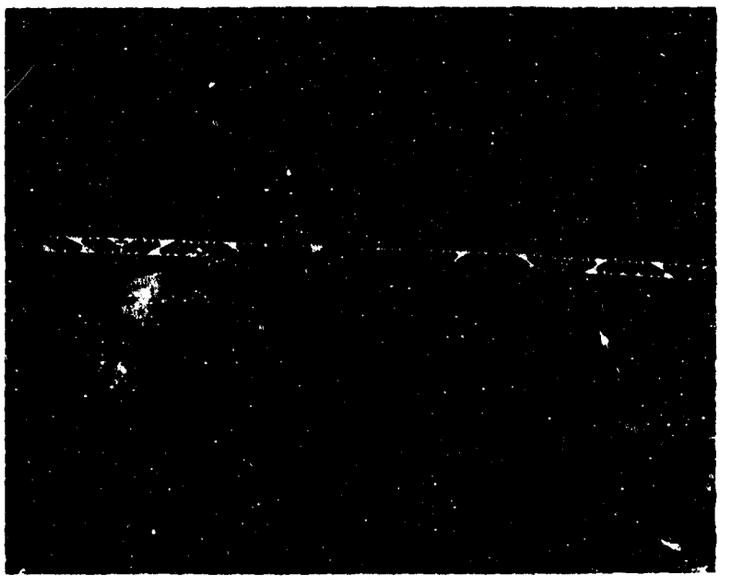

Fig. 103
2000 SAP Bomb 15 Showing Slight Gouging of Nose
Altitude of Release 30,000 Ft

tilted sideways at right angles to the line of flight. Inspection shows that the footwall, or bottom, of the bomb body rather than the hanging-wall, or top, of the bomb body received the more severe abrasion. Where the lugs are on the underneath, or footwall, side of the bomb body at impact, as in Fig. 101, the lugs are sheared off. Where the lugs are on the top, or hanging-wall, side of the bomb body at impact, they remain. (See Fig. 118.)

The photograph, Fig. 102, shows the nose of 1600 AP Bomb 6, released from 18,000 feet above the target and striking a bare, unaltered granite outcrop. The nose has not been blunted, even slightly, by the impact. Figure 103 shows the nose of 2000 SAP Bomb 16 which was released from 30,000 feet above the target. The nose has been gouged slightly, but the depth of the gouge (¼ inch) is not excessive, and no visible indication of rupture is apparent on the bomb body.

The photograph, Fig. 104, shows a crack that has formed in the bomb body of 25,000 SAP Bomb 20, which was released from 26,000 feet above the target. The base plate bolts were not loosened by the impact, but were loosened manually in preparation for attaching a crane sling clip. Other than the crack, no visible damage occurred, and the nose of the bomb was in perfect shape.

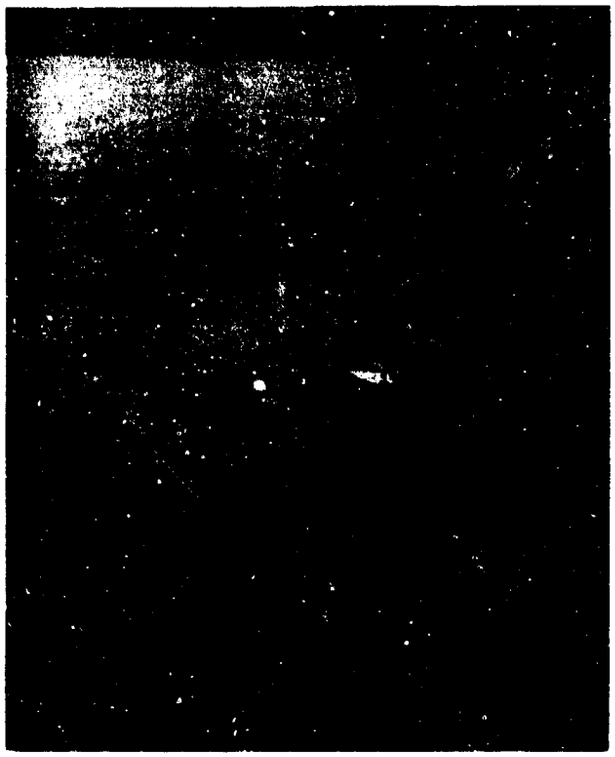

Fig. 104
Crack in Body of 25,000 SAP Bomb 20
Altitude of Release 26,000 Ft

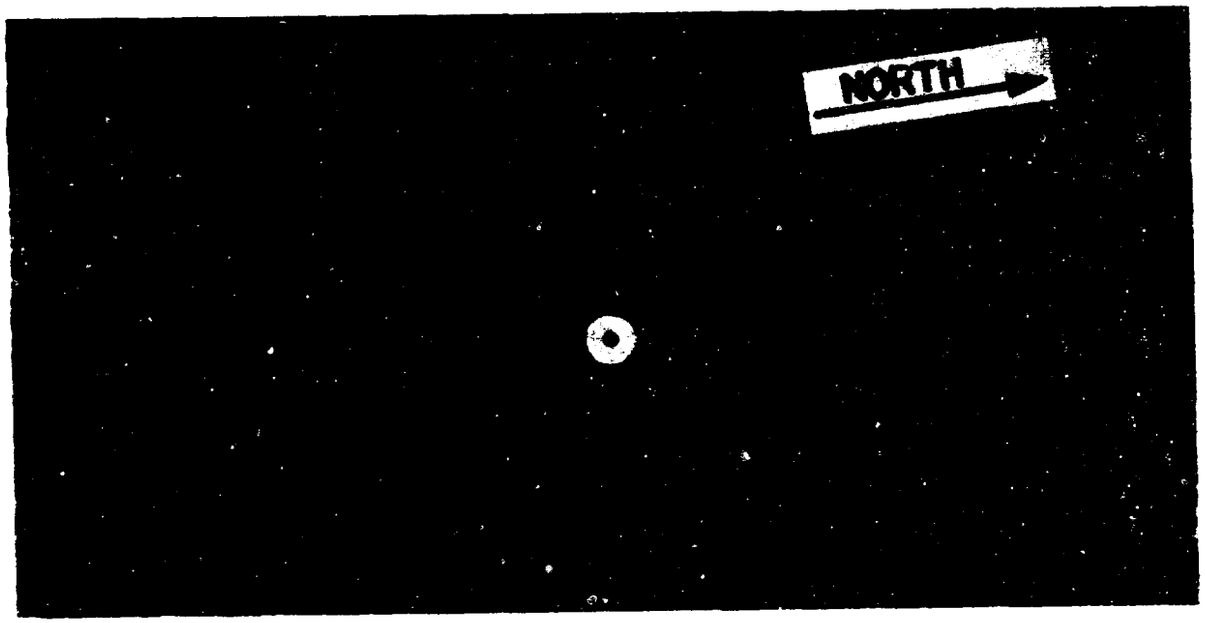

Fig. 105

Putney Mesa Sandstone Bombing Site

PART D—PENETRATION TESTS IN DAKOTA SANDSTONE

SECTION I—TEST PROCEDURE

1—Detail Layout of the Sandstone Site

Figure 105 is an aerial photograph showing the target layout and the pattern of access roads at the Putney Mesa sandstone site. The contrasting background of the buff sandstone and the green trees made the four marker areas stand out clearly and made it unnecessary to cover the markers with pumice. A single bull's-eye target was used throughout the bombing experiments. The outside diameter of the bull's-eye was 150 feet, and the diameter of the black center was 40 feet. Volcanic cinders were used to mark the center, and pumice was used to mark the white circle.

The topography of the Dakota sandstone site was mapped on a scale of 1 inch equals 40 feet, using a contour interval of 5 feet. The map was used as a base map for detailed geologic mapping, and is presented in reduced size as Fig. 106 and in full size in the appendix. The target surface is a gentle-dip slope, and the pattern of grid roads was laid out roughly parallel to and at right angles to the strike of the beds. All bombing runs were made from east to west, or in a direction approximately up the dip. The topography in the central cleared area was mapped on a contour interval of 1 foot and is presented in the appendix.

The attitude of the joints in the Dakota sandstone within the target area is shown in Fig. 106. One set of joints predominates over the others. This set is thought to coincide with the direction of maximum strain, and individual joints having this attitude are classed as longitudinal joints. Cross joints form at right angles to the longitudinal joints, and diagonal joints form a conjugate system at 45 degrees to the longitudinal joints and the cross joints.

2—Description of the Tests in Sandstone

Nine 1600 AP bombs, nine 2000 SAP bombs, and twelve 2000 GP bombs were dropped at the sandstone site. The 1600 AP and the 2000 SAP bombs were released at 9200, 18,000, and 30,000 feet above the target. Essentially three bombs of each type were released from each of three different altitudes. Because of clouds forming over the target it was necessary to release one 2000 SAP bomb at 8700 feet rather than at 9200 feet. The 2000 GP bombs were released at altitudes ranging from 30,000 feet to 7000 feet above the target in an effort to determine the altitude at which rupture begins.

Figures 107 and 108 present in a tabular form the measurements taken to determine the path, the depth of penetration, and the crater shape resulting from impact of each of the bombs dropped at the Putney Mesa sandstone site. The data sheet is in the same form as that used for presenting similar data for bombs dropped at the Paxton Springs granite site.

The crater maps and diagrams of bomb paths in sandstone were constructed in the same way as those for the granite tests. The impact point

was easier to determine in sandstone than in granite because a zone of finely pulverized light-colored rock surrounded the path of the bomb, and because fractures and cracks caused by the impact and penetration were more symmetrical. The uniform lithology of the Dakota sandstone, the more uniform thickness of the soil cover, and the absence of a weathered zone of rock below the soil cover combined to make the dispersion of data in sandstone less than that in the granite.

3—Vertical Penetration of 1600 AP, 2000 SAP, and 2000 GP Bombs in Dakota Sandstone

In Fig. 109 vertical penetration, Y, as recorded on the data sheets, Figs. 107 and 108, is plotted against impact energy for the 1600 AP bombs, the 2000 SAP bombs, and the 2000 GP bombs dropped during the experiments at the Putney Mesa sandstone site. Just as in the presentation of the data for the drops at the granite site, no attempt has been made to correct for soil thickness, topography, obliquity, or geologic properties of the rock. Bombing in an up-dip direction at the granite site resulted in an angle of impact that was on the average about 4 degrees greater than the angle of fall. An increase in the angle of impact resulted in an increase in the depth of penetration.

Bomb 23, a 1600 AP bomb released from 18,000 feet above the target, struck the side of a gully and peeled off a slab of rock instead of creating a true crater. The depth of penetration of Bomb 23 is therefore less than normal.

Bomb 31, a 2000 SAP bomb released from 30,000 feet above the target, missed the target area completely and lit in a talus slope overlying a shale member below the target surface. The bomb passed through the talus and penetrated into shale, but did not encounter any sandstone. The depth of penetration of Bomb 31 is, therefore, more than normal and should not be considered as a drop in sandstone

Bombs 50, 48, 43, and 41, all 2000 GP bombs released from altitudes ranging from 7000 feet to 16,000 feet above the target, did not rupture. Bomb 50, which was released from 7000 feet, was the only one of the four that did not bulge or deform in some manner. Bomb 48, which was released from 8700 feet, missed the target area and struck in a gully where the overburden was unusually thick. Perhaps the slight vertical penetration of Bomb 48 in rock and the lack of rupture are both explainable by the soil thickness. Bomb 43, which was released from 14,000 feet, bulged but did not rupture. Geologic conditions at the point of impact were normal. Bomb 41, which was released from 16,000 feet, bulged more severely than did Bomb 43, but did not rupture.

4—Crater Shape as Related to Impact Energy

The crater maps in the appendix show the apparent and the true craters for each bomb dropped at the sandstone site. The distribution of flyrock and the shape of the ground ring are different in sandstone than in granite. In sandstone, less rock is thrown forward and more is thrown to the sides or to the rear. The steeply dipping longitudinal joints in the Dakota sandstone are more abundant than the cross joints or the diagonal joints and are aligned at right angles to the line of flight. This alignment

100a

NORTH MARKER
WEST MARKER
EAST MARKER
SOUTH MARKER
STRAIN ELLIPSOID
JOINT PATTERNS
CONTOUR INTER
BOND PENETRATION PROJECT
C S M RESEARCH FOU
TOPOGRAPHIC M
-SANDSTONE SIT

100a

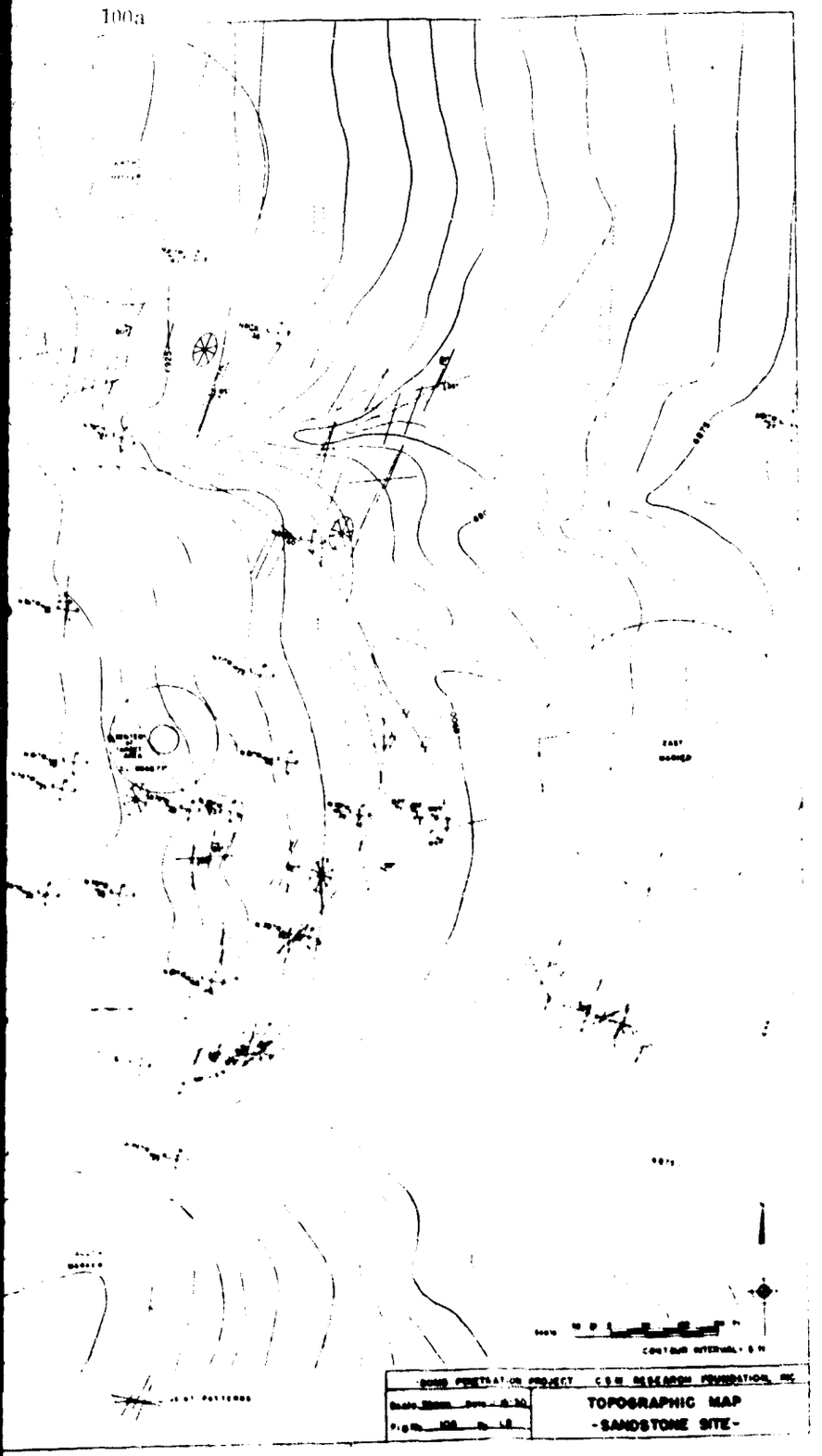

BALLISTIC DATA															CRATER ME												
GROUP NUMBER	C.S.M. BOMB NO.	DATE OF DROP (AUGT)	MISSION NUMBER	AIR FORCE BOMB NUMBER	TYPE OF BOMB	ACTUAL WEIGHT OF BOMB (lbs)	PLANE'S AIR SPEED (mph)	ALTITUDE ABOVE TARGET (ft)	STRIKING VELOCITY (f/s)	ANGLE OF FALL (°)	TIME OF FALL (sec)	PLANE BEARING	ENERGY OF IMPACT (ft-lbs x 10^6)	IMPACT POINT	IMPACT ELEVATION (ft)	ANGLE OF IMPACT (°)	X	X_H	Y	Y_U	Z	Z_F	N_{FR}	P_S	P_{RM}	P_{TM}
VIII	24	22	7	26	AP	1654	268	9200	840	63	—	N 76W	18.16	D6	6964	68 3/4	1.81	2.60	3.45	0.20	0.50	1.28	3.42	1.08	3.90	4.98
	25	22	7	25	AP	1660	269	9200	840	62 1/2	—	N78W	18.22	E2	6928	69 1/4	2.78	-3.20	4.30	1.20	0	1.30	3.00	0.58	5.04	5.62
	26	22	7	21	AP	1654	280	9200	845	62 1/4	22	N81W	18.37	E6	6953	69 3/4	3.18	0.30	4.41	0.35	2.45	0.20	4.30	2.00	5.55	7.55
IX	21	22	7	24	AP	1656	302	18000	1076	68 1/2	34	N76W	29.82	E8	6954	67 3/4	7.15	0	4.90	0	0	0	5.25	0.25	9.00	9.25
	22	22	7	22	AP	1652	300	18000	1076	68 1/2	33	N71W	29.76	D5	6928	74	3.95	-2.00	5.57	1.50	0	1.25	4.20	0.28	6.90	7.18
	23	22	7	23	AP	1652	309	18000	1078	68 1/4	33	N74W	29.86	F9	6922	75 1/4	2.40	14.4	4.10	3.55	0.25	3.30	0	0.55	4.82	5.37
X	27	23	8	27	AP	1643	342	30000	1248	71 1/4	43	N81W	39.81	—	6866	71	3.95	-7.90	4.65	5.15	1.50	0.50	0	0.30	6.25	6.55
	28	23	8	28	AP	1648	350	30000	1250	71	43	N51W	40.06	G2	6916	74	4.10	2.40	5.30	1.60	0.75	1.32	4.05	0.75	6.75	7.50
	29	23	8	29	AP	1651	345	30000	1249	71 1/4	—	N89W	40.06	G5	6976	77 1/4	2.82	0	4.60	0	0.16	0	4.92	0.45	5.48	5.93
	35	25	10	41	SAP	2065	280	8700	809	62	21	N81W	21.02	H4	6951	67	2.01	4.82	2.31	1.55	0	1.92	1.45	0.65	3.20	3.85
XI	33	25	10	43	SAP	2056	280	9200	824	64	22	N81W	21.71	H7	6950	66 1/4	1.90	-0.62	3.05	1.85	0	4.85	1.28	1.00	3.60	4.60
	34	25	10	42	SAP	2065	282	9200	825	64	21	N78W	21.84	G7	6926	69	2.55	2.78	3.70	1.55	0.35	1.40	2.45	0.45	4.90	4.95
XII	36	28	11	45	SAP	2065	295	18000	1035	69	—	N78W	34.41	D3	6960	72	1.97	0	3.90	0	0	0	4.00	3.38	4.37	7.75
	37	28	11	44	SAP	2066	295	18000	1035	69	—	N74W	34.43	H6	6954	72	3.02	2.02	2.97	2.40	0.40	2.35	0.95	1.57	4.30	5.87
	38	28	11	46	SAP	2063	296	18000	1035	69	29	N76W	34.37	F6	6944	74	2.72	0	4.30	0	0	0	4.60	0.65	5.00	5.65
XIII	30	28	11	49	SAP	2061	340	30000	1170	72	—	N81W	43.89	H8	6968	77	2.28	-3.45	3.28	0.95	0.65	3.65	2.15	0.43	4.15	4.58
	31	28	11	47	SAP	2063	342	30000	1170	72 1/4	—	N78W	43.93	—	—	70 1/2	5.90	5.75	4.70	1.45	1.00	1.25	3.20	4.46	7.55	12.20
	32	28	11	48	SAP	2065	338	30000	1170	72	—	N78W	43.97	F9	6928	76	1.80	0.40	3.95	4.50	0	6.55	0	0.52	4.30	4.82

NOTES

(1) Struck the side of an exposed outcrop in the gully; therefore not valid for penetration. Measurements beyond maximum penetration taken to the point of exit from crater.
(2) Missed cliff. Hit in shale and deep soil.
(3) Measurements beyond maximum penetration were taken to point of exit from crater.

CRATER MEASUREMENTS

Y	XH	Y	YU	Z	ZF	NFR	PS	PRM	PTM	P	NS	NR	NT	IS	IR	IT	IN	∠H	∠V	CRATER VOLUME IN ROCK (cu. ft.)	CRATER VOLUME IN SOIL (cu. ft.)	CRATER VOLUME TOTAL (cu. ft.)	CRATER RADUS "R" (ft.)	CRATER DEPTH "D" (ft.)	R/D RATIO	NOTES	CSM BOMB NO.
1.31	2.60	3.45	0.20	0.50	1.28	3.42	1.08	3.90	4.98	7.68	1.07	3.48	4.55	1.00	3.84	4.92	0.18	16 L	2 3/4	176	67	243	4.85	4.30	1.13		24
2.78	-3.20	4.30	1.20	0	1.30	2.00	0.58	5.04	5.62	8.97	0.50	4.50	5.00	0.58	4.97	5.55	0.49	0	5 1/2	151	47	198	4.53	4.90	0.929		25
3.18	0.30	4.41	0.35	2.45	0.20	4.30	2.00	5.55	7.55	8.05	2.08	4.60	6.68	2.00	5.39	7.39	0.95	30 1/2R	10	302	264	566	7.63	6.50	1.17		26
7.15	0	4.90	0	0	0	5.25	0.25	9.00	9.25	9.25	0.25	5.25	5.50	0.25	7.18	7.43	4.82	0	34	382	157	539	5.88	6.90	0.852		21
3.95	-2.00	5.57	1.50	0	1.85	4.20	0.28	6.90	7.18	9.68	0.25	5.90	6.15	0.28	6.65	6.93	1.70	0	14 1/2	388	42	430	5.91	6.00	0.985		22
2.40	14.4	4.10	3.55	0.25	3.30	0	0.55	4.82	5.37	20.3	0.55	4.25	4.80	0.55	4.70	5.25	0.85	6 R	10 1/4	540	60	600	7.63	3.80	2.01	(1)	23
3.95	-7.90	4.65	5.15	1.50	0.50	0	0.30	4.25	6.55	17.08	0.30	4.95	5.25	0.30	5.75	6.05	2.25	22 1/4L	21 1/2	421	29	450	5.56	5.60	0.993	(3)	27
4.10	2.40	5.30	1.40	0.75	1.32	4.05	0.75	5.75	7.50	10.25	0.78	5.48	6.26	0.75	6.40	7.15	2.12	10 1/2R	18 1/2	305	111	416	6.64	6.30	1.05		28
2.82	0	4.60	0	0.16	0	4.94	0.45	5.48	5.93	5.93	0.40	4.92	5.32	0.45	5.30	5.75	1.22	34 1/2R	13	193	71	264	5.35	5.00	1.07		29
2.01	4.82	2.31	1.55	0	1.92	1.45	0.65	3.20	3.85	9.00	0.55	2.50	3.05	0.65	2.96	3.61	0.73	0	14	201	67	268	5.76	3.20	1.80		35
1.90	-0.62	3.05	1.85	0	4.85	1.48	1.00	3.60	4.60	6.55	0.85	3.15	4.00	1.00	3.57	4.57	0.38	0	6	90	74	164	4.77	4.00	1.19		33
2.55	2.78	3.70	1.55	0.35	1.40	[illegible]	0.45	4.50	4.95	8.20	0.50	3.82	4.32	0.45	4.45	4.90	0.70	7 3/4L	9	185	45	230	4.65	4.30	1.08		34
1.97	0	3.90	0	0	0	4.00	3.38	4.37	7.75	7.75	3.22	4.00	7.22	3.38	4.36	7.74	0.51	0	6 3/4	123	295	418	6.21	7.80	0.796		36
3.02	2.02	2.97	2.40	0.40	2.35	0.95	1.57	4.30	5.87	8.82	1.40	3.25	4.65	1.57	3.81	5.38	1.83	7 1/2L	25 3/4	185	104	289	5.65	4.80	1.18		37
2.72	0	4.30	0	0	0	4.60	0.65	5.00	5.65	5.65	0.52	4.60	5.12	0.65	4.98	5.63	1.02	0	11 1/2	227	52	279	5.40	5.10	1.06		38
2.28	-3.45	3.28	0.95	0.65	3.65	2.15	0.43	4.15	4.58	8.13	0.46	3.44	3.90	0.43	3.75	4.18	1.18	16 1/2R	17 1/2	173	66	239	5.51	4.50	1.22		30
5.90	5.75	4.70	1.45	1.60	1.25	3.20	4.66	7.55	12.20	18.20	4.20	4.80	9.00	4.66	6.15	10.73	4.35	9 3/4L	35 1/4	233	738	971	7.92	9.60	0.825	(2)	31
1.30	0.40	3.95	4.50	0	0.55	0	0.52	4.30	4.82	9.32	0.45	4.00	4.45	0.52	4.30	4.78	0.55	0	7 1/4	228	75	303	6.23	4.60	1.33		32

AP & SAP BOMBS

-BOMB PENETRATION PROJECT- CSM RESEARCH FOUNDATION, INC.

Scale ——— Date 2-18-51

Fig. No. 107 By LB

BALLISTIC & CRATER DATA
DAKOTA SANDSTONE

Fig. 107

BALLISTIC DATA															CRATER												
GROUP NUMBER	C.S.M. BOMB NO.	DATE OF DROP (AUG)	MISSION NUMBER	AIR FORCE BOMB NUMBER	TYPE OF BOMB	ACTUAL WEIGHT OF BOMB (lbs)	PLANE'S AIR SPEED (mph)	ALTITUDE ABOVE TARGET (ft)	STRIKING VELOCITY (fps)	ANGLE OF FALL (°)	TIME OF FALL (sec)	PLANE'S BEARING	ENERGY OF IMPACT (ft-lbs x 10^6)	IMPACT POINT	IMPACT ELEVATION (ft)	ANGLE OF IMPACT (°)	X	XH	Y	YU	Z	ZF	NFR	PS	PRM	P
	50	25	10	40	GP	2193	272	7000	760	60	20	W76W	19.72	D6	6964	65 3/4	1.29	6.80	2.40	3.85	0.31	0.85	0	0.76	2.76	3.
XIV	48	25	10	41	GP	2206	275	8700	822	62 1/2	22	W79W	23.19	D9	6933	59	1.40	7.55	0.65	1.95	0.45	1.25	0	3.20	1.54	4.
	49	25	10	39	GP	2202	276	8700	822	62 1/2	21	W81W	23.15	F2	6920	65 1/2	1.84	3.30	1.90	2.52	0	1.90	0	0.34	2.70	3.
	44	24	9	35	GP	2208	280	12000	920	66 1/2	28	W81W	29.07	F8	6938	74 1/2	1.50	7.55	1.43	3.50	0	2.30	0	1.04	2.12	3.
IV	42	24	9	34	GP	2206	285	14000	966	68	26	W79W	32.02	F7	6948	75 1/4	0.98	4.35	1.63	3.10	0	4.10	0	0.92	1.87	2.
	43	24	9	33	GP	2205	280	14000	958	68	27	W78W	31.48	G6	6937	77 3/4	2.58	5.10	3.08	4.90	0.20	0.40	0	0.68	4.03	4.
	41	24	9	38	GP	2194	300	16000	1006	67 1/2	29	W81W	34.54	G6	6928	73	1.35	5.65	2.58	3.85	0	2.10	0	1.16	2.92	4.
XVI	39	24	9	37	GP	2205	310	18000	1038	68 1/2	32	W78W	36.96	H6	6920	73	1.65	2.75	2.74	2.12	0	0.25	0.90	0.85	3.20	4
	40	24	9	36	GP	2212	309	18000	1038	68 1/2	31	W81W	37.08	G3	6922	74 1/2	1.00	3.35	1.00	2.30	0	1.50	0	1.95	1.45	3
	47	23	8	32	GP	2193	300	18000	1036	69	32	W86W	36.62	B6	6976	70 1/4	1.97	4.75	1.90	2.70	0	0.63	0	0.20	2.85	3
XVII	45	23	8	30	GP	2194	342	30000	1140	72 1/2	42	W81W	44.36	A1	6982	76 3/4	0.46	6.45	1.15	2.10	0	0	0	0.32	1.25	1
	46	23	8	31	GP	2200	345	30000	1140	72 1/2	—	W81W	44.48	—	—	78	1.22	3.45	2.17	0	0.22	0.60	2.70	0.30	2.50	2

NOTES

(1) All measurements are taken to the point at which the bomb left the crater for those craters where the bomb hit and then flew out of the crater.

(2) Bomb hit in a gully; soil abnormally thick.

(3) Struck branches of tree before hitting rock.

Bomb No. 50 was the only GP bomb that was not broken or deformed by the impact.

CRATER MEASUREMENTS

PRM	PTM		X	XH	Y	YU	Z	ZF	NFR	PS	PRM	PTM	P	NS	NR	NT	IS	IR	IT	IN	∠H	∠V	CRATER VOLUME IN ROCK (cu ft)	CRATER VOLUME IN SOIL (cu ft)	CRATER VOLUME TOTAL (cu ft)	CRATER RADUS "R" (ft)	CRATER DEPTH "D" (ft)	R/D RATIO	NOTES	C.S.M. BOMB NO.
2.76	3.52	4	1.29	6.80	2.40	3.85	0.31	0.85	0	0.76	2.76	3.52	11.0	0.67	2.52	3.19	0.76	2.76	3.52	0	13 1/4R	0	89	20	109	4.22	3.5	1.21	(1)	50
1.54	4.74		1.40	7.55	0.65	1.95	0.45	1.55	0	3.20	1.54	4.74	13.84	2.20	0.60	2.80	3.06	1.18	4.24	1.80	18 3/4R	23	55	121	176	6.36	2.8	2.27	(2)	48
2.70	3.04	2	1.84	3.30	1.90	2.52	0	1.90	0	0.34	2.70	3.04	7.48	0.30	2.00	2.30	0.34	2.51	2.85	0.80	0	17 3/4	93	12	105	4.03	2.3	1.75		49
2.12	3.16	2	1.50	7.55	1.43	3.50	0	2.30	0	1.04	2.12	3.16	11.2	1.00	1.58	2.58	1.04	1.90	2.94	0.79	0	22 1/2	98	53	151	5.28	3.0	1.76		44
1.87	2.79	4	0.98	4.15	1.63	3.10	0	4.10	0	0.92	1.87	2.79	7.89	0.92	1.70	2.62	0.92	1.84	2.76	0.32	0	9 3/4	46	64	110	3.89	2.6	1.50		42
4.03	4.71	4	2.58	5.10	3.08	4.90	0.20	0.40	0	0.68	4.03	4.71	11.8	0.72	3.40	4.12	0.68	3.81	4.49	1.29	4 1/2R	18 3/4	135	78	213	4.99	4.0	1.25		43
2.92	4.08		1.35	5.65	2.58	3.85	0	2.10	0	1.16	2.92	4.08	10.3	1.20	2.72	3.92	1.16	2.86	4.02	0.40	0	8	142	76	218	5.07	4.1	1.24		41
3.20	4.05		1.65	2.75	2.74	2.18	0	0.25	0.90	0.85	3.20	4.05	7.55	0.85	2.85	3.70	0.85	3.17	4.02	0.65	0	11 1/2	132	77	209	5.21	3.8	1.37		39
1.45	3.40	2	1.00	3.15	1.00	2.30	0	1.50	0	1.95	1.45	3.40	7.65	1.90	1.05	2.95	1.92	1.27	3.19	0.84	0	33 1/2	21	84	105	4.03	2.1	1.92	(3)	40
2.85	3.05	4	1.97	4.75	1.90	2.20	0	0.63	0	0.20	2.85	3.05	8.37	0.20	1.87	2.07	0.20	2.42	2.62	1.23	0	27	176	26	202	5.99	2.4	2.50		47
1.25	1.57	4	0.48	6.45	1.15	2.40	0	0	0	0.32	1.25	1.57	8.52	0.30	1.20	1.50	0.32	1.25	1.57	0.15	0	6 3/4	87	28	115	4.94	1.3	3.80		45
2.50	2.80		1.22	3.15	2.17	0	0.22	0.60	2.70	0.30	2.50	2.80	5.95	0.25	2.30	2.55	0.30	2.40	2.70	0.61	10 1/2R	14 1/4	192	88	280	6.04	2.8	2.16		46

GP BOMBS

- BOMB PENETRATION PROJECT - C S M RESEARCH FOUNDATION, INC

Scale: ——— Date 2-17-51
Fig No 108 By LB

BALLISTIC & CRATER DATA
DAKOTA SANDSTONE

Fig. 108

2

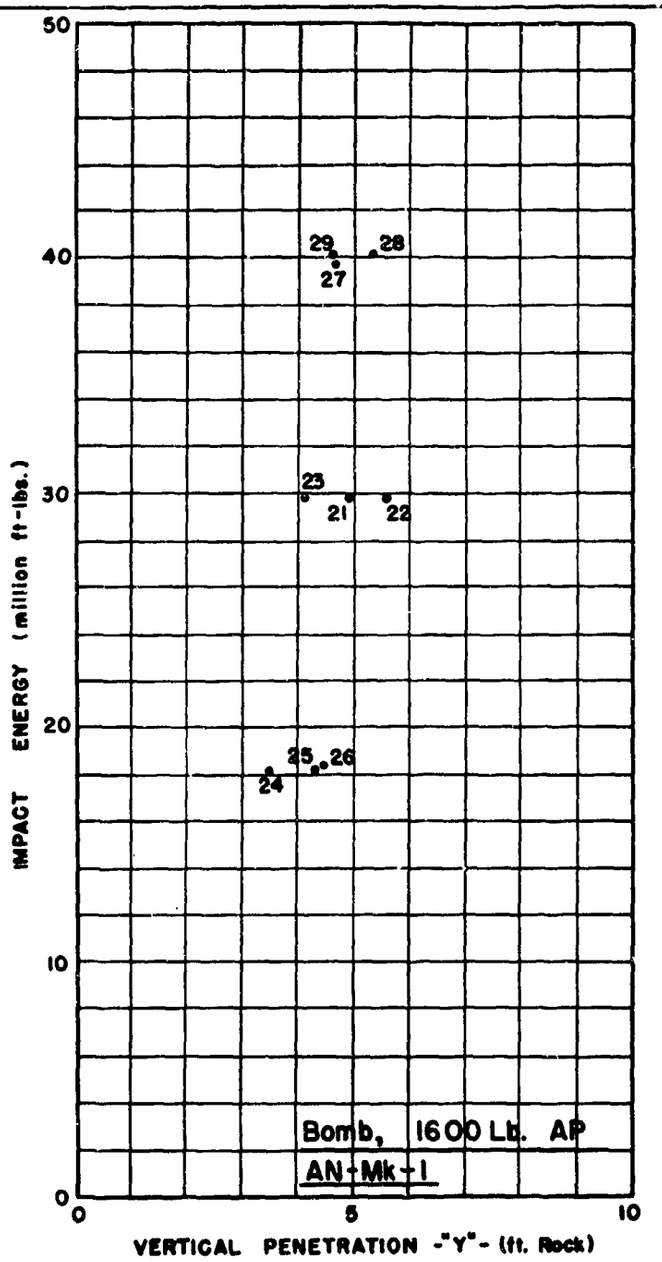
IMPACT ENERGY (million ft-lbs.)
VERTICAL PENETRATION -"Y"- (ft. Rock)
Bomb, 1600 Lb. AP
AN-Mk-1
29
28
27
23
21
22
25
26
24

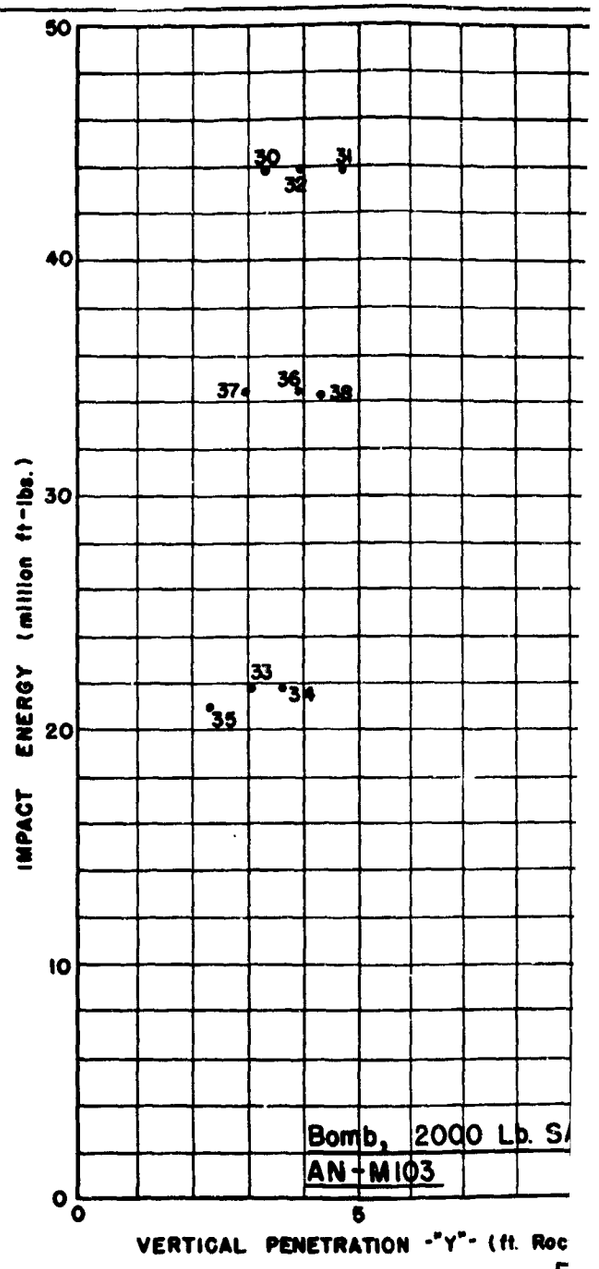
IMPACT ENERGY (million ft-lbs.)
VERTICAL PENETRATION -"Y"- (ft. Roc
Bomb, 2000 Lb. S
AN-M103
30
31
32
37
36
38
33
34
35

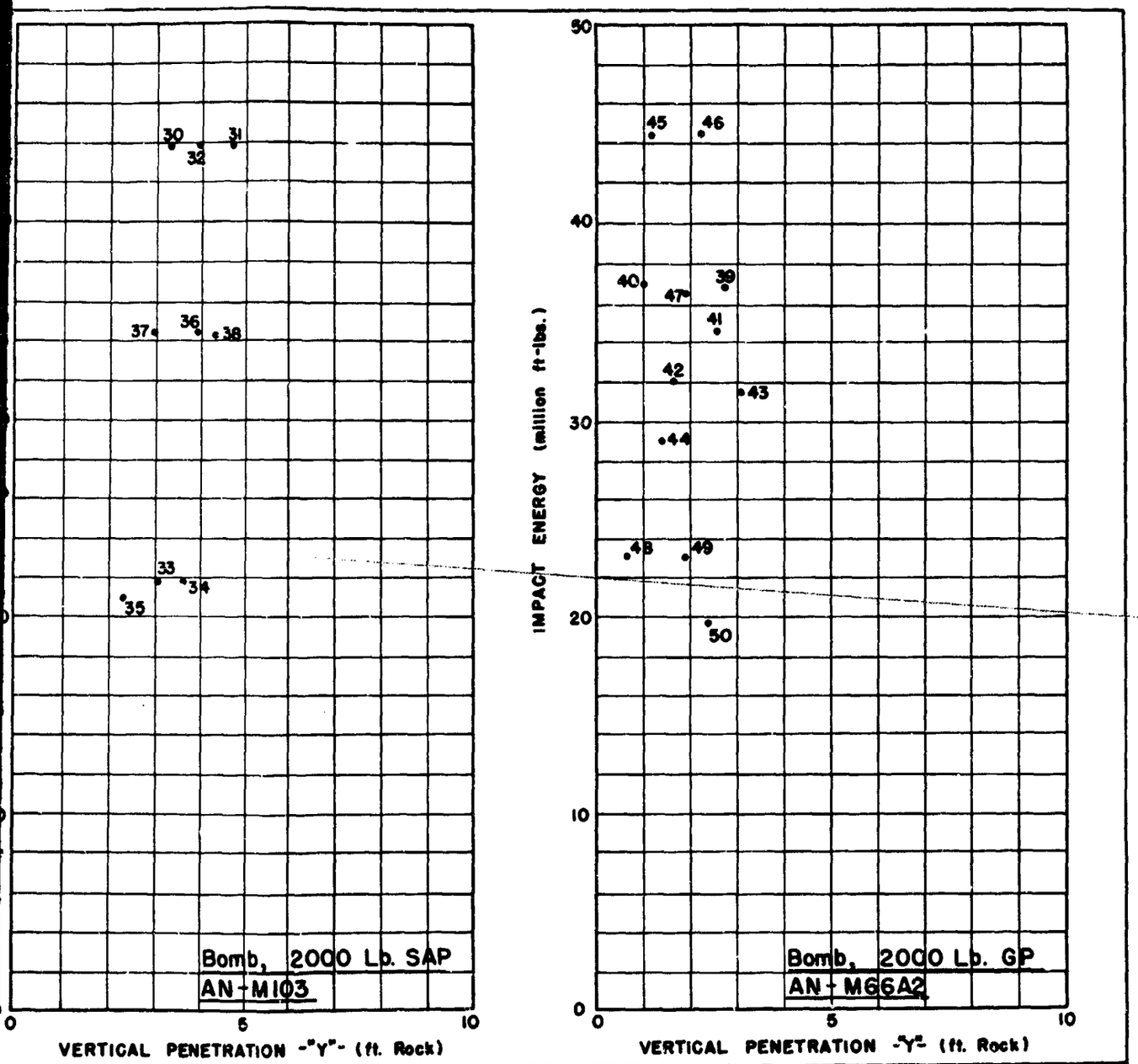

-BOMB PENETRATION PROJECT - CSM RESEARCH FOUNDATION, INC.

Scale ——— Date 3-7-51

Fig. No. 109 By LB

VERTICAL PENETRATION vs IMPACT ENERGY
— DAKOTA SANDSTONE —

Fig. 109

2

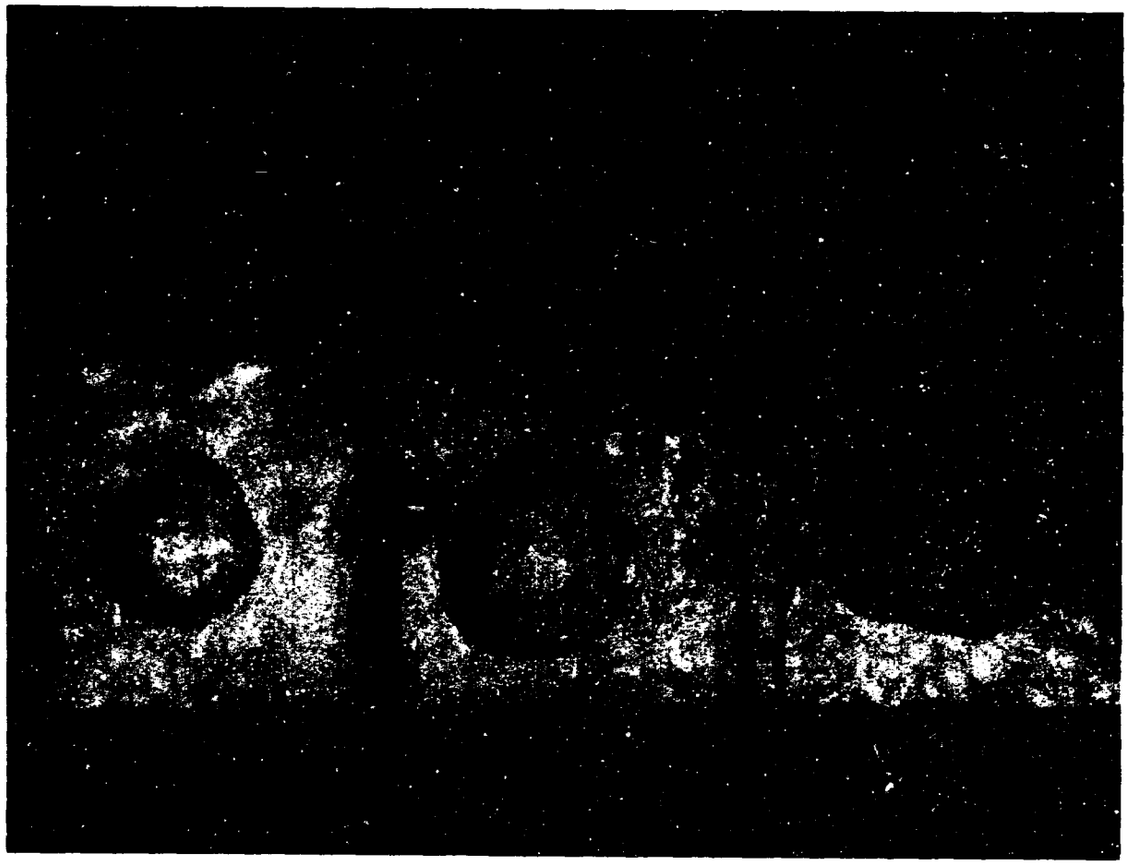

Fig. 110

Plaster Models of Craters 24, 22, and 28 Produced by 1600 AP Bombs in Dakota Sandstone

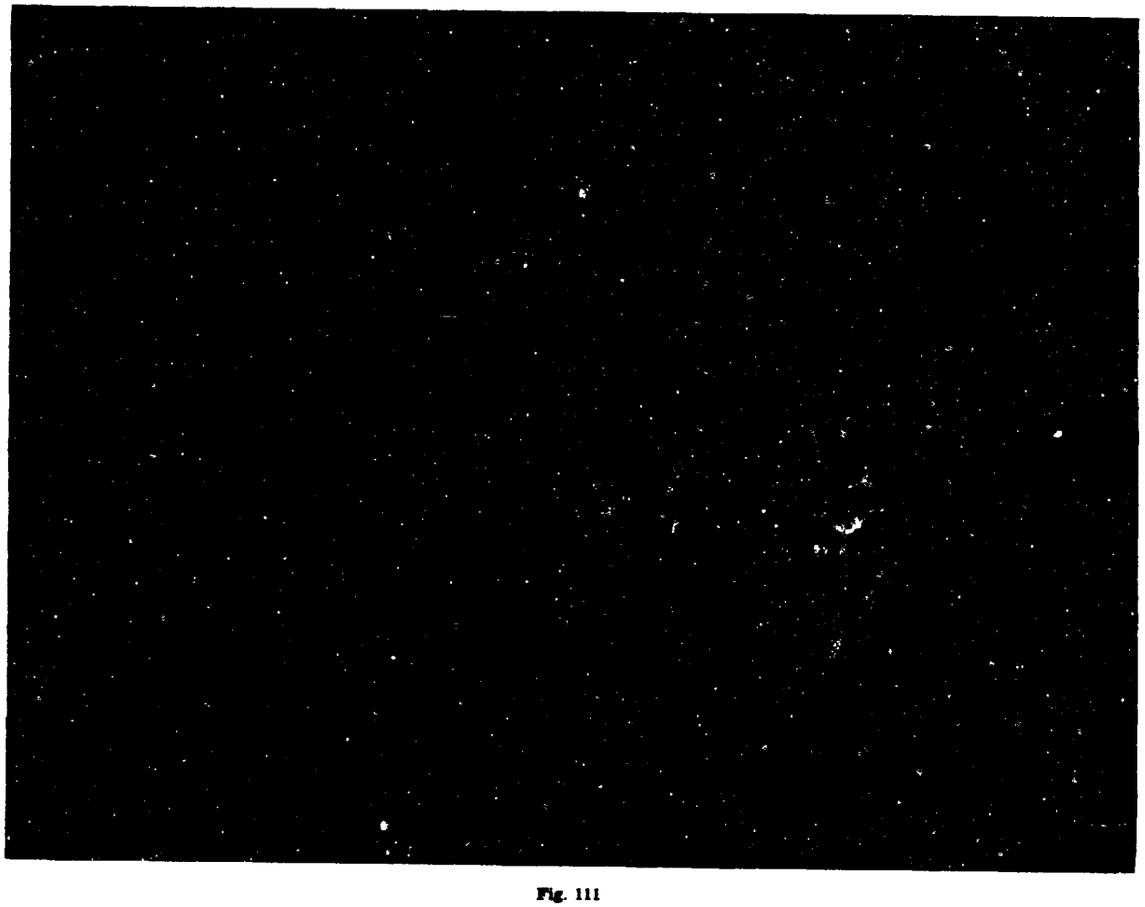

Fig. 111

Plaster Models of Craters 33, 38, and 32 Produced by 2000 SAP Bombs in Dakota Sandstone

Fig. 112

Plaster Models of Craters 48, 39, and 46 Produced by 2000 GP Bombs in Dakota Sandstone

has influenced the manner of rock failure, the shape of the crater, and the distribution of flyrock.

The effect of impact energy upon crater shape is illustrated in Figs. 110, 111, and 112, which are photographs of plaster models of the craters produced by armor-piercing, semi-armor-piercing, and general-purpose bombs in Dakota sandstone. Figure 110 shows the craters produced by 1600 AP Bombs 24, 22, and 28 released from 9200, 18,000, and 30,000 feet. Figure 111 shows the craters produced by 2000 SAP Bombs 33 ,38, and 32 released from 9200, 18,000, and 30,000 feet. Figure 112 shows the craters produced by 2000 GP Bombs 48, 39, and 46 released from 8700, 18,000, and 30,00 feet.

In Fig. 113 the R/D ratio of the craters shown in Figs. 110, 111, and 112 are tabulated, and from the tabular data it may be observed that an increase in the impact energy results in a smaller R/D ratio up to a certain critical value of energy; any increase in energy beyond this critical value results in an increase in the R/D ratio. This is equivalent to saying that energy is more effective in broadening the crater than in increasing the depth of penetration.

Bomb Type	Bomb Number	Kinetic Energy, million ft-lb	R/D Ratio
1600 AP	24	18.2	1.13
1600 AP	22	24.8	0.98 min.
1600 AP	28	40.1	1.05
2000 SAP	33	21.7	1.19
2000 SAP	38	34.4	1.06 min.
2000 SAP	32	44.0	1.33
2000 GP	48	23.2	2.27
2000 GP	39	37.0	1.37 min.
2000 GP	46	44.5	2.16

Fig. 113

Ratio of Crater Radius R to Crater Depth D for 1600 AP, 2000 SAP, and 2000 GP Bombs in Dakota Sandstone

5—Path Shape as Related to Impact Energy

The path shapes comparable to the crater shapes of the 1600 AP, 2000 SAP, and 2000 GP bombs described in preceding paragraphs are arranged in the same sequence and presented graphically in Fig. 114. It can be seen from the figure that the path length increases up to a certain critical energy; then a further immediate increase in impact energy results in a reduced rate of penetration and perhaps a reduced depth of penetration. (See Analysis.)

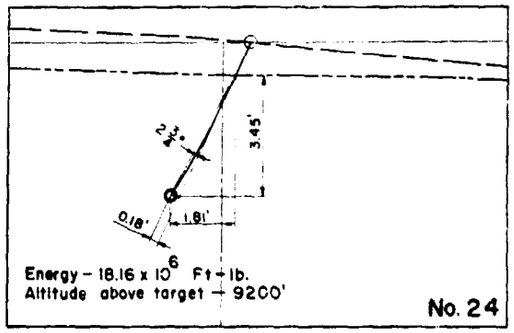

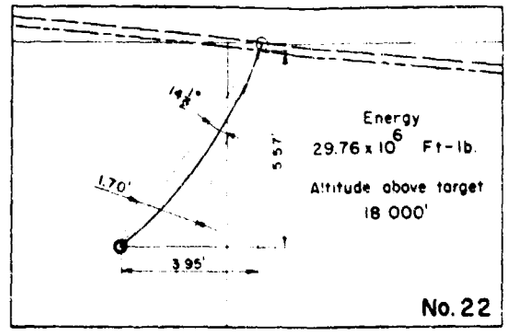

1600 LB. AP BOMB, AN-MK-

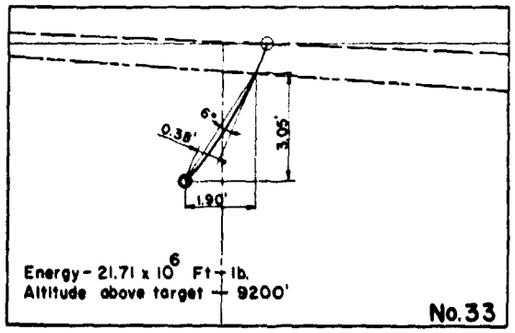

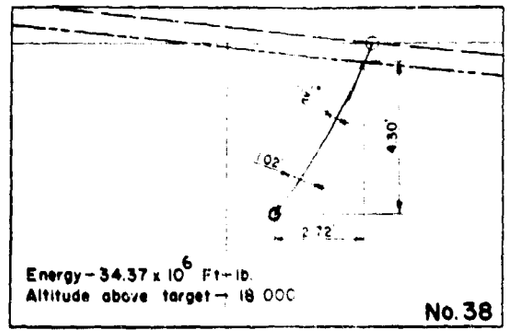

2000 LB. SAP BOMB, AN-M I(

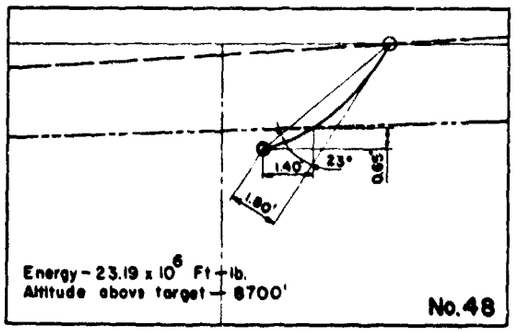

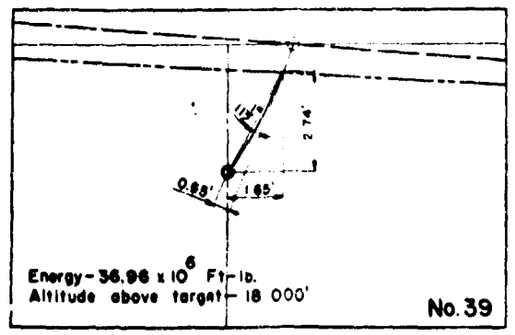

2000 LB. GP BOMB, AN-M 66

NOTE: BOMB 48 WAS DEFORMED; BOMBS 39 AND 46 RUPTURED.

0 1 2 3 4
Feet

-BOMB PENETRAT

Scale Shown Date 2-

Fig. No. 114 By L

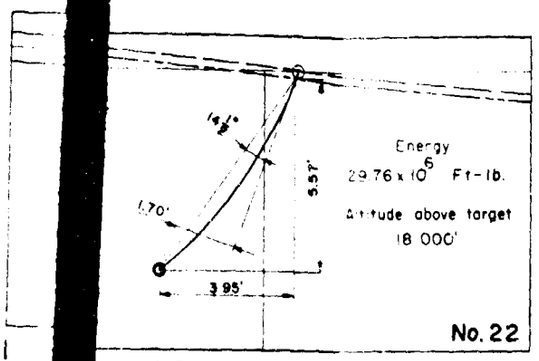

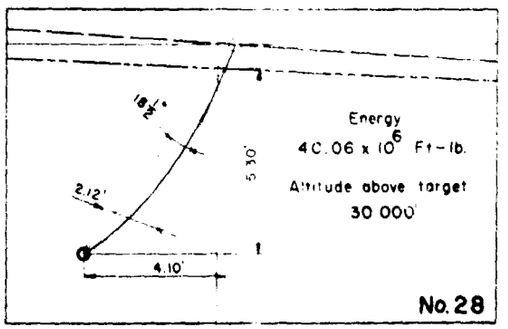

AP BOMB, AN-MK-

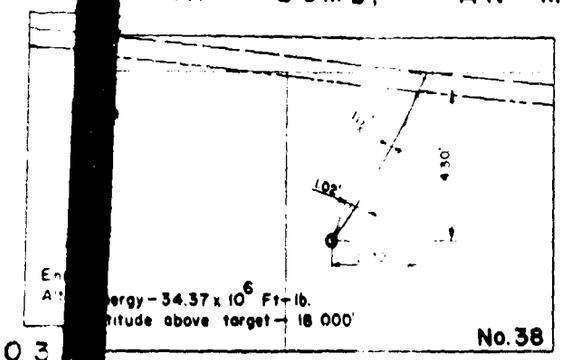

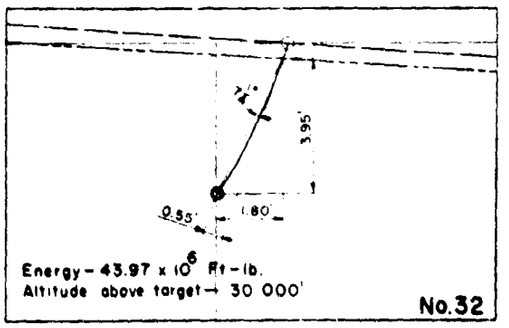

1103 B. SAP BOMB, AN-M103

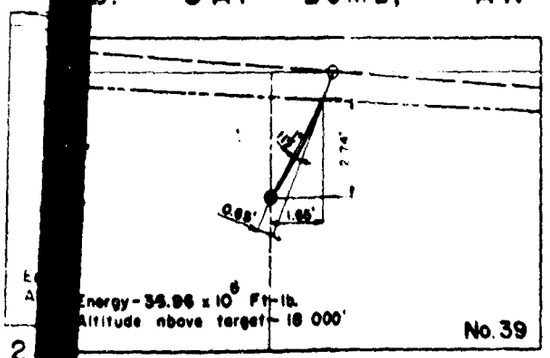

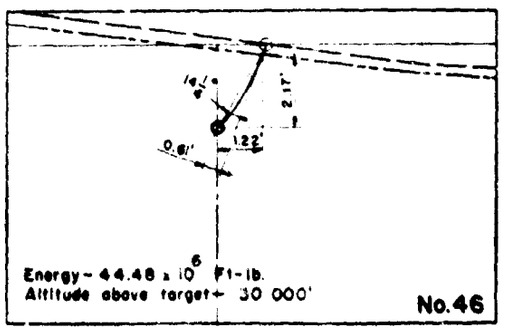

66A2 B. GP BOMB, AN-M66A2

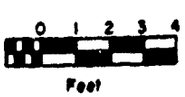

-BOMB PENETRATION PROJECT- CSM RESEARCH FOUNDATION, INC.

Scale Shown Date 2-22-51

Fig. No. 114 By LB

EFFECT OF ENERGY ON PATH SHAPE

-SANDSTONE-

Fig. 114

The angle V is a measure of the curvature of the path and is summarized as follows:

Bomb Type	Bomb Number	Impact Energy	V, degrees
1600 AP	24	18.2	2 3/4
1600 AP	22	24.8	14 1/2 uniform
1600 AP	28	40.1	18 1/2 increase
2000 SAP	33	21.7	6
2000 SAP	38	34.4	11 1/2 max.
2000 SAP	32	44.0	7 1/4
2000 GP	48	23.2	23
2000 GP	39	37.0	11 1/2
2000 GP	46	44.5	14 1/4

Fig. 114 A
Angle "V" as a Function of Impact Energy for Various Bombs

From the preceding table it is apparent that the paths of all three types of bombs have different curvatures. The curvature of the 1600 AP bombs continually increases. The curvature of the 2000 SAP bombs rises to a maximum, then decreases. Because of the rupture of GP Bombs 39 and 46 and because of the excessive soil thickness at the point of impact of Bomb 48, no conclusions can be drawn regarding the path of the general-purpose bombs.

The path of 1600 AP bombs in Navajo sandstone differs from that in Zuni granite. It is thought that the continuous increase in the curvature of the path of the 1600 AP bomb in sandstone indicates that the horizontal component of the resisting force increases more rapidly with depth in sandstone than in granite.

6—Damage to 1600 AP, 2000 SAP, and 2000 GP Bombs in Dakota Sandstone

Damage to the 1600 AP and 2000 SAP bombs striking in sandstone was slight. The fins were knocked off and badly crumpled at impact. No distortion could be detected from measurements of the bomb body. Gouging was less severe than in granite. Lugs were knocked off if they were on the footwall side of the bomb at impact; otherwise they remained on. The least damage to the lugs resulted when they were on the hanging-wall side of the bomb at impact.

Figure 115 shows the condition of 1600 AP Bomb 28 released from 30,000 feet above the target. The nose has not been dented and the bomb body shows no evidence of failure. The condition of the bomb is typical of others of the same type regardless of the altitude of release.

Figure 116 shows the condition of 2000 SAP Bomb 30 released from 30,000 feet above the tarket. There is no evidence of deformation, but

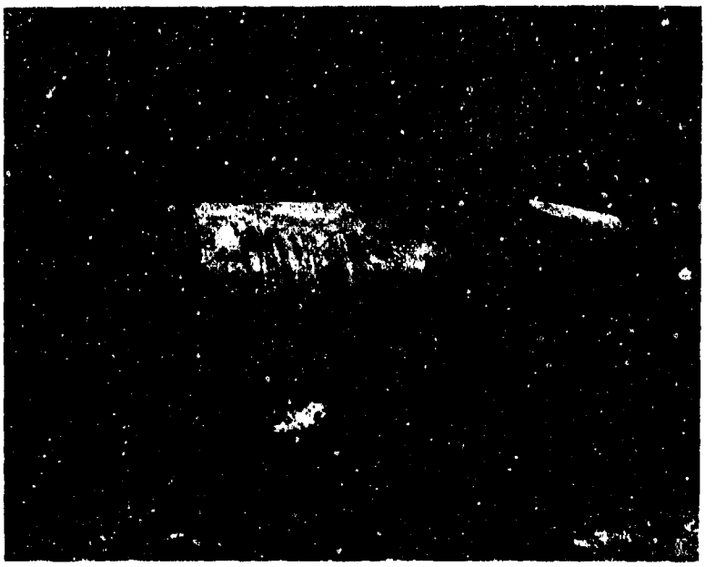

Fig. 115
1600 AP Bomb 28 Released from 30,000 Ft Above the Sandstone Target

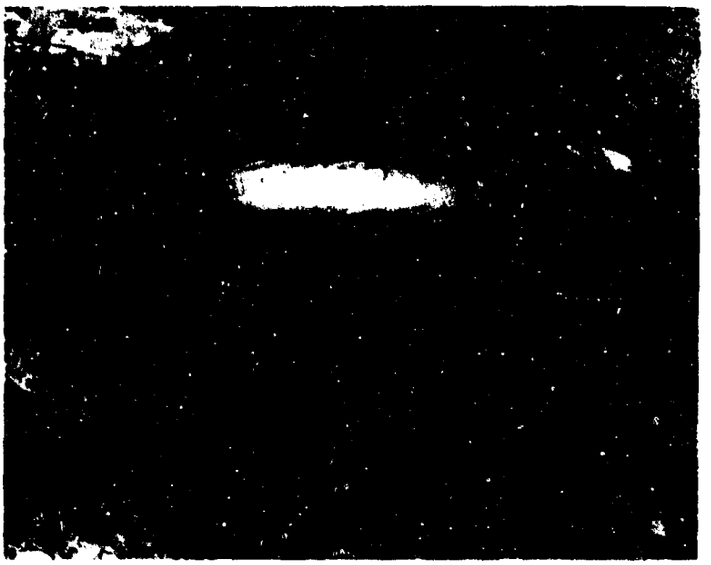

Fig. 116
2000 SAP Bomb 30 Released from 30,000 Ft Above the Sandstone Target

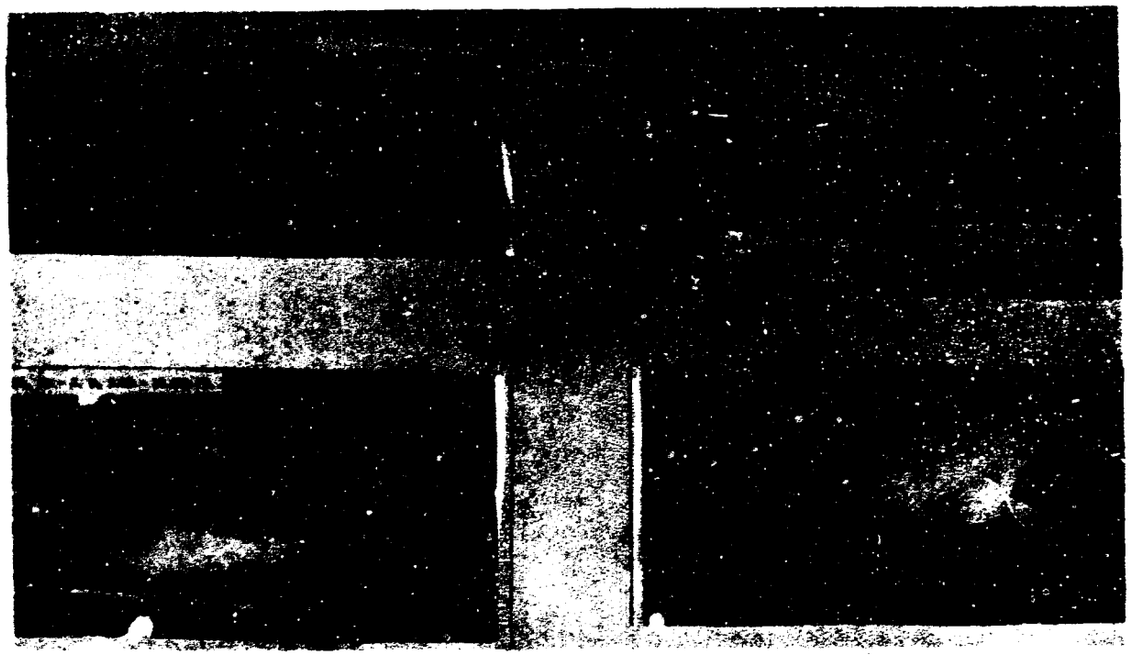

Fig. 117
Sequence of Damage of 2000 GP Bombs Released from 7000, 8700, 18,000, and 30,000 Ft Above the Sandstone Target

as discussed in the metallurgical report, flowed-metal scale is present on the nose and on the body of the bomb. The lugs were bent or broken.

Figure 117 shows the condition of 2000 GP Bombs 50, 49, 39, and 46 arranged in order of increasing height of release. Bomb 50 was released from 7000 feet above the target and did not deform. Only one bomb was released from this altitude, and it would be unwise to state definitely that this is the critical altitude above which damage begins. However, 7000 feet is very close to the altitude at which deformation begins. The first stage of deformation is the formation of a bulge where the curved portion of the nose joins the straight portion of the bomb body, as shown in Fig. 117 for Bomb 49, which was released at 8700 feet above the target.

The bulge in the nose is accompanied by a longitudinal split that extends from the nose to the far end of the cylindrical portion of the bomb body as shown in Fig. 118. Damage is not the same to all bombs at a given altitude. In general, damage is less if the bomb rebounds because of the obliquity at which it strikes. Bomb 43 bulged, but did not split; it was released from 14,000 feet. Thus, it is rather difficult to determine the exact altitude at which a particular stage of failure begins.

All general-purpose bombs released above 18,000 feet were ruptured regardless of the topography or of any other variable. Bomb 39, Fig. 117,

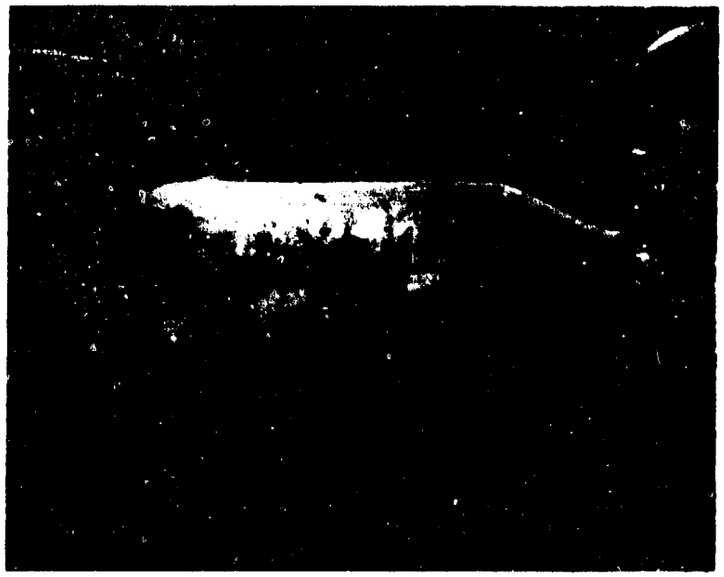

Fig. 118
Longitudinal Rupture Associated with Bulge of Bomb Nose

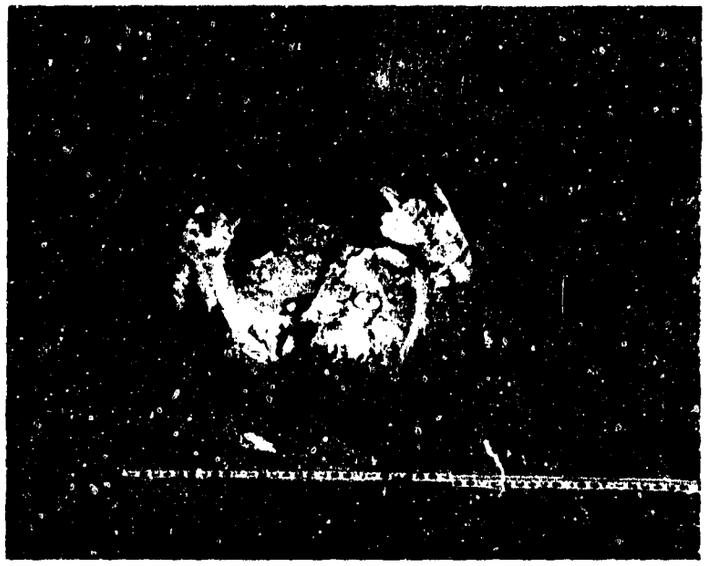

Fig. 119
Rupture and Loss of Filling
2000 GP Bomb 39
Altitude of Release 18,000 Ft

Fig. 120
2000 GP Bomb Released from 30,000 Ft Above the Sandstone Target

released from 18,000 feet above the target shows how the bulge at the nose of the bomb is compressed into a tight fold and how the longitudinal split is extended to the rear and widened. As is shown in Fig. 119, little of the filling remains in the bomb when it comes to rest. The effective diameter of the bomb is greatly increased as a result of the development of the bulge. The resistance to penetration increases as failure proceeds, and the tendency to rebound increases as resistance to penetration increases. All of the general-purpose bombs released from 14,000 feet or above, with the exception of Bomb 43, rebounded and were found at some distance from the crater. Bomb 43 turned around and started out.

All general-purpose bombs released from 30,000 feet ruptured into several parts, rebounded from the crater, and were emptied of filling material. Usually, the buckling of the nose was so severe that the nose came off. Distortion along the longitudinal split sometimes controlled the manner of failure of the bomb, as may be seen in Fig. 120.

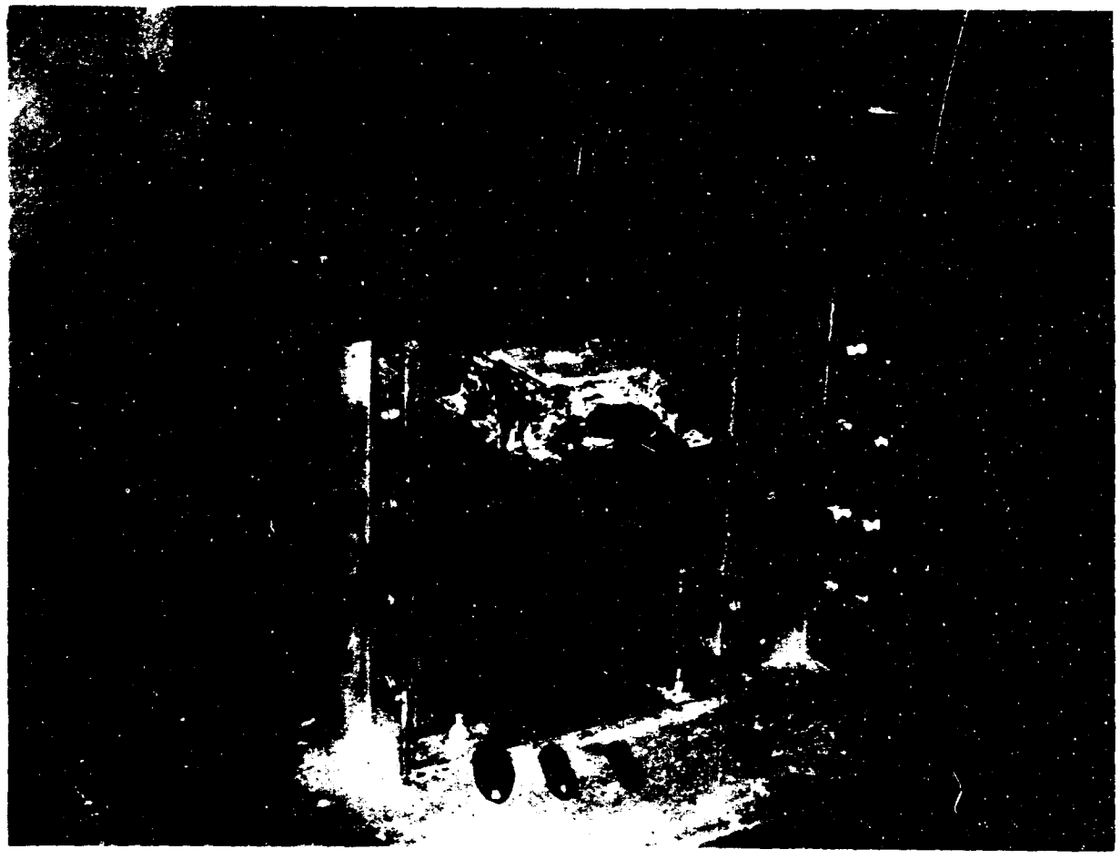

Fig. 121
C.S.M. Model Bombing Apparatus

PART E—LABORATORY EXPERIMENTS AND STRESS ANALYSIS

SECTION I—MODEL BOMBING EXPERIMENTS

1—Introduction

Experiments were conducted in the Barodynamics Laboratory of the Colorado School of Mines to investigate each of several properties of bombs and each of several properties of the medium upon penetration. The experiments were conducted with a precision impossible in the field. The number of "bomb drops" possible in the laboratory was much greater than the number possible during the field experiments; and any given property of the medium upon which the bombs were dropped in the laboratory could be controlled, whereas such control of the rock at the target site is impossible.

It was evident from the results of the field work that penetration of a given type of bomb dropped from a given altitude upon a rock target and particularly upon a granite target, varied greatly, depending upon the physical and geologic properties of the rock at the point of impact and upon the striking angle as influenced by the topography. It was evident also after comparing the penetration of bombs in sandstone, which has an average compressive strength of 5015 pounds per square inch, with the penetration in unweathered Zuni granite, which has an average compressive strength of 24,565 pounds per square inch, that compressive strength alone as determined by a simple compression test cannot be used as a basis for predicting penetration.

Figure 121 is a photograph of the C.S.M. Impact Apparatus modified for use in the model bombing experiments. The impact tup used in impact toughness tests has been replaced by a plate into which model bombs of various types are screwed. In the photograph, a 1600 AP model bomb has been screwed into the plate. Models of 25,000 SAP, 2000 GP, and 2000 SAP bombs are lying on the concrete base of the apparatus. A 3 x 3 x 5-inch block of model material is securely clamped on the adjustable base in position for bombing at zero degrees.

The striking velocity and kinetic energy are varied by changing the height of release. The kinetic energy can also be varied by adding weights to the beam. The weights are bolted to the top flange of the beam symmetrically about the axes of the bomb. By various combinations of weights and model bombs, it is possible to vary either the sectional density or the sectional pressure of the various bombs at constant kinetic energy. The angle of obliquity at which the bomb strikes the model material can be adjusted by changing the angle of the platform upon which the model rests, by means of a rack and pinion that are between the semicircular steel plates visible in the photograph of the apparatus.

The tensile and compressive strengths of the model materials are controlled by the proportions of the mix and are measured at the time of impact using the techniques described in Part A, Section IV, "Physical Rock Tests." A variation in the elastic properties of the medium is obtainable either by varying the proportions of the mix or by using various

model materials. The model materials used in the model bombing experiments are water, sand, cement, Cal-Seal, Zonolite, and plaster.

Certain relations in the model studies are chosen arbitrarily. In the C.S.M. experiments, a scale ratio of 20 to 1 was chosen, and the nature of the apparatus is such that the acceleration of gravity is the same for model and prototype. Dimensional similarity is obtained by controlling the strength of the model material and by controlling the energy at which the model bomb strikes the model material.

Assuming the strength ratio to be properly controlled through the use of model materials of reduced strength, the kinetic energy ratio between prototype and model equals the fourth power of the length ratio, or 160,000 to 1. Thus similarity of penetration between the field experiments for bombing with 1600 AP, 2000 SAP, and 2000 GP bombs between altitudes of 10,000 feet and 30,000 feet is within the range of the laboratory equipment and within the range of kinetic energies between 106 and 275 foot-pounds.

In the special case where the strength ratio between model and prototype is unity, and either Zuni granite or Dakota sandstone is placed in the impact loading device, the kinetic energy ratio between model and prototype equals the cube of the length ratio, or 8,000 to 1, but the density ratio equals 20 to 1 and cannot be satisfied.

Obviously, there is little object in attempting to achieve dimensional similarity in the laboratory unless all of the physical and elastic properties of the model material can be controlled simultaneously, or unless that particular property of the medium that controls penetration can be controlled. We were of the opinion at the beginning of the laboratory work that research has not progressed beyond the empirical stage, and that the specific property of the medium that could be used as a penetration index is unknown. Accordingly, the primary objective of the model bombing experiments was to obtain evidence pointing towards the specific fundamental property of any material that can be used as a penetration index, rather than to achieve dimensional similarity.

2—Comparison of Penetration of Various Bombs

Tests were conducted to determine the depth of penetration of model 1600 AP, 2000 SAP, and 2000 GP bombs in a weak model material of constant strength. The model bombs were constructed of steel to a scale ratio of 20 to 1. The model material was composed of the following ingredients by weight:

19.8 per cent Calseal

15.85 per cent Water

14.85 per cent Fine Sand (−14 mesh)

49.50 per cent Coarse Sand (−8 to + 14 mesh)

After sufficient time had elapsed for the material to reach constant strength (28 days), the compressive strength of test cylinders was found to average 927 pounds per square inch and the tensile strength to average

151 pounds per square inch. The compressive strength ratio between the average of the unweathered Zuni granite specimens and the model material is 26.5 and the tensile strength ratio is 12.6 to 1.

Two preliminary test drops were made to determine the weight and drop necessary to bury completely the nose of the model GP bomb, the largest to be used in the tests. It was found that burial of the nose was satisfactory when 160 pounds was added to the testing machine and when the height of the drop measured at the center of gravity of the beam was 0.776 foot. This drop, the minimum allowable, corresponds to a kinetic energy of 178 foot-pounds.

Using the 1600 AP, 2000 SAP, and 2000 GP model bombs, three drops were made with each value of kinetic energy, and tests were made at three values of kinetic energy for each bomb. For the SAP and GP bombs the ratios of kinetic energies were 1:3:5. The ratios for the AP bombs were 1:2:3.

Critical dimensions of the bombs are as follows:

	Dia., in.	Area, sq. in.	Sectional Density, lb/cu in.	Sectional Pressure, psi
1600 AP	0.700	0.385	563	501
2000 SAP	0.925	0.672	244	287
2000 GP	1.150	1.038	127	156

The sectional density is determined by

$$D = \frac{w}{d^3}$$

where

D = sectional density, pounds per cubic inch

w = weight acting at the center of gravity of the bomb, pounds

d = diameter of the bomb, inches

The sectional pressure equals

$$P = \frac{w}{A}$$

where

P = sectional pressure, pounds per square inch

w = weight acting at the center of gravity of the bomb, pounds

A = cross-sectional area of bomb, square inches

The kinetic energy was held constant for each of the three types of

bombs at 178 and at 534 foot-pounds. Because of the nature of the apparatus, the weight acting at the center of gravity of the AP, SAP, and GP bombs was constant for all practical purposes. The maximum deviation from constant weight equals the difference in weights of the 1600 AP model bomb and the 2000 GP model bombs. This difference equals 0.44 pound. When compared with 229.36 pounds, the weight of the free beam acting at the center of gravity of the beam, the difference is negligible. At 178 foot-pounds and again at 534 foot-pounds the height of drop and striking velocity of each of the three types of bombs were the same.

Accordingly, in a modified Petrie formula:

$$X = KPS$$

where X = depth of penetration

P = the sectional pressure

K = a constant depending upon the nature of the material

S = a constant depending upon the striking velocity

K is constant because the same model material was used for all three types of model bombs; and S is constant for the three types of bombs at the same value of kinetic energy because of the manner in which the experiment was conducted. Therefore, the depth of penetration at a given value of kinetic energy would depend only upon P, the sectional pressure, if the formula is valid within the range of the experimental data.

The laboratory results are shown graphically in Figure 122. In the figure, penetration in inches is plotted against kinetic energy in foot-pounds for each of the three types of model bombs. The sectional pressures of the three types of bombs, the ratio of section pressures compared to a 2000 GP bomb, and the ratio of penetration at 178 and at 538 foot-pounds compared to a 2000 GP bomb are as follows:

Bomb	Sectional Pressure, psi	Ratio of Sectional Pressures	Ratio of Penetrations at 178 ft-lb	Ratio of Penetrations at 538 ft-lb
1000 GP	186	1.000	1.000	1.000
2000 SAP	287	1.543	1.206	1.136
1600 AP	501	2.693	1.523	1.698

By inspection of the tabular data it is apparent that the ratio of penetrations at either 178 foot-pounds or at 538 foot-pounds is not the same as the corresponding ratio of sectional pressures. Inasmuch as the experiment was conducted in such a manner that sectional pressure is the only variable, we conclude that the modified Petrie formula is not valid within the range of the laboratory experiments.

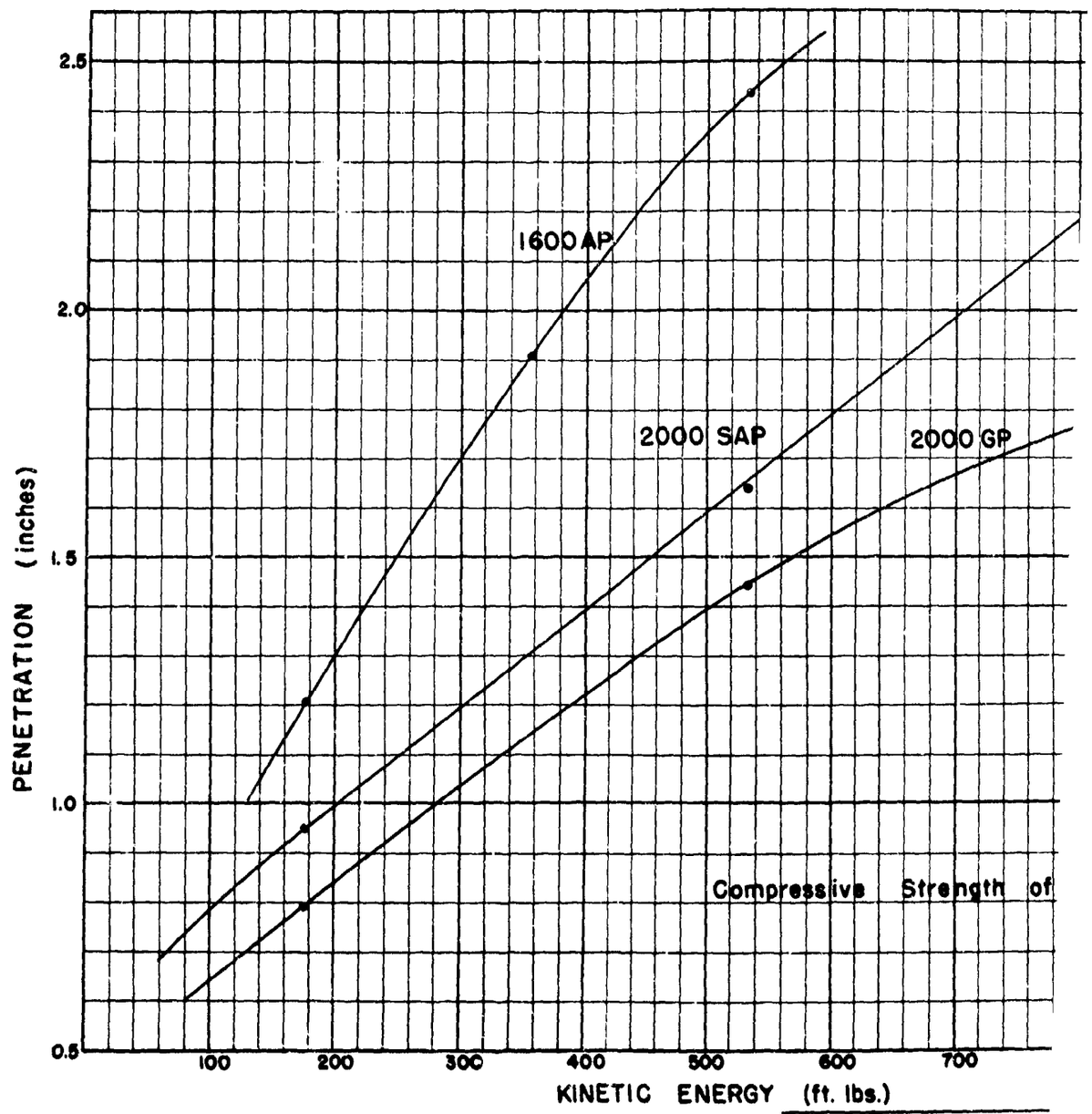

-BOMB PENETRATION PR

Scale ——— Date 3-5-51

Fig. No. 122 By LB

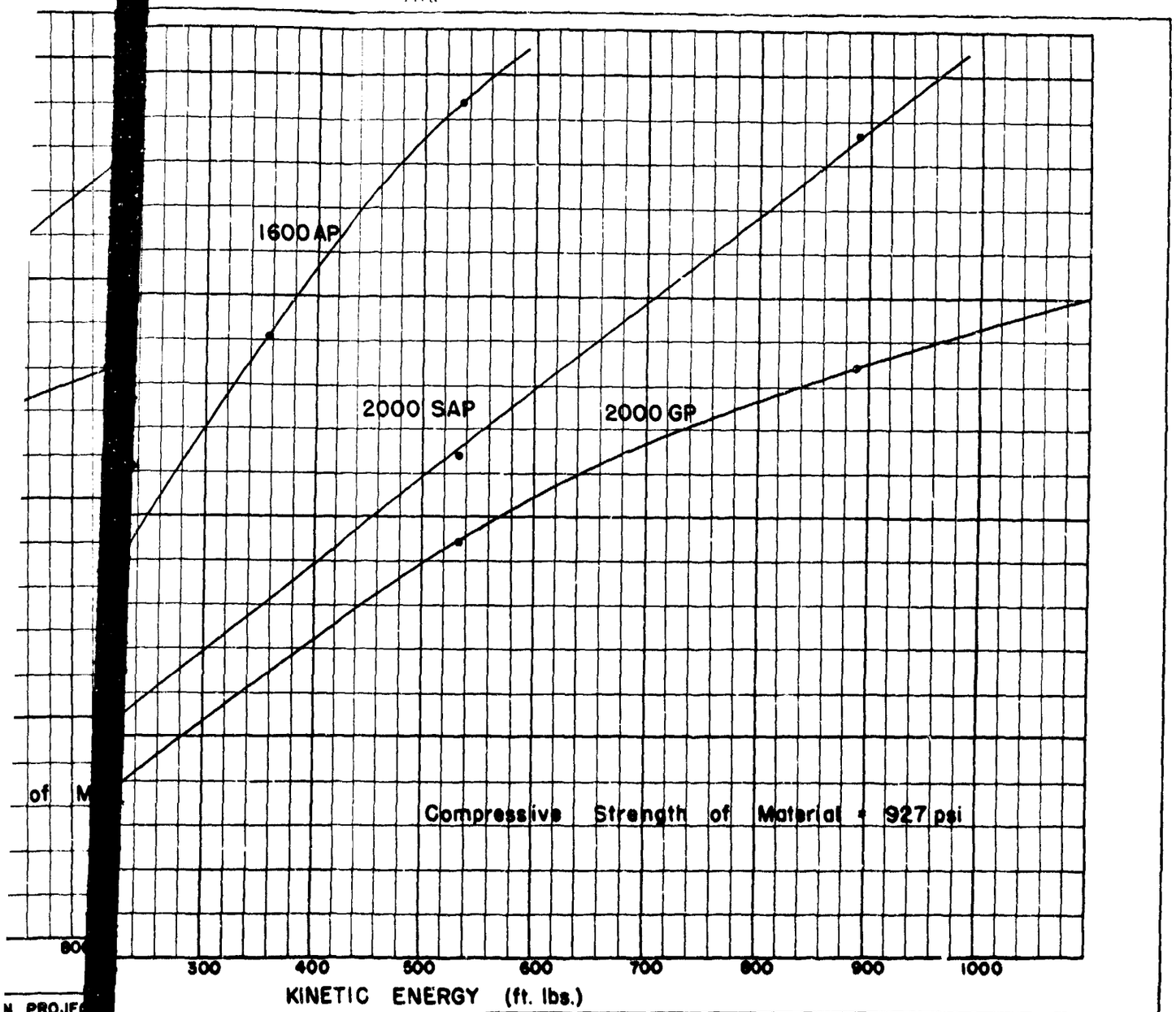

-BOMB PENETRATION PROJECT- CSM RESEARCH FOUNDATION, INC.

Scale ____ Date 3-5-51
Fig. No. 122 By LB

EFFECTS OF BOMB PROPERTIES ON PENETRATION

Fig. 122

2

3—Effect of Sectional Density and of Sectional Pressure Upon Penetration at Constant Kinetic Energy

A second batch of Calseal model material having the following proportions by weight:

18.52—Calseal

12.80—Water

15.88—Fine Sand (—14 mesh)

52.80—Coarse Sand (—8 to + 14 mesh)

was made. It was desired to experiment with a model material in which the ratio of compressive strengths of model and prototype closely approached the scale ratio of 20 to 1. The average compressive strength of the model material proved to be 1314 pounds per square inch and the strength ratio to be 18.7 to 1.

The object of the experiment was to investigate further the relations of sectional density and sectional pressure to penetration. The nature of the impact apparatus is such that the sectional density or the section pressure of a model bomb can be changed by adding or removing weights from the top flange of the beam above the centerline of the model bomb. The addition or removal of weights has the same effect as increasing or decreasing the length of the model bomb.

In this experiment a model 1600 AP bomb was attached to the bomb holder and its sectional density and section pressure were varied by adding weights to the top flange of the beam. The kinetic energy was held constant by decreasing the height of drop. Three drops at constant kinetic energy (533.88 foot-pounds) were made at each of three values of sectional density and sectional pressure. The results are tabulated as follows:

Kinetic Energy, ft-lb	$\frac{w}{d^3}$ Sectional Density, lb cu in.	$\frac{w}{A}$ Sectional Pressure, psi	Average Penetration, in.
533.88	357	316	1.37
533.88	620	553	1.40
533.88	1027	916	1.39

It may be seen from the above results that penetration is independent both of sectional density and of sectional pressure and within all practical limits of measurement is constant at a given value of kinetic energy.

We concluded from the section "Comparison of Penetration of Various Bombs" that penetration does not depend upon sectional pressure only, and we conclude from these experiments that penetration is independent both of sectional density and sectional pressure at constant kinetic energy. Yet, we know that the penetration of different types of bombs at a given value of kinetic energy is different. The smaller diameter bomb penetrates

deeper, and the depth of penetration is not a simple function at any given value of kinetic energy of the ratios of the cross-sectional areas of the bombs.

4—Effect of Compressive Strength Upon Penetration

All of the various available penetration formulas include a constant to represent a material factor or a factor to represent some function of the compressive strength of the material. The results of penetration of bombs into Zuni granite and Dakota sandstone cast considerable doubt upon the use of a constant for a material factor and upon the use of the simple compressive strength of a material as a penetration index. In the following experiments the relations between simple compressive strength, simple tensile strength, and penetration are investigated.

A series of mixtures of cement and Zonolite, a commercial insulating substance used in making light-weight concrete for floors and roof decks, was prepared. Portland cement and ⅛-inch Zonolite in various proportions were mixed, using a water-cement ratio of 0.38. After 28 days, when the mixes had reached constant strength, the tensile strength, compressive strength, and the sclerescope hardness of each of the mixes was determined. The results are as follows:

Ratio		Sclerescope Hardness	Tensile Strength, psi	Compressive Strength, psi
Cement	Zonolite			
1	0	18	404	3410
1	1	7	275	1357
1	3	4.7	104	631
1	5	3.3	68	283

Penetration tests were conducted using each of the four mixtures, and using a model 2000 SAP bomb at a sectional density of 154 pounds per cubic inch. Kinetic energy is the independent variable. Three drops were made at the same value of kinetic energy for each mix. Drops were made at four values of kinetic energy for each mix except the weakest mix. In Figure 123 the depth of penetration is plotted against kinetic energy for each of the four mixes. In Figures 124 and 125 penetration is plotted on logarithmic cross-section paper against the tensile and against the compressive strength. It may be observed that the slope of the lines is not constant, but the curves are concave upward in some regions and concave downward in other regions.

The argument that either the compressive strength or the tensile strength of a material is not a true index of penetration is supported by an experiment in which test specimens were constructed using a mixture of

18.5 per cent Calseal

12.8 per cent Water

68.7 per cent Sand (—16 to + 50 mesh)

Tests with model AP, SAP, and GP bombs at a constant sectional

PENETRATION vs. KINETIC ENERGY

CEMENT-ZONOLITE MIXES

2000 lb SAP Bomb

Sect. Density = 154 lb/in.^{3}

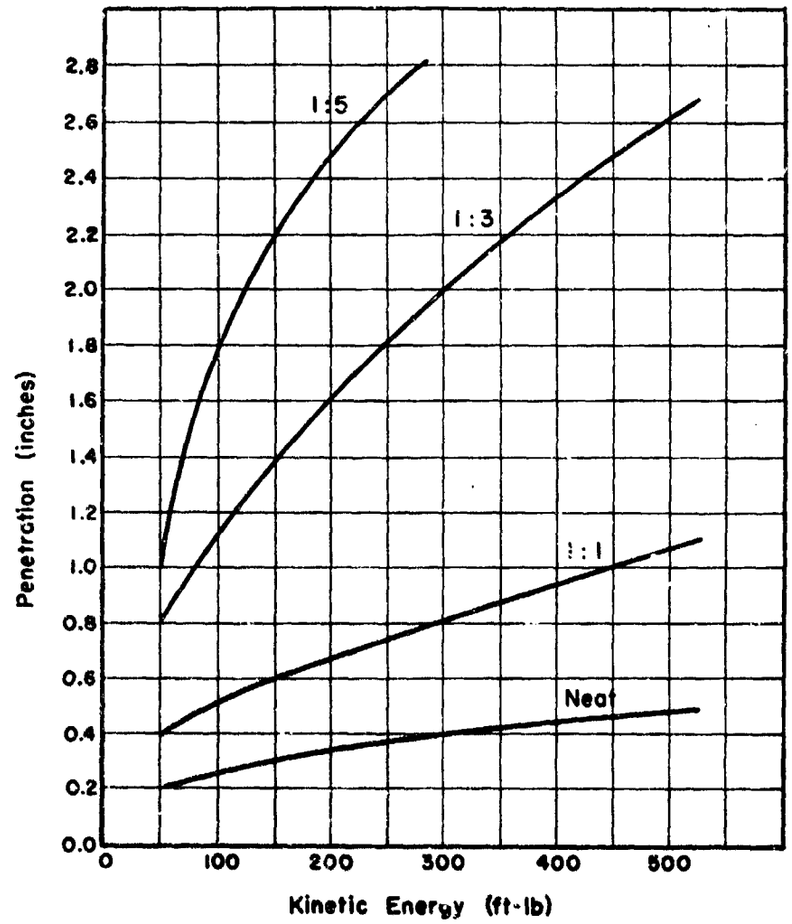

NOTE: Cement to Zonolite = 1:1, 1:3, 1:5 by weight

-BOMB PENETRATION PROJECT- CSM RESEARCH FOUNDATION, INC.	
Scale —— Date 3-20-51 Fig. No. 123 By ADG	PENETRATION IN ZONOLITE MIXTURES OF VARIOUS STRENGTHS

Fig. 123

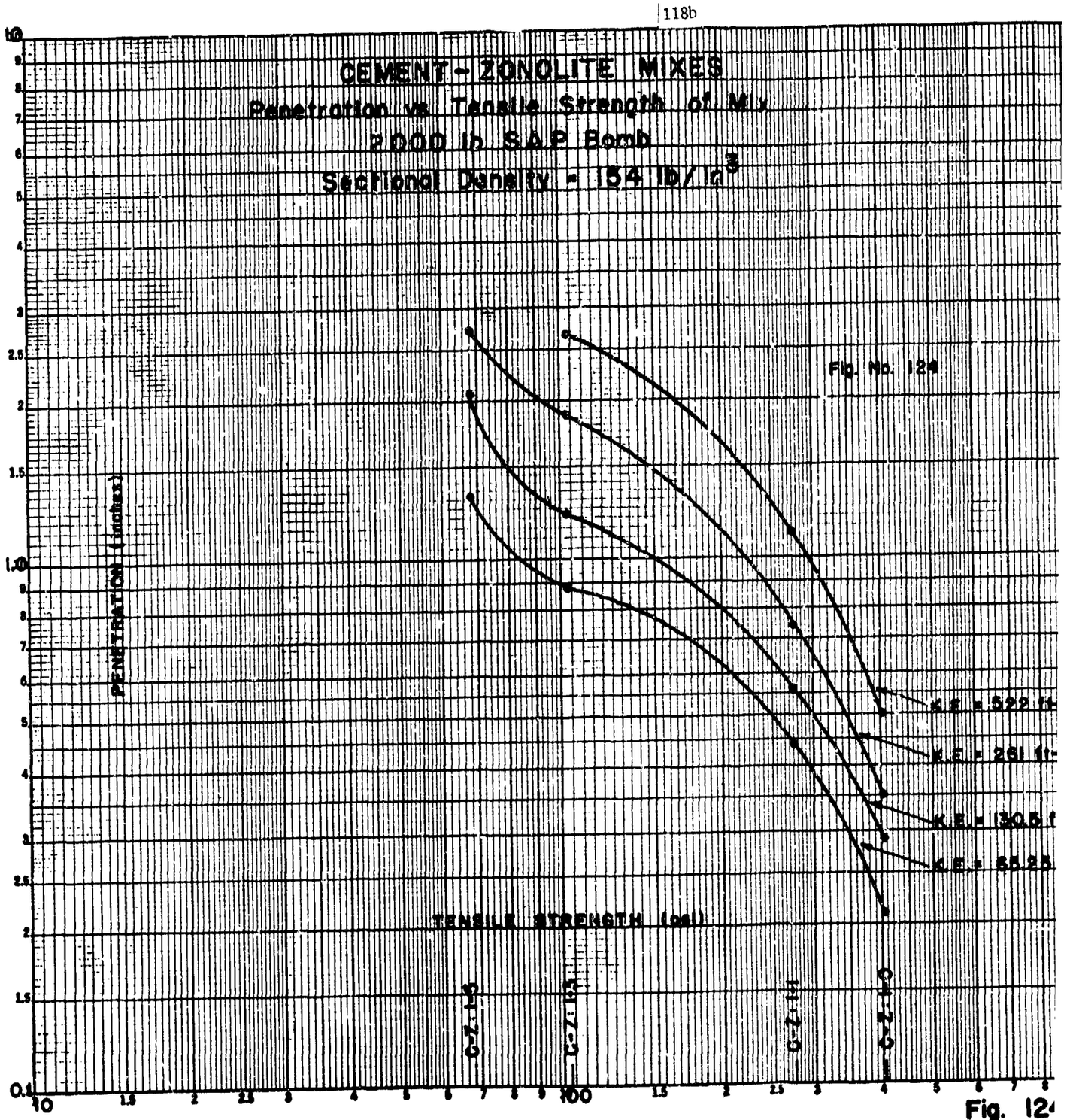
CEMENT - ZONOLITE MIXES
Penetration vs. Tensile Strength of Mix
2000 lb S.A.P. Bomb
Sectional Density = 154 lb/in³
Fig. No. 124
PENETRATION (inches)
TENSILE STRENGTH (psi)
K.E. = 522 ft-
K.E. = 261 ft-
K.E. = 130.5 f
K.E. = 65.25
C-Z-1-5
C-Z-1-3
C-Z-1-1
C-Z-1-0
10
100

Fig. 124

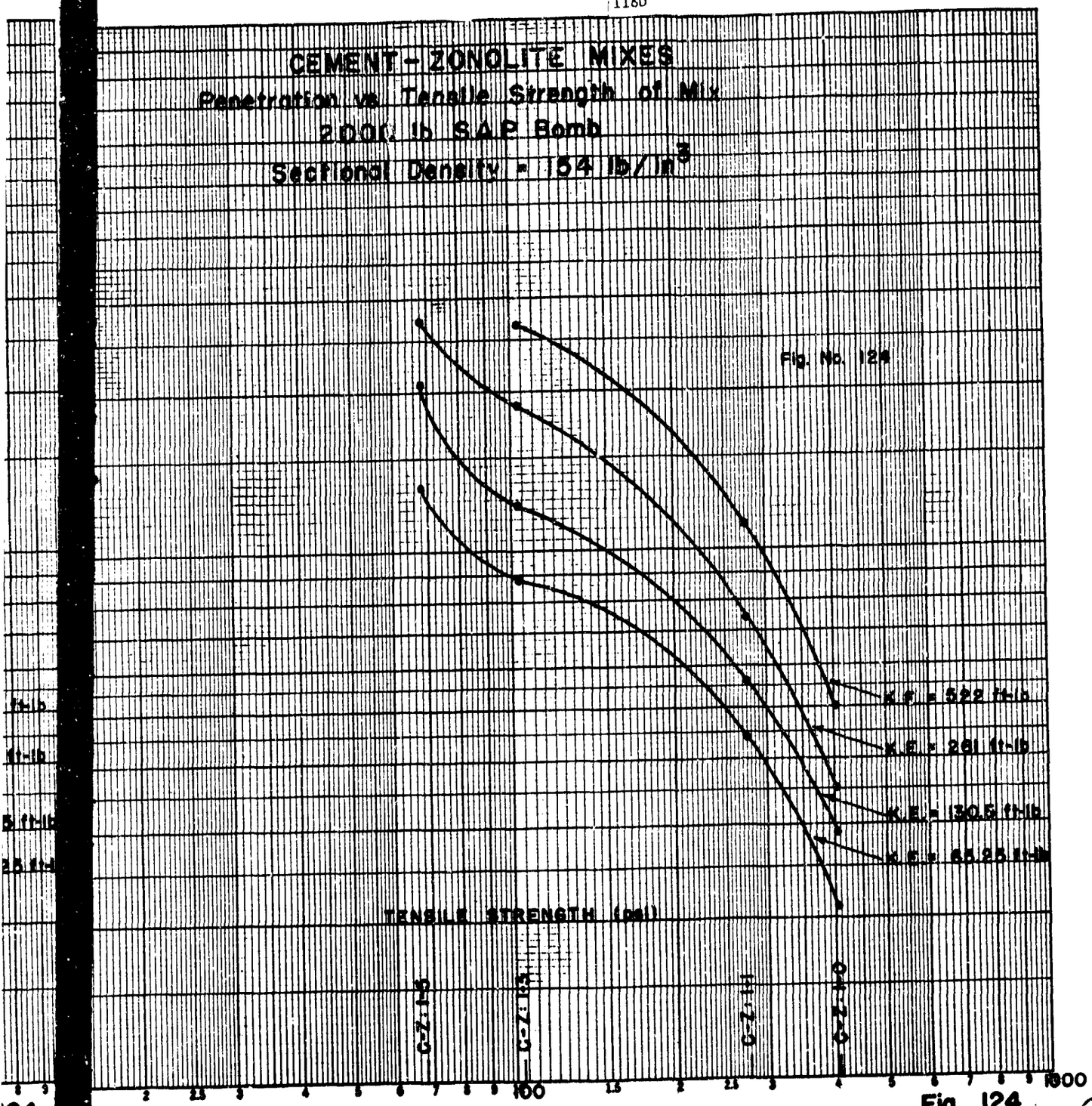

Fig. 124

124

1

2

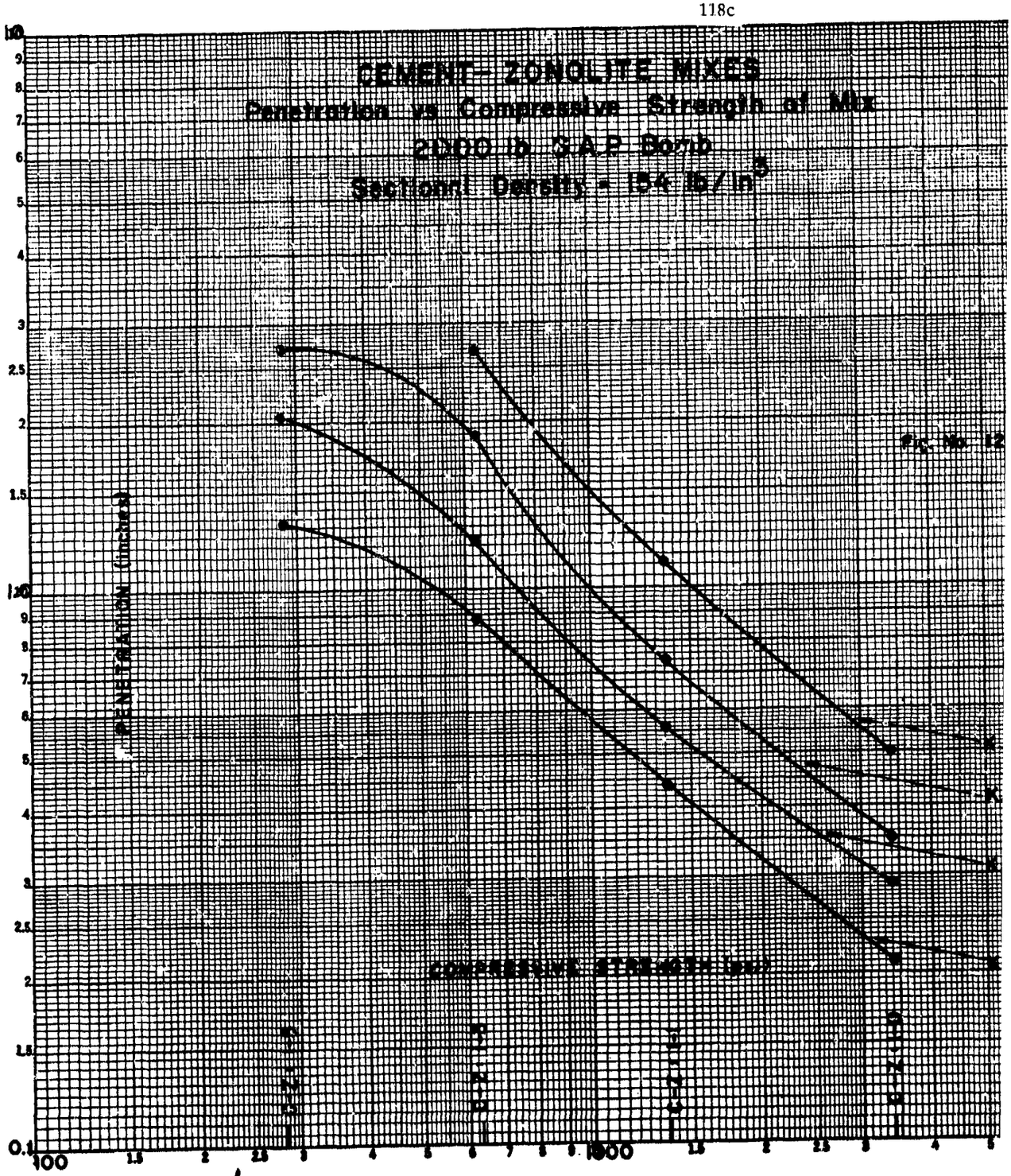
CEMENT-ZONOLITE MIXES
Penetration vs Compressive Strength of Mix
2000 lb S.A.P. Bomb
Sectional Density = 154 lb/in³
Fig. No. 12
PENETRATION (inches)
COMPRESSIVE STRENGTH (psi)
100
1000

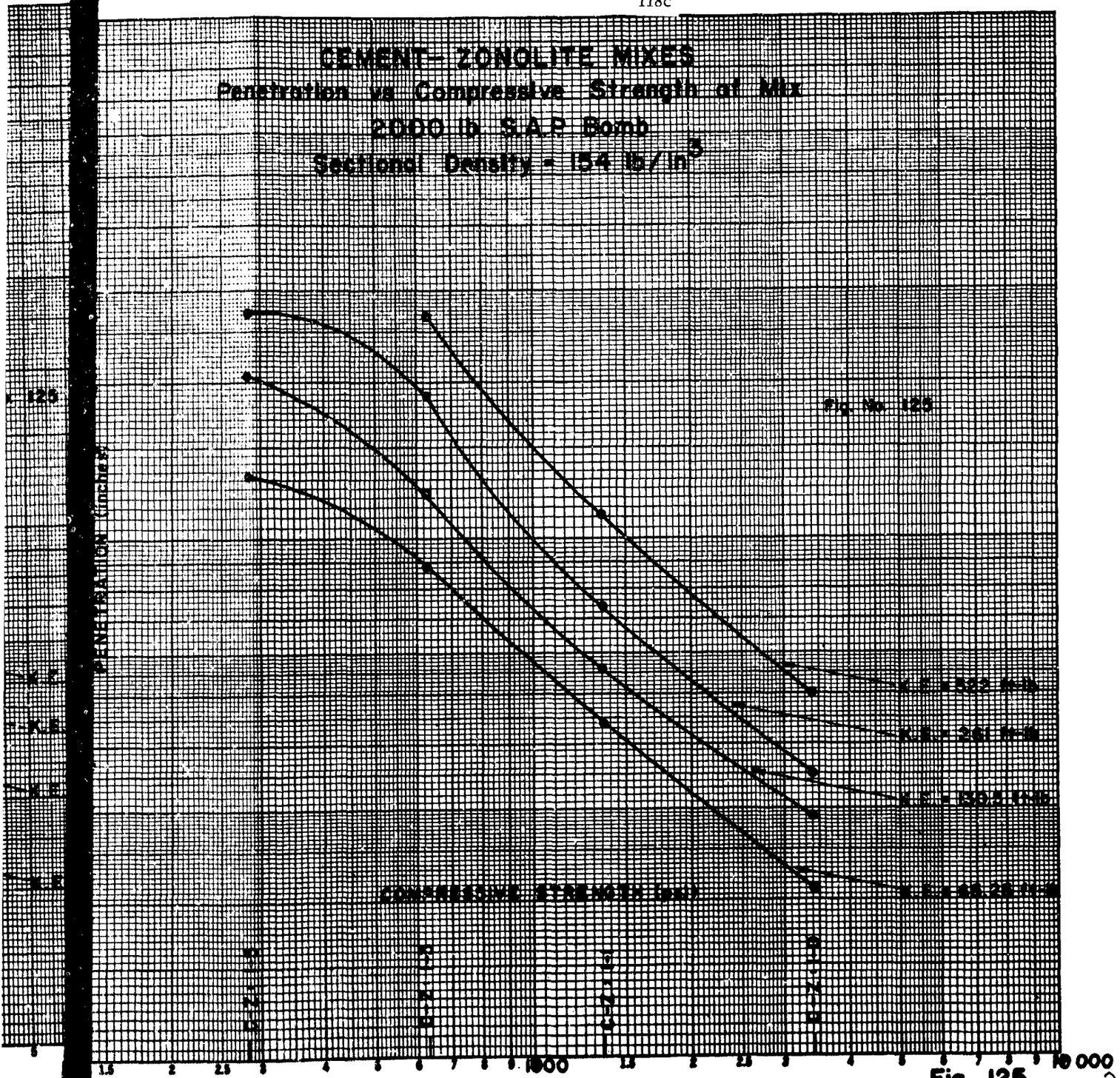
CEMENT- ZONOLITE MIXES
Penetration vs Compressive Strength of Mix
2000 lb S.A.P. Bomb
Sectional Density = 154 lb/in^3
Fig. No. 125
PENETRATION (inches)
COMPRESSIVE STRENGTH (psi)
1.5
2
2.5
3
4
5
6
7
8
9
1000
10 000

Fig. 125

density of 200.9 pounds per cubic inch and a constant value of kinetic energy of 112 foot-pounds were commenced as soon as the mixture reached a compressive strength of 693 pounds per square inch and were continued until the blocks reached a constant strength.

Results are plotted in Figure 126 in the order of increasing compressive strengths. The curves show that penetration of each of the three types of model bombs decreases abruptly at first and then with a further increase in compressive strength the penetration of all three types of bombs increases. Inasmuch as the curves for all three types of bombs follow the same form and inasmuch as both the sectional density of the various bombs and the kinetic energy were held constant, the value of compressive strength as a penetration index is doubtful.

By plotting penetration against time rather than against compressive strength, smooth curves result. The time lag between 770 and 790 pounds per square inch is considerable, and that lag accounts for the abrupt decrease in penetration. It appears, therefore, that some physical or elastic property of the material other than compressive strength should be employed as a penetration index.

5—Variation of Penetration with Kinetic Energy

Laboratory experiments were designed to determine, if possible, the relations between penetration and kinetic energy in a model material of constant strength and constant elastic properties. It was recognized that the particular physical or elastic property to be used as a penetration index was unknown, but that whatever the index was, there must be some relation between it and the depth of penetration at various values of kinetic energy.

The first experiment was conducted using a mixture of

18.52 per cent Calseal

12.80 per cent Water

52.80 per cent Coarse Sand (—8 to +14 mesh)

15.88 per cent Fine Sand (—14 mesh)

Tests were conducted after the mixture reached a constant compressive strength of 1054 pounds per square inch using a model 2000 SAP bomb at a sectional density of 154 pounds per cubic inch. The tests were extended into deeper penetrations, but in order to do so it was necessary to increase the sectional density with the same type of bomb and to use a model mixture of 928 pounds per square inch compressive strength.

The results of the experiment and the change in sectional density and model strength in the higher ranges of kinetic energy are plotted on the graph, Fig. 127.

From the data it is evident that the equation expressing the relation

between penetration and kinetic energy is not a straight-line function of the form

$$P_2 = \frac{KE_2}{KE_1} \cdot P_1$$

where,

P_2 = penetration at KE_2

P_1 = penetration at KE_1

KE_1 = low value of kinetic energy

KE_2 = high value of kinetic energy

The dip in the curve originally was thought to coincide with the change from partial to complete burial of the nose of the bomb. The change in slope of the curve below 400 foot-pounds and above 525 foot-pounds was thought to be due to a difference in the penetration index of the model material.

The next experiment was conducted using molding plaster rather than a Calseal-sand mixture and was designed to investigate the relation between penetration and kinetic energy with SAP and AP model bombs in the region of penetration beyond complete burial of the nose. The molding plaster was composed of two parts of plaster to one of water by volume. The cast blocks were air dried at room temperature for four weeks before being used. At the time of the experiment, the compressive strength of the molding plaster was found to be 1418 pounds per square inch, and the sclerescope hardness of the plaster to be 5. Strain gauges were attached to test cylinders of the plaster, and Young's modulus and Poisson's ratio were measured in the manner described under "Physical Rock Tests." The impact toughness of the plaster also was measured and found to average 13.59 foot-pounds per square inch.

The procedure for the test consisted of making three individual drops at each value of kinetic energy and averaging the depth of penetration of the three drops for various values of kinetic energy ranging from 450 foot-pounds to 790 foot-pounds. Model SAP bombs and model AP bombs were tested at sectional densities of 308 and 522 pounds per cubic inch .

Figures 128 and 129 are photographs of the model blocks after impact. The manner of failure is similar to that observed in the field.

The graphs, Fig. 130, show the relation between penetration and kinetic energy for each of the two types of model bombs. It may be observed from the graph for the AP model bomb that in the region from 550 to 650 foot-pounds the depth of penetration remains nearly constant. This same effect was observed between 30 million and 40 million foot-pounds in the field. The rates of increase of penetration with increasing kinetic energy before and after the period of nearly constant penetration are essentially the same.

The region in which the penetration remains constant for a model SAP bomb is from 625 to 750 foot-pounds kinetic energy. The period of

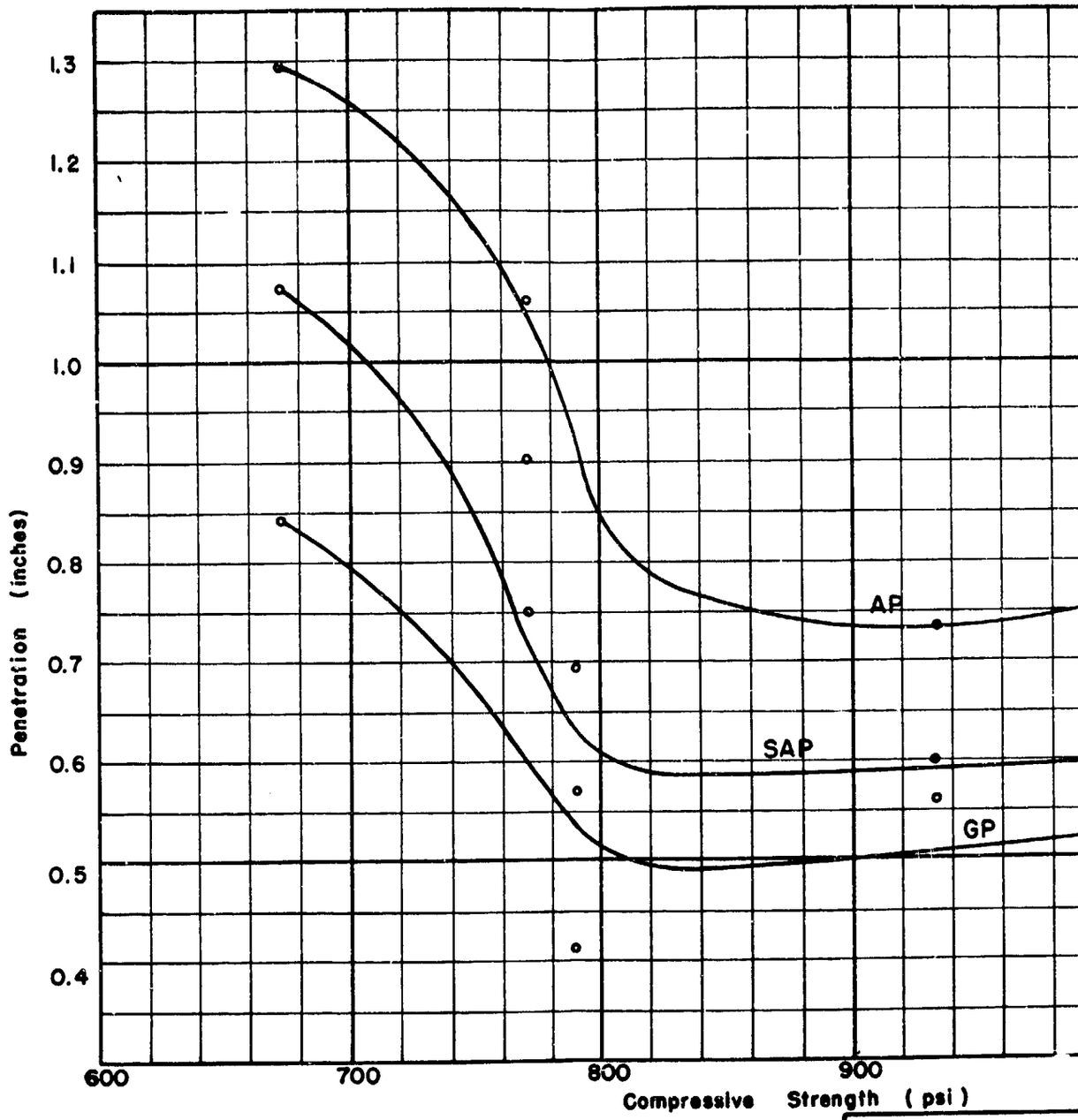

-BOMB PENETRATION

Scale ——— Date 3-6-

Fig. No. 126 By AWG.

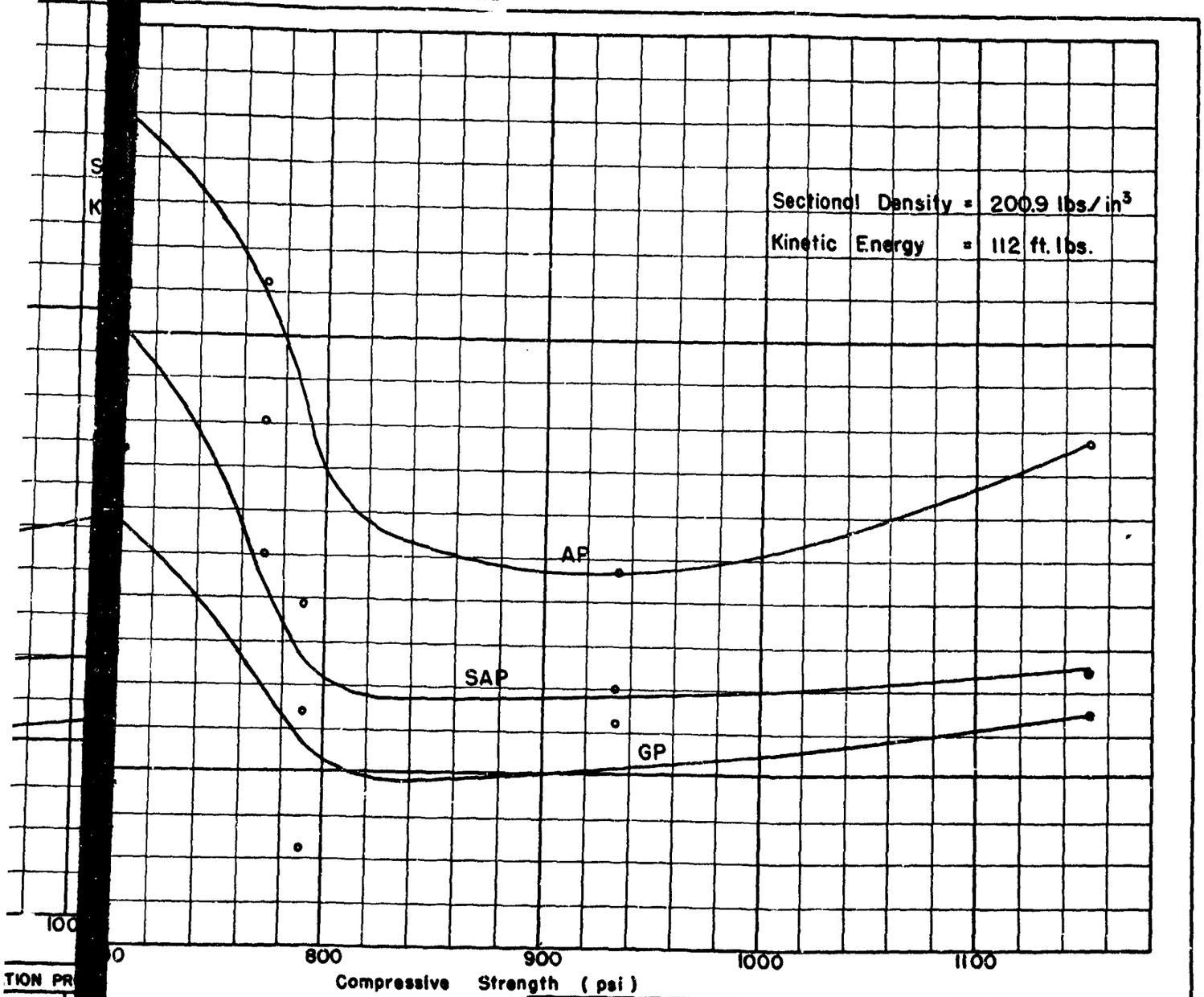

-BOMB PENETRATION PROJECT- CSM RESEARCH FOUNDATION, INC.

Scale ——— Date 3-6-51

Fig. No. 126 By AWG.

PENETRATION vs. COMPRESSIVE STRENGTH

Fig. 126

2

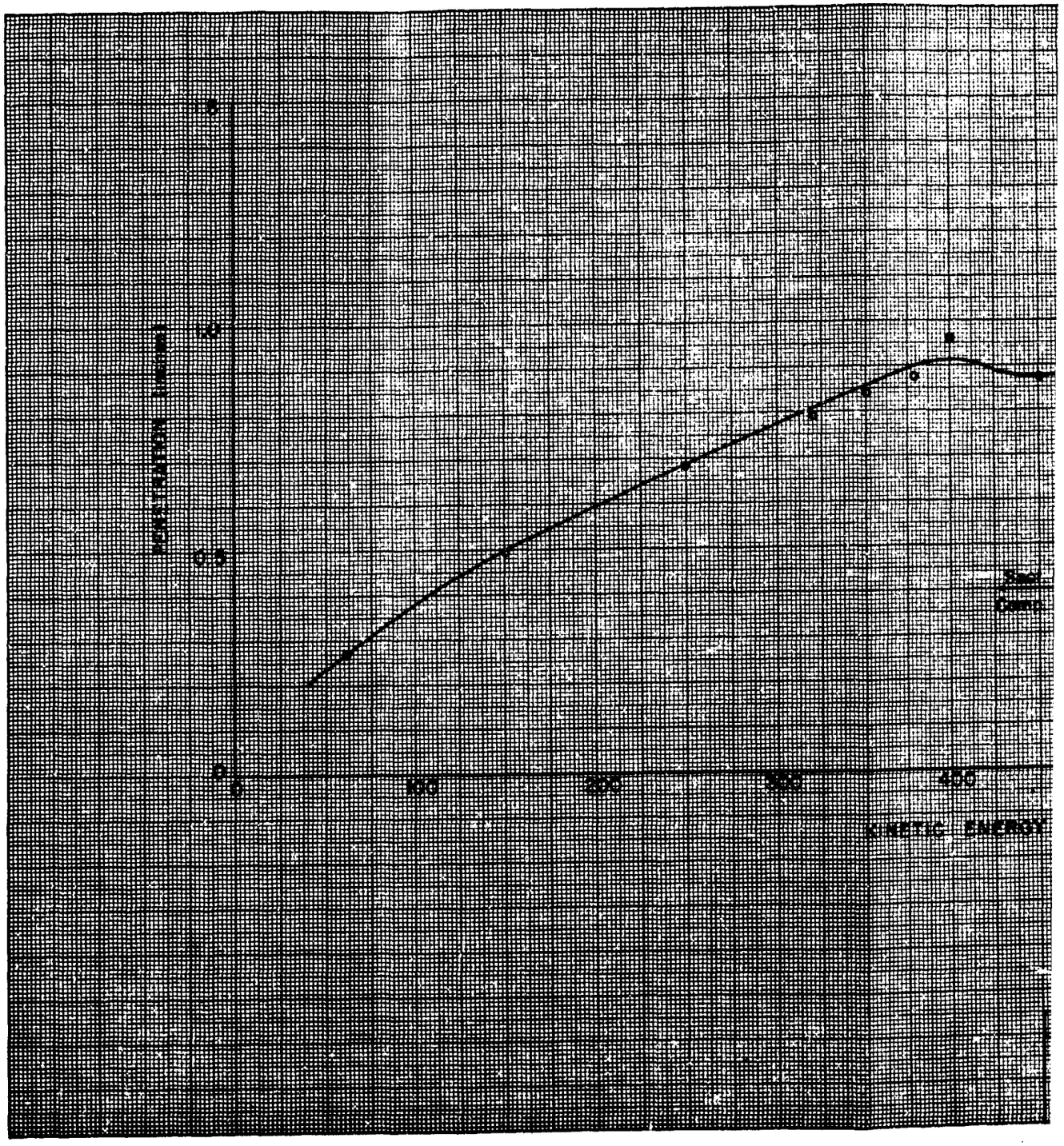
1.0
0.5
0
0
100
200
300
400
KINETIC ENERGY

120b

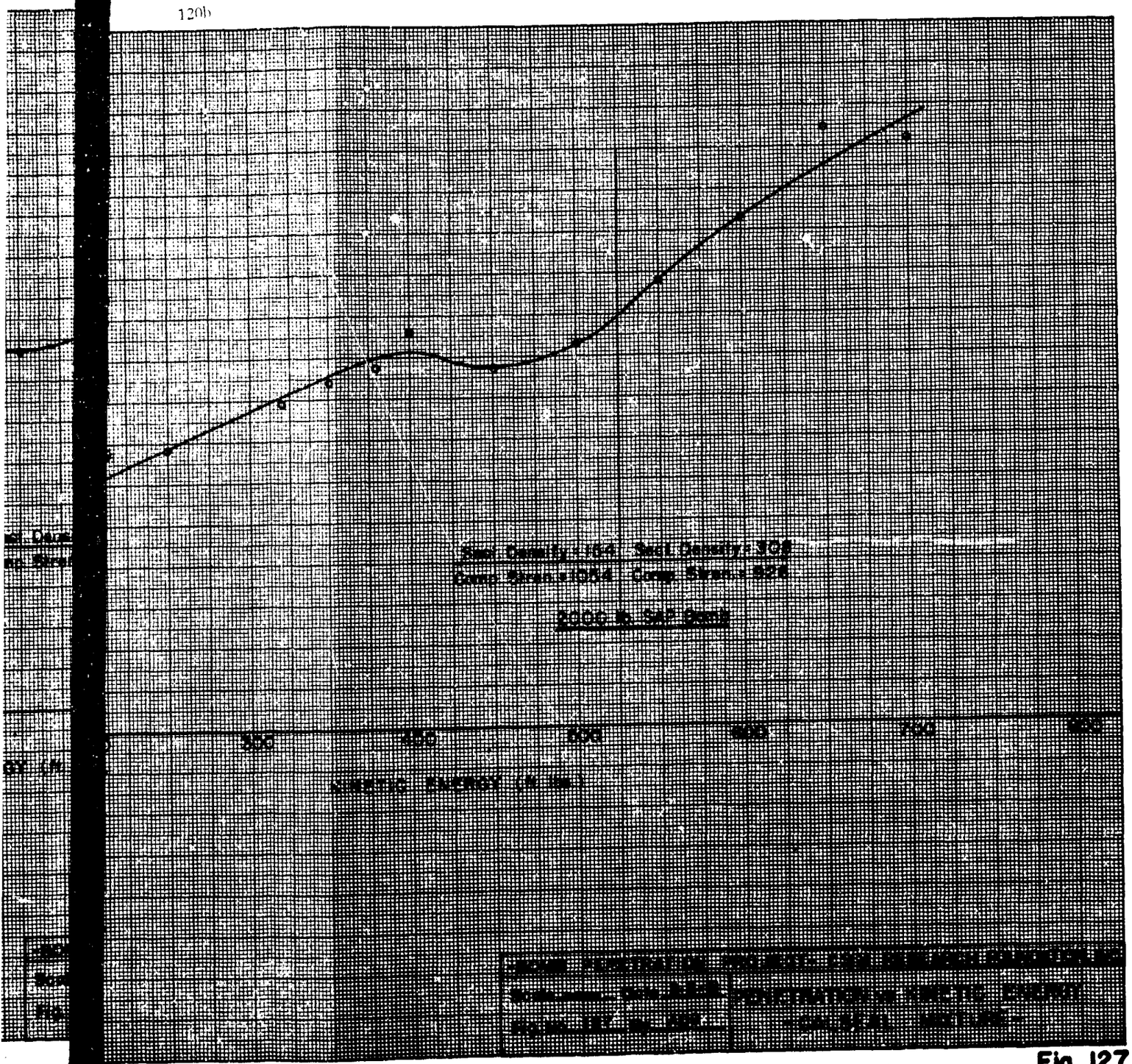

Fig. 127

2

Fig. 128

Plaster Model After Impact—SAP Model Bomb

Fig. 129
Plaster Model After Impact—AP Model Bomb

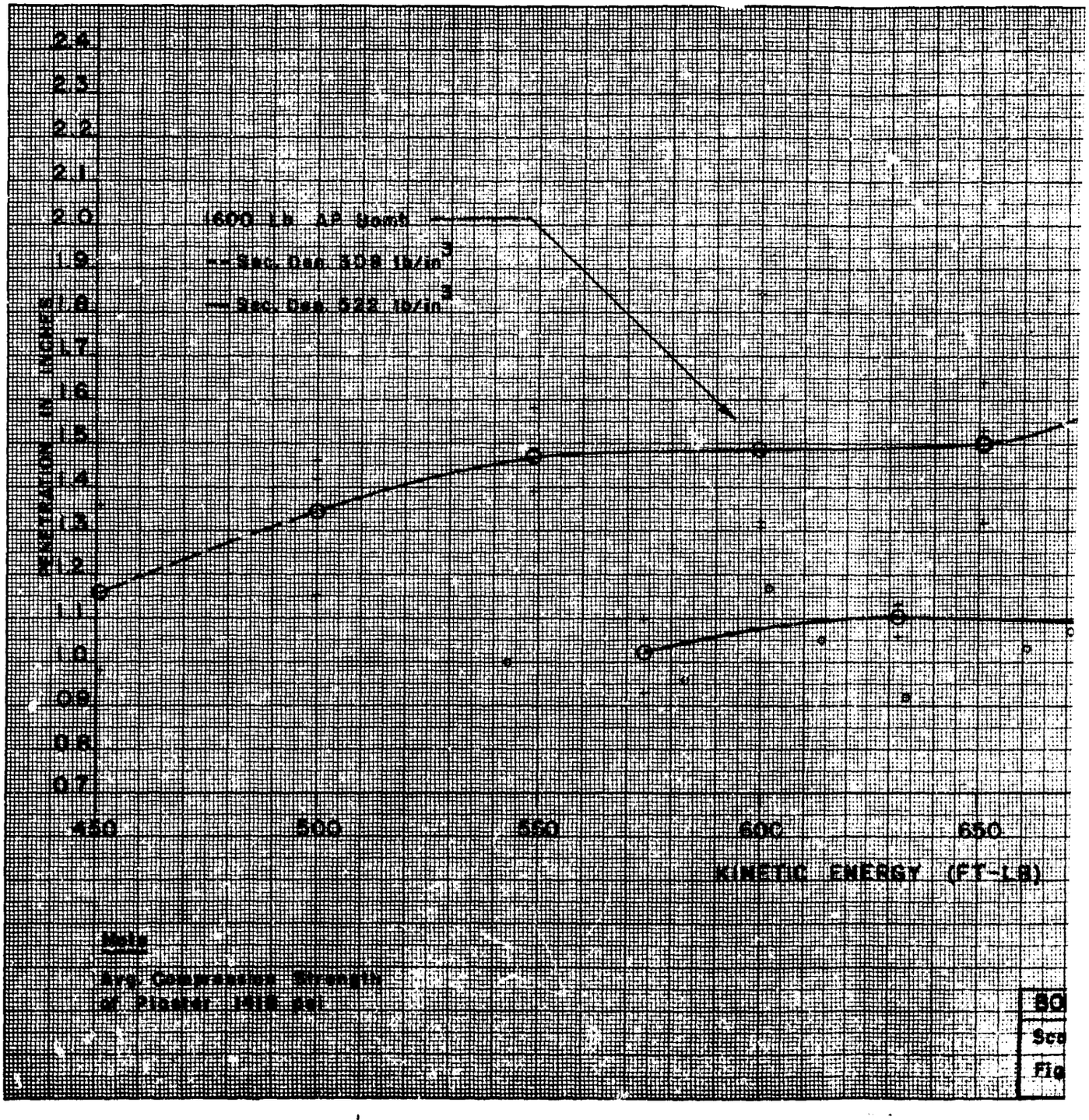
2.4
2.3
2.2
2.1
2.0
1.9
1.8
1.7
1.6
1.5
1.4
1.3
1.2
1.1
1.0
0.9
0.8
0.7
PENETRATION IN INCHES
1600 Lb AP Bomb
-- Sec. Den. 308 lb/in^3
— Sec. Den. 522 lb/in^3
450
500
550
600
650
KINETIC ENERGY (FT-LB)
Note
Avg. Compression Strength
of Plaster 1418 psi

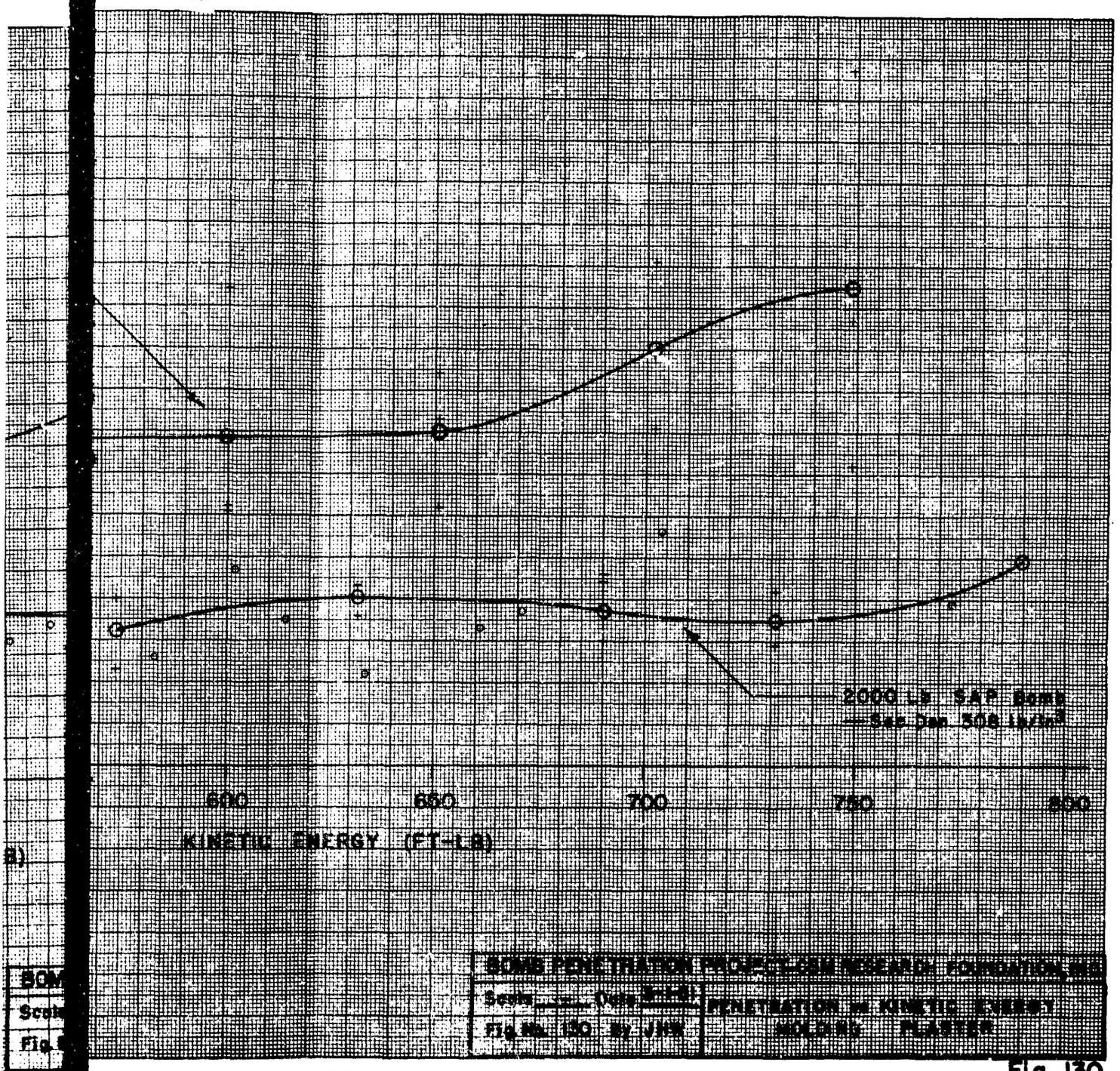
2000 Lb SAP Bomb
Sap Dam 308 lb/in²
600
650
700
750
800
KINETIC ENERGY (FT-LB)
BOMB PENETRATION PROJECT-CSM RESEARCH FOUNDATION, INC.
Scale Date
Fig. No. 130 By JHW
PENETRATION vs KINETIC ENERGY
MODERN PLASTER

Fig. 130

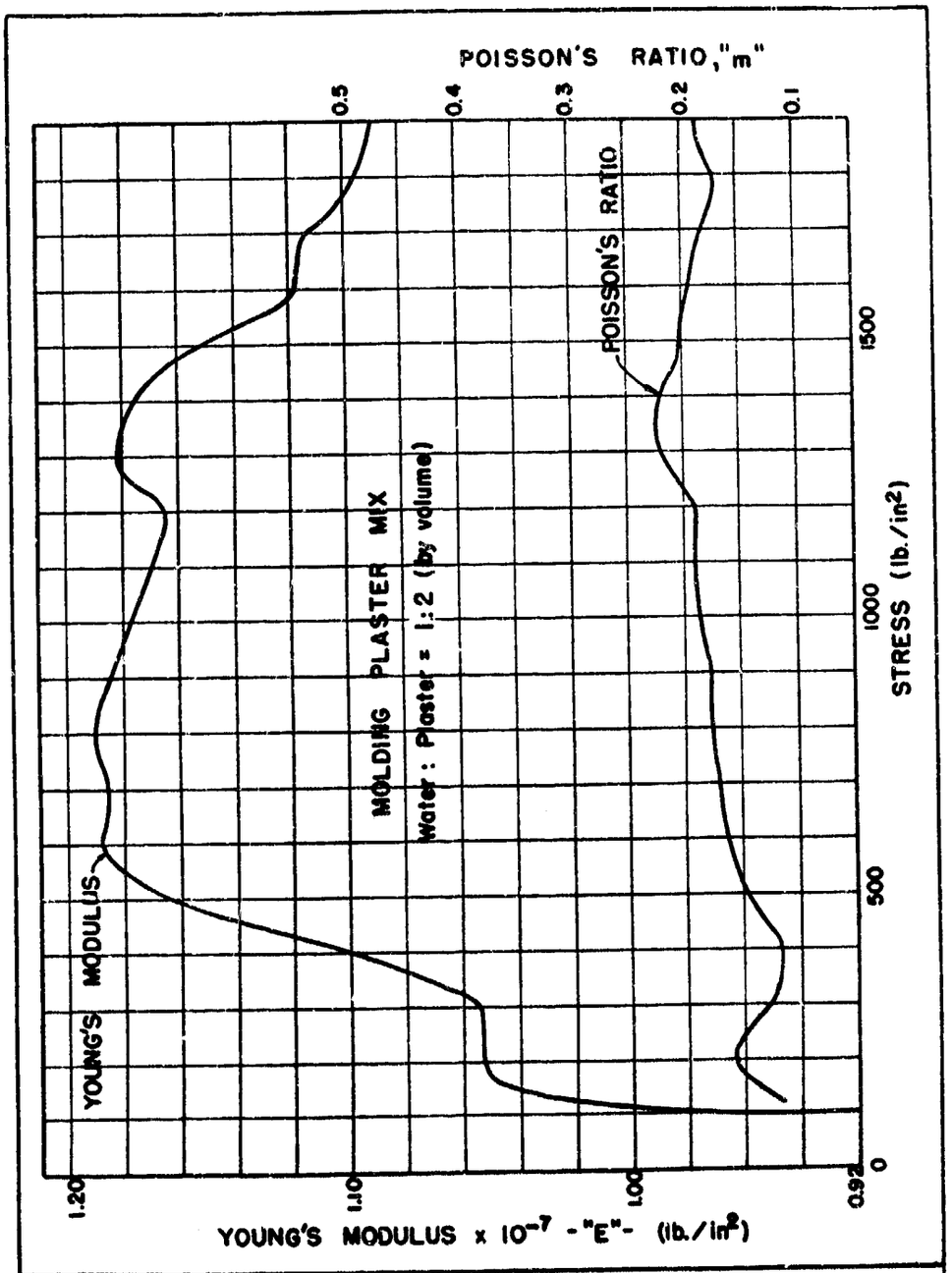

-BOMB PENETRATION PROJECT- CSM RESEARCH FOUNDATION, INC.

Scale ——— Date 3-5-51	POISSON'S RATIO & YOUNG'S MODULUS
Fig. No. 131 By LB	-MOLDING PLASTER-

Fig. 131

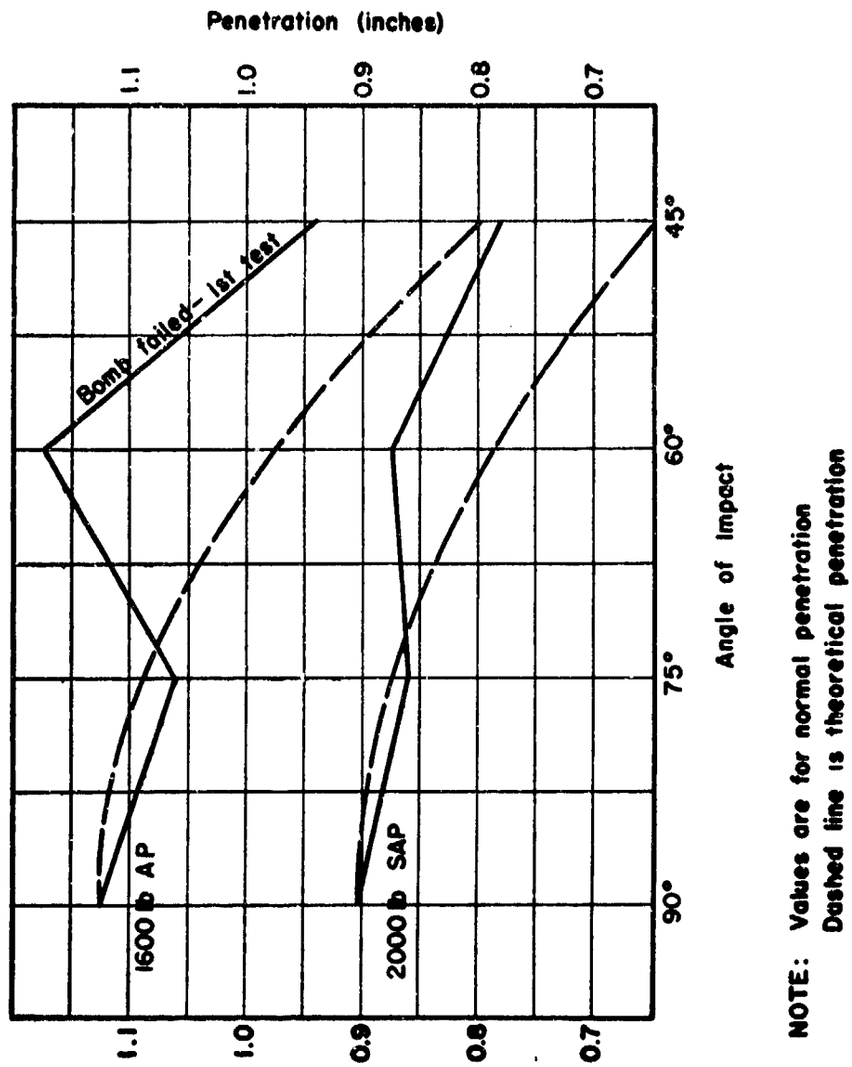

-BOMB PENETRATION PROJECT- CSM RESEARCH FOUNDATION, INC.

Scale ——— Date 3-20-51

Fig. No. 132 By ADG

VARIATION OF PENETRATION WITH ANGLE OF IMPACT-

Fig. 132

constant penetration for an SAP bomb occurs at a larger value of kinetic energy and persists over a larger span of kinetic energies than for an AP bomb. This same effect was observed also in the field.

Figure 131 is a graph showing values of Young's modulus and Poisson's ratio as computed from the results of strain measurements on the plastic model material. Poisson's ratio increases from a minimum of 0.1 to a maximum of 0.225. Young's modulus increases to a maximum of 1.19×10^5 pounds per square inch. The range of values does not differ greatly from the range of values for unweathered Zuni granite, and the shape of the penetration curves for AP and SAP bombs in granite (Fig. 90) and for AP and SAP bombs in sandstone (Fig. 109) is remarkably similar to the curves plotted from the laboratory data (Fig. 130).

6—Variation of Penetration with Angle of Impact

This experiment was designed to study the effect of the angle of impact upon the depth of penetration of the 1600 AP and the 2000 SAP model bombs. The angle of impact was varied by tilting the model confining the mechanism. The material penetrated was a molding plaster consisting of 1 part water to 2 parts plaster. Penetration tests were made at 14 days, at which time the compressive strength of the plaster was 2145 pounds per square inch and the tensile strength was 351 pounds per square inch. Strain measurements were taken to determine Young's modulus and Poisson's ratio.

Drops were made at constant kinetic energy of 500 foot-pounds and constant sectional density of 308 pounds per cubic inch for both bombs so that comparable results could be obtained. These values were selected within the range of former tests in order that a correlation could be made if found desirable. Three drops were made with each model bomb at 90 degrees, 75 degrees, 60 degrees, and 45 degrees and the average normal penetration computed from the inclined penetration. The testing machine is designed to hold the model bombs rigidly, and therefore does not permit curvature of the bomb path, which would result with a free-falling body. The tendency of the bomb to curve was sufficiently great at a 45-degree angle of impact to cause the 1600 AP model bomb to fail at the threads.

The results are presented graphically in Fig. 132. The solid line for each bomb shows the variation in the depth of computed normal penetration with a decrease in the angle of impact. The dashed line is the theoretical penetration. The theoretical penetration equals the normal penetration at zero degrees obliquity, or 90-degree angle of impact, multiplied by the sine of the actual angle of impact.

It may be observed from Fig. 132 that penetration falls below the theoretical from 90 degrees to 75 degrees, but tends to increase as the angle of impact is further decreased to 60 degrees. After 60 degrees a readjustment causes the true penetration to trend parallel to the theoretical, but to remain greater than the theoretical. The relations are similar for both bombs. Probably the shape of the solid line would be less angular if penetration were measured for, say, 5-degree changes in angle of impact rather than 15-degree changes.

A possible explanation of the increased penetration between a 75-

degree and 60-degree angle of impact is that the manner of rock failure may be different because of a difference in the stress distribution in the medium. Whether or not the increased penetration would have occurred if the model bomb had not been fastened rigidly to the striking tup is unknown.

SECTION II—STRESS-COAT EXPERIMENTS

1—Introduction

A novel technique useful in the study of failure of materials under impact loads was developed by George Hesselbacher, Jr.[1] in the Barodynamics Laboratory of the Colorado School of Mines. Hesselbacher's experiments, though of a preliminary nature, demonstrated that one of the directions of principal stress can be determined quickly by use of his apparatus and techniques. The use of brittle coatings for the indication of strains within the elastic range was first reported by Dietrich and Lehr of Germany in 1932. The use of brittle coatings to determine quantitative values was begun at the Massachusetts Institute of Technology in 1937.

A superior brittle coating material developed in the United States and marketed under the trade name "Stress-coat" has the property of fracturing at low values of tensile strain in a direction perpendicular to the direction of principal tensile stress in the area of the crack. At larger values of strain, stress-coat will also flake off in a manner similar to the flaking of mill scale on steel. According to deForest, Ellis, and Stern[2] the flaking occurs in the initial yield region of most metals and correlates directly with the amount of compressive strain produced.

The objectives of the present study were 1) to determine the direction of principal stress in the medium caused by impact of a model bomb at various angle of obliquity, 2) to determine the effect of various depths of penetration and of various types of bombs upon the stress distribution, and 3) to obtain experimental data useful in analyzing the field results of the Bomb Penetration Project.

Figure 133 is a photograph of the Hesselbacher apparatus. It consists of an aluminum beam which is pivoted at one end and to which a striker, or tup, is bolted at the point of impact; curved angle irons which function as supports to position the beam at various heights of drop; and a steel frame within a concrete base which holds and provides lateral support for the model. In the photograph a stress-coated, two-dimensional model representing a vertical slice of the medium is held in position and laterally confined with steel wedges, and a two-dimensional scale model of the medium machined to correspond with complete nose penetration.

Two types of model materials were used in these experiments—allite or Columbia Resin, CR-39, a photoelastic material, and 0.25-in.-thick 2430 Alclad aluminum alloy sheet. The allite model material is the more sensitive and is used when the region of compression spalling is being studied. The aluminum alloy model material is preferable in studying the region of tension cracking, particularly for high values of kinetic energy.

Straight surfaces of the model material were prepared with a milling machine, and curved surfaces were prepared with a jig-saw and a file attachment on the jig-saw. The surfaces of the model material and of a

[1] Hesselbacher, George Jr., A method for the determination of stresses around an opening under impact loads: Master's Thesis, Colorado School of Mines, May 1949.

[2] deForest, A. V., Ellis, G., and Stern, F. B. Jr., Brittle coatings for quantitative strain measurement: Jour. Applied Mechanics, vol. 9, no. 4, pp. A 184-A 188, Dec. 1942.

calibration strip were then cleaned thoroughly with thinners ST-1 or ST-2. An undercoating and a strain-indicating coating were then applied to the model and to the calibration strip.

In all experiments the flaking sensitivity of the brittle coating used was 0.018 inch per inch, and the threshold value for tension cracking was 0.0008 inch per inch.

Fig. 133

Hosselbacher Apparatus for Determining Dynamic Strain Patterns in Stress-Coat

2—Summary of Experimental Results—Aluminum Alloy Models

2a—Areas of Equal Strain

Impact tests were conducted with aluminum models of 1600 AP, 2000 GP, and 25,000 SAP bombs at 0-degree obliquity and at a depth of penetration equal to three-fourths the length of the bomb and for values of kinetic energy of 16 ft-lb, 30 ft-lb, 52 ft-lb, and 97 ft-lb. At 97 ft-lb the aluminum bomb models bent under the impact. For this reason the higher values, although suitable for determining the stress trajectories, were not used to obtain comparative or quantitative data.

Figure 134 is a photograph of the crack pattern produced by impact loading of a model of a 25,000 SAP bomb. The random cracks are drying

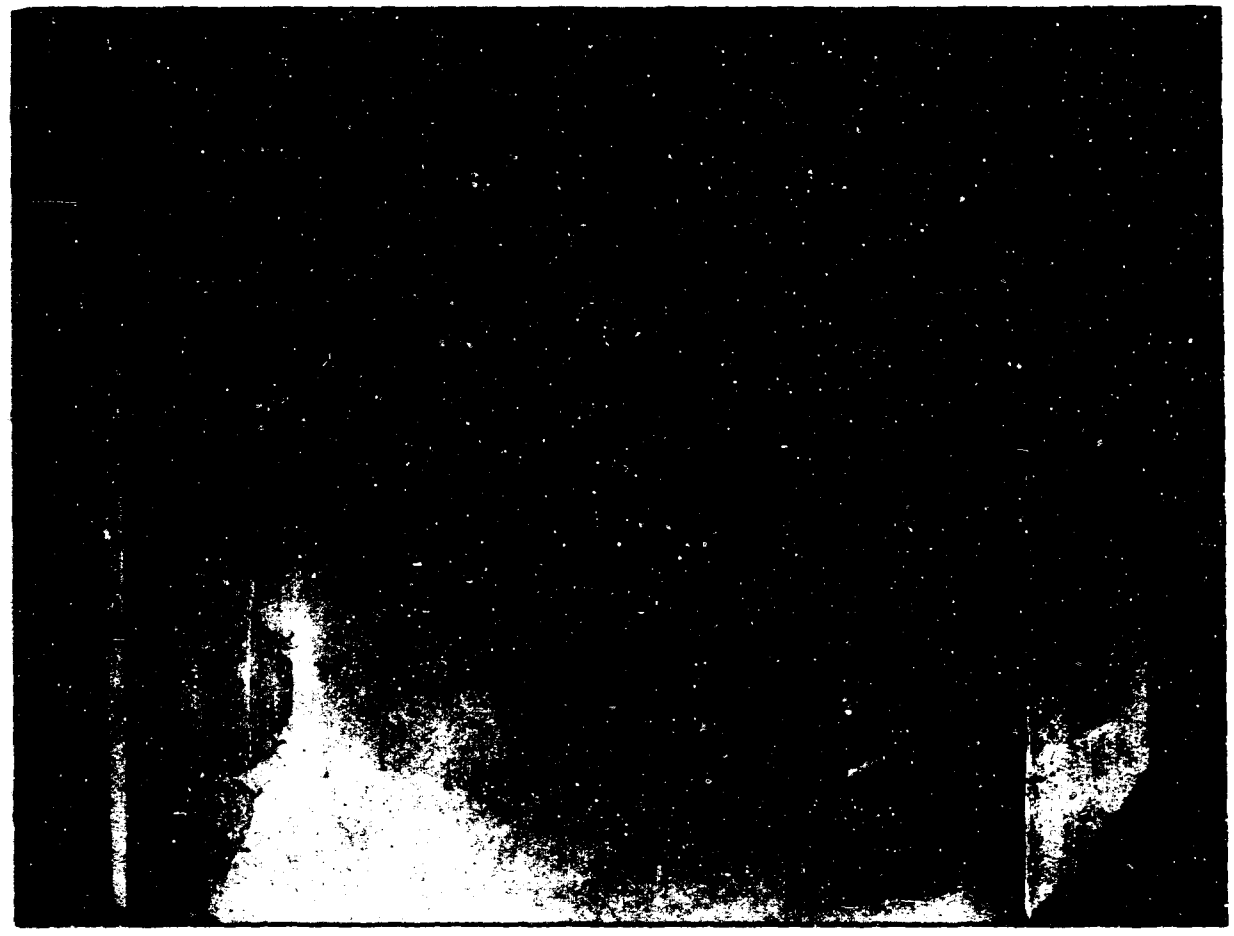

Fig. 134

Dynamic Strain Pattern in a Stress-coat Model by Impact of 25,000 SAP Model Bomb

Fig. 135
Dynamic Strain Pattern—Impact of 1600 AP Model Bomb

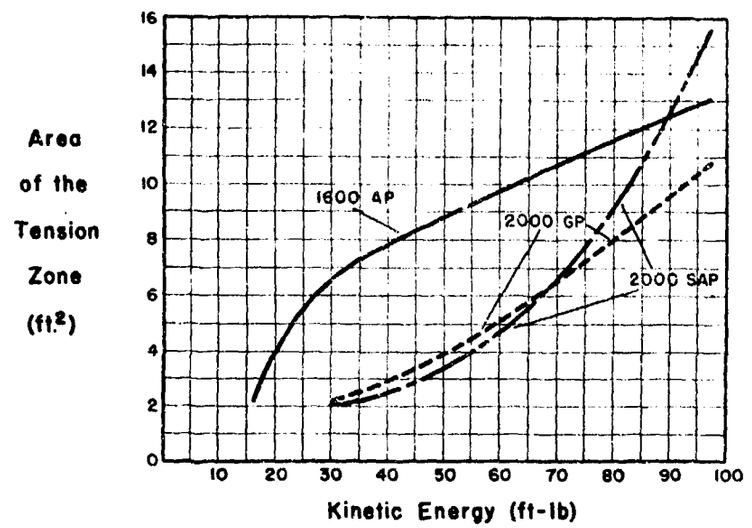

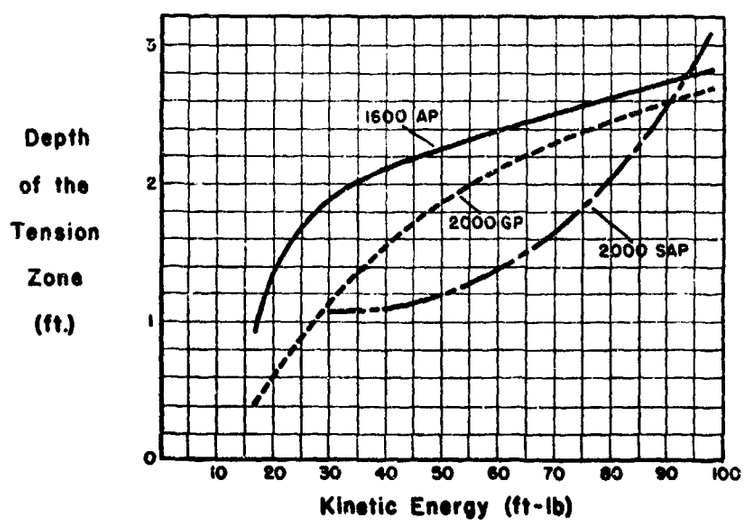

-BOMB PENETRATION PROJECT- C S M RESEARCH FOUNDATION, INC.

Scale ——— Date 2-20-51 Fig.No. 137 By ADG	AREA AND DEPTH OF TENSION ZONE vs KINETIC ENERGY STRESS-COATED MODELS

Fig. 137

cracks and have no significance. The cracks radiating from the nose and the sides of the bomb were produced by successive impacts of 16 ft-lb and 52 ft-lb. The limits of cracking for an impact load of 16 ft-lb are marked by the dotted lines. The ends of the cracks and the expansion of the area of cracking resulting from the greater impact load are apparent.

Figure 135 is a photograph of the crack pattern resulting from successive impact loads of 16, 30, 52, and 97 ft-lb on a model of a 1600 AP bomb. The elliptical lines were scribed on the brittle coating at the ends of the cracks after each successive impact. The scribed lines thus mark the locus of points where the strain in the brittle lacquer equals the calibration strain value of 0.0008 inch per inch for each specific drop.

The areas within the scribed lines (iso-entatics) indicate the region where the strain exceeded the calibration strain value. Since strain and stress are related, the respective areas are a measure of the depth and volume of rock within which the magnitude of the principal stress is not less than a fixed constant value.

The areas affected by tension cracking and the depth of the tension zone for each of the models of types of bombs used in the field work have been converted to units of feet and are as shown in Fig. 136 for various values of kinetic energy.

KE Ft-lb	Area - Square Feet				Depth, Feet			
	1600 AP	2000 SAP	2000 GP	25,000 SAP	1600 AP	2000 SAP	2000 GP	25,000 SAP
16	—	—	2.13	6.05	0.42	—	0.92	2.10
30	2.09	2.01	7.08	—	1.14	1.08	1.99	—
52	4.20	3.66	9.49	41.70	1.94	1.22	2.27	4.55
97	10.75	15.75	13.40	—	2.70	3.11	2.84	—

Fig. 136
Depth and Areas of Equal Minimum Tensile Strain

Because of the necessity of reducing the scale of the 25,000 SAP bombs compared to the three other types, it seems unwise to compare quantitatively results of the 25,000 SAP bomb with those of the other three types. The tabular values of Fig. 136 are presented graphically in Fig. 137.

2b—Stress Trajectories

The tension cracks in the brittle lacquer coating form in a direction perpendicular to the direction of principal tensile stress, and thus are parallel to the direction of maximum principal stress. The direction of minimum principal stress is at right angles to the direction of maximum principal stress. Therefore, it is possible to determine the stress trajectories of both the maximum and minimum principal stresses from the tension cracks in the brittle lacquer.

Figure 138 was constructed using the strain patterns at the highest value of kinetic energy available from the laboratory tests on scale models of 1600 AP, 2000 SAP, 2000 GP, and 25,000 SAP bombs. The following features may be observed from the figure:

1) The direction of maximum principal stress in the medium is perpendicular to the surface of the bomb nose at the point of contact between the bomb and the medium.

2) The maximum principal stress trajectories curve towards a direction parallel to the axis of the bomb; and the rate at which the curvature changes is more rapid for the sharp-nose than for the blunt-nose bombs.

3) The region in the medium from the tip of the bomb nose to the juncture of the nose and the cylindrical portion of the bomb body is the region of stress, whereas little stress develops in the portion of the medium in contact with the cylindrical sides of the bomb.

4) The least principal stress trajectories are curved surfaces somewhat concentric about the nose of the bomb and might be thought of as a "shock front," as a "wave front," or as "flow lines."

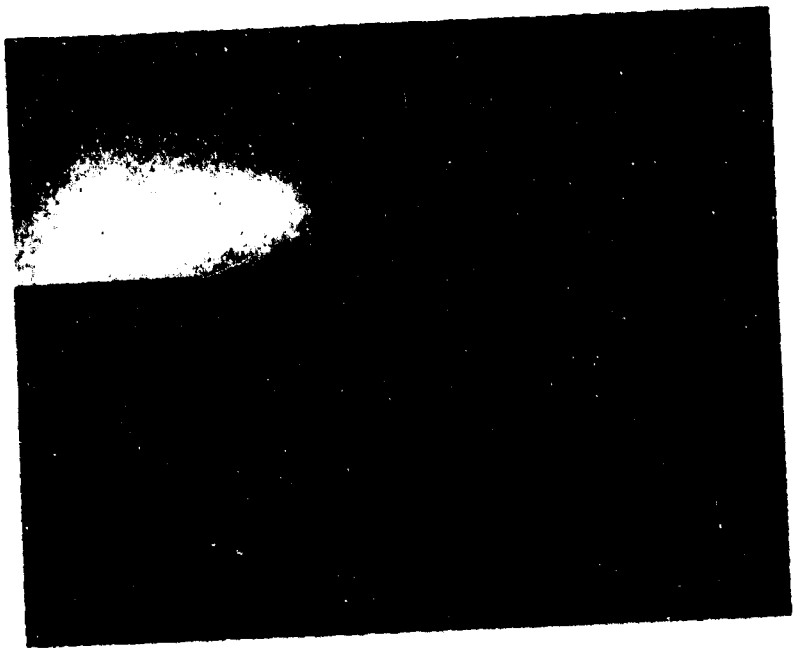

Fig. 139
Area of Flaking Below Model GP Bomb

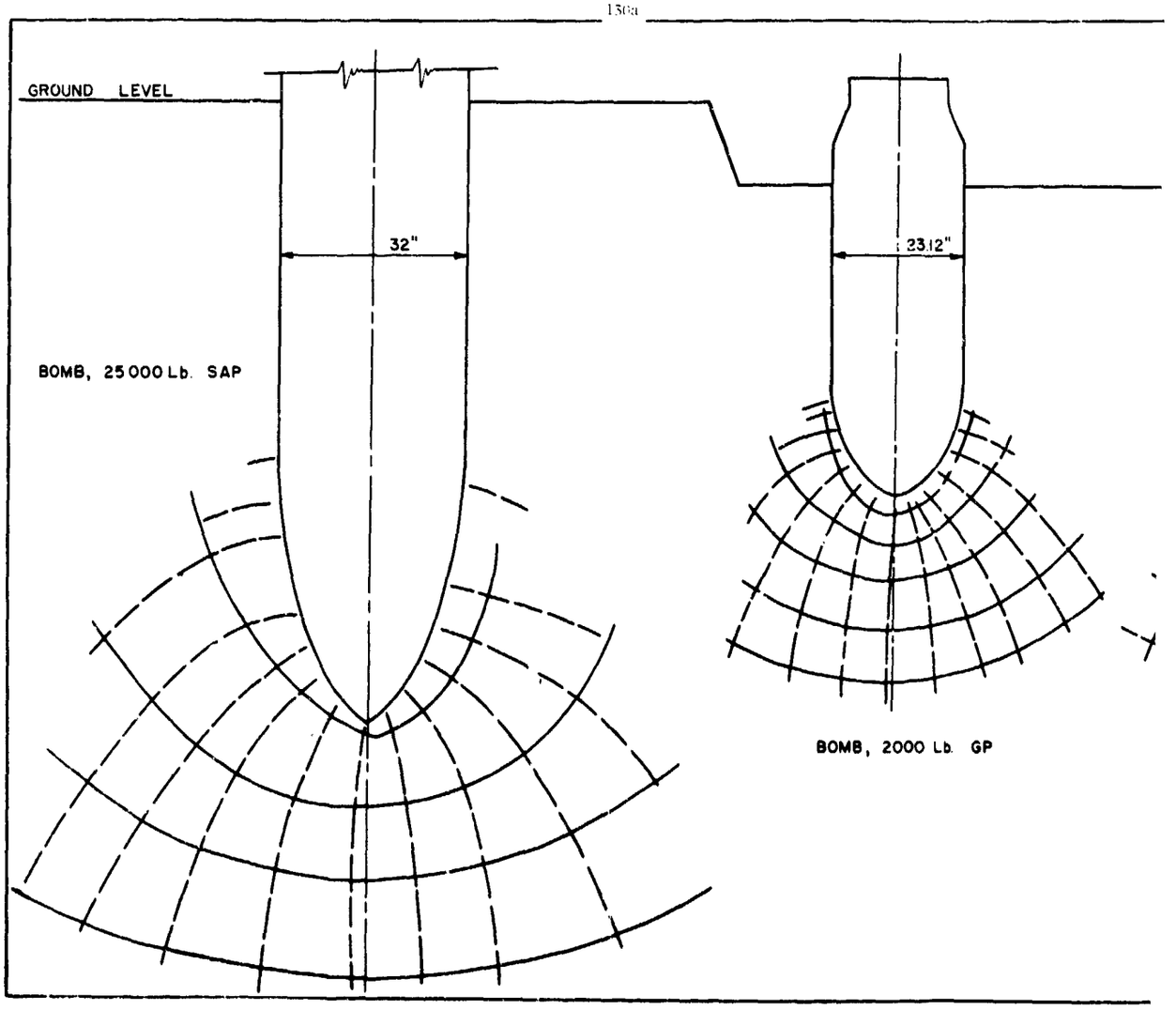
GROUND LEVEL
32"
23.12"
BOMB, 25 000 Lb. SAP
BOMB, 2000 Lb. GP

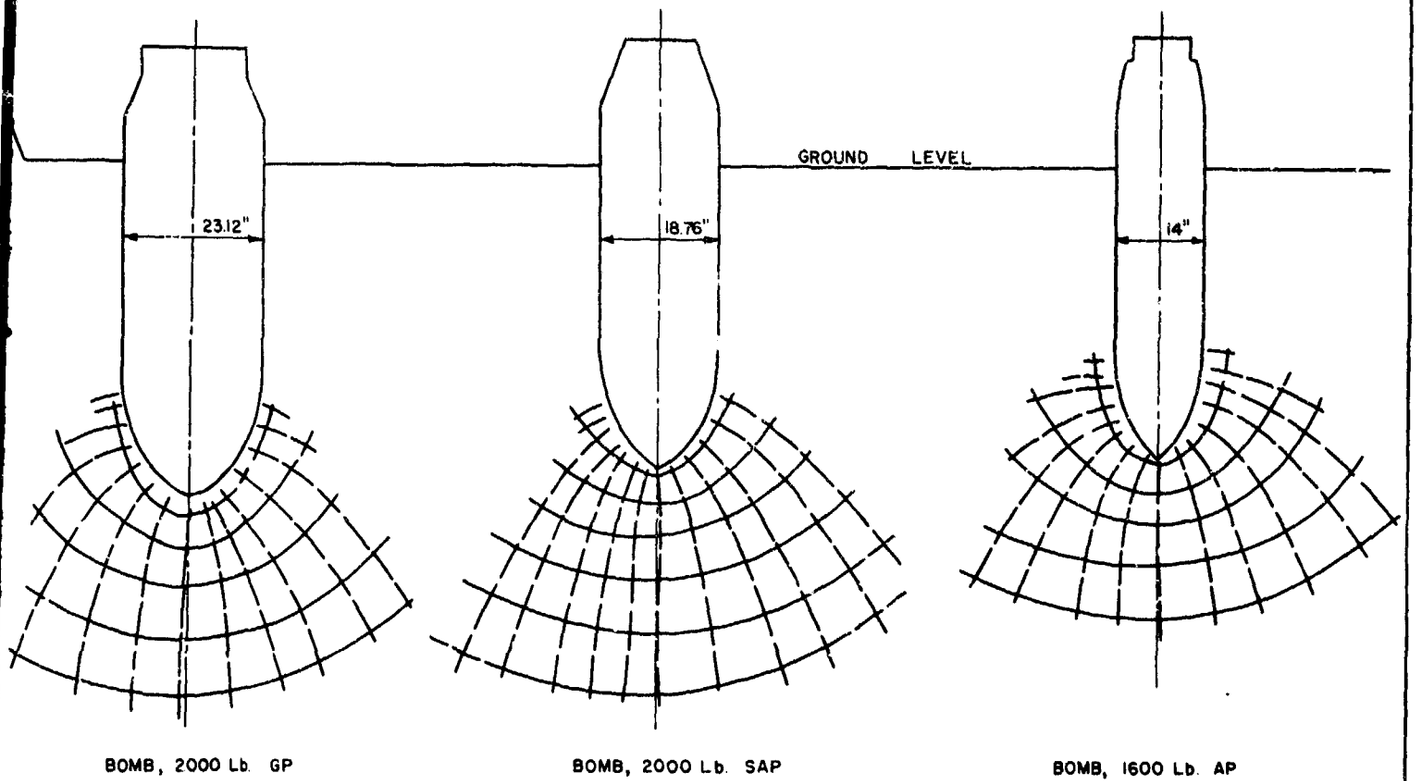

- BOMB PENETRATION PROJECT - C S M RESEARCH FOUNDATION, INC.	
Scale 1" = 17" Date 2-2-51 Fig. No. 138 By LB	STRESS TRAJECTORIES STRESS-COAT MODEL

Fig. 138

2

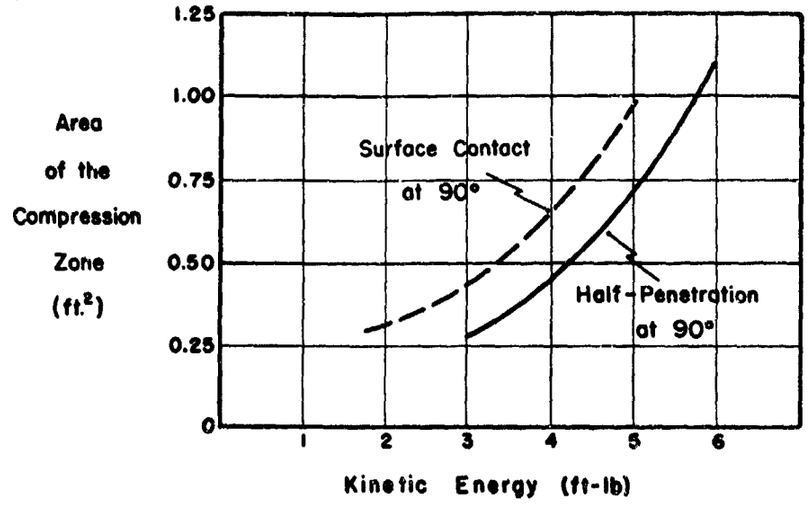

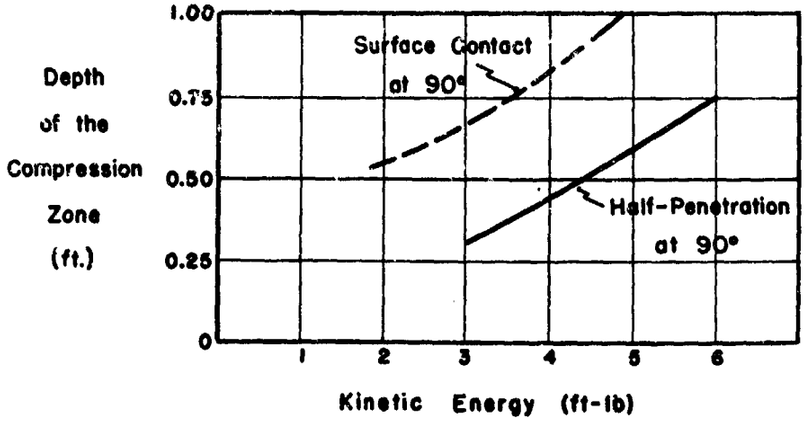

-BOMB PENETRATION PROJECT- C S M RESEARCH FOUNDATION, INC.	
Scale ——— Date 3-9-51 Fig. No. 140 By LB	AREA and DEPTH OF COMPRESSIVE ZONE VS KINETIC ENERGY 2000-LB GP BOMB

Fig. 140

3—Summary of Experimental Results—Allite Models

3a—Area of Compression Spalling—90-Degree Angle of Impact

Allite models coated with Stress-coat are particularly sensitive to flaking at low values of kinetic energy in dynamic loading. With the type of coating used in these experiments, the limits of the spalled area coincide with a strain of 0.018 inch per inch. The area and the depth of flaking increase with the kinetic energy, but differ for each type of bomb.

In the first series of experiments with Stress-coated allite models, the area and depth of flaking were measured at various values of kinetic energy for 0-degree obliquity and for surface contact between an allite ground model and an allite bomb model. Figure 139 shows the area of flaking at the nose of a model of a GP bomb and in the ground below the bomb at 1.8 ft-lb.

The area and depth of the zone of flaking converted to units of feet using the scale ratio of the bomb model to the bomb prototype are presented graphically in Fig. 140. In the same figure the depth and areas of spalling in the ground model after penetration of the same type of bomb into the medium a distance equal to half the length of the bomb is also shown.

The shapes of the curves at zero penetration and at one-half penetration are similar, but the depths and areas of flaking are less at half penetration than at zero penetration. The difference in the depth of flaking is constant for the three values of kinetic energy and equals 0.375 feet. The difference in the area of flaking equals the square of the difference in depth, or 0.1406 square feet.

A possible explanation for the decrease in depth and area of flaking at increased penetration is that the energy absorption of the ground model increases with the volume of material surrounding the energy source. In a two-dimensional model the absorption of energy by the medium would be proportional to the area of material surrounding the energy source. At half penetration, the area of material surrounding the energy source is greater than at zero penetration and is approximately equal to

$$A_2 = 2A_1 - A_m$$

where,

A_2 = energy absorption area at half penetration

A_1 = energy absorption area at zero penetration

A_m = area of the model bomb.

At surface impact the area of the spalled zone is independent of the bomb type, and depends only upon the kinetic energy of the bomb and upon the striking angle of the bomb relative to the surface. Figure 141 is a photograph of a model of a 2000 SAP bomb at 0-degree obliquity and at surface contact with the ground model. The area of flaking at kinetic energies of 0.8 ft-lb and 1.8 ft-lb and the crack pattern beyond the zone of flaking resulting from the larger impact load are shown. The crack pattern records the direction of maximum principal stress in the medium.

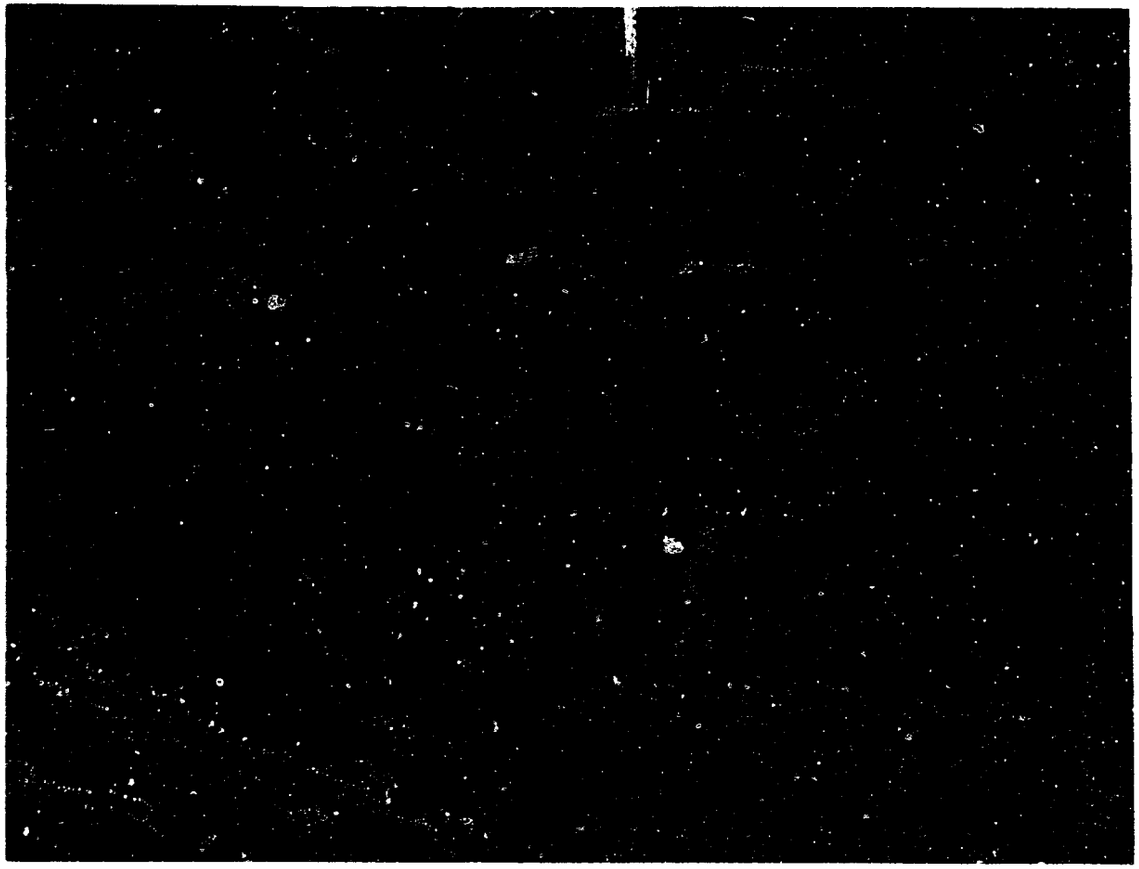

Fig. 141

Compression Spalling and Tension Cracks
Impact Model of a 2000 SAP Bomb

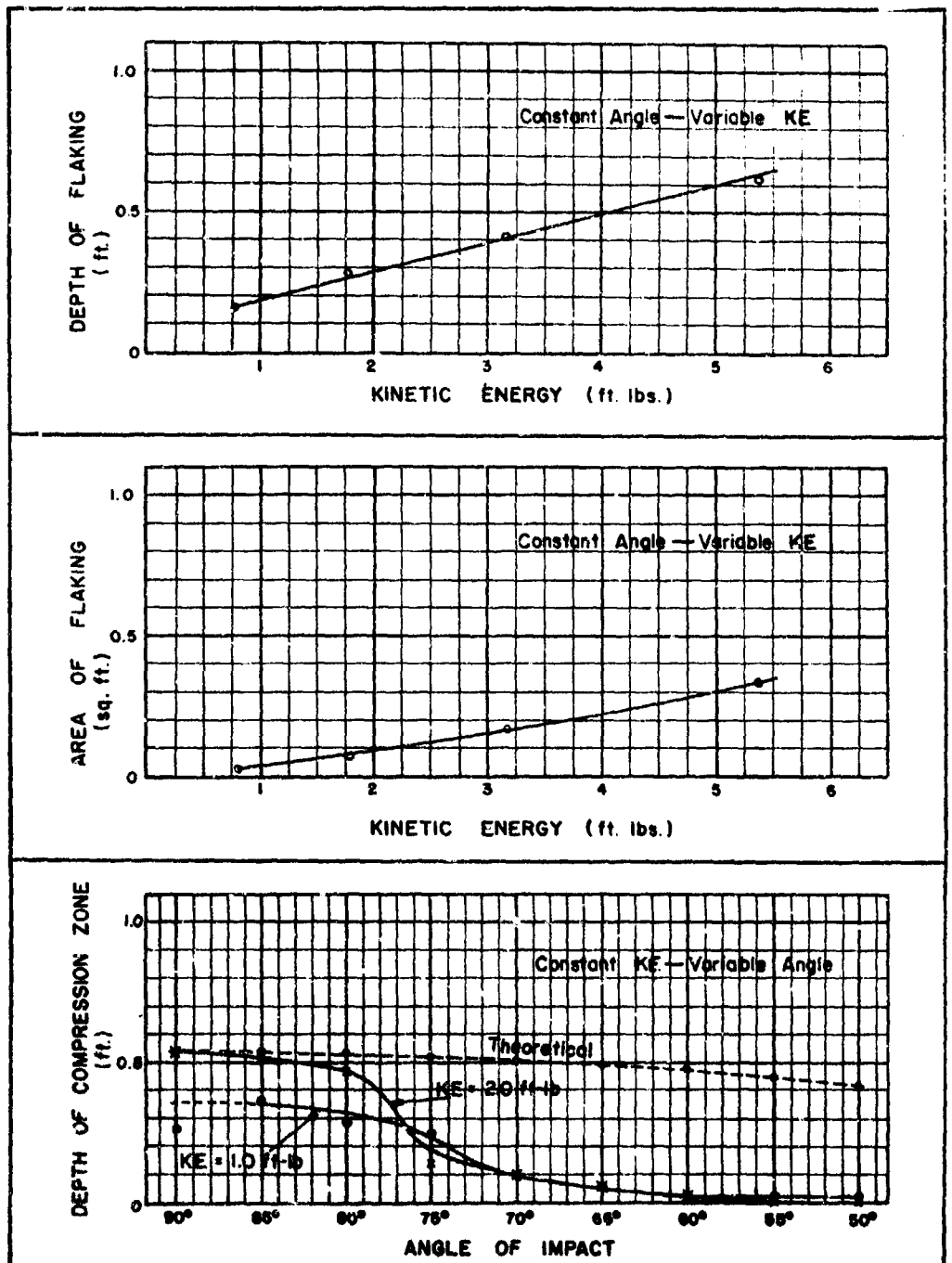

-BOMB PENETRATION PROJECT- CSM RESEARCH FOUNDATION, INC

Scale ——— Date 3-22-51

Fig. No. 142 By LSC

AREA OF FLAKING
2000 lb SAP MODEL BOMB
SURFACE IMPACT

Fig. 142

At surface impact and at 0-degree obliquity the depth and area of flaking are independent of the bomb type. Both the depth and the area of the spalled zone decrease as the obliquity increases. The effect of nose shape upon the rate of decrease of the depth and area of the spalled zone has not been studied. Figure 142 is a graph that shows the variation in the depth of the spalled zone at a constant angle of impact of 65 degrees and at various values of kinetic energy.

At the bottom of Fig. 142, the variation in the depth of the spalled zone for angles of impact ranging from 90 degrees to 50 degrees is shown. It will be noted that the depth of the spalled zone changes abruptly between 80 degrees and 70 degrees at 1 foot-pound kinetic energy and between 80 degrees and 75 degrees at 2 foot-pounds. In the model bombing experiments (see Part E, Section I, item 6) it was noted in connection with the penetration of model AP and model SAP bombs into plaster that at 75 degrees and at 500 foot-pounds, penetration characteristics changed abruptly also, but that the change was possibly due to a difference in the manner of rock failure.

A possible explanation of the abrupt decrease in the depth of the spalled zone below an angle of impact of 80 degrees in the Stress-coated allite models may be that at zero penetration, sliding begins at 80 degrees and the impact energy is absorbed over a broader area and during a greater period of time.

When the depths and areas of the spalled zones at zero penetration of a 2000 SAP bomb at 65 degrees and at various values of kinetic energy are compared with those of a 2000 GP bomb at 90 degrees (Fig. 140), it is apparent that the shape of the nose has had little effect, for the depth of the spalled zone of the model of the 2000 GP bomb at 90 degrees can be obtained as follows:

$$d_1 = \frac{d_2}{F}$$

where,

d_1=depth of spalled zone of GP bomb at 90-degree impact

d_2=depth of spalled zone of SAP bomb at 65-degree impact

F=obliquity factor for SAP bombs, or the ratio of the depth of spalling at 65 degrees to that at 90 degrees with an SAP bomb.

3b—Area of Compression Spalling at Various Angles of Impact

The effect of varying the angle of impact at constant kinetic energy upon the stress distribution in the medium can be illustrated by a comparison of the photographs, Figs. 143 and 144. The calibration strain value of both specimens was the same; thus the stress distribution may be compared qualitatively by comparing the strain patterns. In Fig. 143 the angle of impact is 65 degrees, and in Fig. 144 it is 90 degrees. In both instances, the nose of a model of a 25,000 SAP bomb was buried in the ground model a distance equal to the length of the nose at the instant of impact. The length of the ground model, and the distance from the tip of the bomb measured normal to the lower edge of the specimen were the same.

Fig. 143
Dynamic Strain Pattern at 65-Degree Angle of Impact

Fig. 144

Dynamic Strain Pattern at 90-Degree Angle of Impact

Both specimens split, and the direction of the split coincided with the crack pattern in the brittle lacquer. It is known that the crack pattern indicates the direction of lines of maximum principal stress. The crack pattern in both models below the tip of the bomb is symmetrical about the axis of the bomb. The horizontal cracks in Fig. 144 were caused by clamps used to confine the specimen in the impact-loading device and may be ignored in making the comparison.

The depth of the spalled area at normal penetration is somewhat deeper than at 65 degrees. The length of the cracks normal to the bomb nose and above the spalled area is greater at normal penetration than at 65 degrees. Cracks develop at the surface of the ground model for normal penetration and dip inward toward the bomb nose. Although the crack pattern at the surface is not symmetrical, the lack of symmetry is thought to be due to a slight eccentricity in the application of the impact load. At 65 degrees one inward-dipping crack formed on the hanging-wall side near the bomb and a few short cracks are visible in the model but not in the photograph. No cracks are present on the footwall side.

A possible explanation of the difference in the stress distribution is similar to that previously given as a possible explanation of the decrease in the size of the spalled zone at increased depths of penetration. That is, the energy-absorbing area, measured as a circular-shaped surface whose center is at the point of impact, differs on two sides of the bomb. The side of the bomb having the greater energy-absorbing area will exhibit fewer cracks and less spalling than the side of the bomb having the lesser energy-absorbing area.

SECTION III—STRESSES AND DISPLACEMENTS PRODUCED IN A SEMI-INFINITE SOLID BY A CONCENTRATED FORCE AT THE SURFACE

By W. H. Jurney

1—Introduction

The results presented in this report are derived from the classical theory of elasticity as treated by Boussinesq, Cerrutti, and others in connection with the problem of determining displacements and stresses in a semi-infinite solid bounded by a plane surface, subjected to various types and combinations of types of loading and displacement. The report is an outline of results rather than a complete presentation that includes the derivations of the equation used.

The procedure followed here has been to start with known displacements of a type possible in a continuous body and to compute stresses by means of the stress-strain relations of elasticity (Hooke's Law). For a complete statement of the theory, which cannot be presented here, a reader who desires additional theory is referred to the standard works of Love[1] and of Timoshenko[2].

2—Notation

The notation is that used by Timoshenko[2], and is summarized as follows:

σ_x = normal stress in the x direction

σ_y = normal stress in the y direction

σ_z = normal stress in the z direction

T_{xy} = shear stress parallel to x and perpendicular to y

T_{xz} = shear stress parallel to x and perpendicular to z

T_{yz} = shear stress parallel to y and perpendicular to x

σ_1 = maximum algebraic principal stress

σ_2 = intermediate algebraic principal stress

σ_3 = minimum algebraic principal stress

u, v, w = displacements in the x, y, and z directions respectively

a = shear modulus

m = Poisson's ratio

λ = Lame"s constant

1) Love, A. E. H., The Mathematical Theory of Elasticity, 4th ed.
2) Timoshenko, S., Theory of Elasticity, 1st ed., 1934.

E = Young's modulus

$\epsilon_x, \epsilon_y, \epsilon_z$ = direct strain

$\epsilon_{xy}, \epsilon_{xz}, \epsilon_{yz}$ = shearing strain in planes xy (horizontal), xz (vertical) and yz (vertical) respectively

$e = \epsilon_x + \epsilon_y + \epsilon_z$, or unit volume expansion or contraction

$r = \sqrt{x^2 + y^2 + z^2}$, distance from origin to points having rectangular coordinates (x,y,z)

3—Stress and Coordinate Conventions

Figure 145 shows the attitude of the x, y, and z axes and the direction of the force R and of its horizontal component H and its vertical component V relative to the reference axes. The xy plane is horizontal and is the boundary plane of the semi-infinite solid being considered. The origin of coordinates is the intersection of the horizontal plane xy and the two vertical planes xz and yz. The positive directions are to the right in the direction of H, and downward in the direction of V. Tension is taken as a positive direct stress, and compression as a negative direct stress.

The shear convention is illustrated in Fig. 145. The direction of a positive shear component acting in any plane coincides with the positive axial direction if the normal positive (tensile) stress acts in the corresponding positive axial direction. A negative shear component acts in the opposite direction relative to the normal stress and the positive axial direction. A shearing stress in the x direction lying in a plane perpendicular to the y axis is denoted by T_{xy}. A normal stress in the x direction across a plane perpendicular to the x axis is denoted by σ_x. The six shearing stresses are equal in pairs acting in opposite directions on parallel planes.

4—The Problem

The solutions given are due to Boussinesq[3] and Cerrutti[4] and were computed from displacements given by Love. The procedure for determining principal stresses and principal stress direction was adopted from methods given by Timoshenko.

The problem is divided into two parts, the first dealing with stresses and displacements for the vertical component V of the force R, the second dealing with stresses and displacements for the horizontal component H. In Fig. 145 ϕ is the acute angle between the force R and the xy plane. Therefore, $V = R \sin \phi$ and $H = R \cos \phi$.

5—Stress-Strain Relation

Following are classical stress-strain relations of elasticity expressing Hooke's Law in a continuous, homogeneous, isotropic body:

$$\begin{aligned} \sigma_x &= \lambda e + 2\mu\epsilon_x \\ \sigma_y &= \lambda e + 2\mu\epsilon_y \\ \sigma_z &= \lambda e + 2\mu\epsilon_z \end{aligned} \qquad (1)$$

3) Love, A. E. H., op. cit., p. 191.
4) Idem., p. 243.

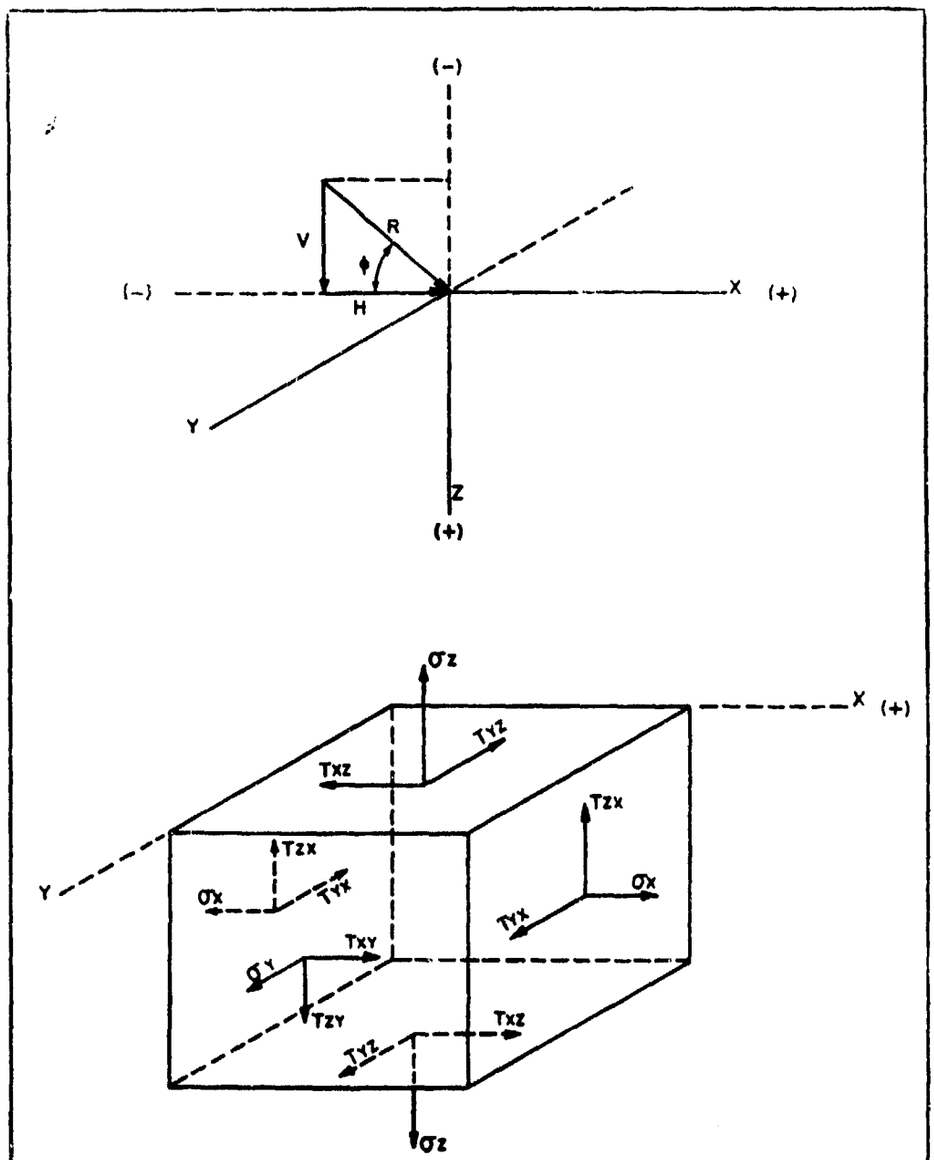

-BOMB PENETRATION PROJECT- CSM RESEARCH FOUNDATION, INC.

Scale _____ Date 3-2-61

Fig. No. 145 By LB

STRESS CONVENTIONS

Fig. 145

$$T_{xy} = T_{yx} = \mu\varepsilon_{xy} \tag{2}$$

$$T_{xz} = T_{zx} = \mu\varepsilon_{xz} \tag{3}$$

$$T_{yz} = T_{zy} = \mu\varepsilon_{yz} \tag{4}$$

$$e = \varepsilon_x + \varepsilon_y + \varepsilon_z \tag{5}$$

$$\varepsilon_x = \frac{\partial u}{\partial x},\ \varepsilon_y = \frac{\partial v}{\partial y},\ \varepsilon_z = \frac{\partial w}{\partial z} \tag{6}$$

$$\varepsilon_{xy} = \frac{\partial v}{\partial x} + \frac{\partial u}{\partial y},\ \varepsilon_{xz} = \frac{\partial u}{\partial z} + \frac{\partial w}{\partial x},\ \varepsilon_{yz} = \frac{\partial v}{\partial z} + \frac{\partial w}{\partial y} \tag{7}$$

Relations between elastic constants that are useful in the calculations are:

$$\frac{2\mu}{\lambda+\mu} = 2(1 - 2m) \tag{8}$$

$$E = \frac{u(3\lambda+2\mu)}{\lambda+\mu} \tag{9}$$

$$m = \frac{\lambda}{2(\lambda+\mu)} \tag{10}$$

6—Displacements and Stresses

Following are summarized the displacement and stresses resulting from the vertical component V of the inclined force R acting at the surface of the solid:

$$u = \frac{V}{4\pi}\left[\frac{xz}{\mu r^3} - \frac{x}{(\lambda+\mu)r(z+r)}\right] \tag{11}$$

$$v = \frac{V}{4\pi}\left[\frac{yz}{\mu r^3} - \frac{y}{(\lambda+\mu)r(z+r)}\right] \tag{12}$$

$$w = \frac{V}{4\pi}\left[\frac{z^2}{\mu r^3} + \frac{(\lambda+2\mu)}{\mu(\lambda+\mu)r}\right] \tag{13}$$

$$\frac{\partial u}{\partial x} = \frac{V}{4\pi}\left[\frac{r^2z-3x^2z}{\mu r^5} - \frac{(r^2-x^2)(z+r) - x^2r}{(\lambda+\mu)r^3(z+r)^2}\right] \tag{14}$$

$$\frac{\partial u}{\partial y} = \frac{V}{4\pi}\left[\frac{-3xyz}{\mu r^5} + \frac{xyr + xy(z+r)}{(\lambda+\mu)r^3(z+r)^2}\right] \tag{15}$$

$$\frac{\partial u}{\partial z} = \frac{V}{4\pi}\left[\frac{r^2x-3xz^2}{\mu r^5} + \frac{x}{(\lambda+\mu)r^3}\right] \tag{16}$$

$$\frac{\partial v}{\partial x} = \frac{V}{4\pi}\left[\frac{-3xyz}{\mu r^5} + \frac{xyr+xy(z+r)}{(\lambda+\mu)r^3(z+r)^2}\right] \tag{17}$$

$$\frac{\partial v}{\partial y} = \frac{V}{4\pi}\left[\frac{r^2z-3y^2z}{\mu r^5} - \frac{(r^2-y^2)(z+r)-y^2r}{(\lambda+\mu)r^3(z+r)^2}\right] \tag{18}$$

$$\frac{\partial v}{\partial z} = \frac{V}{4\pi}\left[\frac{r^2y - 3yz^2}{\mu r^5} + \frac{y}{(\lambda+\mu)r^3}\right] \tag{19}$$

$$\frac{\partial w}{\partial x} = \frac{V}{4\pi}\left[\frac{-3xz^2}{\mu r^5} - \frac{(\lambda+2\mu)}{\mu(\lambda+\mu)}\ \frac{x}{r^3}\right] \tag{20}$$

$$\frac{\partial w}{\partial y} = \frac{V}{4\pi}\left[\frac{-3yz^2}{\mu r^5} - \frac{\lambda+2\mu}{\mu(\lambda+\mu)}\ \frac{y}{r^3}\right] \tag{21}$$

$$\frac{\partial w}{\partial z} = \frac{V}{4\pi}\left[\frac{2r^2z-3z^3}{\mu r^5} - \frac{(\lambda+2\mu)}{\mu(\lambda+\mu)}\ \frac{z}{r^3}\right] \tag{22}$$

$$e = \frac{V}{4\pi}\left[\frac{-2z}{(\lambda+\mu)r^3}\right] \tag{23}$$

$$\sigma_x = \frac{V}{4\pi}\left[\frac{-6x^2z}{r^5} + \frac{2\mu}{\lambda+\mu}\left(\frac{x^2+z^2}{r^3(z+r)} - \frac{y^2}{r^2(z+r)^2}\right)\right] \tag{24}$$

$$\sigma_y = \frac{V}{4\pi}\left[\frac{-6y^2z}{r^3} + \frac{2\mu}{(\lambda+\mu)}\left(\frac{y^2+z^2}{r^3(z+r)} - \frac{z^2}{r^2(z+r)^2}\right)\right] \tag{25}$$

$$\sigma_z = \frac{V}{4\pi}\left[\frac{-6z^3}{r^5}\right] \tag{26}$$

$$\tau_{xy} = \frac{V}{4\pi}\left[\frac{-6xyz}{r^5} + \frac{2\mu}{(\lambda+\mu)}\left(\frac{xy}{r^3(z+r)} + \frac{xy}{r^2(z+r)^2}\right)\right] \tag{27}$$

$$\tau_{xz} = \frac{V}{4\pi}\left[\frac{-6xz^2}{r^5}\right] \tag{28}$$

$$\tau_{yz} = \frac{V}{4\pi}\left[\frac{-6yz^2}{r^5}\right] \tag{29}$$

Following are summarized the displacements and stresses resulting from the horizontal component H of the force, R, acting at the surface of the solid

$$u = \frac{H}{4\pi}\left[\frac{r^2 + x^2}{\mu r^3} + \frac{1}{(\lambda+\mu)(z+r)} - \frac{x^2}{(\lambda+\mu)r(z+r)^2}\right] \quad (30)$$

$$v = \frac{H}{4\pi}\left[\frac{xy}{\mu r^3} - \frac{xy}{(\lambda+\mu)r(z+r)^2}\right] \quad (31)$$

$$w = \frac{H}{4\pi}\left[\frac{xz}{\mu r^3} + \frac{x}{(\lambda+\mu)r(z+r)}\right] \quad (32)$$

$$e = \frac{H}{4\pi}\left[\frac{-2x}{(\lambda+\mu)r^3}\right] \quad (33)$$

$$\frac{\partial u}{\partial x} = \frac{H}{4\pi}\left[\frac{r^2x - 3x^3}{\mu r^5} - \frac{x}{(\lambda+\mu)r(z+r)^2} - \frac{(2xr^2-x^3)(z+r)-2x^3r}{(\lambda+\mu)r^3(z+r)^3}\right] \quad (34)$$

$$\frac{\partial u}{\partial y} = \frac{H}{4\pi}\left[-\frac{r^2y+3x^2y}{\mu r^5} - \frac{y}{(\lambda+\mu)r(z+r)^2} + \frac{x^2y(z+2r)}{(\lambda+\mu)r^3(z+r)^3}\right] \quad (35)$$

$$\frac{\partial u}{\partial z} = \frac{H}{4\pi}\left[-\frac{r^2z+3x^2z}{\mu r^5} - \frac{1}{(\lambda+\mu)r(z+r)} + \frac{x^2(z+2r)}{(\lambda+\mu)r^3(z+r)^2}\right] \quad (36)$$

$$\frac{\partial v}{\partial x} = \frac{H}{4\pi}\left[\frac{r^2y - 3x^2y}{\mu r^5} - \frac{(r^2y-x^2y)(z+r) - 2rx^2y}{(\lambda+\mu)r^3(z+r)^3}\right] \quad (37)$$

$$\frac{\partial v}{\partial y} = \frac{H}{4\pi}\left[\frac{r^2x - 3xy^2}{\mu r^5} - \frac{(r^2x - xy^2)(z+r) - 2xy^2r}{(\lambda+\mu)r^3(z+r)^3}\right] \quad (38)$$

$$\frac{\partial v}{\partial z} = \frac{H}{4\pi}\left[\frac{-3xyz}{\mu r^5} + \frac{(xy)(z+2r)}{(\lambda+\mu)r^3(z+r)^2}\right] \quad (39)$$

$$\frac{\partial w}{\partial x} = \frac{H}{4\pi}\left[\frac{r^2z - 3x^2z}{\mu r^5} + \frac{(r^2-x^2)(z+r) - x^2r}{(\lambda+\mu)r^3(z+r)^2}\right] \quad (40)$$

$$\frac{\partial w}{\partial y} = \frac{H}{4\pi}\left[\frac{-3xyz}{\mu r^5} - \frac{xy(z+2r)}{(\lambda+\mu)r^3(z+r)^2}\right] \quad (41)$$

$$\frac{\partial w}{\partial z} = \frac{H}{4\pi}\left[\frac{r^2x - 3xz^2}{\mu r^5} - \frac{x}{(\lambda+\mu)r^3}\right] \quad (42)$$

$$\sigma_x = \frac{H}{4\pi}\left[\frac{-6x^3}{r^5} + \frac{2\mu}{\lambda+\mu}\left(\frac{x}{r^3} - \frac{x}{r(z+r)^2} - \frac{(2xr^2-x^3)(z+r)-zx^3r}{r^3(z+r)^3}\right)\right] \quad (43)$$

$$\sigma_y = \frac{H}{4\pi}\left[\frac{-6xy^2}{r^5} + \frac{2\mu}{\lambda+\mu}\left(\frac{x}{r^3} - \frac{(r^2x-xy^2)(z+r) - 2xry^2}{r^3(z+r)^3}\right)\right] \quad (44)$$

$$\sigma_z = \frac{H}{4\pi}\left[\frac{-6xz^2}{r^5}\right] \tag{45}$$

$$T_{xy} = \frac{H}{4\pi}\left[\frac{-6x^2y}{r^5} + \frac{2\mu}{\lambda+\mu}\left(\frac{x^2y - r^2y}{r^3(z+r)^2} + \frac{2xy^2r}{r^3(z+r)^3}\right)\right] \tag{46}$$

$$T_{xz} = \frac{H}{4\pi}\left[\frac{-6x^2z}{r^5}\right] \tag{47}$$

$$T_{yz} = \frac{H}{4\pi}\left[\frac{-6xyz}{r^5}\right] \tag{48}$$

7—Principal Stresses and Directions

Consider a tetrahedral element of volume in a solid O-BCD as shown in Fig. 146 (a). Let A be area of face BCD; then the areas of ODC, OBD, and OBC are Am, Al, and An respectively, where l, m, and n are the direction cosines of a normal to plane BCD. The origin is taken at one vertex of the tetrahedron merely to indicate axial directions conveniently. If X, Y, Z are the x, y, z components of the stress N acting across the face BCD, then the following relations result by writing equilibrium conditions for the forces acting on the element:

$$AX = Al\sigma_x + AmT_{xy} + AnT_{xz} \tag{49}$$

$$AY = Am\sigma_y + AlT_{yx} + AnT_{yz} \tag{50}$$

$$AZ = An\sigma_z + AmT_{zy} + AlT_{zx} \tag{51}$$

or dividing out A,

$$X = l\sigma_x + mT_{xy} + n\,T_{xz} \tag{52}$$

$$Y = m\sigma_y + lT_{yx} + n\,T_{yz} \tag{53}$$

$$Z = n\sigma_z + lT_{zx} + m\,T_{zy} \tag{54}$$

The relations are only approximately true as written for the finite tetrahedron but become exact relations between the stresses at a point as the volume of the element approaches zero.

If BCD is a plane of principal stress, then N, the normal stress acting across the plane, becomes S, the principal stress; that is, l, m, and n are direction cosines of a direction of principal stress. In this case

X = Sl, Y = Sm, and Z = Sn, and the above relations become

$$(S - \sigma_x)l = m\,T_{xy} + n\,T_{xz} \tag{55}$$

$$(S - \sigma_y)m = l\,T_{yx} + n\,T_{yz} \tag{56}$$

$$(S - \sigma_z)n = l\,T_{zx} + m\,T_{zy} \tag{57}$$

These are the fundamental equations for determining principal stresses and principal stress directions.

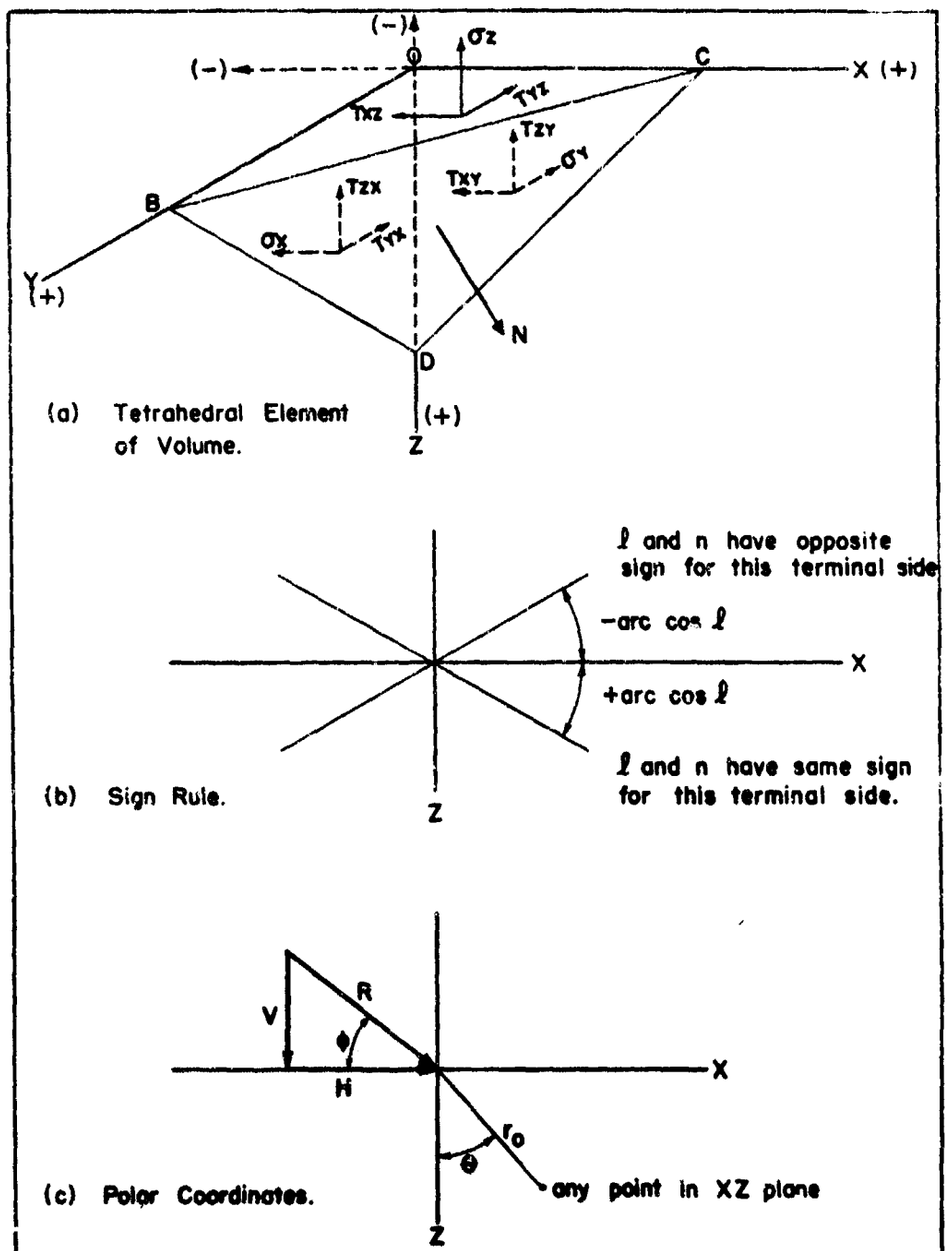

-BOMB PENETRATION PROJECT- CSM RESEARCH FOUNDATION, INC.	
Scale ——— Date 2-28-51 Fig. No. 146 By WHJ-LB	PRINCIPAL STRESS CONVENTIONS

Fig. 146.

A special case of these equations is sufficient for the present investigation of the stress system discussed. For $Y = 0$, T_{xy} and T_{yz} both vanish; hence $Y = 0$ is a principal plane and σ_y is a principal stress. It turns out that σ_y equals σ_2 (the intermediate principal stress) and is therefore of no interest here, for the evaluation of the magnitudes and directions of σ_1 and σ_3 is primary importance. Since σ_y is one principal stress, σ_1 and σ_3 act in the xz plane, and for either direction $m = 0$. This leads to the special case:

$$(S-\sigma_x)l-n\,T_{xz}=0 \qquad (58)$$

$$(S-\sigma_z)n-lT_{xz}=0 \qquad (59)$$

where S is either σ_1 or σ_3.

The last equations can readily be solved for S:

$$S=\tfrac{1}{2}(\sigma_x+\sigma_z)\pm\tfrac{1}{2}\sqrt{(\sigma_x-\sigma_z)^2+4T_{xz}^2} \qquad (60)$$

where σ_1 is obtained if the positive sign is used, σ_3 if the negative sign is used.

Furthermore if σ_1 is substituted in the fundamental equations,

$$(\sigma_1-\sigma_z)n=l\,T_{xz} \qquad (61)$$

and since $\sigma_1 - \sigma_z$ is positive, l and n have the same signs for positive shear T_{xz}; otherwise they have opposite signs. This leads to a rule for choosing the direction of σ_1: "In any case take l as positive and use the acute angle whose cosine is l from the x axis to the direction of σ_1 positive if T_{xz} is positive, negative if T_{xz} is negative." Figure 146 (b) shows the reason for the rule.

The method of computing σ_1 and σ_3 and their directions from the above equations is as follows. Evaluate

$$\sigma_1+\sigma_3=\sigma_x+\sigma_z \text{ and} \qquad (62)$$

$$\sigma_1-\sigma_3=\sqrt{(\sigma_x-\sigma_z)^2+4T_{xz}^2} \qquad (63)$$

By addition and subtraction, σ_1 and σ_3 are then obtained. Next $l^2=\frac{\sigma_1-\sigma_z}{\sigma_1-\sigma_3}$ is computed and the acute angle gives the direction of σ_1. The direction of σ_3 in the xz plane is then determined as perpendicular to that of σ_1.

8—Horizontal and Vertical Component Stress for $y = 0$

It is convenient to use polar coordinates as indicated in Fig. 146(c) to determine the horizontal and vertical components of stress $y = 0$. The following results are obtained by substituting $y = 0$ in the stresses discussed under "Displacements and Stresses." ($x = r_o \sin\theta$, $z = r_o \cos\theta$)

Vertical Component:

$$r_o^2\,\sigma_x = \frac{V}{4\pi}\left[-6\,\mathrm{Sin}^2\theta\,\mathrm{Cos}\,\theta + \frac{2\mu}{\lambda+\mu}\left(\frac{1}{1+\mathrm{Cos}\,\theta}\right)\right] \tag{64}$$

$$r_o^2\,T_{xz} = \frac{V}{4\pi}\left[-6\,\mathrm{Sin}\,\theta\,\mathrm{Cos}^2\,\theta\right] \tag{65}$$

$$r_o^2\,\sigma_z = \frac{V}{4\pi}\left[-6\,\mathrm{Cos}^3\,\theta\right] \tag{66}$$

$$r_o^2(\sigma_x - \sigma_z) = \frac{V}{4\pi}\left[6\,\mathrm{Cos}\,\theta\,\mathrm{Cos}\,2\theta + \frac{2\mu}{\lambda+\mu}\left(\frac{1}{1+\mathrm{Cos}\,\theta}\right)\right] \tag{67}$$

$$r_o^2(\sigma_1 + \sigma_3) = r_o^2\,(\sigma_x + \sigma_z) = \frac{V}{4\pi}\left[-6\,\mathrm{Cos}\,\theta + \frac{2\mu}{\lambda+\mu}\left(\frac{1}{1+\mathrm{Cos}\,\theta}\right)\right] \tag{68}$$

$$2r_o^2\,\tau_{xz} = \frac{V}{4\pi}\left[-12\,\mathrm{Sin}\,\theta\,\mathrm{Cos}^2\theta\right] \tag{69}$$

Horizontal Component:

$$r_o^2\,\sigma_x = \frac{H}{4\pi}\left[-6\,\mathrm{Sin}^3\theta + \frac{2\mu}{\lambda+\mu}\left(\frac{\mathrm{Sin}\,\theta}{(1+\mathrm{Cos}\,\theta)^2}\right)\right] \tag{70}$$

$$r_o^2\,T_{xz} = \frac{H}{4\pi}\left[-6\,\mathrm{Sin}^2\theta\,\mathrm{Cos}\,\theta\right] \tag{71}$$

$$r_o^2\,\sigma_z = \frac{H}{4\pi}\left[-6\,\mathrm{Sin}\,\theta\,\mathrm{Cos}^2\theta\right] \tag{72}$$

$$r_o^2\,(\sigma_x - \sigma_z) = \frac{H}{4\pi}\left[6\,\mathrm{Sin}\,\theta\,\mathrm{Cos}\,2\theta + \frac{2\mu}{\lambda+\mu}\left(\frac{\mathrm{Sin}\,\theta}{(1+\mathrm{Cos}\,\theta)^2}\right)\right] \tag{73}$$

$$2r_o^2\,(T_{xz}) = \frac{H}{4\pi}\left[-12\,\mathrm{Sin}^2\,\theta\,\mathrm{Cos}\,\theta\right] \tag{74}$$

$$r_o^2\,(\sigma_1 + \sigma_3) = r_o^2(\sigma_x + \sigma_z) = \frac{H}{4\pi}\left[-6\,\mathrm{Sin}\,\theta + \frac{2\mu}{\lambda+\mu}\,\frac{\mathrm{Sin}\,\theta}{(1+\mathrm{Cos}\,\theta)^2}\right] \tag{75}$$

8—Explanation of Tables and Computations

Tables based upon solutions given previously were computed for the four following cases:

Case I—A vertical force applied to the surface of the semi-infinite solid for an assumed value of Poisson's ratio of 0.25.

Case II—A vertical force applied as in Case I except for an assumed value of Poisson's ratio of 0.35.

Case III—A force inclined at 60 degrees to the surface of the semi-infinite solid for an assumed value of Poisson's ratio of 0.25.

Case I

Vertical Force - ($m = 0.25$)

θ	$\frac{4\pi}{V}r_o^2(\sigma_x-\sigma_z)$	$\frac{8\pi}{V}r_o^2\tau_{xz}$	$\frac{4\pi}{V}r_o^2\sigma_z$	$\frac{4\pi}{V}r_o^2(\sigma_1-\sigma_3)$	r_o/K^*	$\frac{4\pi}{V}r_o^2\sigma_1$	$\frac{4\pi}{V}r_o^2\sigma_3$	$\sqrt{\frac{4\pi\sigma_1}{V}}r_o$	$\sqrt{\frac{-4\pi\sigma_3}{V}}r_o$	ℓ	Angle from x axis to σ_1
0°	+6.5000	0.00000	-6.0000	6.5000	2.5495	+0.50000	-6.0000	0.70711	2.4495	1.0000	0°
15°	+5.5278	-2.8978	-5.40740	6.2413	2.4982	+0.47717	-5.7641	0.69077	2.4008	0.97100	-14°
30°	+3.1340	-4.50000	-3.8972	5.4838	2.3418	+0.41177	-5.0720	0.64169	2.2521	0.88643	-27°30'
45°	+0.58578	-4.2427	-2.1213	4.2829	2.0695	+0.31302	-3.9699	0.55948	1.9925	0.75391	-41°
60°	-0.83333	-2.5981	-0.75000	2.7285	1.6518	+0.19756	-2.5309	0.44448	1.5909	0.58931	-5°
67.5°	-0.90035	-1.6236	-0.33625	1.8565	1.3625	+0.14158	-1.7147	0.37627	1.3095	0.50733	-59°30'
75°	-0.55048	-0.77647	-0.10403	0.95181	0.97561	+0.09664	-0.85516	0.31087	0.92475	0.45916	-62°30'
77.5°	-0.35490	-0.54883	-0.06084	0.65358	0.80844	+0.08851	-0.56508	0.29751	0.75172	0.47802	-61°30'
80°	-0.12702	-0.35635	-0.03142	0.37832	0.19450	+0.09423	-0.28409	0.30697	0.53300	0.57629	-55°
82.5°	+0.12804	-0.20271	-0.01334	0.23976	0.48965	+0.17056	-0.06920	0.41299	0.26305	0.87580	-29°
90°	+1.0000	0.00000	0.00000	1.00000	1.0000	+1.0000	0.0000	1.0000	0.00000	1.00000	0°

* $K = \frac{4\pi}{V}(\sigma_1 - \sigma_3)$ and $\frac{\sigma_1 - \sigma_3}{2}$ = Maximum Shear

Note: Table terms are symmetric in θ except T_{xz} which changes sign for negative θ.

Fig. 147

Stresses in Dimensionless Form

FORCE ON A SEMI-INFINITE SOLID (MAXIMUM SHEAR CONTOU

ANGLE OF FALL 90° -- POISSON'S RATIO (m) = 0.25

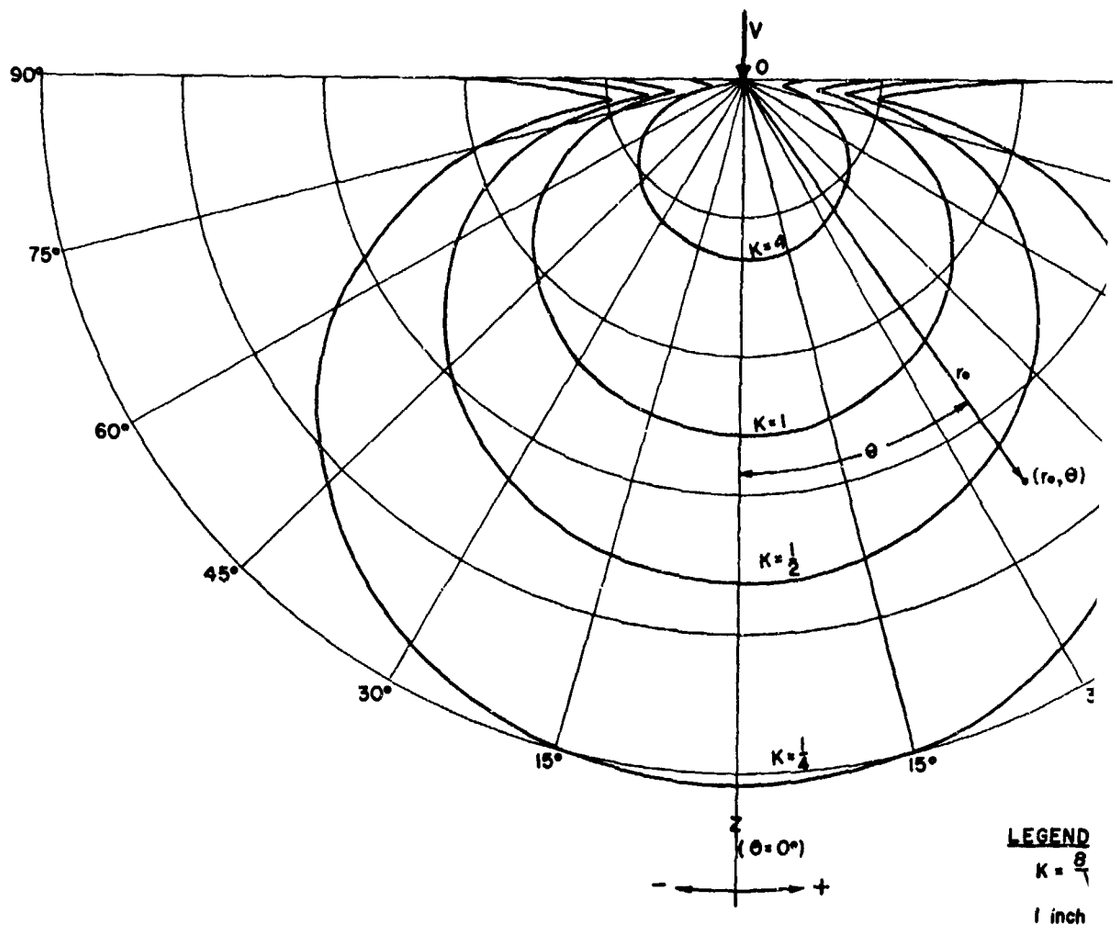

LEGEND

K = θ/

1 inch

Curve

-BOMB PENETRATION PROJEC

Scale 1" = 1 UNIT Date 11-6-50

Dwg. No 148 By W. H. J.

TOURS EMI-INFINITE SOLID (MAXIMUM SHEAR CONTOURS)

5 ALL 90° -- POISSON'S RATIO (m) = 0.25

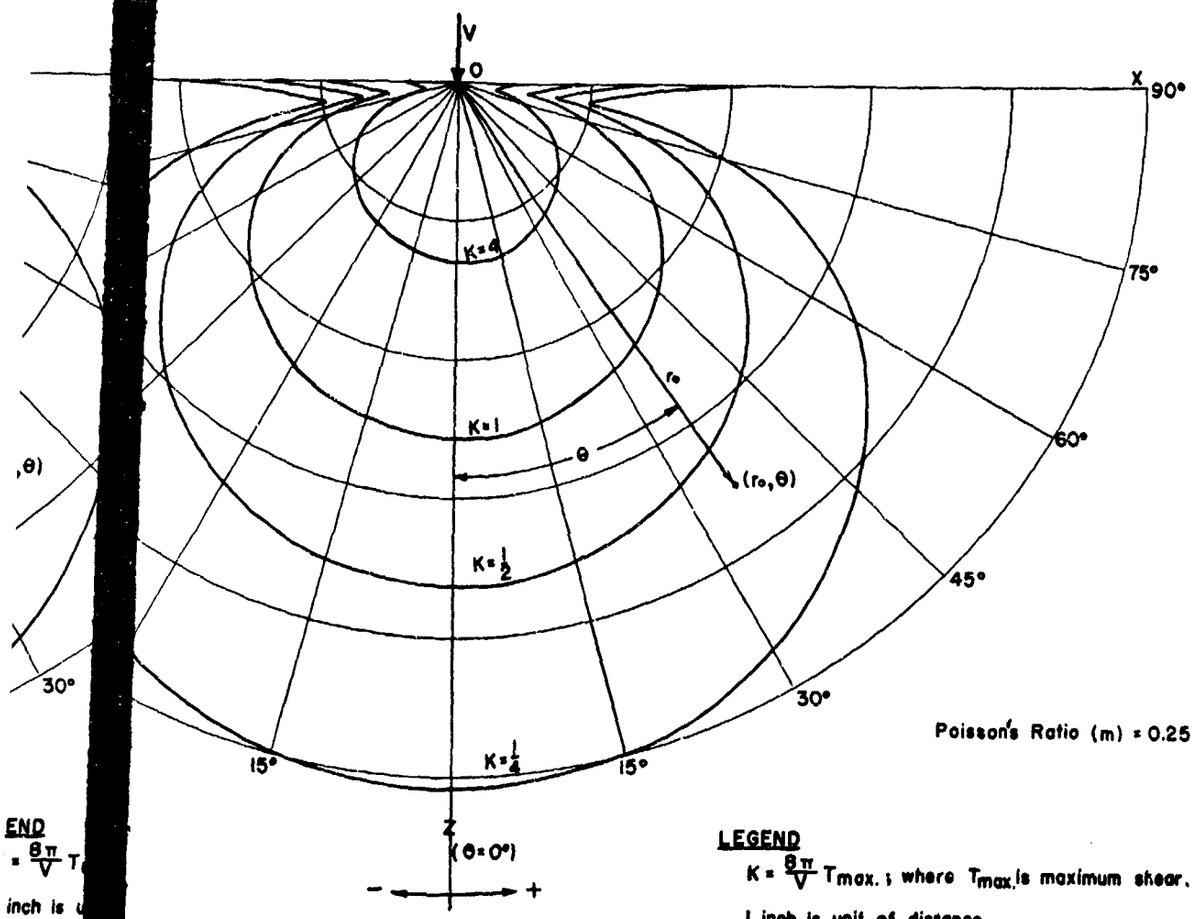

Poisson's Ratio (m) = 0.25

LEGEND

$K = \frac{8\pi}{V} T_{max.}$; where $T_{max.}$ is maximum shear.

1 inch is unit of distance.

Curves plotted are $r_o\sqrt{K}$ = Tabular value

END

$= \frac{8\pi}{V} T$

inch is

urves pl

JECT-

M

-BOMB PENETRATION PROJECT- CSM RESEARCH FOUNDATION, INC.	
Scale 1" = 1 UNIT Date 11-6-50 Dwg. No. 148 By W. K. J.	MAXIMUM SHEAR CONTOURS CASE I

Fig. 148

2

FORCE ON A SEMI-INFINITE SOLID (MAXIMUM SHEAR CONTOU

ANGLE OF FALL 90° -- POISSON'S RATIO (m) = 0.35

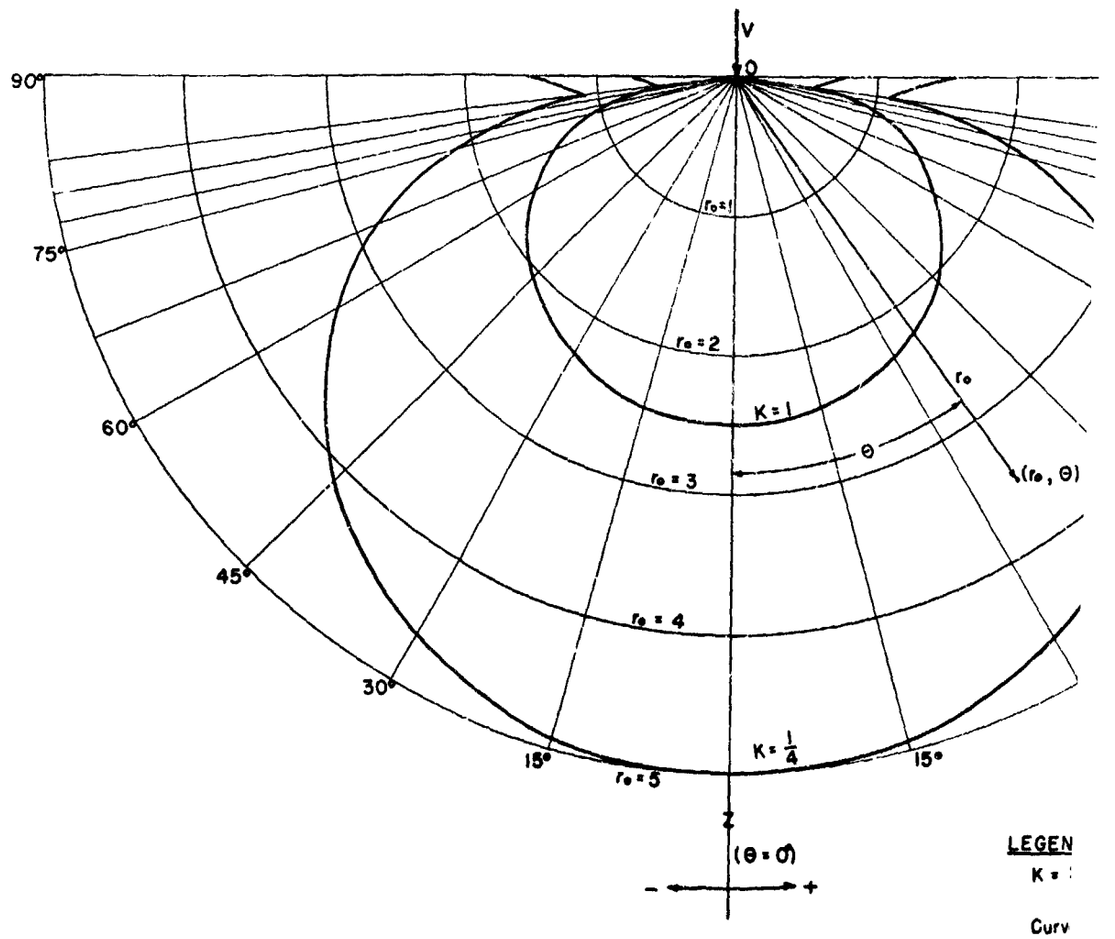

LEGEN

K =

Curv

-BOMB PENETRATION PROJEC
Scale 1" = 1 UNIT Date 18-11-50
Dwg No 149 By W. H. J.

TOURS

.35

FORCE ON A SEMI-INFINITE SOLID (MAXIMUM SHEAR CONTOURS)

ANGLE OF FALL 90° -- POISSON'S RATIO (m) = 0.35

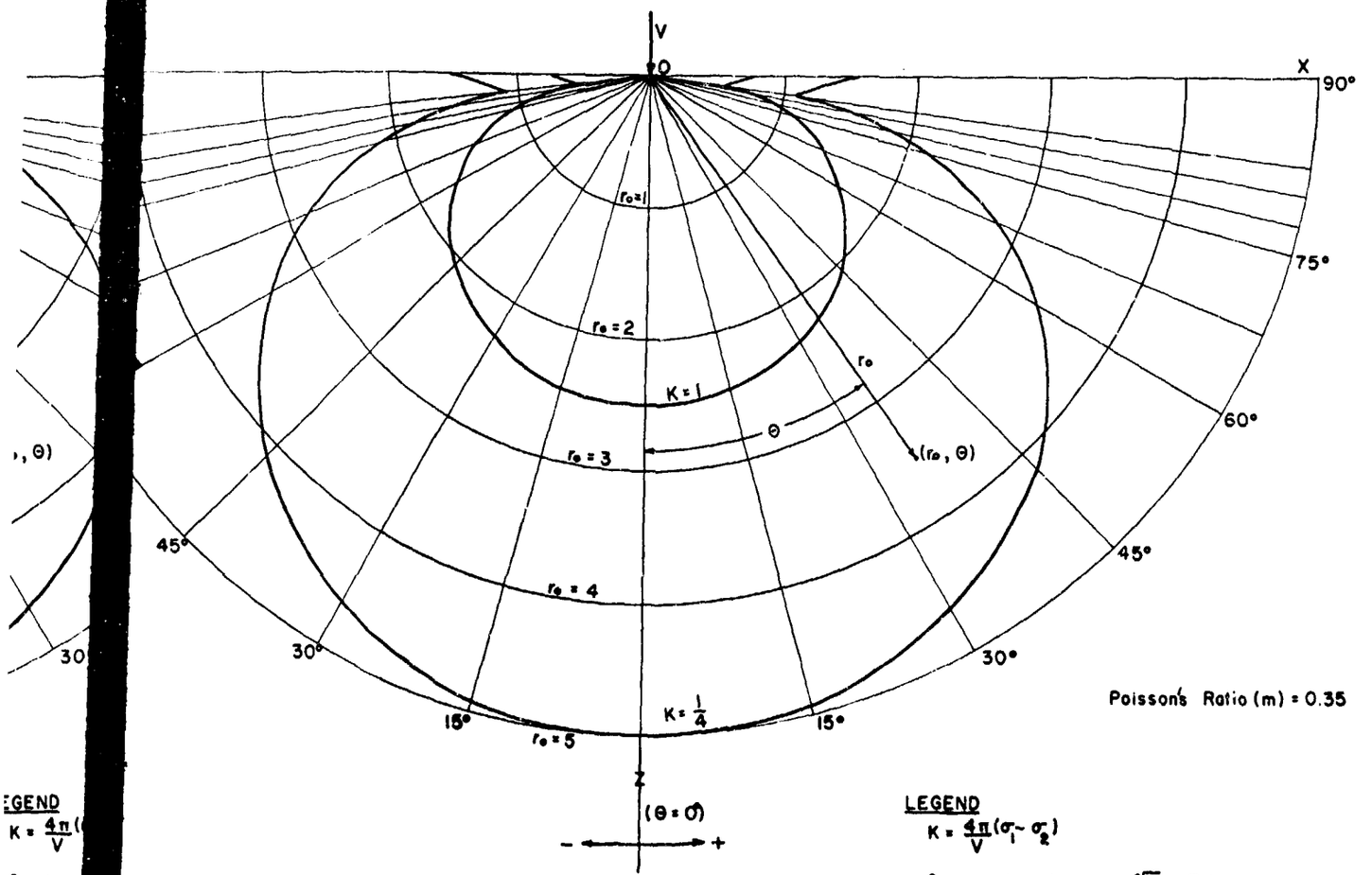

Poisson's Ratio (m) = 0.35

LEGEND

$K = \frac{4\pi}{V}(\sigma_1 - \sigma_2)$

Curves plotted are $r_o\sqrt{K}$ = Tabular value

-BOMB PENETRATION PROJECT- C S M RESEARCH FOUNDATION, INC.

Scale 1" = 1 UNIT Date 12-11-60

Dwg No 149 By W. H. J.

MAXIMUM SHEAR CONTOURS

CASE II

Fig. 149

FORCE ON A SEMI-INFINITE SOLID (MAXIMUM SHEAR CONT

ANGLE OF FALL 60° -- POISSON'S RATIO (m) = 0.2

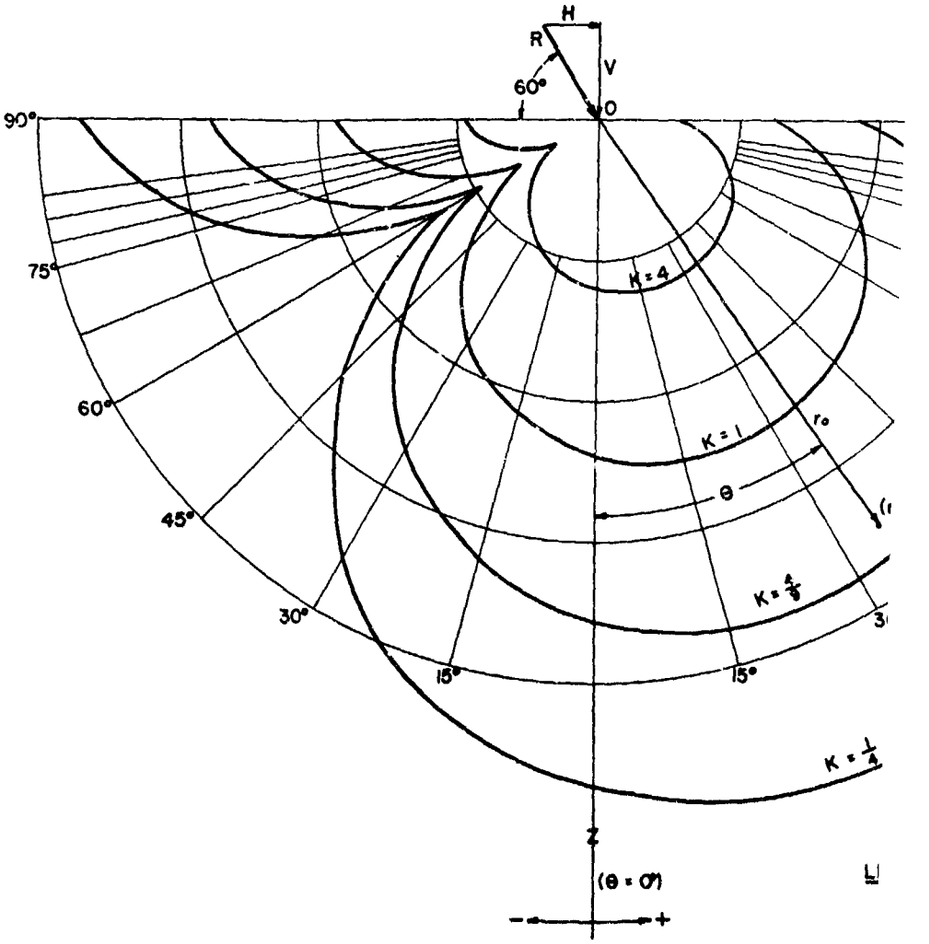

-BOMB PENETRATION

Scale 1" = 1 UNIT Date 1-1-51

Dwg No. 150 By W.H.J.

ORCE ON A SEMI-INFINITE SOLID (MAXIMUM SHEAR CONTOURS)

ANGLE OF FALL 60° -- POISSON'S RATIO (m) = 0.25

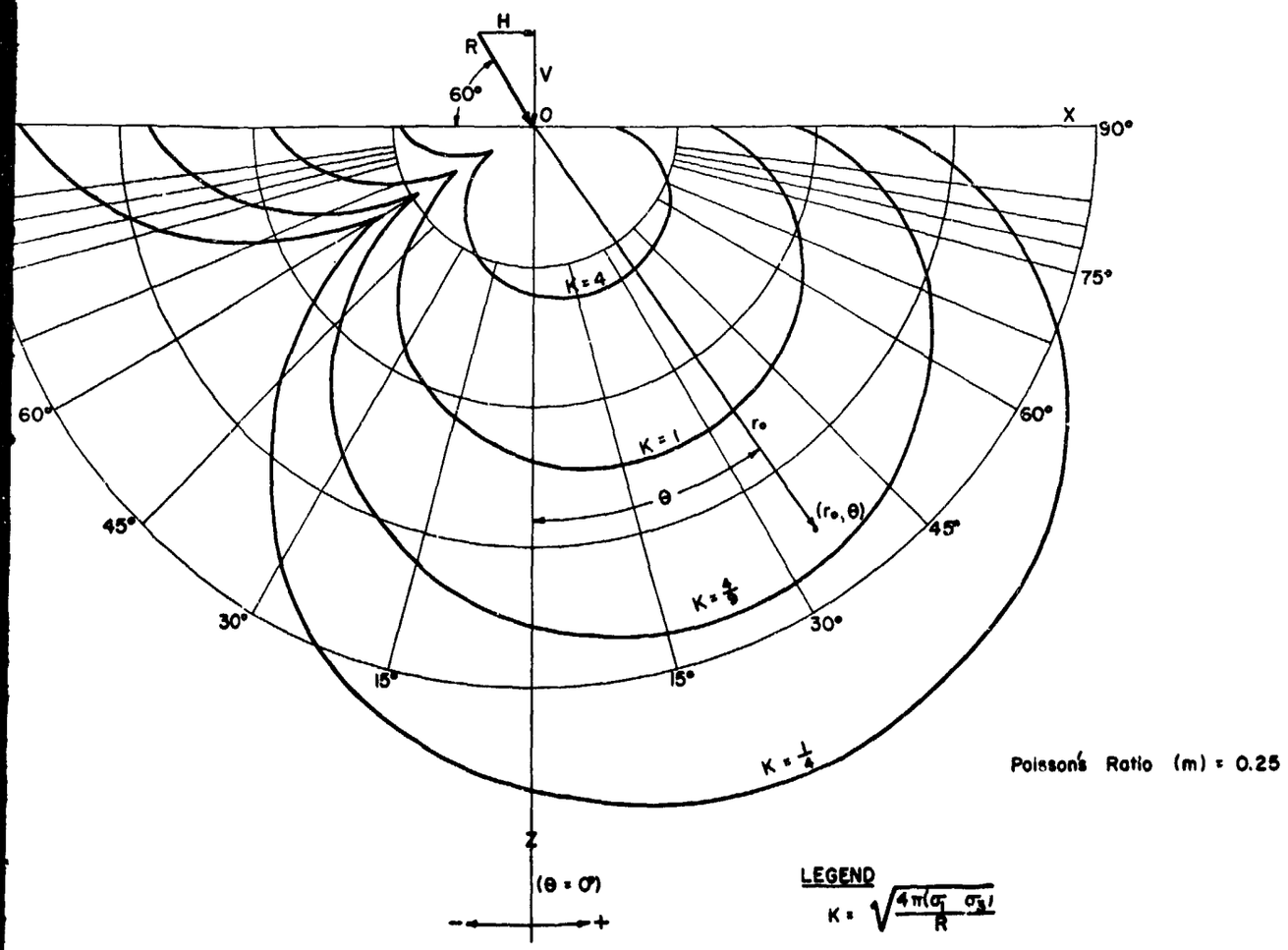

Poisson's Ratio (m) = 0.25

LEGEND

$$K = \sqrt{\frac{4\pi(\sigma_1 - \sigma_3)}{R}}$$

Curves plotted

$\sqrt{K}$ = Tabular value

-BOMB PENETRATION PROJECT- CSM RESEARCH FOUNDATION, INC.	
Scale 1" = 1 UNIT Date 1-1-61 Dwg No. 150 By W.H.J.	MAXIMUM SHEAR CONTOURS CASE III

Fig. 150

FORCE ON A SEMI-INFINITE SOLID (MAXIMUM SHEAR CONTOURS
ANGLE OF FALL 60° -- POISSON'S RATIO (m) = 0.35

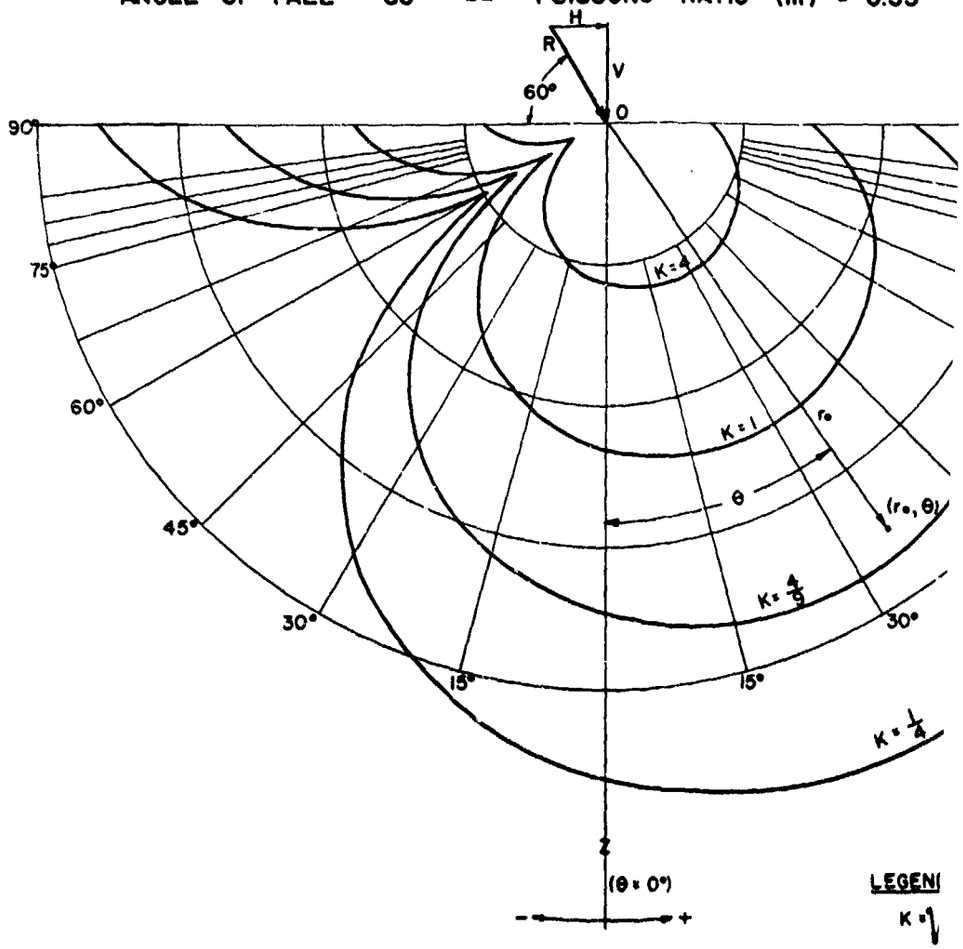

LEGEN
K =
Curv

- BOMB PENETRATION PROJECT
Scale 1" = 1 UNIT Date 1-1-54
Dwg No. 151 By W.H.J.

SEMI-INFINITE SOLID (MAXIMUM SHEAR CONTOURS)
F FALL 60° -- POISSON'S RATIO (m) = 0.35

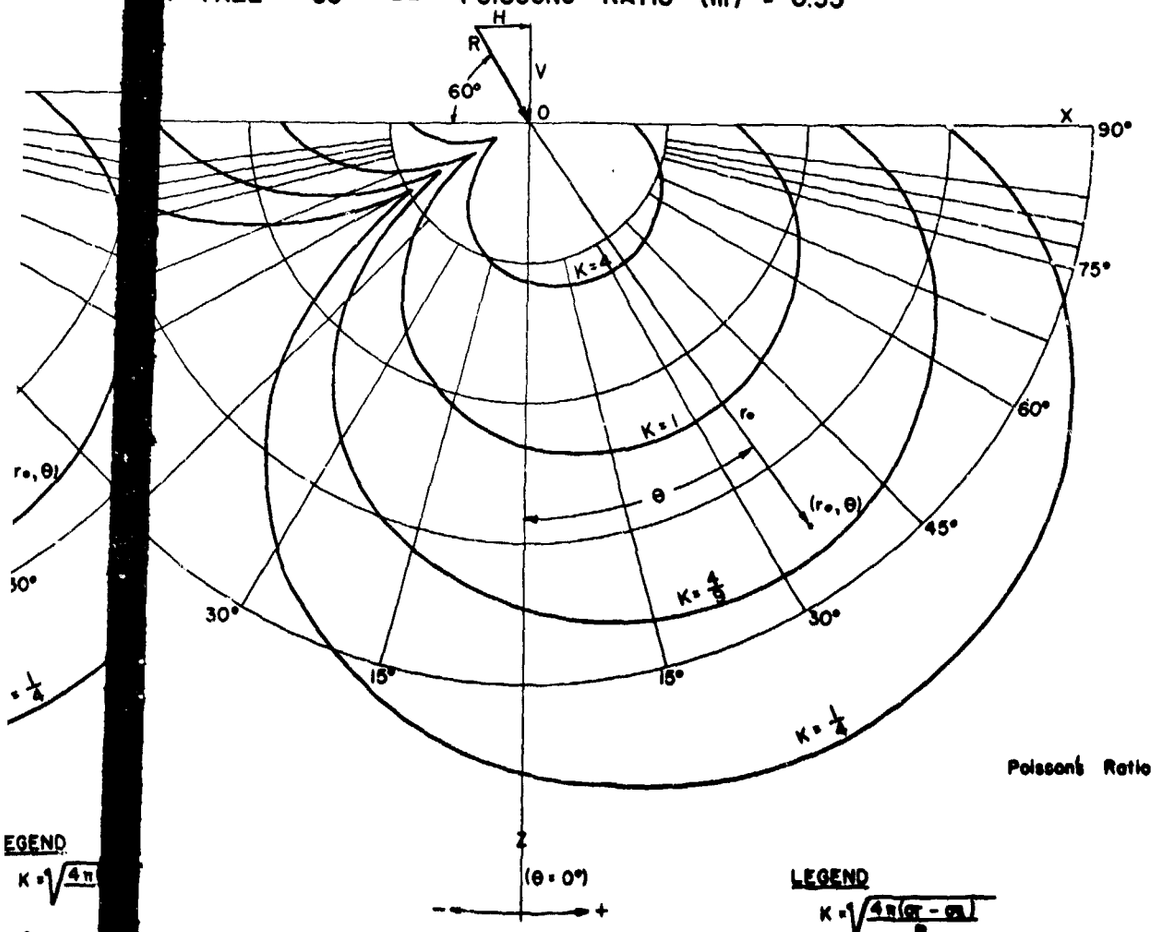

Poisson's Ratio (m) = 0.35

LEGEND

$K = \sqrt{\frac{4\pi(\sigma_T - \sigma_N)}{R}}$

Curves plotted are $r_0\sqrt{K}$ = Tabular value

-BOMB PENETRATION PROJECT- C S M RESEARCH FOUNDATION, INC.	
Scale 1" = 1 UNIT Date 1-1-[illegible] Dwg No. 151 By W. H. [illegible]	MAXIMUM SHEAR CONTOURS CASE IV

Fig. 151

2

Case IV—An inclined force at 60 degrees as in Case III except for an assumed value of Poisson's ratio of 0.35.

Stresses are given in tabular form in Fig. 147 for Case I in dimensionless form as functions of θ, the angle between the positive vertical z axis and the point at which the stress is measured. The manner in which this is accomplished for Case I, Fig. 147, is as follows:

From the equations in the section "Horizontal and Vertical Components of Stress for $y = 0$" and for Case I ($\phi = 90°$, $m = 0.25$), for example,

$$r_o^2\,\sigma_z = \frac{V}{4\pi}\left[-6\,\mathrm{Cos}^3\,\theta\right] \qquad (76)$$

and,

$$\frac{4\pi}{V}\,r_o^2\,\sigma_z = \left[-6\,\mathrm{Cos}^3\,\theta\right] \qquad (77)$$

The quantity $\frac{4\pi}{V}\,r_o^2\,\sigma_z$ is dimensionless, and values of this quantity are tabulated in the fourth column from the left in Fig. 147, for various values of θ from 0 degrees to 90 degrees.

Various values of the vertical component and horizontal component of stress for Cases II, III, and IV respectively are tabulated in the same form as in Fig. 147 and are presented in the appendix.

10—Maximum Shear Contours

Maximum shears act in the plane $y = 0$ and have a magnitude equal to $1/2(\sigma_1 - \sigma_3)$. The quantity $\frac{4\pi}{R}\,r_o^2(\sigma_1 - \sigma_3)$ is given in the tables for each case. For Case I, $R = V$, if $1/2(\sigma_1 - \sigma_3)$ is constant; then the equation of the maximum shear contour is $r_o^2\,K = f(\theta) =$ tabular value or

$$r_o\sqrt{K} = \sqrt{f(\theta)} \qquad (78)$$

where

$$K = \frac{4\pi}{R}(\sigma_1 - \sigma_3) \qquad (79)$$

Values of $r_o\sqrt{K}$ are given in the tables for each of the four cases. To obtain any individual maximum shear contour, an appropriate value of K is selected and substituted in the quantity $r_o\sqrt{K} = f(\theta) =$ tabular value. For example, assume $K = 1/4$, then $r_o\sqrt{K} = \frac{r_o}{2}$ is the tabular value. The curve for $K = 1/4$ is then obtained by multiplying the tabular value corresponding to various values of θ by 2, and plotting the results to scale.

Figures 148, 149, 150, and 151 are maximum shear contours for Case I, Case II, Case III, and Case IV respectively.

11—Stress Trajectories

Stress trajectories are curves whose tangents represent the direction of one of the principal stresses at points of tangency. In the section on principal stresses and directions it was shown that the cosine of the angle from the positive x axis to the direction of σ_1 equals $l^2 = \frac{\sigma_1 - \sigma_y}{\sigma_1 - \sigma_3}$. Now σ_1, σ_y and σ_3 contain r_0^2 as a factor, hence depend only on θ. In other words, the principal stress directions are constant on any radial line through the origin in the plane $y = 0$.

Stress trajectories for Cases I and III are presented in Figs. 152 and 153. The direction of principal stress along any radial line for various values of θ are obtained from the last column in the tables, Fig. 147, and appendix, wherein the stresses are given in dimensionless form for each of the respective cases. These directions are plotted at convenient places along each of the radial lines; then lines are drawn at right angles to them at the same points to indicate the other direction of principal stress. The stress trajectories are then drawn as continuous curves tangent to the directions of principal stress.

12—Principal Stress Contours

Principal stress contours may be drawn for σ_1, the maximum principal stress, or for σ_3, the minimum principal stress. A maximum principal stress contour is a curve along which values of σ_1 are constant; a minimum principal stress contour is a curve along which values of σ_3 are constant. The principal stress contours are constructed from the tabular data in much the same manner as the shear contours. The quantity $\frac{4\pi}{R} r_0^2 \sigma_1$ is given in the tables for each case. For Case I, $R = V$, and if σ_1 is constant,

$$r_0^2 = \left(\frac{4\pi}{V}\sigma_1\right) \div f(\theta) \tag{80}$$

$$r_0 = \sqrt{\frac{4\pi}{V}\sigma_1} \times \sqrt{f(\theta)} \quad \text{tabular value} \tag{81}$$

To obtain any individual maximum principal stress contour, an appropriate value of $n_1 = \sqrt{\frac{4\pi}{V}\sigma_1}$ or $n_1 = \sqrt{\frac{4\pi}{V}\sigma_3}$ is chosen and values of $r_0 = n_1$ (tabular value of σ_1), or of $r_0 = n_3$ (tabular value of σ_3), are plotted.

Figures 154 and 155 are principal stress contours for Case I and Case III.

13—Illustrative Applications of the Diagrams

The following examples illustrate some of the applications of the diagrams and of the tables summarizing the computations.

STRESS TRAJECTORIES (SEMI-INFINITE SOLID)

ANGLE OF FALL 90° -- POISSON'S RATIO (m) = 0.25

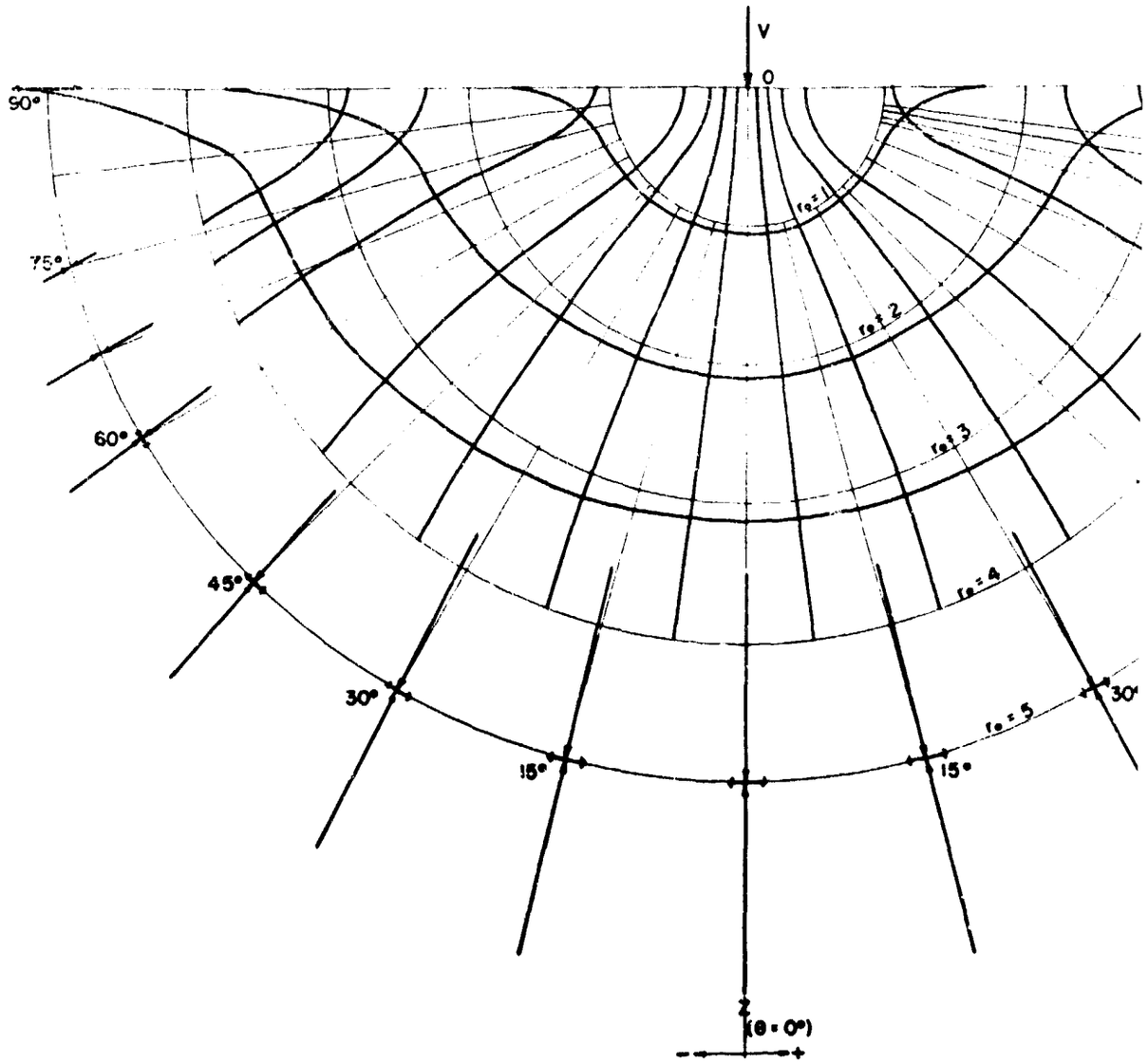

-BOMB PENETRATION PROJECT-	
Scale 40 Date 12-18-50	
Dwg No. 152 By W.H.J.	

SS TRAJECTORIES (SEMI-INFINITE SOLID)

FALL 90° -- POISSON'S RATIO (m) = 0.25

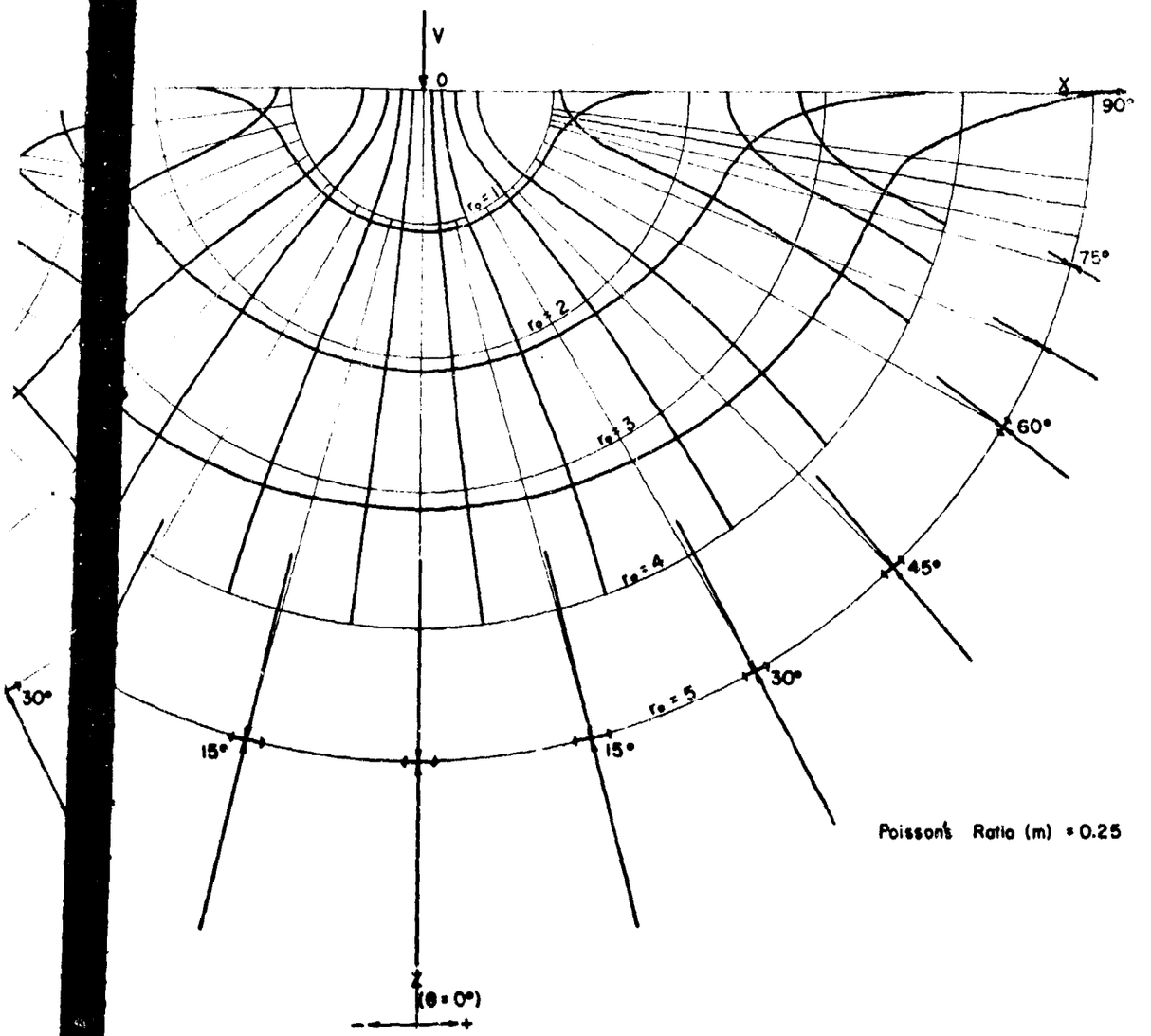

-BOMB PENETRATION PROJECT- C S M RESEARCH FOUNDATION, INC	
Scale 40 Date 12-18-53 Dwg No 152 By W.H.J.	STRESS TRAJECTORIES CASE I

Fig. 152

2

STRESS TRAJECTORIES (SEMI-INFINITE SOLID)

ANGLE OF FALL 60° -- POISSON'S RATIO (m) = 0.25

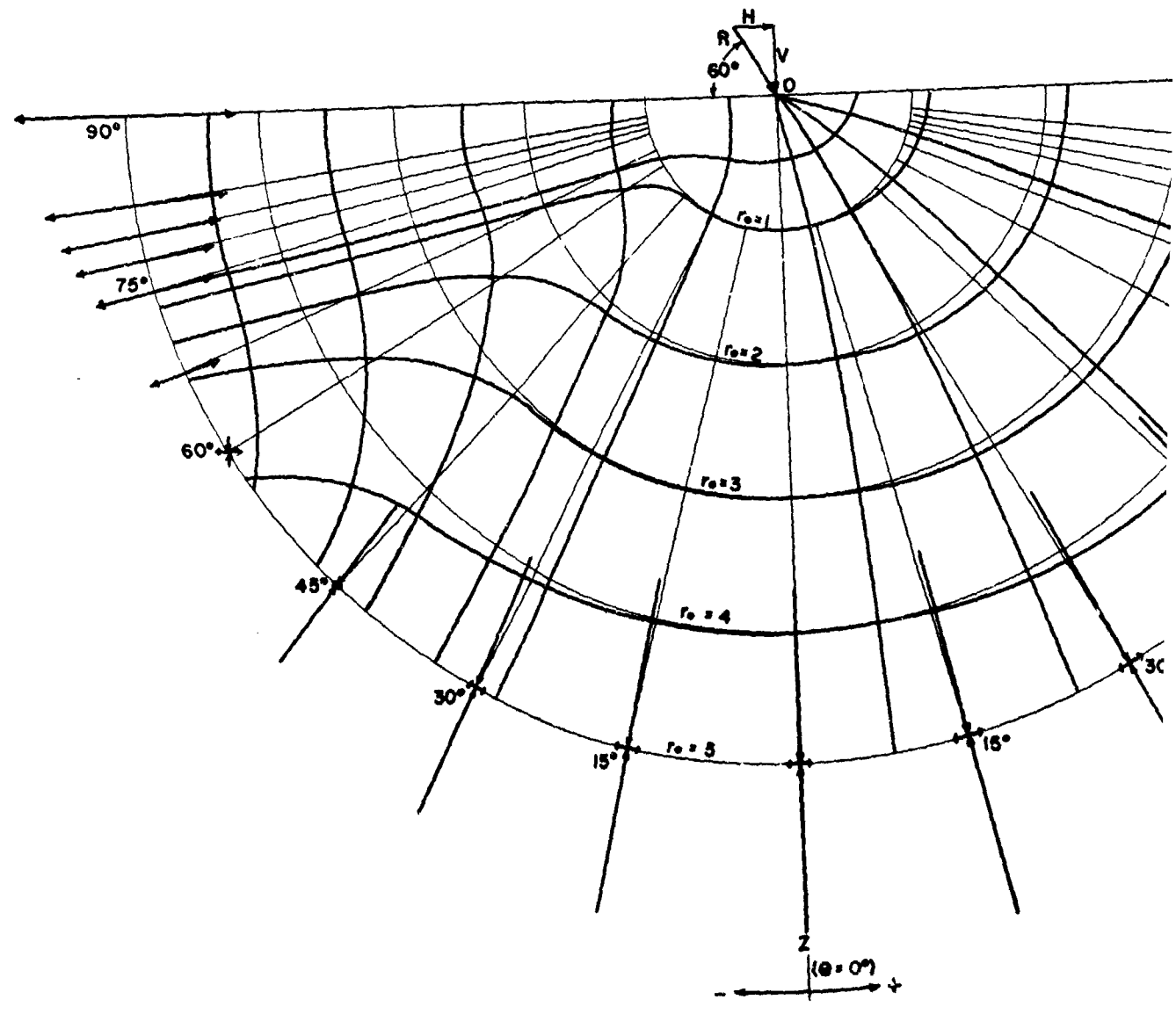

-BOMB PENETRATION PROJECT-

Scale 40 Date 1-1-51

Fig. No. 153 By W.H.J.

STRESS TRAJECTORIES (SEMI-INFINITE SOLID)

ANGLE OF FALL 60° -- POISSON'S RATIO (m) = 0.25

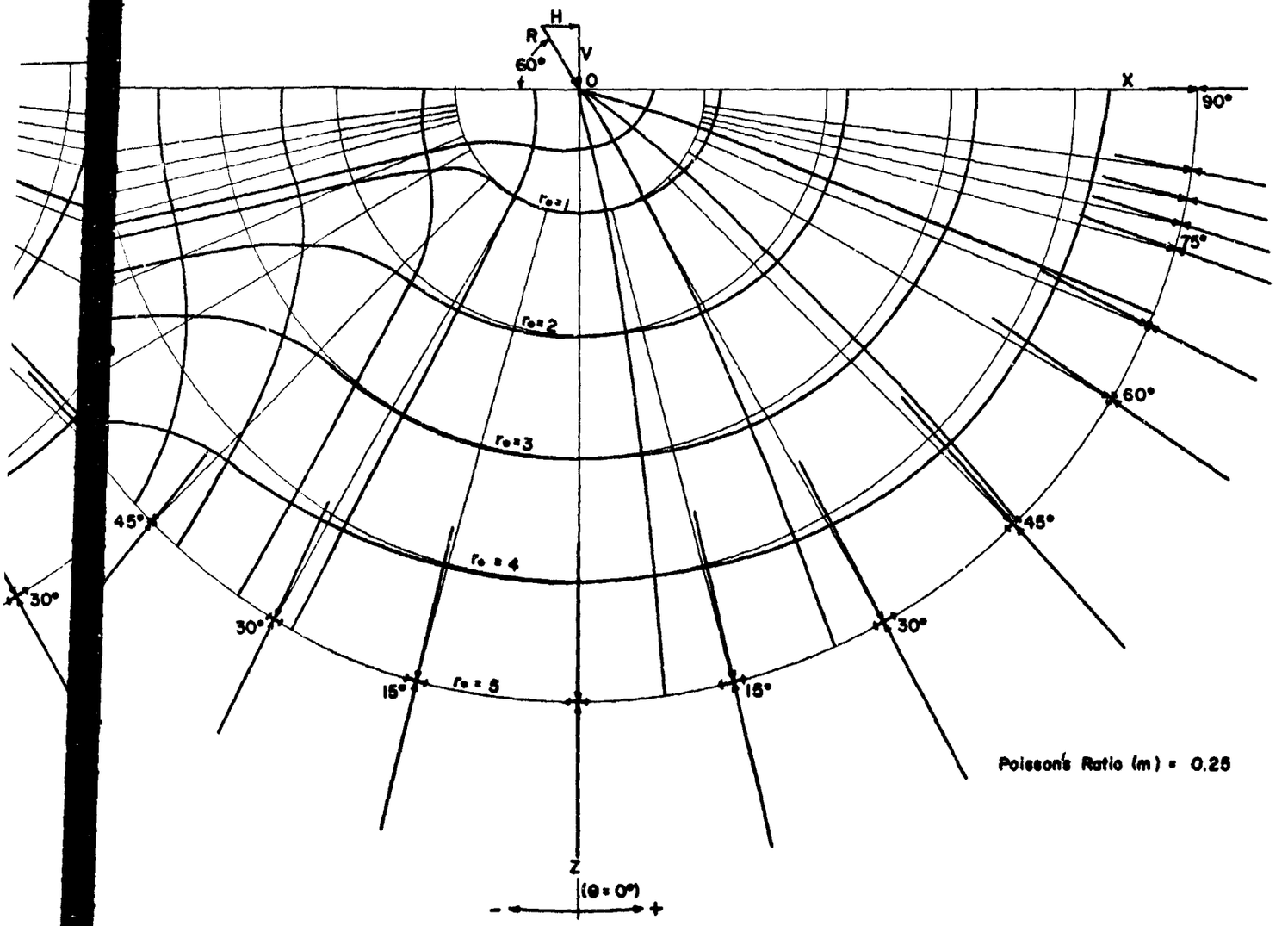

-BOMB PENETRATION PROJECT- CSM RESEARCH FOUNDATION, INC.	
Scale 40 Date 1-1-51 Fig. No. 153 By W.H.C.	STRESS TRAJECTORIES CASE III

Fig. 153 2

PRINCIPAL STRESS CONTOURS (SEMI-INFINITE

ANGLE OF FALL 90° -- POISSON'S RATIO (m)

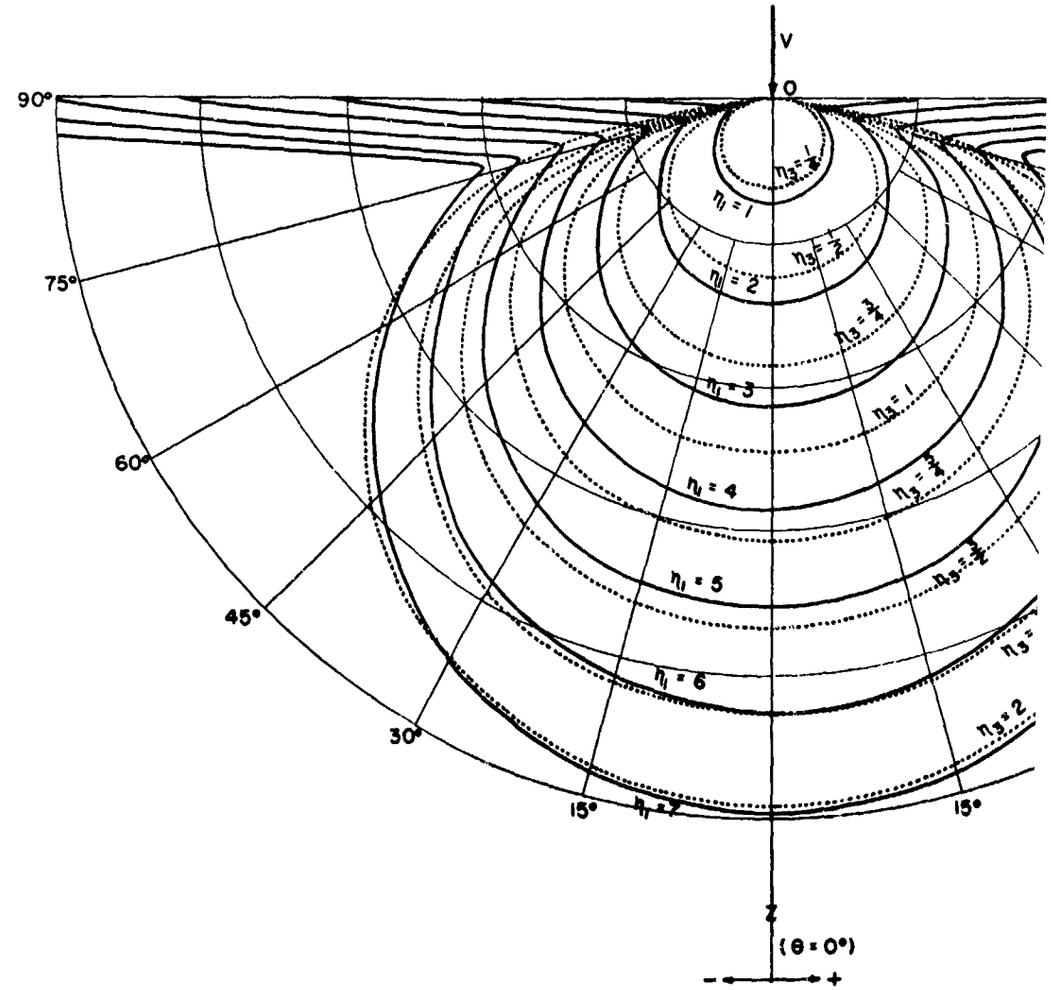

-BOMB PENETRATION

Scale 1" = 1 UNIT Date 12

Dwg No 154 By W.

PRINCIPAL STRESS CONTOURS (SEMI-INFINITE SOLID)

ANGLE OF FALL 90° -- POISSON'S RATIO (m) = 0.25

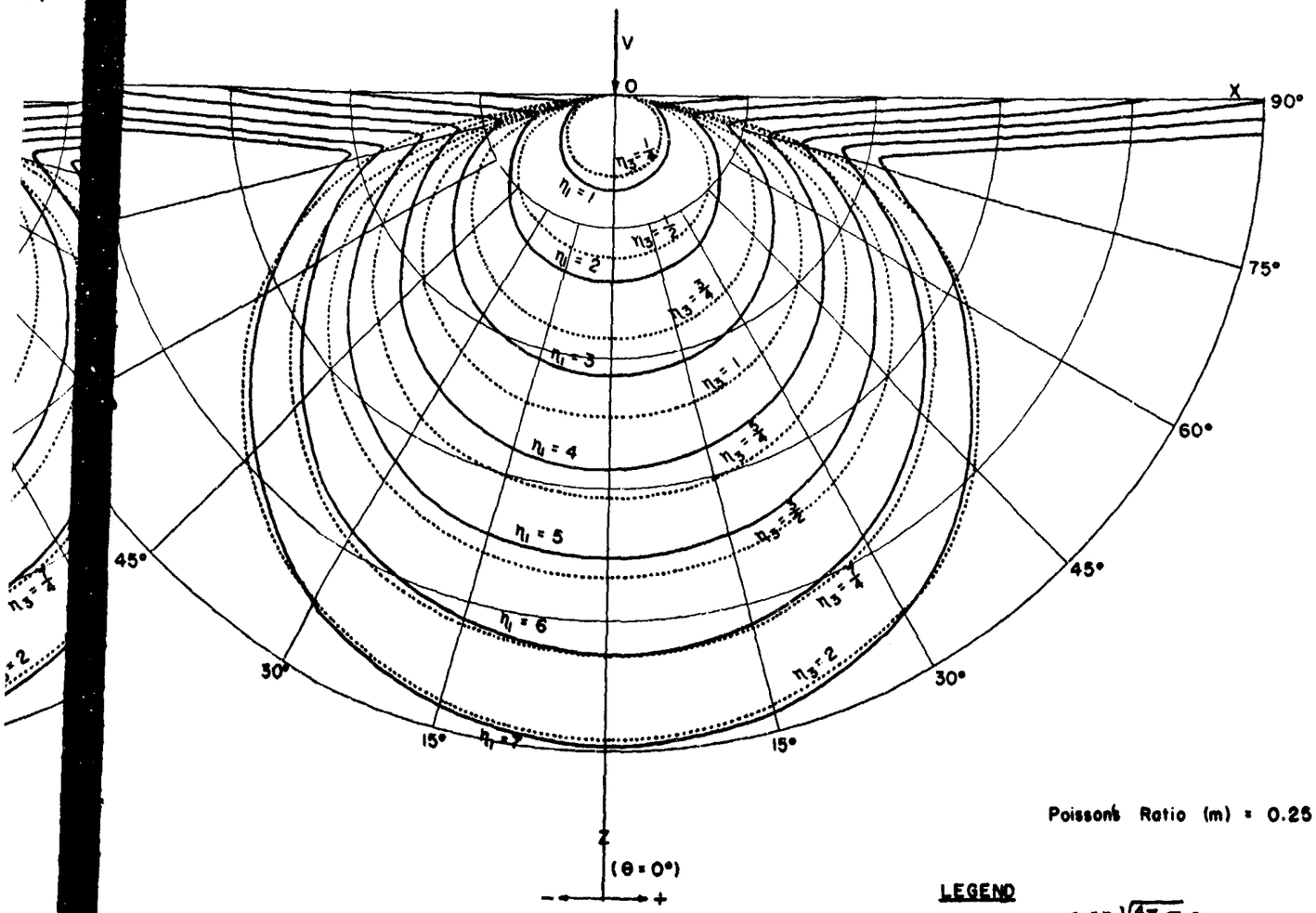

Poisson's Ratio (m) = 0.25

LEGEND

—— σ_1 ; $r_o = \eta_1 \sqrt{\frac{4\pi}{R}\sigma_1}\, r_o$

..... σ_3 ; $r_o = \eta_3 \sqrt{\frac{-4\pi}{R}\sigma_3}\, r_o$

-BOMB PENETRATION PROJECT- C S M RESEARCH FOUNDATION, INC.	
Scale 1" = 1 UNIT Date 12-50 Dwg No. 154 By W. H. J.	PRINCIPAL STRESS CONTOURS CASE I

Fig. 154

PRINCIPAL STRESS CONTOURS (SEMI-INFINITE SOLID)

ANGLE OF FALL 60° -- POISSON'S RATIO (m) = 0.25

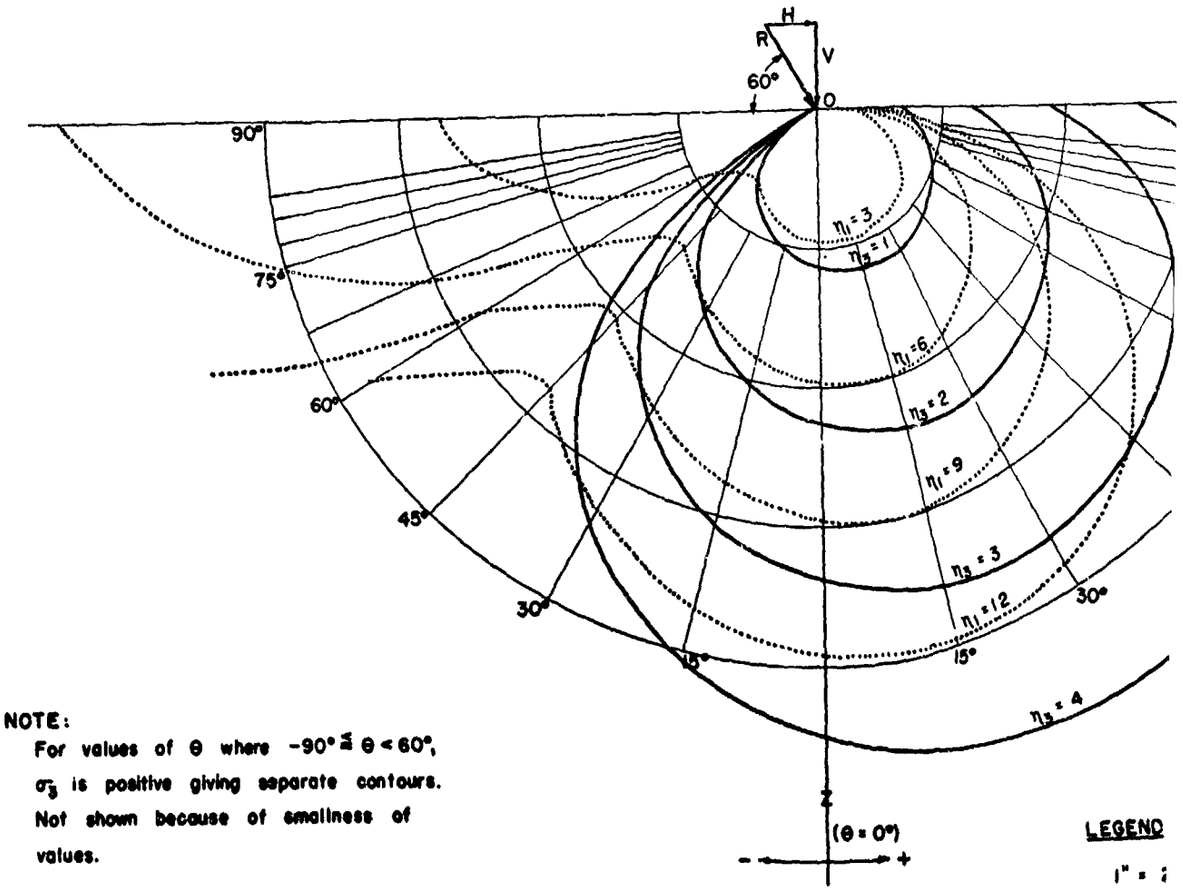

NOTE:
For values of θ where $-90° \leq \theta < 60°$, σ_3 is positive giving separate contours. Not shown because of smallness of values.

LEGEND

1" = 2

Curve

-BOMB PENETRATION PROJECT	
Scale 1" = 2 UNITS Date 1-1-61	
Dwg No. 155 By W.H.J.	

L STRESS CONTOURS (SEMI-INFINITE SOLID)

F FALL 60° -- POISSON'S RATIO (m) = 0.25

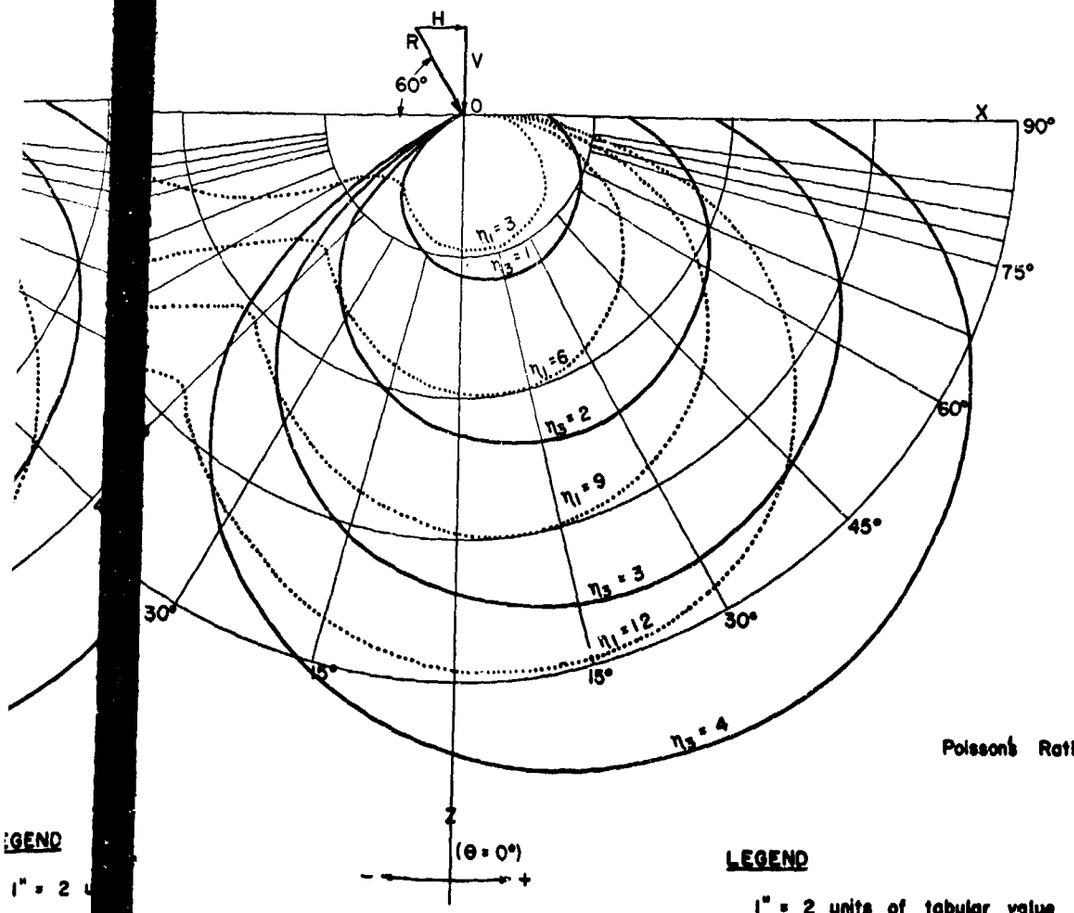

Poisson's Ratio (m) = 0.25

LEGEND

1" = 2 units of tabular value

------- σ_1, a constant

—— σ_3, a constant

Curves plotted: $r_o = \eta_3 \sqrt{\frac{-2\pi}{R}\sigma_3}\, r_o$, &

$r_o = \eta_1 \sqrt{\frac{4\pi}{R}\sigma_1}\, r_o$

-BOMB PENETRATION PROJECT- C S M RESEARCH FOUNDATION, INC.	
Scale 1" = 2 UNITS Date 1-1-54 Dwg No. 155 By W.H.J.	PRINCIPAL STRESS CONTOURS CASE III

Fig. 155

2

Example I

What is the magnitude and direction, a) of the principal stresses b) of maximum shear at a point in a semi-infinite solid of Poisson's ratio 0.25 at a point $\theta = 30$ degrees and $r_o = 10$ in. due to a downward vertical force of 100,000 lb acting at the origin of coordinates?

Solution:

The condition of loading coincides with Case I, and the stresses and directions for this case are tabulated in Fig. 147 in dimensionless units. Enter Fig. 147 opposite $\theta = 30°$ and obtain the following tabular values.

$$\frac{4\pi}{V} r_o^2 \sigma_1 = 0.41177 \tag{82}$$

$$\frac{4\pi}{V} r_o^2 \sigma_3 = -5.0720 \tag{83}$$

angle from x-axis to σ_1 = 27° − 30′.

Substitute V = 100,000 and $r_o = 10$ in the tabular values to obtain stresses in pounds per square inch, and solve for σ_1 and σ_3, the maximum and minimum principal stresses respectively.

$$\frac{4\pi}{100{,}000} \cdot 100\, \sigma_1 = 0.41177 \tag{84}$$

and σ_1 = 33 psi (tension)

$$\frac{4\pi}{100{,}000} \cdot 100 \cdot \sigma_3 = -5.0720 \tag{85}$$

and σ_3 = −404 psi (compression).

From the same table obtain the tabular value

$$\frac{4\pi}{V} r_o^2 (\sigma_1 - \sigma_3) = 5.4838 \tag{86}$$

whence

$$(\sigma_1 - \sigma_3) = \frac{5.4838}{.0125674} = 436 \text{ psi} \tag{87}$$

and

$$\tfrac{1}{2}(\sigma_1 - \sigma_3) = 218 \text{ psi} \tag{88}$$

The stresses and directions are represented in Fig. 156. A Mohr circle representing the normal and shearing stresses is part of the figure.

It is to be noted that the polar coordinate angle θ is positive measured counterclockwise from the z axis, whereas the angle for determining the direction of σ_1 is positive measured clockwise from the x axis.

Example 2

Using the problem data of example 1, estimate the volume in which the minimum principal stress is greater than 1000 psi (compression).

Solution:

From Fig. 154, the principal stress contours for Case I, it may be observed that σ_1 and σ_3 are approximately constant on elliptical-shaped curves within the angular range $\theta = -60$ degrees to $\theta = +60$ degrees. The ratio between the lengths of the minor and major axes of the ellipse is 0.9, and the volume within which the minimum principal stress exceeds any given value is approximately equal to the volume of the ellipsoid obtained by rotating the given ellipse about its minor axis, i.e.,

$$\text{Volume} = \frac{4}{3}\pi a^2 b \tag{89}$$

where

a = half the length of the major axes

b = half the length of the minor axes

The contours for σ_3 were obtained by plotting curves

$$r_o = n_3 \cdot \text{tabular value (Column 10, Fig. 147)} \tag{90}$$

and the tabular value is

$$\sqrt{\frac{-4\pi}{V}\sigma_3} \cdot r_o$$

Hence along any contour

$$r_o = \sqrt{\frac{-4\pi}{V}\sigma_3} \cdot r_o \cdot n_3 \tag{91}$$

or

$$n_3^2 = \frac{V}{4\pi\sigma_3} \tag{92}$$

For this problem

$$n_3^2 = \frac{100{,}000}{4\pi(-1000)} = 7.958 \tag{93}$$

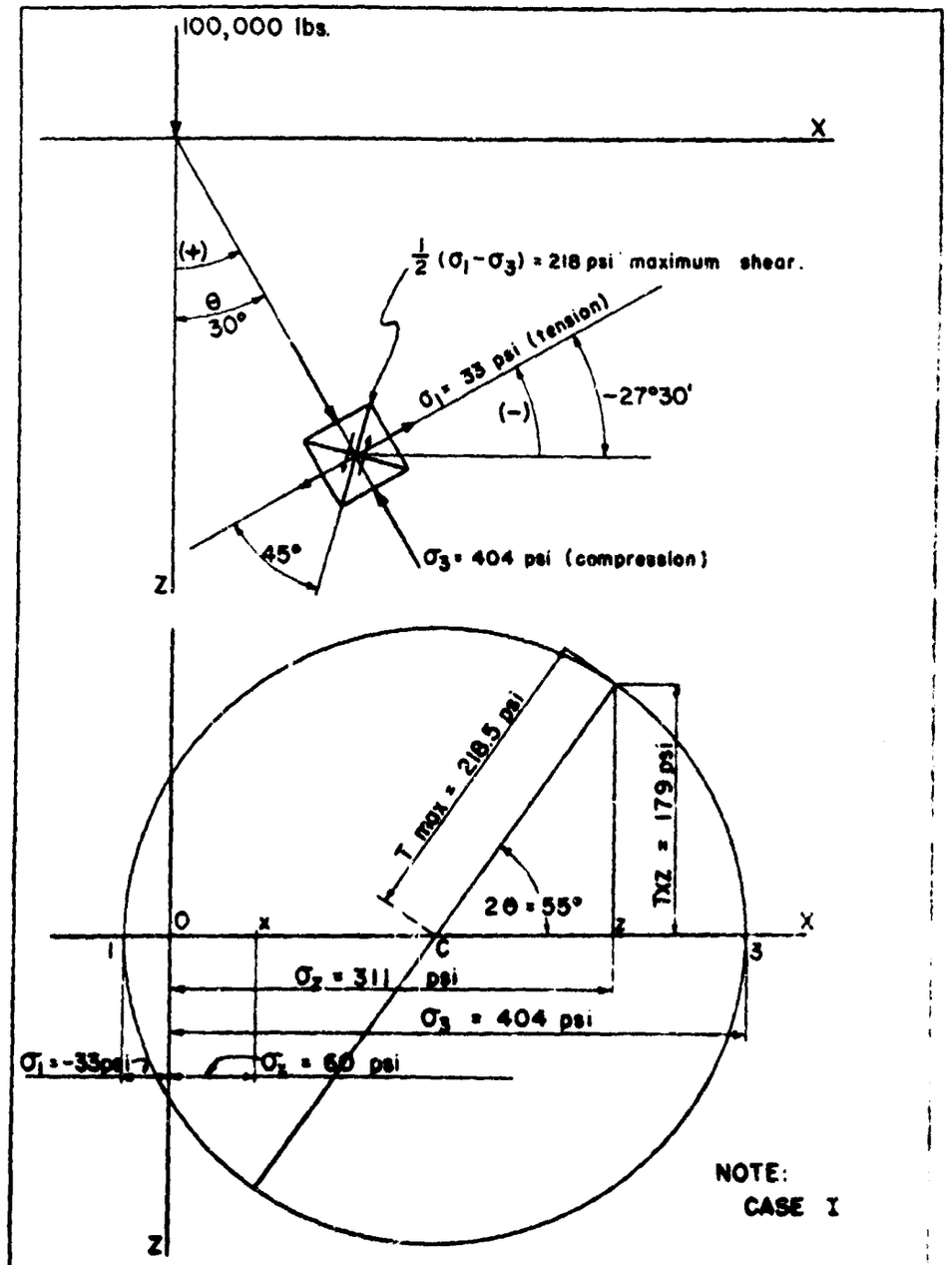

-BOMB PENETRATION PROJECT- CSM RESEARCH FOUNDATION, INC.

Scale ——— Date 3-3-81	FIGURE TO ACCOMPANY
Fig. No. 156 By LB	EXAMPLE I, PART 13

Fig. 156

and

$$n_3 = 2.821 \tag{94}$$

Therefore

$$r_m = 2.821 \cdot \text{(tabular value)} \tag{95}$$

From Fig. 147 the tabular value at θ equals 0 degrees for

$$\sqrt{\frac{-4\pi}{V}}\,\sigma_3 \cdot r_m \text{ is } 2.4495$$

$$r_m = 2.821 \cdot 2.4495 = 6.910 \tag{96}$$

$$\text{But } r_m = 2b \quad \therefore \quad b = 3.455 \tag{97}$$

$$\text{and } a = \frac{b}{0.9} = 3.839 \tag{98}$$

The volume of the ellipsoid is

$$\frac{4}{3}\pi a^2 b = \frac{4}{3}\pi (3.839)^2 \cdot (3.455) = 213.3 \text{ cu. in.} \tag{99}$$

Example 3

Using the problem data of example 2, estimate the ratio of volumes in which the minimum principal stress is greater than 1000 psi if the vertically applied load is increased from 100,000 lb to 200,000 lb.

Solution:

For any value of θ, tabular values of $r_m\sqrt{\frac{-4\pi}{V}}\,\sigma_3$ are given in the table.

Hence for two values of V, say V_1 and V_2, and the same value of σ_3

$$r'_o \sqrt{\frac{-4\pi}{V_1}\sigma_3} = \text{tabular value} \qquad (100)$$

and

$$r''_o \sqrt{\frac{-4\pi\ \sigma_3}{V_2}} = \text{tabular value} \qquad (101)$$

Therefore

$$\frac{r'_o}{r''_o} = \sqrt{\frac{V_1}{V_2}} \qquad (102)$$

and

$$r''_o = r'_o \sqrt{\frac{V_2}{V_1}} \qquad (103)$$

For a load of 100,000 lb and for a value of $\sigma_3 = 1000$ psi from example 2

$$r_o = 6.910 \qquad (104)$$

If the load is increased to 200,000 lb

$$V_2 = 200{,}000 \qquad (105)$$

$$\text{and} \quad \sqrt{\frac{V_2}{V_1}} = \sqrt{\frac{200{,}000}{100{,}000}} \quad 1.4142 \qquad (106)$$

$$r''_o = 6.910 \cdot 1.4142 = 9.772 \qquad (107)$$

The minor axis of the elliptical volume of strain equals

$$2b = 9.772 \text{ in.} \qquad (108)$$

$$b = 4.886 \text{ in.} \qquad (109)$$

$$a = \frac{b}{0.9} = 5.429 \text{ in.} \qquad (110)$$

$$\text{Volume} = \frac{4}{3}\pi a^2 b = \frac{4}{3}\pi (5.429)^2 (4.886) \quad 603 \text{ cu. in.} \qquad (111)$$

$$\text{The ratio of volumes is } \frac{603}{213.3} = \frac{2.83}{1} \qquad (112)$$

SECTON IV—METALLURGICAL STUDIES

By Sigmund L. Smith

1—Introduction

Metal droplets, partly obscured by a white scale, were observed on the noses and on portions of the bomb body of all the various types of bombs dropped during the tests. The photograph, Fig. 157, illustrates the distribution of metal droplets over the nose of a 1600 AP bomb released from 30,000 feet above the target at the granite site. The black strip in which the metal droplets may be seen was first sanded to remove the white silica-bearing scale, washed with water, washed with alcohol, and then painted with india ink. The india ink was then lightly sanded to bring out the relief of the droplets.

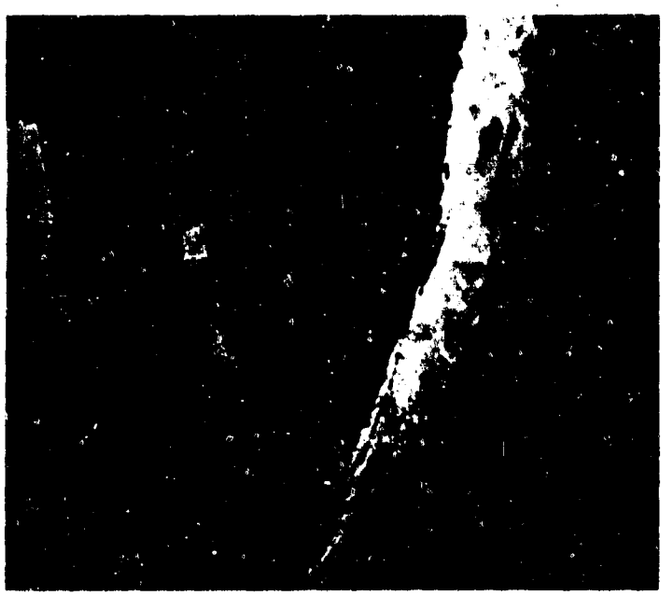

Fig. 157
Distribution of Metal Droplets
Nose of AP Bomb

Metallurgical studies were then undertaken to determine the effect of bomb impact and penetration upon the steel of which the bomb was constructed.

2—Flow Lines and Strain Lines

In order to determine whether strain lines, flow lines, or other changes in the steel of the armor-piercing and semi-armor-piercing bombs might have occurred, one armor-piercing bomb released from 30,000 feet, one armor-piercing bomb released from 18,000 feet, one semi-armor-piercing bomb released from 18,000 feet, and one semi-armor-piercing bomb released from 14,000 feet were treated in the following manner:

1) The sandpapered surface was etched for 30 minutes with a solution of hydrochloric acid at 160 degrees fahrenheit.

2) Subsequently, the surface was etched for 10 seconds with a cold solution of Fry's reagent[1].

From this investigation it was concluded that flow lines were absent at least from the areas investigated, and that the surface failure evidenced by the flow-metal droplets had not penetrated deeply into the body of the bombs.

3—Flow-Metal Droplets

Next, samples of the flow-metal droplets were pried off an armor-piercing bomb released from 30,000 feet above the granite target. It was observed that the metal droplets began to form about 3 inches back from the tip of the nose and then were spread out over the surface by the attrition of the rock. The position of the samples taken for metallurgical study and the photographs of the etched and unetched specimens at various magnifications are shown in Fig. 158.

Photomicrograph 3 (magnification 50X) of a droplet 6 inches from the nose of the bomb shows some of the silicate particles (light gray) embedded in the flow-metal.

A comparison of the several photomicrographs shows that the metal structure of the droplets is very fine-grained or amorphous and is the same for all droplets regardless of position on the bomb body. The number of voids resulting from gases being expelled during solidification is a minimum in the droplets close to the nose and a maximum in the droplets at the juncture of the nose and the body of the bomb.

4—Microstructure

Two of the general-purpose bombs which were dropped at the sandstone site and which broke into fragments upon impact were studied to determine whether any change in composition or hardness had occurred.

One of the bombs, Bomb 42, was released from 12,000 feet above the sandstone target, and the other, Bomb 44, was released from 14,000 feet above the sandstone target. Both ruptured and penetrated less than half the depth of other bombs of the same type released from the same altitude.

---

[1] Fry's reagent is:
[illegible] parts cupric chloride
[illegible] parts concentrated hydrochloric acid
[illegible] parts ethyl alcohol
[illegible] parts water.

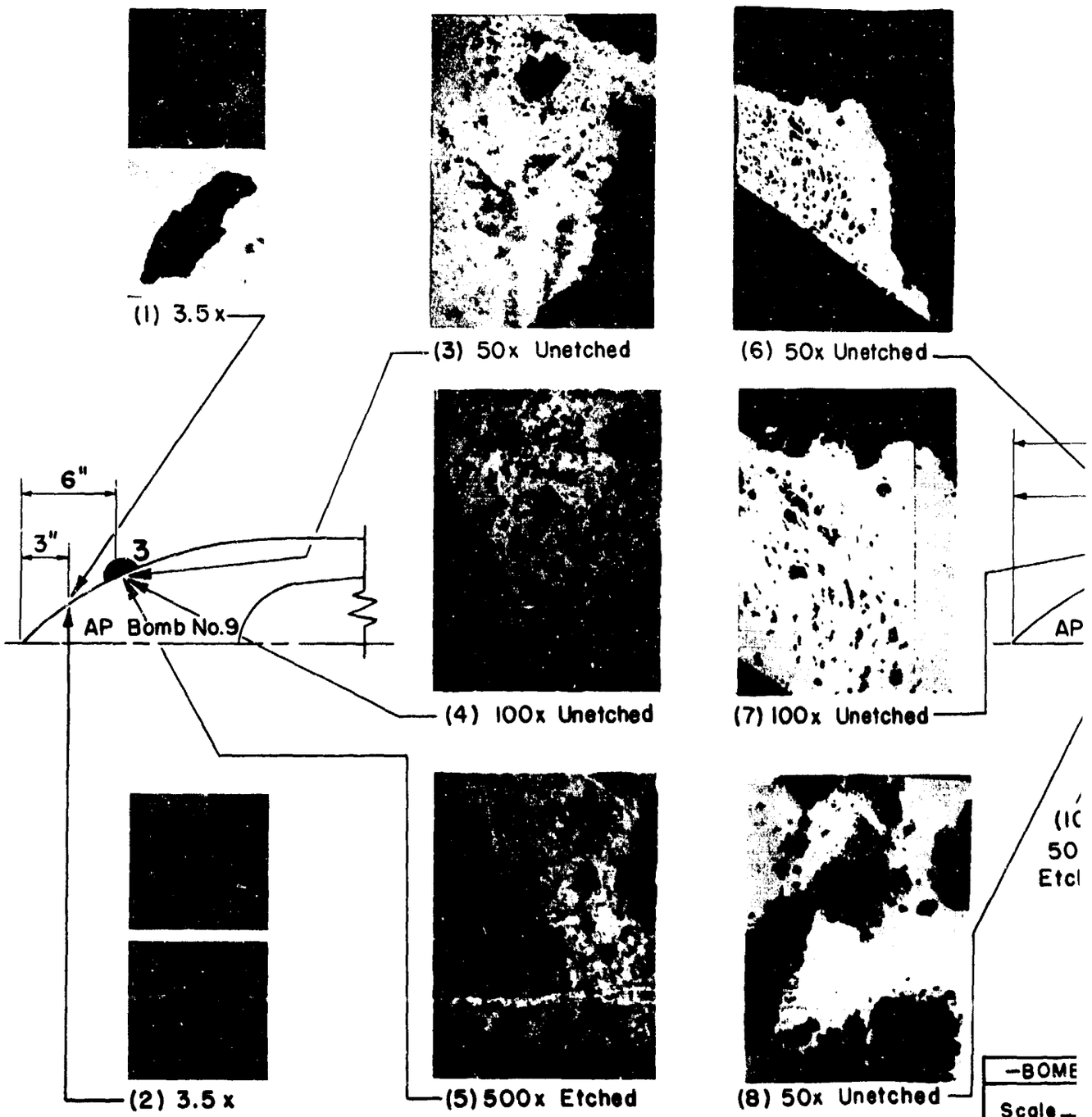
(1) 3.5 x
(3) 50x Unetched
(6) 50x Unetched
6"
3"
3
AP Bomb No.9
(4) 100x Unetched
(7) 100x Unetched
AP
(2) 3.5 x
(5) 500x Etched
(8) 50x Unetched
Scale
Fig. No.

(6) 50x Unetched

(9) 100x Unetched

(11) 50x Unetched

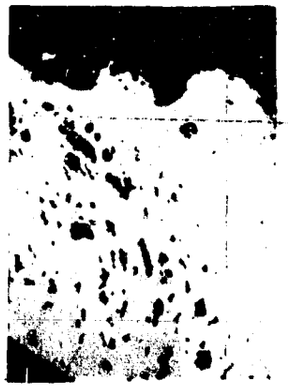

(7) 100x Unetched

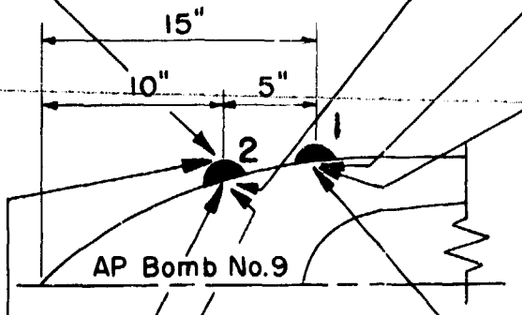

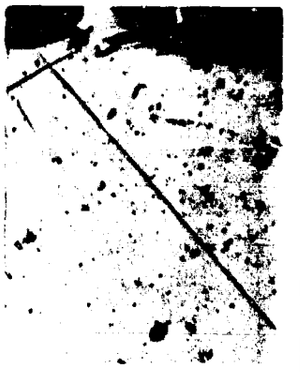

(12) 100x Unetched

(8) 50x Unetched

(10) 500x Etched

(13) 500x Etched

—BOMB PENETRATION PROJECT- CSM RESEARCH FOUNDATION, INC.	
Scale —— Date 3-12-51 Fig. No. 158 By JHW	METALLURGICAL STUDIES 1600 Lb AP BOMB METAL DROPLETS

Fig. 158

2

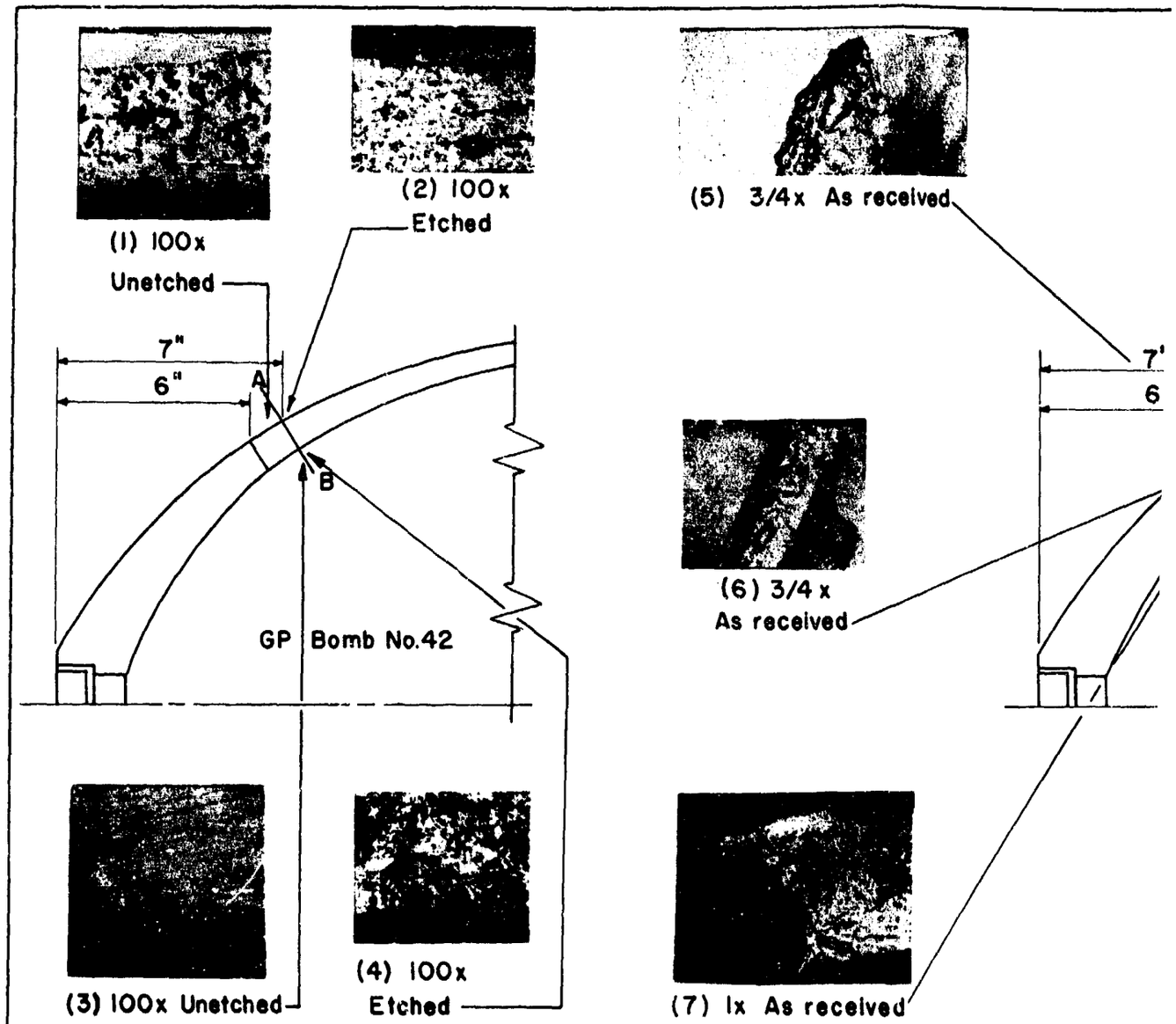
(1) 100x
Unetched
(2) 100x
Etched
(5) 3/4x As received
7"
6"
A
B
GP Bomb No.42
(6) 3/4 x
As received
(3) 100x Unetched
(4) 100x
Etched
(7) 1x As received

-BC
Scal
Fig.

(5) 3/4x As received

(8) 500x Etched

(6) 3/4 x
As received

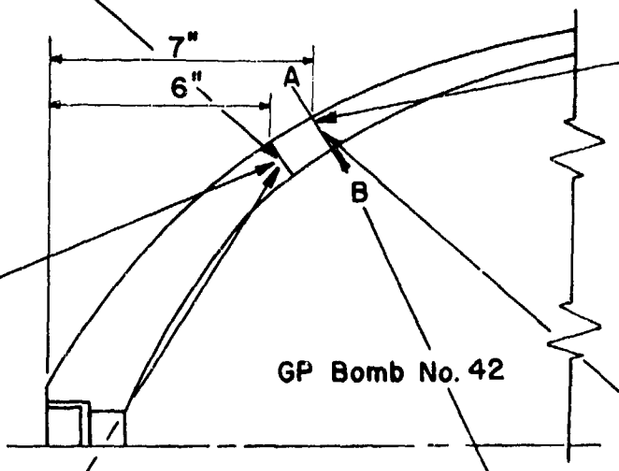

(9) 500x Etched

(7) 1x As received

(10) 500x Etched

-BOMB PENETRATION PROJECT- CSM RESEARCH FOUNDATION, INC.	
Scale — Date 3-12-51 Fig. No. 159 By JHW	METALLURGICAL STUDIES 2000 Lb GP BOMB

Fig. 159

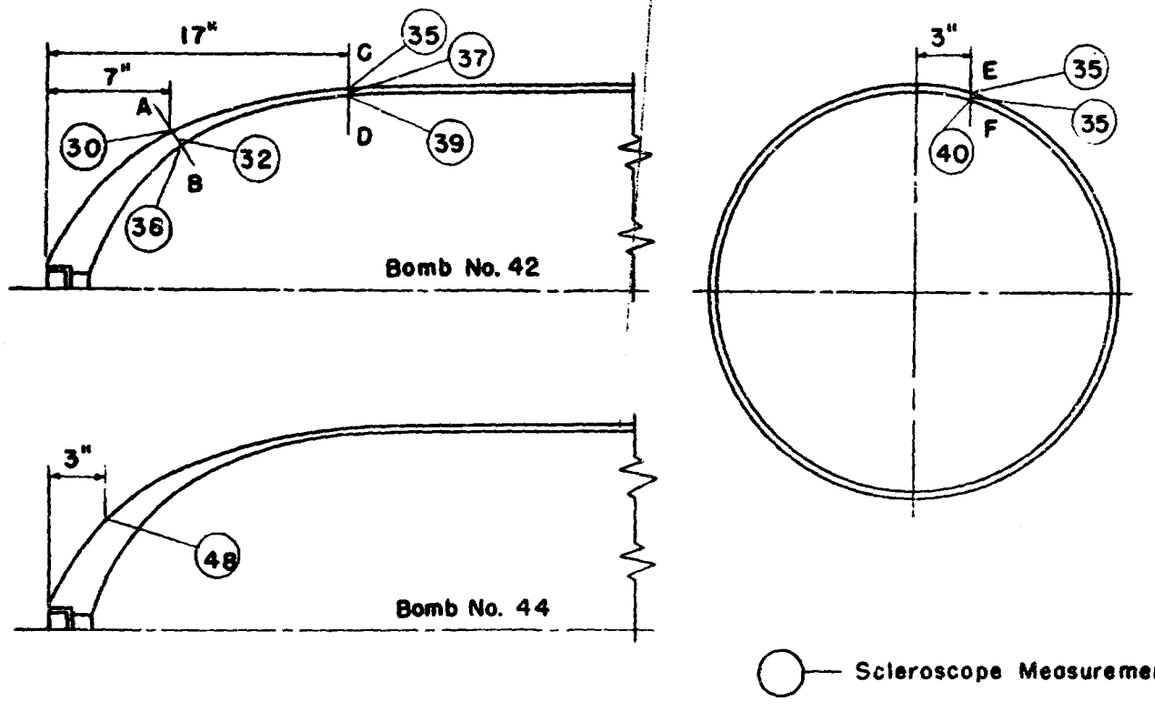

- BOMB PENETRATION PROJECT - COLORADO SCHOOL OF MINES RESEARCH FOUNDATION, INC.	HARDNESS OF GP BOMBS AFTER IMPACT (SHORE SCLEROSCOPE)	Scale 1" = 8" Date 3-9-51 Fig. No. 160 By JHW

Fig. 160

The macrostructure of fragments from GP Bomb 42 and the position on the bomb from which the fragments were taken are shown in Fig. 159, inserts 5, 6, and 7. Cubes were sawed from the bombs and prepared for photography under the metallographic microscope. Inserts 1 and 3 of Fig. 159 are unetched photomicrographs of specimens from the outside and from the inside of the bomb 7 inches behind the nose. Insert 1, a photograph of the outside edge, which shows a layer of metal about to be torn away from the body of the bomb, is in contrast to insert 3, from the inside edge, which shows no such evidence. Microphotographs 2 and 4 have been etched and show the grain structure. The grain structure of the outside edge is similar to that of annealed steel. The grain structure of the inside edge has a typical troostitic appearance such as occurs when cooling is not fast enough to obtain martensite.

The microphotograph, insert 8, at a higher magnification than insert 2, shows the structure near the incipient stage at the outside surface of the bomb. Insert 9 shows the typical pearlitic structure midway between the outside and inside surfaces of the bomb as a result of slower cooling during the normalizing period. Insert 10 shows the troostitic structure of the inside edge at greater magnification.

5—Hardness Changes

Hardness measurements were made on the etched specimens from Bombs 42 and 44. In this test, a Rockwell tester was used with the "C" type of scale; the Rockwell "C" hardness was converted to Shore sclerescope readings in order to have the bomb hardness on the same basis as that used for the rock specimens (see Physical Rock Tests). The position of the specimen and the sclerescope hardness obtained are shown in Fig. 160.

Ordnance specifications require normalizing of the bombs after forging. The purposes of this normalizing treatment are to break up the coarse grain structure and carbides formed by the forging, to remove any residual stresses caused by forging, and to produce a more uniform structure throughout the material. Because of this normalizing, it is reasonable to assume that the inside and outside surfaces of the bomb have an identical microstructure and identical physical properties. The hardness tests showed that the area near the nose had increased in hardness. Tests made 7 inches from the nose showed that the material had softened; further tests at points 11 to 17 inches from the nose showed that the hardness again increased. The increased hardness at the nose can be attributed to work-hardening of the steel. Heat generated at the nose was dissipated into the rock to some extent, and flowed back from the nose to the body of the bomb. The temperature at the tip probably did not rise appreciably, so the internal stresses produced by the cold working remained and caused an increase in the hardness. The lesser hardness found 7 inches from the nose can also be attributed to work-hardening and subsequent annealing. The surface temperature in this zone was high enough so that the steel could reach the incipient point and flow along the surface of the bomb as it moved downward. The non-flowing metal was in the austenitic stage. The cooling from the austenitic stage was slow because the crushed rock acted as a good heat insulator. This slow cooling is typical of the usual annealing methods. The zone 11 to 15 inches from the nose was subjected to a similar process; however, the effects of pressure and temperature became progressively less severe with increased distance from the nose.

SECTION V—PHOTOELASTIC STUDIES OF STRESS DISTRIBUTION IN THE MEDIUM

By M. J. Pandya

1—Introduction

The stress distribution in the interior of a semi-infinite solid due to a concentrated force at the surface can be determined mathematically as presented in Section III, but the mathematical solutions become so complicated if the force is applied at various points and in various directions below the surface that the mathematical approach becomes impractical if not impossible. Accordingly, the photoelastic method of stress analysis was used to investigate the stress distribution in the medium under both conditions of load. The photoelastic method has been used to study three-dimensional problems, but because part of the necessary apparatus was not immediately available, it seemed advisable first to study the stress distribution in the two-dimensional models using standard techniques and available apparatus.

Three problems relative to the validity of the results of the two-dimensional study arise immediately. 1) Is the stress distribution substantially the same in any given plane in a two-dimensional model as it is in the same plane in a three-dimensional model? 2) Is the pattern of the stress distribution in the medium similar in static loading to that in dynamic loading? 3) Is the stress distribution influenced so greatly by the elastic properties of the medium that the usual photoelastic model materials are apt to give distorted results?

The solution to the first problem seemed to be that work should be conducted in such a manner that the three-dimensional mathematical results cited in Section III for a force applied to the surface of a semi-infinite solid could be compared with the two-dimensional photoelastic results. The second problem was met satisfactorily by comparing the strain patterns in Stress-coated models under static and under dynamic loads. The third problem cannot be solved completely until more of the fundamentals are known, but from information now available it appears that within the elastic limit the experimental error is more apt to depend upon the manner of loading and of confining the specimen than upon a great difference between the elastic properties of the photoelastic model material and the rock prototype.

The circumstances surrounding failure of a material are dependent upon the physical properties of that material, such as cohesion and coefficient of friction, but the stress magnitudes and their distribution are entirely unaffected by the physical properties. Changes in physical properties from region to region also affect stress magnitude and distribution.

Figure 161 is a photograph of the C.S.M. photoelastic apparatus and loading frame. The loading frame was designed in the Mining Department of the Colorado School of Mines in such a manner that the specimen is laterally confined and a horizontal component of stress is induced in the

Fig. 161
Photoelastic Apparatus and Loading Frame

medium as a result of application of the vertical load. The induced horizontal stress is

$$P_2 = \frac{m}{1-m} P_1$$

where

P_2 = stress acting horizontally

m = Poisson's ratio

P_1 = stress acting vertically.

2—Comparison of Mathematical and Photoelastic Results

Frocht[1] has shown that the normal stress in a radial direction upon an element in a semi-infinite plate equals

$$\sigma_r = -\frac{2R}{\pi t} \frac{\cos \delta_1}{r_0} \qquad (1)$$

[1] Frocht, Max M., Photoelasticity, vol. II, pp. 55-72, John Wiley and Sons, New York, 1948.

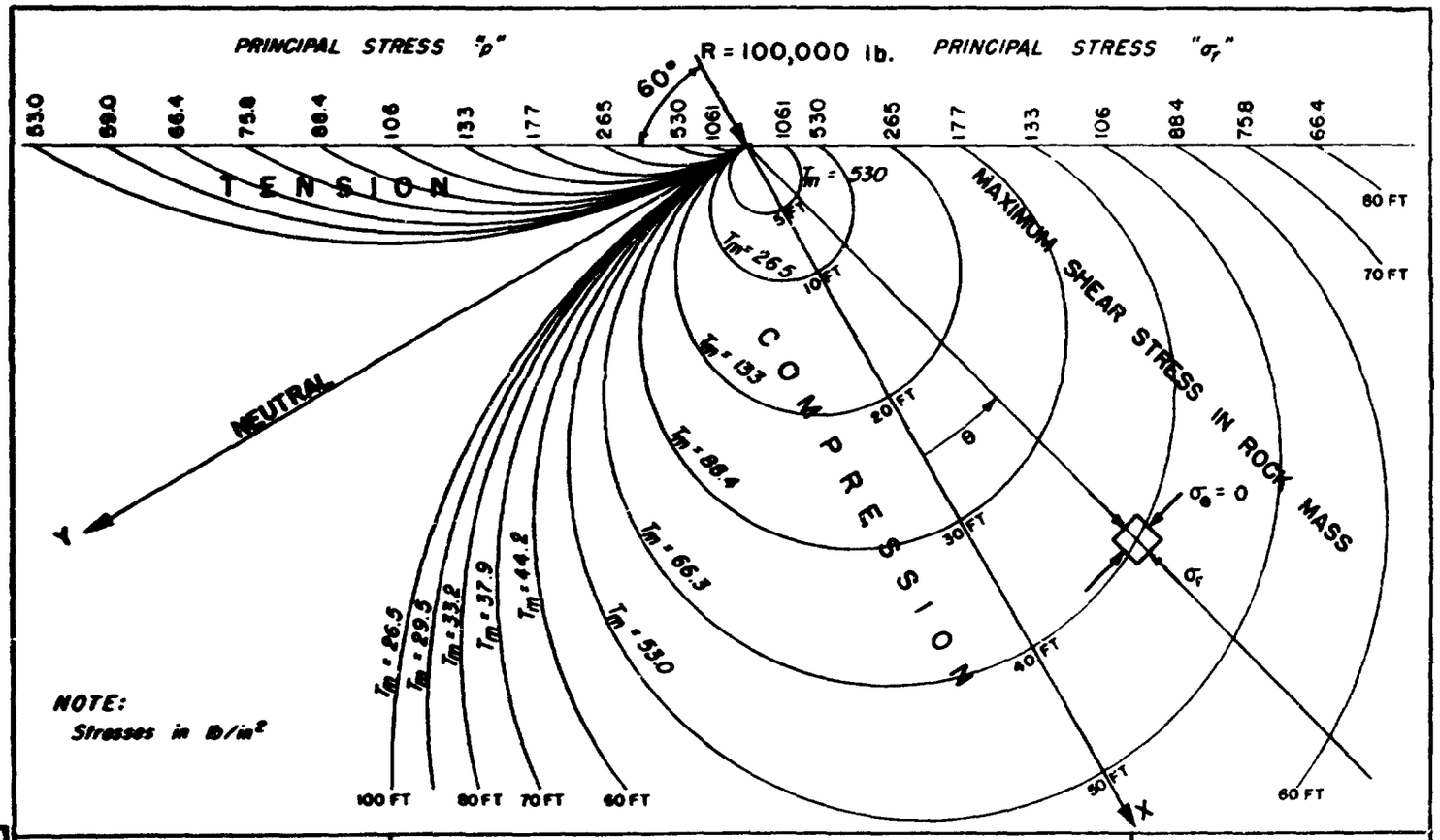

-BOMB PENETRATION PROJECT- COLORADO SCHOOL OF MINES RESEARCH FOUNDATION, INC.	TWO-DIMENSIONAL STRESSES FOR 60° LOADING	Scale 1" = 10' Date 3-28-51 Fig No 162 By LSC

Fig. 162

where

σ_r = radial stress

R = applied load

r_o = radial distance

θ_1 = angle from line of action of the applied force to the element

t = thickness of the plate

The normal stress in a direction at right angles to the radial direction equals σ_θ, and $\sigma_\theta = 0$. The shearing stresses acting on the element are zero, and $t_{r\theta} = 0$. The maximum shear stresses on the element act at 45 degrees to the direction of principal stress and equal

$$T_{max} = \frac{\sigma_\theta - \sigma_r}{2}$$

$$= \frac{R \cos \theta_1}{\pi t r_o} \qquad (2)$$

Now at $\theta_2 = 0°$, $\cos \theta_2 = 1$, $r_o = d$, and

$$T_{max} = \frac{R}{\pi t d} \qquad (2')$$

The shear stresses are constant along a circle of diameter d which bisects the line of action, and at points along the circle are inversely proportional to the diameter. In other words, the shear stress on a circle of d = ¼ is four times as great as that on a circle of diameter d = 1.

If the angle θ_1 is measured from the line of action of the concentrated load R, as in Fig. 162, the angle of obliquity need not be considered. However, the neutral, or zero stress, axis is at right angles to the line of action of the concentrated load. Below the neutral, or zero stress, axis, σ_r is negative (compression); and above the neutral axis, σ_r is positive (tension). The form of the shear contours above the neutral axis is the same as the form of the shear contours below the neutral axis. Both are circles, but the shear contour circles above the neutral axis terminate at the ground line. In Fig. 162 values of σ_r, the normal stress on radial lines, and of T_{max}, maximum shear, for the locus of all points on a series of concentric circles at various distances in feet from a concentrated load of 100,000 pounds acting at 60 degrees to the edge of a plate 1 inch thick, are shown.

The photograph, Fig. 163, shows the fringes in an allite ground model and an allite model of a 26,000 SAP bomb. The allite model and the bomb model are ¼ inch thick, and the fringes are a result of vertical static loading corresponding to an angle of impact of 70 degrees. A device to hold the bomb from slipping on the surface was necessary.

A neutral line is at right angles to the axis of the bomb. Assuming that the diameter of the first dark fringe below the neutral axis is unity, then the diameter of the second fringer equals 1/2, of the third fringe 1/3 and of the nth fringe 1/n. The value of each fringe was found from previous experiments to be 180 pounds per square inch in shear. Thus for the

Fig. 103

Shear Contours as Determined Photoelastically in the Medium below a Model 20000-pound SAP Bomb

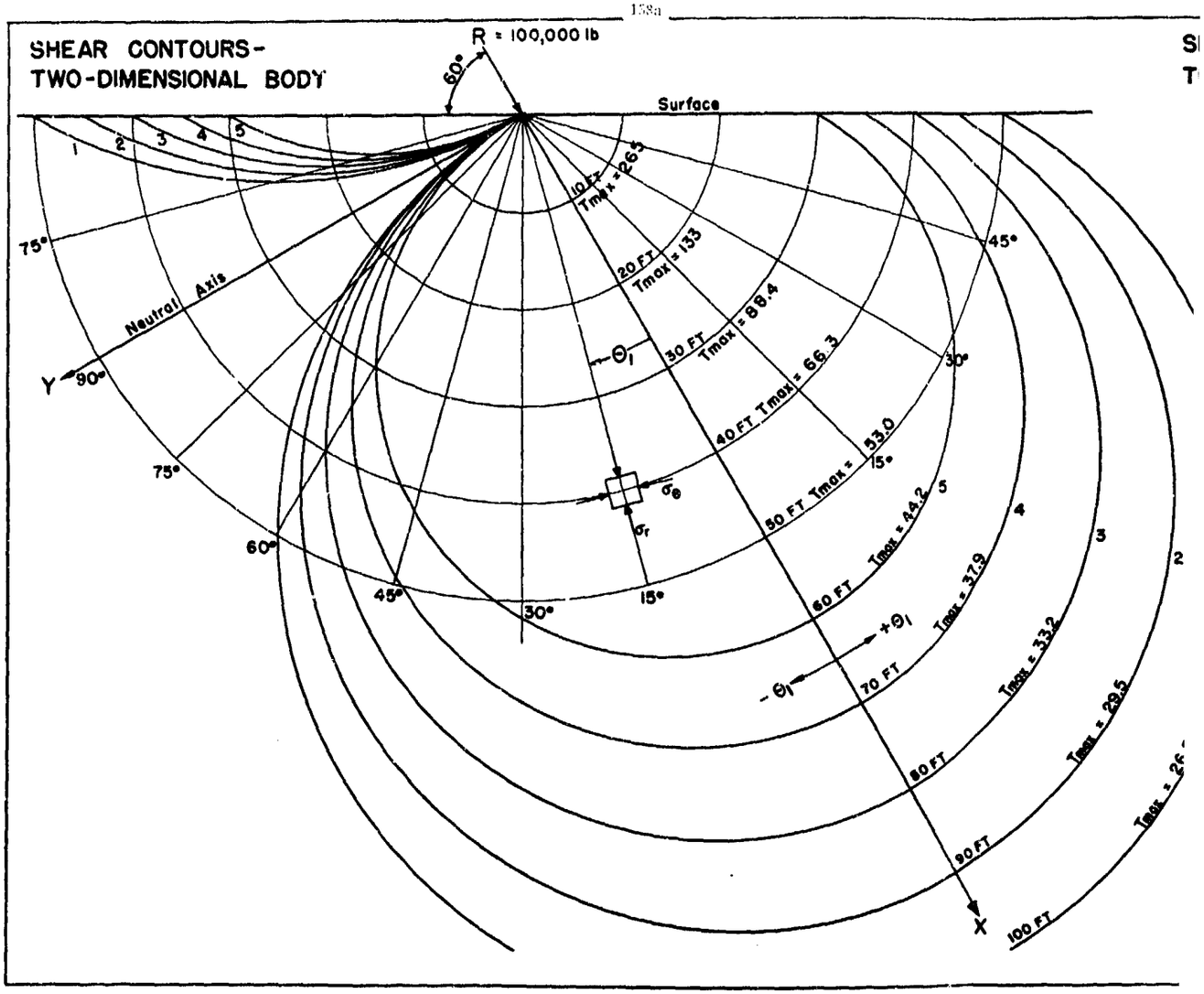
SHEAR CONTOURS-
TWO-DIMENSIONAL BODY
R = 100,000 lb
60°
Surface
1
2
3
4
5
75°
Neutral Axis
Y
90°
75°
60°
45°
30°
15°
45°
30°
15°
10 FT Tmax = 26.5
20 FT Tmax = 133
30 FT Tmax = 88.4
40 FT Tmax = 66.3
50 FT Tmax = 53.0
60 FT Tmax = 44.2
70 FT Tmax = 37.9
80 FT Tmax = 33.2
90 FT Tmax = 29.5
100 FT
X
θ_1
$+\theta_1$
$-\theta_1$
σ_θ
σ_r

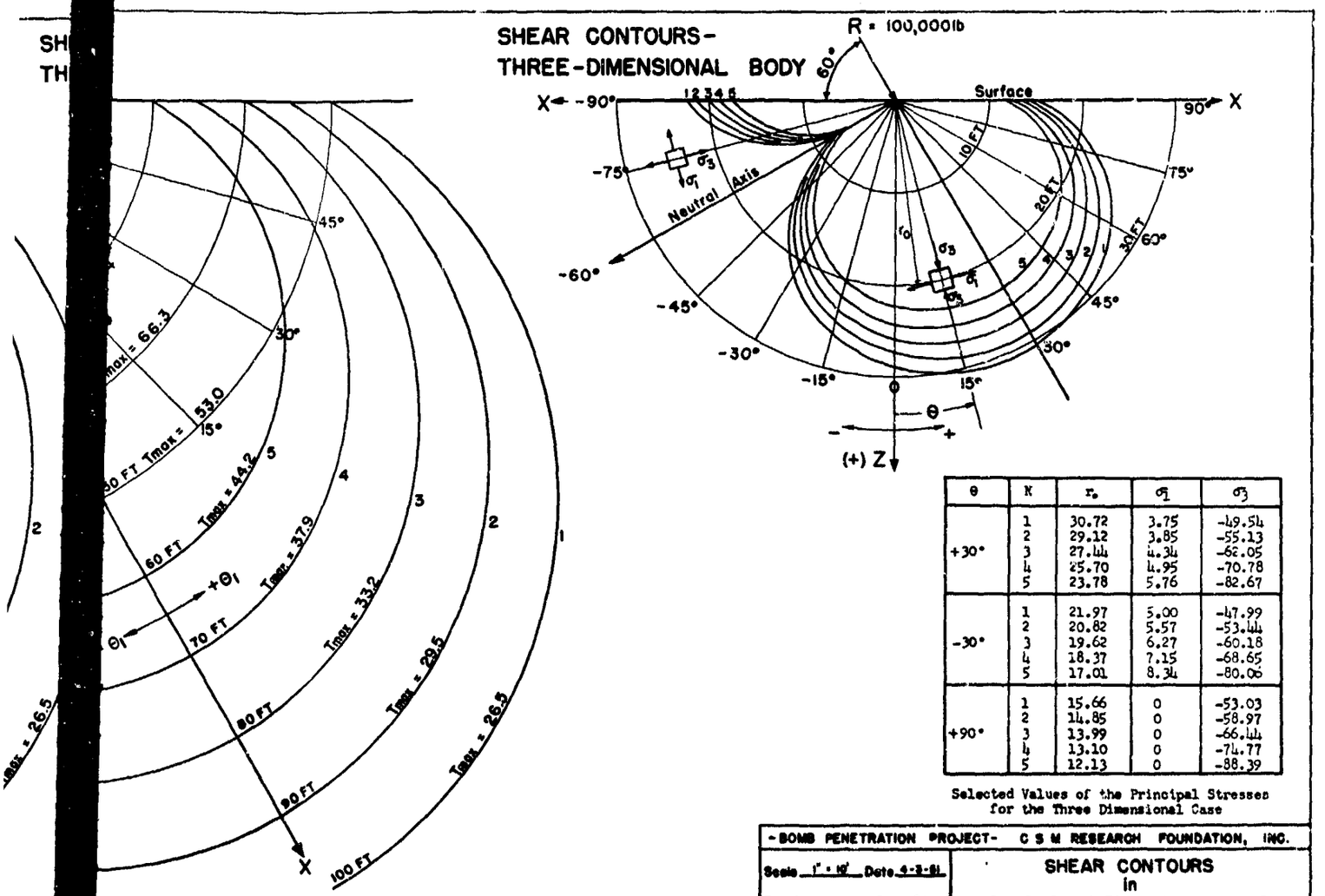

θ	N	r_o	σ_1	σ_3
+30°	1	30.72	3.75	-49.54
	2	29.12	3.85	-55.13
	3	27.44	4.34	-62.05
	4	25.70	4.95	-70.78
	5	23.78	5.76	-82.67
-30°	1	21.97	5.00	-47.99
	2	20.82	5.57	-53.44
	3	19.62	6.27	-60.18
	4	18.37	7.15	-68.65
	5	17.01	8.34	-80.06
+90°	1	15.66	0	-53.03
	2	14.85	0	-58.97
	3	13.99	0	-66.44
	4	13.10	0	-74.77
	5	12.13	0	-88.39

Selected Values of the Principal Stresses for the Three Dimensional Case

- BOMB PENETRATION PROJECT - C S M RESEARCH FOUNDATION, INC.

Scale 1" = 10' Date 4-3-51

Fig. No. _____ By LBG

SHEAR CONTOURS in 2- & 3-DIMENSIONAL BODIES

Fig. 164

2

given load the shearing stress at all points on the first fringe is 180 pounds per square inch; the shearing stress on the second fringe at one-half the distance from the point of application of the load is 360 pounds per square inch, and at one-third the distance is 540 pounds per square inch.

The normal stress, σ_r, on radial lines intersecting the first fringe is twice the maximum shearing stress. The normal stress at all points on the first fringe is 360 pounds per square inch, on all points on the second fringe is 720 pounds per square inch, and on the third fringe is 1080 pounds per square inch.

The shear contours as determined for the two-dimensional body illustrated in Fig. 163 are compared with the shear contours computed mathematically for the three-dimensional body, and the results are presented graphically in Fig. 164. In the figure a cross section through the two-dimensional body is shown to the left, and a cross section through the three-dimensional body to the right. In the two-dimensional body the outermost circle has a diameter of 100 feet, and T_{max} at all points on the circle is 26.5 pounds per square inch. The 100-foot-diameter circle is designated circle 1, the 90-foot-diameter circle is designated circle 2, and the 60-foot-diameter circle is designed circle 5. In the three-dimensional body the shear contours are ellipses rather than circles. The minor diameter of the ellipse is approximately 0.9 the major diameter, and the minor diameter coincides with the direction of the line of action of the applied force. The shear stress along ellipse 1 in the three-dimensional body is the same as the shear stress along circle 1 in the two-dimensional body.

In the three-dimensional body, θ is measured from the z axis and along the line of the applied force; θ equals 30 degrees, and the radial distance to ellipse 1 is 30.72 feet. The shear stress at 30.72 feet in the three-dimensional body and at 100 feet in the two-dimensional body is equal to 26.5 pounds per square inch.

In the two-dimensional body at 100 feet measured along the line of action, the normal radial stress, σ_r, is 53.0 pounds per square inch, and σ_z is zero, whereas in the three-dimensional body and with Poisson's ratio 0.25, σ_z is 49.54 pounds per square inch and σ_r is 2.75 pounds per square inch.

In a two-dimensional body the shear stress and the normal stress in a radial direction vary inversely as the distance from the point of application of the concentrated force, whereas in a three-dimensional body the shear stress, the normal stress in a radial direction, and the normal stress in a tangential direction vary inversely as the square of the distance.

3—The Use of Gelatin as a Photoelastic Material

It proved to be most difficult to prepare an allite model and obtain suitable contact between the bomb and the ground at various stages of penetration. Moreover, field work had shown that penetration is accompanied by rock failure, and it thus would have been necessary to duplicate the rock failure in the allite ground models. Furthermore, it was apparent from the results of the field work that the resistance to penetration was a function of depth and it was difficult, if not impossible, using

allite models, to duplicate the effect of the weight of the rock mass upon the resistance to penetration. These difficulties were overcome by using gelatin as a model material. Farquhasson and Hennes[2] had previously used gelatin models for photoelastic analysis of stress in earth masses.

Because of the difficulty of preparing a simple tension or a simple compression model of gelatin, the method used to determine the fringe values of gelatin was to load the model material over a finite area and to calculate the fringe value from the formula

$$T_{max} = \frac{q_0}{\pi t} \frac{a}{r_0}$$

where

T_{max} = fringe value

q_0 = intensity of load over finite area

t = thickness of finite area (also model)

a = one-half the length of finite area

r_0 = radius of the circular fringe on which the fringe order is being computed

The fringe value for a mixture of 16 per cent gelatin, 25 percent glycerin, and 59 percent water was found to be 0.52 pounds per square inch in shear.

Gelatin ground models were cast between ⅜-inch glass plates in a loading frame of the type shown in Fig. 165. The loading frame was introduced into the standard polariscope setup, and the stress distribution in the medium was determined at various places along the path of the bomb. The path of Bomb 31, which was accurately determined in the field, was used as a prototype path. The model bomb was moved to various positions along the predetermined path by adjusting the position of the rod on the back end of the bomb and by adding weights to the end of the lever arm. The stress distribution was determined after equilibrium between the bomb and the gelatin medium had been established and the bomb had come to rest.

4—Comparison of the Stress Distribution in the Medium at the Noses of 2000 SAP and 25,000 SAP Bombs.

Figure 166 shows the shear contours in the medium at the nose of a 2000 SAP model bomb. It may be observed by comparing Fig. 166 with Fig. 163 that the stress distribution in the gelatin is similar to that in the allite model material. In Fig. 166 the bomb has penetrated a short distance into, rather than being at the surface and making line contact with, the medium. The unstressed medium is dark and extends to the neutral axis on both the footwall and the hanging-wall sides of the bomb. A surface bulge similar to that observed in the field has started to form, and the neutral fringe is within the bulge on both the footwall and the hanging-wall sides of the bomb. In the allite ground model, Fig. 163, as discussed

[2] Farquhasson and Hennes, Gelatin Models for Photoelastic Analysis of Stress in Earth Masses: Civil Engineering, vol. 10, no. 4, pp. 221-224, 1940.

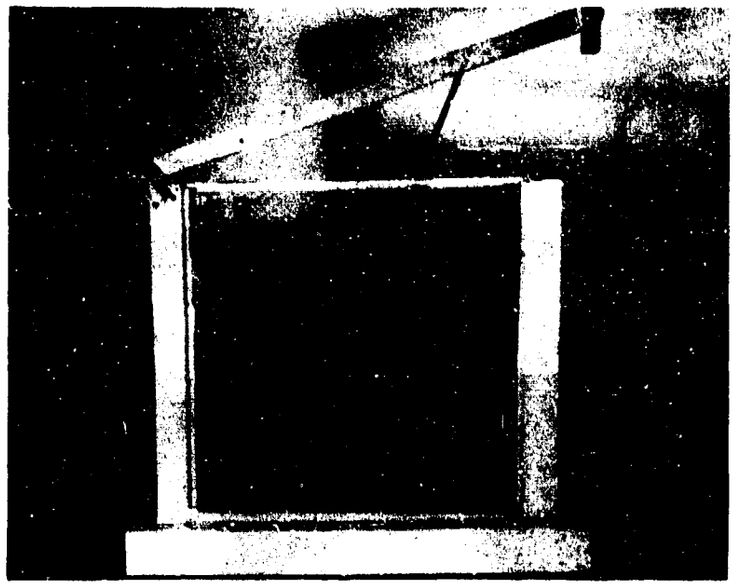

Fig. 165

Gelatin Model Loading Frame

in connection with the two-dimensional mathematical analysis, the neutral axis extends into the medium on the footwall side only. The difference is due to the presence of the surface bulge and to the partial burial of the nose of the 2000 SAP model bomb.

The first white half-fringe above the neutral line indicates negative shear, and tension. The length of the tension zone is greater on the hanging-wall side than on the footwall side of the bomb. The tension zone in the hanging-wall does not show in the allite ground model (Fig. 163) because of the absence of the surface bulge and the point contact on the surface.

The maximum fringe order in the gelatin at the nose of the bomb is 5. The fringes in the gelatin are circular in outline, but the depth of the circles is at a maximum vertically below the nose rather than along the path. The fringes meet the nose of the bomb on both the footwall and hanging-wall sides rather than meeting the tip of the nose as in point loading. As the depth of penetration approaches complete burial of the nose, the type of loading departs further from the point loading of Fig. 163, and the fringes intersect the nose nearer to the cylindrical portion of the bomb body.

Figure 167 shows the shear contours in the medium at the nose of

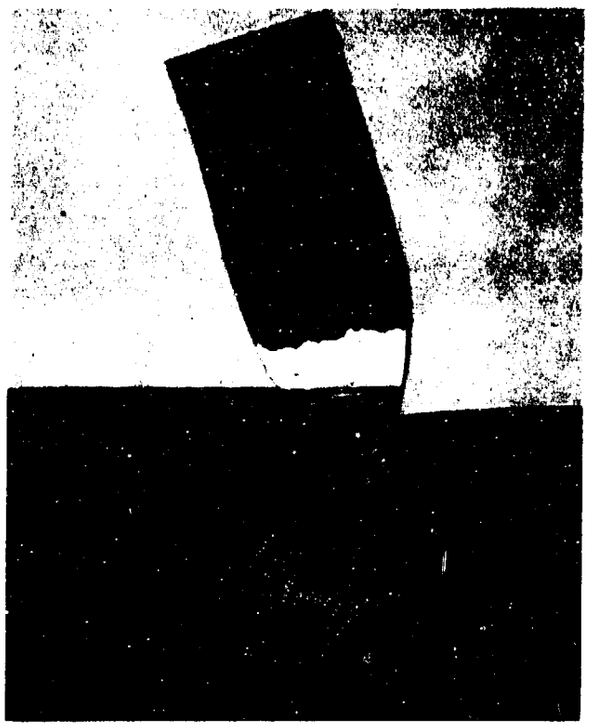

Fig. 166
Stress Distribution in the Medium at the Nose of a 2000-pound SAP Bomb

a 25,000 SAP model bomb. As may be observed, the shear contours differ in shape from those at the nose of the 2000 SAP bomb. The difference is due entirely to the difference in the shapes of the noses of the two bombs, for the manner of loading, the relative depth of penetration, and the fringe value of the model material is the same. The sharp nose of the 25,000 SAP bomb results in a wedging action that parts the medium symmetrically along the line of action of the bomb. The parting of the medium relieves the stress near the zone of plastic failure at the nose than at a greater distance. The stress relief is apparent from a comparison of the shapes of the shear contours.

The wedging action of the 25,000 SAP bomb nose becomes increasingly apparent with an increase in the depth of penetration, as may be observed by comparing the shear contours of the 25,000 SAP model bomb, Fig. 168a, with the shear contours of the 2000 SAP model bomb, Fig. 168b.

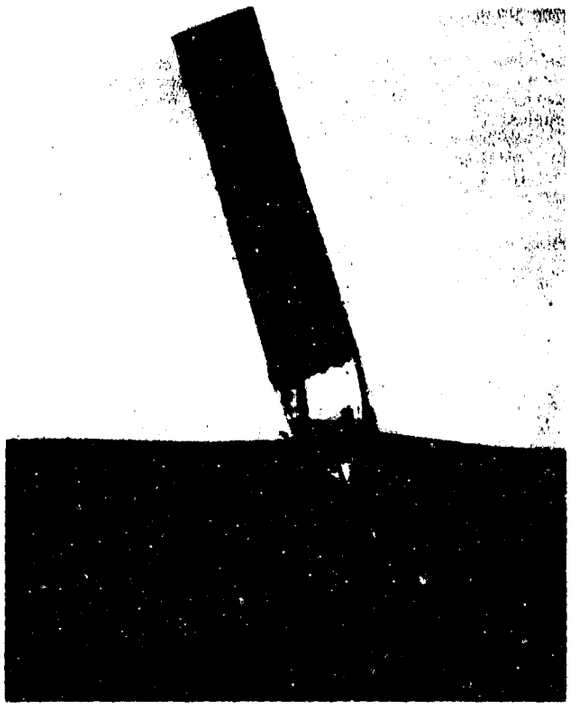

Fig. 167

Stress Distribution in the Medium at the Nose of a 25,000-pound SAP Bomb

The shear contours, fringes 1 and 2 of the 25,000 SAP model bomb, intersect the nose, whereas the shear contours, fringes 1 and 2 of the 2000 SAP bomb, are arranged in a concentric pattern and at a considerable distance beyond the nose. The disturbed area adjacent to both bombs correspond to the "crushed zone" or the "plastic failure zone" observed in the field. The disturbed zone encases the nose of the 2000 SAP model bomb, whereas it is confined for the most part to a region substantially behind the tip of the 25,000 SAP nose.

As the depth of penetration increases, the resistance to penetration also increases, or, in other words, the medium is stronger. Eventually a depth is reached where the nose of the 2000 SAP bomb exerts a wedging action similar to that of the nose of the 25,000 SAP bomb. At any given depth the wedging action is a function of the sharpness of the nose. A perfectly sharp nose would be one in which loading approaches point contact.

5—Stress Distribution in the Medium at Various Stages of Penetration of a 1600 AP Bomb

The shear stress distribution and the directions of principal stress at three stages of the penetration of a model bomb into a gelatin medium were determined, and the force on the model bomb at which equilibrium was reached for each of these three stages was measured. A 1600 AP model bomb constructed of allite to a scale ratio of 1 to 20 was selected, the path of Bomb 31 was used as the prototype path, and the fringe value of the gelatin model material was 0.52 pounds per square inch in shear.

A load was applied to the 1600 AP model, using the apparatus shown in Fig. 165. After equilibrium was reached, the force along the line of action of the bomb was computed to be 4.08 pounds, and the bomb had come to rest at a scale vertical depth of 7.2 feet, which corresponds to a scale incline penetration of 7.5 feet. This point of equilibrium is designated in the following drawings as point 1.

Figure 169a shows the shear fringes in the medium at point 1, the path of prototype Bomb 31, the surface, and the soil-shale contact. The soil-shale contact was formed by filling the loading frame with gelatin to the soil-shale contact and allowing it to cool sufficiently to form a crust before filling the loading frame to the ground line. The fringe orders are numbered in the drawing. The maximum fringe order is 5, and the maximum shearing stress occurs immediately adjacent to the tip of the nose on both the footwall and the hanging-wall side of the nose and also near the tail of the bomb on the footwall side.

From the mathematical analysis and from photoelastic results (see Figs. 162 and 163) it has been shown that the fringe order at the tip of the nose for point loading is greater than at other places in the medium, and from Figs. 167 and 168 it has been shown that as the penetration of a bomb becomes greater, the stress distribution is affected by the shape of the nose. As shown in Fig. 169a, the fringe order is 4 at the tip and is 5 in the medium adjacent to the tip in both the footwall and the hanging-wall at the tip elevation. A possible explanation may be that plastic flow develops at the tip because of high stresses associated with point contact, and the stress is transferred from the plastic zone to the elastic zone that surrounds it.

In the mathematical analysis upon two-dimensional and three-dimensional models it was shown for point loading and for zero penetration that the shear distribution was symmetrical about the line of action of the applied force. In Fig. 169a it may be observed that in the medium below a horizontal plane through the tip of the nose, the shear stress distribution is symmetrical about a vertical line through the nose tip rather than about the line of action. It may be observed also that the distance from the nose tip to any fringe is minimum rather than maximum along the vertical line of symmetry. Further it may be observed that the ratio between the maximum horizontal distance from the tip of the nose to any fringe and the maximum vertical distance to the same fringe is 2 to 1.

An inspection of the shear stress distribution on the nose of the bomb shows 1) that the shear stress is greater on the footwall side than on

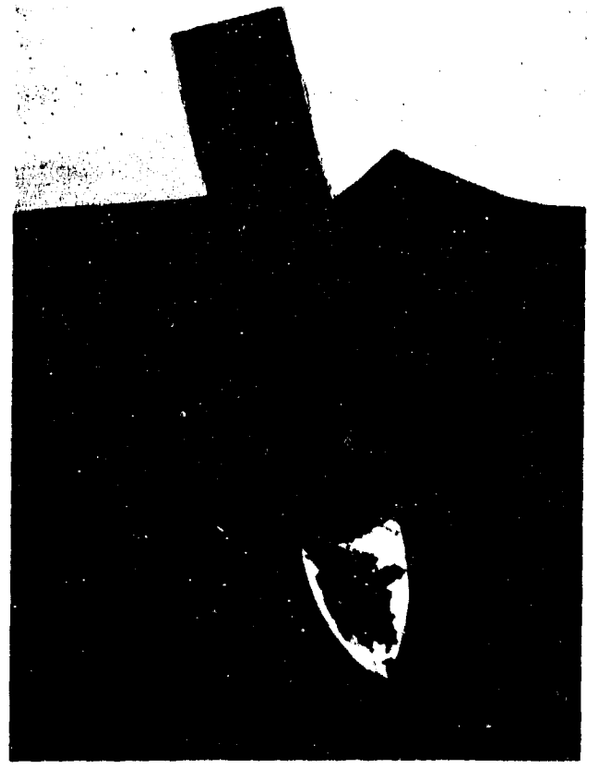

Fig. 168a
Shear Stress Distribution at Nose of 25,000-pound Model Bomb

the hanging-wall side at any given distance measured along the nose from the tip, 2) that the stress increases from the plastic zone at the nose tip to a maximum at some point beyond the plastic zone, then decreases to a minimum near the juncture of the nose and bomb body.

An inspection of the shear stress distribution along the body of the bomb shows 1) that the fringe order at the tail of the bomb on the footwall side is as great as it is at the nose, 2) that the fringe order at the tail end of the bomb on the hanging-wall side is less than on the footwall side, 3) that the fringe order on the hanging-wall side near the juncture of the nose is greater than on the footwall side at the juncture of the nose.

By converting the monochromatic light of the polariscope to white

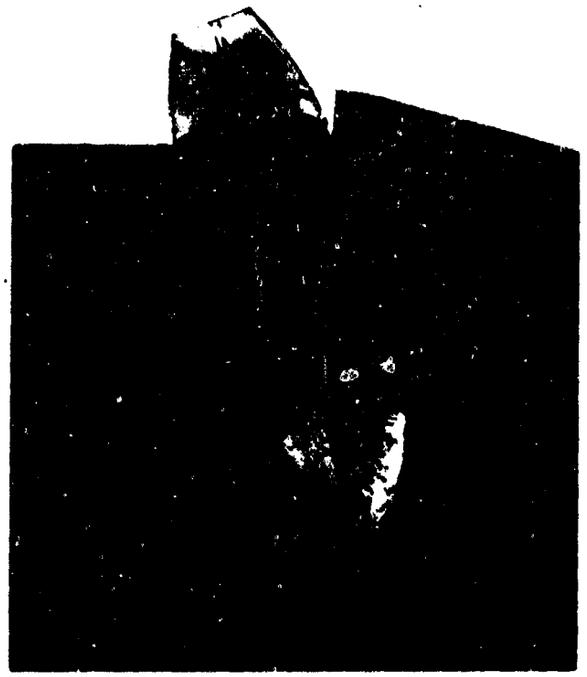

Fig. 168b

Shear Stress Distribution at Nose of 2000-pound SAP Model Bomb

light, removing the quarter-wave plates, and rotating the analyzer and polarizer simultaneously at intervals of 10 degrees, isoclinics were obtained, and the isoclinics were used to construct the stress trajectories at points shown in Fig. 169d. One of the principal directions at any point on a stress trajectory is tangent to the stress trajectory, and the other is at right angles to it. In a two-dimensional semi-infinite solid the principal directions comprise a series of radial lines parallel to σ_r and at right angles to σ_r at any given point as illustrated in Fig 162. The principal directions at the nose of a model 2000 SAP bomb inclined at 75 degrees to the surface and corresponding to a depth of penetration indicated by the shear contours in Fig. 166 are shown in Fig. 170.

It may be observed in Fig. 170 that the principal directions are influenced by the shape of the nose and that the directions are not constant along radial lines. Near the nose of the bomb the departure from radial and tangential directions is not great, but the departure increases as

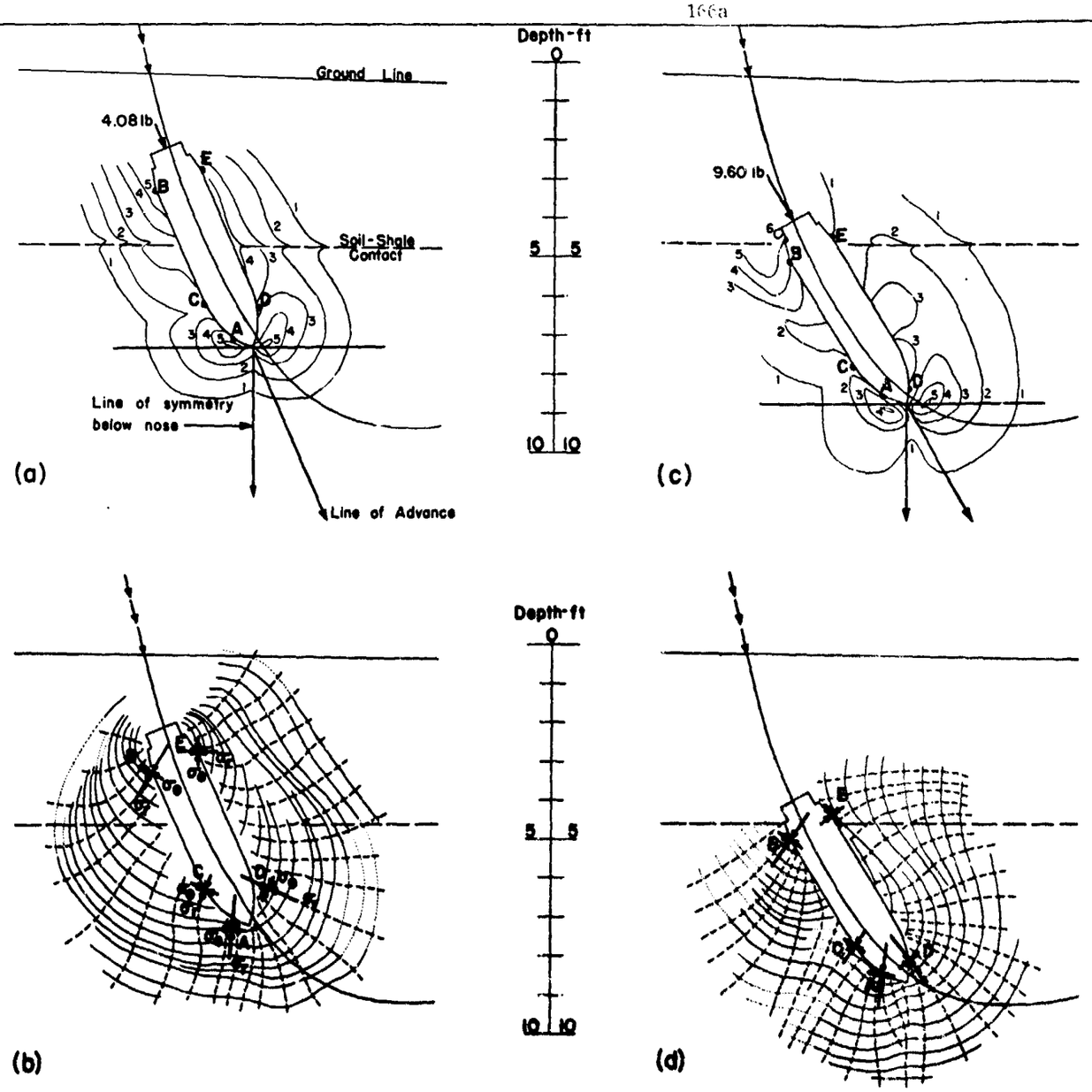
Depth-ft
Ground Line
4.08 lb.
Soil-Shale Contact
Line of symmetry below nose
Line of Advance
(a)
9.60 lb.
(c)
(b)
(d)

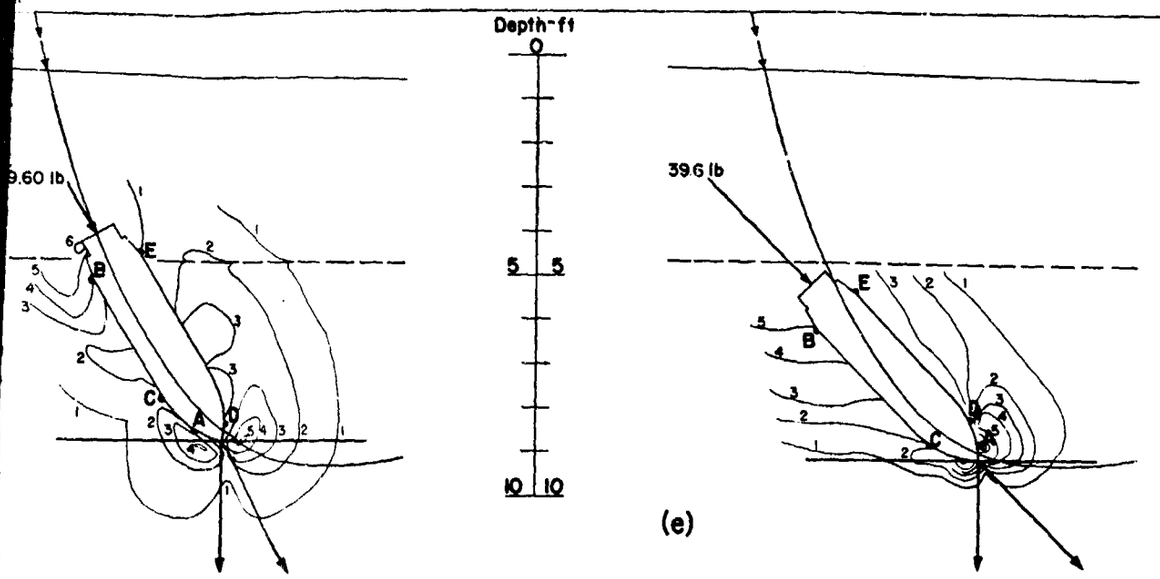

(e)

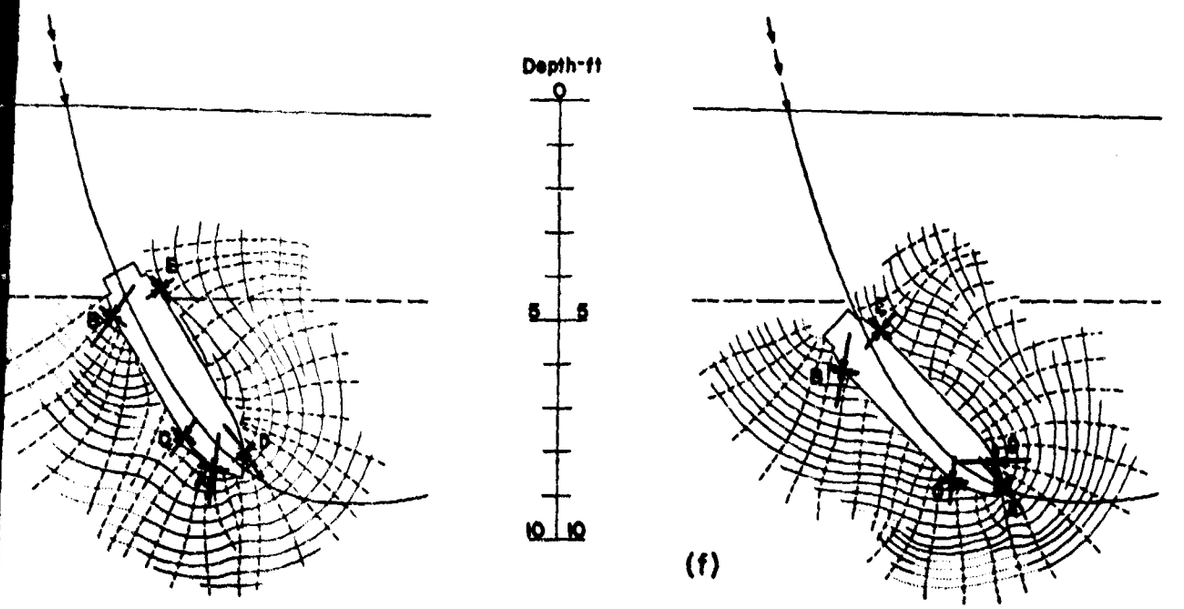

(f)

-BOMB PENETRATION PROJECT- C S M RESEARCH FOUNDATION, INC.	
Scale ——— Date 4-3-61 Fig. No. 169 By L.S.C.	SHEAR CONTOURS & STRESS TRAJECTORIES IN THE MEDIUM 1600 AP BOMB

Fig. 169

2

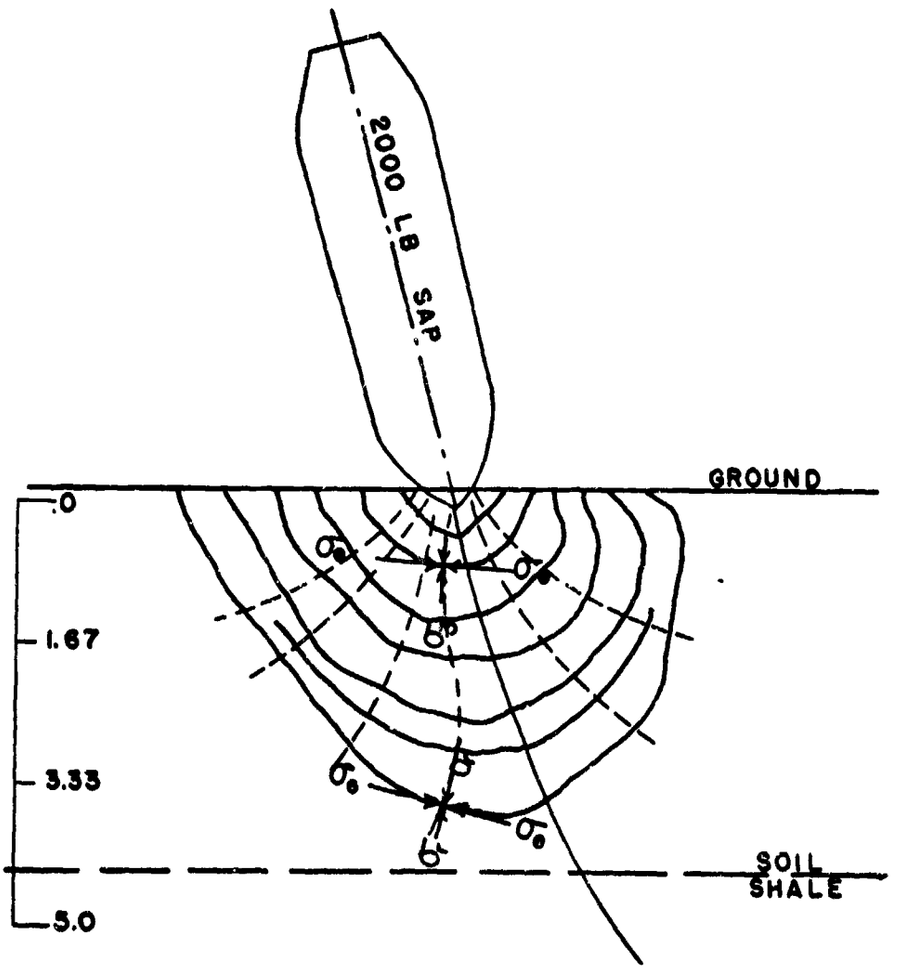

BOMB PENETRATION PROJECT CSM RESEARCH	
Scale 5" = 5' Date 3/30/51 Fig. No 170 By FS	STRESS TRAJECTORIES AT NOSE 2000 lb SAP BOMB

FIG. 170

the distance from the nose increases. The departure is due to the weight of the gelatin, and the effect is comparable with the effect to be expected in a rock mass at depth due to the superincumbent rock load.

Referring to Fig. 169, tangents to the dashed lines are parallel to σ_r and tangents to the solid lines are parallel to σ_θ. At point A, near the nose, and point B, near the tail on the footwall side of the bomb, the fringe order is known to be maximum, and the normal stress, σ_r, at these points is known to be compression. The normal stress in a tangential direction, σ_θ, is also thought to be compressive, but the mathematical and photoelastic analysis is incomplete. At point C, σ_r is thought to be a minimum because the fringe order at that point adjacent to the bomb is minimum. At point D the fringe order is known to be minimum on the hanging-wall sdie, and both σ_r and σ_θ are thought to be compressive. At point E it is known that the fringe order is less than at point B.

The evidence, although incomplete, indicates 1) that the forward thrust along the line of action is combined with a tendency to rotate due to the greater resistance of the medium at depth than near surface, and 2) that somewhere near point C, where the fringe order on the footwall side is minimum, the turning moment is least. Stress relief at the nose is maximum at point D, and stress relief at the tail is maximum at point E. The region on the hanging-wall side of the bomb between E and D may be thought of as a region of minimum compression or maximum tension. As observed in Fig. 168, the maximum surface bulge occurs on the hanging-wall side of the bomb.

The solid lines, or the σ_θ stress trajectories, may be thought of as "flow lines." The displacement on adjacent sides of any flow line increases in the same direction that the fringe order increases. In the region where the σ_θ stress trajectories are dotted, the displacement is so weak that the isoclinics could not be recorded. In the region beyond fringe order 1, the shear stress is so weak that the shear contours cannot be recorded. Thus, the area in Fig. 169d covered by the stress trajectories is a measure of the disturbed area in the medium. The disturbed area remains nearly constant and seems to be a function of the volume of the bomb rather than of the depth of penetration.

In order to increase the depth of penetration of the model 1600 AP bomb in the gelatin, the load on the lever arm of the loading frame was increased. Equilibrium was attained after the movement of the bomb had stopped. The new point of equilibrium was designated point 2. The force on the rear of the bomb at point 2 acting parallel to the line of action was 9.60 pounds; the scale vertical depth of penetration was 8.8 feet; and the scale inclined penetration was 9.6 feet. The shear contours for point 2 are shown in Fig. 169b, and the stress trajectories for point 2 are shown in Fig. 169c.

At point 2 it may be observed that the shear contours extend further into the hanging-wall than the footwall, and that the line of symmetry of the fringe pattern below the tip of the nose corresponds neither with the line of action nor with a vertical line through the nose. In the hanging-wall the ratio between the horizontal distance from the nose to fringe 1 and the maximum vertical distance below the nose to fringe 1 is the same as for point 1, i.e., 2 to 1.

The difference in fringe orders between the hanging-wall side (fringe order 1) and the footwall side (fringe order 6) of the bomb has greatly increased compared to point 1. The maximum fringe order occurs at the base plate rather than at the nose. Points A, B ,C, D, and E of point 2 correspond respectively to points A, B, C, D, and E of point 1.

At point 3, equilibrium was obtained with a force along the line of action of 39.6 pounds, at a vertical depth of penetration of 9.2 feet, and at an inclined penetration of 10.0 feet. The maximum fringe order is 8 and occurs on the hanging-wall rather than the footwall side of the nose tip. The fringe difference between the hanging-wall side at the tail of the bomb is less than for point 2, and the tendency of the bomb to rotate is much less.

SECTION VI—PHOTOELASTIC STUDIES OF THE STRESS DISTRIBUTION IN THE BOMB

By M. J. Pandya and Carl N. Zangar

1—Introduction

A preliminary study of the stress distribution at the nose and near the juncture of the nose and the cylindrical portion of the bomb body was made in which two-dimensional techniques of photoelasticity were employed. It is apparent from this preliminary study that additional work must be done and that new apparatus and techniques must be developed. However, the preliminary work indicates that each of the four types of bombs dropped in the Bomb Penetration Project can be improved in some manner.

As a result of the study of the stress distribution in the medium it has been shown that the forward thrust of the bomb is combined with a torque caused by the increased resistance of the medium at depth. It has been shown also that the maximum shear stress in the medium at the footwall side to the rear of the bomb is as great as the maximum shear stress in the medium at the nose. In the type of loading employed in this preliminary study it was possible to investigate only the stress distribution in the forward part of the bomb at impact and zero penetration. However, this work can be used as a basis of future work.

At first, the model bombs were loaded statically, with the nose of the bomb in contact with the bottom of the loading frame, the axis of the bomb vertical, and a static load applied to the bomb base plate. The model bomb represented a vertical longitudinal slice along the axis of the bomb. This method resulted in excessive bending in the center of the cylindrical portion of the bomb body, and was modified by leaving a solid center area with a hole at the center of gravity of the bomb and hollow forward and rear areas. In this method the bomb was loaded statically at its center of gravity. Stresses at the rear of the bomb body were ignored.

The stress concentration in the forward end of the model general-purpose bombs is in agreement with the observed manner of failure of the 2000 GP bombs in the field. It seems reasonable to believe that the points of weakness in the nose of the 2000 SAP and the 2000 GP bombs can be inferred from the shear contours as determined photoelastically in the model bombs, and that the relative strengths of the four types of bombs dropped during the field tests can be inferred also by the same means. The fracture near the base plate of 25,000 SAP Bomb 19 is due to stress concentration near sharp corners of the base plate and to the resistance to vertical and lateral deviation from the line of action.

2—Maximum Shear Stress Distribution in the Nose of a 1600 AP Bomb

Figure 171 shows the shear stress distribution in the nose and in the walls at the juncture with the nose of a 1600 AP model bomb constructed of allite to scale 1 to 10. The figure shows the growth of fringes as the load

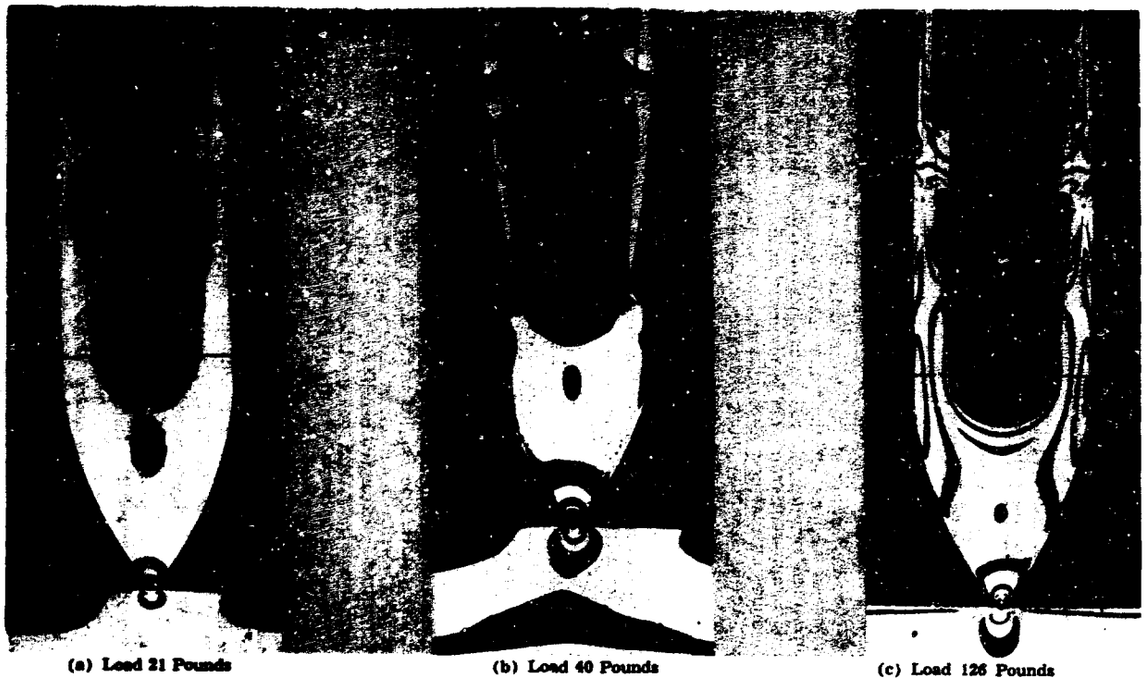

(a) Load 21 Pounds (b) Load 40 Pounds (c) Load 126 Pounds

Fig. 171
Maximum Shear Stress Distribution in the Nose of a 1600 AP Bomb

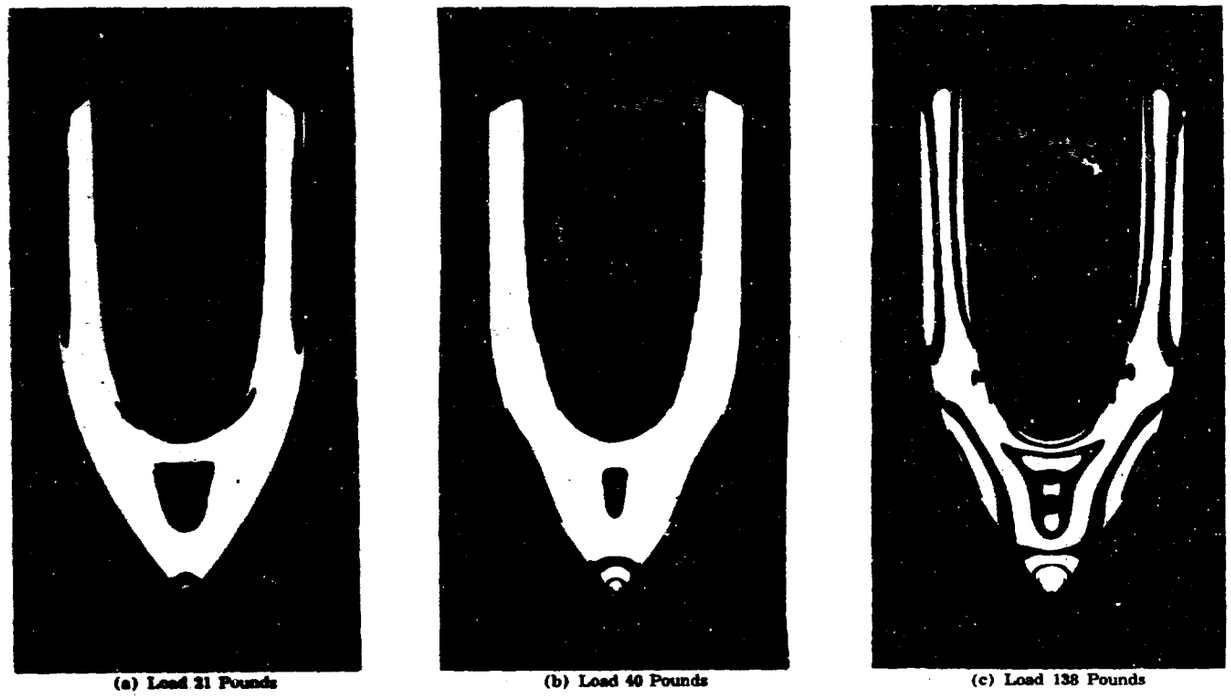

(a) Load 21 Pounds (b) Load 40 Pounds (c) Load 138 Pounds

Fig. 172

Maximum Shear Stress Distribution in the Nose of a 25,000 SAP Bomb

is increased successively from 21.33 pounds, to 40.29 pounds, to 125.61 pounds. The neutral area (fringe order 0) between the tip of the nose and the forward end of the explosive cavity decreases in size as the load increases and then essentially disappears, (Fig. 171c). The nose tip is in compression and the forward semicircular portion of the explosive cavity is in tension. Both the tensile and compressive stresses increase as the load is increased, but the fringe order adjacent to the nose tip is always greater than the fringe order at the semicircular portion of the explosives cavity. The model fringe value is 180 pounds per square inch in shear and 360 pounds per square inch in tension or compression.

3—Maximum Shear Stress Distribution in the Nose of a 25,000 SAP Bomb

Figure 172 shows the shear stress distribution in the nose and walls of a 25,000 SAP bomb, scale 1 to 20. In Fig. 172a the load is 21.33 pounds, in Fig. 172b the load is 40.29 pounds, and in Fig. 172c the load is 137.46 pounds. Because of the scale difference, the fringe orders cannot be directly compared with those in the 1600 AP bomb at the same load.

As the load increases, the neutral zone in the nose diminishes in size. In Fig. 172a, the fringe order at the nose of the bomb is 1, and the nose is in compression. The semicircular portion of the explosive cavity is in tension and the fringe order is ½. Between the nose (fringe order 1) and the neutral area (fringe order 0) the white band represents fringe order ½. Most of the inside surface of the bomb behind the forward semicircular portion lies within the white band and is in compression. In Fig. 172b, fringe order 1 at the nose is in compression, and fringe order 1 along the inside wall of the bomb is in tension. Fringe order ½ (compression) envelopes the neutral area and swings from the inside boundary to the outside boundary at the juncture of the curved portion of the nose with the cylindrical portion of the bomb. In Fig. 172c the neutral area at the center of the nose has decreased in size, the outside of the nose is in high compression, and the inside in tension. The compressive fringe order at the tip of the nose is much greater than the tensile fringe of 3 at the inside surface. Both the inside and the outside of the cylindrical portion of the bomb body are in compression. The fringe order on the inside is 2½, whereas the fringe order on the outside surface is 1½. Maximum bending occurs slightly forward of the juncture of the cylindrical portion of the bomb body with the nose where the white band, fringe order 1½, broadens.

4—Maximum Shear Stress Distribution in the Nose of a 2000 SAP Bomb

Figures 173a and 173b show the maximum shear stress distribution in the nose of a 2000 SAP bomb for loads of 21.33 pounds and 40.29 pounds. The nose tip is in compression and the forward semicircular inside portion of the nose is in tension. The neutral area between the nose tip and the explosives cavity diminishes in size as the load is increased. Greater bending occurs much closer to the nose tip than in either the 25,000 SAP or 1600 AP bombs, and the place of maximum bending is at a section approximately four caliber from the vertical axis of the bomb. Toward the rear of the bomb from the point of maximum bending, the inside wall is in compression and the outside wall is in tension. The point of maximum bending remains fixed as the load is increased. The maximum compressive stress concentration occurs at the tip of the nose and in the section of the nose just forward of the juncture of the nose and the

(a) Load 21 Pounds (b) Load 40 Pounds

Fig. 173

Maximum Shear Stress Distribution in the Nose of a 2000 SAP Bomb

bomb body. Here the maximum fringe order at 40.29 pounds load is 4½ at the inside surface of the bomb and 1½ at the outside surface of the bomb. The region of high stress concentrates is a region of weakness.

From the stress distribution in the nose of the 2000 SAP bomb it may be deduced that the manner of failure of the 2000 SAP bomb would be somewhat similar to that observed in the field for 2000 GP bombs if the striking velocity could be increased or if the resistance of the target to penetration could be increased beyond that in sandstone and granite. The 1600 AP bomb is capable of withstanding nearly four times as much load as a 2000 SAP bomb. The point of rupture of the 1600 AP bomb would be farther from the nose than for the 2000 SAP bomb.

5—Maximum Shear Stress Distribution in the Nose of a 2000 GP Bomb

Figure 174 shows the maximum shear stress distribution in the nose of a 2000 GP bomb due to a load of 26 pounds applied at the center of

Fig. 174

Maximum Shear Stress Distribution in the Nose of a 2000 GP Bomb. Load 26 Pounds

gravity. The maximum shear stress concentration occurs at the juncture of the nose with the cylindrical portion of the bomb body. The fringes are so close together at the point of maximum stress concentration because of extreme bending of the section that it is difficult to determine the maximum fringe order. It is apparent, however, that the general-purpose bomb is several times weaker than the 2000 SAP or the 1600 AP bombs.

When the manner of failure and the position of initial failure of the 2000 GP bombs as observed in the field are compared with the position of maximum shear stress concentration in the models, it appears that the metal of the 2000 SAP bomb fails in maximum shear. It is also apparent that the two-dimensional techniques of determining the position of maximum shear stress concentration are valid, but perhaps the results are qualitative rather than quantitative.

6—Summary

The several types of bombs dropped during the Bomb Pentration Tests are listed in the order of increasing strength as follows:

1—2000 GP (Weakest)

2—2000 SAP

3—25,000 SAP

4—1600 AP (Strongest)

The great strength of the 1600 AP bomb is due to its sharp nose and the thickness of metal between the tip of the nose and the inside of the bomb cavity. Tensile stresses in the cylindrical portion of the bomb body do not exist. The metal thickness in the walls of the cylindrical portion of the bomb body progressively decreases from the forward end toward the rear end. The design of the bomb most closely meets the strength requirements for penetration of rocks, but it is likely that minor modifications can be made to improve both the nose and tail end of the bomb. The tail modification would apply primarily for bombs intended to penetrate great thicknesses of rock, rather than bombs intended to penetrate armor.

The 25,000 SAP bomb is well designed, but the metal distribution in the 1600 AP bomb appears to be superior. It is also possible that the design of the region near the base plate of the 25,000 SAP bomb may be somewhat improved.

It seems reasonable to believe that the shape of the nose of the 2000 SAP bomb can be improved to reduce the stress concentration near the juncture of the curved portion of the nose and the cylindrical portion of the bomb body, and that this change can be made without substantially changing the charge-to-weight ratio.

A greater improvement may be possible in the design of the 2000 GP bombs than in any other type of bomb. The object of the design change would not be to improve the penetration characteristics of the bomb, but would be to minimize low-order detonation associated with casing failure. It seems reasonable to believe that the design change might also improve the accuracy of bombing.

PART F—ANALYSIS AND CONCLUSIONS

SECTION I—A THEORY OF PENETRATION OF PROJECTILES IN ROCK

1—Introduction

The penetration of projectiles in rocks occurs as a result of rock failure. Penetration begins when rock failure begins. Penetration ceases when rock failure ceases. Failure depends upon the magnitude, direction, and position of the applied force; upon the stress distribution in the medium; and upon the physical, elastic, and geologic properties of the rock. Rocks are not homogeneous isotropic substances, and therefore the theoretical attitude of planes of failure is influenced by the attitude of existing geologic planes of weakness. The factors influencing penetration are many, and the problem of penetration in rocks is several times more complex than the problem of penetration in concrete and in soils.

A theory of penetration is desirable if we are to progress beyond the present controversial empirical stage. The theory involves fundamentals of rock failure, a subject that is broad in scope and one in which further fundamental research is necessary. Recognizing the skeletal status of fundamental research in this field, it seems most likely that the theory as presented here will be improved as fundamental research continues. However, it seems that the theory as presented here should aid in the design and selection of bombs to reduce enemy fortifications, and in the design of fortifications to resist enemy bombs. The theory has been derived as a result of the combined analyses of the field results, the laboratory results, the mathematical and photoelastic results, and the physical and elastic properties of the rock. The penetration formula presented in Section II of the analysis summarizes the theory.

2—Rock Failure at Impact

The penetration of a bomb occurs as a result of rock failure. Rock failure does not occur as a result of the penetration of a bomb. Rock failure takes several forms, depending upon a variety of factors. At impact, failure is either by plastic flow or by crushing and fragmentation. The limits of the zone of failure depend upon the kinetic energy of the bomb, the shape of the nose, the diameter of the bomb, and the physical and elastic properties of the rock.

2a) Effect of Kinetic Energy

As the kinetic energy at impact of the bomb with the medium increases, the volume of rock stressed beyond a given value also increases. It has been shown in the mathematical analysis (see pp. 137 to 150) that the volume of rock stressed beyond a given value varies as the ratio of the square roots of the static loads. Thus as the kinetic energy increases, the zone of crushing and fragmentation increases. For a given type of bomb dropped on a given type of rock, the amount of fine material is a measure of the proportion of the rock that has failed by crushing. In the photograph, Fig. 175, the fragmentation of Zuni granite resulting from the release of a 2000 SAP bomb at 9200 feet (Fig. 175a) is compared with the

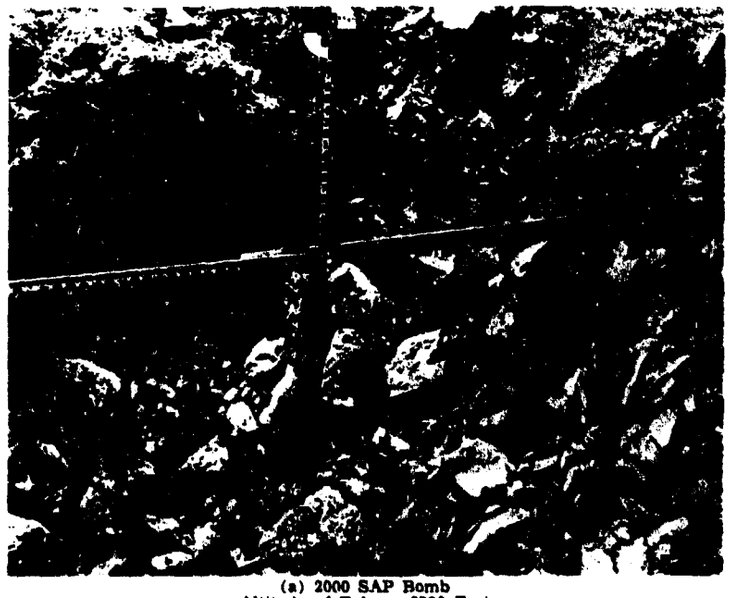

(a) 2000 SAP Bomb
Altitude of Release 9200 Feet

(b) 2000 SAP BOMB
Altitude of Release 30,000 Feet

Fig. 175
Fragmentation in Granite as Related to Impact Energy

greater fragmentation in the same rock type by the same type of bomb at a release altitude of 30,000 feet (Fig. 175b).

2b) Displacement of the Overburden

When the nose of a bomb enters the overburden or soil cover above a solid rock mass, the soil or overburden is displaced outwardly from the point of impact. This displacement is not concentric about the point of impact, nor is it consistent in direction. Apparently the motion of the soil is similar to that of the main current and eddy currents observed in turbulent flow of liquids. It is apparent from the field evidence that the vertical upward component of the ground shock is considerable.

Figure 32, the crater map of Bomb 17, a 2000 SAP bomb dropped from 30,000 feet, shows the displacement of a cinder grid line on the granite target near the point of impact. The soil thickness at the point of impact is 0.8 foot. The displaced grid line is in the footwall of the point of impact. The displacement of the soil has been accomplished by slippage of the soil above the soil-granite contact. The rock below the soil-granite contact in the footwall of the bomb, and outside of the true crater, is undisturbed. The gridline, which was originally straight and 3½ feet behind the point of impact, is now curved and displaced laterally to a maximum of 4 feet from its original position. Farther along the grid line, the direction of displacement is reversed. The maximum amount of the displacement in the reverse direction is 1 foot.

2c) Effect of Nose Shape

The maximum shear stress concentration in the medium at the tip of a sharp-nosed bomb such as a 1600 AP bomb (caliber radius head 2.0) or a 25,000 SAP bomb (caliber radius head 1.56) approaches infinity because the load approaches point loading. (See Fig. 163.) Because of the extremely high stress concentration locally at the tip, the rock fails by plastic flow and the shape of the maximum shear contours is distorted from a circular form to the form shown in Fig. 167. The net effect of the sharp nose is to reduce the amount of crushing at impact and to modify the stress distribution in the medium because of plastic failure at the nose-tip.

2d) Effect of Bomb Diameter

As the cross-sectional area or the diameter of bombs striking and penetrating into a rock surface is increased, the volume of rock that is placed under stress is likewise increased. As will be observed by referring to Fig. 168a and Fig. 168b, the stressed rock extends a considerable distance laterally beyond the sides of the bombs. Fringe order 1 in both instances is at a distance approximately equal to the diameter of the bomb beyond the outside of the bomb. Thus, the net effect of increasing the diameter of the bomb is to increase the volume of rock under stress in proportion to the ratio of increase in diameter.

The combined effect of an increase in the diameter of a bomb and a decrease in the sharpness of the nose upon the degree of fragmentation may be observed in Fig. 176. Figure 176a is a photograph of the apparent crater of 2000 SAP Bomb 35 released 8700 feet above the Dakota sandstone target. Figure 176b is a photograph of the apparent crater of 2000 GP Bomb 49 released 8700 feet above the target. It will be observed that the fineness of the muck pile due to impact of the 2000 GP bomb is much greater than

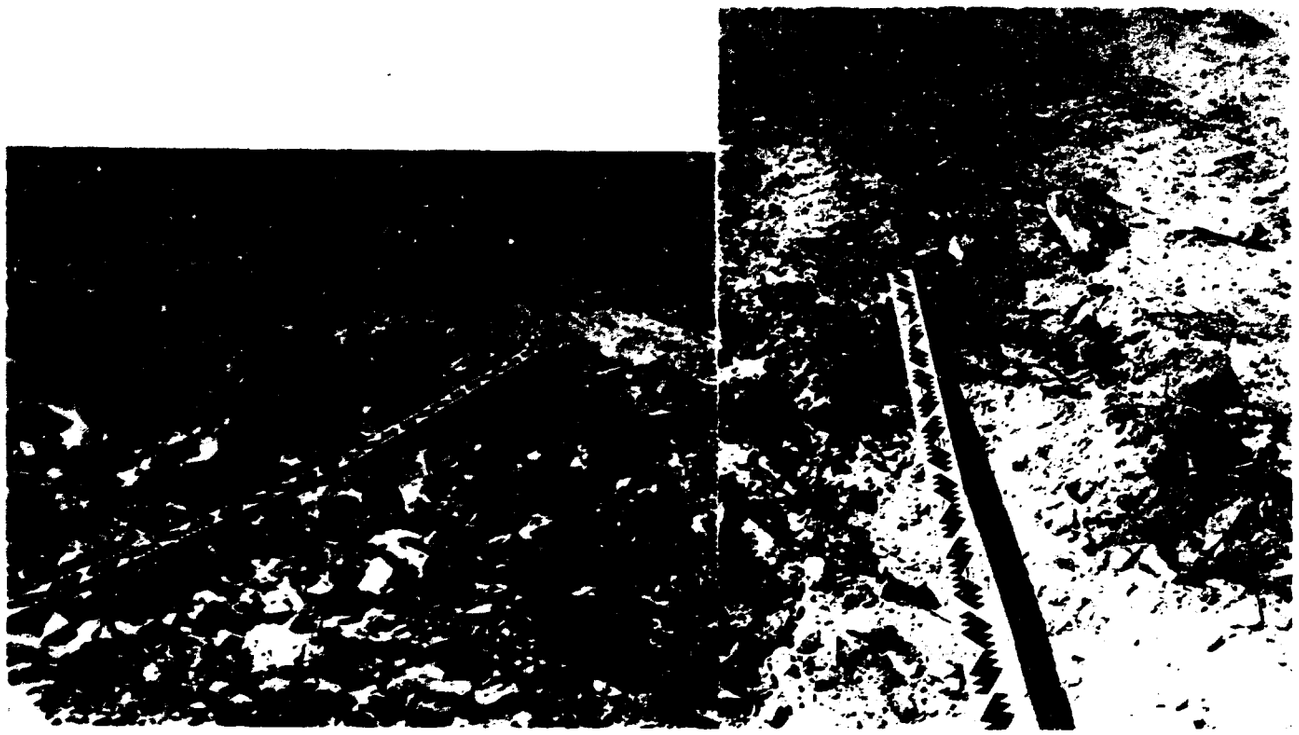

(a) 2000 SAP Bomb
Release Altitude 8700 Feet
Impact Energy 21.82 × 10⁶ Foot-Pounds

(b) 2000 GP Bomb 49
Release Altitude 8700 Feet
Impact Energy 23.15 × 10⁶ Foot-Pounds

Fig. 176
A Comparison of Fragmentation of Dakota Sandstone Relative to Bomb Diameter

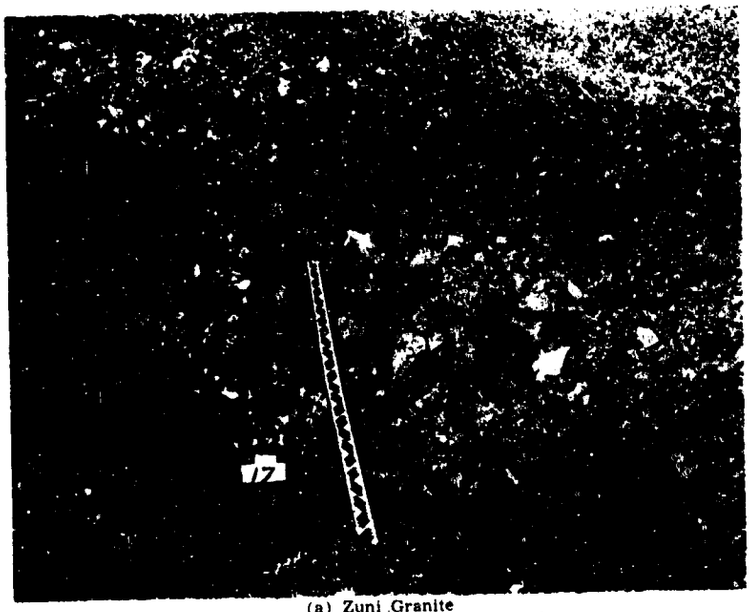

(a) Zuni Granite
Impact Energy 44.42 × 10⁷ Foot-Pounds

(b) Zuni Granite
Impact Energy 43.89 × 10⁷ Foot-Pounds

Fig. 177
The Influence of Rock Type Upon Fragmentation
2000 SAP Bomb; Release Altitude 30,000 Feet

that due to impact of the 2000 SAP bomb. The increased fineness is a measure of the increased resistance to penetration caused by the increase in diameter and by the decrease in sharpness of the nose. A similar effect was observed for bombs striking granite.

2e) Effect of Physical and Elastic Properties of the Rock

The difference in the amount of fine material in sandstone and granite when two bombs of the same type are dropped from the same altitude may be observed in Fig. 177. Figure 177a shows the apparent crater and the fragmentation of Zuni granite produced by 2000 SAP Bomb 17 released 30,000 feet above the target; Fig. 177b shows the apparent crater of 2000 SAP Bomb 30 released at 30,000 feet above the Dakota sandstone. The degree of fragmentation of the sandstone is much less than that of the granite.

The difference in fragmentation is due to the difference in the physical and elastic properties of the rock. The granite has a much greater tensile strength (1905 pounds per square inch compared with 63 pounds per square inch), a much greater compressive strength (24,565 pounds per square inch compared with 5015 pounds per square inch), a much greater impact toughness (54.28 foot-pounds per square inch compared with 24.95 foot-pounds per square inch), and a much greater sclerescope hardness (94.11 compared with 20.74). There can be little doubt that the granite is the stronger rock if the foregoing physical properties of the rock are criteria, but the fact remains that the degree of damage to the granite is much greater than to the sandstone. It is inconsistent to maintain that a "weak" rock will be damaged to a lesser extent than a "strong" rock.

Consider now the results of the triaxial tests and the variation in the so-called "elastic constants" in the higher stress ranges. From the triaxial test data (see pp. 71 to 74) it has been shown that the equation giving the relation of the principal stresses at failure for Dakota sandstone is

$$S_1 = 7110 + 8.68S_2 \qquad (1)$$

and for unweathered Zuni granite is

$$S_1 = 24,360 + 5.6S_2 \qquad (2)$$

where

S_1 = the longitudinal principal stress at failure, pounds per square inch

S_2 = the lateral principal stress at failure, pounds per square inch.

From inspection of the two equations it is apparent that at some stage as the lateral load is increased, the longitudinal principal stress at failure for sandstone will be as great as that for granite. The lateral principal stress can be computed at this stage by solving the two equations simultaneously, and equals

$$S_2 = 5698 \text{ pounds per square inch.}$$

Substituting this value in equation (1) and solving for S_1 we obtain

$$S_1 = 7110 + 8.63 \times 5693$$

$$S_1 = 56{,}240 \text{ pounds per square inch.}$$

If the lateral stress S_3 becomes greater than 5693 pounds per square inch for any given bomb load, the sandstone can withstand a greater axial load than the granite. Below a value of 5693 pounds per square inch for the lateral stress, laboratory tests show that the granite is stronger than the sandstone.

The reason for the increased strength of the sandstone compared to the granite is the difference in the elastic properties of the two rocks. As the strength of the rocks increases with increasing load, the fragmentation decreases and the resistance to penetration increases.

The evidence relative to variation in fragmentation of the rock upon impact of an inert bomb, as presented in preceding pages, is summarized as follows:

1) For a given type of bomb dropped on a given type of rock the amount of fine material increases with the impact energy of the bomb.

2) For a given type of rock and a given impact energy the amount of fine material decreases as the sharpness of the nose increases, but increases as the cross-sectional area of the bomb increases.

3) For a given type of bomb dropped from a given altitude with a given kinetic energy, the amount of fine material depends upon the elastic properties of the rock and upon the stress range rather than upon the compressive strength as determined by a simple compression test.

3—Crushing Failure as Related to Depth

Two factors combine to cause the zone of crushing failure to diminish with increased depth of penetration. First, the kinetic energy of the bomb decreases as work is expended upon the medium. Second, the strength of the medium increases with depth because of increased lateral confinement. The effect of the second factor—increased strength of the medium with depth—is illustrated in Fig. 178. In the figure, three successive stages of penetration of a model 2000 SAP bomb along a prototype path in gelatin model material are shown. The mottled, black and grey area adjacent to the bomb corresponds to the zone of crushing failure, and is a result of failure of the model material. Beyond the mottled area, the material behaves in accordance with the stress-optic law. In Fig. 178a the nose of the bomb is buried, the depth of penetration is less than one-half the length of the model bomb, and the zone of crushing failure is largest. In Fig. 178b, the depth of penetration equals the length of the bomb, and the zone of crushing failure at the nose of the bomb has diminished considerably. In Fig. 178c, the depth of penetration equals one and three-

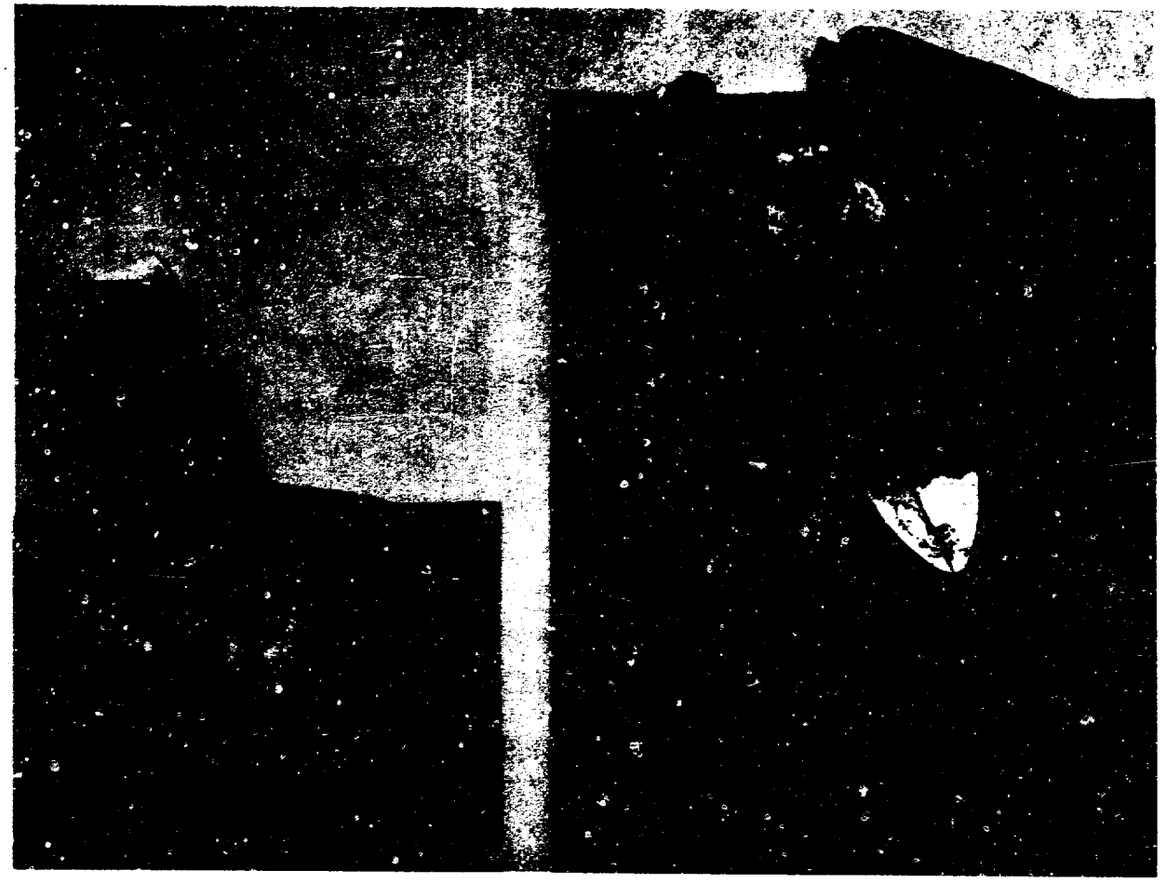

(a) Penetration ½ *l* (b) Penetration 1 *l*

Fig. 178
Crushing Failure as Related to Depth

(c) Penetration 1¾]

Fig. 178
Crushing Failure as Related to Depth

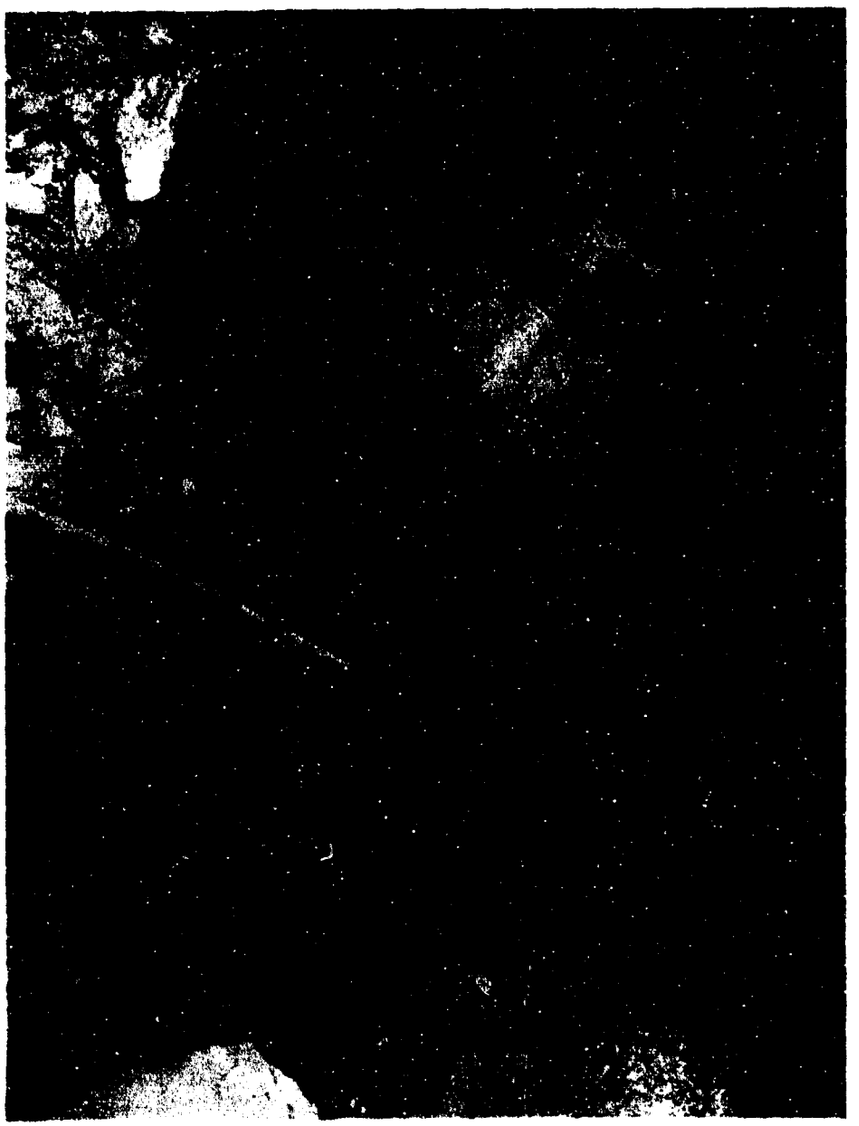

Fig. 179

Crushed Zone in Footwall of 2000 SAP Bomb 11
Altitude of Release, 9200 Feet
Target, Zuni Granite

fourths times the length of the bomb, and the zone of crushing failure at the nose of the bomb has diminished so that it is barely visible.

In the discussion of the stress distribution in the medium, (see pp. 155 to 168) it was pointed out that compression was maximum in the region adjacent to the nose and in the region at the tail of the footwall side of the bomb. The photograph, Fig. 179, shows the zone of crushing in the footwall of Bomb 11, a 2000 SAP bomb released 9200 feet above the granite target. The thickness of the crushed zone in the footwall of the bomb at the position of the 6-foot rule is 0.4 foot.

Figure 180 shows the mold of the nose of 25,000 SAP Bomb 19 in the Zuni granite. The thickness and distribution of the crushed rock is apparent from the dark zone in the photograph. At the extreme tip of the nose, the crushed zone is less than 1 inch thick.

The laboratory evidence and the field evidence substantiate each other and support the theory that the strength of the rock and the resistance to penetration increase with depth.

Fig. 180

Crushed Zone at Nose of 25,000 SAP Bomb 19
Altitude of Release, 18,000 Feet
Target, Zuni Granite

4—Failure in Combined Shear and Tension

Failure of a rock mass due to the penetration of a bomb is characterized by three separate zones of failure. These three zones will be referred to as the "zone of crushing," the "zone of shearing," and the "zone of tension slabbing." In general, the zone of crushing lies nearest to the bomb, the zone of shearing begins at the zone of crushing and extends outwardly to the zone of tension slabbing, and the zone of tension slabbing extends to the surface. Rock failure proceeds concurrently with the advance of the bomb. The tip of the nose of the bomb marks the limit of rock failure in depth.

The "scabbing limit," as described in connection with penetration of projectiles into reinforced concrete slabs, is directly related to the zone of tension slabbing. The distance between the nose of the bomb and the rear face of the concrete slab where scabbing begins is perhaps equal to the critical depth as defined in the Report of the Colorado School of Mines[1] in connection with effect of explosive blasts upon rock. Similarly, the distance from the tip of the bomb to the extreme limits of the uplift area surrounding the visible crater of a bomb is related to the critical distance.

The resistance to rock failure and hence the resistance to penetration increases with depth. At some point a manner of rock failure begins that is referred to as "tunneling." The point at which tunneling begins marks the limit at which plastic flow predominates over failure of the type described in detail in the following pages. Tunneling is beyond the scope of this investigation, for the region in which tunneling is most apt to predominate is the field of extremely-high-altitude bombing, using very large bombs. From the field evidence it appears that tunneling of a 25,000 SAP bomb in granite begins at a release altitude above 18,000 feet and below 26,000 feet. Perhaps the point at which tunneling begins is a function of the elastic properties of the rock, the kinetic energy of the bomb, and the shape of the bomb.

4a) Characteristics of the Zone of Shearing

The term "zone of shearing" is used here to designate a zone in which fragmentation is less intense than in the crushed zone, but more intense than in the zone of tension slabbing. The term is not used in the sense that the rock within the zone fails in pure shear. On the contrary, we find little evidence to indicate that the criterion of failure is any different in the zone of shearing than in the zone of tension slabbing. Failure is dependent upon the stress distribution in the medium. In the zone of shearing the stress distribution is influenced to a greater degree by the position of the bomb than by the position of the surface. The zone of shearing is characterized by two stages of failure: one stage in which the rock fails because of the energy transmitted from the bomb to the medium; the other stage in which the energy imparted to the medium causes the rock to burst into the cavity behind the bomb as in a rock burst in a deep mine. The energy with which the cavity fails causes rock to be carried upward into the upsurge area (see Fig. 88, also p: 84) and in some instances on

[1] Report of the Colorado School of Mines, Series I and Series II Experiments, Underground Explosion Test Program, Footnote, p. 5.

into the atmosphere. The energy also forces rock from the zone of crushing and rock from the first stage of "shearing" failure into fractures described in following paragraphs as being within the zone of tension slabbing.

The first stage of shearing failure is illustrated in the photograph, Fig. 181. In the photograph, the horizontal level rod is parallel with the line of flight. The stake and the other level rod are vertical. The band of finely broken rock which extends diagonally across the photograph and intersects the vertical level rod at 2 feet lies in a warped surface containing the axis of the bomb and marking the path of the bomb through the rock. The fractures in the rock above the path zone terminate at the path zone.

The limits of the zone of shear are arch-shaped in cross sections in three directions. If the attitude of the planes of failure in the rock is

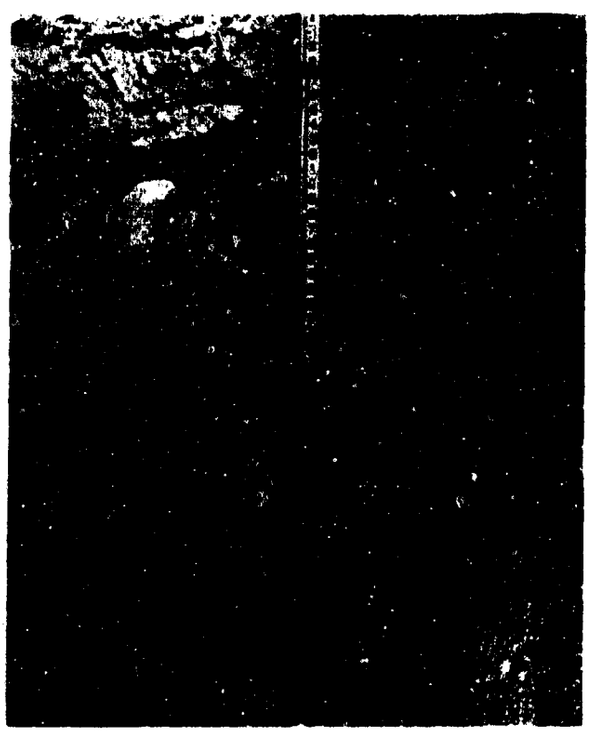

Fig. 181

Rock Failure Within the "Zone of Shearing"
Stage 1—Path Cracks

compared with stress trajectories in the medium as illustrated in Fig. 169, it is apparent that the solid lines representing the σ_θ stress trajectories which intersect the hangingwall of the bomb (see Fig. 169b, d, and f) determine the attitude of one system of the planes of failure. The shear zone viewed in a vertical plane containing the bomb path terminates at a distance measured normal to the bomb and equal to the diameter of the bomb. The shear zone does not progress into the footwall below the bomb. The three principal directions coincide with the σ_r direction, the σ_θ direction, and a direction at right angles to these two. In the three-dimensional case, the σ_r and σ_θ directions develop an interlocking system of natural arches; and the third principal direction coincides with any one of a series of radial fractures which radiate as planes about the axis of the bomb.

Natural planes of weakness such as joints, faults, and bedding planes are present in most rocks. The attitudes of the pre-existing planes of

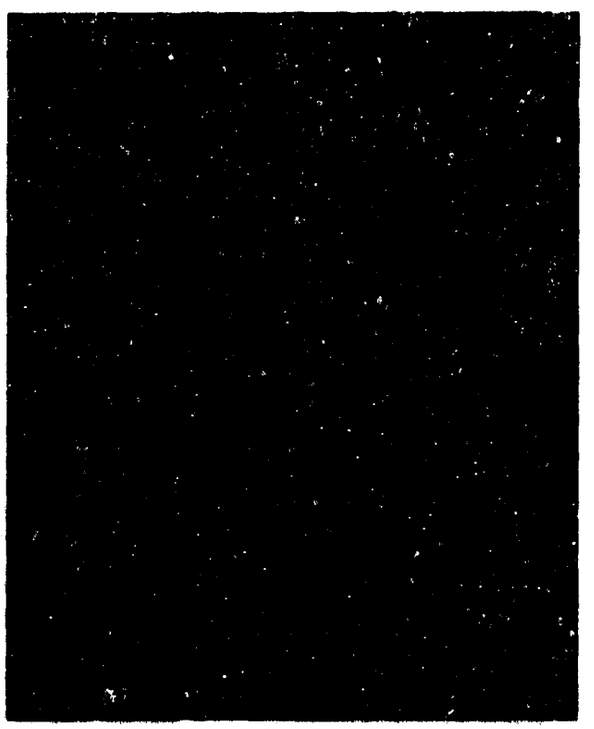

Fig. 162

Rock Failure Within the "Zone of Shearing"
Stage 2—Rock Burst and Release of Strain Energy

weakness influence the attitudes of the planes of failure which accompany and permit the penetration of a bomb into rock. However, in the absence of pre-existing planes of weakness, the attitudes of the planes of failure resulting from the first stage of shearing failure coincide with the principal directions.

The second stage of shearing failure is illustrated in the photograph, Fig. 182. This second stage is referred to here as the "rock-burst" stage. The view in the photograph is looking toward the footwall of the crater of Bomb 17 in a direction opposite to the line of flight. What at first glance appears to be a boulder is in reality evidence of the failure of a uniform-textured granite in the footwall of the bomb path. The explanation offered here is that the energy imparted to the rock by the impact of the bomb is released from the rock with explosive violence after the bomb has passed. The strain-energy stored momentarily in the rock is released into the cavity behind the bomb. Small individual pieces of rock from the footwall region appear to have disintegrated from a central nucleus.

This observed feature has a bearing upon fundamentals of rock failure and of rock bursts, and upon the origin of dusts and the extent of contamination associated with underground atomic bursts.

4b) Characteristics of the Zone of Tension Stabbing

The zone of tension slabbing is characterized by three sets of fractures referred to in the field as "O" cracks, "I" cracks, and "R" cracks. The term "O" crack originated from the first letter of the word "onion," because of the recurrent, more or less concentric, shell-like pattern of the fractures. The term "I" crack originated from the first letter of the word "inward," because of the inward dip of the fractures toward the point of impact. The term "R" crack originated from the first letter of the word "radial," because of the radial strike of the fractures about the point of impact.

Figure 183a is a photograph of the craters of Bomb 8, a 1600 AP bomb released 30,000 feet above the granite target. The stadia rod marks the line of flight, and the photograph was taken from the 6 o'clock position looking toward the hanging-wall of the path of the bomb. Excavation has proceeded to a depth of 5.9 feet, but the rear end of the bomb has not yet been uncovered. The end of a 6-foot rule projects from the flat crack designated in the field as an "O" crack. Figure 183b is another view of the same crater after excavation had proceeded to a greater depth. The view is from the 2 o'clock position, which is nearly at right angles to the line of flight. The recurrent nature and the irregular, jagged surface of the horizontally disposed O cracks are shown. The vertical fractures are referred to as "R" cracks. The R cracks are perpendicular to the O cracks and radiate about the point of impact. The set of cracks referred to as "I" cracks do not show in either photograph. In plan view the I cracks appear as a series of concentric circles. The outer circle defines the limit of the uplift area or the limit of the true crater. The I cracks dip inward toward the point of impact, but the inward dip is due to displacement associated with the surface bulge about the point of impact.

Upon analysis it can be shown that the attitudes of the O cracks, the I cracks, and the R cracks coincide with the three directions of maximum principal stress. The principal stress directions change as the bomb pene-

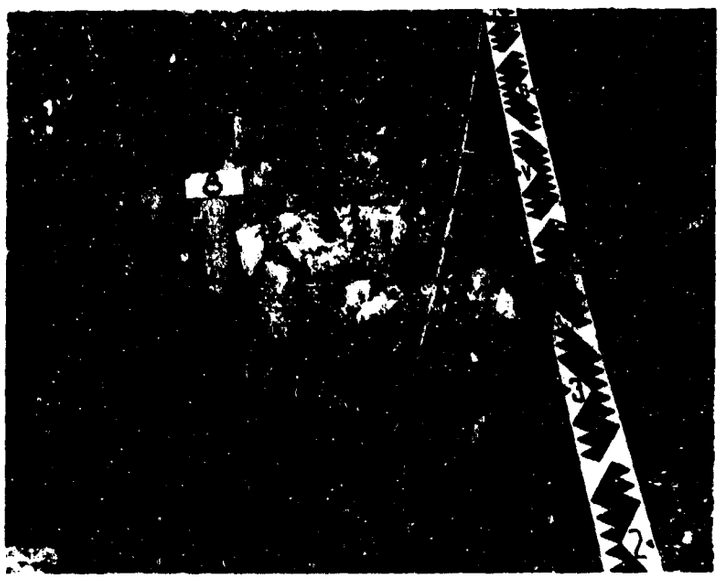

Fig. 183 (a)
Characteristics of the "Zone of Crushing"
"O" Cracks in the Hanging-wall of the Bomb Path

Fig. 183 (b)
Characteristics of the "Zone of Tension Slabbing"

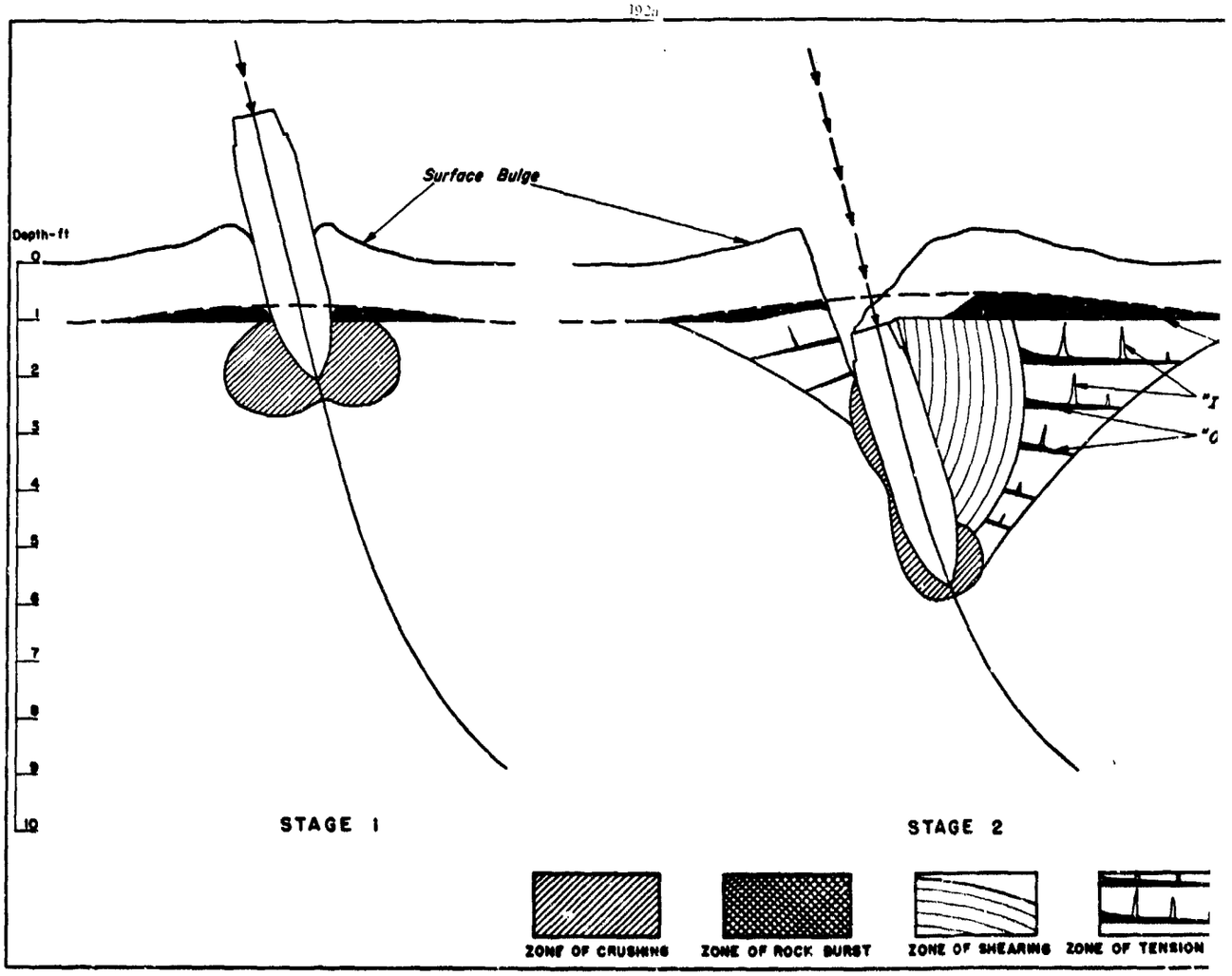
Surface Bulge
Depth-ft
0
1
2
3
4
5
6
7
8
9
10
STAGE 1
STAGE 2
ZONE OF CRUSHING
ZONE OF ROCK BURST
ZONE OF SHEARING
ZONE OF TENSION

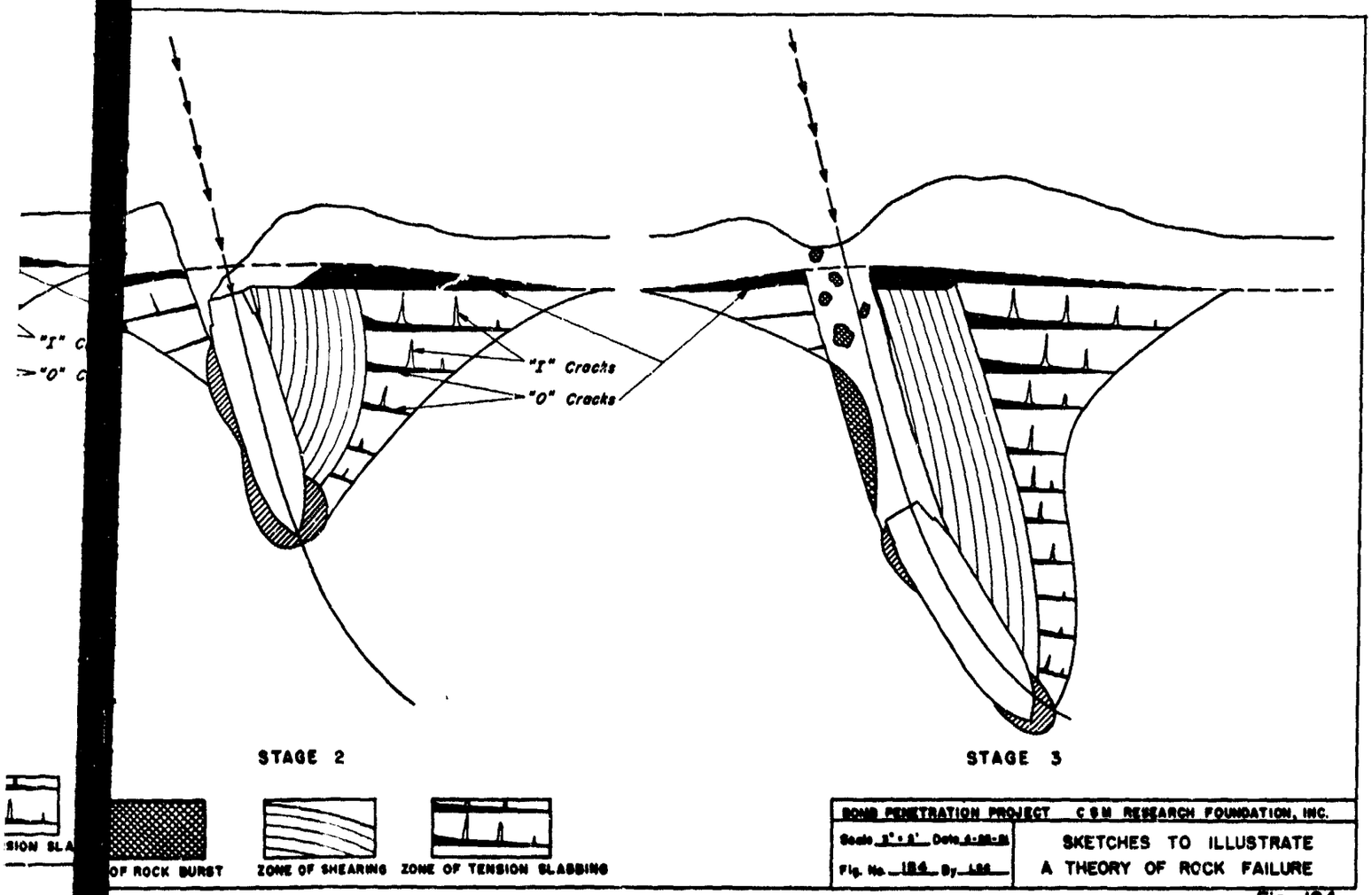
"I" Cracks
"O" Cracks
STAGE 2
STAGE 3
OF ROCK BURST
ZONE OF SHEARING
ZONE OF TENSION SLABBING
BOND PENETRATION PROJECT C & M RESEARCH FOUNDATION, INC.
SKETCHES TO ILLUSTRATE
A THEORY OF ROCK FAILURE

Fig. 184

2

trates deeper into the medium. The attitude of the fractures depends upon the stress distribution at the instant at which the fracture is formed.

5—A Theory of Rock Failure

The sequence of failure and the zones of failure described in preceding paragraphs are illustrated diagrammatically in Fig. 184. In Stage 1, crushing failure predominates. In Stage 2, the zone of crushing is subordinate to the zone of shearing and the zone of tension slabbing. The ratio of the radius of the crater to the depth of the crater (r/d ratio) reaches a maximum. The zone of shearing failure extends into the hangingwall of the bomb path a maximum distance not greatly exceeding the diameter of the bomb. O cracks are a part of the system of fractures within the zone of shearing, but progress beyond the zone of shearing. The I cracks are normal to the O cracks. The displacement accompanying the surface bulge is such that the individual I cracks widen with depth, but the near-surface I cracks are larger than those at successively greater depths. A third system of fractures, referred to as "R" cracks, is present in the zones of shearing and tension slabbing, but these are perpendicular to the other two systems of fractures, and radiate about the axis of the bomb. In Stage 3, the r/d ratio diminishes because of increased resistance to rock failure with increased depth. The decrease in the r/d ratio is accomplished by a reduction in the extent to which the fractures that characterize the zone of tension slabbing extend beyond the zone of shearing. The rock-burst zone is confined principally to the footwall of the bomb path and to the region substantially below the ground surface. The downward advance of the rock-burst zone follows the release of compressive stresses in the medium at the tail of the bomb equal in magnitude to the compressive stresses in the medium at the nose of the bomb.

Criteria of rock failure upon which the theory of penetration is based are as follows:

1—At the instant of impact, the compressive strength of the rock as determined by a single compression test determines the "threshold value" at which penetration begins.

2—As rock failure proceeds, the strength of the rock is increased because of the increase in lateral confinement with depth. The increase in lateral confinement is dependent upon Poisson's ratio of the rock mass. The envelope of rupture, or Mohr's envelope, as determined in a triaxial testing machine, is a measure of the increased strength of the rock.

3—The increase in lateral confinement at any given depth of penetration depends upon the vertical component of force applied at the nose of the bomb in a direction parallel to the axis of the bomb. This vertical component of force results in a vertical stress in an element of the medium equal to P_1, and a corresponding horizontal component of stress, P_3, which

is a measure of the resistance to penetration. The relation between P_3 and P_1 is as follows:

$$P_3 = \frac{m}{1 \quad m} P_1$$

where

P_3 = the stress acting horizontally at the tip of the nose

P_1 = the stress acting vertically at the tip of the nose

m = Poisson's ratio.

4—The attitudes of the planes of failure in the zone of shear and the zone of tension slabbing coincide with the three directions of principal stress at the instant of failure.

5—Plastic failure of the rock occurs particularly at the tip of the nose of sharp-nosed bombs, and in the region of failure referred to here as "the region where tunneling begins." In this region the fundamentals of failure have not been investigated.

SECTION II—THE INFLUENCE OF GEOLOGY AND TOPOGRAPHY UPON PENETRATION

1—The Influence of Soil Cover

A moderately thick cover over granite may have an entirely different effect upon penetration than the same cover over sandstone. Soils containing much clay-size material and much organic matter are apt to accumulate over granitic rocks, whereas sandy soils are more apt to accumulate over sandstone rocks. Chemical agents of weathering are more abundant in the soils formed in place over granite than over sandstone. The thickness of the weathered zone in rock below a soil cover containing abundant agents of weathering increases as the soil thickness increases. Penetration is more easily accomplished in a weathered and party decomposed rock than in an unaltered one. If, as is common at sandstone sites, the soil is relatively free from agents of weathering, then the penetration of a bomb into the rock below the soil cover is more difficult.

It is desirable, therefore, in selecting a site in which openings are to be driven for underground defense, to avoid areas of thick soil cover and areas of deep weathering. A thick cover of windblown sand is less objectionable than a thick cover of soil that has been formed in place. Flat slopes at the portal of the proposed opening are more objectionable than steep slopes, because of both the greater thickness of soil cover and the greater difficulty of excavation.

The question arises as to whether or not the soil cover should be removed or should be left above an underground installation. The cover should not be removed under any circumstances. The soil cover provides protection for the opening against damage; and the greater the thickness of soil above the rock, the less damage to the opening in the rock. The soil cover provides space for the vertical deviation of the bomb, and if the cover is sufficiently thick, the deviation may be such that it is impossible for the bomb to penetrate into the rock.

Perhaps the most important reason for not disturbing the soil cover is to avoid presenting a target for the enemy to aim at. Without a target, the accuracy of bombing cannot be so great as with one. A miss of 100 feet is equivalent to adding more than 100 feet of rock over the roof of the tunnel. Referring to Fig. 18, the spotting map for the sandstone target, it may be observed that the chances of a direct hit such that the bomb penetrates to a point vertically above the center line of an underground tunnel are rather small. Because of the limits of accuracy of bombing, the desirability of excavating underground for protection against airblast and ground shock from the detonation of a bomb increases.

2—The Influence of Joints, Faults, and Bedding Planes

Rocks as they occur in the earth's crust are seldom uniform in composition or in texture. The physical and elastic properties of two specimens from the same drill hole in the same type of rock are seldom identical. The behavior of the two rock masses, in which individual rock specimens

Fig. 186
The Influence of Faulting Upon the Path of a Bomb

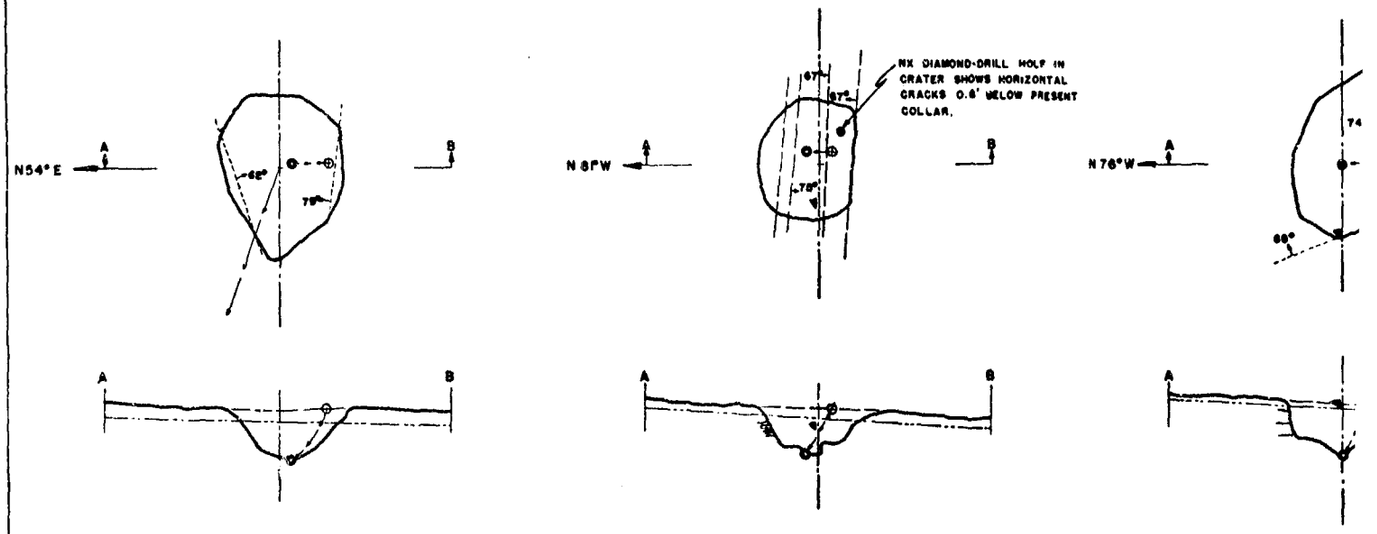

a. Plan and Cross-Section of Crater 16 in Granite

b. Plan and Cross-Section of Crater 33 in Sandstone

c. Plan and Cross Crater 32 in

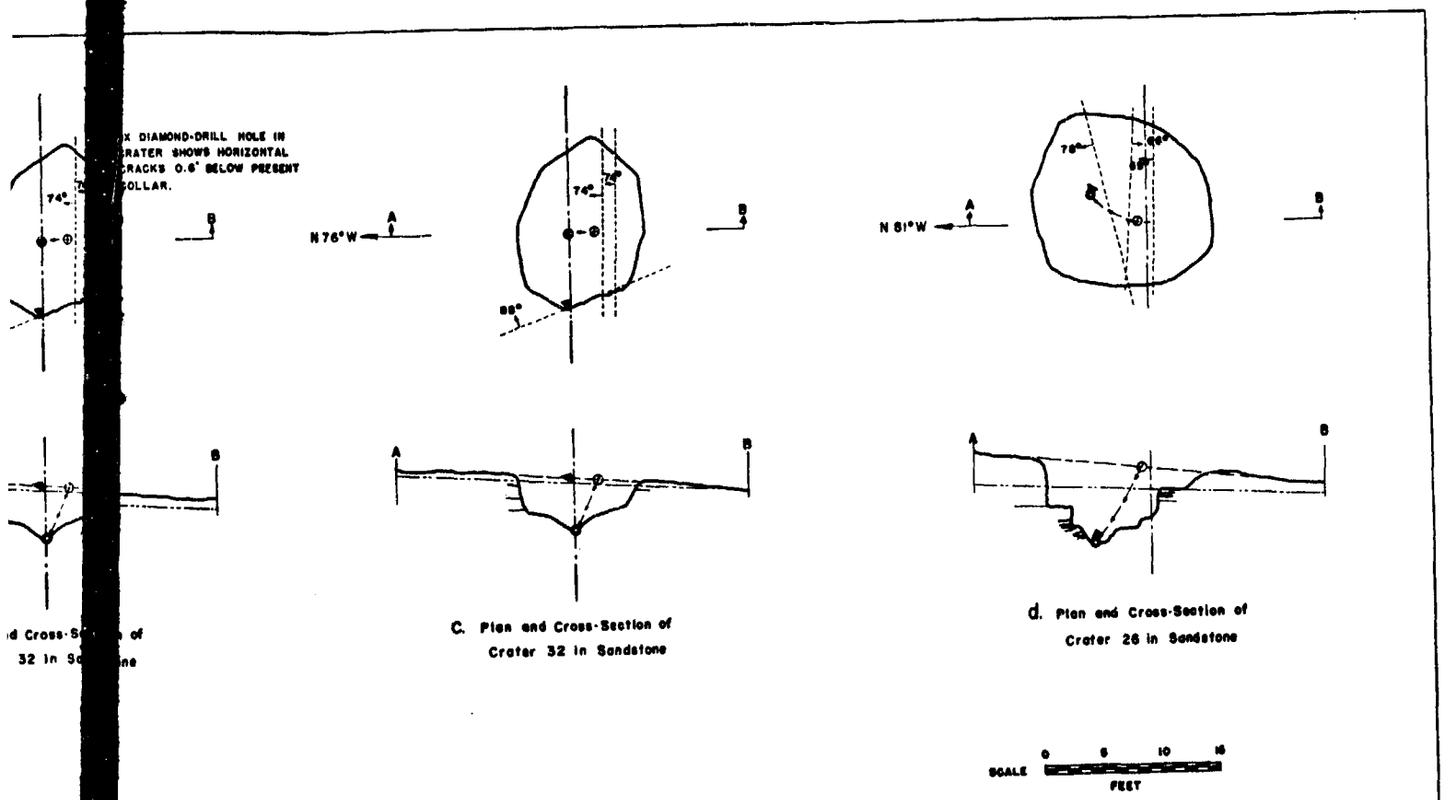

d Cross-S of
32 in S ne

C. Plan and Cross-Section of Crater 32 in Sandstone

d. Plan and Cross-Section of Crater 26 in Sandstone

SCALE 0 5 10 15
FEET

-BOMB PENETRATION PROJECT- C S M RESEARCH FOUNDATION, INC.	
Scale Shown Date 4-28-51 Fig No. 185 By JJK	SKETCHES SHOWING THE EFFECT OF JOINTING UPON CRATER SHAPE AND BOMB PATH

Fig. 185

2

might have identical physical and elastic properties, may differ greatly because of the relative attitude and relative abundance of geologic planes of weakness. The variation in behavior is responsible for the dispersion of the penetration data. The dispersion in a rock such as granite is greater than the dispersion in a rock such as sandstone, because of the greater variation in the geologic properties of the granite.

Geologic planes of weakness such as joints, faults, and bedding planes influence the path of a bomb, and, depending upon their attitude and abundance, may either increase or decrease the depth of penetration. The attitude of the planes of weaknesses relative to the path of the bomb determines the direction of deviation of the bomb.

The effect of joints in the rock upon the path of a bomb depends upon the attitude of each individual joint relative to the line of action of the bomb. Stress is relieved by joints having the same attitude as the theoretical attitude of the planes of failure (see Fig. 184), and a new fracture is not formed. Any joint within the stressed area disturbs the stress distribution in comparison to that in a homogeneous isotropic medium. The presence of joints, faults, bedding planes, or other geologic planes of weakness causes both the shape of the shear contours as presented in the mathematical analysis (see Figs. 148-151) and in the photoelastic analysis (see Figs. 166-169, 171-174), and the shape of the principal stress contours as presented in Figs. 154 and 155 to be modified. Probably the effect of jointing is to relieve stress and to reduce the distance from the point of application of the force to the principal stress contour compared to that in a homogeneous, isotropic medium. Because penetration is the result of rock failure rather than rock failure being the result of penetration, the path of the bomb deviates in the direction of least distortion of the principal stress contours.

The effect of jointing upon the shape of a crater and upon the path of a bomb in rock is illustrated in Fig. 185. The effect of intersecting joints upon the shape of the crater and upon the path of a bomb in granite is illustrated in Fig. 185a, a plan and cross section of crater 16 in granite.

Where, as for Bomb 16 (see Fig. 91) and Bomb 13 (see Fig. 92), the joints dip inwardly toward the point of impact of the bomb, both the bomb and the wedge-shaped mass of rock are likely to be removed before the energy of the bomb has been expended.

Figure 185 b is a plan and cross section of crater 33 in sandstone, which illustrates the effect upon the path of the bomb and upon the shape of the crater of a system of parallel joints which dip steeply towards the point of impact of a bomb and strike at right angles to the line of flight. A similar effect may be observed by referring to the shapes of the craters of Bombs 21, 29, 33, 37, and 47. The craters are elongated in a direction parallel to the strike of the joint system. If the strike of the joints is at right angles to the line of flight, there is little deviation of the bomb from the line of flight in the plan view. The effect of such jointing upon the vertical deviation is to cause the path of the bomb to be steeper than normal.

The photograph, Fig. 186, shows the base plate and enough of the tail of Bomb 7 to indicate the steep dip of the bomb. In this instance the angle

of fall at impact was 72 degrees. The inclination of the axis of the bomb at maximum penetration is 87 degrees. The shape of the path is a compound curve. In the upper part of the path, increased resistance to penetration caused the bomb to flatten until the hanging-wall of the fault zone, visible in the photograph, was reached. The fault acted in the same manner as the jointing of Fig. 185b, to distort the shape of the principal stress contours and to cause the nose of the bomb to be deflected towards the weaker rock.

Figure 185c is a plan and cross section of Crater 32 in sandstone, which illustrates the effect upon the path of the bomb and the shape of the crater of a system of parallel joints which dip in the same direction and at approximately the same angle as the angle of fall. The effect is to minimize the vertical deviation of the bomb and to elongate the crater in a direction parallel to the strike of the joints.

Figure 185d is a plan and cross section of Crater 26 in sandstone, which illustrates the effect upon the path of the bomb and the shape of the crater of a system of steeply dipping joints which strike obliquely to the line of flight. The effect in this particular instance is to cause the bomb to deviate in plan view towards a direction parallel to the strike of the joints.

The net effect of faults and steeply dipping joints is to increase the vertical penetration by reducing the vertical deviation. On the other hand, horizontal and flat-dipping joints, bedding and cross-bedding planes, mud seams, partings, and root-filled cracks reduce the vertical penetration by distributing the load and by increasing the vertical deviation.

The abundance of horizontal planes of weakness in bedded rocks such as the Dakota sandstone is far greater than in igneous rocks such as granite. The photograph of Crater 26, Fig. 187, shows the nature of the bedding planes in Dakota sandstone. Each bedding plane is marked by a mud-filled seam or by the presence of finely crushed rock forced into the cavity from the rock-burst area. In many instances the seams contain an abundance of roots. The effect of the bedding plane is two-fold. First, the mud-filled seam is compacted and the mud or shale fails plastically. The load upon the overlying sandstone at failure is increased by plastic deformation in the bedding planes below, and the load is distributed over a broader area. Second, the natural plane of weakness at the bedding plane functions in the same manner as described for joints to relieve stress. The stress relief disturbs the stress distribution as previously explained, and increases the vertical deviation of the bomb. The photograph, Fig. 188, shows the vertical and the horizontal deviations of 1600 AP Bomb 24 from the line of flight. The bomb was undisturbed during the excavation. The flat inclination of a sharp-nosed bomb such as a 1600 AP bomb at shallow penetration and the flat-bottomed crater are characteristic of craters in the Dakota sandstone.

3—Comparison of the Elastic Properties of Dakota Sandstone and Zuni Granite as Related to Penetration and Path Shape

The photographs, Figs. 189a and 189b, compare the rebound distances of a 1600 AP bomb striking granite and striking sandstone. Figure 189a

Fig. 187
Effect of Bedding in Sandstone Upon Penetration
Stadia Rod Marks the Line of Flight

Fig. 188
Effect of Bedding Upon Vertical Deviation
1000 AP Bomb Undisturbed During Excavation of Crater 24
Stadia Rod Marks the Line of Flight

shows the rebound distance of the nose of Bomb 8 released 30,000 feet above the granite target and striking with an impact energy of 40.14×10^6 foot-pounds. Figure 189b shows much greater rebound distance from the bottom of the crater of Bomb 25 released 9200 feet above the sandstone target and striking with an impact energy of 18.22×10^6 foot-pounds. The greater rebound distance is perhaps due to the much greater strain energy stored in the sandstone than in the granite. The phenomenon cannot be predicted from the results of a simple compression test, nor from the rebound as measured using a Shore scleroscope. Instead, the energy absorbed per unit volume of rock when the rock is stressed to the elastic limit under lateral confinement appears to govern the rebound distance.

The much greater rebound of the bomb in sandstone than in granite, even though the energy of impact is less than half as great, is significant in two respects. First, from the viewpoint of the attack, if the bomb was fused to detonate after rebound, the greater rebound in Dakota sandstone would have the same effect as substantially decreasing the depth of penetration. Second, from the viewpoint of defense, the greater rebound in Dakota sandstone would decrease the coupling factor and thus reduce the efficiency of the explosive blast in producing the ground shock. The degree of damage to an underground opening in the Dakota sandstone would thus be diminished.

If the combined effect of the flat-lying bedding planes and the greater resistance to penetration in Dakota sandstone than in Zuni granite are considered, it is apparent that the path of a bomb designed and released so as to effect substantial penetration in rock would curve much more sharply in Dakota sandstone than in Zuni granite. Thus, the stresses in the medium a tthe tail of the bomb (see pp. 164 to 168 and Fig. 169b) woud be greater in Dakota sandstone than in Zuni granite. Considering this feature from the viewpoint of attack, a bomb striking Dakota sandstone would be much more susceptible to failure at the rear end of the bomb than a bomb striking Zuni granite. Therefore a stronger bomb would be necessary. Considering the same feature from the standpoint of defense, premature rupture of the rear end of the casing would result in reduced penetration and perhaps low-order detonation. Accordingly, the degree of damage to an underground installation in Dakota sandstone would be less than in Zuni granite because of the lower order detonation, greater rebound, and reduced coupling.

The fundamental difference between the Dakota sandstone and the Zuni granite is the increased strength of the Dakota sandstone as the lateral confinement increases. The increased strength is discussed in connection with the results of the triaxial compression tests (see pp. 71 to 74). Furthermore, it has been pointed out in connection with the theory of rock failure (see pp. 193 to 194) that the lateral confinement is a function of Poisson's ratio and of the axially applied stress; also, that the axially applied stress where the sandstone and the granite are of equal strength is 56,240 pounds per square inch (see p. 183). This axial load is beyond the range of the triaxial tests conducted. Accordingly, it is impossible at this time to compare values of Poisson's ratio of sandstone and granite in the region where the sandstone is stronger than the granite.

At the instant of impact of a bomb at the surface of the rock, the

Fig. 189 (a)

Rebound of 1600 AP Bomb in Zuni Granite
Impact Energy: 49.14 × 10^6 Foot-Pounds

Fig. 189 (b)

Rebound of 1600 AP Bomb in Dakota Sandstone
Impact Energy: 18.2 × 10^6 Foot-Pounds

lateral restraint approaches zero and penetration is accomplished by crushing. The axially applied stress causing failure of Dakota sandstone as in a simple compression test is 5,015 pounds per square inch, and the approximate value of Poisson's ratio for Dakota sandstone in this stress range is 0.26 (see Fig. 68). In the same stress range the approximate value of Poisson's ratio for granite is 0.18.

Substituting these values in the equation

$$P_2 = \frac{m}{1-m} P_1$$

where

P_2 = the lateral stress

P_1 = the axial stress, and

m = Poisson's ratio.

For sandstone,

$$P_2 = \left(\frac{0.26}{1.00 - 0.26}\right) P_1 = 0.35\, P_1$$

For granite,

$$P_2 = \left(\frac{0.18}{1.00 - 0.18}\right) P_1 = 0.22\, P_1$$

Thus, the lateral stress in the Dakota sandstone is 1.6 times that in the Zuni granite.

In the stress range where granite fails as in simple compression, the axial stress is 24,565 pounds per square inch. In this stress region the value of Poisson's ratio for the unweathered Zuni granite is 0.22. The stress is beyond the failure stress of Dakota sandstone. The maximum value at the greatest stress range for any specimen of Dakota sandstone is 0.37.

Substituting these maximum values of Poisson's ratio in the equation,

$$P_2 = \left(\frac{m}{1-m}\right) P_1$$

and comparing maximum values of P_2, for sandstone we obtain

$$P_2 = \frac{0.37}{1.00 - 0.37} P_1 = \frac{0.37}{0.63} P_1 = 0.59\, P_1$$

and for granite we obtain

$$P_2 = \frac{0.22}{1.00 - 0.22} P_1 = \frac{0.22}{0.78} P_1 = 0.28\, P_1$$

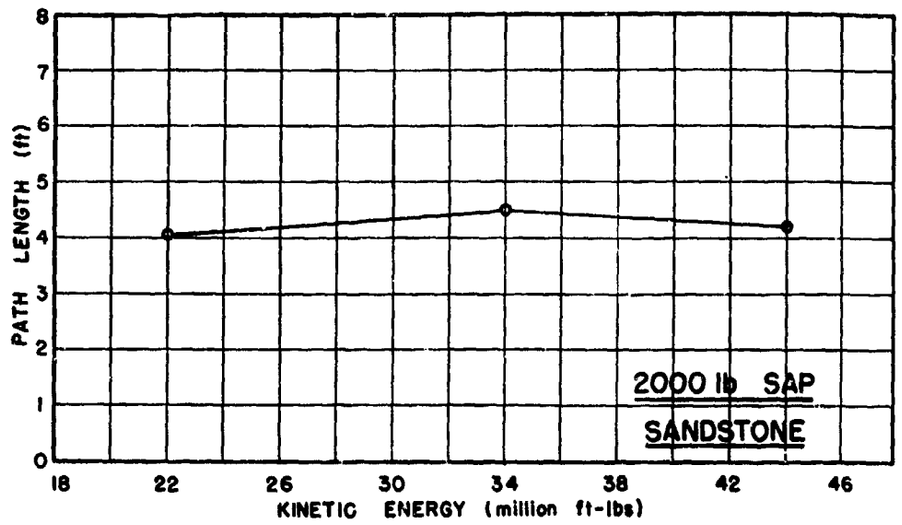
PATH LENGTH (ft)
KINETIC ENERGY (million ft-lbs)
2000 lb SAP
SANDSTONE

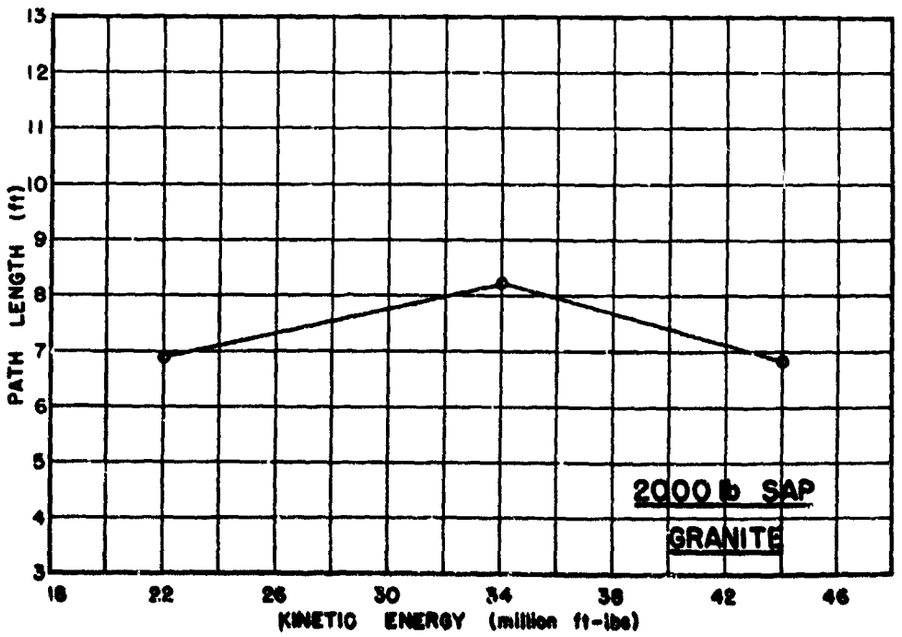
PATH LENGTH (ft)
KINETIC ENERGY (million ft-lbs)
2000 lb SAP
GRANITE

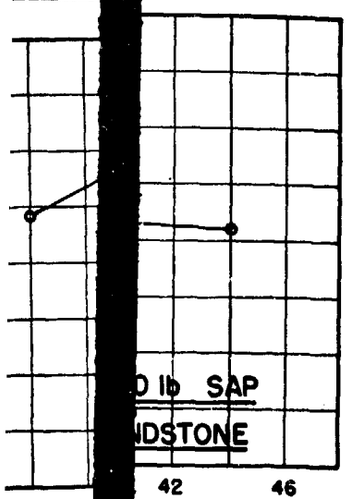

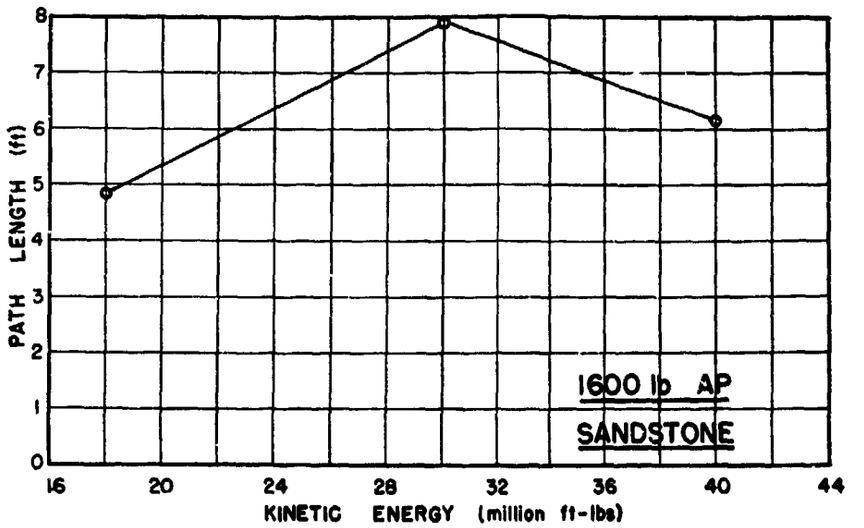

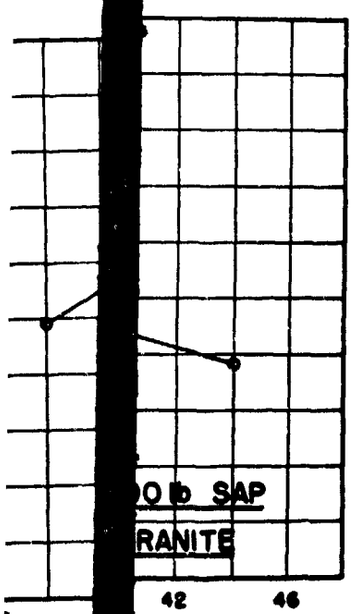

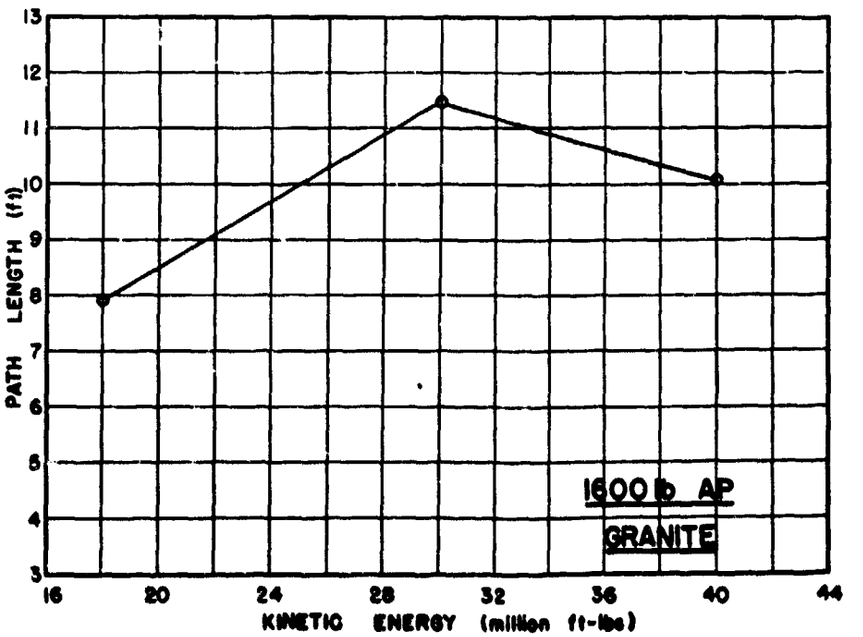

-BOMB PENETRATION PROJECT- C S M RESEARCH FOUNDATION, INC.	
Scale ——— Date 4-22-54	PATH LENGTH vs KINETIC ENERGY
Fig. No 190 By LSC	1600 lb AP ——— 2000 lb SAP
	SANDSTONE & GRANITE

Fig. 190

2

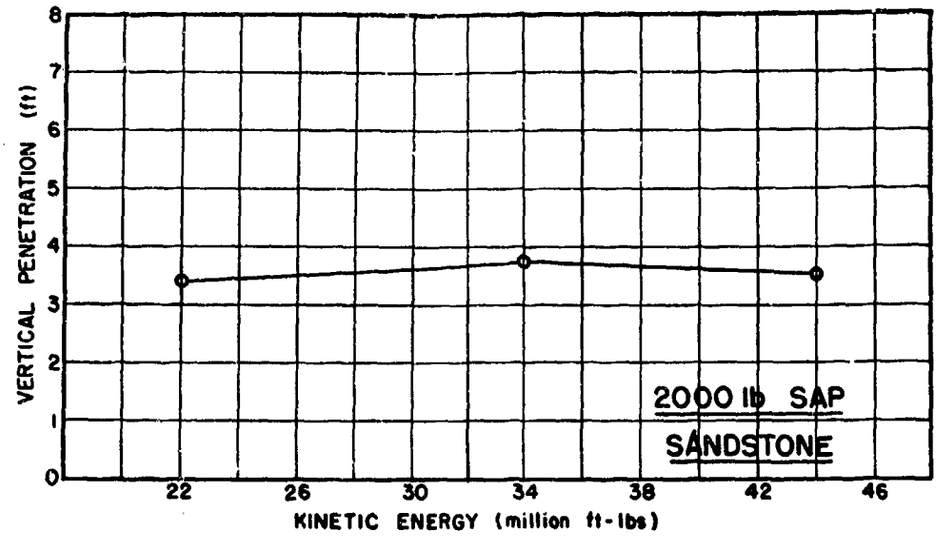

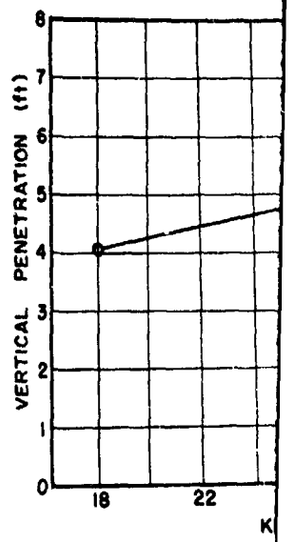

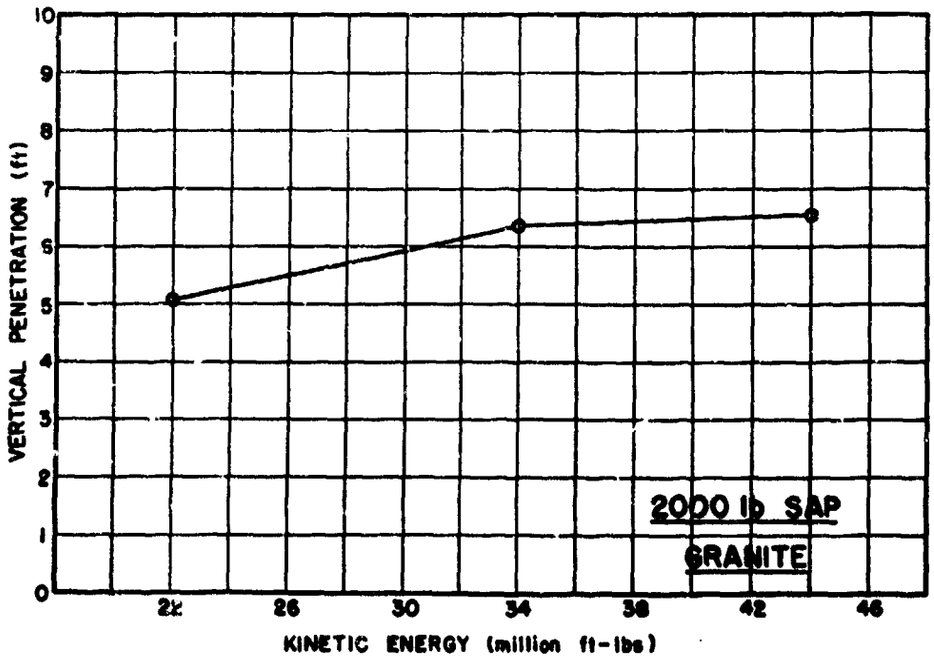

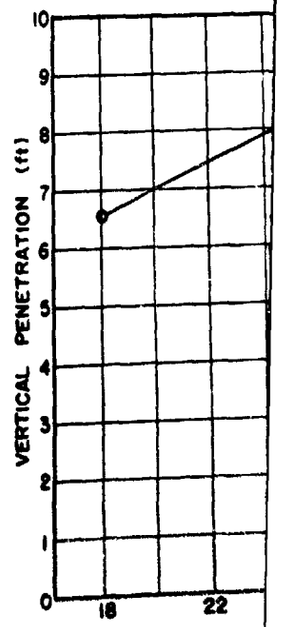

-BOM

Scale

Fig. N

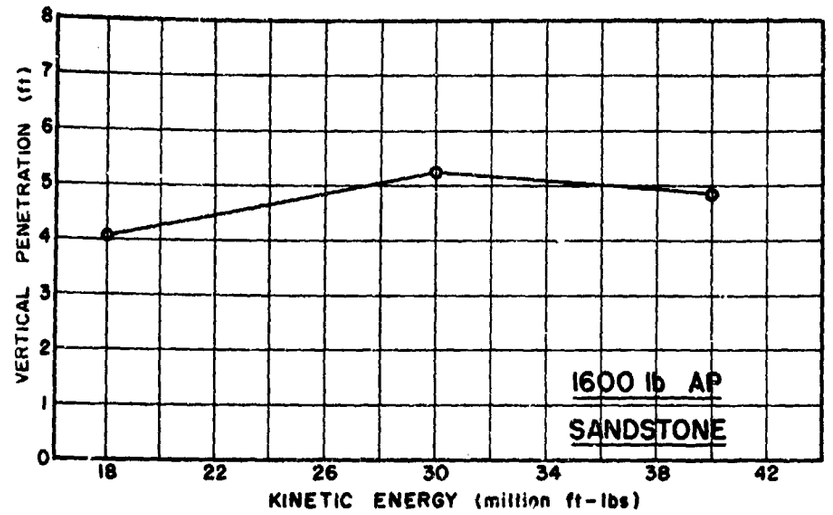

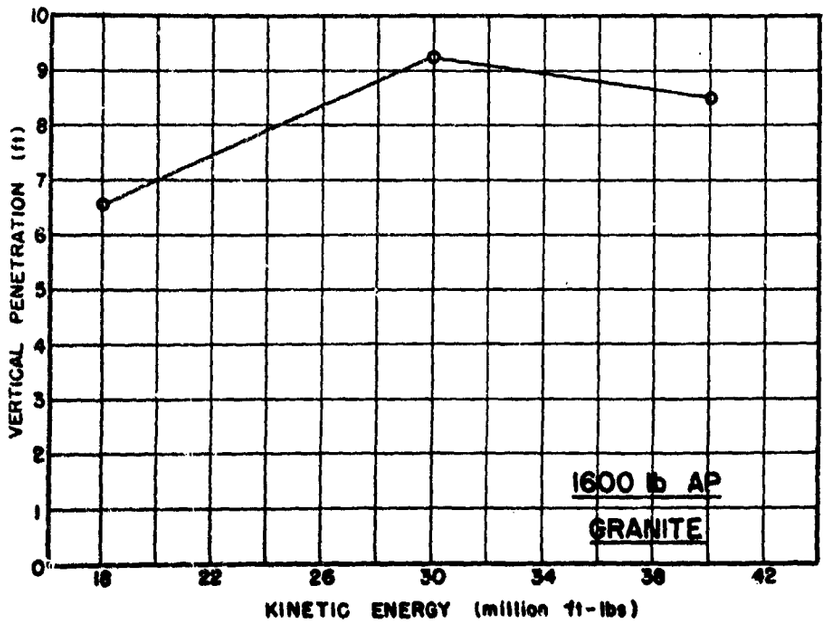

-BOMB PENETRATION PROJECT- C S M RESEARCH FOUNDATION, INC.	
Scale ——— Date 4-28-51	VERTICAL PENETRATION vs KE
Fig. No. 191 By ADG	1600 AP ——— 2000 SAP
	SANDSTONE & GRANITE

Fig. 191

2

Thus, the lateral stress in the Dakota sandstone approaches a maximum of 2.1 times the lateral stress in the Dakota sandstone approaches a maximum of 2.1 times the lateral stress in the Zuni granite. The range in ratios of lateral stress is from 1.6 to 2.1.

If the lateral stress is considered to be a measure of the resistance to penetration of a given bomb in a given type of rock, then the depths of penetration in any two types of rocks for a given type of bomb must vary inversely as the lateral stress. For example, if the penetration in sandstone of a given type of bomb is Xs and the penetration in granite is Xg, then the relation must hold that

$$\frac{X_s}{X_g} = \frac{S_g}{S_s} = \frac{\left(\frac{m_g}{1-m_g}\right) P_1}{\left(\frac{m_s}{1-m_s}\right) P_1} = \frac{m_g\,(1-m_s)}{m_s\,(1-m_g)}$$

where

X_s = penetration in sandstone

X_g = penetration in granite

S_g = lateral stress in granite

S_s = lateral stress in sandstone

m_g = Poisson's ratio for granite

m_s = Poisson's ratio for sandstone

P_1 = axially applied stress.

Specifically, for a given impact energy, the relative depth of penetration in sandstone equals

$$X_s = \frac{m_g\,(1-m_s)}{m_s\,(1-m_g)} X_g$$

and the penetration in granite equals

$$X_g = \frac{m_s\,(1-m_g)}{m_g\,(1-m_s)} X_s$$

In Fig. 190 the path length of 1600 AP and 2000 SAP bombs dropped on Dakota sandstone and on Zuni granite are plotted against kinetic energy. The numerical average path length and the weighted average kinetic energy for each group of bombs has been determined and straight lines have been drawn connecting the points representing the group averages. In Fig. 191 the vertical penetration of 1600 AP and 2000 SAP bombs dropped on Dakota sandstone and on Zuni granite are plotted against kinetic energy, and straight lines have been drawn between group averages as in Fig. 190.

From the data summarized in graphical form in Figs. 190 and 191 the ratio of vertical penetration in granite, Yg, to vertical penetration in

sandstone, Ys; and the ratio of total path length in granite, Pg, to the total path length in sandstone, Ps, have been computed. The data have been grouped separately for each type of bomb and is tabulated in Fig. 192.

Bomb Type	Kinetic Energy million ft-lbs	Vertical Penetration			Path Length		
		Y_s	Y_g	$\frac{Y_g}{Y_s}$	P_s	P_g	$\frac{P_g}{P_s}$
2000	22	3.38	5.03	1.49	4.05	6.91	1.70
SAP	34	3.72	6.41	1.72	4.56	8.21	1.80
	44	3.62	6.50	1.80	4.23	6.88	1.63
1600	18	4.05	6.61	1.63	4.83	7.91	1.64
AP	30	5.23	9.22	1.76	7.95	11.40	1.43
	40	4.85	8.55	1.76	6.16	10.05	1.63
		Avg.		1.69			1.64
				Avg. = 1.665			

Fig. 192

Ratios of Penetration in Zuni Granite and Dakota Sandstone
1600 AP and 2000 SAP Bombs

As may be observed from the tabular data, the average ratio of vertical penetration in Zuni granite to vertical penetration in Dakota sandstone is 1.69. The average ratio of path length, P, in Zuni granite to path length in Dakota sandstone is 1.64. The average of the two is 1.665.

The range in ratios of penetration is from 1.49 to 1.80. The range in ratio of Poisson's ratio is from 1.6 to 2.1. For the stress range at which failure occurs, m_s is equal to 0.287 and m_g is equal to 0.195. Solving the relation

$$\frac{X_g}{X_s} = \frac{m_s\,(1 - m_g)}{m_g\,(1 - m_s)}$$

it is found that

$$\frac{X_g}{X_s} = 1.662$$

Thus the relation is substantiated by the field data.

The very important conclusion may be reached that vertical penetration and path length in any rock varies inversely as the lateral component of stress in the rock in the stress range at which failure occurs. If the path length or vertical penetration of a given type of bomb at a given impact energy in a given type of rock is known, the path length and vertical penetration for the same type of bomb at the same impact energy may be estimated from the relation

$$X_1 = \frac{m_2\,(1 - m_1)}{m_1\,(1 - m_2)}\,X_2$$

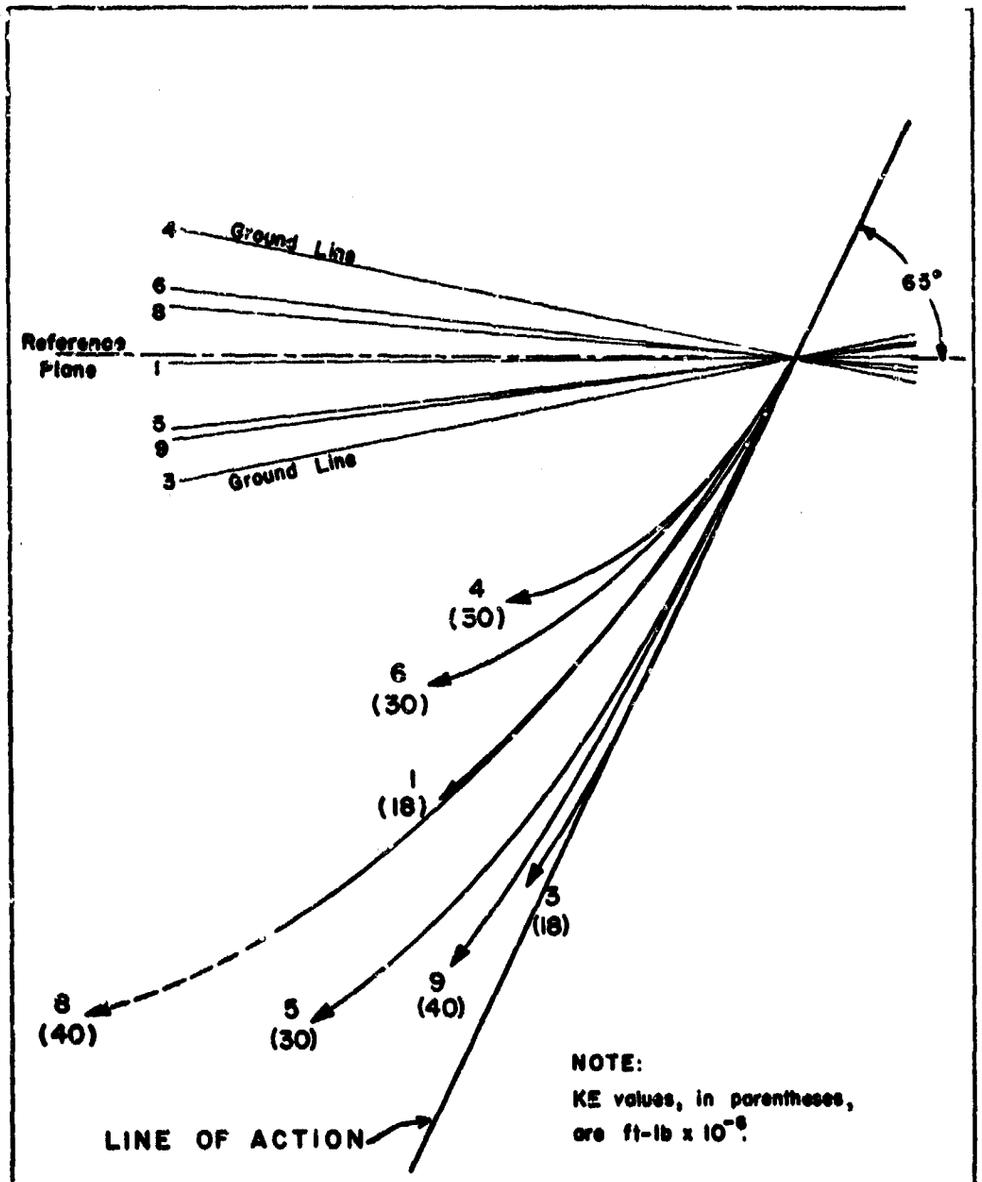

-BOMB PENETRATION PROJECT- C S M RESEARCH FOUNDATION, INC.	
Scale 1" = 5' Date 4-20-51 Fig. No. 193 By APS	PATH OF 1600 LB AP BOMBS REFERRED TO A 65° LINE OF ACTION

FIG. 193

where

X_1 = vertical penetration, or path length to be estimated

X_2 = corresponding vertical penetration, or path length determnied experimentally at a given bombing site.

m_2 = Poisson's ratio at failure stress of rock at known bombing site

m_1 = Poisson's ratio at failure stress of rock at proposed bombing site.

By making use of the above relation, it is possible to eliminate the rock factor and treat all of the bombs dropped at the Putney Mesa Sandstone Site as if they had been dropped at the Zuni Granite Site, and vice versa. Moreover, a means is provided whereby the penetration in any specific rock may be predicted. It should be recognized that the petrographic classification of rocks cannot be used solely as a basis of predicting penetration, for the elastic properties may vary as widely within any rock family, such as granite, as between families, such as granite and sandstone.

4—The Influence of Topography and Striking Angle Upon Penetration and Path Shape

As pointed out in Part C and Part D of this report, the path of a bomb is influenced by the impact energy, the shape of the nose of the bomb, and the slenderness ratio of the bomb. To these factors a fourth may be added —the angle of impact. Upon analysis it becomes apparent that all four factors are related to the manner of rock failure.

It has been pointed out in connection with the photoelastic analysis and the mathematical analysis (Figs. 162, 164) that the stress in the medium due to a concentrated load at the surface is the same at a given distance measured along the line of action of the applied force, regardless of whether the line of action is inclined or vertical. It is possible because of this fact to eliminate one variable, the angle of fall. In doing so, the angle of fall for each bomb dropped during the tests was fixed at 65 degrees (or at approximately the average angle of fall) by an arbitrary reference plane. In order to determine the effect of angle of impact upon penetration and upon path shape, all bomb paths were referred to a line of action at 65 degrees to an arbitrary plane.

Figure 193 shows the paths of the 1600 AP bomb in granite referred to a common line of action. In referring a bomb to the line of action, the AB crater cross-sections (see Appendix) along the line of flight were rotated to cause the angle of fall to coincide with the line of action. Thus the "ground line" in Fig. 193 is a surface profile from the AB crater cross-sections. Each ground line is numbered according to the C.S.M. bomb number and to the corresponding path number. Assuming that the arbitrary reference plane is horizontal, then Bombs 4, 6, and 8 represent uphill, or up-dip, bombing, Bomb 1 represents level surface bombing, and Bombs 5, 9, and 3 represent downhill, or down-dip, bombing.

By inspection of the figure it may be observed 1) that the direction of deviation from the line of action is towards the "free-face"[1] 2) that

[1]The term "free-face" is used as in connection with blasting to indicate the face that fails more easily.

the magnitude of the deviation from the line of action increases progressively for up-dip bombing and decreases progressively for down-dip bombing. Geologic control of Bomb 8 due to the presence of a lamprophyre dike accounts for the only minor discrepancy in the order.

In Fig. 194, the several bombs of Fig. 193 are re-grouped into up-dip bombing, level bombing, and down-dip bombing. The deviation, I_n, for Bombs 6, 1, and 3, which are at comparable depths of inclined penetration, is a visual measure of the decrease in deviation from the line of action as the distance to the free-face decreases. The explanation for the decrease in deviation for down-dip compared to up-dip bombing, is that deviation is a function of the lateral stress component in the medium, P_3. The lateral stress component increases with the depth, and the resistance to penetration increases with depth.

It may be observed by inspection of Fig. 194 that the vertical penetration, Y, does not take into account the slope of the ground as does the normal penetration, N_r. Accordingly, values of N_r more accurately measure the penetration of a bomb than do values of Y. We conclude, therefore, that values of N_r should be summarized and presented as a part of the analysis. Figure 195 presents the normal penetration of 2000 SAP and 1600 AP bombs in Zuni granite and Dakota sandstone in a form similar to Figs. 190 and 191.

The fundamental factor determining the path of a bomb in rock is the manner of rock failure. It seems premature with the data available at this time to explore exhaustively variations in the path of a bomb caused by each of the four factors known to influence the path. It seems more desirable to defer such study until the fundamental problem of rock failure can be pursued further. The basic factor may be re-stated that deviation increases as the resistance to penetration increases. Resistance to penetration increases as the depth of the bomb measured normal to the surface increases, and as the axially applied force on the bomb increases. Within a certain critical range, the ratio of the normal stress, σ_r, to the lateral stress, σ_θ, (see Fig. 169) is such as to minimize deviation and to cause penetration to approach a maximum.

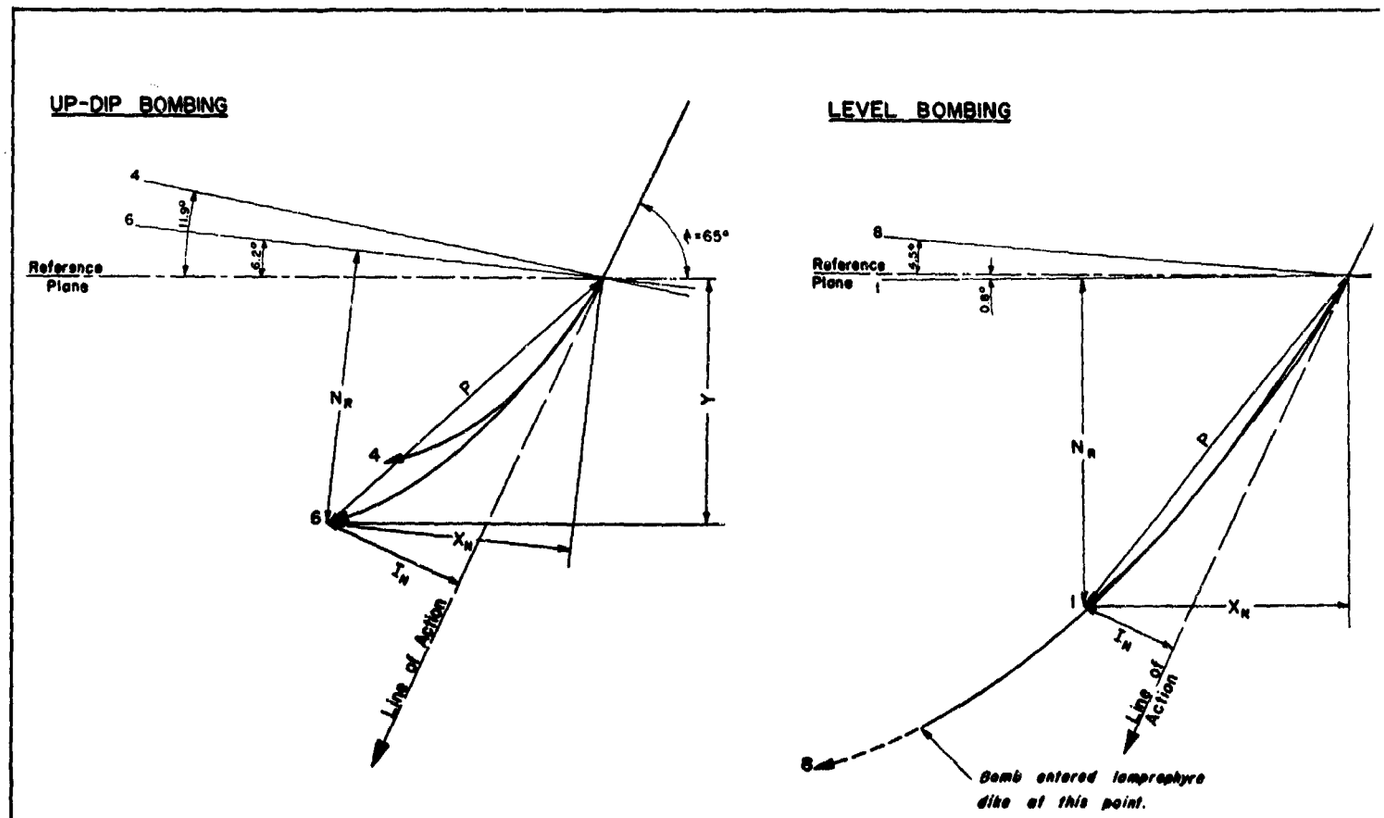
UP-DIP BOMBING
4
6
11.9°
6.2°
Reference Plane
φ=65°
N_R
P
Y
4
6
X_N
T_N
Line of Action
LEVEL BOMBING
8
4.5°
Reference Plane
1
0.8°
N_R
P
1
X_N
T_N
Line of Action
8
Bomb entered lamprophyre dike at this point.

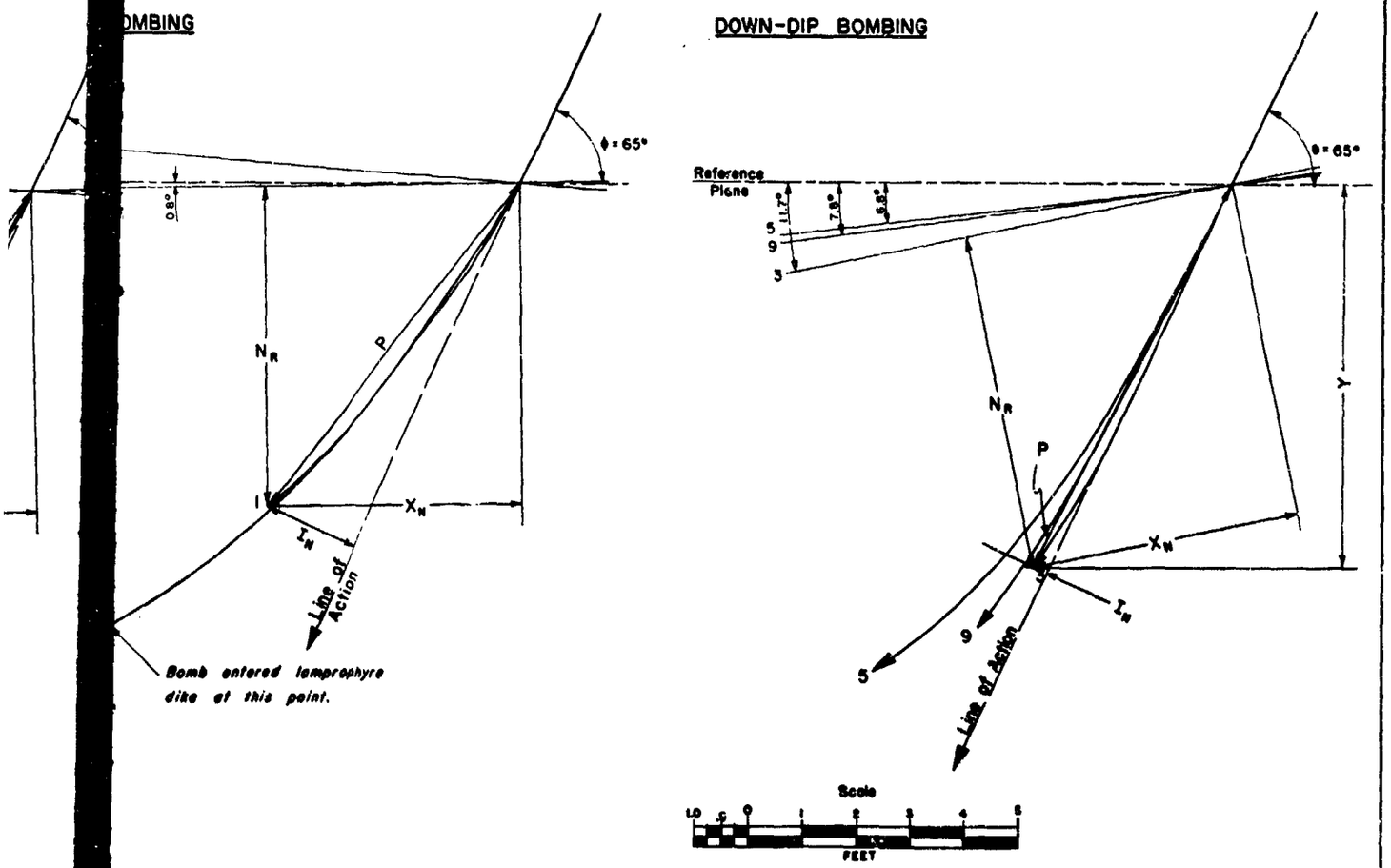

-BOMB PENETRATION PROJECT- C S M RESEARCH FOUNDATION, INC.	
Scale 1" = 2' Date 4-30-51	VERTICAL DEVIATION, I_N, FOR
Fig. No. 194 By LRO	UP-DIP, LEVEL, & DOWN-DIP BOMBING

Fig. 194

2

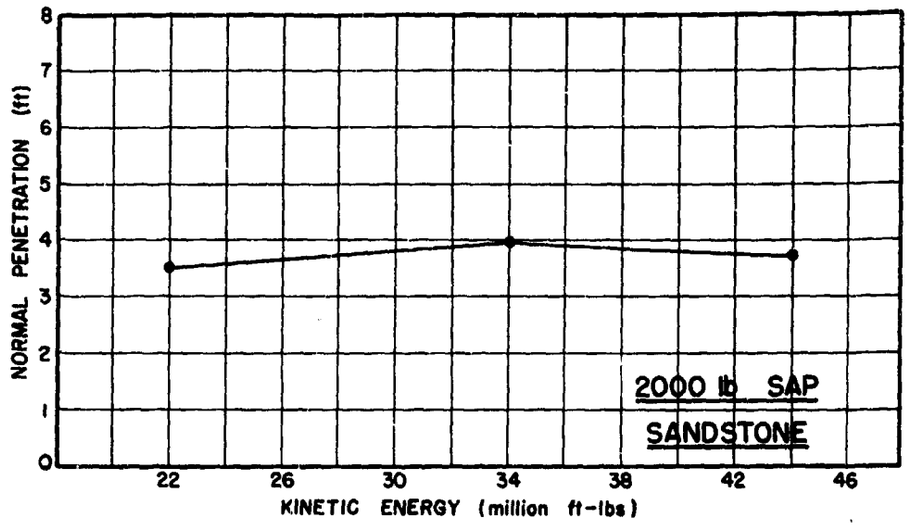
NORMAL PENETRATION (ft)
KINETIC ENERGY (million ft-lbs)
2000 lb SAP
SANDSTONE

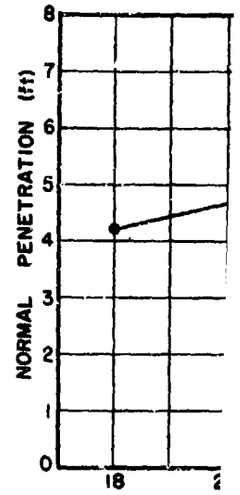
NORMAL PENETRATION (ft)

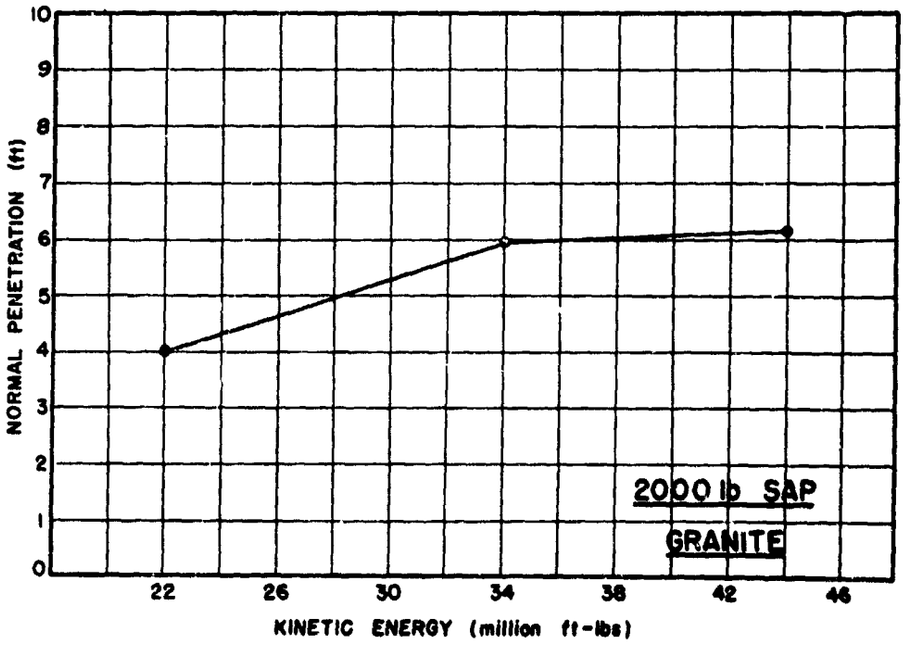
NORMAL PENETRATION (ft)
KINETIC ENERGY (million ft-lbs)
2000 lb SAP
GRANITE

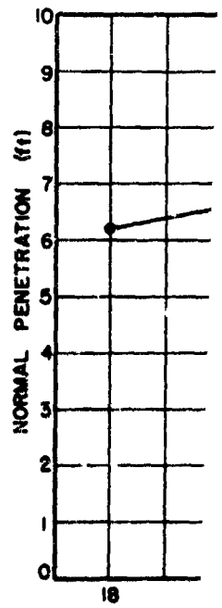
NORMAL PENETRATION (ft)

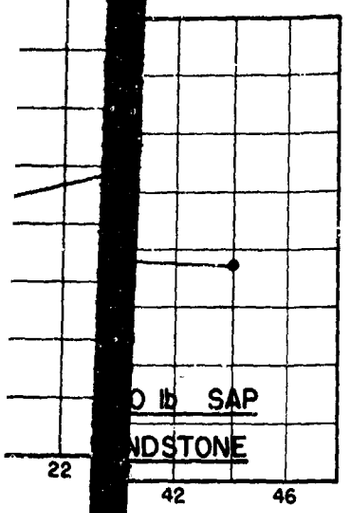

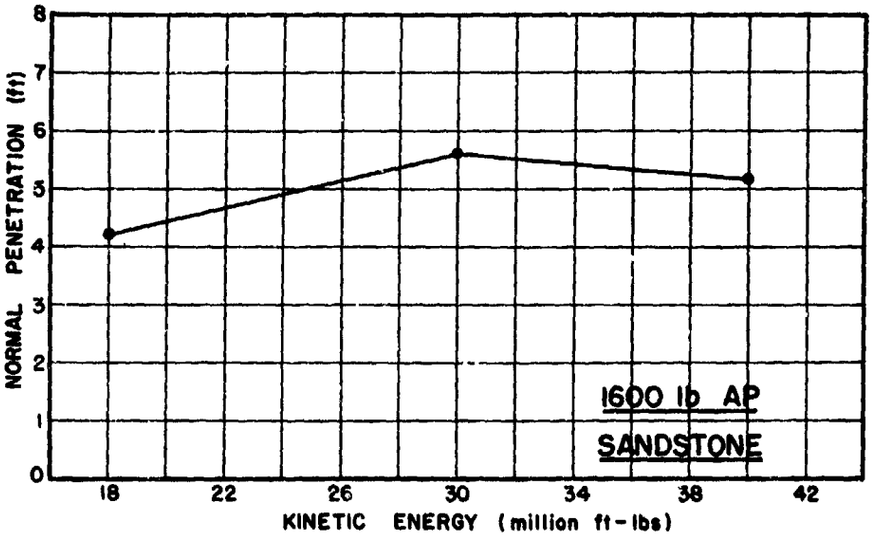

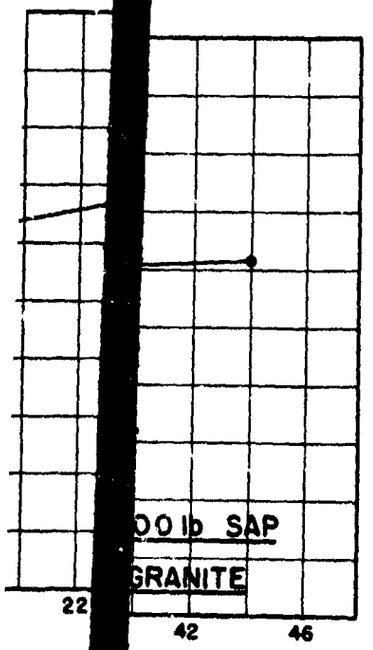

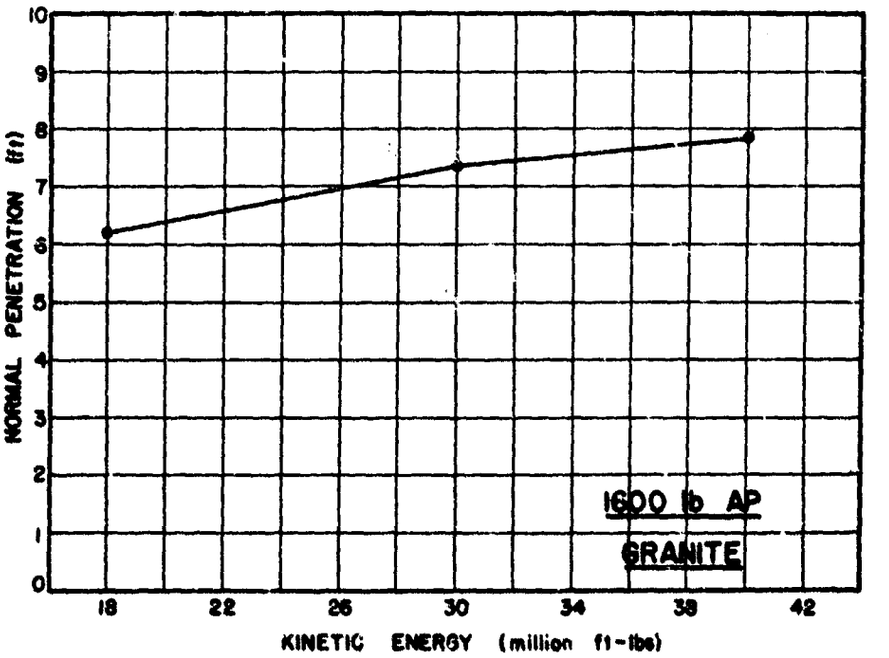

-BOMB PENETRATION PROJECT·· C S M RESEARCH FOUNDATION, INC.

Scale ——— Date 5-15-51

Fig. No. 195 By LPC

NORMAL PENETRATION vs KE
1600 AP ——— 2000 SAP
SANDSTONE & GRANITE

Fig. 195

2

SECTION III—REVIEW AND ANALYSIS OF PENETRATION FORMULAS AND DERIVATION OF THE LIVINGSTON PENETRATION FORMULA

1—Review and Analysis of Penetration Formulas

Perhaps the first attempt to derive a formula for penetration was made by Poncelet in 1829. Starting from Newton's second law, he stated the fundamental differential equation of motion as

$$-F = M\frac{d^2x}{dt^2}$$

where

F = resistance of the material to penetration

M = mass of the projectile

$\frac{d^2x}{dt^2}$ = acceleration of projectile at depth x, and time t.

Poncelet considered the resistance to penetration to be jointly proportional to the strength of the material and the inertia of the material removed from the zone of penetration. Under such assumed conditions, the solution of the equation of motion was found by Poncelet to be:

$$X = \frac{P}{2bgi}\ln_e\left(1 + \frac{b}{a}V^2\right)$$

where

X = maximum penetration

P = sectional pressure

b = inertia coefficient of the particular material

g = acceleration due to gravity, feet per second per second

i = form factor related to the shape of the projectile

a = a constant related to the shatter strength of the material

V = striking velocity, feet per second

Petry, in 1910, assumed that the term b/a in Poncelet's formula could be given a definite value for all materials. The Petry formula is expressed as:

$$X = k\,P\log_{10}\left(1 + \frac{V^2}{216{,}000}\right)$$

where

X = total path length, feet

k = a constant depending on the material

P = sectional pressure of the projectile (weight in pounds divided by maximum cross-sectional area in square inches)

V = striking velocity, feet per second

Values of the constant, k, for various materials may be found in War Department Technical Manual TM 5—310.

Both of the above formulas have a weakness in applying an arbitrary factor, k. The objection to the k factor lies in two assumptions. The first and more evident is the large variation in any specific property from one specimen of a particular kind of rock to another specimen of the same kind. For instance, it is well known that some limestones are soft, easily drilled, and friable and behave like a "weak" rock as ordinarily pictured. Other limestones, however, are hard, tough, difficult to drill or crush and, in general, behave like a "strong" rock as usually visualized. The factor "k" will also undoubtedly vary widely, just as any other rock property does from one specimen of a rock to another specimen of the same rock.

The second, and more serious weakness arising from use of a factor, k, is that such a factor is not determined by any easily measured properties of the rock, and that it would have to be determined by actually dropping bombs upon the rock and finding an average value of k. This is obviously an expensive and time-consuming process. If the k factor could be determined by measuring some properties of the rock in the laboratory and combining them to furnish the k factor, value of the Petry formula would be increased.

During the course of this project, an attempt was made to apply the field data to the Petry formula and determine the k values for a Zuni granite and a Dakota sandstone. Although the Petry formula was the best of the many existing formulas tried, it seemed that a better formula was needed.

In addition to the Petry formula, the following formulas were considered: 1) the old NDRC formula, 2) the new NDRC formula, and 3) the RRL formula.

The "old NDRC" formula is:

$$y = \frac{222P \cdot d^{0.215} \cdot V^{1.5}}{Y} + 0.5\,d$$

where

y = vertical penetration, inches

P = sectional pressure, pounds per square inch

d = maximum bomb diameter, inches

V = striking velocity, units of 1000 feet per second

$Y = \sqrt{S}$ where S = ultimate compressive strength of material.

The "new NDRC" formula is:

$$y = k \cdot N \cdot d^{0.215} \cdot D \cdot V^{1.5} + 1.0$$

where

y = vertical penetration, calibers

k = a "target" factor

N = nose factor = $0.72 + 0.25h$

h = caliber radius of head = radius ogive divided by diameter of bomb

d = diameter of bomb, inches

D = sectional density = weight of bomb divided by diameter cubed

V = striking velocity, units of 1000 feet per second

The "RRL" formula is:

$$y = \frac{k}{S^{1/4}} \left(\frac{w}{d^2}\right) \left(\frac{V}{1750}\right)^n$$

where

y = penetration, inches

w = weight of bomb, pounds

d = diameter of bomb, inches

V = striking velocity, units of 1000 feet per second

S = compressive strength of material, pounds per square inch

$n = \frac{10.7}{S^{1/4}}$

Curves showing the penetration as calculated from each of the preceding formulas were plotted. Arbitrary constants in these formulas were evaluated with representative values of penetration from the field data. The ultimate compressive strength of the rock as determined in the laboratory was substituted for the appropriate quantities in the "old NDRC" formula and the "RRL" formula.

Of the several formulas, none seemed to fit our field data, but the Petrie formula came closest.

3—Zuni Granite and Dakota Sandstone Prototype Composite Curves

By means of the relations discussed in Part F, Section II, item 3,

$$X_1 = \frac{m_2(1 - m_1)}{m_1(1 - m_2)} X_2$$

and because of the interdependence of vertical penetration, Y, normal penetration, N_R, and path length in rock, P, it is possible to construct Zuni granite and Dakota sandstone prototype curves for 2000 SAP and 1000 AP bombs. The prototype curves are obtained by applying a rock factor (the ratio of penetration, 1.665) to all the bombs of a given type

dropped at the sandstone site, so that they may be considered to have been dropped at the granite site, and so that bombs dropped at the granite site may be considered to have been dropped at the sandstone site.

To construct a sandstone prototype curve, the vertical penetrations, or the normal penetrations, or the path lengths of each of the bombs in a group of bombs of comparable impact energies dropped at both the sandstone and the granite sites are combined. An average kinetic energy for the group is computed. The average penetration, either Y, N_R, or P, is computed after converting each penetration of a bomb striking granite to a corresponding penetration in sandstone. For example, Bomb 18, a 2000 SAP bomb striking granite with an impact energy of 34.98×10^6 foot-pounds, has a measured path length in rock of 6.40 feet. The equivalent path length in Dakota sandstone equals

$$6.40 \cdot \frac{1}{1.665} = 3.84 \text{ feet}$$

Given a composite prototype Dakota sandstone curve, a composite prototype Zuni granite curve may be constructed by multiplying any given value of penetration by 1.665.

Figures 196, 197, and 198 are composite prototype granite and sandstone curves for 2000 SAP and 1600 AP bombs for path length, normal penetration, and vertical penetration respectively.

3—Dakota Sandstone Prototype Rock and Prototype Bomb Curves

With the rock factor determined and the medium reduced to a prototype, it becomes expedient to eliminate the variables relevant to the problem which are functions of the bomb. With these variables—the diameter and the nose shape of the bomb—removed, a prototype bomb is achieved, and curves can be constructed for penetration of a prototype bomb in a prototype rock. Rather than carry separate curves for granite and sandstone, only those curves for sandstone will be presented here.

3a) Correction for the Bomb Diameter

As a result of the photoelastic analysis, the mathematical analysis, and the model bombing experiments, it has been shown (see Part F, Section I, item 2d) that the net effect of increasing the diameter of the bomb is to increase the volume of rock under stress in proportion to the increase in diameter. Making use of this fact, it is possible to remove from the rock prototype 1600 AP and 2000 SAP curves one more variable—the bomb diameter.

A prototype bomb is 1.0 foot in diameter. A prototype SAP bomb is an SAP bomb 1.0 foot in diameter having a nose shape of the same caliber radius head as a 2000 SAP bomb. A prototype AP bomb is an AP bomb 1.0 foot in diameter that has a nose shape of the same caliber radius head as a 1600 AP bomb.

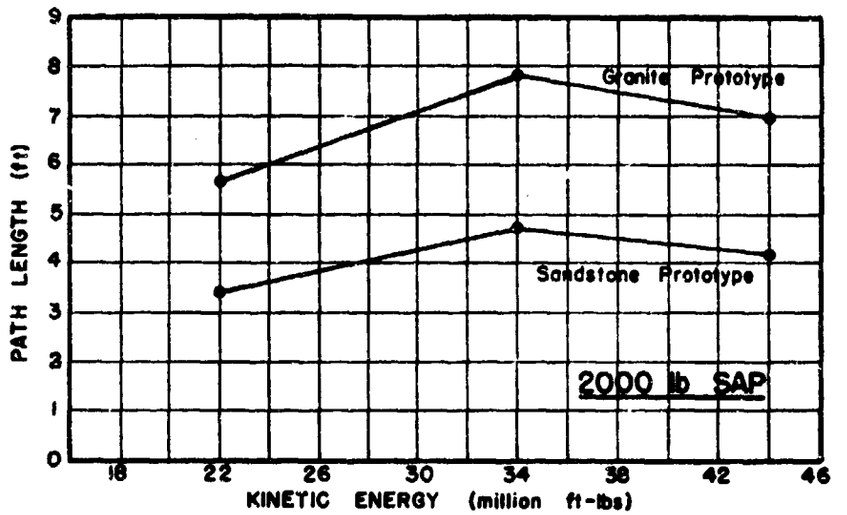

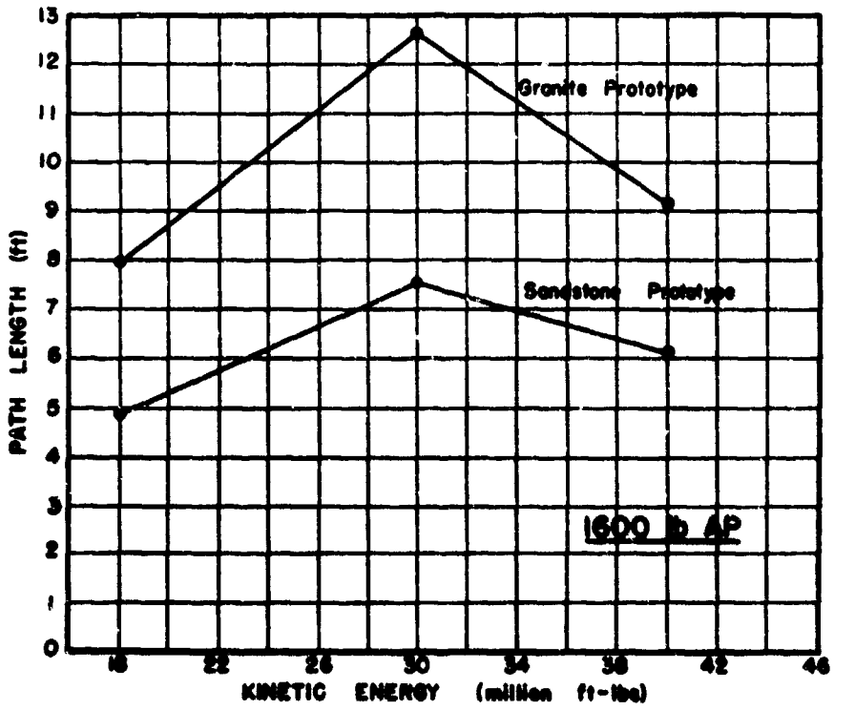

- BOMB PENETRATION PROJECT - C S M RESEARCH FOUNDATION, INC.

Scale ——— Date 8-18-61

Fig. No. 196 By LSG

PATH LENGTH vs KE
1600 AP ——— 2000 SAP
PROTOTYPE ROCK

Fig. 196

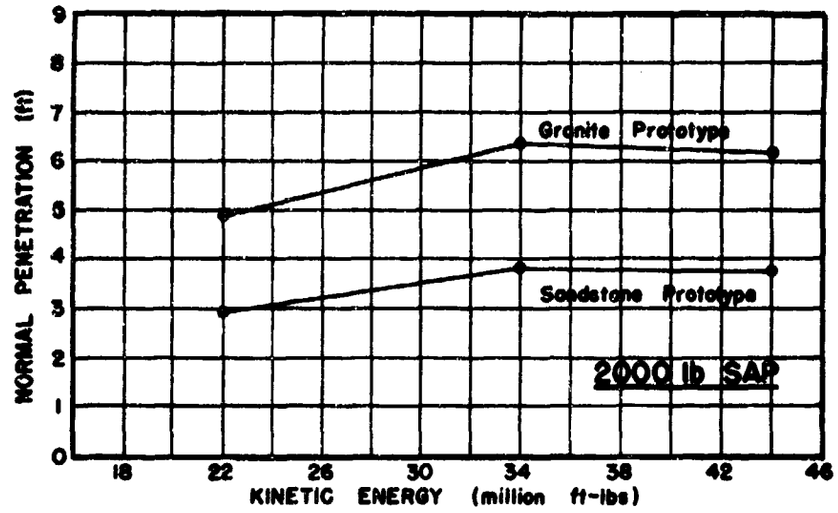

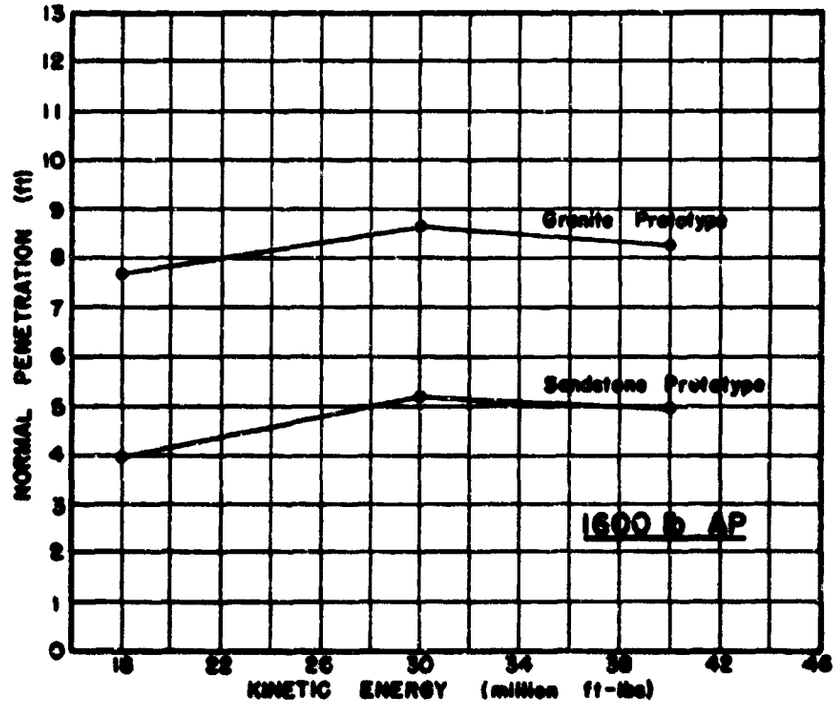

-BOMB PENETRATION PROJECT- C S M RESEARCH FOUNDATION, INC.

Scale ——— Date 5-16-51

Fig. No. 197 By LSG

NORMAL PENETRATION vs KE
1600 AP ——— 2000 SAP
PROTOTYPE ROCK

Fig. 197

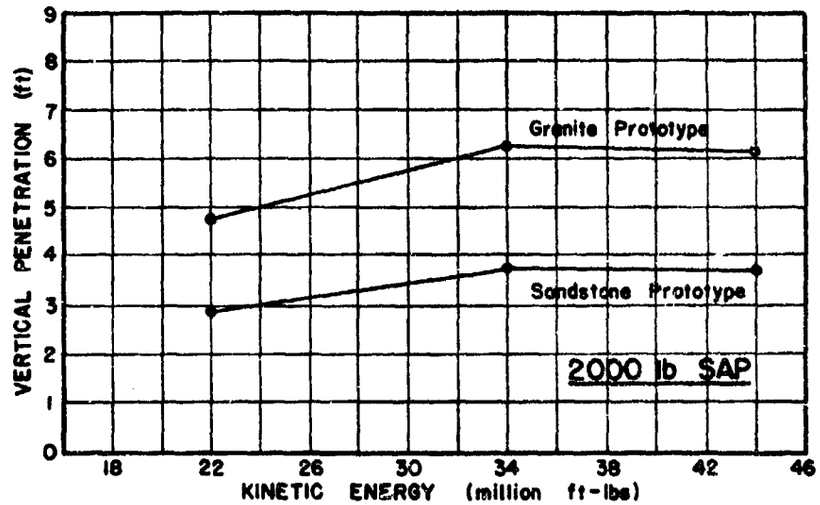

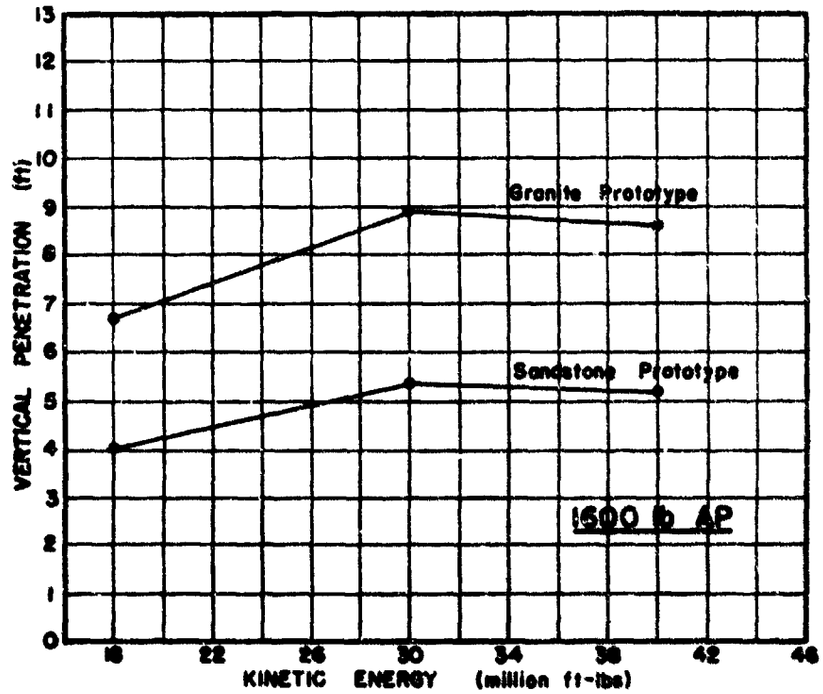

- BOMB PENETRATION PROJECT- C S M RESEARCH FOUNDATION, INC.

Scale ——— Date 3-18-51 Fig. No. 198 By LSO	VERTICAL PENETRATION vs KE 1600 AP ——— 2000 SAP PROTOTYPE ROCK

Fig. 198

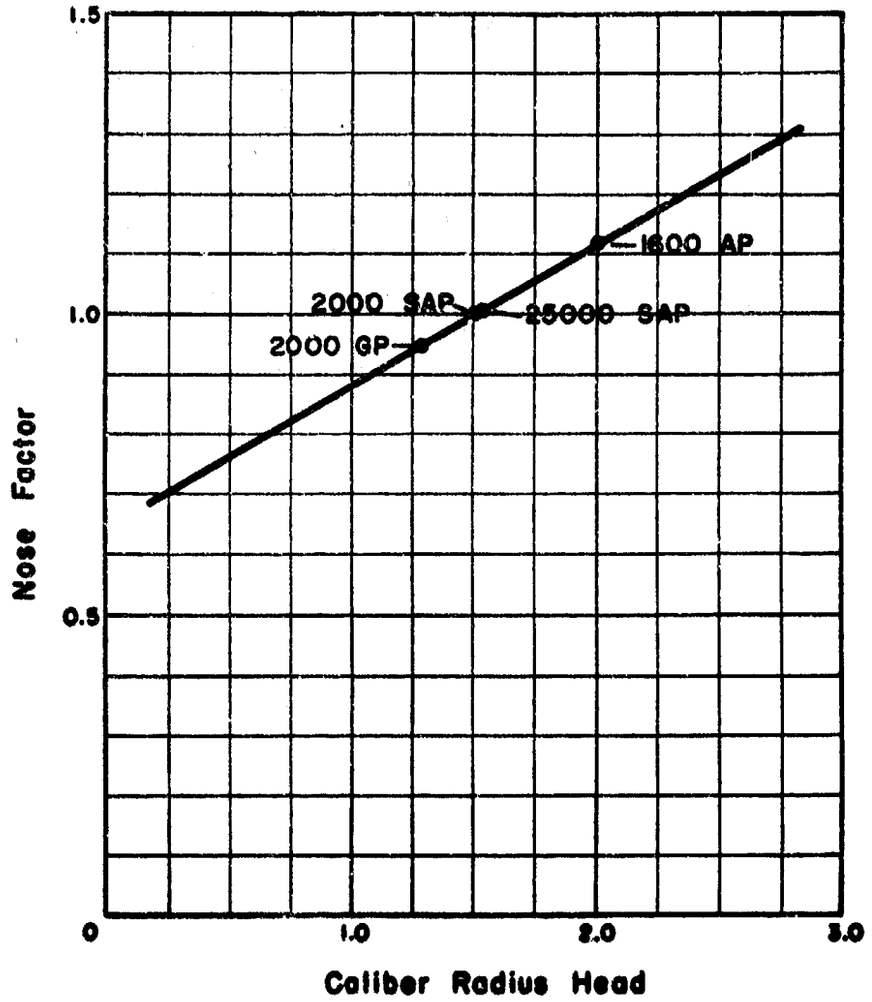

Note: Nose Factors are valid only at energies at which the casing does not break

-BOMB PENETRATION PROJECT- C S M RESEARCH FOUNDATION, INC.	
Scale ——— Date 5-16-51 Fig. No. 199 By ABS	NOSE CORRECTION FACTORS versus CALIBER RADIUS HEAD

Fig. 199

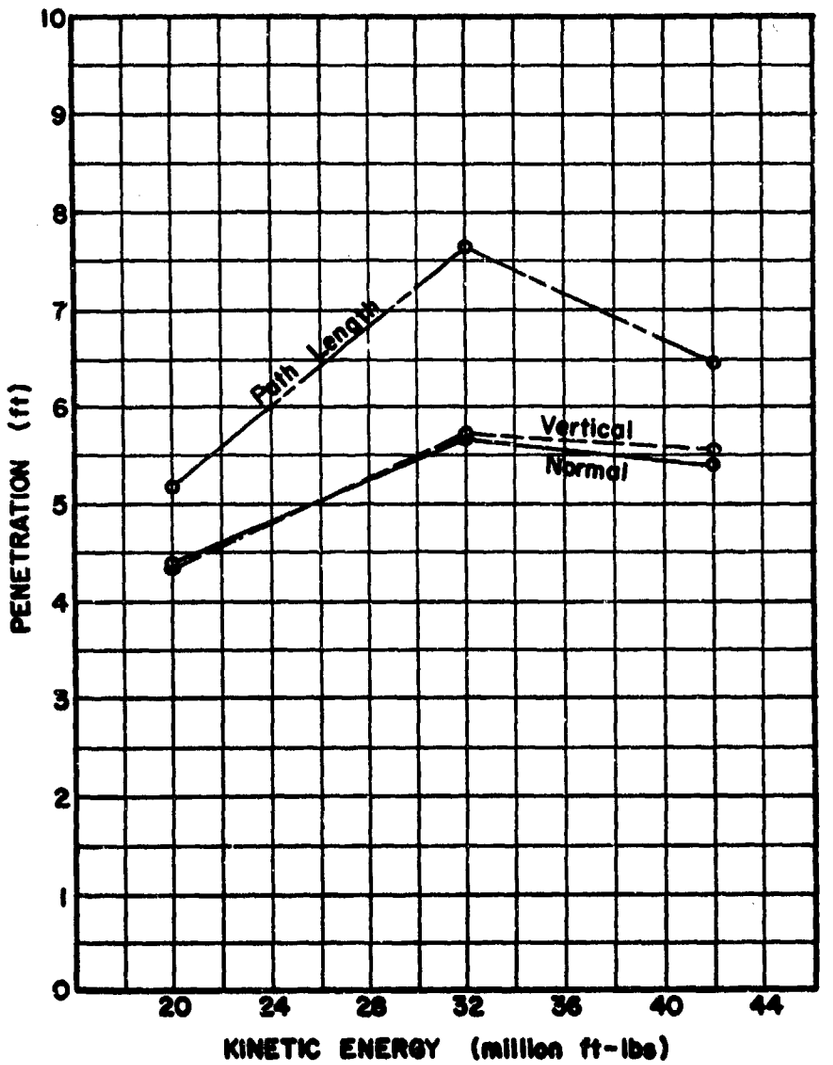

-BOMB PENETRATION PROJECT- C S M RESEARCH FOUNDATION, INC.

Scale ——— Date 5-29-51

Fig. No. 200 By ABS

PENETRATION vs KINETIC ENERGY
1600 AP ——— 2000 SAP
PROTOTYPE BOMB - PROTOTYPE ROCK

Fig. 200

To correct for the bomb diameter, with the prototype rock presumed to be Dakota sandstone, the penetration obtained for each group average, as recorded by the sandstone prototype composite curve, is multiplied by the ratio

$$\frac{d_b}{d_p}$$

where

d_b = the diameter of the bomb dropped during the field experiments

d_p = the diameter of a prototype bomb having the same nose shape

Thus, to correct for the bomb diameter for the 2000 SAP bomb, multiply the path length, normal penetration, or vertical penetration obtained from Figs. 196, 197, and 198 respectively by

$$\frac{d_b}{d_p} = \frac{18.76}{12.00} = 1.563 \text{ feet}$$

To correct for the AP bomb, multiply the respective quantities by

$$\frac{d_b}{d_p} = \frac{14.00}{12.00} = 1.167 \text{ feet}$$

3b) Nose Correction Factors

The effect of the nose shape of a bomb is to modify the stress distribution in the medium. Plastic failure occurs at the tip of a sharp-nosed bomb; thus both the amount of crushing and the rate at which energy is absorbed by the rock are reduced. The shape of the nose of a 2000 SAP bomb was chosen as a prototype shape and assigned a nose correction factor of 1.00. The caliber radius head of a 2000 SAP bomb is 1.49. The caliber radius head of a 1600 AP bomb is 2.00, and the caliber radius head of a 2000 GP bomb is 1.28. Theoretically, the nose correction factor for a sharp-nosed AP bomb should be greater than 1.00, and the correction factor for the round-nosed GP bomb should be less than 1.00.

The nose correction factor for AP bombs is obtained by constructing "prototype rock-prototype AP bomb" curves and dividing the penetration of the AP prototype bomb by the penetration of the SAP prototype bomb. Figure 199 gives tentative nose correction factors for bombs of caliber radius head 2.00 , 1.28, and 1.56 (25,000 SAP), which, because of the comparatively small number of bombs dropped in these tests, should be considered only approximate.

Figure 200 shows "prototype rock-prototype bomb" curves for 2000 SAP and 1600 AP bombs for path length, normal penetration, and vertical penetration in sandstone. As is evident, these are the prototype rock curves (Figs. 196, 197, and 198) corrected for the bomb factors; in other words, penetration of a prototype bomb in a prototype rock.

4—Relation of Sectional Pressure and Sectional Density to Penetration in Rock

Penetration formulas currently in use and developed as a result of experiments with soils and concrete may be grouped into two classes. One group considers penetration to be a function of sectional density

where

$$D = \frac{w}{d^3}$$

D = sectional density

w = weight acting at the center of gravity of the bomb, pounds

d = diameter of the bomb, inches

The other group considers penetration to be a function of sectional pressure

$$P = \frac{w}{A}$$

P = sectional pressure, pounds per square inch

A = cross-sectional area of bomb, square inches

Model bombing experiments conducted in the Barodynamics Laboratory of the Mining Department of the Colorado School of Mines and described in Part E, Section I, have shown that penetration is independent both of sectional density and of sectional pressure.

However, both the quantities w and d influence penetration, but not in the same sense as implied by previous investigators. The weight of the bomb w and the striking velocity determine the impact energy. Impact energy is related to penetration, but the relation is not a simple one, because the resistance to penetration increases as the axially applied force increases. As the diameter of a bomb striking rock increases, the volume of rock that is stressed increases. Penetration is accomplished by rock failure, and the stress distribution in the medium determines the manner of rock failure. Penetration varies inversely as the bomb diameter.

5—Increased Resistance to Penetration as a Function of Depth, Striking Velocity, and Kinetic Energy

Field observations, laboratory work, and theoretical considerations all point to an increased resistance to penetration with increased depth of rock. This is tantamount to saying that the rock is "stronger" at depth.

The increased strength of the rock at depth as a result of the impact and penetration of a bomb is analogous to the increased strength of a rock specimen, subjected to a triaxial compression test, if the lateral confinement is increased. Figure 69 shows how the axially applied stress, S_1, at failure increases with the laterally applied stress, S_3.

If it were possible from existing knowledge to convert a dynamic load to an equivalent static load, and if the relation between the axially applied stress, P_1, and the lateral stress, P^3, were maintained so that

$$P_3 = \frac{m}{1 - m} P_1$$

where

$$m = \text{Poisson's ratio at stress range } P_1$$

and if P_1 were known from impact to maximum penetration, it would be possible to write an equation for penetration without resorting to the use of empirical data. Unfortunately, fundamental research has not yet progressed to the extent where this is possible.

At impact, the energy of bomb causing rock failure and penetration is maximum. The energy decreases as rock failure proceeds. Thus the energy of the bomb decreases with depth, and the strength of the rock increases with depth. Any formula relating penetration to the other variable terms must include a term that expresses this "effect of depth" phenomenon. Until fundamental knowledge beyond that currently available is gained it seems necessary to express the "effect of depth" phenomenon empirically.

6—The Livingston Penetration Formula

In the Livingston Penetration Formula, which is presented in the following paragraphs, the "effect of depth" phenomenon and the impact energy are combined in a "Q" term which depends upon the impact energy.

In previous paragraphs the rock factor, the bomb diameter, and the nose shape factor have been eliminated successively as variables, and generalized "curves" (see Fig. 200) established which are referred to as "prototype bomb-prototype rock" curves. The photoelastic analysis, the mathematical analysis, the physical rock tests, and the model bombing experiments provided the theory upon which the "prototype bomb-prototype rock" curves are based. A 1.0-foot-diameter bomb having a nose shape of the same caliber radius head as a 2000 SAP bomb is defined as a prototype bomb. Dakota sandstone is established as a prototype rock.

These generalized "prototype bomb-prototype rock" curves have been based upon group averages, and the groups have been determined largely from the results of bombing from 9200 feet, 18,000 feet, and 30,000 feet above the target. The points between group averages have been connected by straight lines. As is evident from Fig. 200, the values for vertical penetration and normal penetration of a prototype bomb in a prototype rock do not differ greatly. As previously stated, the normal penetration is thought to be a more exact measure of penetration than the vertical penetration. For these reasons it seems advisable to confine the investigation to normal penetration and to path length.

The formula for the "prototype bomb-prototype rock" curves, and the

effect of the kinetic energy and increased resistance to penetration at depth, can now be stated as follows:

$$P = \frac{m_s (1 - m_x)}{m_x (1 - m_s)} \cdot \frac{N}{d} \cdot Q \qquad (1)$$

where

P = the nose penetration of any type of bomb in rock X, feet

N = the nose factor. A term that expresses the effect of the shape of the nose upon the stress distribution in the medium. (See Fig. 199)

d = the bomb diameter, feet. A term which states that penetration is inversely proportional to the volume of rock under stress.

Q = the nose penetration of a prototype bomb in a prototype rock, feet. A term which is determined empirically and which is a function both of impact energy and of increased resistance to penetration at depth.

m_s = Poisson's ratio at the stress range (5000 psi) at which failure occurs in simple compression for Dakota sandstone, the prototype rock.

m_x = Poisson's ratio of rock X at the same stress range (5000 psi)

$\frac{m_s (1 - m_x)}{m_x (1 - m_s)}$ = the rock factor. A term which states that penetration varies inversely as the lateral component of stress induced in the medium as a result of the axially applied stress.

It is desirable to simplify the form in which the rock factor is stated. This simplification is possible because values of Q are based upon the prototype rock, which is Dakota sandstone. At the stress range at which failure of Dakota sandstone occurs in simple compression (5000 psi), the value of m_s as obtained from Fig. 68 is 0.287. Substituting this value in the factor

$$\frac{m_s (1 - m_x)}{m_x (1 - m_s)}$$

we obtain

$$\frac{1 - m_x}{2.484\, m_x}$$

Thus equation (1) may be stated in the form

$$P = \frac{(1 - m_x)}{2.484\, m_x} \cdot \frac{N}{d} \cdot Q \qquad (2)$$

which in future paragraphs is referred to as the Livingston Penetration Formula.

Obviously, different measures of penetration are dependent only upon the "Q" term. If it is desired to compute the normal penetration of a given

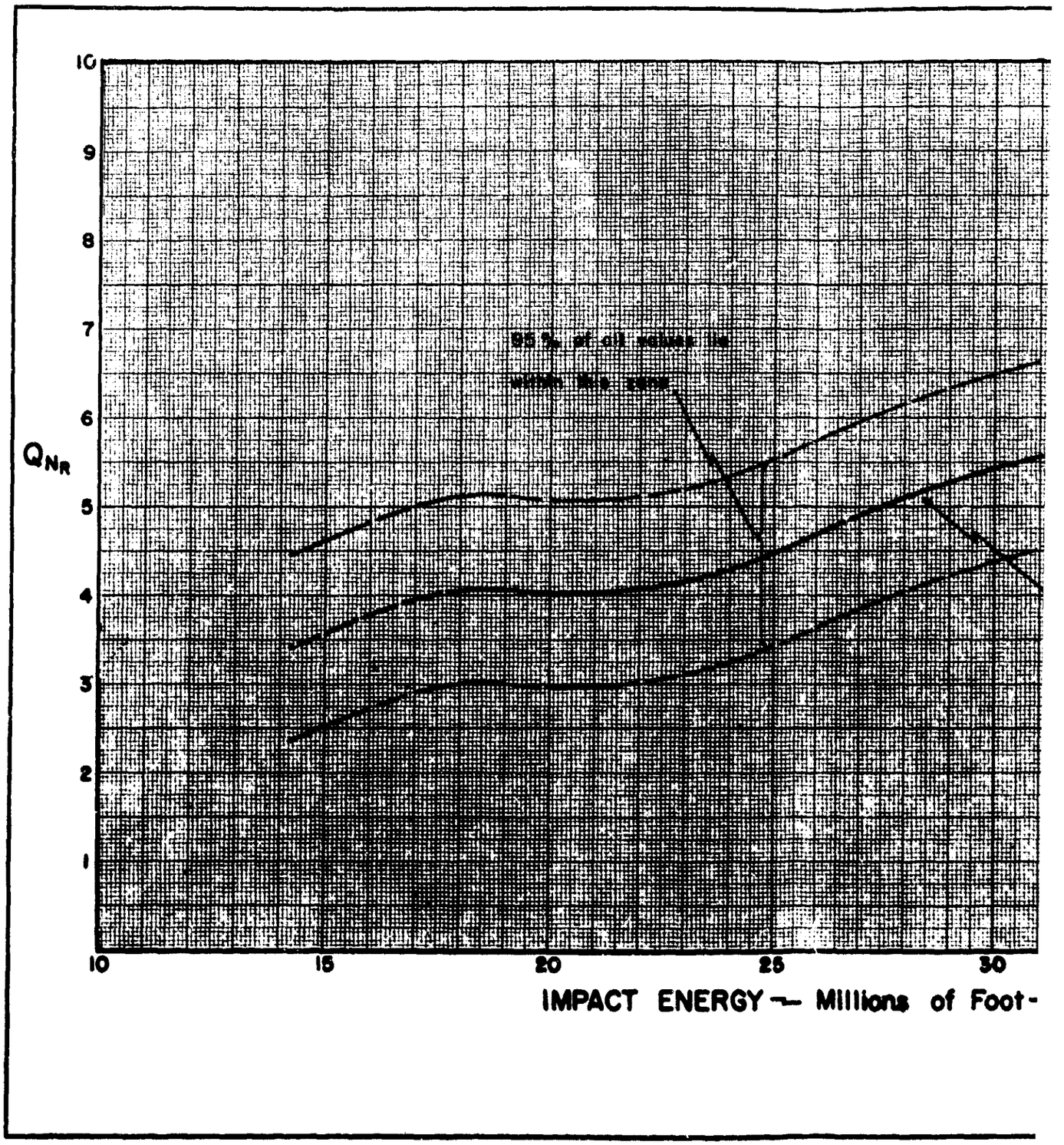
95% of all values lie within this zone
Q_{N_R}
10
9
8
7
6
5
4
3
2
1
10
15
20
25
30
IMPACT ENERGY — Millions of Foot-

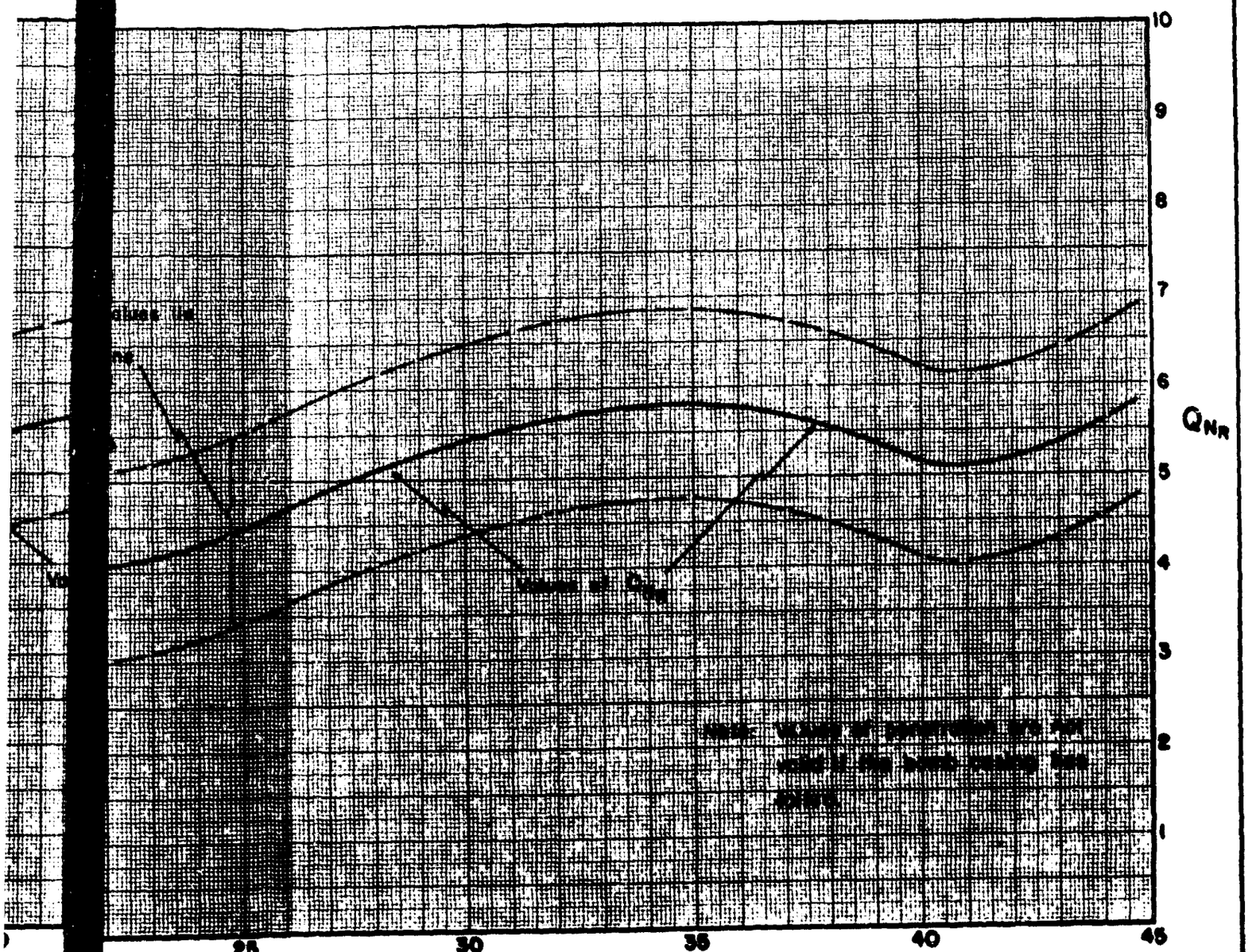

-BOMB PENETRATION PROJECT- CSM RESEARCH FOUNDATION, INC.	
Scale — Date 5-19-51 Fig. No. 201 By ADG	VALUES OF Q_{N_R} IN THE LIVINGSTON PENETRATION FORMULA

Fig. 201

2

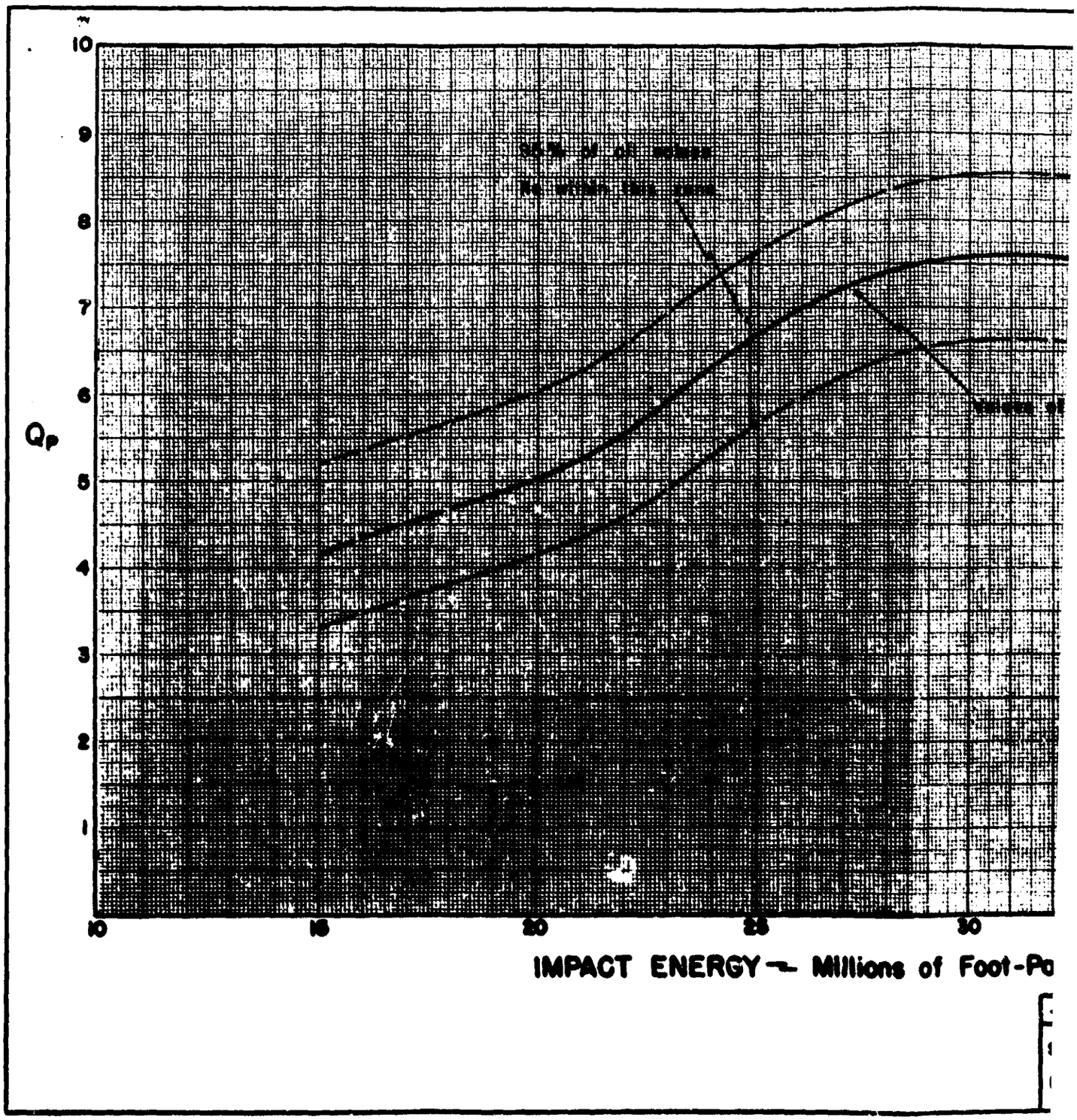
10
9
8
7
6
5
4
3
2
1
Q_P
10
15
20
25
30
IMPACT ENERGY — Millions of Foot-Po

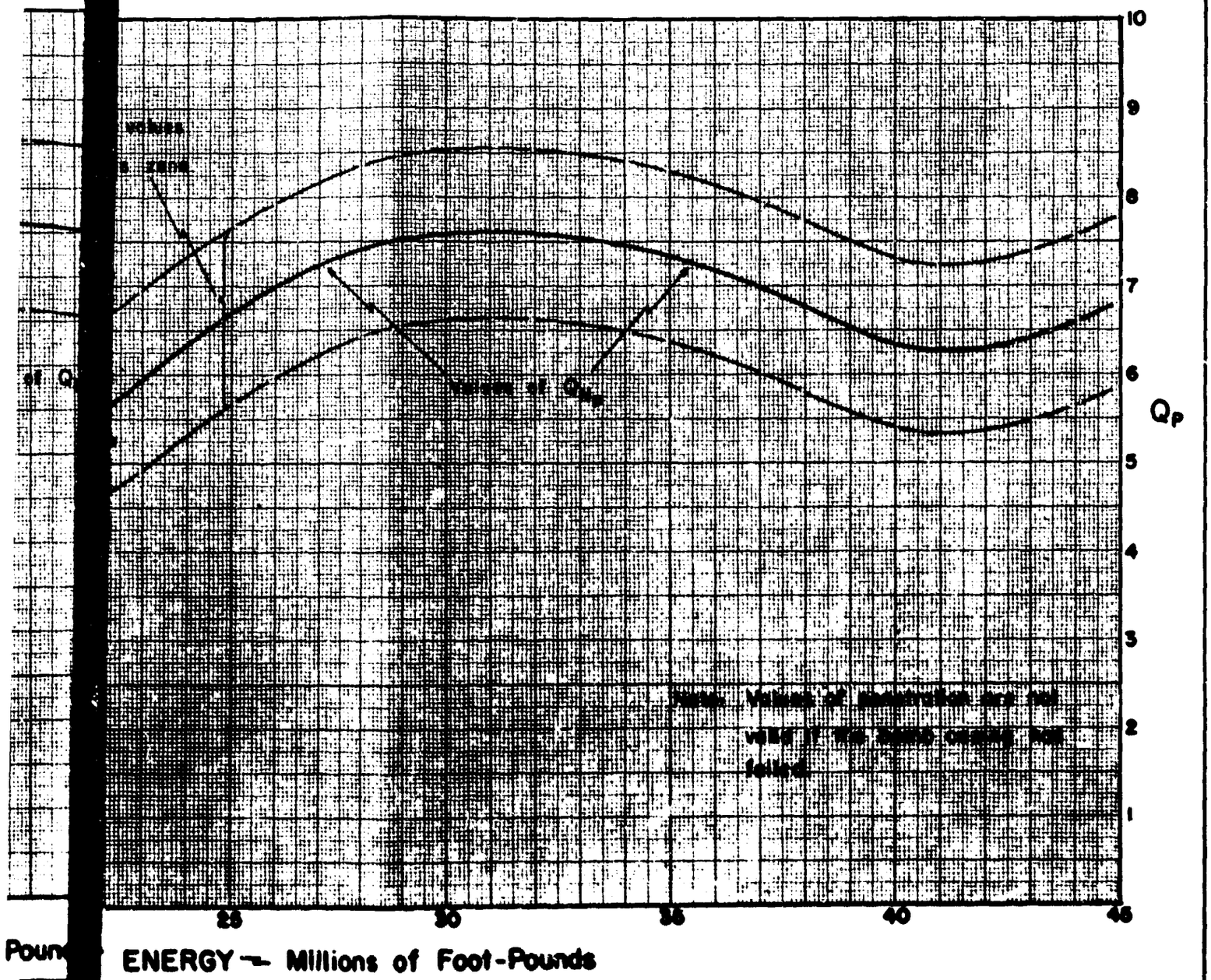

-BOMB PENETRATION PROJECT- C S M RESEARCH FOUNDATION, INC.	
Scale — Date 8-18-51 Fig. No. 202 By ABS	VALUES OF Q_p IN THE LIVINGSTON PENETRATION FORMULA

Fig. 202

type of bomb in a given type of rock, the Livingston Penetration Formula takes the form

$$N_R = \frac{1 - m_x}{2.484\, m_x} \cdot \frac{N}{d} \cdot Q_{NR} \qquad (3)$$

where

N_R = normal penetration of any given bomb in rock X, feet

Q_{NR} = normal penetration of prototype bomb in prototype rock, feet.

If it is desired to compute the path length of a given type of bomb in a given type of rock, the Livingston Penetration Formula takes the form

$$P_{RM} = \frac{1 - m_x}{2.484 m_x} \cdot \frac{N}{d} \cdot Qp \qquad (4)$$

where

P_{RM} = path length of any given bomb in rock X, measured to the point of maximum normal penetration, feet

Q_P = path length of prototype bomb in prototype rock, feet

Equations (3) and (4) can now be applied to each bomb dropped during the tests, including the general-purpose bombs that did not rupture and including bombs released from altitudes other than 9200 feet, 18,000 feet, and 30,000 feet. The resulting curves are referred to as "Q" curves. Figure 201 gives values of Q_{NR} for various values of kinetic energy ranging from 14 million foot-pounds to 45 million foot-pounds. The range of kinetic energies does not include the two 25,000 SAP bombs dropped during the tests, but does include all others. As may be observed, the dashed lines of the figure indicate the dispersion of the test data due to variations in geologic properties of Dakota sandstone and Zuni granite. Ninety-five per cent of all values lie within the zone between the dashed lines.

Figure 202 gives values of Q_P for various values of kinetic energy between 15 million and 45 million foot-pounds. Values of Q_P from the figure are substituted in the Livingston Penetration Formula to obtain the length of the path of the bomb in rock to the point of maximum normal penetration.

If the shapes of the "Q" curves, Figs. 201 and 202, are compared with the laboratory results of the model bombing experiments the similarity is readily apparent. For example, compare Fig. 201 with Fig. 127 in which the normal penetration of a model 2000 SAP bomb in a Calseal mixture at various impact energies is plotted. Compare Fig. 201 also with Fig. 130 in which the normal penetration of a model 1600 AP bomb and of a model 2000 SAP bomb in molding plaster at various impact energies is plotted. A characteristic feature of the field and of the laboratory results is the paradoxical behavior wherein penetration decreases with an increase of impact energy in certain ranges.

When this behavior was first observed during the field tests it was thought that a possible explanation might be that the bombs were unstable in flight in certain ranges. In the interim report it was suggested that there is a critical altitude for each given bomb type above which penetration decreases rather than increases. Upon completion of our analysis it was apparent that there is a series of critical points rather than a single critical point. Over a broad range of impact energies, such as between 15 million and 700 million foot-pounds, penetration increases with an increase in impact energy, but within a local range such as between 35 million and 41 million foot-pounds, penetration decreases rather than increases.

Inasmuch as rock failure precedes penetration and permits the penetration of a bomb into rock, rather than that penetration causes rock failure, it appears that the true explanation for local decreases in penetration with increase in impact energy is that energy is stored or absorbed by a rock mass between stages of rupture. Perhaps, if a large number of bombs were dropped, the strain-energy relation might be observable for each set of "O" cracks that forms.

7—Extrapolation of the Data

Although the hazards of extrapolation are recognized and appreciated, it seems desirable to venture into the unknown. A total of 50 bombs was dropped during the Bomb Penetration Project; 48 of the 50 were dropped within the range of impact energies from 20 million to 45 million foot-pounds, 1 was dropped at 514 million foot-pounds; and 1 was dropped at 683 million foot-pounds.

The trend of the Q_{NR} curve through the range 20 to 45 million foot-pounds impact energy and the maximum deviation above and below the trend line, together with the trend of the Q_P curve and the deviation above and below the trend line are shown in Figure 203. The "Q_{NR}" and the "Q_P" values for bombs 19 and 20 and the same deviation as observed at the lower impact energies are plotted in the figure. When the size of the unknown region is compared with the size of the known region, it is apparent that much work remains to be done in the field of this investigation. However, Figure 203 serves as a means of extrapolating beyond the range of the Bomb Penetration Project to obtain values of Q_P and Q_{NR} to be substituted in the Livingston Penetration Formula.

Based upon the change in slope of the "Q" curves at 540 million foot-pounds impact energy, a tentative limit between the elastic zone and the plastic zone is indicated in Fig. 203. It seems particularly desirable to conduct further research in the plastic zone.

8—Use of the Formula

The following example problems illustrate the application of Figs. 201, 202, and 203 to the Livingston Penetration Formula.

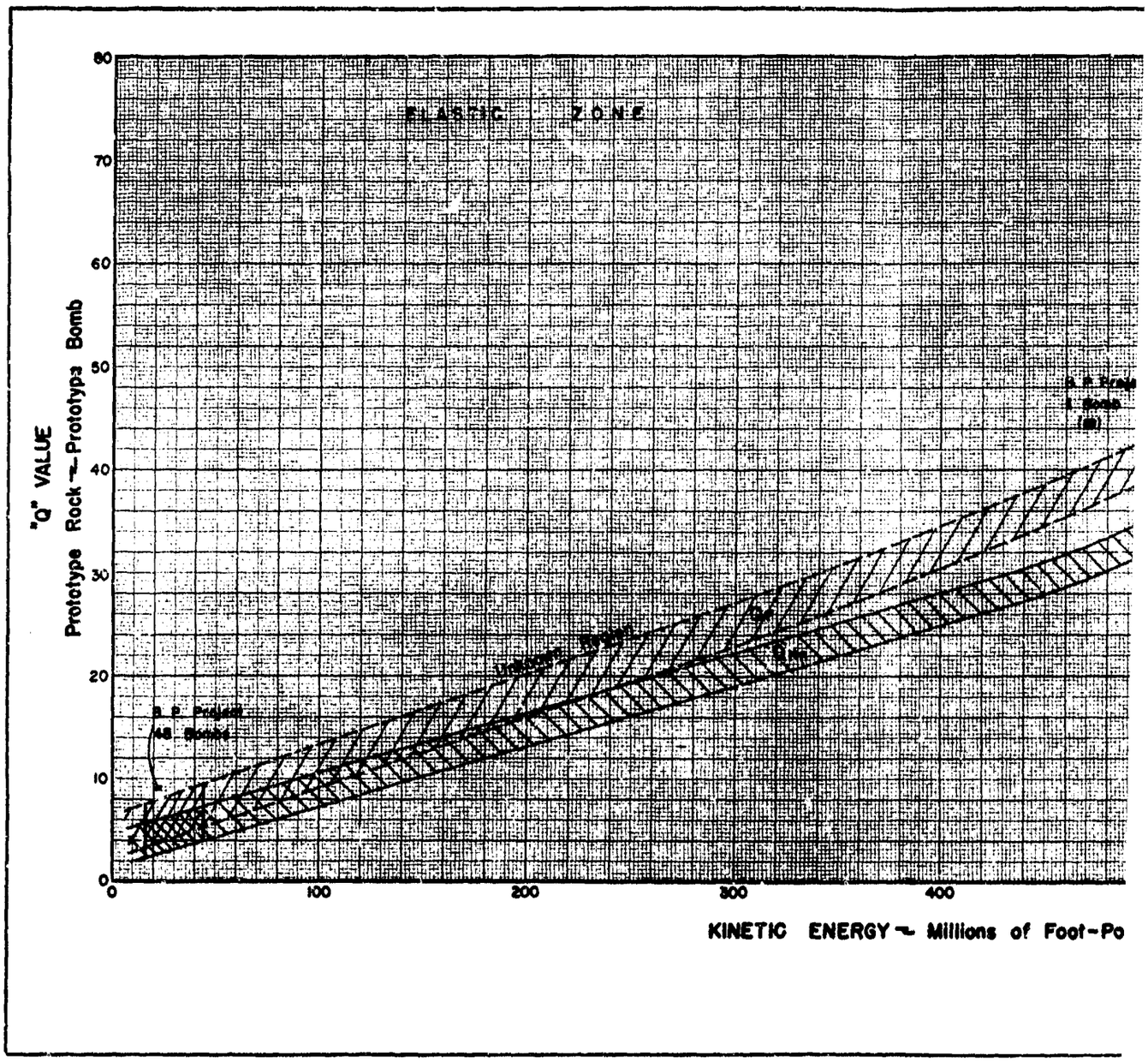
ELASTIC ZONE
"Q" VALUE
Prototype Rock — Prototype Bomb
0
10
20
30
40
50
60
70
80
0
100
200
300
400
KINETIC ENERGY — Millions of Foot-Po

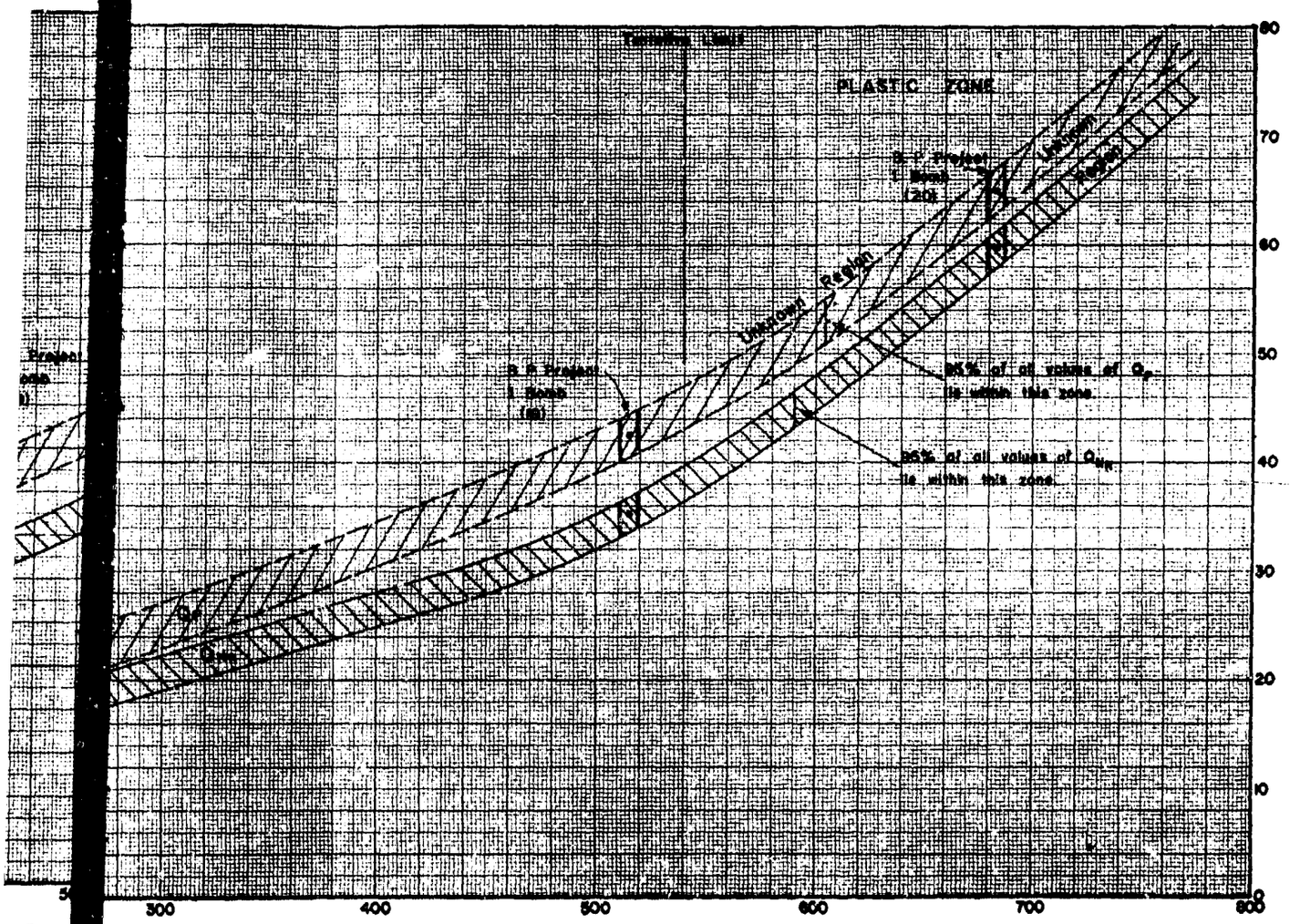

KINETIC ENERGY — Millions of Foot-Pounds

-BOMB PENETRATION PROJECT- C S M RESEARCH FOUNDATION, INC.	
Scale ——— Date 5-21-51 Fig. No. 203 By LSC	EXTRAPOLATION OF PENETRATION DATA

Fig. 203

2

Example 1

What normal penetration and what path length in Dakota sandstone is anticipated if a 25,000 SAP bomb is released at 38,000 feet above sea level at a true air speed of 350 miles per hour and strikes a target 2000 feet above sea level?

Solution

Enter Fig. 84 which records the striking velocity versus the height of target. From the curves for a 25,000 SAP bomb the striking velocity is 1500 feet per second. The impact energy is

$$KE = \frac{wV^2}{2x32.14}$$
$$= \frac{25{,}000 \cdot (1500)^2}{64.28}$$
$$= 388.92 \cdot 2.25 \cdot 10^6$$
$$= 762.57 \cdot 10^6 \text{ foot-pounds}$$

Enter Fig. 203 to obtain values of Q_P and Q_{NR}.

From Fig. 203, at $KE = 763 \cdot 10^6$

$$Q_P = 78.4, \quad Q_{NR} = 73.2$$

Substitute in the formula

$$N_R = \frac{1 - m_s}{2.484 m_s} \cdot \frac{N}{d} \cdot Q_{NR}$$

where

$$m_s = 0.287 \text{ (Dakota sandstone)}$$
$$\frac{1 - m_s}{2.484 m_s} = 1.0$$

The diameter of the 25,000 T28E4 Bomb is 32 inches, or 2.67 feet. The nose factor of the 25,000 SAP bomb, caliber radius head 1.56, is 1.0 (See Fig. 199).

$$N_R = 1.0 \cdot \frac{1.0}{2.67} \cdot 73.2 = 27.42 \text{ feet}$$

Also

$$P_{RM} = \frac{78.4}{2.67} = 29.36 \text{ feet}$$

Example 2

What normal penetration in rock X, which has a Poisson's ratio of 0.22 at a stress range of 5000 pounds per square inch, is possible with a bomb that has a caliber radius head of 1.8 and a diameter of 2.5 feet, and strikes with an impact energy of 300 million foot-pounds?

Solution

Normal penetration, from Formula 3, is

$$N_R = \frac{1 - m_x}{2.484\, m_x} \cdot \frac{N}{d} \cdot Q_{NR}$$

For an impact energy of 300 million foot-pounds, enter Fig. 203 to obtain the value of Q_{NR}. From the figure,

$$Q_{NR} = 20.6$$

The value of m_x in the formula (Poisson's ratio for rock X) is 0.22.

The diameter of the bomb, d, is 2.5 feet, and the nose factor, N, obtained from Fig. 199, is 1.07.

The normal penetration is

$$N_R = \frac{1 - 0.22}{2.484\,(0.22)} \cdot \frac{1.07}{2.5} \cdot 20.6$$

$$= 1.417 \cdot 0.428 \cdot 20.6$$

$$= 12.58 \text{ feet}$$

Example 3

At what range of altitude of bombing can a 1600 AP bomb be expected to give constant penetration if it is released at a true air speed of 250 miles per hour and strikes a target 5000 feet above sea level?

Solution

From the curves of Figures 201 and 202 it can be seen that values of Q_P and Q_{NR} are relatively constant for values of kinetic energy between 28 million foot-pounds and 36 million foot-pounds.

The striking velocity at these energy limits equals

$$KE = \frac{WV^2}{2g}$$

$$V = \sqrt{\frac{2g\ (KE)}{w}}$$

For $KE = 28 \cdot 10^6$

$$V = \sqrt{\frac{2 \cdot 32.14 \cdot 28 \cdot 10^6}{1600}}$$

$$V = 1061 \text{ feet per second}$$

and for $KE = 36 \cdot 10^6$

$$V = \sqrt{\frac{2 \cdot 32.14 \cdot 36 \cdot 10^6}{1600}}$$

$$V = 1203 \text{ feet per second}$$

Entering Fig. 80, which shows the altitude above target versus striking velocity for the 1600 AP bomb, it is found that for a true air speed of 250 miles per hour, the altitude above target giving these striking velocities will be

18,100 feet at 1061 feet per second

27,000 feet at 1203 feet per second.

After adding to these values the altitude of the target above sea level, 5000 feet, the range of altitude of bombing which will give constant penetration will be from

18,100 + 5000 = 23,100 feet to

27,000 + 5000 = 32,000 feet.

It is notable, from an inspection of Figs. 201 and 202, that at altitudes of bombing just over 32,000 feet a decrease in penetration in this target can be expected.

Example 4

How will the slope of the target surface affect the normal penetration, the path length, and the horizontal displacement of a 1600 AP bomb released at 27,000 feet above the target at a true air speed of 250 miles per hour? Assume that Poisson's ratio for the rock of this target area equals 0.24. As in example 3, the impact energy is 36 million foot-pounds, and the angle of fall at impact is 75 degrees.

Solution

The value of m_s, Poisson's ratio for this rock, is 0.24.

The diameter of the 1600 AP bomb is 1.167 feet and the nose factor, from Fig. 199, is 1.12.

From Figs. 201 and 202, Q_{NR} is 5.78 and Q_P is 7.15.

Using formulas (3) and (4)

$$N_R = \frac{1 - 0.24}{2.484\,(0.24)} \cdot \frac{1.12}{1.167} \cdot 5.78$$

$$= 1.27 \cdot 0.96 \cdot 5.78$$

$$= 7.08 \text{ feet}$$

$$P_{RM} = 1.27 \cdot 0.96 \cdot 7.15$$

$$= 8.75 \text{ feet}$$

It can now be shown that values for normal penetration and path length are independent of the slope of the target area, but that the magnitude of the horizontal displacement, X, (see Fig. 88), is partially dependent upon this slope. Although this horizontal displacement is difficult to establish analytically, a simple graphical solution, for three assumed slopes of target surface and based upon an angle of fall of 75 degrees, is illustrated in Fig. 204.

Figure 204b shows the bomb striking a level surface. For this condition,

Angle of Impact	= 75°
Normal Penetration, N_R	= 7.08 feet
Path length, P_{RM} (assumed as being a straight line from the point of impact to the nose position of the bomb at deepest penetration)	= 8.75 feet
Horizontal Displacement, X	= 5.15 feet

For up-dip bombing with an assumed inclination of the target surface equal to plus 8 degrees, shown in Fig. 204a, the quantities listed above become

Angle of Impact	= 83°
Normal Penetration, N_R	= 7.08 feet
Path Length, P_{RM}	= 8.75 feet
Horizontal Displacement, X	= 6.09 feet

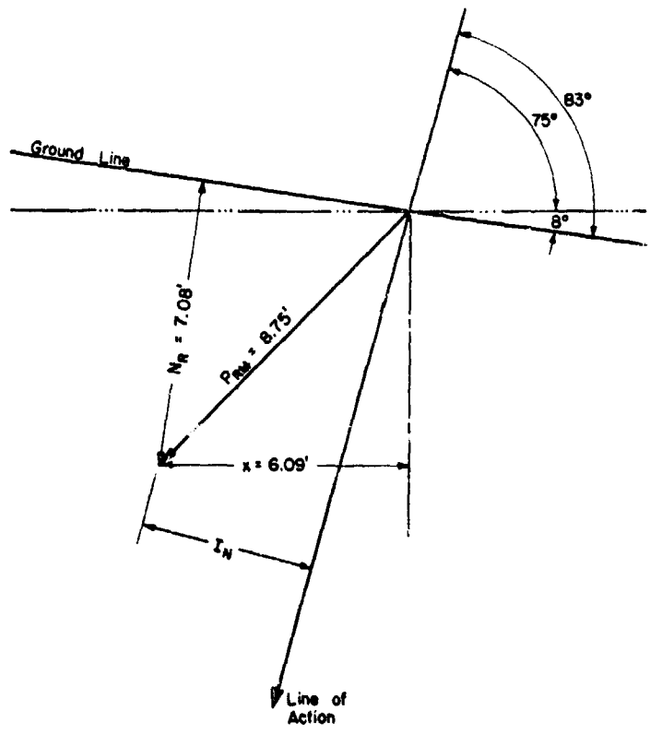

(a)

UP-DIP BOMBING

Angle of Fall 75°
Angle of Impact 83°

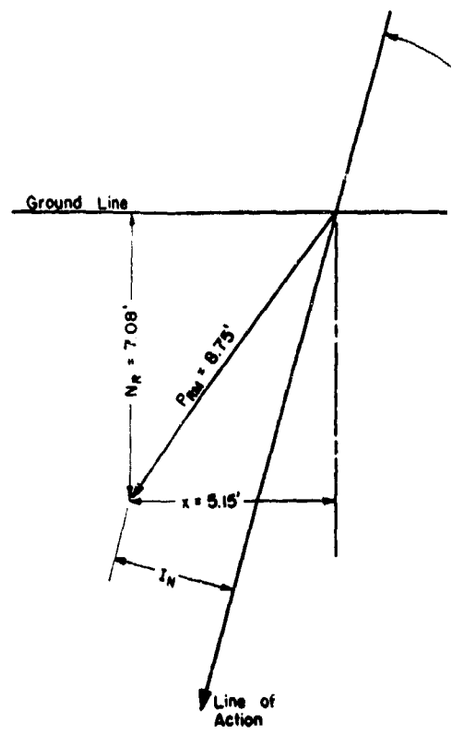

(b)

LEVEL SURFACE BOMBING

Angle of Fall 75°
Angle of Impact 75°

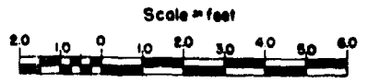

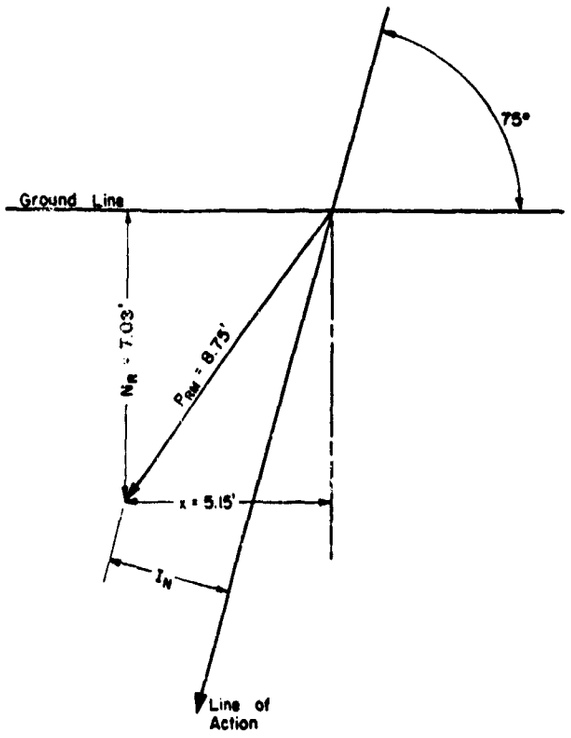

(b)

LEVEL SURFACE BOMBING

Angle of Fall 75°
Angle of Impact 75°

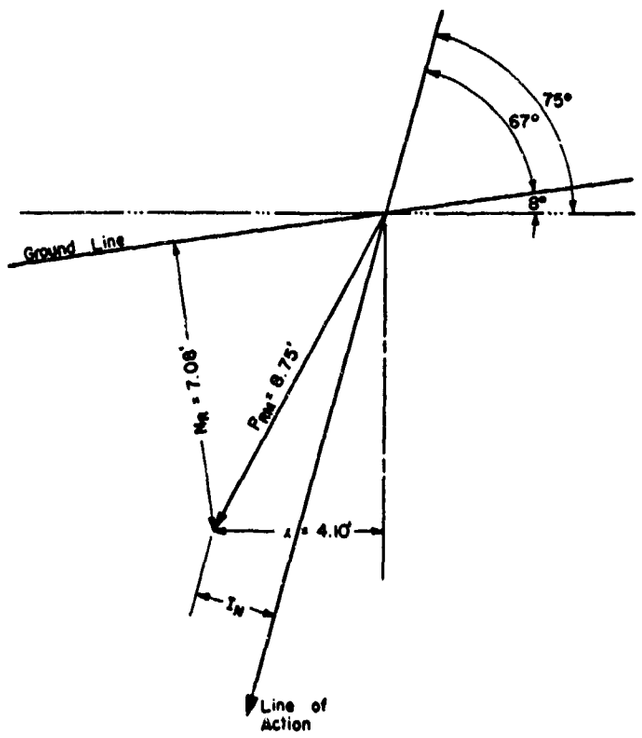

(c)

DOWN-DIP BOMBING

Angle of Fall 75°
Angle of Impact 67°

-BOMB PENETRATION PROJECT - C S M RESEARCH FOUNDATION, INC.	
Scale 1" = 3' Date 5-22-51 Fig. No. 204 By L.S.O.	HORIZONTAL DISPLACEMENT AS INFLUENCED BY THE INCLINATION OF THE TARGET SURFACE

Fig. 204

2

Thus, although the normal penetration and path length are unaffected, the horizontal displacement is increased by 0.94 feet.

In the third condition, Fig. 204c, for down-dip bombing with an assumed inclination of the target surface equal to minus 8 degrees, the quantities become

Angle of Impact	67
Normal Penetration, N_R	7.08 feet
Path Length, P_{RM}	8.75 feet
Horizontal Displacement, X	4.10 feet

As in up-dip bombing, normal penetration and path length are unaffected, but the horizontal displacement, based upon the value for level bombing, is decreased by 1.05 feet.

A more apparent measure of the effect of the inclination of the target surface is evident in the magnitude of the I_N values (see Fig. 204), the deviation of the bomb from the line of action. However, when applying the procedure to problems of the attack, or defense, of underground installations, the use of the value of the horizontal displacement, X, is logical and more applicable.

The following conclusions have been illustrated in example 4:

a) The horizontal displacement and the vertical deviation increase as the angle of impact increases; conversely, the horizontal displacement and vertical deviation decrease as the angle of impact decreases.

b) It is desirable, when planning an attack upon an enemy underground installation, to study the topography in advance of the bombing so that the effect of the horizontal displacement may be appraised.

c) When planning an attack against underground installations, it should be recognized that up-dip bombing is more apt to result in damage to the rear end of the bomb and, possibly, in lower-order detonation than would result with down-dip bombing.

The procedure followed in these examples has demonstrated the use of the Livingston Penetration Formula in studying and analyzing the penetration of bombs. Example 4, especially, stressed the importance of employing this knowledge in planning bombing attacks against enemy underground installations and in designing such installations for protection against enemy bombs. However, to fully appreciate the problem, the knowledge concerning penetration must be supplemented with an understanding of the effects of the explosion of the bomb. Of importance to this report, therefore, is the following section which deals with the overall effect of bombing on underground installations.

SECTION IV—THE EFFECT OF BOMBING ON UNDERGROUND INSTALLATIONS

1—Accuracy of Bombing

The accuracy of bombing is important to the study of damage to underground openings because of the ability of rock masses to withstand damage from explosions. It will be shown later in this section that there is an optimum area within which a bomb must strike in order to create a desired degree of damage to a particular underground structure. This effective region is rather small when the accuracy of the bombing attained in the field work is considered.

An analysis of the attained accuracy of the field bombs was made. Those bombs that were dropped without using the bombsight were not included in the study; the 25,000-pound SAP bombs were also omitted. The number of bombs included is, of course, too small to be entirely satisfactory in a statistical study. The trend is, however, indicative.

Combined results from both sites show that the mean error was 390 feet. The median error was 312 feet. A circle of 455-foot radius would include 68 per cent of all bombs dropped; a circle 850-foot radius would contain 95 per cent of all the hits. The range of accuracy was from 105 feet to 990 feet. On the basis of the limited number of bombs dropped, a circular area of 105-foot radius would not be hit. The AP and SAP bombs are equally accurate, and are more accurate than the GP bombs. The height of release up to 18,000 feet does not seem to affect the accuracy. The accuracy of all types of bombs released from above 18,000 feet decreased with increased height of release. The GP bombs were decidedly less accurate than the AP and SAP bombs, even at a low height of release.

If, as in these experiments, none of the bombs strike nearer than 105 feet to an underground tunnel, the error of bombing becomes the equivalent of adding at least 105 feet to the depth of rock cover. Thus, it would seem unprofitable to bomb underground fortifications with bombs of the type dropped in the Bomb Penetration Project unless the accuracy of bombing can be greatly improved.

2—Preliminary Discussion

The basic questions involved in planning the attack or defense of any underground installation are: "What is the best type of bomb to use against an enemy's structure?" and, "How may be best design an installation to resist damage from an enemy bomb?" The answers to these questions depend upon 1) the size of the structure, 2) the kind of rock in which it is located, 3) the thickness of rock covering the opening, 4) the penetration that the bomb will attain, and 5) the explosive force that can be brought to bear against the structure.

This section will discuss the relative merits of each bomb used in the course of the field work. By using data obtained from the Bomb Penetration Project in conjunction with data obtained from Series I and II Experiments[1], it is possible to evaluate both the effect of the penetration of the bomb and the effect of its explosive pay-load upon the structure. Although Series I and II Experiments pertain to Navajo sandstone and Unaweep granite and the Bomb Penetration experiments pertain to Dakota sandstone and Zuni granite, it may be presumed, at least for the purpose of illustrating the method of evaluation, that the two sandstones behave alike and the two granites behave alike. In practice, it is likely that the penetration of a bomb in Navajo sandstone would differ somewhat from the penetration of the same bomb in Dakota sandstone. It is also likely that the penetrations into the two granites would differ. Moreover, it is likely that the radii of damage for a given weight of explosive will differ from sandstone to sandstone and from granite to granite.

The curves constructed in the Series I and II Experiments were based upon an explosive confined within a borehole and in contact with the rock. The steel casing of the bomb will have two influences upon the explosion. First, the better confinement of the gaseous products of the explosion increases the explosion pressure and the energy of the explosion until the casing ruptures. Second, the influence of the steel casing decreases the energy available for breaking or compressing rock by an amount equal to the energy used in rupturing the case. Since these two influences oppose each other, and since the importance of each is unknown, the damage distances have not been adjusted. In other words, it has been assumed that the explosive contained in the bomb after penetration produces the same results as the explosive confined in a borehole. It is also assumed that detonation of the explosive takes place at the instant of maximum penetration.

Figure 205 tabulates various quantities pertaining to the rock and the bomb that are needed in predicting the damage to an underground opening. Quantities are given for sandstone and granite. The first column of the table gives the weight and type of bomb, the weight of explosive (here taken to be TNT), and the distance from the nose of the bomb to the center of mass of the explosive. The second column gives the height of release above the target. The third column, x, is the average of the x distances (see Figs. 88, 89, 107, and 108) for the bombs of the group considered. The average is weighted on the basis of the impact energies. The fourth column, y, is the weighted average of the vertical penetrations, for the groups. The fifth and sixth columns, x_a and y_a, are the adjusted values of the x's and y's of the two preceding columns. The adjustments are of two kinds: namely, an adjustment for the slope of the target, measured in the line of flight of the bomb, and an adjustment for the distance from the nose of the bomb to the center of gravity of the explosive. The two remaining columns, R_D and R_T are the distances at which "destruction" and "tension failure" occur when the explosive in the bomb is detonated in Navajo sandstone and in Unaweep granite. The distances are those given in the curves of Series I and II Experiments[2].

---

[1] Report of the Colorado School of Mines, Underground Explosion Tests, Series I and II Experiments, Protective Construction Branch, Office, Chief of Engineers, U. S. Army.

[2] Op. cit. Figure 89 gives the R_D and R_T distances for Navajo sandstone; Figure 204 gives distances for Unaweep granite

Sandstone

Type and Weight Explosive, and cg Explosive	Altitude ft	x	y	x_a	y_a	R_D	R_T
1600 AP	9200	2.59	4.05	0.03	3.19		
215 lbs TNT	18000	5.55	5.23	2.99	4.37	8.9	16.0
3.42 ft	30000	3.62	4.85	1.06	3.99		
2000 SAP	9200	2.24	3.38	-0.09	2.60		
556.5 lbs TNT	18000	2.57	3.72	0.24	2.94	11.8	21.2
3.11 ft	30000	2.04	3.62	-0.29	2.84		
2000 GP	7000	1.29	2.40	-0.93	1.66		
1045.6 lbs TNT	8700	1.84	1.90	-0.38	1.16		
2.96 ft	14000	1.77	2.35	-0.45	1.61	13.9	25.9
	18000	1.54	1.88	-0.68	1.14		
	30000	0.85	1.66	-1.37	0.92		

Granite

Type and Weight Explosive, and cg Explosive	Altitude ft	x	y	x_a	y_a	R_D	R_T
1600 AP	9200	4.60	6.61	2.04	5.76		
215 lbs TNT	18000	6.20	9.22	3.64	8.37	6.8	14.0
3.42 ft	30000	6.29	9.34	3.73	8.48		
2000 SAP	9200	4.71	5.03	2.38	4.25		
556.5 lbs TNT	18000	5.03	6.41	2.70	5.63	9.6	19.2
3.11 ft	30000	2.64	4.90	0.31	4.12		
25,000 SAP	18000	14.90	22.30	7.89	19.96		
3860 lbs TNT	26000	15.10	38.00	8.09	35.66	17.0	34.0
9.35 ft							

Fig. 205

Quantities Used in Predicting Damage to an Underground Opening

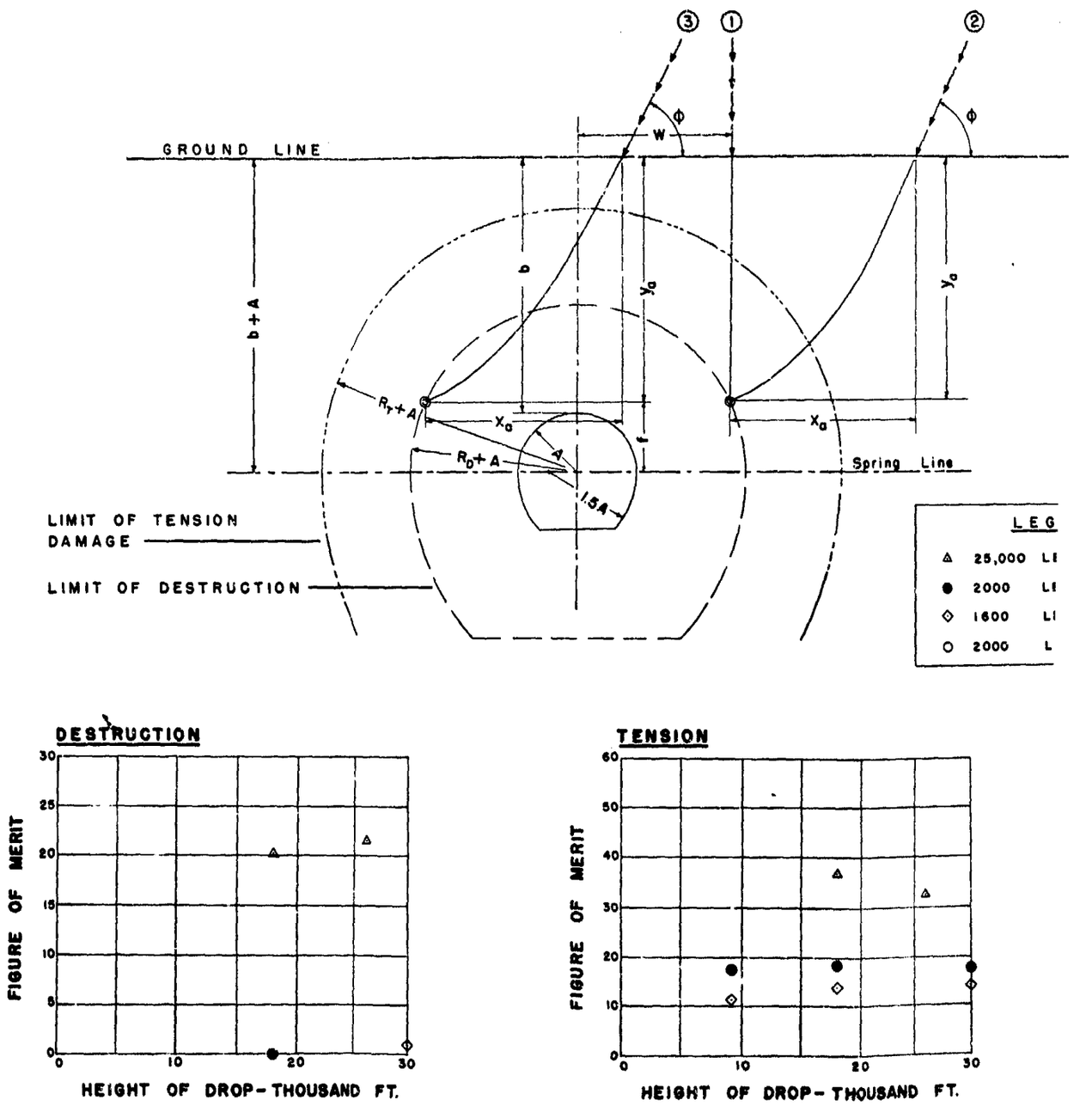

③ ① ②
GROUND LINE
W
Φ
b
b+A
y_a
R_T+A
X_a
R_D+A
A
1.5A
f
Spring Line
LIMIT OF TENSION DAMAGE
LIMIT OF DESTRUCTION
LEG
25,000
2000
1600
2000
DESTRUCTION
FIGURE OF MERIT
HEIGHT OF DROP-THOUSAND FT.
TENSION
FIGURE OF MERIT
HEIGHT OF DROP-THOUSAND FT.

GRANITE

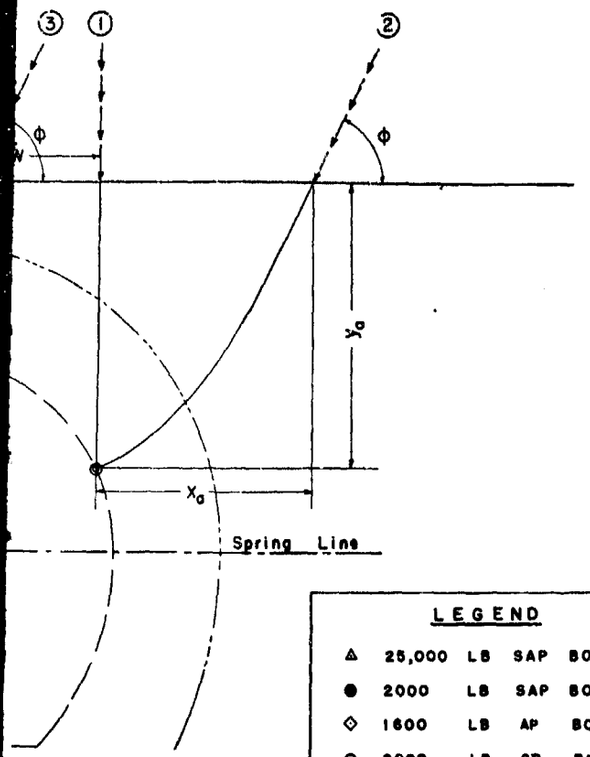

LEGEND			
△	25,000 LB	SAP	BOMB
●	2000 LB	SAP	BOMB
◇	1600 LB	AP	BOMB
○	2000 LB	GP	BOMB

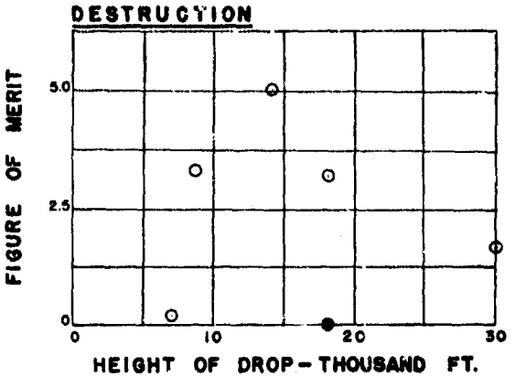

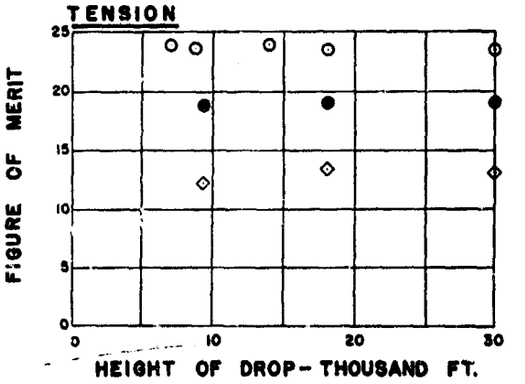

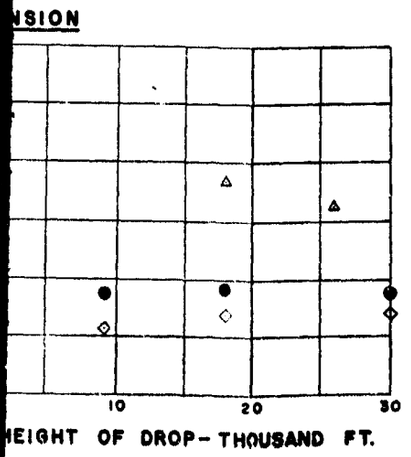

SANDSTONE

FORMULA:

$$W = \sqrt{(R+A)^2 - (b+A-y)^2}$$

$$W = \sqrt{(R+A)^2 - f^2}, \quad \text{where } f = b+A-y$$

— BOMB PENETRATION PROJECT — CSM RESEARCH FOUNDATION, INC.	
Scale _____ Date 4-25-51 Fig. No. 206 By FLS	DAMAGE TO AN UNDERGROUND OPENING BY VARIOUS BOMBS

Fig. 206

2

Figure 206 shows a tunnel located beneath a level surface. The symbols illustrated on the figure have the following meanings:

A = radius of arch of the tunnel, feet

b = depth of rock from the surface to the roof of the tunnel, feet

y_n = vertical penetration, in feet, adjusted for the inclination of the ground and for the location of the center of gravity of the explosive in the bomb

x_n = horizontal distance from the point of impact to the center of gravity of the explosive at maximum penetration, feet

A proper adjustment to locate the center of gravity of the explosive would depend upon the inclination of the bomb at the instant of detonation, but data concerning this inclination are not available. Accordingly, the x_n distance was arbitrarily computed by subtracting ¾ of the distance from the nose of the bomb to the center of gravity of the explosive from the x distance. The y_n distance was computed by subtracting ¼ of the distance from the nose of the bomb to the center of gravity of the explosive from the y figure.

W = figure of merit, or the horizontal distance on either side of the projected center line of the tunnel within which a given bomb dropped from a given altitude must strike in order to cause the required degree of damage. The formula for W^2 is

$$W^2 = (R + A)^2 - f^2$$

where

$$f = \text{the criterion quantity} = b + A - y_n$$

The criterion quantity is a measure of whether a given degree of damage is possible with a specified bomb at a specified height of drop. To cause the damage, f must be less than or equal to (R + A).

Figure 206 shows the three ways a bomb can be dropped to damage a tunnel. The first is to drop the bomb so that the line of flight is parallel to the center line of the tunnel; the second is to drop the bomb so that the line of flight is at right angles to the center line, with the bomb striking short of center line; the third is to drop the bomb with the line of flight at right angles to the center line so that the bomb overshoots the target and comes to rest beyond it.

3—Comparison of Various Bombs for Damage to Underground Openings

The following arbitrary definitions are used in comparing the merits of the several bombs.

Standard Tunnel: A standard tunnel is a horseshoe-shaped opening 6 feet high. The radius of the arch is 3 feet; the radius of the sides below spring line is 4½ feet. The invert is flat. These dimensions were selected as giving a tunnel of minimum practical size. The tunnel section drawn in Fig. 206 is a standard tunnel.

Standard Depth of Cover: The standard depth of cover for a particular kind of rock is a thickness of the rock overlying a standard tunnel such that a 2000-pound SAP bomb loaded with TNT and dropped from 18,000 feet above the target causes damage defined in Series I and II Experiments as "destruction" if the bomb comes to rest vertically above the centerline of the tunnel.

From Fig. 206 and from the algebraic expressions, it is evident that the standard depth of cover in a hypothetical Navajo-Dakota sandstone is

$$b_s = R_D + y_s = 11.8 + 2.94 = 14.74 \text{ feet}$$

where

b_s = the standard depth of cover.

The table, Fig. 207, compares the various bombs as to their relative merits in causing destruction in sandstone. The figures of merit for the destruction case in sandstone are also plotted in Fig. 206. Only destruction damage to the roof of the tunnel is possible for the assumed configuration of a standard tunnel covered by 14.74 feet of sandstone, and then only with the 2000-pound SAP bomb from 18,000 feet if it strikes on the center line, or with the GP bombs striking as shown by the figure of merit. None of the AP bombs will do the job, chiefly because they do not carry enough explosive. The GP bombs will cause destruction because of their comparatively high explosive content. However, because rupture of the casings occurred if bombs were dropped above 8700 feet, it would be better to release the bombs from 7000 feet in order to prevent low-order detonation caused by rupture of the casing. Because the figure of merit is also the width of the strip within which the bomb must fall when the line of flight is in the same direction as the center line, a GP bomb dropped from 7000 feet must hit within 0.2 feet left or right of center. If the aircraft approaches at right angles to the center line, the bomb must strike within 1.13 and 0.73 feet short of the center line.

The table, Fig. 208, sets forth the same type of data for the case where tension damage to the roof of the tunnel is to be caused. All the bombs will cause this type of failure; the GP bomb from 7000 feet is again the best bomb because of its figure of merit. The greater the width of the strip, as determined by the figure of merit, the greater the chance of bombs falling within the required strip.

Assume that a bomber is approaching this tunnel in the same direc-

SANDSTONE - DESTRUCTION
A = 3.00 ft, b = 14.74 ft

Type, Weight Explosive, cg Explosive, R_D	Altitude	R_D+A	$(R_D+A)^2$	x_a	y_a	f	f^2	W_D^2	W_D	W_D+X	W_D-X
1600 AP	9200			0.03	3.19	14.55*	—	—	—	—	—
215 lbs TNT	18000	11.9	141.61	2.99	4.37	13.37*	—	—	—	—	—
3.42 ft R_D = 8.9 ft	30000			1.06	3.99	13.75*	—	—	—	—	—
2000 SAP	9200			-0.09	2.60	15.14*	—	—	—	—	—
556.5 lbs TNT	18000	14.8	219.04	0.24	2.94	14.80	219.04	0	0	0.24	-0.24
3.11 ft R_D = 11.8 ft	30000			-0.29	2.84	14.90*	—	—	—	—	—
2000 GP	7000			-0.93	1.66	16.08	258.57	0.04	0.20	-0.73	1.13
1045.6 lbs TNT	8700			-0.38	1.16	16.58	274.90	10.71	3.27	2.89	3.65
2.96 ft R_D = 13.9 ft	14000	16.9	285.61	-0.45	1.61	16.13	260.18	25.43	5.04	4.59	5.49
	18000			-0.68	1.14	16.60	275.56	10.05	3.17	2.49	3.85
	30000			-1.37	0.92	16.82	282.91	2.70	1.64	0.27	3.01

* Since $A + b - y = F$ is greater than $(R_D + A)$, these bombs will not produce any destructive damage.

Fig. 207

Figure of Merit for Various Bombs to Give Destruction in Sandstone

SANDSTONE - TENSION

A = 3.00 ft b = 14.74

Type, Weight Explosive, cg Explosives, R_T	Altitude	R_T+A	$(R_T+A)^2$	x_a	y_a	f	f^2	W_T^2	W_T	W_T+X	W_T-X
1600 AP	9200			0.03	3.19	14.55	211.70	149.30	12.22	12.25	12.19
215 lbs TNT	18000	19.0	361.0	2.99	4.37	13.37	178.76	182.24	13.50	16.49	10.51
3.42 ft R_T = 16.0	30000			1.06	3.99	13.75	189.06	171.94	13.11	14.17	12.05
2000 SAP	9200			-0.09	2.60	15.14	229.22	356.42	18.88	18.79	18.97
556.5 lbs TNT	18000	24.2	585.64	0.24	2.94	14.80	219.04	366.60	19.15	19.39	18.91
3.11 ft R_T = 21.2	30000			-0.29	2.84	14.90	222.01	363.63	19.07	18.78	19.36
2000 GP	7000			-0.93	1.66	16.08	258.57	576.64	24.01	23.08	24.94
1045.6 lbs TNT	8700			-0.38	1.16	16.58	274.89	560.32	23.67	23.29	24.05
2.96 ft R_T = 25.9	14000	28.9	835.21	-0.45	1.61	16.13	260.18	575.03	23.98	23.53	24.43
	18000			-0.68	1.14	16.60	275.56	559.65	23.66	22.98	24.34
	30000			-1.37	0.92	16.82	282.91	552.30	23.50	22.13	24.87

Fig. 208

Figure of Merit for Various Bombs to Give Tension in Sandstone

GRANITE - DESTRUCTION

A = 3.00 ft b = 15.23 ft

Type, Weight Explosive, cg Explosive, R_D	Altitude	R_D+A	$(R_D+A)^2$	x_a	y_a	f	f^2	W_D^2	W_D	W_D+X	W_D-X
1600 AP	9200			2.04	5.76	12.47*	—	—	—	—	—
215 lbs TNT	18000	9.8	96.04	3.64	8.37	9.86*	—	—	—	—	—
3.42 ft R_D = 6.8	30000			3.73	8.48	9.75	95.06	0.98	0.99	4.72	2.74
2000 SAP	9200			2.38	4.25	13.98*	—	—	—	—	—
556.5 lbs TNT	18000	12.6	158.76	2.70	5.63	12.60	158.76	0	0	2.70	-2.70
3.11 ft R_D = 9.6	30000			0.31	4.12	14.11*	—	—	—	—	—
25,000 SAP	18000	20.0	400.00	7.89	19.96	-1.73	2.99	397.01	19.92	27.81	12.03
3860 lbs TNT	26000			8.09	35.66	-17.43	303.80	96.20	9.81	17.90	1.72
9.35 ft R_D = 17.0											

* Since A + b - y = F is greater than (R_D+A), these bombs will not produce any destructive damage

Fig. 209

Figure of Merit for Various Bombs to Give Destruction in Granite

GRANITE - TENSION

A 3.00 ft b 15.23 ft

Type, Weight Explosive, cg Explosives, R_T	Altitude	R_T+A	$(R_T+A)^2$	x_a	y_a	f	f^2	W_T^2	W_T	W_T+X	W_T-X
1600 AP	9200			2.04	5.76	12.47	155.50	133.50	11.55	13.59	9.51
215 lbs TNT	18000	17.0	289.00	3.64	8.37	9.86	97.22	191.78	13.85	17.49	10.21
3.42 ft $R_T = 14.0$	30000			3.73	8.48	9.75	95.06	193.94	13.93	17.66	10.20
2000 SAP	9200			2.38	4.25	13.98	195.44	297.40	17.24	19.62	14.86
556.5 lbs TNT	18000	22.2	492.84	2.70	5.63	12.60	158.76	334.08	18.28	20.98	15.58
3.11 ft $R_T = 19.2$	30000			0.31	4.12	14.11	199.09	293.75	17.14	17.45	16.83
25,000 SAP	18000	37.0	1369.00	7.89	19.96	-1.73	2.99	1366.01	36.96	44.85	29.07
3860 lbs TNT	26000			8.09	35.66	-17.43	303.80	1065.20	32.64	40.73	24.55
9.35 ft $R_T = 34.0$											

Fig. 210

Figure of Merit for Various Bombs to Give Tension in Granite

tion as the center line. The direction of center line is assumed to be known to the pilot. The plane is carrying 2000-pound GP bombs and will release them from a height of 7000 feet above the level ground surface. All bombs in order to create tension damage must fall within a strip 24.01 feet on either side of the center line, or a strip 48.02 feet wide. If the aircraft approaches at right angles to the center line, all bombs can fall short 23.08 feet, or overshoot center line 24.94 feet on a total strip width of 48.02 feet. In general, then, if enough bombs to provide a statistical sample are dropped, it will not matter what the direction of flight is.

The tables, Figs. 209 and 210, give the same sort of information for a standard tunnel located in granite. Here the standard depth of cover is:

$$9.6 + 5.63 = 15.23 = b,$$

where

$$y_s = 5.63 \text{ feet.}$$
$$R_D = 9.6 \text{ feet}$$

To create destructive damage to this tunnel, a 1600-pound AP bomb from a height of 30,000 feet, a 2000-pound SAP from a height of 18,000 feet, or a 25,000-pound SAP bomb must be used. (See Fig. 209.) It will be seen that a deep-penetrating bomb, such as the 25,000-pound SAP, might, under some circumstances, penetrate too deeply to do any damage. To create tension damage, any of the bombs listed in Fig. 210 will serve the purpose.

4—Attack or Defense of Any Underground Opening

The methods used in the above section can be applied to select the best bomb to drop against a given underground installation, or, conversely, to determine how deep a structure must be located in order to withstand a given bomb. The formula for calculating the figure of merit as given on Fig. 206 is general, and may be applied to any tunnel in any rock and for any bomb. One must, however, know the x_s and y_s values and the R_D or R_T distances for the particular bomb and the particular rock.

Example 1.

Let us consider what type of bomb to use in attacking the 0.2 scale tunnel of the Underground Explosion Test Program. This tunnel is located in the Navajo sandstone member of the Glen Canyon series of rocks east of Castledale, Utah. The following data apply to this opening:

Radius of arch, $A = 3.5$ feet

Depth of cover, $b = 21$ feet

For destructive damage we apply the criterion

$$f = b + A - y_s = 24.5 - y_s.$$

This must be less than or equal to $R_D + A$. For an AP bomb carrying 215 pounds of TNT, Fig. 205 shows $R_D = 8.9$ feet. Therefore

$$24.5 - y_n = 8.9 + 3.5$$

or

$$y_n = 24.5 - 12.4 = 12.1$$

Reference to Fig. 205 shows that the largest value, y_n, for the 1600-pound bombs is 4.37 feet from an altitude of 18,000 feet. Therefore, AP bombs will not produce any destructive damage to the tunnel.

For an SAP bomb carrying 556.5 pounds of TNT, the R_D distance is 11.8 feet. Therefore, y_n for a 2000-pound bomb must be at least

$$y_n = 24.5 - (11.8 + 3.5) = 9.2 \text{ feet.}$$

No SAP bombs will penetrate to this depth, so this bomb is also unsuitable.

For a GP bomb carrying 1045.6 pounds of TNT, $R_D = 13.9$. Therefore

$$y_n = 24.5 - (13.9 + 3.5) = 7.1 \text{ feet.}$$

Since these bombs will not penetrate the required distance, they, too, are unsuitable.

If these are the only bombs available, we cannot expect to cause destructive damage to the 0.2 scale tunnel. However, we know that between tension damage and destructive damage there is a range of heavy damage, the so-called combined shear and tension damage, which grades into the destructive damage. Reference to Fig. 89 of the Series I and II Report shows that the R for combined shear and tension is as follows for the three bombs considered:

1600 AP 215 lbs TNT = 11.3 feet

2000 SAP 556 lbs TNT = 15.2 feet

2000 GP 1046 lbs TNT = 18.2 feet.

Applying the criterion quantity for the 1600 AP bomb, we see that:

$$y_n = 24.5 - (11.3 + 3.5) = 9.7 \text{ feet.}$$

The AP bomb, is therefore, not suitable.

For the 2000 SAP bomb,

$$y_n = 24.5 - (15.2 + 3.5) = 5.8.$$

None of the SAP bombs are suitable.

For the GP bombs,

$$y_n = 24.5 - (18.2 + 3.5) = 2.8.$$

The GP bomb approaches, but does not quite reach, the necessary penetration. It would, therefore, cause damage between combined shear and tension and tension damage, but not between combined shear and tension and destruction.

Reference to Fig. 205 shows that the deepest penetrating GP bomb will be one dropped from 7000 feet and attaining a penetration of the center of gravity of the explosive, $y_a = 1.66$ feet. To calculate the figure of merit for this bomb in tension, we proceed as follows:

$$R_T \quad 25.9; \qquad A = 3.50; \qquad R_T + A = 29.40.$$

$$f = b + A - y_a = 21.00 + 3.50 - 1.66 = 22.84.$$

Since f is less than $R_T + A$, tension damage is possible with this bomb from this altitude, if the impact is within the figure of merit:

$$W^2 = (29.40)^2 - (22.84)^2 = 342.70$$

$$W = 18.51 \text{ feet,}$$

or for cross bombing if the bomb falls short of the projected center line

$$18.51 + (-0.93) = 17.58 \text{ feet,}$$

or overshoots the center line

$$18.51 - (-0.93) = 19.44 \text{ feet.}$$

This discussion concerning a relatively shallow tunnel illustrates the inherent strength of an opening in rock for defense against bombing.

Example 2.

From a different point of view, it may be of interest to calculate what weight of TNT can be exploded near a tunnel without causing any damage. The 1.0 scale tunnel of the Underground Explosion Tests has an arch radius of about 15.5 feet and is covered by 60 feet of Navajo sandstone. Assume one bomb is dropped and strikes 100 feet short of the projected center line of the tunnel. The bomb penetrates such a distance that the center of gravity of its explosive content penetrates to the spring line of the tunnel. Assume further that the angle of impact and angle of fall are equal and are 70 degrees, and that the bomb continues on this angle until it comes to rest and detonates. What maximum weight of explosive may be contained in the bomb if the tunnel is to suffer no tension damage?

The conditions given are:

$$A + b = 75.5 \text{ feet}$$

$$y_a = 75.5 \text{ feet}$$

$$x_a = 75.5 \cot 70^\circ = 75.5 \times 0.364 = 27.5 \text{ feet}$$

The figure of merit, W, for the bomb is, therefore,

$$W + x_a = 100 \quad \text{or} \quad W = 72.5 \text{ feet}$$

Because this is measured from the center of the tunnel, the thickness of rock between the explosion and the wall of the tunnel is:

$$72.5 - 15.5 = 57 \text{ feet}$$

Entering the curves in Fig. 89 of the Series I and II Report, we find that R is 57 feet, and is the tension distance for 17,500 pounds of TNT. Referring to the destructive line on the same figure, we see that 57 feet is the destructive distance for 310,000 pounds of TNT.

Suppose, however, that the same bomb strikes 27.5 feet short of the projected center line. This means that the bomb will perforate the tunnel and explode inside. This illustrates the critical influence of bombing accuracy upon damage to an underground structure.

Example 3.

What must be the minimum depth of granite cover in order to protect an arched opening with a 50-foot span from damage by a 25,000-pound bomb dropped from 26,000 feet and striking at the optimum point?

The optimum point for bombing with the direction of the tunnel would be a strike on the projected center line. For cross bombing, the point would be short of center line by the x_s distance.

Suppose the line of flight to be parallel to the center line of the tunnel and the bomb is to fall directly on the center line and not deviate right or left of this line during its downward course.

Then

$$W^2 = (R_T + A)^2 - f^2$$

where

$$f = A + b - y_s.$$

The 25,000-pound SAP bomb contains 3860 pounds of TNT. The R_T distance from Fig. 205 is equal to 34 feet. The radius of the tunnel arch is 25 feet. Therefore,

$$R_T + A = 34.0 + 25.0 = 59 \text{ feet}$$

Because the bomb struck on center line, the center of gravity of the explosive must not be closer to the spring line of the tunnel than 59 feet. Reference to Fig. 205 shows that the bomb will penetrate to a distance $y_s = 35.66$ feet.

The minimum depth from surface to the center of the tunnel should then be:

$$35.66 + 59 = 94.66 \text{ feet.}$$

This calculated depth should be increased to provide a margin of safety. Good practice requires that a safety factor be based upon a knowledge of the effect of the static forces acting upon the opening, upon the chance of the enemy's having an improved bomb, and upon the probability of a bomb penetrating deeper than assumed in the calculation.

SECTION V—CONCLUSIONS

1—The Livingston Penetration Formula

The depth of penetration of various types and sizes of bombs into rock masses can be predicted by means of the Livingston Penetration Formula

$$P = \frac{1 - m_x}{2.484\, m_x} \cdot \frac{N}{d} \cdot Q$$

If it is desired to compute the path length in rock to the point of maximum normal penetration, the formula takes the form

$$P_{RM} = \frac{1 - m_x}{2.484\, m_x} \cdot \frac{N}{d} \cdot Q_P$$

If it is desired to compute the normal penetration in rock, the formula takes the form

$$N_R = \frac{1 - m_x}{2.484\, m_x} \cdot \frac{N}{d} \quad Q_{NR}$$

where

P_{RM} = path length of any given bomb in rock X, measured to the point of maximum normal penetration, feet

Q_P = path length of a 1.0-foot-diameter prototype bomb in a prototype rock, feet (See Fig. 202)

N_R = the maximum depth of penetration measured normal to the rock surface of any given bomb in rock X, feet

Q_{NR} = the normal penetration of a 1.0-foot-diameter prototype bomb in a prototype rock, feet. (See Fig. 201)

m_x = Poisson's ratio of rock X at 5000 pounds per square inch, the stress range at which failure occurs in simple compression for Dakota sandstone, the prototype rock.

N = the nose factor. (See Fig. 199)

d = the diameter of the bomb, feet.

The Livingston Penetration formula differs in several respects from other formulas for penetration. In part, the difference may be due to the massive nature of the target which influences the stress distribution in the medium and the manner of rock failure . In part, the difference may be due to the stress range which influences the stress distribution in the medium and the manner of rock failure. And in part, the difference may be due to the difference in the physical and elastic properties of the target material—such as the difference between soil and rock, or the difference between reinforced concrete and rock.

The first term of the Livingston Penetration Formula

$$\frac{1 - m_x}{2.484\, m_x}$$

has been referred to as "the rock factor." The constant 2.484 is present because the formula has been set up for a prototype rock. The prototype rock is Dakota sandstone which fails in simple compression at 5000 pounds per square inch and which has a value of Poisson's ratio equal to 0.287 at failure. Any rock that has the same value of Poisson's ratio and fails at 5000 pounds per square inch in simple compression is a prototype rock.

The rock factor is a measure of the lateral stress in the medium, and the lateral stress is a function of Poisson's ratio and of the axially applied force. Neither the axial force or Poisson's ratio is a constant. Moreover, Poisson's ratio is dependent upon the stress range (See Fig. 68). Therefore it is necessary to establish a prototype stress range and a prototype rock. The prototype rock has been referred to repeatedly as Dakota sandstone, but perhaps it should be stated that the prototype Dakota sandstone is from the Putney Mesa sandstone bombing site. For, it is probable that the elastic properties of the Dakota sandstone formation vary widely, depending upon the environment of deposition and upon the lithology of the beds.

By means of the rock factor term it is possible to predict penetration in any type of rock from any part of the world. The mistake should not be made, as is commonly made, of assuming a constant rock factor for each family of rocks such as granite, limestone, basalt, sandstone, or shale. Instead, the rock factor may vary as greatly within a given family of rocks such as granite, as between families—for example between granite and sandstone. In order to predict penetration accurately, specimens of the rock in which penetration is desired should be tested in the laboratory to obtain m_x, Poisson's ratio at the prototype stress range.

A significant feature that is apparent from analysis of the rock factor is that penetration decreases as m_x increases. Moreover, the theoretical maximum value of Poisson's ratio is 0.5. If the theoretical maximum value of m_x is substituted in the rock factor term, the theoretical minimum value of the rock factor is obtained and equals,

$$\frac{1.0 - 0.5}{2.484 \cdot 0.5} = 0.40$$

Inasmuch as the value of the rock factor for the prototype rock is 1.00, it follows that perhaps some type of rock may be found that is superior to Dakota sandstone for resistance against bombing.

The second term in the Livingston Penetration Formula

$$\frac{N}{d}$$

involves the nose factor and the bomb diameter. Evidence regarding both the nose factor and the bomb diameter was obtained in the laboratory using techniques of photoelasticity. It was determined (See Part E, Sec-

tion V, Item 4) that the form of the shear contours in the medium depends upon the shape of the nose, and that a sharp nose such as that of a 25,000 SAP bomb or of a 1600 AP bomb results in a wedging action that parts the medium and relieves the stress in front of the nose. It was shown also (See Part F, Section 1, Items 2c and 2d) that the degree of fragmentation of Dakota sandstone and of Zuni granite decreases as the sharpness of the nose increases.

Perhaps at some future time it may be possibe to determine the nose factor N either from photoelastic studies or by measuring the area of new surface produced. It was necessary in this work to determine the nose factor from the field data by constructing prototype rock—prototype bomb curves for each of the four types of bombs dropped in the tests. Because of the comparatively small number of bombs of each type dropped, the nose factors presented in this report (See Fig. 199) should be considered to be tentative values.

The second term of the Livingston Penetration Formula states that penetration varies inversely as the diameter of the bomb. This relation was determined from photoelastic studies and is at variance with the sectional pressure formulas in which penetration varies inversely as the square of the diameter of the bomb. The effect of an increase in the diameter of a bomb upon the rock is to increase that volume of rock under stress in proportion to the increase in diameter. In any given type of rock and at any given value of impact energy, the fragmentation of the muck pile increases as the diameter increases. Thus the effect of an increase in the diameter of a bomb upon the manner of rock failure is to increase the rate of energy consumption per unit volume of rock.

In the model bombing experiments conducted in the Barodynamics Laboratory of the Mining Department of the Colorado School of Mines (See Part E, Section 1, Item 3) in which sectional pressure and sectional density were the only variables it was shown that penetration is independent both of sectional pressure and of sectional density at a given impact energy. If the Colorado School of Mines apparatus had not been developed, it would have been impractical, if not impossible, to vary the sectional pressure or the sectional density of a projectile at constant impact energy. Accordingly, the true relations between penetration and bomb diameter would not have been discovered if the apparatus had not been developed.

The third and final term in the Livingston Penetration Formula is called here a "Q" term. "The "Q" term expresses the path length, or the normal penetration of a prototype bomb in a prototype rock. A prototype bomb is a bomb 1.0 foot in diameter that has the same nose shape as a 2000 SAP bomb. Values of Q_{NR} may be obtained from the graphs, Figs. 201 and 203, and are used to compute normal penetration. Values of Q_P may be obtained from the graphs, Figs. 202 and 203, and are used to compute path length. Rather than present similar curves giving values to Q to be used in computing vertical penetration, a procedure similar to that presented in Part F. Section III, Item 7, Example 4 should be used. Using the recommended procedure, values of the vertical deviation I_N, values of the horizontal displacement X, and values of the vertical

penetration Y (See Fig. 88) may be obtained, and these values will take into account variations in the inclination of the target surface.

Values of "Q" depend upon the impact energy and have been determined from the field results after eliminating the rock factor, the nose factor, and the bomb diameter factor. The "Q" term thus expresses empirically two factors that cannot be separated without further fundamental research. One of these factors is the decrease in kinetic energy of the bomb between impact and maximum penetration. The other is the increased resistance to peneration with depth. The increased resistance to penetration with increased depth was measured in a gelatin model material at various stages of penetration (See Fig. 169, and Part C, Section V, Item 3). Perhaps through continued research it may be possible to state the "Q" term theoretically rather than empirically.

The following conclusions may be stated relative to those objectives of the Bomb Penetration Project listed on page 2 that are closely related to the Livington Penetration Formula.

5) *Is penetration a function of the sectional pressure or of the sectional density of a bomb?*

Penetration of projectiles in rock masses is independent of both sectional pressure and of sectional density. Penetration varies inversely as the diameter of a bomb and is a function of the impact energy. The "Q" term in the Livingston Penetration Formula includes the effect of the impact energy in combination with the effect of increased resistance to penetration with increased depth.

6) *Does the resistance to penetration increase with depth?*

Resistance to penetration depends upon the lateral stress in the medium. The lateral stress acts at right angles to the direction of maximum principal stress. The lateral stress is induced by an axial load tangent to the path of the bomb and to a horizontal component of stress that depends upon Poisson's ratio and upon the weight of the rock mass. The horizontal component increases with depth, but the lateral stress decreases as the impact energy of the bomb is dissipated. The net effect is to increase the strength of the rock beyond that indicated by a simple compression test, but the increased strength is not a simple function of the increase in depth. The "Q" term in the Livingston Penetration Formula includes the effect of increased resistance to penetration with increase in depth.

13) *Do all standstones or granites behave alike? How can the results of the Bomb Penetration Project be applied to similar rocks?*

The behavior of a rock depends upon the physical and elastic properties of the rock rather than the petrographic classification. Some sandstones, particularly those cemented by silica or by iron oxides, may behave in the same manner as an igneous rock such as granite. The variation in

physical and elastic properties may be as great within a given rock family as between different rock families.

By means of the first term of the Livingston Penetration Formula, "the rock factor," it is possible to compute the depth of penetration in an unknown rock if Poisson's ratio at a prototype stress range of 5000 pounds per square inch is measured using standard techniques described in the section of the report dealing with the determination of the elastic "constants" by the static method (see Part A, Section IV, Item 11).

10) *What geologic and topographic conditions minimize the penetration of a bomb into rock and provide the maximum protection against bombing?*

A type of rock that has a high value of Poisson's ratio at a low stress range is desirable because of its high resistance to penetration, and because of the resulting abrupt vertical deviation of the path of the bomb which may cause bending or rupture of the bomb case. A type of rock that absorbs a large amount of energy before rupture is desirable because it will cause rebound and poor coupling for the explosive blast. A type of rock that contains an abundance of flat-lying natural planes of weakness is desirable because planes of weakness so oriented increase the vertical deviation of the bomb and decrease the vertical penetration. Rocks that are highly weathered or hydrothermally altered and traversed by numerous faults and fissures should be avoided.

A very rough topography and a surface containing large boulders and a minimum of overburden is desirable, because these features all tend to cause a bomb to either to ricochet or to deviate greatly both in a horizontal and a vertical plane.

2—Effect of the Bomb Upon the Rock

Penetration is the result of rock failure. The manner of rock failure depends upon the stress distribution in the medium and upon the physical and elastic properties of the medium. Failure of a rock mass is characterized by three zones of failure—the zone of crushing, the zone of shearing, the zone of tension slabbing—and a stage of rock burst. These zones are illustrated in Fig. 184 and described in detail in Part F. Section I. The attitude of the planes of failure coincide with the three directions of principal stress in the medium. Field evidence indicates that the rock fails predominantly in tension as a result of a constant stress-difference between the maximum and the minimum principal stresses. Strain energy is imparted to the medium between each of a series of stages of rupture. The footwall of the path of the bomb becomes a rock burst zone as the strain energy is released from the zone of maximum compression.

Failure of a rock mass and the penetration of a bomb proceed concurrently. Rock failure does not take place far ahead of the nose of the bomb. The zone of crushing (See Fig. 184) is the deepest zone of failure, and as the depth of penetration increases, the thickness of the zone of crushing decreases. The decrease in thickness of the crushed zone is due both to the decrease in energy of the bomb and to the increase in strength of the rock. It is evident from a comparison of the distribution of stress in the medium (See Fig. 164) and the distribution of the zones of failure

(See Fig. 184), that rock failure occurs predominately within the region shown by photoelastic studies to be above the neutral axis.

If instead of penetrating into a semi-infinite solid free from openings, a bomb should penetrate into a rock mass in which tunnels had been driven, or into a thick concrete slab, then the manner of failure of the rock mass would differ from that observed in the Bomb Penetration Tests. The free face at the tunnel opening or the free face at the underneath side of the thick slab would be a potential zone of failure. Scabbing of the slab or scabbing of the tunnel would occur at what might be referred to as the "critical distance" (which is not a constant distance but depends upon the kinetic energy of the bomb at any instant). Upon approaching the scabbing limit, the resistance to penetration would no longer increase with depth, and the "Q" term of the Livingston Penetration Formula would no longer be valid.

The field evidence indicates that the manner of rock failure for very high altitude bombing with larger bombs may differ from that observed in the Bomb Penetration Project. From the meager data available, it appears that the change occurs at roughly 540 million foot-pounds for projectiles striking with a velocity of 1300 feet per second. The change is thought to mark the lower limit of plastic failure. Further fundamental research in this region is desirable, for it is probable that the "Q" values of Fig. 203 must be modified in the region where plastice failure predominates.

The following conclusions may be stated relative to those objectives of the Bomb Penetration Project that are closely related to the effect of the bomb upon the rock.

1) *How does a rock fail as a result of bomb impact?*

Rock failures due to the impact of a bomb may be classified in one of two zones. These zones are termed here "the zone of elastic failure" and "the zone of plastice failure." The limit between the two zones is tentatively placed at 540 million foot-pounds for bombs striking at 1300 feet per second. Perhaps the true limit between the two zones may vary; the plastic zone may coincide with the region above Mohr's envelope of rupture (See Fig. 71), and the elastic zone may coincide with the region below Mohr's envelope of rupture.

Rock failure as observed in the Bomb Penetration Project is thought to be primarily in the "zone of elastic failure." The manner of rock failure differs in each of four zones of failure illustrated in Fig. 184 and described in detail in Part F, Section I. The rock is thought to fail predominantly in tension as a result of a constant stress difference between the maximum and the minimum principal stress. The attitude of the planes of failure coincides with the three directions of principal stress.

2) *Is the method of failure the same in granite as in sandstone?*

The method of failure is identical in the two types or rock. The Dakota sandstone is more resistant to penetration than the granite when bombing at impact energies in excess of 15 million foot-pounds. Part F, Section I, presents a theory of penetration of projectiles in rock and discusses the

effect of the elastic properties of the two types of rocks upon the resistance to penetration and upon the degree of fragmentation of the rock in the apparent craters.

3) *How are the physical and elastic properties of rocks related to their ability to resist penetration?*

The effect of the physical and elastic properties of rocks upon penetration is discussed in Part F, Section I, Items 2c, and in Part F, Section II, Item 3. The first terms of the Livingston Penetration Formula expresses the effect mathematically and states that penetration is a function of Poisson's ratio and of the lateral stress in the medium.

4) *What determines the shape of the path of a bomb in rock?*

The shape of the path of a bomb in rock is determined by the relative magnitudes of the components of stress in the medium parallel to the axis of the bomb and at right angles to the axis of the bomb. The component parallel to the axis of the bomb is determined by the impact energy and by the rate at which energy is dissipated into the medium. The component at right angles to the axis of the bomb is determined by the impact energy and by the stress induced in the medium because of lateral confinement.

The inclination of the target surface, the angle of fall at impact, the shape of the nose of the bomb, the diameter of the bomb, the ratio of the length of the bomb to the diameter of the bomb, and the attitude of geologic planes of weakness all influence the stress distribution in the medium, the manner of rock failure, and the path of the bomb.

7) *What factors determine the size and shape of the bomb crater in rock?*

The factors that determine the size and shape of a bomb crater in rock are discussed in Part C, Section I, Items 4 and 5; and Part D, Section I, Items 4 and 5. The relations are complex, but in general the rock factor, the nose factor, the diameter of the bomb, the impact energy, and the attitude of geologic planes of weakness determine the size and shape of the crater, the path of the bomb, and the depth of penetration.

8) *How do geologic planes of weakness influence the crater shape and the depth of bomb penetration?*

Geological planes of weakness such as joints and bedding planes relieve stress and distort the shape of the shear contours and the principal stress contours. The bomb is caused to deviate in the direction of least distortion of the principal stress contours. The influence of joints, faults, and bedding planes upon the crater shape and upon the depth of penetration is illustrated in Fig. 185 and described in detail in Part F, Section II, Item 2. The effect of a fault, as distinguished from a joint, is to reduce the resistance to penetration. Although a fault might be thought of as a series of closely spaced joints, the fault zone usually is brecciated and the broken rock altered to a greater extent than the rock walls. The effect of the brecciation and alteration is to modify the elastic properties of the

rock within the fault zone and to cause the rock to fail by plastic flow, rather than in the manner illustrated in Fig. 184.

9) *How and why does tunneling of a bomb in a rock occur?*

The point at which "tunneling" begins is thought to mark the limit between the region in which plastic flow predominates over rock failure of the type described in Part F, Section I, Item 5. Plastic flow may occur at a low stress range in a weak rock or at a high stress range in a strong rock. Future fundamental research in this field is needed.

11) *What types of damage to underground installations in sandstone and granite is possible using the types of bombs dropped in the Bomb Penetration Tests?*

Sandstones differ substantially in their elastic properties as likewise do granites. The types of damage to underground installations in Dakota sandstone and Zuni granite are discussed in detail in Part F, Section IV and in Part F, Section V. The area above a tunnel where bombs of the type dropped in the Bomb Penetration Tests must strike to damage the tunnel is small. In general it would seem unprofitable to attack underground installations with the types of bombs used in the Bomb Penetration Tests.

12) *What is the relative effectiveness of various types of bombs in damaging underground installations?*

The relative effectiveness of the various types of bombs are listed as follows in order of decreasing effectiveness.

1—25,000 SAP	Most effective
2— 2,000 SAP	
3— 1,600 AP	
4— 2,000 GP	Least Effective

The criteria upon which the above list is based are 1) accuracy, 2) weight of the explosive charge and the resistance of the casing to rupture, 3) the depth of penetration, and 4) the figure of merit (See Fig. 206). The effectiveness of an underground installation and the selection of bombs for attack are discussed in following pages.

14) *How can the theory of penetration of bombs be used to improve the design of fortifications?*

Resistance to penetration of a massive fortification is probably a function of Poisson's ratio of the construction material. Therefore, materials having a high value of Poisson's ratio should be considered. The placement of reinforcing rods on the front and rear faces of thick slabs perhaps can be improved to minimize the development of "O" cracks (See Fig. 184). The path and the depth of penetration of projectiles striking the fortification can be calculated for various angles of impact. The thickness of the fortification to resist the combined effects of impact and explosion can be calculated.

15) *How can the vulnerable portal area of an underground installation best be protected against bombing?*

The best protection for the portal is camouflage. The next best protection is by means of the practice of "roof bolting," in which the sides of the opening and in some instances also the roof of the opening are reinforced. If it is free from overburden, the surface above the opening may also be reinforced with roof-bolts.

3—Effectiveness of an Underground Installation

An underground structure that is capable of withstanding an explosion in the rock mass itself will not be damaged by an explosion that takes places on the surface or in the air above the installation. Air blast will cause some stress in the rock, but examination of Fig. 164 shows that the stress in a three-dimensional body decreases very rapidly with increasing depth. The peak overpressure of the shock wave 1000 feet from the explosion of a nominal atomic bomb is only 100 pounds per square inch.[1] Figure 164 was constructed for an assumed load of 100,000 psi. Thus, it is evident that air blast will have no effect upon a buried opening in rock.

Under some circumstances, the portal and auxiliary structures, such as ventilation and escape shafts, might suffer damage as a result of air blast or flying rock. Proper design would prevent such damage.

Rock masses are singularly well adapted to resist shock because of their inherent strength and because of the rapid damping of a shock front in the rock. The discussion of Part F, Section IV, brings out the fact that an increase in the rock cover greatly increases the resistance of an opening to damage. The amount of rock protecting an opening is determined not only by the depth at which the opening is placed, but also by the lateral distance from the opening at which the bomb may strike.

Part F, Section IV, also shows how inaccurate bombing is equivalent to adding rock cover to an underground opening. The area above a tunnel where a bomb must strike to do the required damage is small; thus a premium is placed upon bombing accuracy.

In view of the necessity for extreme bombing accuracy, additional protection is obtained by camouflage of the access roads and the portal and by not disturbing the surface above an installation. If the target is well-concealed, it will be difficult to attain the required accuracy.

4—Effect of the Rock Upon the Bomb

From photoelastic studies of the stress distribution in the medium (See Part E, Section V, Item 5) it has been determined that the forward thrust of a bomb along the line of action is combined with a tendency to rotate. The resistance offered to rotation by a long bomb in rock is greater than that offered by short bomb. Thus, a long bomb is more likely to be bent or to be damaged near the base plate than a short bomb. However,

---

[1] U. S. Atomic Energy Commission, The Effects of Atomic Weapons, page 32, fig. 3.13b, McGraw Hill, New York, 1950.

if the long bomb is designed to withstand the stress at the tail, the vertical deviation will be reduced and the normal penetration will be increased.

The shear stress distribution in the nose and at the juncture of the nose and the cylindrical part of each of the types of bombs dropped in the tests is presented in Part E, Section VI. Because failure of a bomb occurs in maximum shear, those places showing a high stress concentration are weakest. It is desirable to eliminate zones of high stress concentration by changing the metal distribution. The 1600 AP bomb is the strongest of the four types of bombs dropped. The design of the 1600 AP bomb most nearly meets the requirements of ideal stress distribution, but it is apparent that the bomb is stronger than necessary for penetrating rock.

The Livingston Penetration Formula summarizes three relations to be observed in designing bombs to achieve maximum penetration. First, the bomb must have a sharp nose. (See Nose Factors, Fig. 199). Second, the bomb must have as small a diameter as is possible, because penetration varies inversely as the diameter. Third, the bomb must have as great a mass as is possible, because the "Q" factor (See Figs. 201, 202, and 203) depends upon the mass.

Now consider the three requirements that a bomb suitable for attack must fulfill.

1) The bomb must be ballistically accurate.
2) The bomb must be released from the proper altitude.
3) The bomb must carry the highest possible amount of explosive.

If we combine the requirements for penetration with the requirements for attack we obtain the specifications of future bombs intended for attacking underground installations. The technical difficulty imposed by item 3 above can be eliminated by restating the requirement in the form:

3a) The bomb must contain the greatest possible explosive energy, in the smallest possible space near the nose of the bomb.

The following conclusions may be stated relative to those objectives of the Bomb Penetration Project that are closely related to the effect of the rock upon the bomb.

1) *Which of the various bombs tested is most effective for penetration?*

For a given rock and a fixed impact energy, the penetration is proportional to the nose factor, N, and inversely proportional to the diameter of the bomb, d. Therefore, the best bomb for penetration is the one with the greatest N d ratio: This is tabulated for each of the bombs dropped.

1600 AP	0.96	(most effective)
2000 SAP	0.64	
2000 GP	0.48	
25,000 SAP	0.38	(least effective)

Thus, it is seen that the 1600 AP bomb is the best for penetrating a given rock at a fixed impact energy. The 25,000 SAP penetrates more because of its great energy, not because of its better penetration characteristics. Possibly, when rating the effectiveness of various types of bombs, further consideration might be given both to the scaling laws and to the limits of elastic and plastic failure.

2) *Can the design of bombs be improved to increase their penetration into rocks?*

Each of the four types of bombs dropped in the tests has certain advantages. It seems desirable to improve the stress distribution in each of the four types of bombs, but it does not seem desirable to design each of the four types to increase penetration into rock. Instead it seems more desirable to develop a new type of bomb that combines the requirements for penetration with the requirements for attack.

3) *At what altitude can low-order detonation be expected when bombing with general-purpose bombs?*

Only one 2000 GP bomb dropped in the tests did not deform. It was released from 7000 feet above the target. It is unwise from the evidence obtained from only one bomb drop to state that 7000 feet is the critical altitude above which damage begins. (See Part D, Section I, Item 6). All 2000 GP bombs released above 18,000 feet ruptured regardless of topography or any variable. All of the 2000 GP bombs released from above 14,000 feet rebounded and were found at some distance from the crater. From available evidence it seems that rupture and low-order detonation of 2000 GP bombs may begin at a release altitude of approximately 8700 feet.

4) *Can the design of 2000 GP bombs be improved to minimize low-order detonation?*

Although new laboratory techniques must be developed for applying loads to model bombs in the photoelastic laboratory and three-dimensional studies should be undertaken, it seems from present evidence possible to improve the stress distribution in 2000 GP bombs without substantially altering the present charge-weight ratio. Points of high stress concentration as observed in the photoelastic laboratory coincide with points of failure as observed in the field. By changing the inside and outside shape of the bomb to eliminate bending at the nose, it seems possible that low-order detonation due to casing failure at impact can be reduced.

5) *What structural changes and hardness changes take place in the metal of the bomb at impact?*

The metal near the nose of the bomb is affected to a greater degree than the metal near the tail of the bomb, and the metal on the footwall side of the bomb is affected to a greater degree than the metal on the hangingwall side of the bomb. Flow-metal droplets form near the nose of the bomb and spread out along the nose and on the footwall side of the bomb. Hardness changes occur which result in a greater hardness than the original in some places and a lesser hardness in other places.

The metallurgical and hardness changes due to impact are described in Part E, Section IV.

6) *What is the stress distribution in the nose and in the forward part of the cylindrical portion of each of the types of bombs dropped in the Bomb Penetration Project?*

The stress distribution in each of the bombs for various degrees of loading is shown in the photographs and discussed in Part E, Section VI.

7) *Can the shape of the nose and the distribution of metal be improved to increase the strength of the various bombs tested without increasing the weight of the bombs?*

The shape of the nose is the key to the stress distribution in the forward end of all bombs. The stress distribution in sharp-nosed bombs is superior to that in the blunt-nosed bombs. The penetration of sharp-nosed bombs is superior to that of blunt-nosed bombs. Of the four types of bombs, improvement of the 2000 GP bombs seems most desirable and most feasible.

8) *What future types of bombs will be most effective against underground installations?*

It is doubtful if a bomb has yet been developed that is truly effective against underground installations. The prerequisites for effective bombing of underground installations are discussed in Part F, Section V, Item 4. The effect of bombing on underground installations is discussed in Part F, Section IV, and each of the bombs dropped in the Bomb Penetration Project is assigned a figure of merit which is a measure of damage to a "standard" tunnel.

5—Selection of Bombs for Attack

A bomb that is suitable for attack must fulfill three requirements:

1) The bomb must be ballistically accurate.
2) The bomb must be dropped from an altitude that will result in the impact kinetic energy's falling in a range of maximum penetration but still being below the energy at which rupture of the casing and low order detonation of the explosion will occur.
3) The bomb should carry the highest possible amount of explosive.

The first condition is necessary to meet the requirements of accuracy. The second is necessary to ensure that the pay-load of the bomb is delivered as near as possible to the target. The third requirement makes for the creation of maximum damage with whatever penetration can be attained.

It can be shown from the Livingston Pentration Formula that if a 1600 AP bomb and a 2000 SAP bomb are dropped with the same energy upon a given rock, the AP bomb will penetrate 1.5 times deeper than

the SAP, but because the SAP bomb carries 2.58 times as much explosive as the AP carries, the damage distance for a given degree of damage is about 1.35 times more for an SAP than for an AP bomb. The GP bomb carries 1.88 times as much explosive as the SAP bomb does, but because it ruptures easily and thereby causes a low order detonation, it is not suitable for attack purposes unless dropped from low altitudes.

The 2000 SAP bomb is the best of the three small bombs to use. The 25,000 SAP bomb is necessary for the attack of relatively deep installations because of its greater penetration and greater explosive capacity.

6—Recommendations

We believe that fundamentals of rock failure previously unknown have been set forth in this report. Moreover, theories are presented here which are on the frontiers of knowledge. Considering the importance of these theories relative to the extent of the field and laboratory work upon which they are based, it is evident that the work begun here is but a skeleton of that which remains to be done.

1) It is our recommendation that the Bomb Penetrationt Project be continued, particularly at the Putney Mesa sandstone site in the prototype rock. It is recommended that more types of bomb and more of each type of bomb be tested. It is recommended that experiments be conducted in both the elastic and the plastic zones as set forth in Fig. 203.

It has been pointed out in this report that pin-point accuracy is a primary prerequisite for attacking underground installations. A 10-foot miss of an underground installation is more serious than a 100-foot miss of a surface target. In these experiments it was observed 1) that 1600 AP and 2000 SAP bombs are equally accurate, 2) that the accuracy at 9,000 feet is better than at 18,000 feet, 3) that both the accuracy and the penetration are better at 18,000 feet than at 30,000 feet, 4) that the accuracy of the 25,000 SAP bomb may be superior to that of the 1600 AP and 2000 SAP bombs at 18,000 feet.

2) It is our recommendation that a statistical study be made of the accuracy of various types of bombs from various altitudes, and that the results of these findings be used as a basis of

   a) determining what qualities cause a bomb to be stable in flight,

   b) determining the ballistic characteristics of future bombs designed for penetrating rocks.

A distinct possibility exists that penetration may be much greater in the plastic range than in the elastic range. There are four possible ways to enter the plastic range, a) to decrease the diameter of the bomb, b) to increase the sharpness of the nose, c) to increase the striking velocity, and d) to increase the mass of the bomb. If recommendations 1 and 2 are adopted, fundamental data will be achieved whereby the limits of elastic and plastic failure may be defined. If recommendation 2 is adopted, the shape and the ballistic characteristics of a super-bomb may be estab-

lished. If the following recommendation is adopted and the evidence is combined with the prerequisite listed in Part F, Section IV and V, a super-bomb may be developed that will be more effective against underground installations than anything yet conceived.

3) Continue a) the study of the stress distribution in a semi-infinite solid due to the impact and penetration of bombs and b) the study of the stress distribution in the nose, the body, and the tail of bombs at various stages of penetration. Determine, if possible, the proper length-to-diameter ratio and the proper shape of the tail end of the bomb body. Determine, if possible, preferred shapes for each of several standard types of bombs, and improve, if possible, the charge-weight ratio of each.

We have pointed out a) that the "Q" factor of the Livingston Penetration Formula (See Part F, Section V, Item 2) expresses two factors that can not be separated without further fundamental research, b) that the nose correction factors of Fig. 199 are tentative because of the limited data available.

4) It is our recommendation that fundamental research in the photoelastic laboratory and the barodynamics laboratory continue towards the objective that the "Q" factors may be stated in a mathematical form, as has been accomplished for the rock factor. It is suggested that this laboratory work proceed concurrently with recommendation 1.

The Bomb Penetration Project was conducted in Dakota sandstone and Zuni granite, and the Livingston Penetration Formula was developed from the evidence obtained from these two types of rock. It is desirable to check the evidence upon which the formula is based by extending the Bomb Penetration Project to include other types of rocks. When selecting the other types of rocks it seems desirable to select, if possible, a rock type that may be more resistant to penetration than Dakota sandstone and a rock type that may be less resistant to penetration than Zuni granite.

5) It is recommended that the Bomb Penetration Project be extended to include rocks that are more resistant to penetration than the prototype Dakota sandstone and less resistant than Zuni Granite. In order to determine what geological classes of rocks meet these requirements, it is suggested that drill cores from many localities be tested in the barodynamics laboratory. It is suggested that subsequent to the laboratory work that reconnaissance surveys be conducted to determine the suitability of proposed bombing sites in the types of rocks selected from the laboratory studies.

It has been pointed out (See Part F, Section V) that the theoretical maximum value of Poisson's ratio is 0.5 and that when this theoretical maximum is substituted in the rock factor term of the Livingston Penetration Formula, the theoretical minimum value of the rock factor is 0.4 compared to a Dakota sandstone value of 1.0. It is known that hydrostatic

conditions prevail where Poisson's ratio is 0.5. Furthermore, it is apparent that the vertical deviation of a bomb increases as the resistance to penetration increases. It is known also that as the vertical deviation increases, the stress at the tail of a bomb likewise increases. Since water has a Poisson's ratio of 0.5, it becomes a distinct possibility that the principles set forth here as applying to rocks may be applicable also when designing bombs to attack submarines. Now, it is obviously impractical to measure the path of a bomb through water, or to observe the damage to a bomb casing upon impact with water. However, by conducting experiments in a rock that behaves plastically (perhaps a shale) it may be possible to improve the design of areial torpedoes and of bombs released from high altitudes against ships and submarines.

6) It is recommended that the path of army- and navy-type bombs in shale and the effect of the impact upon the bomb casing be studied. Bombs of various diameter, various nose-shapes, and various length-to-diameter ratios should be included in the tests.

Roof-bolting has been suggested as a means of reinforcing the surface above a tunnel and of reinforcing the sides and back of a tunnel. The suggestion is based upon the theory of crater formation (See Part F, Section I, Item 4b) and upon the theory of tunnel damage (Series I and Series II Experiments).

7) It is recommended that upon completion of the Underground Explosion Test Program at the Navajo Sandstone Site, that the 0.1 scale tunnel and the 0.2 scale tunnel be reinforced underground and on the surface, and that live bombs be dropped in an effort to destroy the openings.

TABLE OF ERRATA

Page 5—Paragraph 5, read sites instead of cites.

Figure 9—Read 89.5% instead of 895%.

Page 20—Paragraph 4, read northwest instead of southwest.

Page 43—Paragraph 6, read dike instead of like.

Page 64—Figure 60, read Zuni Granite instead of Zuni Sandstone.

Page 69—Read V_n to V instead of V_n to U.

Page 118—Paragraph 1, read or instead of "of".

Page 157—Last Paragraph, read fringe instead of fringer.

Page 213—First paragraph, read P_3 instead of P^3.